City Research Online

City, University of London Institutional Repository

PhD Thesis

Gauge Theories, Toric Varieties and Machine Learning

Author:
Jiakang Bao

Supervisor:
Prof. Yang-Hui He

Submitted in partial fulfillment of the requirements for the degree of Doctor of Philosophy of City, University of London

CITY
UNIVERSITY OF LONDON
—— EST 1894 ——

CITY, UNIVERSITY OF LONDON

Abstract

Department of Mathematics

PhD in Mathematics

Gauge Theories, Toric Varieties and Machine Learning

by Jiakang Bao

We discuss some recent study on quiver gauge theories in the setting of toric geometry. After mentioning some basic geometric and topological properties, we consider some mathematical concepts, namely the Mahler measure and the dessins d'enfants, in this context. We then focus on the quiver BPS algebras and their connections to different aspects in physics. We also have a discussion on the stability of chiral rings for more general geometry. Besides, we make some comments on the applications of machine learning to relevant topics. This thesis is based on the works [1–16].

Acknowledgements

First and foremost, I wish to express my utmost gratitude to my supervisor, Prof. Yang-Hui He. His guidance with fascinating insights, immense knowledge, heartening encouragement and vast patience has been a beacon illuminating my PhD study and my life. Only with his considerate care can I voyage to the wonderland of physics and mathematics. *Plurimum illi debeo et gratiam habeo sempiternam.*

I would like to thank the PhD cohort for all the laughter and tears, all the hopes and fears that we share with each other. With my academic siblings Ed Hirst and Elli Heyes, I had the best memories of the days of our lives. I am fortunate to have Ed, who is always kind and supportive, as my friend and my colleague from the first day of my PhD study. I really admire Suvajit Majumder, who exerts his great efforts running our journal club, for his passion and wisdom in physics. It is my pleasure to be a friend with Takanobu Taira who is full of charisma and does intriguing works on quantum field theory. I would always remember Gabriel Bliard for his great friendliness and exceptional brilliance. I am proud to know Dmitrii Riabchenko with whom I had many invaluable discussions and unforgettable chats. I am also thankful to all the other mathematical scientists in the PhD office, including Johann Bauer, Alberto Bracci, Bob Dabson, Cecilia de Fazio, Hasan Haq, Amin Mekacher, Will Murphy, Sotiris Papadopoulos, Alan Scaramangas. Moreover, a special thanks goes to my "Cubbie buddy" Xiangnan Feng.

I am obliged to Ali Zahabi who introduced me to many splendid concepts in mathematical physics. I had amazing conversations when working with him. I am grateful to Futoshi Yagi. I have learnt so much from him, and his research attitude is always an inspiration to me. I am also indebted to Antoine Bourget, Siqi Chen, Sebastián Franco, Julius Grimminger, Amihay Hanany, Zezhuang Hao, Johannes Hofscheier, Yusheng Jiao, Alexander Kasprzyk, Ziwen Kong, Chunhao Li, Deshuo Liu, Gregg Musiker, Rak-Kyeong Seong, Yan Xiao, Masahito Yamazaki, Zhenghao Zhong for fruitful disscusions and/or enjoyable collaborations, as well as all the little things in life.

I would like to earnestly thank the London Institute for Mathematical Sciences (LIMS) for hospitality during my PhD study. All the members, including Robert Bywater, Ali Emamy, Rob Farr, Andrey Fedosyeyev, my "chips ally" Thomas Fink, Madeleine Hall, Victoria Harrison, Thomas Hodgkinson, Alana Ker Mercer, Sarah Myers Cornaby, Sasha Ochirov, Roman Rybiansky, Forrest Sheldon, Ilya Shkredov, are always friendly and welcoming to me. Their efforts make LIMS a wonderful place, and I will miss the warm atmosphere there.

I am thankful to my family for their enduring support during my study.

As a tradition in one's thesis, I wish to thank my girlfriend whose existence has not yet been proven. So far, she does not even behave like an instanton in my worldvolume. This allowed me to spend more time on my PhD study.

I am grateful to the examiners Valentina Forini, Sanjaye Ramgoolam who devoted their time to reading the thesis and providing invaluable suggestions. I would like to thank Laure Daviaud for kindly being the chair of my viva. I also appreciate Ann-Marie de Here's help on dealing with the university system.

I need to make sincere apologies to those who I should acknowledge but are not mentioned explicitly here. There is not enough space in the margin (and in my head).

To my grandfather

Contents

美麗有兩種
一是深刻又動人的方程
一是你汎著倦意淡淡的笑容
<div style="text-align: right">ukim (ID) from PKUBBS</div>

Chapter 1

Introduction

After the great success of relativity, quantum mechanics and then quantum field theories, quantizing gravity becomes the core of high energy theory. There are quite a few candidates for quantum gravity, but string theory seems to be the most promising one. Although we cannot find more evidences from current experiments, string theory already explains many things as postdictions, which are also important as tests for our theories. Moreover, string theory is mathematically consistent and has led to many profound discoveries in mathematics. See [17] and the references therein for summaries on the current status of string theory, ranging from physical mathematics to possible future experimental evidences.

Superstring theories demand our spacetime dimension to be 10, which means we should reduce them to an effectively 4-dimensional theory. The standard solution of string compactification, as a generalization of Kaluza-Klein compactification, renders the extra six dimensions Calabi-Yau (CY). Thus, the study of Calabi-Yau and algebraic geometry has entered the field of theoretical physics.

For Type II string theory on toric CY threefolds, the 4d $\mathcal{N} = 1$ gauge theories arised therefrom can be beautifully described by quivers [18, 19]. With various techniques developed in the past few decades, including brane tilings [20–24], Hilbert series and plethystics [25–40], and crystal melting [41–45], many salient features of our physical theories have been extensively investigated and understood. They have also shown deep connections to a vast range of areas in mathematics such as algebraic geometry and enumerative geometry.

In this thesis, we shall explore some recent progress in these directions. There have been vigorous interactions with not only geometry but also number theory, quantum algebras and representation theory. Of course, toric CYs are non-compact. Nevertheless, in principle, we can turn on the Ω-background so that the theory would be localized at the fixed point under the isometry of CY threefolds and effectively get compactified. More importantly, there is still little known for the compact cases, and we hope that our study would shed light on our investigations in the compact geometry. Broadly speaking, further study on mathematical physics and physical mathematics should lead us to a more comprehensive picture of the nature of spacetime and more insights of unification.

1.1 Organization of the Thesis

The thesis is organized as follows. In Chapter 2, we will start with some rudiments of quiver gauge theories, brane tilings and toric geometry. As an illustration, we shall then consider the cases associated to convex lattice polygons with two interior points. They serve as the toric diagrams of certain toric CY_3 cones, as well as those of compact base surfaces. In particular, the volume functions of the Sasaki-Einstein base manifolds can be computed so as to get the R-charges of the fields via volume minimization. As we will see, there are differences between the non-reflexive cases and the reflexive cases (with one single interior point) regarding certain geometric and topological properties.

More specifically, we shall analyze the minimized volumes in terms of the topological quantities of the compact toric varieties constructed from the polygons. To obtain the compact varieties, we need the fans over the polytope followed by complete resolutions. However, unlike reflexive cases, we have two choices of origins here, which we call zeroth-grade and first-grade points. It turns out for most of the cases, the Chern numbers and even the Chern classes coincide for the two compact varieties. For those with first-grade points, they do not have such property, but if we further resolve the smooth surface with an extra ray added to the fan, we find that the Chern numbers and classes are again the same for the two varieties. As we will see, whether the two varieties are the same surface can completely determined by the symmetries of the polygon, namely whether it is axial symmetric or centrosymmetric.

Similar to the reflexive cases studied in [46], all the relevant topological invariants, including Chern numbers, Betti numbers and Hodge numbers, are dependent to each other. Hence, all the non-trivial quantities can be expressed with Euler numbers. Thus, we only need to consider the relation between $V_{\min}$ and χ. It turns out that the volume bounds relation from the reflexive cases does not hold for the non-reflexive ones, and we will raise a generalized conjecture.

In Chapter 3, we will introduce the concept of Mahler measure [47] which originates from number theory. We will see that Mahler measure enjoys many nice properties in the context of toric quiver gauge theories. We find that maximizing the Mahler measure at the so-called isoradial point leads to the correct R-symmetry in the infrared. In other words, maximization of the Mahler measure is equivalent to the a-maximization.

We will also discuss how the Mahler measure, its logarithmic derivative, and the Ronkin function behave under Seiberg/toric duality and specular duality. We conjecture that they are all invariant under Seiberg duality. As a byproduct, this provides ways to treat the non-isoradial brane tilings and the isoradial ones on an equal footing. It is worth noting that the logarithmic derivative of the Mahler measure can be viewed as the generating function of the master space in terms of perfect matchings/gauged linear sigma model fields. As a result, we will see that the Mahler measure have remarkable features for toric and specular duals.

In Chapter 4, we will discuss the relations of the Mahler measure and the dessins d'enfants [48]. Dessins are essentially collections of black and white nodes connected by edges. However, such simple graphs actually encode information of rational maps and quadratic differentials due to Belyi's theorem [49]. For reflexive polygons, as their Newton polynomials define elliptic curves, we can consider the so-called modular Mahler measure [50]. We will see that with certain choices of the coeffcients in the Newton polynomials, there can be a one-to-one correspondence between the Mahler measure and the dessins. In fact, such choices are different from the ones that are used in determining the R-charges. Nevertheless, both of them reflect certain aspects of the brane tilings and the gauge theories. We also hope that the discussions therein would elucidate the study on the consistency of brane tilings.

As we shall discuss, different complex structures of the torus arised from different contexts are actually extrapolated by the Mahler flow. In other words, by varying the parameter in the Mahler measure, we can reach different points for these complex structures. As some further applications, we will mention how the brane monodromies can be related to the monodromies for dessins in the context of F-theory. In particular, the 7-branes correspond to not only the faces of the dessins but also some of the black nodes. On the other hand, we will see that certain expansions in the Mahler measure can recover the Gromov-Witten (GW) invariants of local vanishing surfaces in the CY spaces. From enumerative geometry, we learn that they reveal the BPS states from F-theory compactified on the toric threefolds. We will give a dictionary between the GW and the Mahler sides.

In Chapter 5, we will focus on the BPS algebras in the Type IIA setting. Studying the BPS spectrum [51, 52] of particles has been an important topic in quantum field theory and string theory. As aforementioned, although there is little known for the case of compact CY manifolds, the techniques

have been greatly developed in the context of non-compact, or local, CYs, especially when they afford a toric description. As the lattice polygons nicely encode combinatorial information from the toric CY threefolds, crystal melting and quivers have become extremely useful tools in BPS counting.

Mathematically, BPS counting has a close relation with Donaldson-Thomas (DT) invariants[1], and are hence also connected to Gromov-Witten and many other geometric invariants. Going one step further, we would also like to understand more about the Hilbert space of the BPS states, which can be recast as the cohomology of chain complexes. This then leads to the categorification of BPS indices and wall crossings [53–56]. Although we will not discuss such categorification in this paper, they should be intimately related to the algebraic structure of BPS states.

For Type IIA string theory compactified on a general toric CY threefold, the BPS states are the bound states formed by Dp-branes wrapping holomorphic p-cycles therein. Here, we shall focus on the following setting: (i) a single D6 wrapping the whole CY$_3$; (ii) D0-branes supported on points which are trivially compact in the CY; (iii) D2-/D4-branes wrapping either compact or non-compact 2-/4-cycles. The compact D-branes are then light BPS particles that are dynamical. In contrast, non-compact D-branes are heavy line operators which become non-dynamical in our compactified theory.

Recently, the quiver Yangians are introduced as realizations of the BPS algebras in this setup [57]. We will give a definition of these algebras and their trigonometic and elliptic counterparts. We will discuss various properties for them, including the coproducts, their transformaions under toric duality etc. Moreover, we shall consider its connections to integrability as well as vertex operator algebras (VOAs).

Similar to the ordinary Yangian algebras, we can consider the $\mathcal{R}$-matrix formalisms for the quiver BPS algebras. We will discuss the actions of quiver Yangians on the crystal representations as well as their coproduct structures. In fact, there are still many interesting directions for future study. For instance, there are obstructions for the Bethe/gauge correspondence for chiral quivers [58]. Also, the precise connections to the Maulik-Okounkov (MO) Yangians are still not clear [59]. Moreover, recent progress on 4d Chern-Simons theory [60–63] could provide more insights as well.

On the other hand, the $\mathcal{W}$-algebras [64–70] should play a crucial role in the tensionless limit of string theory in AdS$_3$ [71–74]. In particular, the rectangular $\mathcal{W}$-algebra can be realized as the symmetry algebra of the coset CFT whose holographic dual gives higher spin gravity [75]. Such vertex algebras have been well-studied in mathematics literature such as [76–78].

Therefore, we shall discuss the BPS/CFT (aka AGT, 2d/4d) correspondence [79, 80] here as well. The BPS algebras and the VOAs are expected to be contained in a broader picture under the BPS/CFT correspondence. In the finite cases, the relations between Yangians and $\mathcal{W}$-algebras have been explored in [81–83]. For $\widehat{\mathfrak{gl}}_1$ whose associated CY is the simplest $\mathbb{C}^3$, it was shown in [84, 85] that the affine/quiver Yangian is isomorphic to the universal enveloping algebra of the $\mathcal{W}_{1+\infty}$-algebra. Moreover, in such case, the AGT conjecture was proven in [86] with a surjective homomorphism from the quiver Yangian for $\mathbb{C}^3$ to the universal enveloping algebra of the principal $\mathcal{W}$-algebra. Physically, the Nekrasov partition function of the 4d supersymmetric gauge theories can be identified with the conformal blocks of the corresponding VOAs. From a geometric perspective, the Verma module of the VOA results from its action on the equivariant intersection cohomology of the instanton moduli space [87].

Similar to the $\mathcal{W}_{1+\infty}$-algebra case whose truncation gives the algebra at the corner [88], the matrix-extended $\mathcal{W}$-algebra (called $\mathcal{W}_{M|N\times\infty}$ in [69]) for any generalized conifold is expected to truncate to VOAs describing certain interface of a 4d supersymmetric gauge theory. We will see that the

---

[1]In the usual canonical crystal melting setting, we are working in the non-commutative Donaldson-Thomas chamber.

universal enveloping algebras of the VOAs are indeed the truncations of the BPS algebras, and the quiver Yangians can in this sense be viewed as some realization of $U(\mathcal{W}_{M|N\times\infty})$.

In Chapter 6, we will switch gears and consider general varieties including non-toric cases. Whether a chiral ring describes any CFT was related to the concept of K-stability in [89]. We shall apply the tools of Hilbert series, plethystics and Gröbner basis to study this. We will illustrate this with a few examples. In particular, we will see that K-stability does not always imply that the chiral ring is a ring of some CFT. Nevertheless, it is still natural to conjecture that K-stability gives a necessary condition.

In Chapter 7, we will mention some recent applications of machine learning in mathematics and physics. We will consider two examples where the analysis on the machine learning results could help us find analytic results. In the first example, we will use the Ehrhart polynomials to get the volumes of the associated lattice polytopes. In the second example, we shall analyze the data for amoebae in tropical geometry to find the conditions on their genus. Although these examples are rather simple and the analytic results are already known before, it could be possible that future developments would be used in numerical analysis and even conjecture formulations. Thus, whether AI can be a "witness" of our study in physics and mathematics and how we should apply machine learning properly have become interesting questions in our future research.

In the appendices, we give some supplementary materials as well as more discussions that are not covered in the main context. In Appendix A, we list all the lattice polygons with two interior points, along with their volume functions. In Appendix B, we give an explicit example on computing the Mahler measure and some plots of the amoebae. We discuss some more aspects of the dessins in Appendix C. In particular, we consider their relations with Seiberg-Witten curves and conformal blocks. We will give some criteria to determine how dessins could correspond to conformal blocks in minimal models. In Appendix D, as a comparison with the dessins and Mahler measure in the main context, more choices on the coefficients in the Newton polynomials are mentioned. In Appendix E, we review how to construct the quivers associated to the generalized conifolds. In Appendix F, we discuss possible connections of the BPS partition functions to the Kac polynomials. We give some more examples on the $\mathcal{R}$-matrices acting on the crystal configurations in Appendix G. A quick review on rectangular $\mathcal{W}$-algebras can be found in Appendix H. Some comments on the modes of quiver BPS algebras are mentioned in Appendix I. In Appendix J, we have a recap on the Gröbner basis. In Appendix K, we derive the conditions on the genus for some (lopsided) amoebae.

1.2 Summary

Although we have mentioned some results of the thesis in the previous section, for clarity, let us make a brief list of the summary here. More concrete details of the results can be found at the beginning of each chapter.

Chapter 2 is mainly a review part. Nevertheless, we analyze the relation between the minimized volumes and the topological quantities associated to the toric CYs, extending the previous conjecture for reflexive polygons to non-reflexive ones.

In Chapter 3,

- We define different "limits" known as the isoradial and tropical limits, and discuss the behaviour of the Mahler measure and amoebae in these limits.

- We report the theorem stating that for isoradial dimers, the maximization of the Mahler measure is equivalent to the a-maximization, and we conjecture this to hold for non-isoradial dimers as well.

- We study the properties of Mahler measure under Seiberg duality and specular duality. In particular, it is expected to be invariant under Seiberg duality. A crucial quantity (u_0) is

shown to encode the master space, and hence lead to how Mahler measure transform under specular duality.

In Chapter 4,

- We connect the Mahler measure to dessins under modularity. On the Mahler measure/Newton polynomial side, we find the Hauptmoduln of some congruence subgroup arised from the parameter thereof. The congruence group of the corresponding dessin is conjectured to be the subgroup of the one on the Mahler side.

- We argue that the Mahler measure is a period in the sense of Kontsevich and Zagier when the j-invariant is algebraic. We also write the differential equation of the Mahler measure with respect to the j-invariant ((4.2.17)).

- We illustrate how the 7-branes can be "placed" on the dessins in the context of F-theory.

- We give the dictionary between the Mahler measure and certain Gromov-Witten invariants.

In Chapter 5,

- We propose the crystal models for different chambers under wall crossing in the study of the BPS spectra.

- We discuss how one can obtain the Bethe ansatz equations from the BPS algebras via the $\mathcal{R}$-matrix construction.

- For generalized conifolds, we give the coproduct of the BPS algebras. We also argue that Seiberg dual theories have isomorphic BPS algebras. Moreover, these BPS algebras can be truncated to rectangular $\mathcal{W}$-algebras.

- We also report some results for toroidal and elliptic versions of the BPS algebras.

In Chapter 6,

- We discuss how one can determine the K-stabiliity of a chiral ring with illustrations of various examples.

- We find a counterexample of the conjecture which states that a chiral ring describing a ring of a CFT is equivalent to it being K-stable.

In Chapter 7, we give some examples of the application of machine learning, including

- how the machine predicts the volumes of lattice polytopes from the Ehrhart series;

- how the machine determines the genus of the (lopsided) amoebae.

Some of the appendices include the supplementary materials and/or some lists of the calculation results. We also put some results that slightly digress from the discussions in the main context in the appendices. In Appendix C, we discuss how one can bridge the dessins and conformal blocks (for minimal models) via their connections to Seiberg-Witten curves. In Appendix D, we consider a different choice of coefficients of the Newton polynomials and study the relation of the corresponding Mahler measure and (possible) dessins. In Appendix F, we discuss the relations of BPS partition functions and Kac polynomials. In Appendix G, we give examples on how to compute the $\mathcal{R}$-matrix actions on the crystal representations at higher levels.

Chapter 2

Quivers and Toric Varieties

Let us start with a quick review on toric varieties and their associated quivers. Then we shall discuss some topological and geometric properties following [2, 8]. In particular, we analyze the relation between the geometric quantity (minimized volumes) and the topological quantities (Chern classes and Euler numbers) for (the geometry associated to) the Newton polygons with 2 interior points. We conjecture that the minimized volume for the Sasaki-Einstein base manifold of any toric CY satisfies $1/\chi \leq V_{\min} < m_n \int c_1^{n-1}$ for some number m_n, where χ and c_1 are the Euler number and the first Chern class respectively.

2.1 Preliminaries

The worldvolume theory of a stack of D3-branes probing a toric CY cone-type singularity is a 4d $\mathcal{N} = 1$ supersymmetric gauge theory. Such gauge theories can be represented by quivers in which the matter contents and the superpotentials are encoded[1] [90]. Each toric CY_3 corresponds to a toric diagram which is a 2-dimensional lattice polytope, viz, a lattice polygon. The geometry of the CY_3 can thus be studied via their toric diagrams.

Hence, it is natural to expect that there are some connections between the quivers and toric diagrams. From one diagram, we can find the other following the approaches in [91, 92]. Given a quiver diagram, the process of finding the toric diagram is called the forward algorithm. Conversely, obtaining quivers from a toric diagram is known as the inverse algorithm. Generally speaking, the correspondence between the two kinds of diagrams is often one-to-many. A toric diagram may give rise to more than one quivers while many quivers can have the same toric diagram. As a matter of fact, these quiver theories are related by toric duality, which can be understood as Seiberg duality in the toric phases [90, 93].

If we consider the back reaction to the geometry from D3s, then we get an AdS near-horizon geometry. As a result, the gauge/gravity duality [94] gives another point of view to the above problem. The 4d $\mathcal{N} = 4$ SYM theory is related to the string theory in AdS$\times S^5$. If we replace the 5-sphere with a Sasaki-Einstein manifold Y of real dimension 5, then the SUSY is broken down to $\mathcal{N} = 1$ [95, 96].

In fact, we can use Type IIB brane configurations to study this. Consider D5-branes suspended between an NS5-brane wrapping a holomorphic surface Σ as tabulated in Table 2.1.1. Then the Newton polynomial of the toric diagram defines this holomorphic surface. The system is compactified along directions 5 and 7 on a torus $\mathbb{T}^2$. After performing a T-duality on each of these two directions, the D5s would be mapped back to D3s probing the CY 3-fold.

We can draw a 5-brane web diagram on $\mathbb{T}^2$. The dual graph of the web diagram is then a bipartite periodic graph on the torus. Such dual graphs are known as dimers/brane tilings [20–24]. With the help of brane tilings, we are able to bridge the toric diagrams and the quivers.

---

[1]Saying this, we should bear in mind that the superpotential is generally additional data for defining a theory, unless we are considering periodic quivers for toric theories.

	0	1	2	3	4	5	6	7	8	9
D5	×	×	×	×		×		×		
NS5	×	×	×	×	——	Σ	——			

<div align="center">TABLE 2.1.1</div>

2.1.1 Lattice Polytopes

A lattice polytope Δ is a convex hull of a finite number of points in $\mathbb{Z}^n$, and its vertices form the set $\Delta \cap \mathbb{Z}^n$. A polytope is said to be reflexive if its dual polyotpe

$$\Delta^\circ = \{ \boldsymbol{v} \in \mathbb{Z}^n : \boldsymbol{u} \cdot \boldsymbol{v} \geq -1, \forall \boldsymbol{u} \in \Delta \} \tag{2.1.1}$$

is also a lattice polytope in $\mathbb{Z}^n$. For $n = 2$, it is not hard to show that Δ is reflexive iff there is only one interior point[2]. Hence, we can always choose this unique interior point as the origin.

However, in this chapter, we will contemplate 2d polytopes with two interior points. Hence, they are not reflexive, and we have two choices of origins. This would lead to a different discussion on the compact toric surface $X(\Delta)$ in §2.3. Here, we will first focus on the rational polyhedral cone generated by the vertices of the polytope/toric diagram Δ in 3d.

The affine toric CY 3-fold We take the origin $(0,0,0) \in \mathbb{Z}^3 =: M$, and let the vertices in the polygon be $\boldsymbol{u}_i' = (\boldsymbol{u}_i, 1) \in \mathbb{Z}^3$. Then these vectors generate a cone σ with the origin as the apex to the vertices of Δ:

$$\sigma = \left\{ \sum_i \lambda_i \boldsymbol{u}_i' : \lambda_i \geq 0 \right\} \subset M \otimes_{\mathbb{Z}} \mathbb{R} =: M_{\mathbb{R}}. \tag{2.1.2}$$

The dual cone lives in the dual lattice $N_{\mathbb{R}}$ where $N := \mathrm{Hom}(M, \mathbb{Z})$:

$$\sigma^\vee = \{ \boldsymbol{w} \in N_{\mathbb{R}} : \boldsymbol{w} \cdot \boldsymbol{u} \geq 0, \forall \boldsymbol{u} \in \sigma \}. \tag{2.1.3}$$

Then we have the algebra $\mathbb{C}[\sigma^\vee \cap N]$ spanned over $\mathbb{C}$ by the points in $\sigma \cap M$. We can therefore define an affine toric variety $\mathcal{X}$ to be the spectrum of this ring:

$$\mathcal{X} \cong \mathrm{Spec}\,\mathbb{C}[\sigma^\vee \cap N]. \tag{2.1.4}$$

Since the endpoints of σ live on the same (hyper)plane, $\mathcal{X}$ is a Gorenstein singularity, and hence can be resolved to a CY 3-fold, although being co-hyperplanar makes it non-compact [46, 97, 98].

The Higgs-Kibble mechanism The Higgs-Kibble mechanism [99–101] has a natural interpretation in the toric diagrams. As studied in [102], higgsing of a theory corresponds to blowing down a compact 2-cycle to a point in the toric geometry while unhiggsing blows up a point to a compact 2-cycle. All the 45 toric diagrams with 2 interior points (and their corresponding quiver gauge theories) can be obtained by higgsing the same parent theory as given in Appendix A.

2.1.2 Brane Tilings

As mentioned above, the junction of N D5-branes and one NS5-brane can be plotted on the torus. Given a toric diagram, we can draw the outer normal vector to each segment separated by the perimeter points of the polytope. Then we put these vectors on the torus, which will divide the torus into different regions. Each region is a bound state of 5-branes, including $(N, 0)$ and $(N, \pm 1)$ 5-branes. Every time when we move from one region to another, we will cross a vector. If we cross

---

[2]This statement (namely the "if" part, in other words, the "⇐" direction) is not generally true when $n \neq 2$.

the vector from left (right) to right (left), then the NS5 charge is increased (decreased) by 1. For instance, the NS5 cycles of $\mathbb{C}^3/\mathbb{Z}_5$ (1,2,2) is (figure taken from [103, Figure 29]):
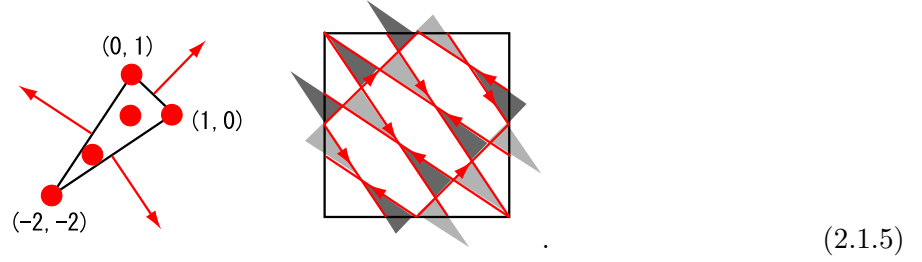
$$(2.1.5)$$

Then we can obtain a bipartite graph by taking the $(N,\pm 1)$ regions to be white/black nodes. The $(N,0)$ regions give faces in the tiling. The intersection points of the branes, for which we have massless open strings, correspond to edges in the tiling. As the open strings are oriented, every loop surrounding the white/black node is clockwise/counterclockwise, which gives a sign in the corresponding superpotential term. For instance, the above example leads to the brane tiling in (2.2.2). Since the bipartite graph is periodic, the fundamental region is in a red box. From fivebrane diagrams/brane tilings, we can read off the quivers. This is summarized in Table 2.1.2. Readers are referred to [1, 103] for a detailed discussion.

Fivebrane diagram	Brane Tiling	Quiver
$(N,1)$ brane	white node	superpotential term $(+)$
$(N,-1)$ brane	black node	superpotential term $(-)$
$(N,0)$ brane	face	gauge node/group
open string	edge	bifundamental

TABLE 2.1.2

Quivers   In our context, the quivers only have two objects: round nodes and arrows. Each round node corresponds to a gauge group, which is always unitary here. For toric quivers, viz, quivers in the toric phases, the ranks of nodes in one quiver are always the same. Each arrow connects two gauge nodes. These arrows correspond to the matter fields transform under fundamental and anti-fundamental representations under the two gauge groups. We can write a $G \times E$ matrix, where G is the number of gauge nodes[3] and E is the number of edges/bifundamentals, called incidence matrix d to encode the quiver data. If the arrow leaves the node a, viz, the bifundamental X_{ab}, then the corresponding entry is assigned 1. Likewise, if the arrow comes into the node a, viz, the bifundamental X_{ba}, then the entry is -1. Otherwise, the entry is 0.

Perfect matchings and charges   It is always to possible to find a set p_α of bifundamentals that connect all the nodes in the brane tiling precisely once. This set p_α is known as a perfect matching. A new basis of fields in the language of gauged linear sigma model (GLSM) [104] can be naturally defined from the bifundamental fields [91]. The number of GLSM fields is the number of perfect matchings c. Then we can write the $P_{E \times c}$ perfect matching matrix P which encodes the relation between the two sets of matter fields as $X_{ab} = \prod p_\alpha$ for all p_α containing X_{ab}.

As the F-terms come from $\partial W/\partial X_{ab} = 0$, one can show that the charges of GLSM fields under the F-term constraints are given by the F-term charge matrix of size $(c - G - 2) \times c$:

$$Q_F = \ker(P). \tag{2.1.6}$$

---

[3]Notice that the number of nodes G is always equal to the number of unit simplices under full triangulation of the toric diagram. This in turn equals the normalized area of the toric diagram.

From [104], we know that the D-terms in terms of the bifundamentals X_I are

$$D_i = -e^2(\sum_A d_{iA}|X_I|^2 - \zeta_i), \tag{2.1.7}$$

where e is the gauge coupling[4] and d is the incidence matrix. The ζ_i are Fayet-Iliopoulos (FI) parameters. In fact, as shown in [90,91], the FI parameters encode the resolutions of toric singularities. In the matrix form, this reads

$$\delta \cdot |X_I|^2 = \boldsymbol{\zeta}, \tag{2.1.8}$$

where δ is the reduced quiver matrix of size $(G-1) \times E$. This can be related to the perfect matching matrix via [91, 105]

$$\delta = Q_D P^{\mathrm{T}}, \tag{2.1.9}$$

where Q_D is a $(G-1) \times c$ matrix. As Q_D encodes the GLSM charges under D-term constraints, this is known as the D-term matrix.

In light of GLSM, the F- and D-terms can be treated on an equal footing. Hence, the two charge matrices can be concatenated to a $(c-3) \times c$ matrix, known as the total charge matrix [91]:

$$Q_t = \begin{pmatrix} Q_F \\ Q_D \end{pmatrix}. \tag{2.1.10}$$

As the F-terms must vanish while the D-terms are adjusted by the FI parameters, the last column is always in the form $(\mathbf{0}, \boldsymbol{\zeta})^{\mathrm{T}}$. Hence, we will always omit the last column. Then taking the kernel yields

$$G_t = \ker(Q_t). \tag{2.1.11}$$

This matrix G_t exactly encodes the information of the toric diagrams. Each column is the coordinate of a lattice point in the polytope (thus, the last row of G_t is $(1,\ldots,1)$). Therefore, every point is assigned to some GLSM field(s). Each corner (aka extremal) point/vertex always correspond to one GLSM field with non-zero R-charge. On the other hand, non-extremal points correspond to multiple GLSM fields all with zero R-charges.

Toric/Seiberg duality   The toric/Seiberg duality [93, 106, 107] is a duality among theories that have the same IR fixed point under RG flow. As we are always staying in the toric phases in this chapter, there will be no fractional branes, and hence our theories keep superconformal and the quivers have nodes of the same rank as aforementioned. The dual quiver gauge theories all have the same moduli space/Higgs branch, which is exactly the toric CY cone corresponding to the toric diagram.

Therefore, we can use toric duality to obtain different quivers of the same toric diagram with the following steps:

1. As Seiberg duality takes $\mathrm{SU}(N_c)$ gauge group with N_f fundamentals and N_f bifundamentals to $\mathrm{SU}(N_f - N_c)$ gauge group, in the toric phase, only nodes satisfying $N_f = 2N_c$ can be dualized[5]. We first scale the gauge couplings of gauge groups other than the chosen node a to zero, and the fields not connected to a decouple. Then the bifundamentals connected to a is reduced to (anti-)fundamentals under the flavour symmetry. Since duality requires the dual quarks to transform in the conjugate (flavour) representations to the original ones, the directions of the $2N_f$ arrows should be reversed. The overall result is that every time we perform such duality, we reverse all the arrows connected to the dualized node.

2. Then we add an arrow from the flavour node i to the flavour node k for each 2-path $i \to j \to k$ in the *original* quiver. This is just the quarks-to-meson map $Q_a \tilde{Q}^b \to M_a^b$. As the flavours

---

[4]In general, the gauge coupling should be e_i, but one often sets $e = e_i$ for all i in GLSM.
[5]For simplicity, we shall mainly focus on U(1) gauge groups unless otherwise specified.

groups will be gauged back at the end, these mesons will be promoted to bifundamentals. In the superpotential, the factors $X_{ij}X_{jk}$ should be replaced with $\mathcal{M}_{ik}$, and terms $\mathcal{M}_{ik}X_{kj}X_{ji}$ need to be added.

3. There could exist arrows that should be removed. This is checked from the superpotential. More specifically, quadratic terms in the superpotential should be removed. In physical parlance, this means that the quadratic terms are mass terms. We need integrate out the massive fields say $\mathcal{X}$ in terms of the F-term relations. As a result, the corresponding arrows should be discarded in the quiver. Finally, we "gauge back" all the flavour nodes.

In cluster algebra, this is exactly the mutation for quivers (without adjoint loops and 2-cycles) [108]. In terms of brane tilings, the technique called urban renewal can be applied to obtain dual tilings. For more details in Seiberg duality in quiver gauge theories, one is referred to, for example, [21, 109–111].

2.1.3 The Moduli Spaces

The master space $\mathcal{F}^\flat$ [28, 112] is a combination of baryonic and mesonic moduli spaces defined as the symplectic quotient of the perfect matching ring[6]:

$$\mathcal{F}^\flat = \mathbb{C}[p_1, \ldots, p_c]//Q_F. \tag{2.1.12}$$

The global symmetry The master space has global symmetry that can be divided into two parts:

- The mesonic symmetry is $\mathrm{U}(1)^3$ or its enhancement with rank 3. It may be enhanced to $\mathrm{SU}(2)\times\mathrm{U}(1)^2$, $\mathrm{SU}(2)^2\times\mathrm{U}(1)$ or $\mathrm{SU}(3)\times\mathrm{U}(1)$. The enhancement is determined by the duplicated columns in Q_t. In particular, there is always a $\mathrm{U}(1)$ which is the R-symmetry.

- The baryonic symmetry is $\mathrm{U}(1)^{G-1}$ or its enhancement with rank $(G-1)$. It consists of non-anomalous and anomalous symmetries. The non-anomalous symmetry is always $\mathrm{U}(1)^{N_P-3}$, where N_P is the number of perimeter points in the polytope. The anomalous symmetry is $\mathrm{U}(1)^{2I}$ or an enhancement of rank $2I$, where I is the number of interior points. The enhancement is determined by the repeated columns in Q_F. The non-abelian enhancement of anomalous symmetry is also known as hidden symmetry.

Notice that the combination in the baryonic symmetry is actually the Pick's theorem:

$$\frac{G}{2} = I + \frac{N_P}{2} - 1 = A, \tag{2.1.13}$$

where A is the (unnormalized) area of the toric diagram.

The mesonic moduli space and Hilbert series The mesonic moduli space $\mathcal{M}$ is a subspace of $\mathcal{F}^\flat$:

$$\mathcal{M} = \mathcal{F}^\flat//Q_D = (\mathbb{C}^c[p_1, \ldots, p_c]//Q_F)//Q_D. \tag{2.1.14}$$

We can use the (mesonic) Hilbert series (aka Hilbert-Poincaré series) to desribe the moduli space. The Hilbert series is a generating function that enumerates the invariant monomials under the group action. Physically, it counts the gauge invariant operators of each degree in the chiral ring. As aforementioned, the moduli space coincides with the toric CY 3-fold $\mathcal{X}$. Hence, we can use the following formula to compute the Hilbert series. The (refined) Hilbert series for a toric CY n-fold cone can be computed as [113, 114]

$$\mathrm{HS} = \sum_{i=1}^{r} \prod_{j=1}^{n} \left(1 - \boldsymbol{t}^{\boldsymbol{u_{i,j}}}\right)^{-1}. \tag{2.1.15}$$

---

[6]Strictly speaking, this is the largest irreducible component, known as the coherent component, of the master space rather than $\mathcal{F}^\flat$ itself. Nevertheless, we will solely focus on the coherent component and make this abuse.

The number r is the number of $(n-1)$-dimensional simplices under triangulation. The index j runs over the n faces of each simplex. The vector $\boldsymbol{u_{i,j}}$ is an n-vector inner normal to the jth face of the ith simplex, and $\boldsymbol{t}$ are the fugacities $t_1,\ldots,t_n$. Then $\boldsymbol{t^{u_{i,j}}} = \prod_{k=1}^{n} t_k^{\boldsymbol{u_{i,j}}(k)}$, multiplied by the kth component of $\boldsymbol{u}$. One can also use *Molien-Weyl integral* to compute Hilbert series of the Higgs branch [25]. The two results should be the same under some fugacity map.

2.1.4 Volume Minimization

As $\mathcal{X}$ of complex dimension n is the Kähler cone over the Sasaki-Einstein manifold $Y = \mathcal{X}|_{r=1}$ of real dimension $(2n-1)$:

$$\mathrm{d}s^2(\mathcal{X}) = \mathrm{d}r^2 + r^2\mathrm{d}s^2(Y), \tag{2.1.16}$$

the volume of Y is then [113, 114]

$$\mathrm{vol}(Y) = 2n \int_0^1 \mathrm{d}r \; r^{2n-1}\mathrm{vol}(Y) = 2n \; \mathrm{vol}(\mathcal{X}|_{r\leq 1}) = 2n \int_{r\leq 1} \frac{\omega^n}{n!}, \tag{2.1.17}$$

where ω is the Kähler form of $\mathcal{X}$. We are now going to see that the volume of the Sasaki-Einstein base is closely related to the R-charges of the fields in our theory.

The Reeb vector $K := \mathcal{J}(r\partial/\partial r)$ is the Killing vector of Y, where $\mathcal{J}$ is the complex structure of $\mathcal{X}$. Since the torus action $\mathbb{T}^n$ of the toric $\mathcal{X}$ leaves ω invariant, we can take the vector fields $\partial/\partial\phi_i$ to be the generators of the action with $\phi_i \sim \phi_i + 2\pi$. Then the reeb vector reads $K = b_i\partial/\partial\phi_i$, where the components b_i's are algebraic numbers, with the last component b_n set to be n.

In [113, 114], the volume function of Y, which is shown to be related to the Reeb vector components, is introduced to be

$$V(b_i; Y) = \frac{\mathrm{vol}(Y)}{\mathrm{vol}(S^{2n-1})} \tag{2.1.18}$$

such that the volume of the $(2n-1)$-sphere,

$$\mathrm{vol}(S^{2n-1}) = \frac{2\pi^n}{(n-1)!}, \tag{2.1.19}$$

is normalized. Then the volume function is related to the Hilbert series of $\mathcal{X}$ via[7]

$$V(b_i; Y) = \lim_{\mu\to 0} \mu^n \; \mathrm{HS}(t_i = \exp(-\mu b_i); \mathcal{X}). \tag{2.1.20}$$

It is known that V always admits precisely one positive minimum $V_{\min}$. Since the Reeb vector is algebraic, $V_{\min}$ is also an algebraic number.

For toric threefolds, in [115], it was shown that the a-function, in terms of the volume function, can be expressed as

$$a(R) = \frac{1}{4V}, \tag{2.1.21}$$

where R denotes the R-charges of the superconformal theory. A procedure known as a-maximization can be used to determine the R-charges [116–118]. The central charges a and c of the SCFT in 4d are

$$a(R) = \frac{3}{32}(3\mathrm{Tr}R^3 - \mathrm{Tr}R), \quad c = \frac{1}{32}(9\mathrm{Tr}R^3 - 5\mathrm{Tr}R), \tag{2.1.22}$$

where $\mathrm{Tr}R^3$ and $\mathrm{Tr}R$ are 't Hooft anomalies. In general, as we have flavour symmetries in IR, a possible candidate is

$$R_t = R_0 + \sum_i t_i F_i, \tag{2.1.23}$$

---

[7]If we are taking outer normal vectors to the faces of simplices when computing the Hilbert series, the Hilbert series would just change by the fugacity map $t_i \to 1/t_i$. As a result, the volume function would only differ by a minus sign.

where F_i's are the charges of global non-R symmetries and R_t is called the trial R-charge. According to [116], the U(1) R-symmetry should satisfy

$$9\text{Tr}(R^2 F_i) = \text{Tr}F_i, \ \text{Tr}(RF_iF_j) < 0, \tag{2.1.24}$$

which can be translated into the maximization of $a(R_t)$. When the trial a-function is maximized, only the R-charge R_0 will make contribution. Thus, we see that $V_{\min}$ plays a crucial role in determining the R-charges.

In light of quiver diagrams, let X_I be the R-charges of the bifundamentals. Then the vanishing β-function from the theory being conformal yields

$$\sum_I X_I = 2, \ \sum_I (1 - X_I) = 2, \tag{2.1.25}$$

where the first sum is taken in each superpotential term and the second sum is taken with respect to each gauge node. Let N_W be the number of superpotential terms, then we have $(G + N_W)$ equations for E parameters in all, which in general are not all independent though $G + N_W = E$ as the bipartite graph is embedded on a torus. With these conditions, the a-function can be written as[8]

$$a = \frac{3}{32}\left(2G + \sum_I (3(X_I - 1)^3 - (X_I - 1))\right). \tag{2.1.26}$$

Anomaly cancellation implies $a = c$, viz, $\text{Tr}R = 0$ [119, 120][9]. Thus, we have

$$a = \frac{9}{32}\left(G + \sum_I (X_I - 1)^3\right). \tag{2.1.27}$$

As we have seen, this is equivalent to minimizing V, together with (2.1.25), we can solve for the R-charges of the bifundamentals, and hence the R-charges of GLSM fields as well.

Example   Let us consider the abelian orbifold $\mathbb{C}^n/\mathbb{Z}_n$ with orbifold action $(1,\ldots,1)$ as an example. The Hilbert series reads

$$\text{HS} = \left(\left(1 - t_n^{-s}\prod_{i=1}^{n-1} t_i^s\right)\prod_{j=1}^{n-1}\left(1 - t_j^s\right)\right)^{-1} + \sum_{i=1}^{n-1}\left(\left(1 - t_i^{-s}\right)\left(1 - t_i^{sn}t_n^s\prod_{j=1}^{n-1} t_j^s\right)\prod_{\substack{k=1\\k\neq i}}^{n-1}\left(1 - t_k^s t_i^{-s}\right)\right)^{-1}, \tag{2.1.28}$$

where $s = (-1)^n$. As the limit picks out the leading order of μ, the volume function is

$$V = \frac{(-1)^n n^{n-1}}{\prod\limits_{j=1}^{n-1}\left(\sum\limits_{i=1}^{n-1} b_i - nb_j - b_n\right)}. \tag{2.1.29}$$

Then taking $b_n = n$, we find that $V_{\min} = 1/n$ at $b_1 = \cdots = b_{n-1} = 0$. In quiver gauge theories, we have a unique toric quiver for each n. The R-charges of all the bifundamentals are $2/n$. Hence, the R-charges of the n GLSM fields corresponding to extremal points are all $2/n$, with others vanishing. Interestingly, the Sasaki-Einstein base of $\mathbb{C}^n$ (whose toric diagram is the unit simplex) is the $(2n-1)$-sphere. Hence, the volume function equals 1. As we will see in §2.3.2, it is not a coincidence to have $1/n = V(S^{2n-1})/|\mathbb{Z}_n|$ here.

---

[8] Notice that this expression itself (normalized by N^2), which is generally true when we assume all the gauge groups have the same rank N, does not require that the dimer is embedded on $\mathbb{T}^2$.

[9] The relevant anomalies are the ones of the R-symmetry current with itself or with the stress tensor, namely $\langle RRR\rangle$ or $\langle RTT\rangle$.

2.2 Example: $\mathbb{C}^3/\mathbb{Z}_5$ $(1,2,2)$

Here, let us consider $\mathbb{C}^3/\mathbb{Z}_5$ with action $(1,2,2)$ as a concrete example. The analysis for other polygons with two interior points can be found in [2]. The polytope is
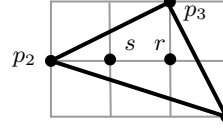
$$(2.2.1)$$

The brane tiling and the corresponding quiver are
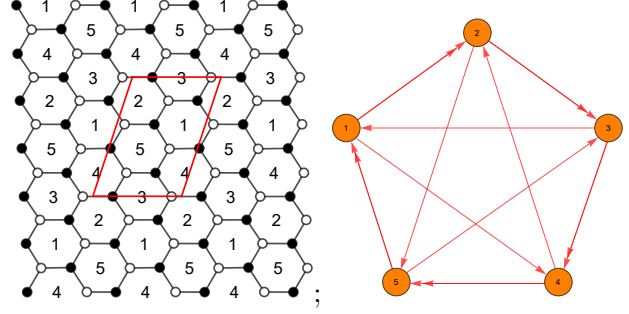
$$(2.2.2)$$

The superpotential is

$$
\begin{aligned}
W \;=\; & X_{12}^1 X_{25} X_{51}^2 + X_{12}^2 X_{23}^1 X_{31} + X_{23}^2 X_{34}^1 X_{42} + X_{34}^2 X_{45}^1 X_{53} + X_{45}^2 X_{51}^1 X_{14} \\
& - X_{12}^2 X_{25} X_{51}^1 - X_{12}^1 X_{23}^2 X_{31} - X_{23}^1 X_{34}^2 X_{42} - X_{34}^1 X_{45}^2 X_{53} - X_{45}^1 X_{51}^2 X_{14}.
\end{aligned}
\tag{2.2.3}
$$

The perfect matching matrix is

$$
P = \left(
\begin{array}{c|ccccccccccccc}
 & p_1 & p_2 & s_1 & s_2 & s_3 & r_1 & s_4 & r_2 & s_5 & r_3 & r_4 & r_5 & p_3 \\
\hline
X_{12}^1 & 1 & 0 & 0 & 0 & 1 & 0 & 1 & 0 & 0 & 0 & 0 & 1 & 0 \\
X_{12}^2 & 0 & 1 & 0 & 0 & 1 & 0 & 1 & 0 & 0 & 0 & 0 & 1 & 0 \\
X_{23}^1 & 1 & 0 & 0 & 1 & 0 & 0 & 0 & 0 & 1 & 0 & 1 & 0 & 0 \\
X_{23}^2 & 0 & 1 & 0 & 1 & 0 & 0 & 0 & 0 & 1 & 0 & 1 & 0 & 0 \\
X_{34}^1 & 1 & 0 & 1 & 0 & 0 & 0 & 1 & 1 & 0 & 0 & 0 & 0 & 0 \\
X_{34}^2 & 0 & 1 & 1 & 0 & 0 & 0 & 1 & 1 & 0 & 0 & 0 & 0 & 0 \\
X_{45}^1 & 1 & 0 & 0 & 1 & 1 & 1 & 0 & 0 & 0 & 0 & 0 & 0 & 0 \\
X_{45}^2 & 0 & 1 & 0 & 1 & 1 & 1 & 0 & 0 & 0 & 0 & 0 & 0 & 0 \\
X_{51}^1 & 1 & 0 & 1 & 0 & 0 & 0 & 0 & 0 & 1 & 1 & 0 & 0 & 0 \\
X_{51}^2 & 0 & 1 & 1 & 0 & 0 & 0 & 0 & 0 & 1 & 1 & 0 & 0 & 0 \\
X_{31} & 0 & 0 & 1 & 0 & 0 & 1 & 0 & 1 & 0 & 1 & 0 & 0 & 1 \\
X_{25} & 0 & 0 & 0 & 1 & 0 & 1 & 0 & 1 & 0 & 0 & 1 & 0 & 1 \\
X_{42} & 0 & 0 & 0 & 0 & 1 & 1 & 0 & 0 & 0 & 1 & 0 & 1 & 1 \\
X_{14} & 0 & 0 & 0 & 0 & 0 & 0 & 1 & 1 & 0 & 0 & 1 & 1 & 1 \\
X_{53} & 0 & 0 & 0 & 0 & 0 & 0 & 0 & 0 & 1 & 1 & 1 & 1 & 1 \\
\end{array}
\right),
\tag{2.2.4}
$$

where the relations between bifundamentals and GLSM fields can be directly read off. Then we can get the total charge matrix:

$$
Q_t = \left(
\begin{array}{ccccccccccccc}
p_1 & p_2 & s_1 & s_2 & s_3 & r_1 & s_4 & r_2 & s_5 & r_3 & r_4 & r_5 & p_3 \\
2 & 2 & -1 & -1 & -1 & 0 & -1 & 0 & -1 & 0 & 0 & 0 & 1 \\
1 & 1 & 0 & 0 & -1 & 0 & -1 & 0 & -1 & 0 & 0 & 1 & 0 \\
1 & 1 & 0 & -1 & 0 & 0 & -1 & 0 & -1 & 0 & 1 & 0 & 0 \\
1 & 1 & -1 & 0 & -1 & 0 & 0 & 0 & -1 & 1 & 0 & 0 & 0 \\
1 & 1 & -1 & -1 & 0 & 0 & -1 & 1 & 0 & 0 & 0 & 0 & 0 \\
1 & 1 & -1 & -1 & -1 & 1 & 0 & 0 & 0 & 0 & 0 & 0 & 0 \\
\hline
0 & 0 & -1 & 1 & 0 & 0 & 1 & 0 & -1 & 0 & 0 & 0 & 0 \\
0 & 0 & -1 & 0 & -1 & 0 & 2 & 0 & 0 & 0 & 0 & 0 & 0 \\
0 & 0 & -2 & 0 & 0 & 0 & 1 & 0 & 1 & 0 & 0 & 0 & 0 \\
0 & 0 & -1 & -1 & 1 & 0 & 1 & 0 & 0 & 0 & 0 & 0 & 0 \\
\end{array}
\right)
\tag{2.2.5}
$$

with kernel

$$
G_t = \left(
\begin{array}{ccccccccccccc}
p_1 & p_2 & s_1 & s_2 & s_3 & r_1 & s_4 & r_2 & s_5 & r_3 & r_4 & r_5 & p_3 \\
-3 & 0 & -1 & -1 & -1 & 0 & -1 & 0 & -1 & 0 & 0 & 0 & 1 \\
5 & 0 & 2 & 2 & 2 & 1 & 2 & 1 & 2 & 1 & 1 & 1 & 0 \\
1 & 1 & 1 & 1 & 1 & 1 & 1 & 1 & 1 & 1 & 1 & 1 & 1 \\
\end{array}
\right).
\tag{2.2.6}
$$

From G_t, we can get the GLSM fields associated to each point as shown in (2.2.1), where

$$
r = \{r_1, \ldots, r_5\}, \quad s = \{s_1, \ldots, s_5\}.
\tag{2.2.7}
$$

From Q_t (and Q_F), the mesonic symmetry reads $\mathrm{SU}(2) \times \mathrm{U}(1) \times \mathrm{U}(1)_{\mathrm{R}}$ and the baryonic symmetry reads $\mathrm{U}(1)_{\mathrm{h}}^4$, where the subscripts "R" and "h" indicate R- and hidden symmetries respectively.

The Hilbert series of the toric cone is

$$
\text{HS} = \frac{1}{\left(1 - \frac{t_1}{t_3}\right)\left(1 - \frac{t_1 t_2}{t_3}\right)\left(1 - \frac{t_3^3}{t_1^2 t_2}\right)} + \frac{1}{(1 - t_2)\left(1 - \frac{t_2}{t_1}\right)\left(1 - \frac{t_1 t_3}{t_2^2}\right)} + \frac{1}{\left(1 - \frac{1}{t_2}\right)\left(1 - t_1 t_2^2\right)\left(1 - \frac{t_3}{t_1 t_2}\right)}
$$
$$
+ \frac{1}{\left(1 - \frac{1}{t_2}\right)\left(1 - \frac{1}{t_1 t_2^2}\right)\left(1 - t_1 t_2^3 t_3\right)} + \frac{1}{(1 - t_2)\left(1 - \frac{t_1}{t_2}\right)\left(1 - \frac{t_3}{t_1}\right)}.
$$

$$(2.2.8)$$

The volume function is then

$$
V = -\frac{25}{(b_1 - 2b_2 + 3)(2b_1 + b_2 - 9)(b_1 + 3b_2 + 3)}.
\tag{2.2.9}
$$

Minimizing V yields $V_{\min} = 1/5$ at $b_1 = 2$, $b_2 = 0$. Thus, $a_{\max} = 5/4$. Together with the superconformal conditions, we can solve for the R-charges of the bifundamentals, which are $X_I = 2/3$ for any I, viz, for all the bifundamentals. Hence, the R-charges of GLSM fields are $p_i = 2/3$ with others vanishing.

2.3 The Toric Variety $\widetilde{X(\Delta)}$

Given a lattice polytope Δ of (complex) dimension n, besides the $(n+1)$-dimensional Calabi-Yau cone which is non-compact, we can also get a compact toric variety $X(\Delta)$ under the construction of inner normal fan $\Sigma(\Delta)$. Here, we only give a quick review on the ingredients that will be used below. A detailed treatment can be found in [97, 98].

To build $X(\Delta)$, we choose one interior point as the origin, then the fan $\Sigma(\Delta)$ is constructed out of cones having rays going through the vertices of each face with origin as the apex, viz,

$$
\Sigma(\Delta) = \{\text{pos}(F) : F \in \text{Faces}(\Delta)\},
\tag{2.3.1}
$$

where

$$
\text{pos}(F) = \left\{\sum_i \lambda_i \boldsymbol{v}_i : \boldsymbol{v}_i \in F, \lambda_i \geq 0\right\}
\tag{2.3.2}
$$

is the positive hull of the n-cone over face F. For instance, choosing the left interior point as the origin, the polygon in §2.2 has

$$(2.3.3)$$
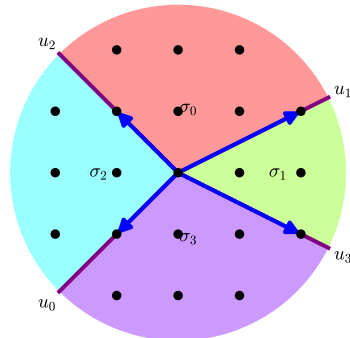
with the cones σ_i as affine patches.

Then following the standard construction in [97, 98], we can get the compact $X(\Delta)$. Here, the information of the fans suffices for our discussions on the geometric and topological properties. Such $X(\Delta)$ may not be smooth. In fact, the toric variety built from (2.3.3) is not smooth. This can be solved by the following definition:

Definition 2.3.1. *The polytope and the corresponding fan are regular if every cone in the fan has generators that form part of a $\mathbb{Z}$-basis.*

The regularity can be determined by the determinant of *all* n-tuple vectors of each cone. If all the determinants are ± 1, then we have a regular polytope and a regular fan. With regularity, we have the following theorem [98]:

Theorem 2.3.1. *The toric variety $X(\Delta)$ is smooth iff Δ is regular.*

For example, in (2.3.3), $\det(u_0,u_2)=-2$, and therefore the corresponding toric variety is singular. Nevertheless, we can always resolve the singularities via triangulations of the polytope. For reflexive polytopes, FRS triangulations are considered [46, 121], where

- "Fine" stands for all the lattice points of the polytope involved in the triangulation;

- "Regular" stands for the polytope being regular;

- "Star" stands for the origin being the apex of all the triangulated cones.

Now that we are dealing with polygons having two interior points, F and S can not be simultaneously satisfied. Hence, we will drop the condition F, and contemplate RS triangulations. Under such triangulations, we get a complete resolution, $\widetilde{X(\Delta)}$, of $X(\Delta)$. For instance, (2.3.3) can be resolved to

$$(2.3.4)$$
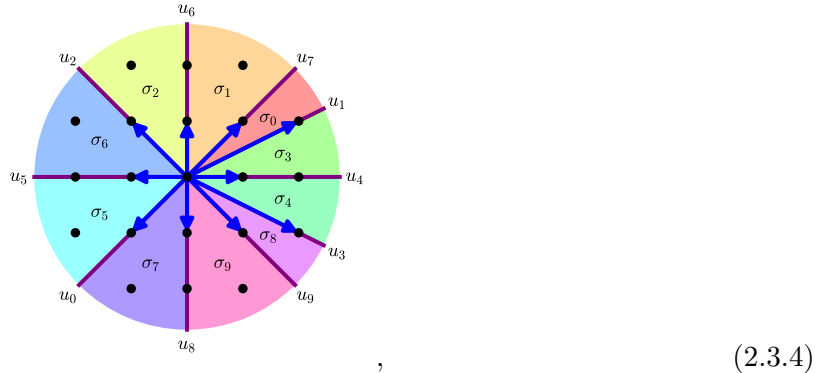
which is complete and smooth.

2.3.1   The Two Interior Points as Origins

From [122], we know that $X(\Delta)$ constructed from reflexive polytopes are Gorenstein Fano, i.e., its anticanonical divisor K_X is Cartier and ample. However, as we have two interior points here, $X(\Delta)$ does not hold this property any more. Actually, since we have two choices of the origin, we can build two compact toric varieties, which may or may not be the same[10].

For the two $\widetilde{X(\Delta)}$'s built from Δ to coincide, it is necessary for them to have the same Euler number. As we will discuss in §2.3.2, the Euler number of $\widetilde{X(\Delta)}$ equals to the number of triangles under the triangulation, viz, the number of two-dimensional cones. Hence, this can be checked by counting the numbers of triangles under triangulations. After complete resolutions, we find that there are only 12 polygons that have $\widetilde{X(\Delta)}$'s with different Euler numbers. In terms of the ordering in Appendix A, they are (2), (4), (10), (12), (15), (18), (19), (23), (37), (38), (39) and (40).

As the two interior points is connected by a straight line, now for simplicity, let us call this line the "spine" of the polygon[11]. Since the Euler number is related to triangulation, it is not hard to see that when we have zero or two perimeter points lying on the spine, the two Euler numbers are

---

[10] Notice that even though we have this choice on the level of the toric 2-fold, the affine 3-fold is the same and hence the gauge theories are the same.

[11] This should not be confused with the spines for amoebae in tropical geometry.

equal[12]. On the other hand, if there is only one perimeter point on the spine, the two complete resolutions would yield different Euler numbers. This is because for these three points on the spine, if the interior point is in the middle (which we will refer to as the "zeroth-grade" point), the fan will have rays extending to both of the other two points on the spine. For the other interior point (which we will refer to as the "first-grade" point), the fan will only have one ray on the spine. Thus, the zeroth-/first-grade Euler numbers will differ by 1:

$$\chi_0 - \chi_1 = 1. \tag{2.3.5}$$

As will be discussed in §2.3.2, the first Chern numbers will then satisfy $C_{1,1} - C_{1,0} = 1$ where $C_{1,i}$ denotes the first Chern number of $\widetilde{X_i(\Delta)}$ from the ith-grade point[13].

For the remaning 33 polygons who have two zeroth-grade points, it turns out that not only the corresponding Chern numbers of $\widetilde{X(\Delta)}$, but also the two Chern classes (and hence the two Euler numbers) are *equal*. For the 12 polygons with first-grade points, consider the complete resolution whose fan has the first-grade point as the apex. If we add another ray opposite to the original ray on the spine, i.e., we further resolve the complete smooth surface, then we will reach a new variety with Euler number $\chi_1' = \chi_1 + 1 = \chi_0$. As a matter of fact, we find that the total Chern classes of $\widetilde{X_0(\Delta)}$ and $\widetilde{X_1'(\Delta)}$ are equal:

$$c\left(\widetilde{X_1'}\right) = c\left(\widetilde{X_0}\right). \tag{2.3.6}$$

As an example, the different resolutions of (2.2.1) in §2.2 is depicted in Figure 2.3.1.

(A) (B) (C)
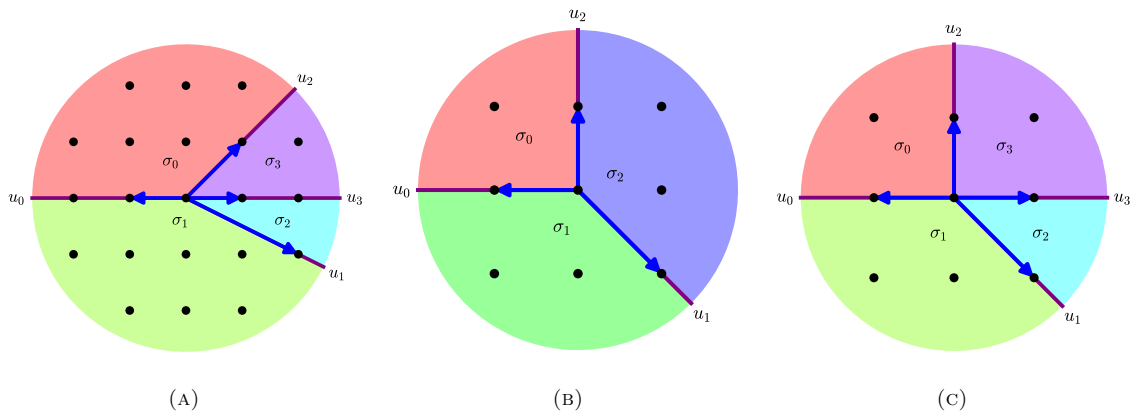
FIGURE 2.3.1: (a) The complete resolution $\widetilde{X_0}$ is constructed from the zeroth-grade point. The Euler number χ_0 is 4. (b) The toric variety X_1 is already smooth, viz, $X_1 = \widetilde{X_1}$. The Euler number χ_1 is 3. (c) We make a further blow-up on X_1 by adding the ray $u_3 = (1,0)$. The new variety $\widetilde{X_1'}$ has Euler number $\chi_1' = 4$.

It is worth noting that all the 12 polygons with first-grade points can be higgsed from a minimal parent theory which also has a first-grade point (and two zeroth-grade points). This minimal parent theory is

$$\tag{2.3.7}$$
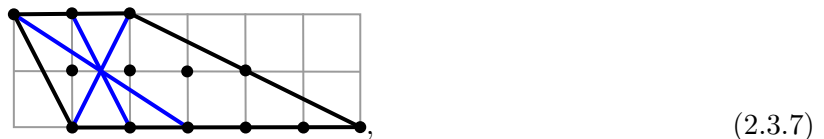
where the blue lines indicate three of the higgsed polygons each from blowing down three points. The remaining 9 can be obtained from these three polygons. Notice that the first-grade point

---

[12]Hence, none of the hexagons belongs to the 12 polygons as it has been proven in [123] that the two interior points of a hexagon must lie on the same diagonal.

[13]For polytopes with arbitrarily many interior points, the zeroth-grade points will be those which give the largest possible Euler number n while the mth-grade points will give Euler number $(n - m)$.

in (2.3.7) is always higgsed away, and one zeroth-grade point becomes a first-grade point after higgsing.

As the first-grade point trivially yields a different $\widetilde{X_1(\Delta)}$ from $\widetilde{X_0(\Delta)}$, we will consider $\widetilde{X_1'(\Delta)}$ which has an extra step of resolution when comparing the two compact smooth complete varieties built from each toric diagram. Since the characteristic classes are always the same for the two varieties, we need a new approach to distinguish them. Our strategy is the same as classifying inequivalent lattice polygons, that is, checking whether the two fans are related by SL(2,$\mathbb{Z}$) transformations (along with translations and reflections)[14]. One way to see this is to tell whether the vectors ending on the each row/column are properly shifted. Another way is to consider the determinants since all the transformations have determinant ± 1 and all the 2×2 matrices with determinant ± 1 is such a transformation. Then if we pick out any corresponding pairs of vectors from the two fans, the matrices they form should have the same determinant up to a sign.

It turns out that this can be directly read off from the symmetries of the toric diagrams since we only have one spine (which is a result of always having two interior points). Due to the existence of the unique spine, the vectors above and below the spine should be shifted along *opposite* directions. However, as we are moving from one interior point to the other along the spine, the vectors above and below the spine would always be shifted along the *same* direction. An example is illustrated in Figure 2.3.1(a, c).

Hence, reflection or rotation[15] is necessary to make the two varieties coincide. As a result,

Proposition 2.3.2. *The two $\widetilde{X(\Delta)}$'s are the same iff the lattice polygon (under certain* SL(2, $\mathbb{Z}$) *transformations) satisfies either of the following two: (1) axially symmetric with respect to the perpendicular bisector of the two interior points; (2) centrosymmetric*[16].

Therefore, only 8 out of the 45 toric diagrams give rise to two same $\widetilde{X(\Delta)}$'s. In terms of the ordering in Appendix A, they are (14), (20), (22), (24), (26), (43), (44) and (45).

Before moving on to the next subsection, let us briefly discuss the smoothness of $X(\Delta)$. Although it is not always the case, some Δ still lead to smooth $X(\Delta)$. There are 9 such polygons. In terms of the ordering in Appendix A, they are (2), (6), (7), (8), (18), (25), (26), (41) and (42). In particular, since (2) and (18) have both zeroth- and first-grade points, only the first-grade points in both of the cases can give smooth varieties directly. The other 7 toric diagrams can all give rise to two smooth complete surfaces without any further resolutions. It is straightforward that all the perimeter points need to be corner points for $X(\Delta)$ to be smooth. If the toric diagram has a first-grade point as well, then the zeroth-grade point cannot yield a smooth $X(\Delta)$.

2.3.2 Minimized Volumes and Topological Quantities

As we have obtained the volume data of the 45 cases in Appendix A, we plot $1/V_{\min}$ against the number of lattice points N in Figure 2.3.2. Now we would like to relate the minimized volume functions of Sasaki-Einstein manifolds to the topological quantities of $\widetilde{X(\Delta)}$'s. From [97, 98], we have

Theorem 2.3.3. *For the smooth projective variety $\widetilde{X(\Delta)}$ of (complex) dimension n, the Betti numbers satisfy*

$$b_{2k-1} = 0, \ b_{2k} = \sum_{i=k}^{n} (-1)^{i-k} \binom{i}{k} d_{n-i}, \tag{2.3.8}$$

---

[14]More precisely, as the origin is always the apex of the cones, we have no translations here, and thus the transformations lie in SL(2,$\mathbb{Z}$)×$\mathbb{Z}_2$.

[15]Due to reflection, without loss of generality, rotation can be restricted to inversion, viz, rotation by π.

[16]These two properties then rule out all the toric diagrams with a first-grade point. Even though we further resolve them to make the Chern classes match, we still cannot have the same toric varieties.
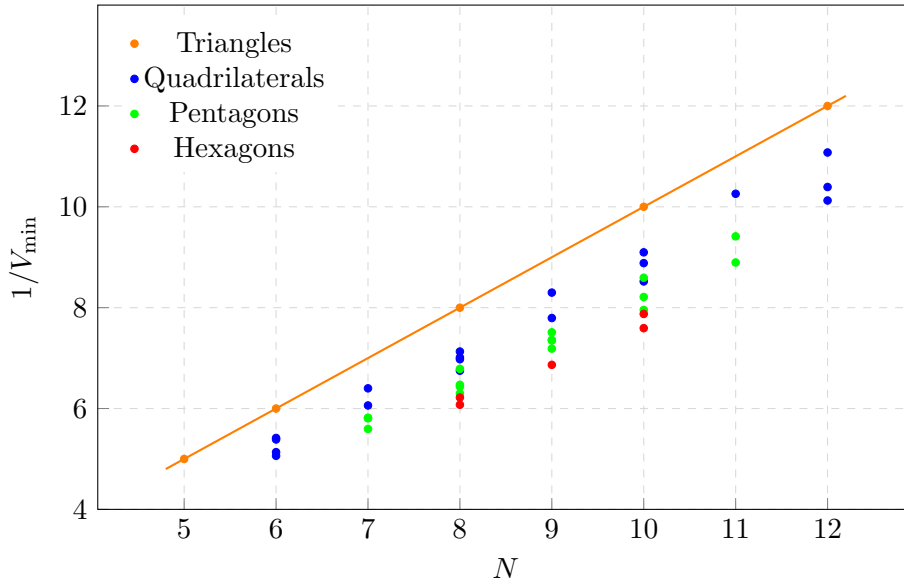
FIGURE 2.3.2: The reciprocals of minimized volumes against the number of lattice points N. This is bounded by the straight line $1/V_{\min} = N$ where the triangles live.

where $k = 0, 1, \ldots, n$ and d_j is the number of j-dimensional cones in $\widetilde{\Delta}$. As the Euler number $\chi = \sum\limits_{i=0}^{n} (-1)^i b_i$, then

$$\chi = d_n. \tag{2.3.9}$$

This verifies our statement that the Euler number is the number of triangles under the triangulation used in §2.3.1. Then

Corollary 2.3.3.1. *For the lattice polygons, we have*

$$b_0 = b_4 = 1, \ \ b_1 = b_3 = 0, \ \ b_2 = d_1 - 2d_0 = d_1 - 2 = \chi - 2. \tag{2.3.10}$$

Since $b_k = \sum\limits_{i=0}^{k} h^{i,k-i}$, we get

$$\chi = \sum_{r,s} (-1)^{r+s} h^{r,s} = h^{2,2} + h^{2,0} + h^{1,1} + h^{0,2} + h^{0,0} = 2 + 2h^{2,0} + h^{1,1}. \tag{2.3.11}$$

In fact, we find that the dimension of the Kähler cone over $\widetilde{X(\Delta)}$ is always $\chi - 2$. Thus,

$$h^{2,2} = h^{0,0} = 1, \ h^{2,0} = h^{0,2} = 0, \ h^{1,1} = \chi - 2. \tag{2.3.12}$$

The vanishing $h^{2,0}$ ($h^{0,2}$) shows that there is no global sections to the (anti-)canonical bundle. Then the only remaining interesting Hodge number $h^{1,1}$ is determined by the Euler number. As we are now going to see, the (first) Chern number is also determined by the Euler number.

For surfaces, we have two Chern numbers: $C_1 = \int_{\widetilde{X}} c_1^2$ and $C_2 = \int_{\widetilde{X}} c_2 = \chi$. In Figure 2.3.3, we plot $1/V_{\min}$ against the first and second Chern numbers respectively, following the strategy of [46]. First of all, putting the two graphs together, we can see that the two sets of points are symmetric with respect to $x = 6$. Indeed, we find

Theorem 2.3.4. *For a smooth complete toric surface $\widetilde{X}$, we have*

$$C_1 + \chi = 12. \tag{2.3.13}$$
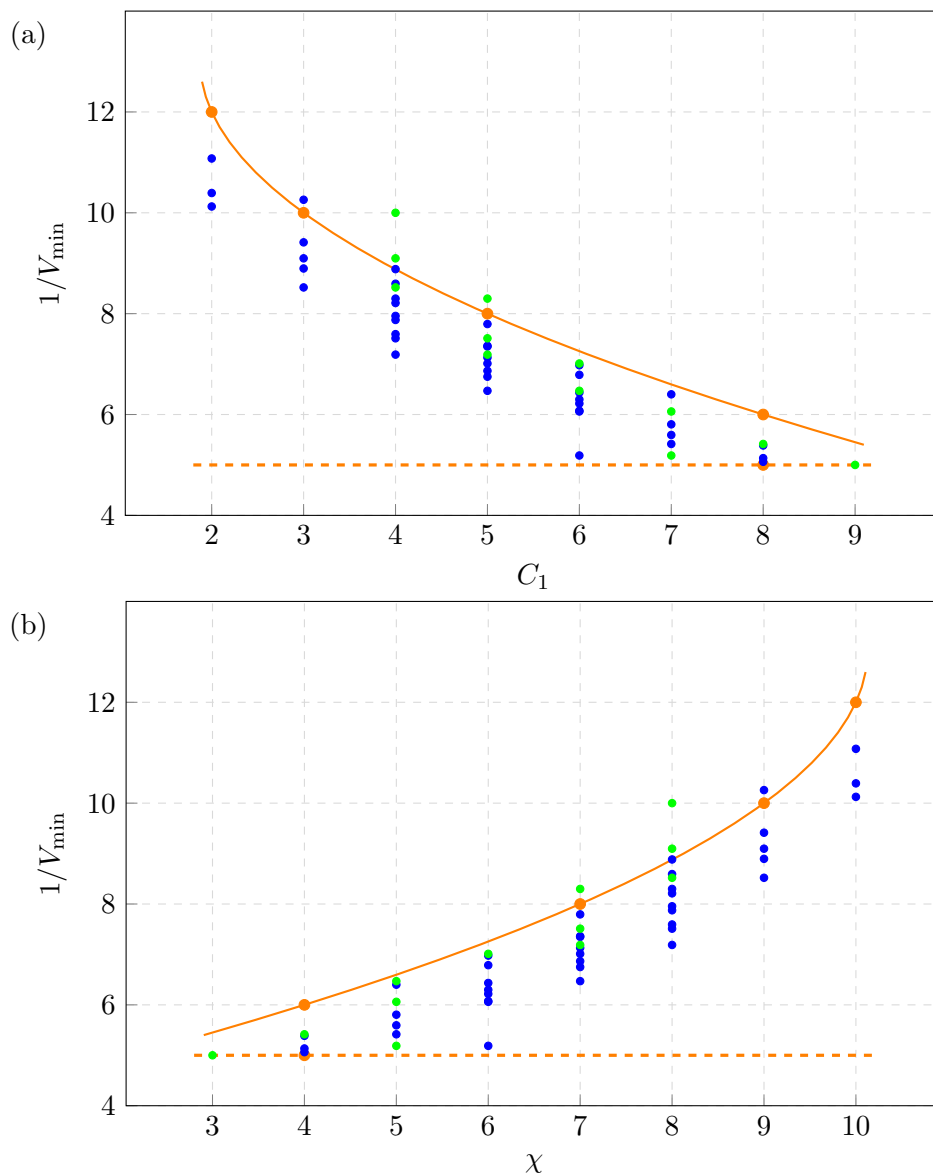
FIGURE 2.3.3: The green points correspond to $\widetilde{X(\Delta)}$ built from first-grade points. The varieties (from zeroth-grade points) of triangles are in orange.

A proof of this can be found in [2, §7.2].

It is conjectured in [46] that the lower bound of minimized volumes is $1/\chi$, and the bound is saturated when $\mathcal{X}$ is an abelian orbifold of $\mathbb{C}^3$ for reflexive polytopes in any dimensions. However, as we can see from Figure 2.3.3, $1/V_{\min}$ can be greater than the Euler number. Furthermore, the volumes of triangles do not form a lower bound any more[17]. There are two cases (13 and 17) that are above the orange curve even if we ignore the green points. Nevertheless, we still find the orange curve seems to follow some pattern. For reflexive cases, such curve would be $\chi = 1/V_{\min}$ as this is the bound mentioned above. For the cases with two interior points, the curve is

$$\chi = \frac{1}{8}\left(14 - \frac{1}{V_{\min}}\right)\left(12 - \frac{1}{V_{\min}}\right) + 2. \tag{2.3.14}$$

We suspect that for polygons with arbitrarily many interior points, such curves would follow some specific pattern.

---

[17]However, we should emphasize that such bound may still be true for reflexive polytopes in any dimension, though we do not have available data to test this.

On the other hand, the upper bounds of minimized volumes for reflexive cases in any dimensions are fibrations of dP_3 [46]. Here, for polygons with two interior points, we find that the upper bound is $\mathbb{C}^3/\mathbb{Z}_5$ (1,2,2), which is the only $\mathbb{C}^3$ orbifold not on the orange curve.

It is conjectured in [46] that the bounds of the minimized volumes for toric CY n-folds $\mathcal{X}$ with reflexive $(n-1)$-dimensional polytopes as the toric diagrams are

$$\frac{1}{\chi} \leq V_{\min} \leq m_n \int c_1^{n-1}, \tag{2.3.15}$$

where $m_3 \sim 3^{-3}$, $m_4 \sim 4^{-4}$ and $m_n > m_{n+1}$. We have already seen that the first inequality does not hold for non-reflexive cases (while the second one still holds here). In Figure 2.3.4, we plot the χ-$1/V_{\min}$ diagram again. It is obvious that the area bounded by $1/V_{\min} = \chi/m_3$ and $1/V_{\min} = (12 - \chi)/m_3$ is much larger than the region where our data points live. Hence, it is
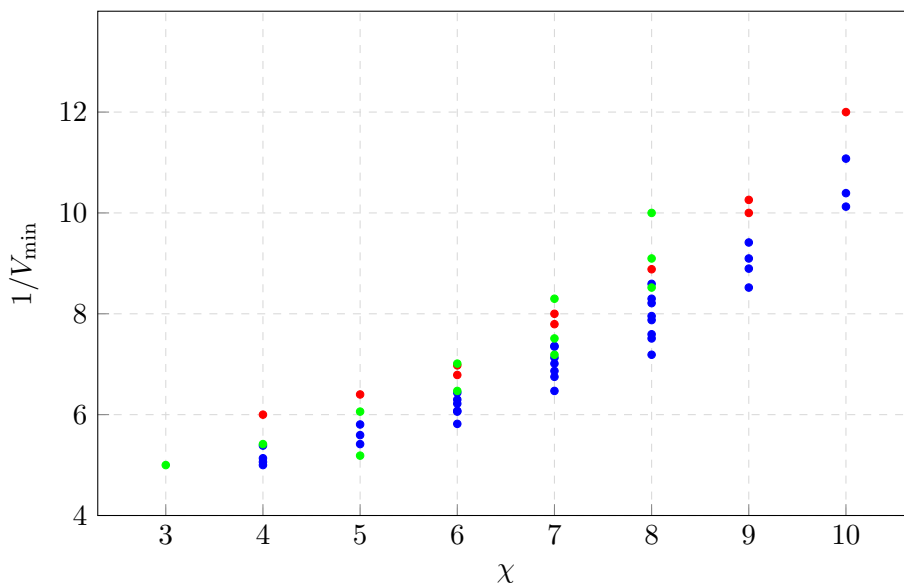
FIGURE 2.3.4: There are large gaps between red points and others. In other words, the red points are much closer to the lower bound of volumes.

possible that we may extend the above conjecture to the following[18].

Conjecture 2.3.5. *For polytopes (either reflexive or non-reflexive), we have*

$$\frac{1}{\chi} \leq V_{\min} < m_n \int c_1^{n-1}. \tag{2.3.16}$$

It is worth noting that such bounds for 2d lattice polygons in terms of their areas are obtained in [92]:

$$\frac{1}{A} \leq V_{3,\min} < \frac{4\pi^2}{27A}, \tag{2.3.17}$$

where A is the normalized area of the polygon. Moreover, the lower bound is saturated for triangles while the upper bound is the case for ellipses (as limit shapes of polygons) and hence can never be saturated. If we compare (2.3.17) with (2.3.16) with $n = 3$, we find that the lower bounds agree: χ is the Euler number for a complete resolution which corresponds to a fine triangulation, and hence $\chi = A$. Furthermore, they take equalities under the same condition. For the upper bound, (2.3.16) becomes $m_3 C_1 = m_3(12 - \chi)$, whose connection to (2.3.17) is more subtle to understand.

We would also like to know whether the minimized volume of Y with an arbitrary polytope Δ can be arbitrarily close to 0, viz, unbounded from above in the χ-$1/V_{\min}$ diagram[19]. The answer is yes

---

[18]There is a typo in [2], but this is corrected in [8].
[19]For polygons, this can also easily be seen from 2.3.17.

and can be seen from considering the orbifolds. We know that the volume of an orbifold is the volume of its parent divided by the order of the quotient group, regardless of the action:

$$\mathrm{vol}(M/\Gamma) = \frac{\mathrm{vol}(M)}{|\Gamma|}. \tag{2.3.18}$$

From [113], we know that the volume of a (finite) cone is proportional to the volume of the Sasaki-Einstein manifold. Then the minimized volume function should also follow[20]

$$V(M/\Gamma) = \frac{V(M)}{|\Gamma|}. \tag{2.3.19}$$

For instance, this provides a quick way to see that $V_{\min}(\mathbb{C}^n/\mathbb{Z}_n) = 1/n$ as we have shown in §2.1.4. Also, this does not depend on the orbifold action. The lattice rectangle of size 2×1 and the toric diagram of F_0 are both the conifold quotiented by $\mathbb{Z}_2$, but with different actions. However, they both have $V_{\min} = 8/27$.

Outlook   In this chapter, we have only considered 2d polygons with two interior points. This is quite a strict constraint which only gives us 45 inequivalent toric diagrams. For instance, the classification of 3d lattice polytopes with two interior points has been done in [124], which gives 22673449 of them up to unimodular equivalence. Therefore, a general method needs to be found to get a more detailed understanding of the geometric and topological properties for any polytopes. It would also be interesting to randomize over the space of toric diagrams and try volume-topolgy plots.

For reflexive polytopes of dimension n, besides the affine CY_{n+1} cone which is non-compact, we know that compact smooth CY_{n-1} can be constructed as hypersurfaces in $X(\Delta)$ from [125–130]. However, for non-reflexive ploytopes, we do not have the defining polynomials any more. It would be interesting to study the hypersurfaces for such cases.

---

[20]As it should be clear, we will use the corresponding orbifold to denote the volume function of Y in our notation.

Chapter 3

Mahler Measure

In this chapter, we shall mention the statistical aspect of dimer models/brane tilings. In particular, the crystal melting models [41–43, 131] turn out to be crucial in the study of BPS spectra, which will be discussed in more detail in Chapter 5. Here, let us consider a concept from number theory, that is, the Mahler measure [47]. We will see that it enjoys nice properties in the context of quiver gauge theories and dimer models[1]:

- We introduce the isoradial and tropical limits that depend on the coefficients of the Newton polynomials. When the Newton polynomial is restricted to have one single parameter, we show that when a tropical limit is reached in the large limit of the free parameter. We argue that the Mahler measure (and the Ronkin function) increases monotonically from the isoradial limit to this tropical limit. Moreover, we propose that this free parameter could be related to the (single) FI parameter of the gauge theory with the constraints of the D-term relations.

- We give the asymptotic expressions ((3.2.19) and (3.2.20)) of the areas of the holes in the amoeba in this tropical limit.

- We find that when the Newton polynomial takes the coefficients with the canonical choice (introduced below), the maximization of the Mahler measure is equivalently to the a-maximization which determines the R-charges for isoradial dimers. We also conjecture that this holds for non-isoradial cases.

- We conjecture that with the canonical choice of the coeffcients, the Newton polynomial (and hence the Mahler measure in the isoradial limit) is invariant under Seiberg duality.

- We will see that the quantity u_0 (defined below) appeared in the calculations of the Mahler measure can be viewed as a generating function of the master space of the gauge theory. One then find how the Mahler measure transforms under the specular duality ((3.2.58)).

3.1 Prelude

Since we are attempting to connect a multitude of concepts from mathematics and physics, it is expedient to present an introductory summary here, as much to motivate the reader as to set notation. Let us start with the Mahler measure. Then we will see how this is connected to dimer models/brane tilings.

3.1.1 The Mahler Measure

Originating in algebraic number theory, the Mahler measure is a seemingly innocuous object. Given a Laurent polynomial in n complex variables, the Mahler measure can be considered as an average on the n-torus:

---

[1]A short summary can also be found in [132].

Definition 3.1.1. *For a (non-zero) Laurent polynomial $P(\boldsymbol{z}) = P(z_1, \ldots, z_n) \in \mathbb{C}[z_1^{\pm 1}, \ldots, z_n^{\pm 1}]$, the* **Mahler measure** *is*

$$m(P) := \int_0^1 \cdots \int_0^1 \log |P(\exp(2\pi i \theta_1), \ldots, \exp(2\pi i \theta_n))| \mathrm{d}\theta_1 \ldots \mathrm{d}\theta_n. \tag{3.1.1}$$

By convention, we set $m(0) = \infty$.

We emphasize that the name Mahler measure often means the exponential $\exp(m(P))$ in the literature. However, since we will exclusively work with $m(P)$ in this paper, we will always refer to $m(P)$ in (3.1.1) as the Mahler measure.

The Mahler measure enjoys many salient features, such as additivity, meaning that $m(PQ) = m(P) + m(Q)$ for any two Laurent polynomials P, Q. Furthermore, for a univariate polynomial $P(z) = a \prod_{i=1}^{n} (z - \alpha_i)$, we have Jensen's formula:

$$m(P) = \log |a| + \sum_{i=1}^{n} \max\{0, \log |\alpha_i|\} . \tag{3.1.2}$$

However, for more than one variable, the integral in (3.1.1) is already highly non-trivial. Since in this paper we are mainly considering bivariate Laurent polynomial $P(z, w)$, and already no such simple formula as Jensen's is known[2].

What we do know about the n variable case is that the Mahler measure is $\mathrm{GL}(n, \mathbb{Z})$ invariant [134, 135]:

Theorem 3.1.1. *Let $0 \neq (M_{ij})_{n \times n} \in \mathrm{GL}(n, \mathbb{Z})$. Then*

$$m(P(\boldsymbol{z})) = m(P(\boldsymbol{z}^M)) = m(P(-\boldsymbol{z}^M)), \tag{3.1.3}$$

where $\boldsymbol{z}^M = \left(\prod_{i=1}^{n} z_i^{M_{i1}}, \ldots, \prod_{i=1}^{n} z_i^{M_{in}} \right)$.

Other than the few nice properties mentioned above, perhaps the most extraordinary about the Mahler measure is that for certain polynomials, it evaluates to special values of zeta and L-functions [50, 136, 137].

Here, we will mainly apply the expansion of the integrand and residue theorem to calculate the integral. Writing $\boldsymbol{z} := (z_1, \ldots, z_n)$, and extract the constant term of the polynomial P as k, i.e.,

$$P(\boldsymbol{z}) := k - p(\boldsymbol{z}) , \tag{3.1.4}$$

we have the series expansion (formally in p)

$$\log(k - p(\boldsymbol{z})) = \log k - \sum_{n=1}^{\infty} \frac{p^n(\boldsymbol{z})}{n} k^{-n}. \tag{3.1.5}$$

Since we are integrating on the n-torus, we need the restriction $|k| \geq \max_{\boldsymbol{z} \in T^n} |p(\boldsymbol{z})|$. This then ensures the series expansion converges uniformly on the support of the integration path and hence we are also allowed to exchange the sum and integral in our calculation. Therefore, we may write the Mahler measure as

$$m(P) = \mathrm{Re} \left(\frac{1}{(2\pi i)^n} \int_{|z_i|=1} \log(P(z_1, \ldots, z_n)) \frac{\mathrm{d}z_1}{z_1} \ldots \frac{\mathrm{d}z_n}{z_n} \right). \tag{3.1.6}$$

---

[2]By writing $P(z, w)$ as $a(w) \prod_{i=1}^{n} (z - \alpha_i(w))$, we can still use Jensen's formula to compute $m(P(z, w))$, but the expression is much more involved [133] and no analytic results are known explicitly.

By the residue theorem and integrating over $|k| > \max\limits_{\boldsymbol{z} \in T^n} |p(\boldsymbol{z})|$, only the constant term in (3.1.5) contributes. Therefore, we have that

$$m(P) = \operatorname{Re}\left(\log k - \int_0^{k^{-1}} (u_0(t) - 1)\frac{\mathrm{d}t}{t}\right), \tag{3.1.7}$$

where

$$u_0(k) = \frac{1}{(2\pi i)^n} \int_{|z_i|=1} \frac{1}{1 - k^{-1}p(z_1, \ldots, z_n)} \frac{\mathrm{d}z_1}{z_1} \cdots \frac{\mathrm{d}z_n}{z_n}. \tag{3.1.8}$$

An example of the above process can be found in Appendix B.

In fact, (3.1.8) means that $u_0(k)$ is a period of a holomorphic 1-form ω_Y on the curve Y defined by $1 - k^{-1}P = 0$ [50, 138], that is, $\int_\gamma \omega_Y$ where γ is a 1-cycle on Y. We shall also refer to this as the period of the curve Y. Therefore, u_0 also satisfies the Picard-Fuchs equation:

$$A(k)\frac{\mathrm{d}^2 u_0}{\mathrm{d}k^2} + B(k)\frac{\mathrm{d}u_0}{\mathrm{d}k} + C(k)u_0 = 0, \tag{3.1.9}$$

where $A(k), B(k), C(k)$ are polynomials in k.

We may also extend the definition of Mahler measure.

Definition 3.1.2. *The generalized Mahler measure extends definition* (3.1.1) *to an arbitrary torus with variable sizes a_i:*

$$m(P; a_i) = \frac{1}{(2\pi i)^n} \int_{|z_i|=a_i} \log P(z_1, \ldots, z_n)\frac{\mathrm{d}z_1}{z_1} \cdots \frac{\mathrm{d}z_n}{z_n}. \tag{3.1.10}$$

3.1.2 More on Dimer Models

To discuss how $P(z, w)$ and Mahler measures are related to dimer models, we need to introduce a few more concepts supplementary to the reviews in §2.1.2. Recall that the brane tiling gives a bipartite graph $\mathcal{G}$, and the dimer model is the study of its (random) perfect matchings. As we shall always take $\mathcal{G}$ to be $\mathbb{Z}^2$-periodic, it always constitutes a doubly-periodic tiling of the plane. In other words, $\mathcal{G}$ is embedded in the $\mathbb{Z}^2$ lattice[3]. Now, the plane quotiented by $\mathbb{Z}^2$ is a torus, of genus 1, and we will use $\mathcal{G}_1 := \mathcal{G}/(\mathbb{Z}^2)$ to denote the fundamental domain of the bipartite graph. More generally, we use $\mathcal{G}_n$ to denote the quotient $\mathcal{G}/(n\mathbb{Z}^2)$, where $n\mathbb{Z}^2$ is the n-times enlarged fundamental domain.

Given a perfect matching M, we can define a unit flow ω that flows by one along each edge in M from white node to black node. Consider a reference perfect matching M_0 with flow ω_0, and let γ be a path from face f_0 to f_1 in the graph. Then for any matching q with flow ω, the total flux of $\omega - \omega_0$ across γ is independent of γ and defines a height function of M. The difference of height functions of any two perfect matchings is independent of the choice of M_0. A perfect matching M_1 on the fundamental domain $\mathcal{G}_1$ gives a periodic perfect matching M on $\mathcal{G}$. The **height change** of M_1 is defined to be (h_x, h_y) if the horizontal and vertical height changes of M for one period are h_x and h_y respectively.

We can define a real function $\mathcal{E}(e)$ on the edges e of $\mathcal{G}$. This is known as the **energy** of the edges [139].

Definition 3.1.3. *Given a perfect matching (or more generally, any set of edges) M, its energy is $\mathcal{E}(M) := \sum\limits_{e \in M} \mathcal{E}(e)$. For any edge e in the graph, its **edge weight** is defined to be $\mathrm{e}^{-\mathcal{E}(e)}$. Let $\mathcal{M}(\mathcal{G})$ be the set of perfect matchings on $\mathcal{G}$, then the **partition function** of $\mathcal{M}$ is $Z(\mathcal{G}) := \sum\limits_{M \in \mathcal{M}(\mathcal{G})} \mathrm{e}^{-\mathcal{E}(M)}$.*

---

[3]More generally, one may also consider any 2-dimensional lattice instead of $\mathbb{Z}^2$. Indeed, one can consider high-genus tilings.

Given the edge weights, one can define the **Kasteleyn matrix** K.

Definition 3.1.4. *A Kasteleyn matrix has rows (columns) representing the white (black) nodes in $\mathcal{G}$. Its entries are the corresponding edge weights multiplied by ± 1 as follows. Around each face there are an odd number of edge weights multiplied by -1 if the face has $0 \pmod 4$ edges and an even number if it has $2 \pmod 4$ edges.*

It was shown in [140] that this construction is always possible, and

Theorem 3.1.2. *The absolute value of the determinant is the partition function, that is,*

$$|\det(K)| = Z(\mathcal{G}) = \sum_{M \in \mathcal{M}(\mathcal{G})} e^{-\mathcal{E}(M)}. \tag{3.1.11}$$

As $\mathcal{G}_1$ is embedded on a torus, let γ_x and γ_y be paths winding horizontally and vertically around the torus. Then we can multiply an edge weight by z (or z^{-1}) if the γ_x crosses the edge with the black node on its left (or right). Likewise, we multiply an edge weight by $w^{\pm 1}$ if γ_y crosses the edge. This leads to the "magnetically altered" Kasteleyn matrix $K(z, w)$ [139]. We may then construct a Laurent polynomial from this.

Definition 3.1.5. *The **Newton** or **charateristic polynomial** of $\mathcal{G}$ is $P(z, w) := \det(K(z, w))$ in formal complex variables z, w. It defines a so-called **spectral curve** $P(z, w) = 0$, as a Riemann surface.*

For each monomial $c_{(m,n)} z^m w^n$ in $P(z, w)$ with coefficient $c_{(m,n)}$, we can associate a point (m, n) on the lattice. These points form a lattice polygon known as the **Newton polygon**. In toric geometry, this is precisely the toric diagram discussed in the previous chapter. In particular, each vertex/corner point in the polygon is associated with a toric divisor of the Gorenstein singularity.

Example 1. *Let us consider the dimer in Figure 3.1.1(a). The fundamental region is the square*
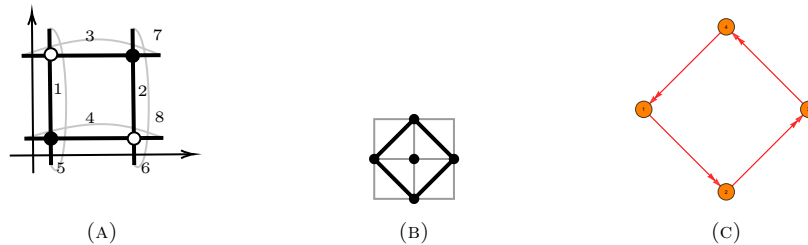
FIGURE 3.1.1: (a) The dimer model. (b) The toric diagram. (c) The quiver diagram.

where the numbers are the labels of the edges (rather than weights). Let us take the weight of each edge to be $\sqrt{2}$ (for the reason to be discussed shortly). Now consider for instance the vertex correponding to the monomial z in the Newton polygon. Its perfect matching is composed of X_2, X_5 where X_I is the arrow dual to edge I [105]. Therefore, this gives rise to $(-1) \times \sqrt{2} \times \sqrt{2} z = -2z$ in the spectral curve. Overall, one may check that this agrees with the Kasteleyn matrix

$$K = \begin{pmatrix} -\sqrt{2} + \sqrt{2} z & \sqrt{2} - \sqrt{2} w \\ -\sqrt{2} + \sqrt{2} w^{-1} & -\sqrt{2} + \sqrt{2} z^{-1} \end{pmatrix}, \tag{3.1.12}$$

where the signs and variables assigned to the edges are $\{1, -1, -1, -1, z, z^{-1}, -w, w^{-1}\}$ (ordered by the labelling of edges). The curve is then given by

$$-2z - 2z^{-1} - 2w - 2w^{-1} + (2 + 2 + 2 + 2) = 0, \tag{3.1.13}$$

or equivalently,

$$-z - z^{-1} - w - w^{-1} + 4 = 0. \tag{3.1.14}$$

It is straightforward to get the Newton polygon as in Figure 3.1.1(b). The quiver in Figure 3.1.1(c) is the dual graph of the dimer.

Isoradial dimers We have introduced some rudiments of dimer models and brane tilings. Of particular interest is the isoradial embedding of a dimer model.

(a)   (b)
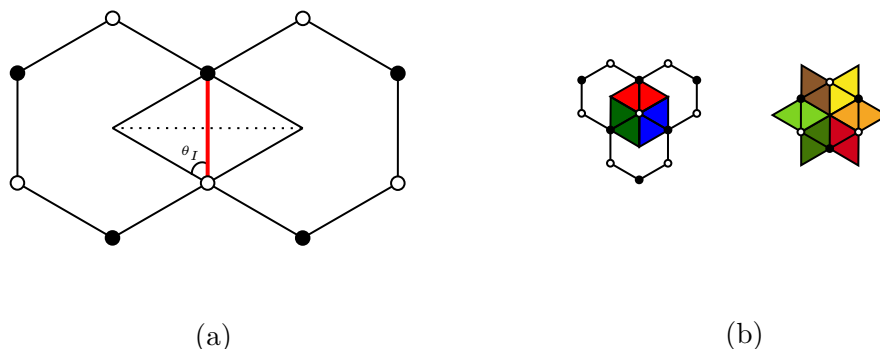
FIGURE 3.1.2: (a) The edge in red has length l. Its dashed dual edge is of length $\sqrt{4-l^2}$ which equals the weight of the edge. The rhombus angle is labelled by θ_I. The corresponding internal angle $2\theta_I$ of the rombus gives the R-charge physically. (b) The left plot indicates $\sum 2\theta_I = 2\pi$ which corresponds to each superpotential term while the right plot indicates $\sum(\pi - 2\theta_I) = 2\pi$ which correpsonds to (the fields connected to) each node in the quiver.

Definition 3.1.6. *A dimer is* **isoradial** *if every face is inscribed in a circle of the same radius, which we can take to be* 1. *In this paper, we will mostly choose the weight of an edge to be* $\sqrt{4-l^2}$ *for an isoradial dimer where l is the length of the edge.*

The reason for this choice is that the edge weight is equal to the distance of the circumcentres of the two faces adjacent to the edge (i.e., its dual, perpendicular, edge). We illustrate this in Figure 3.1.2(a) in a hexagonal tiling example. As we will see shortly, we can always construct a spectral curve of certain kind (a so-called genus 0 Harnack curve) from such isoradial embedding of a dimer. According to [141], this choice of edge weight is *critical* in the sense that it uniquely maximizes the (normalized) determinant of Dirac operator. We will also later see that it is closely related to the Mahler measure for isoradial embeddings.

We can also express this edge weight in terms of the **rhombus angle** θ_I, as shown in Figure 3.1.2(a). In our convention, $2\theta_I$ is the angle of the rhombus at the vertex that has in common with the edge. It is easy to see that our chosen edge weight is $\sqrt{4-l^2} = 2\sin(\theta_I)$. In other words, $l = 2\cos(\theta_I)$. The energy function associated to this edge e_I, recalling that edge weight is $e^{-\mathcal{E}}$, is then $\mathcal{E}(e_I) = -\log(2\sin(\theta_I))$.

Now, the internal angle $2\theta_I$ is essentially the R-charge of the corresponding chiral multiplet in the dual quiver gauge theory [142]: for a field X_I with R-charge R_I,

$$2\theta_I = \pi R_I. \tag{3.1.15}$$

Indeed, we have (i), that $\sum 2\theta_I = 2\pi$, which is the geometric recasting of the condition on R-charges from the vanishing β-function, that $\sum R_I = 2$. Likewise, we have (ii), that $\sum(\pi - 2\theta_I) = 2\pi$. Notice the difference between the two sums: (i) is a sum over the angles whose edges are connected to the same black or white node while the (ii) is a sum of angles in the same face. We depict this in Figure 3.1.2(b), where a coloured rhombus has rhombus angle θ_I. The left plot represents (i), a sum over the parts of rhombi surrounding a *vertex* (drawn as white in the middle). Every such sum corresponds to a term in the superpotential. The right plot represents (ii), a sum over the part of rhombi surrounding the (circum)centre of the dimer *face*. Each contributes an angle of $(\pi - 2\theta_I)$ so that $\sum(\pi - 2\theta_I) = 2\pi$. Every such sum corresponds to arrows attached to a node in the dual quiver.

Example 2. *Recall the dimer in Figure 3.1.1. Since the rhombus angles are all $\pi/4$, each edge weight equals $2\sin(\pi/4) = \sqrt{2}$.*

Isoradial spectral curve and GLSM fields It is straightforward to obtain the spectral curve in terms of the rhombus angles from Kasteleyn matrix. When taking determinant, each term we get is simply a product of edge weights $2\sin(\theta_I)$ contributed from the corresponding rhombus angles/R-charges[4]. Therefore, we need to figure out which edges contribute to each monomial in the Newton polynomial. This can be seen from the perfect matching(s) associated to each lattice point in the Newton polygon. Recall that each perfect matching can be interpreted as a GLSM field. Every lattice point in the Newton polygon is associated with one or more GLSM fields.

For a vertex/corner point v_i, we only have one corresponding GLSM field p_i. It can be written as $p_i = \sum_I X_I$ where X_I's are the arrows in the quiver. Recall that X_I's are arrows dual to the edges e_I in the dimer. When computing $\det(K)$, we would get the monomial corresponding to v_i as a product of these e_I's. Since they have weights $2\sin(\theta_I)$, this gives the term

$$(-1)^\delta \prod_I 2\sin(\theta_I) z^a w^b \tag{3.1.16}$$

where the factor $z^a w^b$ can be directly read off from the Newton polygon, and we will explain what δ means shortly.

This can be generalized to any lattice point. For interior points and other boundary points, they correspond to multiple GLSM fields. Suppose one of such points is associated to GLSM fields $q_1, \ldots, q_k$, then each q_i can be written as $q_i = \sum_I X_I$. As a result, each q_i gives rise to a product of $2\sin(\theta_I)$ from the determinant. Then the corresponding monomial in the spectral curve is the sum of these products for every q_i,

$$(-1)^\delta \sum_i \begin{bmatrix} \text{weight} \\ \text{of } q_i \end{bmatrix} z^a w^b = (-1)^\delta \sum_i \left(\prod_I 2\sin(\theta_I) \right) z^a w^b. \tag{3.1.17}$$

Now let us determine δ. Given a reference perfect matching M_0, denote the horizontal (vertical) height change of the perfect matching M to be h_x (h_y). Then the above rules of writing the Newton polynomial should agree with the result in [139]:

$$P(z,w) = \sum_M e^{-\mathcal{E}(M)} z^{h_x} w^{h_y} (-1)^{h_x h_y + h_x + h_y}. \tag{3.1.18}$$

It is straightforward to see that the energy of M is consistent with (3.1.16) and (3.1.17), that is, $\mathcal{E}(M) = \sum_I \mathcal{E}(e_I) = -\log\left(\prod_I 2\sin(\theta_I) \right)$. Now different reference M_0 may give different signs for each term, but it would preserve certain properties of the spectral curve (such as its Mahler measure). Here, we will stick to the perfect matching corresponding to $a = b = 0$ (i.e. the origin of the Newton polygon) as the reference M_0 so that the powers of variables agrees with (3.1.16) and (3.1.17) [5]. Then the parity of $(h_x h_y + h_x + h_y)$ is fully determined by $a = h_x$ and $b = h_y$. Thus, we may write δ as

$$\delta = \begin{cases} 0, & \text{both } a \text{ and } b \text{ are even} \\ 1, & \text{otherwise} \end{cases}. \tag{3.1.19}$$

Example 3. *Recall the example in Figure 3.1.1(a). Let us choose the matching consisting of edges 1 and 2 as the reference perfect matching. As the matching consisting of edges 4 and 7 has height*

---

[4]Note that so far by R-charges, we mean all possible trial R-charges that satisfy the conformality condition. In other words, the rhombus angles are still variables in the spectral curve. We will determine their exact values (and hence exact coefficients for the curve) in §3.2.4.

[5]Notice that in [139], there is also a total factor $z^{x_0} w^{y_0}$ in the front of the right hand side in (3.1.18), where x_0 and y_0 are the total flows across the horizontal and vertical cycles respectively. This would ensure that the overall powers $z^{x_0 + h_x} w^{y_0 + h_y}$ is the same as $z^a y^b$. For simplicity, we remove this factor in (3.1.18) as long as we choose the one with $x_0 = y_0 = 0$ as our reference perfect matching.

change $(0, -1)$, *we have* $\delta = 1$ *and this gives rise to the term* $-2w^{-1}$. *Altogether, we have the spectral curve*

$$-2z - 2z^{-1} - 2w - 2w^{-1} + (2 + 2 + 2 + 2) = 0, \tag{3.1.20}$$

or equivalently,

$$-z - z^{-1} - w - w^{-1} + 4 = 0. \tag{3.1.21}$$

This agrees with (3.1.14).

3.1.3   Amoebae and Harnack Curves

Now that we have some familiarity with dimers and Newton polynomials/spectral curves, let us collect some facts on amoebae and Harnack curves, adhering to the notation of [139, 143].

Definition 3.1.7. *An **amoeba** is the set of points in the real plane, of the logarithmic projection of the spectral curve* $P = 0$:

$$\mathcal{A}_P = \Big\{ \big(\log |z|, \log |w| \big) \ \big| \ P(z, w) = 0 \Big\}. \tag{3.1.22}$$

The definition of the amoeba can be easily extended to polynomials of more variables, but in this paper, we will only focus on Newton polynomials in two variables (z, w), and everything will be planar: the Newton polynomial lives in $\mathbb{C}^2$; the amoeba lives in $\mathbb{R}^2$ and the toric diagram lives in $\mathbb{Z}^2$. Let us also introduce the spine as a deformation retract of the amoeba. For simplicity, we shall use the result in [22] as our definition. For the original definition, see [144].

Definition 3.1.8. *The **spine** $\mathcal{S}$ of the amoeba is the dual* (p, q)-*web of the toric diagram associated to* $P(z, w)$.

In parallel, we have

Definition 3.1.9. *A real algebraic curve* $C \subset \mathbb{RP}^2$ *of degree* d *is an **M-curve** if it has the maximal number of connected components, i.e.,* $\frac{(d-1)(d-2)}{2} + 1$. *Following [143], we shall call the connected components **ovals**. Ovals that do not intersect the coordinate axes are known as **compact ovals**. An isolated real point on the curve is regarded as a **degenerate oval**. The **genus** g is the number of non-degenerate compact ovals. For an M-curve, the genus is also maximal and equals* $\frac{(d-1)(d-2)}{2}$.

A Harnack curve is a special type of M-curve in the sense that its ovals have the "best" possible topological configurations (see Figure 2 in [143] for an illustration). The definition of Harnack curves is quite intricate [145]. Here, we will take the following characterization as the working definition:

Definition 3.1.10. *A **Harnack curve** C possesses the map*

$$C(\mathbb{C}) \ni (z, w) \mapsto (\log |z|, \log |w|) \in \mathcal{A}_C \tag{3.1.23}$$

such that it is 2-to-1 from the curve to its amoeba (except for a finite number of real nodes where it is 1-to-1). The amoeba of Harnack curve with genus g *has exactly* g *holes (i.e., compact complementary regions). Hence, the number of holes for an amoeba is also called the genus of the amoeba.*

From [139], we have a practical way to identify Harnack curves associated with amoebae and dimers.

Theorem 3.1.3. *For any choice of non-negative edge weights on a dimer, the spectral curve* $P(z, w) = 0$ *is a Harnack curve of degree* d *with* $\frac{(d-1)(d-2)}{2}$ *compact ovals.*

There is another remarkable theorem [146] that will be crucial to us:

Theorem 3.1.4. *A curve is Harnack if and only if its amoeba has the maximal possible area for a given Newton polygon* Δ. *That is,* $A(\mathcal{A}_P) = \pi^2 A(\Delta)$ *where* $A(\Delta)$ *is the unnormalized area of the Newton polygon.*

In fact, the 2-to-1 feature for Harnack curves leads to the two important propositions [139]:

Proposition 3.1.5. *The boundary of the amoeba is the image of the real locus of the spectral curve* $P(z, w) = 0$. *It follows that the amoeba of a Harnack curve can be determined by*

$$\prod_{n_1, n_2 \in \mathbb{Z}^2} P\left((-1)^{n_1} e^x, (-1)^{n_2} e^y\right) \leq 0. \tag{3.1.24}$$

Proposition 3.1.6. *Any interior lattice point of the Newton polygon Δ corresponds to either a bounded complementary region (i.e., a hole) of the amoeba or an isolated real node in the spectral curve. In particular, the number of holes of the amoeba is equal to the genus g of the curve.*

Finally, we have a theorem from [143] for isoradial dimers:

Theorem 3.1.7. *A dimer corresponding to a genus zero Harnack curve is isoradial if and only if its amoeba contains the origin.*

On the log plane, we can always shift the amoeba so that it contains the origin, which corresponds to a rescaling of z and w of the spectral curve. This gives a canonical family of isoradial parameterizations for any genus-zero Harnack curve.

Example 4. *The spectral curve* (3.1.14) *is Harnack and of genus* 0. *In fact,* $-z - z^{-1} - w - w^{-1} + k = 0$ *is Harnack when $k \geq 4$, with $g = 0$ for $k = 4$ and $g = 1$ otherwise.*

Ronkin functions   Closely related to the amoeba is the so-called Ronkin function. In fact, to probe different regions of the amoeba, we can use this analytic tool.

Definition 3.1.11. *In two dimensions, the generalized Mahler measure* (3.1.10) *with $a_1 = \exp(x)$, $a_2 = \exp(y)$ defines the* **Ronkin function** $R(x, y) := m(P; e^x, e^y)$. *In particular, $R(0, 0) = m(P; 1, 1) = m(P)$.*

Following [144, 147–149], we have[6]

Theorem 3.1.8. *The Ronkin function $R(x, y)$ is convex. It is strictly convex over $\mathcal{A}_P$ and linear over each component of $\mathbb{R}^2 \backslash \mathcal{A}_P$. The gradient $\nabla = (\partial_x, \partial_y)$ of the Ronkin function satisfies*

- *$\text{Int}(\Delta) \subset \nabla R(\mathbb{R}^2) \subset \Delta$, where Δ is the Newton polygon for P and $\text{Int}(\Delta)$ is its interior;*

- *for each component E_i of $\mathbb{R}^2 \backslash \mathcal{A}_P$, $\nabla R(E_i) = (a_i, b_i)$, where (a_i, b_i) is the lattice point in Δ corresponding to E_i.*

Given a Harnack curve with ovals (either degenerate or non-degenerate), we can always shift the amoeba such that a hole or a critical point[7] is located at the orgin. In terms of $P(z, w)$, this is a rescaling/redefinition of the variables z, w (we will make this more precise in §3.2.1). Since the Mahler measure is the Ronkin function at $(0, 0)$ (which is always a lattice point in Δ), we have $\nabla R(0, 0) = (0, 0)$ following this theorem. Moreover, as the Ronkin function is always convex, we have

Corollary 3.1.8.1. *Given a Laurent polynomial P (with possible rescaling of variables), the Mahler measure $m(P)$ is the minimum of $R(x, y)$.*

3.1.4   Crystal Melting and D-branes

Another physical system, in contrast to quiver gauge theories of brane tiling, that arise from dimer models is the so-called crystal melting model, which counts certain BPS bound states [43, 131].

---

[6]We are focusing on $\mathbb{R}^2$ in this paper, but the discussions on Ronkin functions here can be directly extended to any $\mathbb{R}^n$.

[7]By critical point, we mean that this point in the amoeba corresponds to a node in the spectral curve.

In Type IIA string theory, consider D0- and D2-branes with a single D6 on a toric Gorenstein 3-fold $\mathcal{X}$. More generally, we also include D4-branes [150–152]. Denote the charges of Dp-branes as Q_p, where $Q_{6,4}$ are magnetic while $Q_{2,0}$ are electric. In this configuration, the D4s wrap an ample divisor class $[C] = \sum\limits_{i=1}^{b_2(\mathcal{X})} Q_{4,i}[C_i] \in H_4(\mathcal{X}, \mathbb{Z})$ where C_i is a basis of the 4-cycles and $b_2 = b_4$. Likewise, the D2s wrap the 2-cycle $[S] = \sum\limits_{i=1}^{b_2(\mathcal{X})} Q_{2,i}[S_i] \in H_2(\mathcal{X}, \mathbb{Z})$. Then, the D6-D4-D2-D0 bound states are counted by the partition function [150]

$$Z_{\text{BPS}} = \sum_{Q_0, \boldsymbol{Q}_2} \Omega(Q_0, \boldsymbol{Q}_2, \boldsymbol{Q}_4, Q_6) \mathrm{e}^{-Q_0 \phi_0 - \boldsymbol{Q}_2 \boldsymbol{\phi}_2}, \tag{3.1.25}$$

where ϕ_p are the chemical potentials for Dp-branes and Ω is the degeneracy (Witten index) of the bound states. In fact, the chemical potentials ϕ_0 and ϕ_2 can be identified with string coupling g_s and Kähler moduli respectively [131].

The profound results of [41, 43, 131] then relate the BPS states to the crystal models. A crystal is also a dual diagram of the dimer in the following sense. In the crystal, there are different types of atoms. Each type corresponds to a node in the quiver, and the chemical bonds between atoms are represented by the arrows.

Given an initial crystal, one can melt it by removing atoms from the top of it. The BPS degeneracy is equal to the number of melting crystal configurations with Q_0 being the total number of atoms removed and $\boldsymbol{Q}_2$ the numbers of atoms of different types.

In the thermodynamic limit where a large number of atoms are removed, the shape of the molten crystal is exactly the (minus) Ronkin function, whose 2d projection is the amoeba of Newton polynomial P associated to the Gorenstein 3-fold $\mathcal{X}$. Therefore, using saddle point approximation, we have [131]

Proposition 3.1.9. *In the thermodynamic limit,*

$$Z_{\text{BPS}} \sim \exp\left(\int \mathrm{d}x \, \mathrm{d}y \, R(x,y) \right) \tag{3.1.26}$$

*(where we have omitted a factor of $4/g_s^2$ in the exponential). We may then define the **free energy** as $F \equiv -\log Z_{\text{BPS}}$ [139].*

In general, (3.1.26) is divergent. Hence, we need to normalize the partition function by Z/Z_0 where Z_0 is the partition function of the initial unmolten crystal. Then the volume between the Ronkin functions for Z and Z_0 would remain finite[8].

In particular, the phase structures of crystals are given by amoebae.

Definition 3.1.12. *An unbounded complementary region of the amoeba corresponds to an unmolten part in the crystal and is hence called the **solid phase**. For the parts where atoms are removed in the crystal, the interior of the amoeba is known as the **liquid phase** while a bounded complementary region of the amoeba is known as the **gas phase**.*

With D6-D2-D0 bound states, there would only be liquid and solid phases. Gas phases would appear when we further add D4 branes.

Following Proposition 3.1.6, the number of gas phases of a dimer/crystal model is equal to the genus of $P(z,w) = 0$. In general, every solid/frozen phase corresponds to a boundary point on Δ and every gas phase corresponds to an interior point (except for degenerate cases).

Example 5. *The Ronkin function and amoeba with $P = k - z - z^{-1} - w - w^{-1}$ ($k > 4$) are sketched in Figure 3.1.3. As we can see, the bounded (unbounded) linear facets in a Ronkin function correspond*

---

[8]Note that this volume is different from the volume under Ronkin function discussed in [143].
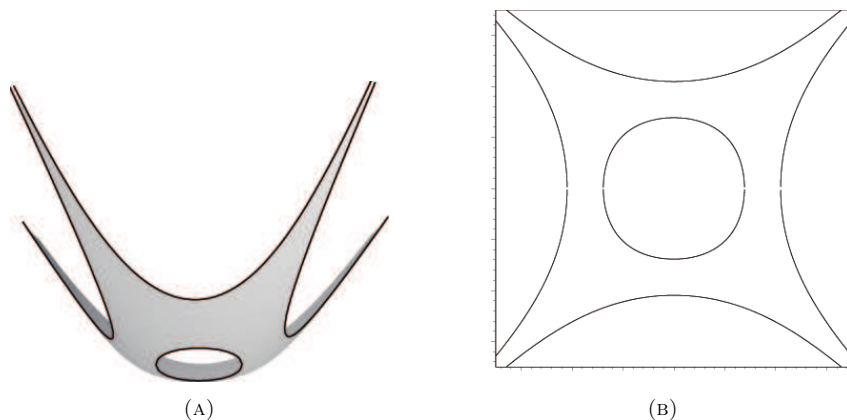
FIGURE 3.1.3: The Ronkin function (a) and the amoeba (b) of F_0. Figures are taken from [139] (with slight modifications). The grey part in (a) gives the interior of amoeba in (b), which corresponds to the liquid phase. The hole in (a)/(b) is the gas phase. The unbounded white parts in (a) gives the unbounded complementary regions in (b). They correspond to solid phases.

to the bounded (unbounded) complementary regions in the amoeba while the non-linear part in the Ronkin function is projected to the interior of the amoeba. The (minus) Ronkin function is the limit shape of the crystal.

Quiver quantum mechanics   Let us think of $\mathcal{X}$ as a fibre bundle of $\mathbb{T}^2 \times \mathbb{R}$ over the $\mathbb{R}^3$ base. Then we can recover the quiver and brane tiling by performing T-dualities along the $\mathbb{T}^2$ directions. The low energy effective 1d quantum mechanics is in fact the dimensional reduction of the 4d $\mathcal{N} = 1$ gauge theory. In the toric diagram, its boundaries specify the singular loci where the $\mathbb{T}^2$ fibre degenrates to a circle. This becomes the NS5-branes under T-dualities, which are (straightened) zig-zag paths on the brane tiling. The D0s become D2s wrapping the whole torus while the D2s are still D2s but restricted in certain domains separated by the NS5 branes. In some of these domains, there would also be NS5s stretched parallel to the D2s. Based on the charges of these NS5s, different domains correspond to black/white nodes and faces in the dimer model. Thus, we can also get the quiver as the dual graph of the dimer. Readers are referred to Figure 1 and 2 in [43] for illustrations.

For the single D6 brane, as it fills the whole CY 3-fold, it will become a point on the torus after T-dualities. Hence, it acts as a flavour brane and there is a flavour node added to the quiver. Likewise, the D4s will become flavour D2-branes which are again points on the torus. These would lead to flavour D4-nodes in the quiver diagram [152].

3.2   Mahler Measure in Quiver Gauge Theories

After going over some fundamentals of Mahler measures and dimer models, we can now study the roles Mahler measures play in quiver gauge theories. As discussed in (3.1.4), we can recast the Newton polynomials into the form (up to shifting the Newton polygon and/or overall multiplication of sign)

$$P(z,w) = k - p(z,w) \ , \qquad k > 0, \tag{3.2.1}$$

where $p(z,w)$ has no constant terms and no free parameters. When we start to increase k, holes might appear in the amoeba of P. For any dimer, let us call the weights $2\sin(\pi R_I/2)$ the **canonical weight choice**. Nevertheless, let us start with a more general set-up where all coefficients $c_{(m,n)}$ depend on k in the following definition.

Definition 3.2.1. *For a spectral curve associated to a dimer with one free parameter k, write it as $P(z,w) = \sum\limits_{(m,n)} c_{(m,n)}(k) z^m w^n$. The **isoradial limit** is defined to be $k = k_{\mathrm{iso}}$ such that $c_{(m,n)}(k)$ agrees with the coefficients from the canonical choice.*

Remark 1. *So far, the canonical choice only has special properties for isoradial dimers. As we will see later, the weights $2\sin(\pi R_I/2)$ which physically come from R-charges also have interesting features for non-isoradial dimers. One may then view a non-isoradial dimer as some sort of "isoradial dimer" with "zero" or "negative" edge lengths. Therefore, we shall always call it the isoradial limit as long as the edge weights follow the canonical choice $2\sin(\pi R_I/2)$ for any dimer regardless of its isoradiality.*

Remark 2. *For $P(z,w) = k - p(z,w)$, the amoeba would have $g = 0$ when $k \leq k_{\mathrm{iso}}$. If $k > k_{\mathrm{iso}}$, the holes would emerge in the amoeba. In particular, the number of holes would always be the same as the number of interior points in the Newton polygon. These holes would evolve simultaneously when we vary k.*

Another interesting limit in the parametrization $P = k - p$ would be the large k limit. First, we introduce a well-known concept.

Definition 3.2.2. *The **Hausdorff distance** between two closed sets $A, B \subset \mathbb{R}^n$ is*

$$d_H = \max\{\sup_{a \in A}(d_E(a, B)), \sup_{b \in B}(d_E(b, A))\}, \tag{3.2.2}$$

where d_E is the usual Euclidean distance.

We shall define a tropical limit using Hausdorff distance.

Definition 3.2.3. *For a Harnack curve associated to a dimer with one free parameter k, write it as $P(z,w) = \sum\limits_{(m,n)} c_{(m,n)}(k) z^m w^n$. Denote its amoeba to be $\mathcal{A}(k)$ and the spine to be $\mathcal{S}$. The **tropical limit** is $k = k_{\mathrm{trop}}$ such that $d_H(\mathcal{A}(k), \mathcal{S})$ is minimized at k_{trop}.*

Theorem 3.2.1. *For $P(z,w) = k - p(z,w)$, $k \to \infty$ is a tropical limit.*

A proof of this can be found in [9, §3].

Remark 3. *Notice that $k \to \infty$ is **a** tropical limit, but may or may not be **the** only tropical limit. For instance, as illustrated in Appendix B, $k = 0$ is also a tropical limit for the F_0 example. Nevertheless, throughout, we will mainly focus on the tropical limit at infinity.*

Since most of the relevant objects diverge at $k_{\mathrm{trop}} = \infty$, we will mainly discuss sufficiently large k.

Definition 3.2.4. *Given an amoeba $\mathcal{A}_P$, denote the set of all vertices v_i of the spine as $\mathcal{V}$. Let $V \subset \mathcal{V}$ be a non-empty proper subset of $\mathcal{V}$. We say that $\mathcal{A}_P$ is **locally** an amoeba $\mathcal{A}_{\mathrm{loc}}$ around V if in a neighbourhood of V, P can be approximated by dropping some of its terms. The dropped terms correspond to the vertices v^* in the dual graph that are outside the neighbourhood. Moreover, the approximated Newton polynomial has amoeba $\mathcal{A}_{\mathrm{loc}}$.*

*Let $\mathcal{P}(\mathcal{V}) \neq \{\mathcal{V}\}$ be a non-trivial partition of $\mathcal{V}$. If $\mathcal{A}_P$ is locally some $\mathcal{A}_{\mathrm{loc}}$ for every $V \in \mathcal{P}(\mathcal{V})$, then we say k is **subtropical**. If $\mathcal{P}(\mathcal{V}) = \{\{v_1\}, \{v_2\}, \ldots, \{v_n\}\}$, i.e., there is a local amoeba around every single vertex v_i, then we say k is **high-subtropical**[9].*

3.2.1 The Mahler Flow

As mentioned above, the Newton polynomials here are constructed by writing down an initial $P_{\mathrm{iso}} = k_{\mathrm{iso}} - p(z,w)$ with certain choice of edge weights. Then we simply vary k to get a family of curves.

---

[9]Analogous to the term "tropical", we also borrow words "subtropics" and "subtropical high" from climate science.

When varying k, the Mahler measure changes continuously. We shall refer to this as the **Mahler flow**. As discussed before, $k_{\min}$ gives the isoradial limit while a tropical limit is reached when $k \to \infty$.

Recall that when $k > \max(|p(z,w)|) = p(1,1)$, we can compute $u_0(k)$ from (3.1.8) using its Taylor expansion just like $m(P)$. It is not hard to see that

$$\frac{\mathrm{d}m(P)}{\mathrm{d}\log k} = u_0(k). \tag{3.2.3}$$

We may also integrate the Mahler flow equation to get

$$\int_{m_{k_0}}^{m_{k_1}} \frac{\mathrm{d}m(P)}{u_0(k)} = \log \frac{k_1}{k_0}, \tag{3.2.4}$$

where we shall take $k_0 = p(1,1)$. Then from their Taylor expansions, we can see that $u_0(k)$ grows no faster than $m(P)$. As a result, both sides would diverge at large k.

For $k \leq p(1,1)$, the behaviour of $u_0(k)$ could be very different. In fact, the right hand side of (3.2.3) is not the same u_0 as the integral of $\frac{1}{1-k^{-1}p}$ any more. This is because the Taylor expansion has radius of convergence $k > p(1,1)$. Consequently, the right hand side in (3.2.3) is no longer a period of the elliptic curve for sufficiently small k. Hence, we shall take (3.2.3) as the definition of $u_0(k)$ for *any* k.

When $k > p(1,1)$, it is straightforward to see that the left hand side of (3.2.3) is positive since $u_0(k)$ should be positive as a period. Its positivity can also been seen from its Taylor expansion $u_0(k) = \sum_{n=0}^{\infty} \frac{p^n(z,w)}{k^n}$. Therefore[10],

Lemma 3.2.2. *The Mahler measure strictly increases when k increases along the Mahler flow, from $k_0 = \max\limits_{|z|=|w|=1} (|p(z,w)|)$ to $k \to \infty$.*

In many cases, $k_{\mathrm{iso}} < k_0$. In terms of amoeba, this means that the holes would not open up at the origin. Then we can always shift the amoeba by

$$(\log|z|, \log|w|) \to (\log|z| - \log a, \log|w| - \log b) \tag{3.2.7}$$

for some positive numbers a and b such that a node is moved to the origin. This gives a rescaling/redefinition of the variables in $P(z,w)$ [11]:

$$k_{\mathrm{iso}} - p(z,w) \to k_{\mathrm{iso}} - p(z/a, w/b). \tag{3.2.8}$$

Since $k_{\mathrm{iso}} - p(z,w) = 0$ is Harnack, the pair (a,b) is unique by the 1-to-1 property between amoeba and spectral curve at nodes. In other words, there is a unique solution to $k_{\mathrm{iso}} - \tilde{p}(z,w) = 0$ where $\tilde{p}(z,w) \equiv p(z/a, w/b)$. As the parametrization of $k - \tilde{p}$ (for fixed $\tilde{p}$) is continuous, we can see that this unique solution is given by

$$k_{\mathrm{iso}} = \max\limits_{|z|=|w|=1} (|\tilde{p}(z,w)|) = \tilde{p}(1,1) = p(1/a, 1/b). \tag{3.2.9}$$

---

[10] Alternatively, we may also take the derivative of $m(P)$ with respect to k:

$$\frac{\mathrm{d}}{\mathrm{d}k} m(P) = \int_0^1 \int_0^1 \frac{\mathrm{d}}{\mathrm{d}k} (\log|k - p|) \, \mathrm{d}\theta \mathrm{d}\phi. \tag{3.2.5}$$

Now,

$$\frac{\mathrm{d}}{\mathrm{d}k} \log|k - p| = \frac{1}{|k-p|} \frac{\mathrm{d}}{\mathrm{d}k} ((k-p)(k-\bar{p}))^{1/2} = \frac{k - \mathrm{Re}(p)}{|k-p|^2}. \tag{3.2.6}$$

This leads to the same result as $\max(|p|) = \max(\mathrm{Re}(p)) = p(1,1)$.

[11] As this is just a shift of the amoeba, the 2-to-1 property between the spectral curve and amoeba still holds. Hence, the curve is still Harnack.

More importantly, this shows that a hole would now open up at the origin for the amoeba when k gets increased from k_{iso}, and we have $k \geq \max\limits_{|z|=|w|=1} (|\tilde{p}|)$ for any $k \geq k_{\text{iso}}$. Therefore, we can now rewrite the above lemma as

Proposition 3.2.3. *The Mahler measure (with possible rescaling of variables) strictly increases when k increases along the Mahler flow, from k_{iso} to $k \to \infty$.*

Remark 4. *Although the Mahler measure would vary under the rescaling of z, w, this is essentially a translation on the xy-plane for the Ronkin function as the amoeba is shifted. The change of Mahler measure is just indicating different points on $R(x, y)$. Therefore, the physics would not change. The partition function, which is the volume under $R(x, y)$, remains invariant under the rescaling of variables.*

More generally, we may also consider any $k > 0$ (without any rescaling of variables) and compute the integration for Mahler measure numerically. Although the spectral curve is non-Harnack and hence the correspondence between solid/liquid phases and regions of amoeba is not clear, we find that $m(P)$ always increases monotonically for all Newton polynomials $P(z, w)$ we have encountered along the Mahler flow. Thus, we are led to:

Conjecture 3.2.4. *The Mahler measure monotonically increases when k increases along the Mahler flow, from $k = 0$ to $k \to \infty$.*

From the viewpoint of crystal melting in the thermodynamic limit, it is natural to expect the increasing of Mahler measure when we increase k since more atoms are removed from the crystal. In terms of amoeba, the size of the hole is controlled by the value of k. When k increases, the hole would also become larger and larger, which is consistent with the growing gas phases. When k is (sub)tropical, the gas phase would become dominant. Moreover, k_{iso} is the critical point for the existence of the holes/gas phases. The holes would open up for $k > k_{\text{iso}}$ (even if the holes do not appear from the origin). For $k \leq k_{\text{iso}}$ (though only k_{iso} gives a Harnack curve), the amoeba is of genus zero, and its area would become larger when increasing k.

Moreover, the partition function for the crystal melting model should also become larger when increase k [12]. In terms of (3.1.26), this implies that we may extend the above conjecture to Ronkin functions.

Conjecture 3.2.5. *The Ronkin function $R(x, y)$ (for any fixed (x, y)) does not decrease when we increase k along the Mahler flow for $k > 0$. More precisely, when $k_2 > k_1$,*

$$\begin{cases} R_{k_2}(x, y) > R_{k_1}(x, y), & (x, y) \text{ in a non-linear or bounded linear region for } k_2; \\ R_{k_2}(x, y) = R_{k_1}(x, y), & (x, y) \text{ in an unbounded linear facet for } k_2. \end{cases} \tag{3.2.10}$$

Notice that for $k_2 > k_1 \geq k_{\text{iso}}$, the non-linear region is the liquid phase and a bounded (unbounded) facet is a gas (solid) phase.

Since the Ronkin function at (x, y) is essentially the Mahler measure for $P(\mathrm{e}^x z, \mathrm{e}^y w)$, $R(x, y)$ for $P(z, w)$ is exactly the Mahler measure for $\tilde{P}(z, w) = P(\mathrm{e}^x z, \mathrm{e}^y w)$ and shifted amoeba. Hence, we conclude that

Proposition 3.2.6. *Conjecture 3.2.4 and Conjecture 3.2.5 are equivalent.*

Remark 5. *Notice that the increase of Mahler measure is strict in Proposition 3.2.3 while the increase is monotonic (i.e., only non-decreasing required) in Conjecture 3.2.4. The reason for non-strict increasing is more clear in terms of Conjecture 3.2.5: the Mahler measure $m(P) = R(0, 0)$ may lie in an unbounded linear facet of the Ronkin function.*

---

[12] Again, for $k < k_{\text{iso}}$, the physical interpretation of Ronkin functions, in particular for different phases, may not be clear. Nevertheless, this would still make sense mathematically. More importantly, it is still possible that Ronkin functions for non-Harnack curves are closely related to crystal melting etc in physics, but in a more subtle way.

Example 6. *For F_0 with $P = 4 - z - z^{-1} - w - w^{-1}$, we have*

$$m(P) = \log k - 2k^{-2}{}_4F_3\left(1,1,\frac{3}{2},\frac{3}{2}; 2,2,2; 16k^{-2}\right), \quad u_0(k) = {}_2F_1\left(\frac{1}{2},\frac{1}{2};1;16k^{-2}\right) \quad (3.2.11)$$

for $k \geq 4$. One may check that they satisfy the Mahler flow equation. At $k = k_{\mathrm{iso}} = 4$, we have

$$m(P) = \frac{4\mathcal{K}}{\pi}; \quad u_0(4) \to \infty \quad (3.2.12)$$

where $\mathcal{K}$ is Catalan's constant. At $k \to k_{\mathrm{trop}} = \infty$, we have

$$m(P) \to \log k_{\mathrm{trop}} = \infty; \quad u_0(k_{\mathrm{trop}}) = 1. \quad (3.2.13)$$

We can also plot the Mahler flow and $u_0(k)$ from k_{iso} to k_{trop} as follows:

$$(3.2.14)$$
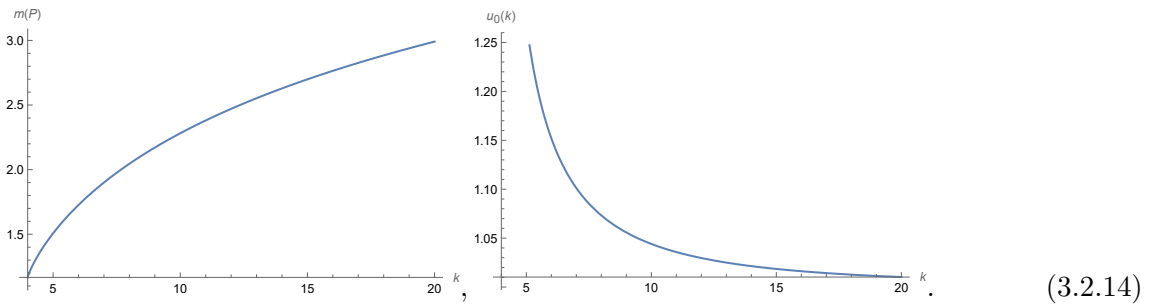
3.2.2   Tropical Geometry of the Mahler Flow

A geometric interpretation of the Mahler flow could be revealed by the holes of the amoeba. In general, it is hard to determine the area(s) of the holes A_h. However, when k is sufficiently large, we might be able to calculate A_h using the spines as a tropical limit of the amoeba.

Consider an example, say, $Y^{2,2}$ with vertices of Δ being $\{(0,0),(1,0),(0,-1),(1,-1),(-1,-1)\}$. The associated $P = -w - z^{-1}w^{-1} - zw^{-1} - 2w^{-1} + k$. For very large k, we find that the amoeba is close to its spine as in Figure 3.2.1(a). As further shown in Figure 3.2.1(b), the spine (in red)
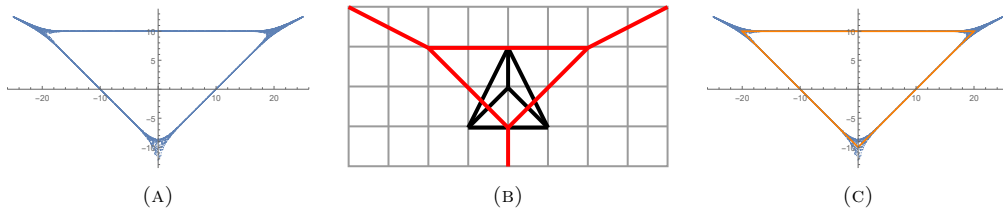
FIGURE 3.2.1: (a) The amoeba for the Newton polynomial $P(z,w) = -w - z^{-1}w^{-1} - zw^{-1} - 2w^{-1} + k$. As an example, we choose $k = \mathrm{e}^{10}$. (b) The spine (in red) is the dual of the triangulated Newton polygon Δ (in black). (c) The internal triangle in the spine is drawn explicitly in orange in the amoeba. In this example, we can see that the three vertices of the orange triangle are $(20,10)$, $(-20,10)$ and $(0,-10)$ respectively.

is the dual of the triangulation (in black) of the Newton polygon Δ. Of particular interest here is the red triangle which is the dual of the three internal lines of the triangulation of Δ as shown. This is made more clear in Figure 3.2.1(c): the interior of the orange triangle (i.e., the bounded lines of the spine) consists of the hole and certain parts of the amoeba. At large k here, the hole approaches to this triangle.

Quantitatively, we observe that the three vertices in the spine are $(2\log k, \log k)$, $(-2\log k, \log k)$ and $(0, -\log k)$. Note that this is not only true for large k but also for **any** k since this is the consequence of the spine. Around each vertex of the spine, the amoeba locally looks like an amoeba $\mathcal{A}_{\mathrm{loc}}$ whose Newton polygon is the corresponding subdivision in Δ. These local parts then

connect with each other through their thin tentacles. For instance, the upper left part in Figure 3.2.1 is locally a $\mathbb{C}^3$-amoeba. For a (global) $\mathbb{C}^3$-amoeba, its tentacles would become thinner and thinner (i.e., asymptotic to the spines) when it goes to infinity. This ensures that the area of the amoeba remains finite ($\pi^2/2$).

Now, in the $Y^{2,2}$ amoeba, the local $\mathbb{C}^3$ part becomes semi-infinite. The thin finite tentacles will become longer and thinner when k is increased. Therefore, it is natural to conjecture that the area of the local amoeba would be divided equally by the spine. One may check that the sum of areas of the local parts is equal to the area of the whole amoeba since they are all proportional to the areas of the Newton polygons and the local parts correspond to subdivisions of the whole polygon. Then the area of the hole A_h for large k may be computed as

$$A_h \simeq A(\blacktriangle) - 2 \times \frac{1}{3} A(\mathcal{A}_{\mathbb{C}^3}) - \frac{1}{3} A(\mathcal{A}_{Y^{1,1}}), \qquad (3.2.15)$$

where $\blacktriangle$ denotes the bounded polygon in the spine of Δ (e.g. the orange triangle here), and $Y^{1,1}$ corresponds to the black triangle at the bottom in the tessellation in Figure 3.2.1(b). Therefore,

$$A_h \simeq 4\log^2 k - 2 \times \frac{1}{3} \times \frac{\pi^2}{2} - \frac{1}{3} \times \pi^2 = 4\log^2 k - \frac{2}{3}\pi^2. \qquad (3.2.16)$$

If we increase the coefficient for the term w^{-1}, we find that the shape of the amoeba (especially its tentacles) would change as shown in Figure 3.2.2(a,b). As we can see, the tentacle at the bottom

(A)　　　　　　　　　　(B)　　　　　　　　　　(C)
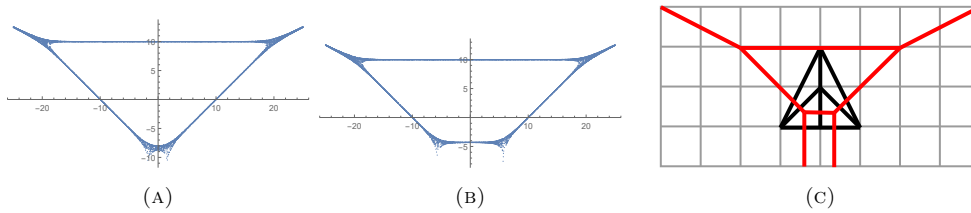
FIGURE 3.2.2: (a) The amoeba for the Newton polynomial $P(z,w) = -w - z^{-1}w^{-1} - zw^{-1} - 2ew^{-1} + e^{10}$. (b) The amoeba for the Newton polynomial $P(z,w) = -w - z^{-1}w^{-1} - zw^{-1} - 2e^5w^{-1} + e^{10}$. (c) The spine (in red) is the dual of the triangulated Newton polygon Δ (in black).

has now been divided into two. The subdivision of the Newton polygon and its dual spine have changed as in Figure 3.2.2. Now the bottom local part becomes the triangulated $Y^{1,1}$ for (a) and two $\mathbb{C}^3$ for (b).

In general, it turns out that for the canonical choice of coefficients, there is no split in the spines caused by boundary lattice points that are not at the corner. In the Ronkin function, this means that the unbounded linear facets would only appear for vertices in the Newton polygon.

We shall make the above discussion more rigorous using the definition for (sub)tropical k. The amoebae sketched in Figure 3.2.1(a) and Figure 3.2.2(a,b) all have subtropical k. However, only Figure 3.2.1(a) and Figure 3.2.2(b) have high-subtropical k. Now consider $P = -w - z^{-1}w^{-1} - zw^{-1} - 2w^{-1} + k_{\text{st}}$ in Figure 3.2.1. When $|w|$ is large enough while $|z|$ is small enough such that $\log|w| \sim \mathcal{O}(\log(k_{\text{st}}))$, $\log|z| \sim \mathcal{O}(1/\log(k_{\text{st}}))$ and $1/|zw| \sim \mathcal{O}(1)$, the Newton polynomial can be approximated by $-w - z^{-1}w^{-1} + k_{\text{st}}$. This corresponds to the local $\mathcal{A}_{\mathbb{C}^3}$ at the upper left corner in Figure 3.2.1(a).

For (high-sub)tropical k, we may try to compute A_h for any amoeba using the above method. We first need to determine the vertices of $\blacktriangle$. Let us consider $\mathbb{C}^3$ whose Harnack curve $c_1 z + c_2 w + k$ (for fixed $c_{1,2}$) as an example. Then by looking at its asymptotic behaviour, we can find its spine

as follows:

$$x \to 0: \ y = \log|w| = \log|k/c_2|;$$
$$y \to 0: \ x = \log|z| = \log|k/c_1|; \tag{3.2.17}$$
$$x, y \to \infty, z/w \sim \mathcal{O}(1): \ y = \frac{x + \log|c_1|}{\log|c_2|}.$$

Hence, the intersection point of the three lines is $(\log|k/c_1|, \log|k/c_2|)$. Now we can use the following theorem [153, 154].

Theorem 3.2.7. *For $(\alpha, M) \in (\mathbb{C}^*)^2 \rtimes \mathrm{GL}(2, \mathbb{Z})$ and $P(\boldsymbol{z}) \equiv P(z, w) \in \mathbb{C}\left[z, w, z^{-1}, w^{-1}\right]$, the map $\Psi: (\mathbb{C}^*)^2 \rtimes \mathrm{GL}(2, \mathbb{Z}) \to \mathrm{Aut}\left(\mathbb{C}\left[z, w, z^{-1}, w^{-1}\right]\right)$ defined by $\Psi(\alpha, M)(P(\boldsymbol{z})) = P\left(\alpha \cdot \boldsymbol{z}^M\right)$ is an isomorphism. Moreover, their Newton polytopes satisfy $\Delta(\Psi(P)) = M \cdot \Delta(P)$. Denote the amoeba of P as $\mathcal{A}_P$, then for $\det(M) \neq 0$, we have $\mathcal{A}_P = M\mathcal{A}_{\Psi(P)} - \mathrm{Log}(\alpha)$.*

Then for $M = (M_{ij})$ (and $\alpha = (1, 1)$), the curve becomes $P = c_1 z^{M_{11}} w^{M_{21}} + c_2 z^{M_{12}} w^{M_{22}} + k$. The vertex has coordinates

$$\frac{1}{\det M}(M_{22} \log|k/c_1| - M_{21} \log|k/c_2|, -M_{12} \log|k/c_1| + M_{11} \log|k/c_2|). \tag{3.2.18}$$

For instance, the local approximation $-w - z^{-1}w^{-1} + k$ is a $\mathrm{GL}(2, \mathbb{Z})$ transformation of $-z - w + k$ given by $\begin{pmatrix} -1 & 0 \\ -1 & 1 \end{pmatrix}$. This gives the vertex $(-2\log k, \log k)$ for $Y^{2,2}$ in Figure 3.2.1. For any local amoebas, the corresponding vertex in the spine can be obtained in this way. Once we know the coordinates of the vertices, we may compute the area of the hole.

Conjecture 3.2.8. *Given a Newton polygon with Newton polynomial $P(z, w) = k - p(z, w)$ and k high-subtropical, the area of a hole (labelled by i) in the amoeba reads*

$$A_{h,i} \simeq A(\blacktriangle_i) - \sum_{v_j \in \mathcal{V}_i} \frac{1}{n_j} A(\mathcal{A}_{\mathrm{loc},j}) = A(\blacktriangle_i) - \sum_{v_j \in \mathcal{V}_i} \frac{\pi^2}{n_j} A(\Delta_j), \tag{3.2.19}$$

where $\blacktriangle_i$ denotes the corresponding separated polygon in the spine and $A(\blacktriangle_i) \propto \log^2(k)$. Moreover, $\mathcal{V}_i$ is the set of spine vertices surrounding the hole i. The local amoeba $\mathcal{A}_{\mathrm{loc},j}$ around the vertex v_j of the spine corresponds to the n_j-gon Δ_j in the tessellation of Δ.

The total area A_h of the holes is then

$$A_h \simeq A(\blacktriangle) - \sum_{v_j \in \mathcal{V}} \frac{m_j}{n_j} A(\mathcal{A}_{\mathrm{loc},j}) = \sum_i A(\blacktriangle_i) - \sum_{v_j \in \mathcal{V}} \frac{m_j \pi^2}{n_j} A(\Delta_j), \tag{3.2.20}$$

where m_j is the number of $\blacktriangle_i$'s that have v_j as a vertex, and $\mathcal{V}$ is the set of all vertices of the spine.

Example 7. *For polygons with a single interior lattice point, we have $m_j = 1$, and there is a single $\blacktriangle$.*

Remark 6. *It is often more useful to consider the simplification as follows. For Newton polynomials of form $P(z, w) = k - p(z, w)$ considered in this paper, the (high-sub)tropical k is also the large k limit. We always have the dominating contribution $A_h \sim \log^2(k)$. We may also recast the Mahler flow equation in terms of the area of the hole $\frac{dm(P)}{dA_h}$. Then at large k, $\frac{dm(P)}{dA_h} \sim \frac{1}{2\log k} > 0$.*

Integral approximations As a byproduct, this helps us understand certain integrals in the large k limit. For instance, for F_0, by solving $e^y + e^{-y} - e^x - e^{-x} - 1 = 0$, we get part of the boundary of $\mathcal{A}_{F_0}$ (i.e., one solution to the equation) which reads[13]

$$y = \log\left(\frac{1}{2}e^{-x}\left(1 + e^{2x} + ke^x + \sqrt{-4e^{2x} + (-1 - e^{2x} - ke^x)^2}\right)\right). \tag{3.2.21}$$

---

[13]Recently, the analytic boundaries for more amoebae were found in [155].

As we can see, this is the upper right boundary of the amoeba:
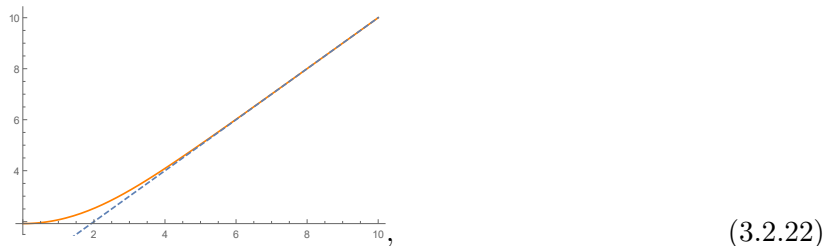
$$(3.2.22)$$

where we have used $k = 5$ to illustrate this and the dashed line indicates the spine. Therefore, the area of the hole is

$$A_h = 8 \left(\int_0^\infty y\mathrm{d}x - \int_0^\infty x\mathrm{d}x \right) - A(\mathcal{A}_{F_0}) = 8 \int_0^\infty (y - x)\mathrm{d}x - 2\pi^2. \qquad (3.2.23)$$

In general, it is not straightforward to determine the large k behaviour for such kind of integral with integrand

$$I \equiv y - x = \log \left(\frac{1 + \mathrm{e}^{2x} + k\mathrm{e}^x + \sqrt{-4\mathrm{e}^{2x} + (-1 - \mathrm{e}^{2x} - k\mathrm{e}^x)^2}}{2\mathrm{e}^{2x}} \right) \qquad (3.2.24)$$

because x is also integrated to ∞. Nevertheless, from the above analysis, we learn that $A_h \sim \log^2(k)$ for large k. Therefore,

$$\int_0^\infty I \, \mathrm{d}x \sim \log^2(k) \qquad (3.2.25)$$

in the large k limit.

Higher dimensions It would also be natural to conjecture that similar patterns would happen for any dimension n.

Conjecture 3.2.9. *Let $P(\boldsymbol{z}) = k - p(\boldsymbol{z})$ be a Laurent polynomial of $\boldsymbol{z} \in \mathbb{C}^n$. In the large k limit, we have $V_{\mathrm{bdd}} \sim \log^n k$, where V_{bdd} is the volume of a bounded complementary region of the amoeba $\mathcal{A}(P)$.*

3.2.3 The Kähler Parameter

So far, the variable k has not been endowed with any further physical interpretations, except being the scale of the Mahler flow and controlling the size of the hole in the amoeba. In this subsection, we shall discuss the physical interpretations of the parameter k in quiver theories.

It is well-known that the variables in the coefficients of $P(z, w)$ are related to Kähler moduli of the toric CY singularity [156, 157]. In quiver quantum mechanics, these Kähler moduli are FI parameters. Since every FI parameter is associated with a gauge node in the quiver, or equivalently, a face in the dimer, they should be related to edge weights/energies and magnetic fluxes on the dimer model as pointed out in [44].

Hence, it would be natural to relate k to the Kähler/FI parameters. However, there are more than one FI parameter in general while we only have one variable k in our Newton polynomial. In fact, the discrepancy between the numbers of parameters are compensated by D-term relations. Let G be the number of nodes. Recall from Chapter 2 that the D-term charge matrix Q_D with $(G - 1)$ rows encodes the GLSM charges under D-term relations. As the coefficients in the Newton polynomial are obtained from perfect matchings/GLSM fields in the dimer model, there is only one free parameter left with the constraints from Q_D. Varying k along the Mahler flow can therefore be interpreted as varying this free parameter. In general, all the coefficients should be functions of these FI parameters while we consider a simplification where we only have one variable k as constant term in this paper.

General coefficients Let us also make a brief comment on more general choices of coefficients in $P(z, w)$. Since these coefficients are determined by the FI parameters, they would be related to wall crossings in the moduli space of the quiver quantum mechanics. Following the 4d/1d correspondence [158], wall crossing corresponds to Seiberg duality in the 4d $\mathcal{N} = 1$ gauge theories. As the Ronkin function is closely related to the 4d superconformal index and topological string partition function (see §3.2.7 and also [158]) which are invariant under Seiberg duality and wall crossing respectively, we expect that the Mahler measure and Ronkin function would enjoy certain property under Seiberg duality/wall crossing. We will discuss this explicitly for the isoradial limit shortly.

Intercepts of Ronkin functions Different coefficients in the Newton polynomial would also lead to different intercepts of the linear facets in the Ronkin function. When a solid phase corresponds to a vertex/corner point (m, n) in the Newton polygon, the facet would have slope (m, n) in the Ronkin function. Besides, the Newton polynomial would contain a term $c_{(m,n)} z^m w^n$. According to [144],

Theorem 3.2.10. *The intercept of this facet is* $\log |c_{(m,n)}|$.

As a result, if the coefficients of these linear facets do not equal, their extension would not meet at the origin in the plot of Ronkin function[14]. In crystal melting, this means that the unmolten crystal would not have a point as the tip. Instead, the top of the crystal would be some ridge or face. In [43], the one-to-one correspondence between crystal melting and dimer model was proven for the crystal with a single atom at the tip. Nevertheless, different coefficients for crystal melting has also been considered in various literature, and it would be natural to expect that this one-to-one correspondence could be extended to such situation for crystal melting[15]. In light of [139], this would imply a non-trivial magnetic field.

When Newton polynomials cannot be rescaled to have coefficients 1 for corner points, there are actually two different types.

Example 8. *The Newton polynomial for* $L^{1,3,1}/\mathbb{Z}_2$ $(0, 1, 1, 1)$ *reads*

$$P = -\frac{AB}{C}(zw + w) - \frac{C}{AB}(zw^{-1} + z^{-2}w^{-1} + 3w^{-1} + 3z^{-1}w^{-1}) - (2z + 2z^{-1}) + k, \quad (3.2.26)$$

where

$$A = \sin\left(\frac{5 - \sqrt{7}}{12}\pi\right), B = \sin^2\left(\frac{5 - \sqrt{7}}{6}\pi\right), C = \sin^3\left(\frac{1 + \sqrt{7}}{12}\pi\right). \quad (3.2.27)$$

Although it does not have same coefficients for the corner points, we can absorb the extra factor by $\frac{AB}{C}w \to w$ *so that the four coefficients would all become* 1. *As we can see, this is a rescaling of* z, w.

However, there is another type whose coefficients cannot be made the same even with such rescaling. For instance, the Newton polynomial for PdP_{4a} *reads*

$$P = -B_1^2 B_2^2(z + z^{-1}) - B_2^2 B_3 B_4(zw^{-1} + w^{-1}) - B_5^4 z^{-1}w^2 - 2B_1 B_2 B_5^2(z^{-1}w + w) + k, \quad (3.2.28)$$

where $B_i = \sin(\pi b_i / 2)$ *and*

$$b_1 \approx 0.427 \text{ is a root of } 3x^3 - 340x^2 - 24x + 72 = 0;$$
$$b_2 \approx 0.725 \text{ is a root of } 3x^3 - 134x^2 + 228x - 96 = 0;$$
$$b_3 \approx 0.298 \text{ is a root of } 3x^3 + 206x^2 - 384x + 96 = 0; \quad (3.2.29)$$
$$b_4 \approx 0.596 \text{ is a root of } 3x^3 + 412x^2 - 1536x + 768 = 0;$$
$$b_5 \approx 0.550 \text{ is a root of } 3x^3 + 250x^2 - 124x - 8 = 0.$$

---

[14]If these (extensions of) facets meet at the same point but not the origin, we can always rescale the whole Newton polynomial to make $c_{(m,n)} = 1$ and hence shift it to $(0, 0, 0)$.

[15]We should emphasize that the analysis of quiver gauge theories should not be affected since they can be directly read off from the dimers with different edge weights.

It turns out that no matter how we rescale the variables, the five vertices z, z^{-1}, zw^{-1}, w^{-1} and $z^{-1}w^2$ would not have same coefficients.

3.2.4 Isoradial Limit

Now, let us focus on one of the special points, that is, k_{iso}, in the Mahler flow. When the embedding is isoradial with $2\sin(\theta_I)$ as (canonical) edge weights, we shall call $m(P)$ and $R(x, y)$ the isoradial Mahler measure and Ronkin function respectively. For a different choice of coefficients in the Newton polynomial, it is still possible to have an isoradial point $k = k_{iso}$. Now we will show that there is a set of θ_I^* that maximizes the isoradial Mahler measure and this coincides with the R-charges in a-maximization. More importantly, after our discussion on Seiberg duality below, we will find that the followings in this subsection can be applied to any toric quivers and brane tilings regardless of isoradiality.

Isoradial Mahler measure It is useful to introduce a simple and remarkable formula for isoradial Mahler measure obtained in [159]:

$$m(P) = \sum_I \left(\frac{\theta_I}{\pi} \log(2\sin(\theta_I)) + \frac{1}{\pi}\Lambda(\theta_I) \right), \tag{3.2.30}$$

where

$$\begin{aligned} \Lambda(x) &= -\int_0^x \log(2\sin(t))\mathrm{d}t \\ &= \frac{i}{12}\pi^2 - \frac{i}{2}x^2 + x\log(1 - \mathrm{e}^{2ix}) - x\log(\sin(x)) - \frac{i}{2}\mathrm{Li}_2(\mathrm{e}^{2ix}) \end{aligned} \tag{3.2.31}$$

is the *Lobachevsky function*. In terms of the energy functions, we may also write (3.2.30) as

$$m(P) = -\frac{1}{\pi}\sum_{I=1}^m \left(\theta_I \mathcal{E}(e_I) + \int_0^{\theta_I} \log(2\sin(t))\mathrm{d}t \right). \tag{3.2.32}$$

It is important to notice that

$$\frac{\partial m(P)}{\partial \theta_I} = \frac{\theta_I}{\pi}\cot(\theta_I). \tag{3.2.33}$$

Example 9. *Consider our running example of $m(4 - z - z^{-1} - w - w^{-1})$ for F_0. Since $\theta_I = \pi/4$ for all I, we get*

$$\begin{aligned} m(P) &= \frac{1}{(2\pi i)^2}\int_0^1\int_0^1 \left(\log(8 - 2z - 2z^{-1} - 2w - 2w^{-1}) - \log(2) \right) \frac{\mathrm{d}z}{z}\frac{\mathrm{d}w}{w} \\ &= m(8 - 2z - 2z^{-1} - 2w - 2w^{-1}) - \frac{\log(2)}{(2\pi i)^2}\int_0^1\int_0^1 \frac{\mathrm{d}z}{z}\frac{\mathrm{d}w}{w} \\ &= 8\left(\frac{\pi}{4\pi}\log(2\sin(\pi/4)) + \frac{1}{\pi}\Lambda(\pi/4) \right) - \log(2) \\ &= \frac{4\mathcal{K}}{\pi}. \end{aligned} \tag{3.2.34}$$

This agrees with our result in (3.2.12).

Maximization of isoradial Mahler measure When finding R-charges under RG trajectory in 4d, we need to maximize the a-function,

$$a = \sum_I (R_I - 1)^3 = \sum_I \left(\frac{2\theta_I}{\pi} - 1 \right)^3, \tag{3.2.35}$$

where we have normalized the coefficient and omitted the part from number of quiver nodes (which corresponds to faces in the dimer). On the other hand, the isoradial Mahler measure is also explicitly given in terms of θ_I by (3.2.30). As θ_I is a rhombus angle in the dimer model, we have $\theta_I \in [0, \pi/2]$. The shapes of the two functions are sketched in Figure 3.2.3, heuristically drawn against 1 and 2 of the θ_I angles. The derivatives for the two functions are respectively
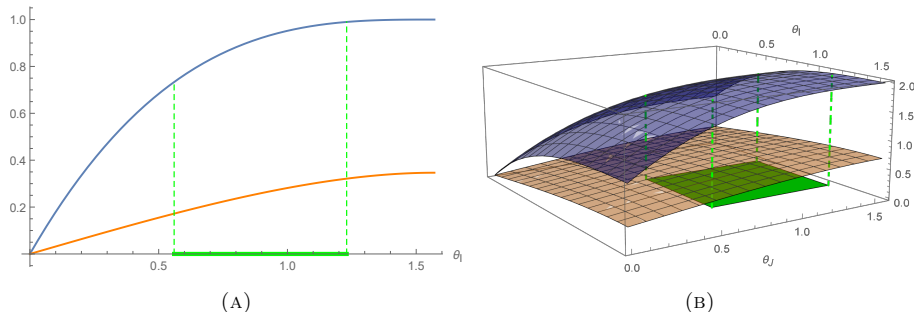
FIGURE 3.2.3: The a-function (blue) and isoradial Mahler measure (orange) plotted as functions of θ_I. We can only visualize the (a) 1d and (b) 2d versions while physically there should be at least 3 θ_I's (R_I's) in our theory. Notice that we have shifted the a-function by (a) +1 and (b) +2 for better visualization and comparison. The green region is the conformal manifold on the θ_I axis/θ_I-θ_J plane.

$$\frac{\partial a}{\partial \theta_I} = \frac{6}{\pi}\left(\frac{2\theta_I}{\pi} - 1\right)^2 > 0 \ , \qquad \frac{\partial m_{\text{iso}}}{\partial \theta_I} = \frac{\theta_I}{\pi}\cot(\theta_I) > 0 \ ; \qquad \theta_I \in [0, \pi/2] \ . \tag{3.2.36}$$

Hence, both of the functions are strictly increasing for any R-charges. For a-maximization, the rhombus angles are also subject to the conditions $\sum 2\theta_I = 2\pi$ and $\sum(\pi - 2\theta_I) = 2\pi$. The region of rhombus angles/R-charges that satisfy these conditions is the so-called conformal manifold $\mathcal{M}$. Pictorially, we sketch the conformal manifold in green in the θ_I-space in Figure 3.2.3, and the dashed lines cut out the possible values for a and m_{iso}. In other words, we need to find the maximum of a for the set of points $\{(\theta_1, \ldots, \theta_n) \in \mathcal{M}\}$. Suppose that a is maximized at $(\theta_1^*, \ldots, \theta_n^*)$, then the isoradial Mahler measure would also reach its maximum at $(\theta_1^*, \ldots, \theta_n^*)$ on the conformal manifold as a and m_{iso} are both monotonically increasing. Therefore, we have shown that

Theorem 3.2.11. *For toric quiver gauge theories, we have*

$$m_{\text{iso}}\text{-}maximization = a\text{-}maximization. \tag{3.2.37}$$

Remark 7. *Following this proposition, we may also conclude that m_{iso}-maximization is equivalent to volume minimization [115] and K-semistability (for product test configurations) [160]. We will not expound upon this here, and readers are referred to [4, 89, 160, 161] for more details (see also Chapter 6).*

Remark 8. *Since the weights for the dimer edges are always non-negative for any trial R-charges, the spectral curve is always Harnack. Hence, with different trial R-charges, the amoeba is deformed but its area is invariant. Furthermore, it would always be genus 0.*

We emphasize that this theorem is still valid for non-isoradial dimers. Though for the latter we do not have a well-defined rhombus angle, but we can write the edge weights as $2\sin(\pi R_I/2)$. In other words, we replace θ_I by $\pi R_I/2$ in (3.2.30). Then (3.2.30), which we shall still call m_{iso} for convenience, again reaches its maximum at R_I^*, where R_I^* maximizes the a-function. Therefore, it is always true that m_{iso}-maximization is equivalent to a-maximization[16].

---

[16]Strictly speaking, so far we can only say that maximizing (3.2.30) (rather than m_{iso}) is equivalent to a-maximization as we have not shown that (3.2.30) gives the correct Mahler measures for non-isoradial embeddings with canonical weight choices. We will come back to this point shortly.

Example 10. *Let us vary the shape of the isoradial dimer for F_0 in the following way:*
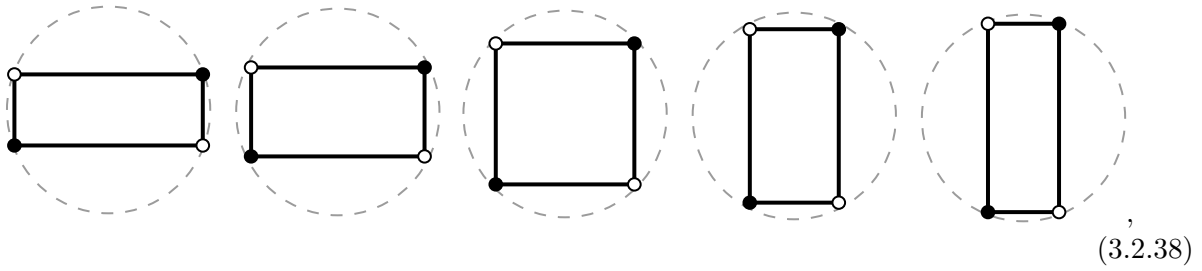
$$\tag{3.2.38}$$

where we are restricting to rectangles as an illustration. Suppose the two distinct edges have weights $2\nu_1^{1/2}$ and $2\nu_2^{1/2}$, then we have $\nu_I = \sin^2(\theta_I)$ and $\nu_1 + \nu_2 = 1$. The Mahler measure reads

$$m_{\mathrm{iso}} = \int_0^{2\pi} \int_0^{2\pi} \log|2\nu_1 + 2\nu_2 - \nu_1 e^{is} - \nu_1 e^{-is} - \nu_2 e^{it} - \nu_2 e^{-it}| \mathrm{d}s \mathrm{d}t. \tag{3.2.39}$$

The isoradial Mahler measure as a function of ν_1 and its derivative are plotted in Figure 3.2.4. We
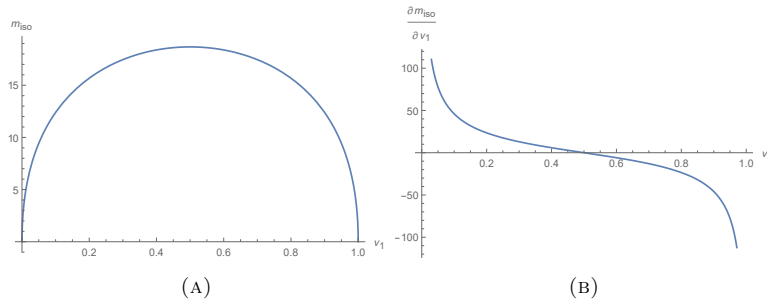
FIGURE 3.2.4: The plot of (a) m_{iso} and (b) $\partial m_{\mathrm{iso}}/\partial\nu_1$. Here $\nu_2 = 1 - \nu_1$.

can see that the maximum is reached at $\nu_1 = 1/2$. Indeed, (3.2.30) yields

$$m_{\mathrm{iso}} = 4\left(\frac{\theta_1}{\pi}\log(2\sin(\theta_1)) + \frac{1}{\pi}\Lambda(\theta_1)\right) + 4\left(\frac{\theta_2}{\pi}\log(2\sin(\theta_2)) + \frac{1}{\pi}\Lambda(\theta_2)\right) \tag{3.2.40}$$

with $\theta_2 = \pi/2 - \theta_1$. Its derivatives read

$$\begin{aligned}
\frac{\partial m_{\mathrm{iso}}}{\partial\theta_1} &= \frac{4\theta_1}{\pi}\cot(\theta_1) + \frac{4\theta_1 - 2\pi}{\pi}\tan(\theta_1), \\
\frac{\partial^2 m_{\mathrm{iso}}}{\partial\theta_1^2} &= \frac{4\cot(\theta_1) - 4\theta_1\csc^2(\theta_1) + 2\sec^2(\theta)(2\theta_1 + 2\sin(\theta_1) - \pi)}{\pi}.
\end{aligned} \tag{3.2.41}$$

One can find that the first derivative vanishes when $\theta_1 = \pi/4$ (and the second derivative equals $8/\pi - 4 < 0$). Therefore, the Mahler measure is maximized at $\theta_1 = \theta_2 = \pi/4$ (or equivalently, $\nu_1 = \nu_2 = 1/2$). This agrees with the result from a-maximization. In general, if the faces in the dimer are not rectangles but general isoradial quadrilaterals, the Mahler measure should still be maximized at $\theta_{1,\dots,8} = \pi/4$, that is, $R_{1,\dots,8} = 1/2$.

Seiberg Duality   Theories engineered by D-branes on toric Gorenstein singularities enjoy certain dualities including Seiberg duality and specular duality. In this subsection, we show that the Mahler measure also exhibits certain properties under these dualities. Let us start with Seiberg duality [93, 106, 107]. In terms of quivers, this is essentially mutations (plus non-trivial superpotentials). For brane tilings, this gives rise to so-called urban renewal [21]. Seiberg duals correspond to the same toric diagram as moduli space. However, there is no reason why the Newton polynomials for the duals would remain the same since the coefficients are obtained from different brane tilings whose perfect matchings can change. Nevertheless, we will see that at the isoradial point, the polynomials are the same.

Assume that the dimer is embedded isoradially on the torus, then we can use our canonical choice of edge weights to write down the Newton polynomial. It turns out that for all the duals we checked, although the total numbers of multiplets/rhombus angles change, the coefficient for every single monomial, viz, $\sum e^{-\mathcal{E}(M)} = \sum \left(\prod_I 2 \log(\sin(2\theta_I)) \right)$, is invariant up to a factor of $2^{n_2 - n_1}$ for some integers n_i. In fact, n_1 and n_2 are nothing but the numbers of edges/multiplets in each perfect matching/GLSM field for the two tilings respectively. Therefore, we can simply cancel the factor 2^{n_1} or 2^{n_2} from every monomial in the two Newton polynomials.

Note that there is a subtlety in the above discussion. In general, a dimer (which is a dual of an isoradial one) does not admit an isoradial embedding. Nevertheless, let us still use $2 \sin(\pi R_I / 2)$ as the edge weights[17]. It turns out that the resulting Newton polynomial is again the same as its Seiberg dual(s). To ensure that this is the desired $P(z, w)$ even though the embedding is non-isoradial, one may check that in such case the Mahler measure is equal to the value computed from (3.2.30) using $\theta_I = \pi R_I / 2$ for the physical R-charges R_I. In fact, this is because the non-isoradial dimer has been continuously deformed so that some of the edges shrink to zero (or even negative lengths). After such deformation, the non-isoradial dimer degenerates to an isoradial dimer with some of the rhombus angles being $\pi/2$ (or even obtuse). Therefore, the formula (3.2.30) for isoradial Mahler measures would still work in this situation.

Conjecture 3.2.12. *Seiberg duals have exactly the same Newton polynomials. Hence, Mahler measure is trivially invariant under Seiberg duality.*

Equivalently, we may keep the two factors 2^{n_1} and 2^{n_2} such that the Newton polynomials are related by $P_2(z, w) = 2^{n_2 - n_1} P_1(z, w)$, where n_i is the number of edges/multiplets in each perfect matching/GLSM field. Then we can say that the Mahler measure is invariant under Seiberg duality up to $\log(2^{n_2 - n_1})$, that is, $m_2 = m_1 + \log(2^{n_2 - n_1})$.

Remark 9. *Since the Newton polynomial $P(z, w) = k_{\text{iso}} - p(z, w)$ is invariant, if we leave the isoradial point and increase k, the resulting $P = k - p$ and its Mahler measure would also be the same for Seiberg duals.*

Example 11. *Let us consider $L^{1,3,1}/\mathbb{Z}_2 \, (0, 1, 1, 1)$ as an example. It has two toric phases whose brane tilings are*

$$, \qquad . \tag{3.2.42}$$
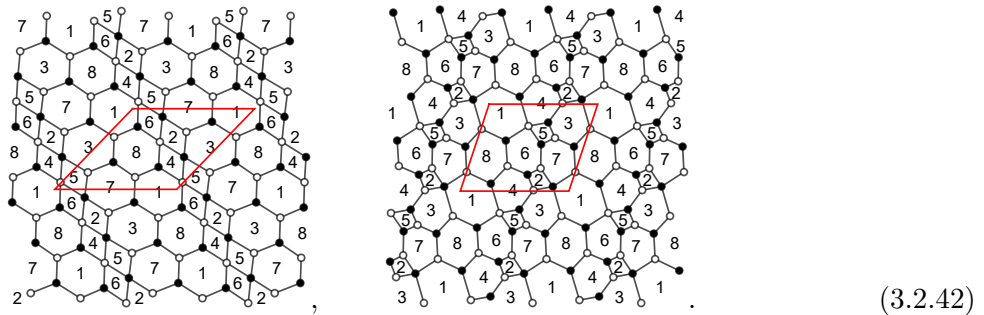
Using the data including perfect matrices in [105], we find that both of them yield (after cancelling a common factor of 2^n for each case respectively)

$$ P = -\frac{AB}{C}(zw + w) - \frac{C}{AB}(zw^{-1} + z^{-2}w^{-1} + 3w^{-1} + 3z^{-1}w^{-1}) - (2z + 2z^{-1}) + 12, \tag{3.2.43}$$

where A, B, C are given in (3.2.27). The dual theories have 20 and 22 bifundamentals respectively, but the corresponding edges weighted by their R-charges lead to the same Newton polynomial. In particular, the second dimer does not admit an isoradial embedding. However, we find that two of the R-charges in this case become 1. This is equivalent to two of the edges shrinking to zero in the dimer. One edge e_{34} is between face 3 and 4 while the other e_{67} is between face 6 and 7. After such

---

[17]We can only write the weights in terms of the R-charges as the concept of rhombus angle is not really well-defined for non-isoradial embeddings.

deformation, the dimer degenerates to an isoradial embedding with two rhombus angles being $\pi/2$. One may also check that (3.2.30) in this case agrees with the result from the first dimer and gives the correct Mahler measure.

It is worth noting that when the two edges shrink in the second brane tiling, it does not degenerate to the first tiling but instead some dimer that is "partially urban renewed". More precisely, from the second tiling to the first one under Seiberg duality, $e_{34,67,64}$ would vanish while a new edge e_{73} would be created. In the "partially renewed" dimer, only the removal of e_{34} and e_{67} has been done. In terms of the quivers, Seiberg duality flips node 2 in the quiver. The "partially renewed" dimer has bifundamentals X_{34} and X_{67} removed in the quiver while X_{64} has not yet been removed and X_{73} has not not been added. Therefore, this partially mutated quiver theory is anomalous[18].

In fact, one may also check that some of the matter fields have $R_I > 1$ in some toric phases. In such cases, we find that the above discussion still holds. We may therefore say that the weights are assigned to be $2\sin(\theta_I)$ with $\theta = \pi R_I/2 > \pi/2$. Eqvuialently, we can also regard the edges as of "negative" lengths, that is, $2\cos(\pi R_I/2) < 0$.

Example 12. *Let us consider* PdP_{4a} *as an example. It has three toric phases whose brane tilings are*

$$\tag{3.2.44}$$
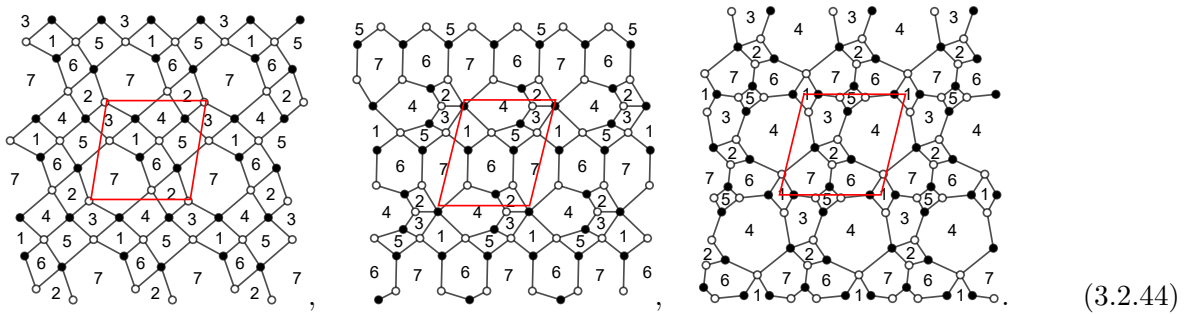
Using the data including perfect matrices in [105], we find that all of them yield (after cancelling a common factor of 2^n for each case respectively)

$$
\begin{aligned}
P = &- B_1^2 B_2^2 (z + z^{-1}) - B_2^2 B_3 B_4 (zw^{-1} + w^{-1}) - B_5^4 z^{-1} w^2 - 2B_1 B_2 B_5^2 (z^{-1} w + w) \\
&+ 2B_1^2 B_2^2 + 4B_1 B_2 B_3 B_5 + 2B_2^2 B_4 B_5 + B_3^2 B_5^2,
\end{aligned}
\tag{3.2.45}
$$

where $B_i = \sin(\pi b_i/2)$ are given in (3.2.45). The dual theories have 15, 17 and 19 bifundamentals respectively, but the corresponding edges weighted by their R-charges lead to the same Newton polynomial.

In particular, for the second tiling, X_{67} has R-charge $R_{67} = \mathfrak{R}$, where

$$\mathfrak{R} \approx 1.023 \text{ is a root of } x^3 + 24x^2 - 96x + 72 = 0. \tag{3.2.46}$$

Therefore, the edge e_{67} (not to be confused with e_{76}) has "negative" length in the dimer. When performing Seiberg duality between the second tiling to the first one. Node 2 in the quiver is flipped. Therefore, the white node where face 2, 6, 7 meet in the second dimer would become black. Then the edge e_{67} would have its white and black nodes reversed, and hence of negative length. Notice that e_{67} vanishes in the first dimer. This is because the "isoradial" embedding for the second dimer with negative e_{67} degenerates to one being "partially urban renewed".

Likewise, in the third tiling, the fields X_{37} and X_{67} would both have R-charge $\mathfrak{R} > 1$. Again, compared to the first dimer, the two edges e_{37} and e_{67} would have their white and black nodes reversed, and hence of negative lengths.

---

[18]We should emphasize that when we say the tiling *degenerates*, it only "looks like" the "partially renewed" dimer but does *not* "become" that dimer. The tiling still gives an anomaly-free physical quiver theory. Only the two edges $e_{34,67}$ have length 0 (viz, weight 2) due to the R-charges for $X_{34,67}$ being 1.

From the above discussion, we have actually found a canonical choice for edge weights regardless of isoradiality.

Remark 10. *For any brane tiling, the canonical choice (in the sense of m_{iso}-/a-maximization and Seiberg duality) for the weight of edge e_I is $2\sin(\pi R_I/2)$. The Mahler measure for the corresponding Newton polynomial can be computed using* (3.2.30).

For isoradial embedding, this edge weight is just the critical choice (in the sense of [141]) $2\sin(\theta_I)$. For non-isoradial embedding, we have two equivalent viewpoints:

- *The dimer still has the original shape with positive edge lengths, and hence non-isoradial. We are just assigning the so-called canonical weights to the edges.*

- *As before, we may also say that the dimer degenerates and becomes isoradial. However, as we have emphasized, it is* different *from the dimer that leads to anomalous theory. Some of the edges are* not *removed, and they just have zero or negative lengths.*

The first point of view emphasizes the universal weight choice for all (both isoradial and non-isoradial) embeddings. On the other hand, the second one explains why we can always apply (3.2.30) in the calculations of Mahler measures for any toric quiver theories.

In fact, when computing Mahler measures using (3.2.30) for Seiberg duals, they would imply some non-trivial mathematical identities. For instance,

Remark 11. *In the example for* PdP_{4a} *above, we have*

$$\alpha\log(2\sin(\alpha)) + \Lambda(\alpha) + \beta\log(2\sin(\beta)) + \Lambda(\beta) = \pi\log(2), \tag{3.2.47}$$

where

$$\frac{2\alpha}{\pi} = 10 - \frac{24(1-i\sqrt{3})}{\left(\frac{1}{2}(233+i\sqrt{1007})\right)^{1/3}} - (1+i\sqrt{3})\left(\frac{1}{2}(233+i\sqrt{1007})\right)^{1/3} \approx 0.977473,$$

$$\frac{2\beta}{\pi} = -8 - \frac{24(1-i\sqrt{3})}{\left(\frac{1}{2}(-233+i\sqrt{1007})\right)^{1/3}} - (1+i\sqrt{3})\left(\frac{1}{2}(-233+i\sqrt{1007})\right)^{1/3} \approx 1.02253. \tag{3.2.48}$$

When there are some R-charges equal to 1 (such as the above example for $L^{1,3,1}/\mathbb{Z}_2$), we always have the same identity

$$\Lambda(\pi/2) \equiv -\int_0^{\pi/2} \log(2\sin(t))\mathrm{d}t = 0. \tag{3.2.49}$$

This is expected due to the periodicity of $\sin(t)$.

To end this subsection, let us make a comment on the Ronkin functions. Although there is no simple formula like (3.2.30) for Mahler measures,

Conjecture 3.2.13. *The Ronkin function is invariant under Seiberg duality since the Newton polynomial (with the canonical weight choice) does not change (regardless of the isoradiality of the dimer).*

Remark 12. *We mainly focused on $k = k_{iso}$ in this subsection. However, we may also leave the isoradial point and consider general $P(z,w) = k - p(z,w)$. Since Seiberg duals have the same starting isoradial point, the Newton polynomials, Mahler measures and Ronkin functions would also be the same for these dual theories along the Mahler flow.*

3.2.5 The Master Space

So far, we have engaged in many discussions on Mahler measures at $k = k_{\text{iso}}$. Let us now leave the isoradial point and treat k as a general variable. As we are now going to see, this would encode certain information of the master space.

Recall that for $k > \max\limits_{|z|=|w|=1} (|p(z,w)|) = p(1,1)$, we have the expansions

$$m(P) = \log k - \sum_{n=2}^{\infty} \frac{f_n}{nk^n}; \quad u_0(k) = 1 + \sum_{n=2}^{\infty} \frac{f_n}{k^n}, \tag{3.2.50}$$

for some expansion coefficients f_n. Since the coefficients of $p(z,w)$ come from the perfect matchings/GLSM fields, we shall write it as

$$p(z,w) = \sum_i r_i z^{m_i} w^{n_i}, \tag{3.2.51}$$

where each r_i denotes a perfect matching that does not correspond to a constant term in $P(z,w)$. Likewise, we shall denote the perfect matchings giving a constant term in P as s_i. Henceforth, we will refer to them as r-matchings and s-matchings respectively. Note that here we are keeping the coefficients general (rather than just the canonical choices). Following the multinomial theorem, we have [50]

$$f_n = \sum_{\substack{\boldsymbol{l}=(l_1,\ldots,l_N)\in\mathbb{Z}_{\geq 0}^N \\ l_1+\cdots+l_N=n \\ M\boldsymbol{l}=0}} \frac{n!}{l_1!\ldots l_N!} r_1^{l_1}\ldots r_N^{l_N}, \tag{3.2.52}$$

where N is the number of r-matchings and

$$M = \begin{pmatrix} m_1 & m_2 & \ldots & m_N \\ n_1 & n_2 & \ldots & n_N \end{pmatrix} \tag{3.2.53}$$

is the $2 \times N$ matrix of the corresponding lattice points. Notice that there could be duplicated columns in M since some lattice points can correspond to multiple (r-)matchings. We have that

Theorem 3.2.14. *The period $u_0(k)$ is a generating function of the master space in terms of F-term charge matrix.*

A proof of this can be found in [9, §3.5].

Remark 13. *Since we are working with general coefficients for $P(z,w)$, the canonical choice would certainly satisfy this proposition. We can simply replace r_i with $\prod\limits_I 2\sin(\pi R_I/2)$ for every perfect matching.*

Remark 14. *Since we always have $D4$-branes as flavour branes in the system when the Taylor expansion is valid, the superpotential would change from W_0 to $(W_0 + W_{\text{flav}})$. Nevertheless, the F-term relations would still be $\partial W_0/\partial X_I = 0$ as shown in [152]. Alternatively, Q_F is only determined by perfect matchings on the dimer which remain unchanged regardless the existence of $D4$-branes. Therefore, the above theorem should always hold[19].*

It is best to illustrate the foregoing discussions with an example.

Example 13. *Consider $Y^{2,2}$ whose Newton polynomial is $P = k - (r_1 w + r_2 w^{-1} + r_3 z^2 + r_4 z^{-1} + r_5 z^{-1})$. Then*

$$u_0(k) = 1 + \frac{2r_3 r_4 + 2r_3 r_5}{k^2} + \frac{12r_1 r_2 r_3^2 + 12r_3^2 r_4 r_5 + 6r_3^2 r_4^2 + 6r_3^2 r_5^2}{k^4} + \ldots \tag{3.2.54}$$

The F-term charge matrix is

$$Q_F = \begin{pmatrix} r_1 & r_2 & r_3 & r_4 & r_5 & s_1 & s_2 & s_3 & s_4 \\ 0 & 0 & -1 & -1 & 0 & 1 & 1 & 0 & 0 \\ 0 & 0 & -1 & 0 & -1 & 0 & 0 & 1 & 1 \\ 1 & 1 & 0 & -1 & -1 & 0 & 0 & 0 & 0 \end{pmatrix}. \tag{3.2.55}$$

---

[19]Incidentally, the moduli space of D4-D2-D0 states is just a subspace of the moduli space of D6-D2-D0 states [152].

At order two, the coefficients give the first two rows in Q_F: $r_3 + r_4 = s_1 + s_2$ and $r_3 + r_5 = s_3 + s_4$. The factors 2 are just equivalent ways of writing the relations, e.g. $r_3 + r_4$ and $r_4 + r_3$. At order four, $r_1 r_2 r_3^2$ decodes the third row in Q_F since

$$r_1 + r_2 = r_4 + r_5 = s_1 + s_2 - r_3 + s_3 + s_4 - r_3. \tag{3.2.56}$$

Again, the factor 12 is just the number of ways to arrange r_1, r_2 and two r_3's. The second term $12 r_3^2 r_4 r_5$ reveals the same relation but with $r_4 + r_5 + 2r_3 = s_1 + s_2 + s_3 + s_4$ instead. The remaining two terms are (redundant) relations of lower-order relations: $2(r_3 + r_4) = 2(s_1 + s_2)$ and $2(r_3 + r_5) = 2(s_3 + s_4)$.

Specular Duality For toric quiver gauge theories, a duality known as specular duality was proposed in [105, 162]. In general, specular duality does not preserve the mesonic moduli spaces (except for self-dual cases) although Hilbert series for duals are the same up to some fugacity map. Instead,

Definition 3.2.5. *Specular duality is a duality that preserves master spaces.*

Therefore, a consequence of Theorem 3.2.14 is:

Corollary 3.2.14.1. *Given a pair of specular duals a and b, suppose the GLSM fields p_i^a and p_i^b are mapped under*

$$p_1^a \leftrightarrow p_1^b, \quad p_2^a \leftrightarrow p_2^b, \quad \ldots, \quad p_L^a \leftrightarrow p_L^b. \tag{3.2.57}$$

If their Newton polynomials are $P_a(z, w) = k - p_a(z, w)$ and $P_b(z, w) = k - p_b(z, w)$, then for $k \geq \max\limits_{|z|=|w|=1} (|p_a(z, w)|, |p_b(z, w)|)$, the two Mahler measures have the series expansions

$$m(P_a) = \log(k) - \sum_{n=2}^{\infty} \frac{f_n(p_i^a)}{nk^n}, \quad m(P_b) = \log(k) - \sum_{n=2}^{\infty} \frac{f_n(p_i^b)}{nk^n}. \tag{3.2.58}$$

Likewise,

$$u_0(P_a) = 1 + \sum_{n=2}^{\infty} \frac{f_n(p_i^a)}{k^n}, \quad u_0(P_b) = 1 + \sum_{n=2}^{\infty} \frac{f_n(p_i^b)}{k^n}. \tag{3.2.59}$$

Here, f_n are functions of $p_i^{a,b}$ whose variables are ordered as

$$f_n(p_1^a, p_2^a, \ldots, p_L^a) \text{ and } f_n(p_1^b, p_2^b, \ldots, p_L^b). \tag{3.2.60}$$

Remark 15. *Since the Newton polynomials and Mahler measures are invariant under Seiberg duality, Corollary 3.2.14.1 is transitive. If a toric phase of polygon Δ_1 is specular dual to toric phase A of Δ_2 and a toric phase of Δ_3 is dual to toric phase B of Δ_2, then the Mahler measures and u_0 for Δ_1 and Δ_3 would also satisfy Corollary 3.2.14.1.*

Example 14. *One of the toric phases for F_0 is specular dual to the single phase for $Y^{2,2}$. Their Newton polynomials are*

$$P_{F_0} = k - 8(z + w + z^{-1} + w^{-1}), \quad P_{Y^{2,2}} = k - 9(z + z^{-1}w^{-1} + z^{-1}w + 2z^{-1}), \tag{3.2.61}$$

where the coefficients are taken to be the canonical choice from R-charges, and k_{iso} is reached at $k = 32, 36$ respectively. For instance, at order 2, one of the "internal perfect matchings" on $2\mathcal{G}_1^{F_0}$

is

<div align="right">(3.2.62)</div>
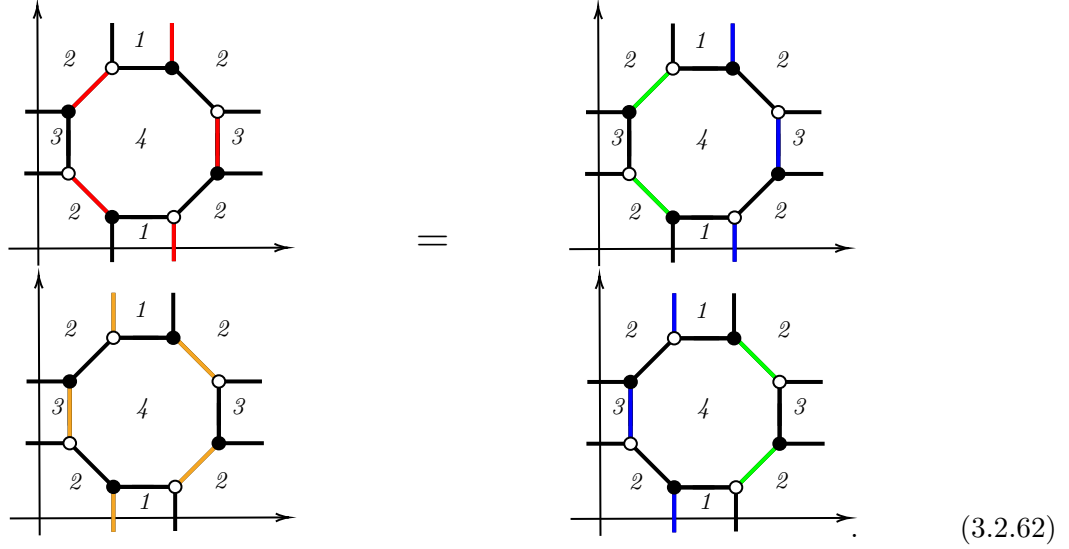
On the left hand side, we have two external perfect matchings on $\mathcal{G}_1^{F_0}$ (in red and orange respectively). Together they form an internal perfect matching on $2\mathcal{G}_1^{F_0}$. This can be regrouped into two internal perfect matchings on $\mathcal{G}_1^{F_0}$ as shown on the right hand side in blue and green respectively.

Under specular duality, the perfect matchings in different colours are mapped to

<div align="right">(3.2.63)</div>
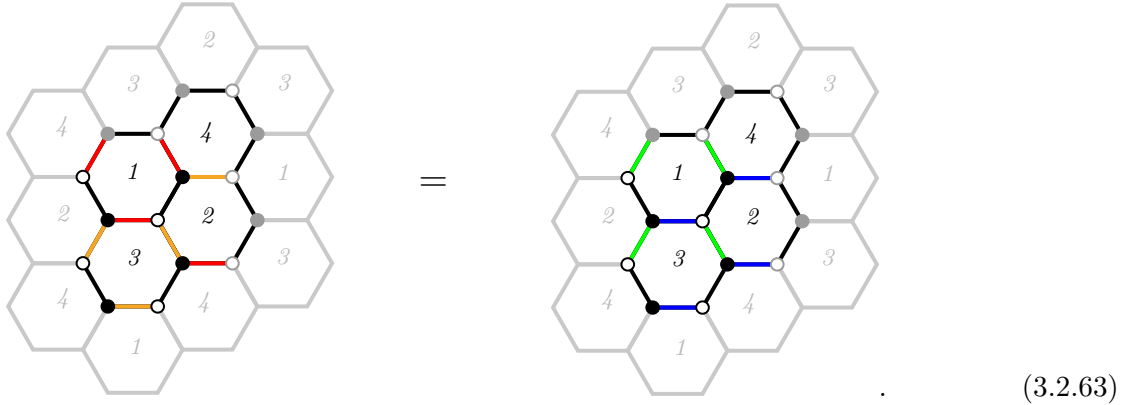
Notice that now the red and orange ones are internal perfect matchings while the blue and green ones are external on $\mathcal{G}_1^{Y^{2,2}}$.

Overall, at order 2, we have

$$
\begin{aligned}
f_2 =\; & 2 \times 2^8 \sin\left(\frac{\pi R_H}{2}\right) \sin\left(\frac{\pi R_A}{2}\right) \sin\left(\frac{\pi R_B}{2}\right) \sin\left(\frac{\pi R_G}{2}\right) \\
& \times \left(\sin\left(\frac{\pi R_K}{2}\right) \sin\left(\frac{\pi R_L}{2}\right) \sin\left(\frac{\pi R_C}{2}\right) \sin\left(\frac{\pi R_D}{2}\right) \right. \\
& \left. + \sin\left(\frac{\pi R_I}{2}\right) \sin\left(\frac{\pi R_J}{2}\right) \sin\left(\frac{\pi R_E}{2}\right) \sin\left(\frac{\pi R_F}{2}\right) \right),
\end{aligned}
$$

<div align="right">(3.2.64)</div>

where the subscripts of the R-charges follow the notations in the perfect matching matrices in [162, §4.2]. One may check that f_n for the two theories should match at any order n.

In the above example, if we plug in the R-charge values for the two theories, we find that

$$
\begin{aligned}
m(P_{F_0}) &= \log(k) - \frac{128}{k^2} - \frac{36864}{k^4} - \frac{5242800}{3k^6} - \frac{10276044800}{k^8} - \frac{34093450395648}{k^{10}} - \cdots, \\
m(P_{Y^{2,2}}) &= \log(k) - \frac{162}{k^2} - \frac{59049}{k^4} - \frac{35429400}{3k^6} - \frac{52732233225}{2k^8} - \frac{110712378300552}{5k^{10}} - \cdots
\end{aligned}
$$

<div align="right">(3.2.65)</div>

At different orders, the ratios of the coefficients are

$$\sigma_2 = \frac{81}{64}, \; \sigma_4 = \frac{6561}{4096}, \; \sigma_6 = \frac{531441}{262144}, \; \sigma_8 = \frac{43046721}{16777216}, \; \sigma_{10} = \frac{3486784401}{1073741824}, \ldots \tag{3.2.66}$$

One can actually find that

$$\sigma_n = \frac{f_n^{Y^{2,2}}}{f_n^{F_0}} = \left(\frac{9}{8}\right)^n. \tag{3.2.67}$$

This means that we can rescale/normalize the Newton polynomial by dividing P_{F_0} ($P_{Y^{2,2}}$) by a factor of 8 (9):

$$P_{F_0} = k - (z + w + z^{-1} + w^{-1}), \quad P_{Y^{2,2}} = k - (z + z^{-1}w^{-1} + z^{-1}w + 2z^{-1}), \tag{3.2.68}$$

where we have absorbed the factor for the constant term under the redefinition $k \to k/8$ ($k \to k/9$). Then the two normalized Newton polynomials have equal Mahler measures (as well as $u_0(k)$).

More generally, if the duals have Mahler measures

$$m(P_a) = \log(k) - \sum_{n=1}^{\infty} \frac{f_a^n C_n}{nk^n}, \quad m(P_b) = \log(k) - \sum_{n=1}^{\infty} \frac{f_b^n C_n}{nk^n} \tag{3.2.69}$$

for $C_n, f_{a,b}^n \in \mathbb{C}$, then we can normalize $P_{a,b} = k - p_{a,b}$ to be $P_{a,b}^{\text{norm}} = k - p_{a,b}^{\text{norm}} = k - \frac{p_{a,b}}{f_{a,b}}$ such that the two would have equal Mahler measures. However, this is not true in general, and we have found several counterexamples. For instance, the third tiling for PdP$_{4a}$ in (3.2.44) is dual to the single toric phase of PdP$_{4b}$ (see [105, 162] for its details). It turns out that no matter how we normalize the Newton polynomials, their Mahler measure expansions would not have the same numerical coefficients though the discrepancies are very small[20].

Remarkably, for all the examples whose *numerical* f_n's are different from their specular duals (under any normalization), we find that they coincide with polynomials of second type in Example 8. It would be interesting to explore this more deeply in future.

It is also natural to ask how specular duals are related at isoradial point. Since the number of chiral multiplets is invariant under specular duality, the number of summands in (3.2.30) would not change. Moreover, a **zig-zag path** is mapped to a face in the specular dual tiling [162]. A zig-zag path is a collection of edges that forms a closed path on the brane tiling. It maximally turns left/right at a black/white node. The winding number (p,q) of the zig-zag path corresponds to a direction in the dual web of the toric diagram. Physically, zig-zag paths can be interpreted as gauge invariant operators [163]. On the other hand, a node in the tiling is mapped to a node in the dual tiling. In terms of superpotentials, this reverses the order of half the terms based on the convention of untwisting the zig-zag paths. Now that we have the zig-zag $\leftrightarrow$ face and node $\leftrightarrow$ node mappings, we can write down how Mahler measures would transform.

Proposition 3.2.15. *Suppose a brane tiling G has c perfect matchings. Then for the specular dual tiling G' with edges e_I, the Mahler measure is*

$$m = \sum_I \left(\frac{\theta_I}{\pi} \log(2\sin(\theta_I)) + \frac{1}{\pi} \Lambda(\theta_I) \right), \tag{3.2.70}$$

where θ_I (and m) can be obtained by maximizing m subject to the conditions

$$\sum_{e_I \in \mathcal{I}} \theta_I = \pi, \quad \sum_{e_I \in \mathcal{Z}} (\pi - 2\theta_I) = 2\pi \tag{3.2.71}$$

for all nodes $\mathcal{I}$ in G [21] and all zig-zag paths $\mathcal{Z}$ in G.

---

[20]To avoid any possible confusion, we should emphasize that only the numerical coefficients differ in these cases. Corollary 3.2.14.1 holds for any polygons.

[21]In this case, "$\in$" indicates the edges attached to a node.

Notice that specular duality, in particular for non-reflexive polygons, may require the dimers to be embedded on a Riemann surface of any genus g rather than just a torus. Nevertheless, the discussions in this subsection would still hold for any polygons. This is because Corollary 3.2.14.1 only requires the invariance of the master spaces, and for Proposition 3.2.15, (3.2.30) is always true for dimers which are (doubly) periodic on general bi-dimensional lattices [159].

3.2.6 Tropical Limit

In this part, we shall focus on another special point in the Mahler flow, that is, k_{trop}. Recall that in the large/(sub)tropical k limit, the amoeba tends to its spine and the gas phase becomes dominant. In particular, in this limit the k^{-n} terms in the Mahler measure tend to zero and we have $m(P) \sim \log k$. Moreover, the area of the hole in the amoeba is $A_h \sim \log^2 k$. Therefore, in the large k limit, the Mahler measure in the tropical limit follows an area law

$$m(P) \sim A_h^{1/2}. \tag{3.2.72}$$

Likewise, the Ronkin function would be dominated by the linear facets. More precisely,

$$R(x,y) \simeq \log |c_{(m,n)}| + mx + ny \tag{3.2.73}$$

for $P = \sum_{(m,n)} c_{(m,n)} z^m w^n$. For each linear facet, this equality is exact. For the liquid phases, it gives a good approximation as the non-linear regions tends to the spine at large k. In fact, as the amoeba $\mathcal{A}$ in the (sub)tropical limit is a union of local amoebae $\mathcal{A}_{\text{loc}}$, the (local) non-linear part of $R(x,y)$ for $\mathcal{A}$ would be the translations and rotations of the Ronkin functions for $\mathcal{A}_{\text{loc}}$, where the detailed translations and rotations can be determined by the neighbour linear facets.

From the perspective of crystal melting, (almost) the whole crystal is molten. In other words, the system becomes a gas of atoms. Since the linear facets of the Ronkin function are sent to infinity, the partition function would also diverge as expected.

In this large k limit, we may then estimate the free energy in (3.1.26) as

$$F = -\log Z \sim -A_h \log k \sim -\log^3 k. \tag{3.2.74}$$

In other words,

$$F \sim -m^3(P). \tag{3.2.75}$$

Now we shall consider the meaning of tropical limit from the perspective of gauge theories. The F-term relations are encoded by $u_0(k)$ for the master space. In the large k limit, we have $u_0 \to 1$. Therefore, all the constraints on the GLSM fields from Q_F are lost in the tropical limit. As a result, the master space would become the trivial $\mathbb{C}^n$, and all the GLSM fields become free.

This is also reflected by the amoeba. In the large k limit, the amoeba is composed of local vertices in the spine. These vertices are only connected by thin long channels/lines.

3.2.7 Discussions and Outlook

There is a very straightforward implication of the Ronkin functions if we consider the GLSM fields. From [139], we know that the partition function for perfect matchings (in the thermodynamic limit) can be determined by Ronkin functions. Therefore,

Proposition 3.2.16. *The partition function Z for GLSM fields can be determined via*

$$\log Z = \int \mathrm{d}x\, \mathrm{d}y\, R(x,y), \tag{3.2.76}$$

which also defines the free energy of the dimer/GLSM as $F \equiv -\log Z$.

Of course, such expression would diverge, so we need to normalize it by Z/Z_0, where Z_0 is the partition function whose Ronkin function only has linear (solid) facets.

A more non-trivial interpretation would be the connection to 4d superconformal index I_{4d} on $S^3 \times S^1$. As studied in [158, 164], when the radius of S^1 goes to 0, I_{4d} would reduce to the partition function Z_{3d} on the ellipsoid $S_b^3 = \{(z_1, z_2) \in \mathbb{C}^2 | b^2 |z_1|^2 + b^{-2} |z_2| = 1\}$. By further taking $b \to 0$, the 3d partition function would give the partition function for 2d $\mathcal{N} = (2, 2)$ theory:

$$Z_{2d} = \int d\sigma \exp\left(-\frac{1}{\pi b^2} W_{2d}(\sigma)\right), \tag{3.2.77}$$

where σ is the scalar in the vector multiplet. The effective twisted superpotential W_{2d} can then be identified with the volume of some hyperbolic 3-fold $\mathcal{M}$. This 3-fold can be determined by (the zig-zag paths on) the dimer model. Moreover, the genus-0 prepotential for topological B-model is

$$F_0 = \int dx \, dy \, R(x, y) = \int dx \, dy \, \mathcal{L}(\text{vol}(\mathcal{M})), \tag{3.2.78}$$

where $\mathcal{L}$ denotes the Legendre transformation. As we can see [158],

Proposition 3.2.17. *The 4d superconformal index under dimensional reduction is related to topological string partition function and Ronkin function via Legendre transformation.*

The topological string partition functions are invariant under wall crossing. Its counterpart in 4d, i.e., the superconformal indices, are also invariant under Seiberg duality. This would provide a further evidence that the Mahler measure/Ronkin function should be invariant under Seiberg duality. Moreover, it also seems to have some connections to F-theorem in 3d [158]. A more detailed study would give us a better understanding of the physics for Mahler measure in gauge theories.

Since the Mahler measure and Ronkin function are related to the degeneracy of D-brane bound states, it would be possible to define a quiver entropy from this. It would also be important to study if relation with the surface tension of the crystal model, which is the Legendre dual of the Ronkin function. In [26, eqn(2.25)], another quiver entropy was defined in terms of the plethystic exponential of the Hilbert series. How this would be connected to the quiver entropy from the Mahler measure is still an interesting open question. On the other hand, the famous OSV conjecture [165] says that $Z_{BH} = |Z_{topo}|^2$ when the D-brane bound states become black holes with smooth event horizon. it is worth noting that the black hole entropy in the supergravity approximation is also the Legendre transformation of the free energy of topological A-model at genus 0.

Chapter 4

Dessins d'Enfants

In this chapter, we shall discuss the dessins d'enfants (children's drawings) which have constituted a core object in algebraic geometry and number theory since Grothendieck's Esquisse d'un Programme (sketch of a programme) [48]. Following Belyi's theorem [49], these bipartite graphs can be nicely connected to algebraic curves. The study of dessins has then been led to the vast areas of Galois theory, modularity, and, more recently, congruence subgroups and monstrous moonshine [166–170]. Due to the relationship to polynomial equations defining Riemann surfaces, dessins appear in the study of Seiberg-Witten (SW) theory, as points in the Coulomb branch [171]. They have then applied to various aspects in physics, including both $\mathcal{N} = 1$ and $\mathcal{N} = 2$ quivers, conformal blocks etc [5, 172–174]. See also Appendix C for relevant discussions.

Now, it was demonstrated in [50] that the Mahler measure[1] has certain expansion whose building blocks behave as modular forms. Therefore, it would be natural to expect some deep connection between Mahler measure and dessins due to the emergence of modularity. In particular, the reflexive polygons provide a nice playground since their Newton polynomials define elliptic curves.

The family of the elliptic curves defined by these Newton polynomials with parameter k furnishes the Klein's j-invariant as a meromorphic function $j(k) : \mathbb{P}^1 \to \mathbb{P}^1$. Of particular interest here would be the so-called tempered families that put certain restrictions on the coefficients of the Newton polynomials. We find that a subset of these families, which we call *maximally tempered*, give a one-to-one correspondence between Mahler measures and dessins.

A priori, there does not seem to be anything special for the maximally tempered coefficients except that they are non-zero binomial numbers along each edge of a reflexive polygon. However, it has a salient interpretation in physics. When constructing quiver theories from brane tilings, each lattice point in the Newton polygon is associated with some perfect matchings/gauged linear sigma model fields [21, 22, 175]. The maximally tempered coefficients are exactly the numbers of perfect matchings for the lattice points.

We find that the dessins obtained in such way are invariant under specular duality. On the other hand, we have discussed how Mahler measures behave under specular duality in the previous chapter. Here, with the special maximally tempered coefficients, we find that Mahler measures are invariant for specular duals. Thus, the one-to-one correspondence between Mahler measures and dessins are automatic. As is known, specular duality preserves the master space of the gauge theory. However, different toric phases are often not related by such a duality[2]. Therefore, the Mahler measure and the dessin should encode some information of the master space.

Calculations of the modular Mahler measure show that certain modular quantities are related to some congruence subgroups via their Hauptmoduln. In fact, they contain the congruence subgroups associated to the dessin. Besides, as the Mahler measure is derived from several modular forms (with singularities), one can naturally apply the results in [176] and study the Mahler measure in

---

[1] In this chapter, we shall mainly focus on the expression without "Re" in (3.1.6) and refer to this complex quantity as the Mahler measure.

[2] Yet, they have the same Mahler measure and dessin as the Newton polynomial does not change.

terms of j-invariants. We will also discuss the appearances of dessins and modular Mahler measure in quiver gauge theories and F-theory in this chapter.
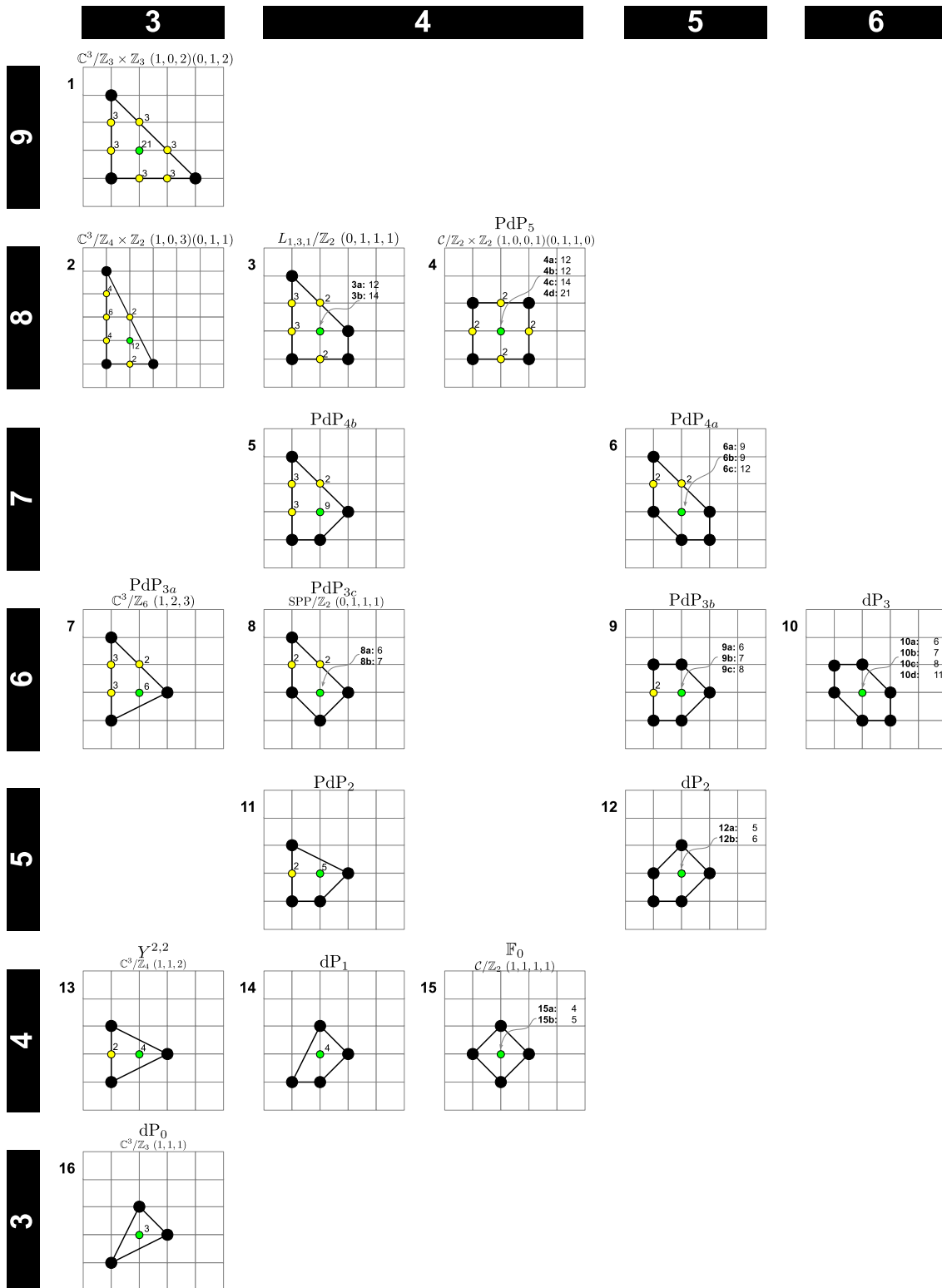
FIGURE 4.0.1: The 16 inequivalent reflexive polygons (up to $\mathrm{SL}(2,\mathbb{Z})$). Figure taken from [105] (with slight modifications). The reflexive polygons are arranged such that the dual pairs are mirror symmetric with respect to the middle line (fourth row), and the four polygons in the middle line are therefore self-dual. In each row, the polygons have the same number of boundary points/(normalized) area. In each column, the polygons have the same number of vertices.

4.1 Dramatis Personae

In this section, we give a brief review on the relevant conecpts used in this chapter. First, let us list all the reflexive polygons in Figure 4.0.1.

As shown in [156], the Laurent/Newton polynomial $P(z,w)$ specifies the mirror geometry of the CY singularity by $P(z,w) = W = uv$ with $u,v \in \mathbb{C}$. Hence, it can be viewed as a double fibration over the W-plane. In particular, $P = 0$ is known as the spectral curve. See [22] for more details.

Tempered Polynomials   Given a Newton polygon, it is easy to construct the Newton polynomial. Nevertheless, we still have the freedom to choose the complex coefficients in $P(z,w)$. In the previous chapter, we have the canonical choice of the coefficients that specifies the R-charges of the fields. Here, we consider the so-called tempered families that are of particular interest in number theory and related study of Mahler measure [50, 136].

Given a Newton polygon $\mathfrak{P}$, we obtain the Newton polynomial $P(z,w) = \sum c_{(m,n)} z^m w^n$ with coefficients $c_{(m,n)}$ for each of the lattice points. Now, consider a bounding edge F of the polygon $\mathfrak{P}$. There might also be lattice points on it (the yellow points in Figure 4.0.1), in addition to the 2 endpoints (the black points in Figure 4.0.1) which are vertices of $\mathfrak{P}$. Suppose there are N lattice points on F, indexed from 0 to $N-1$, and we call the associated coefficients $c_{(m,n)}$ as $c_{F,l}$. Then, we can create an auxiliary polynomial $P_F(t) \in \mathbb{C}[t]$ as

$$P_F(t) = \sum_{l=0}^{N-1} c_{F,l} t^l \ , \tag{4.1.1}$$

for each edge F.

Notice that this automatically requires that the boundary point $c_{F_1,N-1}$ to coincide with $c_{F_2,0}$ for any two adjacent edges F_1 and F_2. A Laurent polynomial is then said to be **tempered** if the set of roots of $\prod_{F \in \mathfrak{P}} P_F(t)$ consists of roots of unity only. In other words, each P_F in $\mathfrak{P}$ would only have roots on the unit circle.

Notice that being tempered only gives restrictions to the coefficients for the boundary points. For the reflexive polygons considered in this paper, we always take the single interior point as the origin, corresponding to the constant term k in the Newton polynomial as discussed before: $P(z,w) = k - p(z,w)$.

Example 15. *For F_0, $P = k - z - z^{-1} - w - w^{-1}$ is tempered. For instance, the lattice points $(1,0)$ and $(0,-1)$ corresponds to the monomials $-z$ and $-w^{-1}$ in P. The edge linking them is associated to the polynomial $-1 - t$ which only has one root $t = -1$. In fact, every one of the 4 edges has the same polynomial $P_F = -1 - t$. Thus, P is tempered.*

t^0	1	1	1	1	1	1	1	1	1	1	1	1	1	1	1	1	1	1	1	1	1	1	1	1	1
t^1	0	0	0	0	0	0	0	0	0	1	1	1	1	1	1	1	1	2	2	2	2	2	3	3	4
t^2	-2	-2	-1	0	0	0	1	1	2	-1	0	0	0	1	1	1	2	0	1	2	2	3	3	4	6
t^3	0	0	0	0	0	1	0	0	0	-1	-1	0	1	0	1	1	1	-2	0	1	2	2	1	3	4
t^4	1	0	1	-1	1	0	0	1	1	0	-1	0	1	0	0	1	1	-1	0	0	1	1	0	1	1

TABLE 4.1.1: Each column gives a set of coefficients for $P_F(t)$ such that the solutions to $P_F(t) = 0$ only have roots of unity.

For reflexive polygons, all the possible P_F's that make P tempered have been classified in [50]. We reproduce it here in Table 4.1.1; there are 25 possibilities. For convenience, given a tempered Newton polynomial, if it only has non-zero coefficients for vertices, we shall call such choice *minimally tempered coefficients*. If all the boundary points have non-zero coefficients and the coefficients for every edge are binomial, that is, $P_F = (t+1)^N$ for all $F \in \mathfrak{P}$, then we shall call such choice *maximally tempered coefficients*. When a polygon has no boundary lattice points other than vertices (i.e., each edge has exactly the 2 endpoints which are lattice points), the minimally and maximally tempered coefficients coincide and this is the only set of tempered coefficients.

Example 16. *As we have seen, F_0 has only one possible set of tempered coefficients. On the other hand, for $\mathbb{C}^3/(\mathbb{Z}_4 \times \mathbb{Z}_2)$ $(1,0,3)(0,1,1)$ (No.2 in Figure 4.0.1), there are $2 \times 2 \times 4 = 16$ tempered choices. When all the three faces have $P_F(t) = -t - 1$, $P(z, w)$ is minimally tempered. If $P_{F_{1,2}} = -t^2 - 2t - 1 = -(t+1)^2$ and $P_{F_3} = -t^4 - 4t^3 - 6t^2 - 4t - 1 = -(t+1)^6$, then $P(z, w)$ is maximally tempered. Notice that the minus sign is just a convention here as it would not change the spectral curve $P = 0$. All the maximally and minimally tempered Newton polynomials are listed in Appendix D.*

Elliptic curves Since the reflexive polygons give elliptic curves, we here review some of the requisites from the geometry and number theory of elliptic curves. In general, any elliptic curve E can be transformed into Weierstrass normal form

$$y^2 = x^3 + fx + g. \tag{4.1.2}$$

The curve is non-singular if and only if $\Delta \neq 0$, where

$$\Delta = -16(4f^3 + 27g^2) \tag{4.1.3}$$

is known as the discriminant. Then the j-invariant is given by

$$j = \frac{4 \times (24f)^3}{\Delta}. \tag{4.1.4}$$

This is a crucial concept since isomorphic (isogenous) elliptic curves have the same j-invariant. Notice that however j-invariant is only able to distinguish elliptic curves over algebraically closed fields.

Topologically, an elliptic curve E is the torus $\mathbb{T}^2$. Hence, it is endowed with a complex structure specified by the two periods which are integrals along the two cycles A and B of the torus: $\int_{A,B} \frac{\mathrm{d}x}{y}$. This complex structure should coincide with the τ computed from $u_{0,1}$ in (4.1.8) up to $\mathrm{SL}(2, \mathbb{Z})$. As a function of τ, $j(\tau) : E \to \mathbb{P}^1$ is a modular function, i.e., invariant under $\mathrm{SL}(2, \mathbb{Z})$ transformations. It is in fact the only modular function in that any meromorphic function which is $\mathrm{SL}(2, \mathbb{Z})$-invariant is a rational function in $j(\tau)$.

Now, because our Newton polynomial always has a parameter k, any reflexive polygon defines for us a family of elliptic curves. Geometrically, when $k \in \mathbb{C} \sqcup \infty$, this defines an elliptic fibration over $\mathbb{P}^1$, giving us a complex surface which is called a modular elliptic surface [166, 177]. In this case, all the crucial quantities, such as Δ and j, depend on k. In particular, $j(k)$ can be seen as a map from $\mathbb{P}^1$ with coordinate k to $\mathbb{P}^1$. We will make use of this map shortly.

4.1.1   Modular Mahler Measure

In general, the spectral curve $P(z, w) = 0$ defines a Riemann surface as an algebraic curve Σ. Since each reflexive polygon has a single interior point, Σ is of genus one. For all but finitely many k, the curve would be a smooth elliptic curve. For convenience, let us define $\lambda := k^{-1}$, then we have (where we explicitly write out the dependence of the elliptic curve on the parameter λ)

$$\Sigma_\lambda \ : \ 1 - \lambda \, p(z, w) = 0 \ . \tag{4.1.5}$$

As pointed out in [50], u_0 is a period of a holomorphic 1-form on Σ_λ. Hence, it satisfies the Picard-Fuchs equation

$$A(\lambda)\frac{\mathrm{d}^2 u_0}{\mathrm{d}\lambda^2} + B(\lambda)\frac{\mathrm{d}u_0}{\mathrm{d}\lambda} + C(\lambda)u_0 = 0, \tag{4.1.6}$$

where $A(\lambda), B(\lambda), C(\lambda)$ are polynomials in λ. As we will see in §4.2.3, this is actually a consequence of Theorem 4.2.8 [176]. We may then use the Picard-Fuchs equation to find the dual period u_1 of the form

$$u_1(\lambda) = u_0(\lambda)\log(\lambda) + v(\lambda), \tag{4.1.7}$$

where v is a holomorphic function with $v(0) = 0$. This defines

$$\tau = \frac{1}{2\pi i}\frac{u_1}{u_0}, \quad q = \mathrm{e}^{2\pi i\tau} = \lambda + \dots. \tag{4.1.8}$$

As usual, τ gives the complex structure of the elliptic curve $P = 0$ as a torus. The monodromy around $\lambda = 0$ (i.e., at k infinity) acts as $\tau \to \tau + 1$. This fixes q and we may locally invert it to get

$$\lambda(\tau) = q + \dots, \quad u_0(\tau) = 1 + \dots. \tag{4.1.9}$$

Recall that Mahler flow equation reads

$$\frac{\mathrm{d}m}{\mathrm{d}\log\lambda} = \lambda\frac{\mathrm{d}m}{\mathrm{d}\lambda} = -u_0(\lambda), \tag{4.1.10}$$

where we have used $\lambda = k^{-1}$. Using the nome q, we can also express the Mahler flow equation as

$$q\frac{\mathrm{d}m}{\mathrm{d}q} = \frac{\mathrm{d}m}{\mathrm{d}\lambda}\frac{q\mathrm{d}\lambda}{\mathrm{d}q} = \frac{u_0}{\lambda}\frac{q\mathrm{d}\lambda}{\mathrm{d}q} =: e(\tau). \tag{4.1.11}$$

In fact, λ, u_0, e are modular forms (with singularities) of weights 0, 1, 3 respectively under the monodromy of Picard-Fuchs equation, namely a congruence subgroup of $\mathrm{SL}(2,\mathbb{Z})$ acting on τ [50]. We may therefore call (4.1.11) the modular Mahler flow equation.

Write the Fourier series of $e(\tau)$ as $e(\tau) = 1 + \sum\limits_{n=1}^{\infty} e_n q^n$. Then from (4.1.11), we have

Theorem 4.1.1 (Rodriguez-Villegas [50]). *Locally around $\tau = i\infty$ (i.e., $\lambda = 0$), we have*

$$m(P) = -2\pi i\tau - \sum_{n=1}^{\infty}\frac{e_n}{n}q^n. \tag{4.1.12}$$

Because of the modularity of $e(\tau)$, the Mahler measure for elliptic curves is referred to as *modular Mahler measure* though $m(P)$ itself is not modular.

Example 17. *Let us consider $P(z,w) = \lambda^{-1} - z - z^{-1} - w - w^{-1}$. Since u_0 is hypergeometric, it is easy to see that the Picard-Fuchs equation is*

$$\mu(16\mu - 1)\frac{\mathrm{d}^2 u}{\mathrm{d}\mu^2} + (32\mu - 1)\frac{\mathrm{d}u}{\mathrm{d}\mu} + 4u = 0, \tag{4.1.13}$$

where we have used $\mu := \lambda^2$ for convenience. This leads to [50]

$$u_1 = u_0\log(\mu) + 8\mu + 84\mu^2 + \frac{2960}{3}\mu^3 + \dots, \tag{4.1.14}$$

and

$$u_0 = 1 + 4\sum_{n=1}^{\infty}\sum_{d|n}\chi_{-4}(d)q^n, \quad e = 1 - 4\sum_{n=1}^{\infty}\sum_{d|n}\chi_{-4}(d)d^2\,q^n, \quad \mu = \frac{1}{c^2}\left(\sum_{\substack{n=1 \\ n\text{ odd}}}^{\infty}\sum_{d|n}d\,q^n\right), \tag{4.1.15}$$

where χ_{-4} is the Dirichlet character/Kronecker symbol satisfying $\chi_{-4}(n) = 1, 0$ when $n \equiv 0, 1 \pmod{2}$. Then, we have

$$m(P) = \frac{16\,\mathrm{Im}\tau}{\pi^2}\sum_{\substack{n_1, n_2 \in \mathbb{Z} \\ (n_1, n_2) \neq (0,0)}}\frac{\chi_{-4}(n_1)}{(n_1 + 4n_2\tau)^2(n_1 + 4n_2\bar{\tau})}, \tag{4.1.16}$$

which under modular transformations, we have

$$\tau \to -\frac{1}{\tau}: \quad m = \frac{16\,\mathrm{Im}\bar{\tau}}{\pi^2} \sum_{\substack{n_1,n_2\in\mathbb{Z}\\(n_1,n_2)\neq(0,0)}} \frac{\chi_{-4}(n_1)\tau}{(4n_2 - n_1\tau)^2(4n_2 - n_1\bar{\tau})},$$

$$\tau \to \tau+1: \quad m = \frac{16\,\mathrm{Im}\tau}{\pi^2} \sum_{\substack{n_1,n_2\in\mathbb{Z}\\(n_1,n_2)\neq(0,0)}} \frac{\chi_{-4}(n_1)}{(n_1 + 4n_2\tau)^2(n_1 + 4n_2\bar{\tau})}. \tag{4.1.17}$$

Hence, m is invariant under monodromy ($\tau \to \tau + 1$) at $k \to \infty$ while we have $m \to 0$ as $\tau \to 0$. We expect this to be true in general for reflexive polygons.

4.1.2 Esquisse de Dessins

The discussions on elliptic curves above are initmately related to the profound theorem by Belyi [49]:

Theorem 4.1.2. *Let $\mathcal{X}$ be a compact, connected Riemann surface. Then $\mathcal{X}$ is a non-singular, irreducible projective variety of complex dimension 1 and can be defined by polynomial equations. The defining polynomial has algebraic coefficients if and only if there exists a rational map $\beta : \mathcal{X} \to \mathbb{P}^1$ which is ramified at exactly three points, that is, has three critical values.*

We will be primarily concerned with the case of $\mathcal{X} = \mathbb{P}^1$, so that the Belyi map is a rational function $p(x)/q(x) : \mathbb{P}^1 \to \mathbb{P}^1$. Now, on the target $\mathbb{P}^1$, any three points can be taken to be 0, 1 and ∞ (that is, $[0:1]$, $[1:1]$ and $[1:0]$ in homogenous coordinates) by linear-fractional Möbius transformations, so that the three ramified points can be thus chosen. Following Grothendieck [48], a bipartite graph called **dessin d'enfant** (or child's drawing) can be associated to β by

$$\begin{aligned}
&B = \beta^{-1}(0) = \{x \in \mathbb{P}^1 \mid p(x) = 0\}, \quad W = \beta^{-1}(1) = \{x \in \mathbb{P}^1 \mid p(x) = q(x)\},\\
&E = \beta^{-1}([0,1]) = \{x \in \mathbb{P}^1 \mid p(x) = tq(x), \text{ for some } t \in [0,1]\}, \tag{4.1.18}\\
&F = \beta^{-1}(\infty) = \{x \in \mathbb{P}^1 \mid q(x) = 0\},
\end{aligned}$$

where B, W, E and F denote the black, white vertices, edges and faces respectively. As β is $\mathbb{P}^1 \to \mathbb{P}^1$, the graph is embedded on a sphere. Moreover,

Proposition 4.1.3. *Let $\beta : \mathbb{P}^1 \to \mathbb{P}^1$ be a Belyi map. Then the associated bipartite graph $(V = B \sqcup W, E, F)$ is loopless, connected and planar. It has $|V| = |\beta^{-1}(\{0,1\})|$ vertices, $|E| = \deg(\beta)$ edges and $|F| = |\beta^{-1}(\infty)|$ faces, satisfying $|V| - |E| + |F| = 2$.*

As we will plot the dessin on a plane via stereographic projection, all the bounded faces on the plane are called internal faces while the face containing $k \to \infty$ is known as the external face. As β is a multi-covering of the target $\mathbb{P}^1$, we can consider the monodromy around each vertex in the dessin. Essentially, each monodromy acting on a vertex permutes the edges connected to that vertex. We shall denote the set of such permutations around black (white) vertices as σ_0 (σ_1). Then σ_0 and σ_1 generate a free group known as the monodromy/cartographic group G of the dessin. In particular, the monodromies σ_∞ around faces can be obtained by $\sigma_\infty \circ \sigma_1 \circ \sigma_0 = 1$. As the dessin has $|E|$ edges, G is a subgroup of the symmetric group $\mathfrak{S}_N$ where $N = |E|!$.

In our context, recall that all our elliptic curves E are parametrized by k so that the Klein invariant $j(k)$ is a function of the parameter k and is thus a map from $\mathbb{P}^1$ (instead of E) to $\mathbb{P}^1$. We will show in §4.2.1 that $j(k)$ is actually Belyi for maximally tempered coefficients in the Newton polynomials:

$$\beta = \frac{j}{1728} \ . \tag{4.1.19}$$

Congruence subgroups and coset graphs A coset graph is a graph associated with a group K generated by elements $\{x_i\}$ and a subgroup H. Then each vertex (drawn in black so as to

reconstruct the dessin) in the coset graph represents a right coset Hg for $g \in K$. An edge is of form (Hg, Hgx_i) which connects the coset Hg and $H(gx_i)$.

As we will see shortly, the dessins associated to reflexive polygons (with maximally tempered coefficients) are *clean*, namely that the white vertices all have valency 2. Therefore, the dessins can be viewed as coset graphs by removing the white vertices. Conversely, we can insert a white vertex on each edge to get the dessin from the coset graph.

In particular, the dessins we will consider in §4.2 are associated with the modular group (P)SL$(2, \mathbb{Z})$ and the congruence subgroups. Hence, the generators can be taken as the usual S and T, viz,

$$S = \begin{pmatrix} 0 & -1 \\ 1 & 0 \end{pmatrix}, \quad T = \begin{pmatrix} 1 & 1 \\ 0 & 1 \end{pmatrix} \quad \text{s.t. PSL}(2, \mathbb{Z}) = \langle S, T | S^2 = (ST)^3 = 1 \rangle. \tag{4.1.20}$$

The **congruence groups** of level n are defined as

$$\Gamma(n) := \left\{ M \in \text{(P)SL}(2, \mathbb{Z}) \middle| M \equiv \begin{pmatrix} 1 & 0 \\ 0 & 1 \end{pmatrix} \pmod{n} \right\},$$

$$\Gamma_1(n) := \left\{ M \in \text{(P)SL}(2, \mathbb{Z}) \middle| M \equiv \begin{pmatrix} 1 & b \\ 0 & 1 \end{pmatrix} \pmod{n} \right\}, \tag{4.1.21}$$

$$\Gamma_0(n) := \left\{ M \in \text{(P)SL}(2, \mathbb{Z}) \middle| M \equiv \begin{pmatrix} a & b \\ 0 & d \end{pmatrix} \pmod{n} \right\}.$$

In particular, we have $\Gamma(n) \leq \Gamma_1(n) \leq \Gamma_0(n)$ and $\Gamma_0(n_2) \leq \Gamma_0(n_1)$ if $n_1 | n_2$. The fact that every congruence subgroup of (P)SL$(2, \mathbb{Z})$ has a coset graph (called Schreier-Cayley graph) which is a clean trivalent dessin was discussed in [166, 169, 178].

Given a congruence subgroup Γ, the quotient space $\mathfrak{h}/\Gamma$ (where $\mathfrak{h}$ is the upper half plane) can be compactified by adding a few isolated points (aka cusps of Γ). Such compactified curve $X(\Gamma)$ is called the **modular curve**. The genus of Γ is then defined to be the genus of $X(\Gamma)$. When $X(\Gamma)$ is of genus 0, the field of meromorphic functions on $X(\Gamma)$ is generated by a single element known as a **Hauptmodul** of Γ.

4.1.3   Dimers and Reflexive Polygons

Recall that $u_0(k)$ is the generating function of the master space in terms of F-term charge matrix though the F-term relations in higher orders are just redundant. Besides, $k \to \infty$ is known as a tropical limit when $P(z, w) = k - p(z, w)$. As a result, this is equivalent to $q \to 0$ and hence $\tau \to i\infty$. Physically, τ can be interpreted as the complexified gauge coupling in Type IIB string theory, that is, $\tau = \frac{\theta}{2\pi} + \frac{i}{g_{\text{IIB}}}$. Therefore, this gives the weak coupling $g_{\text{IIB}} \to 0$. For the modular forms (with singularties) introduced before, we have $\lambda \to 0$, $u_0 \to 1$ and $e \to 1$. In particular, $u_0 \to 1$ indicates a free theory in the tropical limit as the master space become trivial. This is consistent with the weakly coupled gauge theory with $\tau \to i\infty$.

Moreover, we have m tends to ∞ for tropical k. On the other hand, m would go to 0 in the strong coupling regime (as $\tau \to 0$).

For reflexive polygons, the specular duals are [162]

$$1 \leftrightarrow 1 , \tag{4.1.22}$$

$$2 \leftrightarrow 4d , \ 3a \leftrightarrow 4c , \ 3b \leftrightarrow 3b , \ 4a \leftrightarrow 4a , \ 4b \leftrightarrow 4b , \tag{4.1.23}$$

$$5 \leftrightarrow 6c , \ 6a \leftrightarrow 6a , \ 6b \leftrightarrow 6b , \tag{4.1.24}$$

$$7 \leftrightarrow 10d , \ 8a \leftrightarrow 10c , \ 8b \leftrightarrow 9c , \ 9a \leftrightarrow 10b , \ 9b \leftrightarrow 9b , \ 10a \leftrightarrow 10a , \tag{4.1.25}$$

$$11 \leftrightarrow 12b , \ 12a \leftrightarrow 12a , \tag{4.1.26}$$

$$13 \leftrightarrow 15b , \ 14 \leftrightarrow 14 , \ 15a \leftrightarrow 15a , \tag{4.1.27}$$

$$16 \leftrightarrow 16 \ , \tag{4.1.28}$$

where the letters following the number label different toric phases as in Figure 4.0.1. As we can see, their internal and external perfect matchings get exchanged under specular duality.

Remark 16. *The red numbers in the above list contain polygons that are called exceptional cases due to the following two reasons [9].*

- *With canonical weights, most of the specular duals can have the same Mahler measure (with the constant term taken to be k) up to an additive constant, that is, $m(P_2) = m(P_1) + \kappa$. Hence, by an overall scaling of factor $\mathrm{e}^{-\kappa}$, we have $k - p_1 \to k - \mathrm{e}^{-\kappa}p_1$ (notice that this does not change the spectral curve $P_1 = 0$). Thus, $m(P_2) = m(P_1)$. As a result, for example, polygons No.2 and No.3 have the same Mahler measure as they are connected by different toric phases of No.4 even though they are not specular duals. However, it turns out that No.5, 6, 9 and 11 do not satisfy this property.*

- *Moreover, with canonical weights (with constant term k), most Newton polynomials can have equal coefficients for vertices under rescaling of z and/or w. However, this is not possible for No.5, 6, 9 and 11.*

It is worth noting that the exceptions of the above two properties coincide (though the reason why they coincide is still unclear). It is still not known why No.5, 6, 9, 11 are exceptional. In §4.2.1, we will see that they are further exceptional regarding a third property.

4.2 Modularity and Gauge Theories

Having introduced all the background, we are now ready to discuss how modular Mahler measures connected the various different areas in mathematics and physics. From §4.1, the readers may have already noticed that

Proposition 4.2.1. *The maximally tempered coefficients in the Newton polynomials are equal to the numbers of perfect matchings associated to the exterior lattice points of the toric diagrams.*

Hence, we will mainly focus on the maximally tempered coefficients in the following discussions, and we will see various properties implying potential physical relevance. As listed in [2], all the non-reflexive polygons with two interior points also have maximally tempered coefficients equal to the numbers of perfect matchings associated to the boundary points (it would also be interesting to see what happens for higher dimensional reflexive polytopes [46]). Furthermore, the consistent brane tilings for all polygons presented in [179] also have maximally tempered coefficients equal to the numbers of perfect matchings while the remaining inconsistent tilings do not[3]. Therefore, it is natural to conjecture that

Conjecture 4.2.2. *A brane tiling is consistent if and only if the corresponding toric diagram (either reflexive or non-reflexive) has maximally tempered coefficients for its boundary points, which are equal to the numbers of the associated perfect matchings.*

It is curious that maximal tempered coefficients appear in two completely different contexts, one from perfect matching in physics and another from considering Mahler measure in mathematics.

4.2.1 Dessins and Mahler Measure

As mentioned throughout, we will focus on the 16 reflexive polygons with maximally tempered coefficients. The Newton polynomials are listed in Table D.0.1. Recall that the spectral curve $P(z, w) = 0$ for each reflexive polygon is an elliptic curve (except for finitely many k values). We can transform the spectral curves into Weierstrass normal form $y^2 = x^3 + f(k)x + g(k)$ (recall

---

[3]See [180] for a general discussion on consistency of brane tilings.

that all our elliptic curves depend on the parameter k). This is computationally rather involved (Nagell's algorithm) but can luckily be done with SAGE.

In Table 4.2.1, we list the Weierstrass form of all 16 reflexive polygons with maximally tempered coefficients, where the coefficients $f(k)$ and $g(k)$ all assume the form

$$f = -\frac{1}{48}k^4 + a(k), \quad g = \frac{1}{864}k^6 + b(k). \tag{4.2.1}$$

Polygon(s)	No.1	No.2, 3, 4
$a(k)$	$\frac{9}{2}k^2 + 36k + 81$	$\frac{5}{3}k^2 + 8k + \frac{32}{3}$
$b(k)$	$-\frac{3}{8}k^4 - 4k^3 - \frac{27}{2}k^2 + 54$	$-\frac{5}{36}k^4 - \frac{2}{3}k^3 + \frac{8}{9}k^2 + \frac{32}{3}k + \frac{448}{27}$
Singular k	$-6, 21$	$-4, 12$
Polygon(s)	No.5, 6	No.7, 8, 9, 10
$a(k)$	$\frac{5}{6}k^2 + \frac{5}{2}k + \frac{5}{3}$	$\frac{1}{2}k^2 + k$
$b(k)$	$-\frac{5}{27}k^4 - \frac{5}{24}k^3 + \frac{5}{9}k^2 + \frac{19}{6}k + \frac{395}{108}$	$-\frac{1}{24}k^4 - \frac{1}{12}k^3 + \frac{1}{4}k^2 + k + 1$
Singular k	$-3, \frac{5}{2}(1 \pm \sqrt{5})$	$-3, -2, 6$
Polygon(s)	No.11, 12	No.13, 15
$a(k)$	$\frac{1}{3}k^2 + \frac{1}{2}k - \frac{1}{3}$	$\frac{1}{3}k^2 - \frac{1}{3}$
$b(k)$	$-\frac{1}{36}k^4 - \frac{1}{24}k^3 + \frac{5}{36}k^2 + \frac{1}{3}k + \frac{35}{108}$	$-\frac{1}{36}k^4 + \frac{5}{36}k^2 + \frac{2}{27}$
Singular k	$-1, \kappa_{1,2,3}$	$0, \pm4$
Polygon(s)	No.14	No.16
$a(k)$	$\frac{1}{6}k^2 + \frac{1}{2}k - \frac{1}{3}$	$\frac{1}{2}k$
$b(k)$	$-\frac{1}{72}k^4 - \frac{1}{24}k^3 + \frac{1}{18}k^2 + \frac{1}{6}k + \frac{19}{108}$	$-\frac{1}{24}k^3 + \frac{1}{4}$
Singular k	$\kappa_{5,6,7,8}$	$-3, \frac{3}{2}(-1 \pm i\sqrt{3})$

TABLE 4.2.1: The data of the elliptic curves for reflexive polygons with maximally tempered coefficients. We also list the values of k when the spectral curve becomes singular for each case. Here, $\kappa_{1,2,3}$ are the three roots to $k^3 + k^2 - 18k - 43 = 0$ ($\kappa_1 \approx 4.73$, $\kappa_{2,3} \approx -2.86 \pm 0.94i$) while $\kappa_{5,6,7,8}$ are the four roots to $k^4 + k^3 - 8k^2 - 36 - 11 = 0$ ($\kappa_5 \approx -0.33$, $\kappa_6 \approx 3.80$, $\kappa_{7,8} \approx -2.23 \pm 1.94i$).

We find that specular duals have exactly the same elliptic curve. Notice that this property only holds for maximally tempered coefficients[4]. Recall that the maximally tempered coefficients indicate the number of perfect matchings for each lattice point and that specular duality exchange internal and external perfect matchings. Again, we see that maximally tempered coefficients are of particular physical interest.

We also tabulate all the values of k that make each spectral curve $P = 0$ singular in Table 4.2.1. They can be obtained by checking whether the discriminant of the curve vanishes. It is worth mentioning that in many cases, there exists a singular k such that $|k|$ is equal to the minimal number of internal perfect matchings for the polygon. For instance, No.4 has four toric phases, the numbers of internal perfect matchings are 12, 12, 14 and 21 respectively. Indeed, there is a singular

---

[4]In Appendix D.1, for example, we list the elliptic curves for the same polygons but with minimally tempered coefficients, and specular duals do not give the same elliptic curves anymore.

$k = |k| = 12$. However, five of the reflexive polygons do not obey this observation: No. 5, 6, 11, 14 and 12. We find that the first four polygons coincide with the exceptional cases in Remark 16 while No.12 is the specular dual of (the exceptional) No.11.

Dessins d'Enfants Given the elliptic curves in Table 4.2.1, we can then compute their j-invariants as in Table 4.2.2. Notice that in terms of the k parameter, this is a map $j : \mathbb{P}^1 \to$

Polygon(s)	No.1	No.2, 3, 4	No.5, 6	No.7, 8, 9, 10
$j(k)$	$\frac{(k-18)^3(k+6)}{k-21}$	$\frac{(k^2-8k-32)^3}{k^2-8k-48}$	$\frac{(k^4-40k^2-120k-80)^3}{(k+3)^5(k^2-5k-25)}$	$\frac{k^3(k^3-24k-48)^3}{(k-6)(k+2)^3(k+3)^2}$
Polygon(s)	No.11, 12	No.13, 15	No.14	No.16
$j(k)$	$\frac{(k^4-16k^2-24k+16)^3}{(k+1)^2(k^3+k^2-18k-43)}$	$\frac{(k^4-16k^2+16)^3}{k^2(k^2-16)}$	$\frac{(k^4-8k^2-24k+16)^3}{k^4+k^3-8k^2-36k-11}$	$\frac{k^3(k^3-24)^3}{k^3-27}$

TABLE 4.2.2: The j-invariants for the elliptic curves.

$\mathbb{P}^1, k \mapsto j(k)$. In particular, the preimage $\mathbb{P}^1 \cong S^2$ is the space of k, and hence parametrizes the Mahler flow. We will discuss this in more details in §4.2.4. By further checking $j(k)/1728$, we find that all of them are Belyi. Therefore, we can plot the corresponding dessins as in Figure 4.2.1 based on the `Mathematica` package from [181].

(A) No.1: $\{1^1 3^1, 2^2, 1^1 3^1\}$, $\Gamma_0(3)$

(B) No.2, 3, 4: $\{3^2, 2^3, 1^2 4^1\}$, $\Gamma_0(4)$

(C) No.5, 6: $\{3^4, 2^6, 1^2 5^2\}$, $\Gamma_1(5)$

(D) No.7, 8, 9, 10: $\{3^4, 2^6, 1^1 2^1 3^1 6^1\}$, $\Gamma_0(6)$

(E) No.11, 12: $\{3^4, 2^6, 1^3 9^1\}$, $\Gamma_0(9)$

(F) No.13, 15: $\{3^4, 2^6, 1^2 2^1 8^1\}$, $\Gamma_0(8)$

(G) No.14: $\{3^4, 2^6, 1^3 9^1\}$, $\Gamma_0(9)$

(H) No.16: $\{3^4, 2^6, 1^3 9^1\}$, $\Gamma_0(9)$
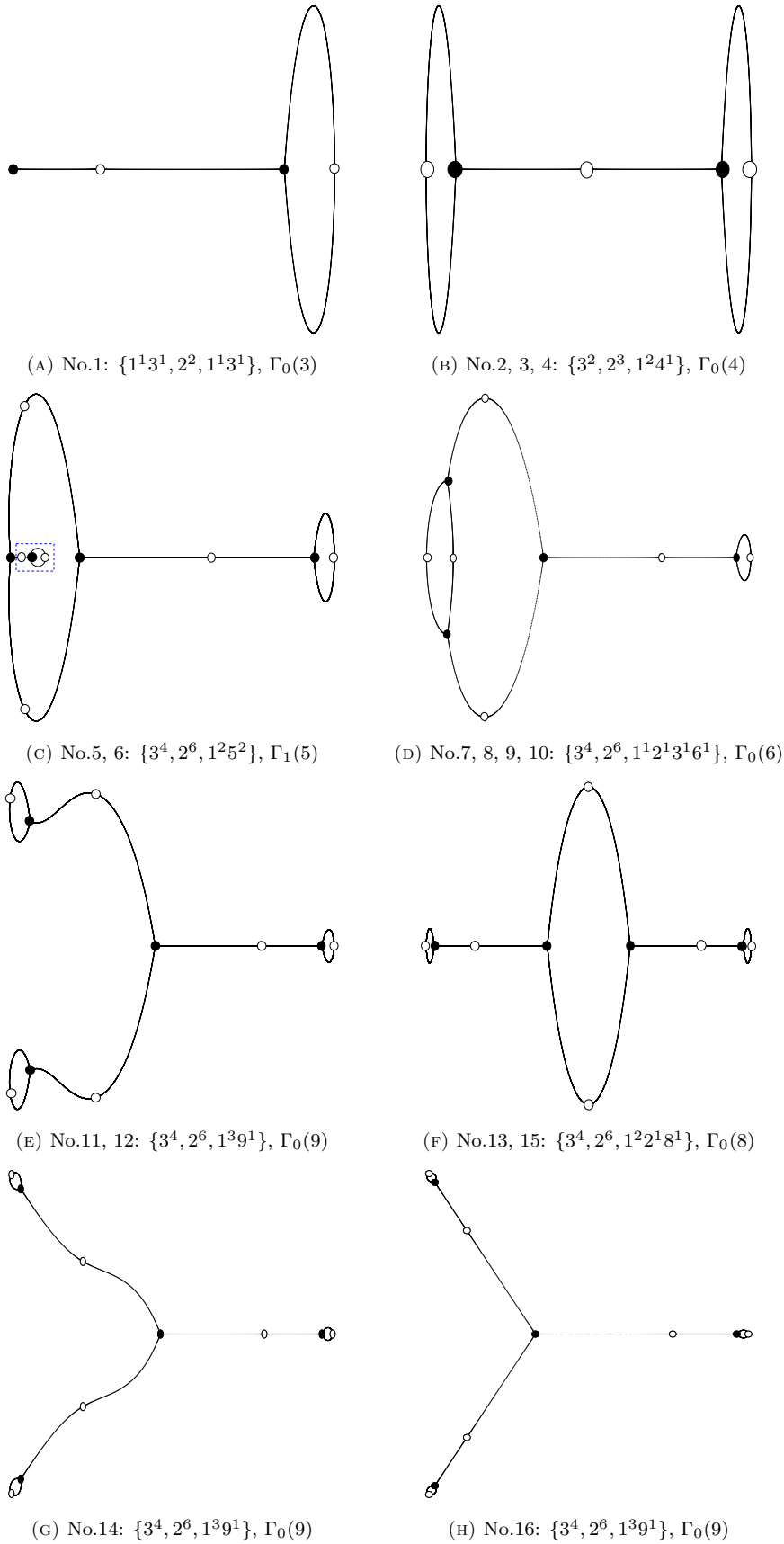
FIGURE 4.2.1: The dessins for reflexive polygons with maximally tempered coefficients, their passports and the corresponding congruence subgroups.

Here, the plots for the dessins are rigid in the sense that the vertices and edges are at the precise

positions of $k = j^{-1}$ on $S^2 \cong \mathbb{C} \sqcup \{\infty\}$ (except the part in the dashed blue box in (c) where we have to zoom in since the vertices $j^{-1}(0)$ and $j^{-1}(1)$ are too close to each other). As a result, the dessins in (e, g, h) have different "shapes" though they are isomorphic graphs[5].

As we have checked the reflexive polygons case by case, we conclude that

Proposition 4.2.3. *With maximally tempered coefficients for all 16 reflexive polygons, the family of elliptic curves, depending on k, are modular elliptic surfaces such that the j-invariants $j(k)$ are Belyi maps. Furthermore, specular dual reflexive polygons, regardless of which toric phases, give rise to the same elliptic curve, and hence the same j-invariant and dessin.*

Remark 17. *Different toric phases for a reflexive polygon are often not related by specular duality, but they would still lead to the same elliptic curve/dessin as these phases would only differ by the multiplicity of the interior point. Since the master space is invariant under specular duality, this hints that the corresponding elliptic curve and dessin should encode some common features of the master spaces in different phases.*

Remark 18. *In fact, $j(k)/1728$ being Belyi is generally true only for maximally tempered coefficients. For any other coefficient choices which are not physical in the sense of counting perfect matchings, the maps may or may not be Belyi. See Appendix D.1 for example.*

Although specular duals have the same elliptic curve, this does not directly imply that they should have the same Mahler measure as the Weierstrass normal form is obtained from the spectral curve under some bi-rational transformation while Mahler measure is only $GL(2, \mathbb{Z})$ invariant. Of course, we can compute the Mahler measures for reflexive polygons and likewise check case by case to show that specular duals have the same Mahler measure. Nevertheless, there is a more general proof using the Corollary 3.2.14.1, which we recall here for convenience:

Lemma 4.2.4. *Given a pair of specular duals a and b, suppose that the perfect matchings are mapped under $M_i^a \leftrightarrow M_i^b$. If their Newton polynomials are $P_{a,b}(z, w) = k - p_{a,b}(z, w)$, then for $|k| \geq \max\limits_{|z|=|w|=1} (|p_a|, |p_b|)$, the two Mahler measures have the series expansions*

$$m(P_{a,b}) = \log(k) - \sum_{n=2}^{\infty} \frac{f_n(M_i^{a,b})}{nk^n}, \qquad (4.2.2)$$

where f_n are functions of $M_i^{a,b}$, and we have simply used $M_i^{a,b}$ to denote the weight for the corresponding perfect matching.

Now we can "unrefine" this by taking $M_i^{a,b} = 1$. Then, we get the maximally tempered coefficients since they give the numbers of corresponding perfect matchings for the lattice points. Therefore,

Proposition 4.2.5. *With maximally tempered coefficients, the Mahler measure is invariant under specular duality.*

In particular,

Corollary 4.2.5.1. *The reflexive polygons with maximally tempered coefficients have the same Mahler measure under specular duality.*

Remark 19. *As Proposition 4.2.5 is a general statement, if two non-reflexive polygons have specular dual phases, then they would also have the same Mahler measure. Notice however the maximally tempered coefficients would now also fix all the coefficients for the interior points to be the corresponding numbers of perfect matchings except the origin with coefficient k.*

Remark 20. *As Mahler measure is $GL(2, \mathbb{Z})$ invariant, equivalent lattice polygons which are classified up to $SL(2, \mathbb{Z})$ transformations would have the same Mahler measure.*

---

[5]It is worth noting that as shown in [182], the Coulomb branches of rank-1 E_n 5d SCFTs, whose brane web constructions are dual to the (P)dP$_n$ polygons, are exactly the modular curves associated to the congruence of the dessins, except $\tilde{E}_1$ (No.14) and E_2 (No.12). The k parameter is closely related to the U-plane in such context.

For reference, we list the Mahler measures for reflexive polygons with maximally tempered coefficients in Table 4.2.3.

No.1	$\log(k) - \frac{27}{k^2} - \frac{164}{k^3} - \frac{4941}{2k^4} - \frac{31752}{k^5} - \frac{479940}{k^6} - \frac{7426080}{k^7}$ $- \frac{482173965}{4k^8} - \frac{6030521840}{3k^9} - \frac{171779570802}{5k^{10}} - \cdots$
No.2, 3, 4	$\log(k) - \frac{10}{k^2} - \frac{32}{k^3} - \frac{297}{k^4} - \frac{2112}{k^5} - \frac{55720}{3k^6} - \frac{163200}{k^7}$ $- \frac{3038665}{2k^8} - \frac{43406720}{3k^9} - \frac{141433992}{k^{10}} - \cdots$
No.5, 6	$\log(k) - \frac{5}{k^2} - \frac{10}{k^3} - \frac{135}{2k^4} - \frac{312}{k^5} - \frac{5675}{3k^6} - \frac{11100}{k^7}$ $- \frac{280175}{4k^8} - \frac{1346800}{3k^9} - \frac{2962386}{k^{10}} - \cdots$
No.7, 8, 9, 10	$\log(k) - \frac{3}{k^2} - \frac{4}{k^3} - \frac{45}{2k^4} - \frac{72}{k^5} - \frac{340}{k^6} - \frac{1440}{k^7}$ $- \frac{27405}{4k^8} - \frac{96880}{3k^9} - \frac{794178}{5k^{10}} - \cdots$
No.11, 12	$\log(k) - \frac{2}{k^2} - \frac{2}{k^3} - \frac{9}{k^4} - \frac{24}{k^5} - \frac{245}{3k^6} - \frac{200}{k^7}$ $- \frac{2065}{2k^8} - \frac{12320}{3k^9} - \frac{75852}{5k^{10}} - \cdots$
No.13, 15	$\log(k) - \frac{2}{k^2} - \frac{9}{k^4} - \frac{200}{3k^6} - \frac{1225}{2k^8} - \frac{31752}{5k^{10}} - \cdots$ $= \log k - 2k^{-2}\,{}_4F_3\left(1, 1, \frac{3}{2}, \frac{3}{2}; 2, 2, 2; 16k^{-2}\right)$
No.14	$\log(k) - \frac{1}{k^2} - \frac{2}{k^3} - \frac{3}{2k^4} - \frac{12}{k^5} - \frac{55}{3k^6} - \frac{60}{k^7}$ $- \frac{875}{4k^8} - \frac{1400}{3k^9} - \frac{9576}{5k^{10}} - \cdots$
No.16	$\log(k) - \frac{2}{k^3} - \frac{15}{k^6} - \frac{560}{3k^9} - \cdots$ $= \log(k) - 6k^{-3}\,{}_4F_3\left(1, 1, \frac{4}{3}, \frac{5}{3}; 2, 2, 2; 27k^{-3}\right)$

TABLE 4.2.3: The Mahler measure up to order 10 for reflexive polygons with maximally tempered coefficients. Here, we restrict $k \geq \max\limits_{|z|=|w|=1}\{|p(z,w)|\}$.

It is then also straightforward to get the expression for $u_0(k)$, which reads

$$u_0(k) = 1 + \sum_{n=2}^{\infty} \frac{nc_n}{k^n}, \quad \text{if } m(P) = \log(k) - \sum_{n=2}^{\infty} \frac{c_n}{k^n}. \tag{4.2.3}$$

Remark 21. *When the Newton polynomials have maximally tempered coefficients, as both Mahler measure/$u_0(k)$ and the dessins are invariant under specular duality and should encode certain information of the master space, it would be natural to associate Mahler measures and dessins with each other.*

4.2.2 Hauptmoduln and the k parameter

In this subsection, we shall give more clues on the connection between Mahler measure and dessins, as well as to congruence groups. Let us consider the modular expansion of Mahler measure and illustrate this with a few examples.

Example 1: No.15 As reviewed in §4.1.1, the Mahler measure for $P = k - z - z^{-1} - w - w^{-1}$ reads

$$m(P) = \frac{16\mathrm{Im}\tau}{\pi^2} \sum_{\substack{n_1,n_2\in\mathbb{Z} \\ (n_1,n_2)\neq(0,0)}} \frac{\chi_{-4}(n_1)}{(n_1 + 4n_2\tau)^2(n_1 + 4n_2\bar{\tau})}. \tag{4.2.4}$$

Of particular interest here would be the parameter k, where [183]

$$k^2 = \frac{\eta^{24}(2\tau)}{\eta^8(\tau)\eta^{16}(4\tau)} = q^{-1} + 8 + 20q - 62q^3 + 216q^5 - \dots, \tag{4.2.5}$$

with $\eta(\tau)$ being the Dedekind eta function. This is a Hauptmodul for $\Gamma_0(4)$. In particular, the congruence subgroup associated to the dessin in this case is $\Gamma_0(8)$, which is a subgroup of $\Gamma_0(4)$.

Example 2: No.16 The Newton polynomial is $P = k - z - w - z^{-1}w^{-1}$. One can compute that

$$u_0(k) = {}_2F_1\left(\frac{1}{3}, \frac{2}{3}; 1; \frac{27}{k^3}\right). \tag{4.2.6}$$

For convenience, we write $\mu \equiv 1/k^3$. Then we have [50]

$$u_0 = 1 + 6\sum_{n=1}^{\infty}\sum_{d|n} \chi_{-3}(d)q^n, \quad e = 1 - 9\sum_{n=1}^{\infty}\sum_{d|n} d^2\chi_{-3}(d)q^n,$$

$$\mu = \frac{1}{27}\left(1 - \frac{e}{c^3}\right) = q - 15q^2 + 171q^3 - 1679q^4 + \dots, \tag{4.2.7}$$

where $\chi_{-3}(n) = 0, 1, -1$ when $n \equiv 0, 1, 2 \pmod 3$. The Mahler measure is

$$m(P) = \frac{81\sqrt{3}\mathrm{Im}\tau}{4\pi^2} \sum_{\substack{n_1,n_2\in\mathbb{Z} \\ (n_1,n_2)\neq(0,0)}} \frac{\chi_{-3}(n_1)}{(n_1 + 3n_2\tau)^2(n_1 + 3n_2\bar\tau)}. \tag{4.2.8}$$

Moreover, we have [183]

$$k^3 = 1/\mu = 27 + \left(\frac{\eta(\tau)}{\eta(3\tau)}\right)^{12} = 27 + \frac{1}{q} - 12 + 54q - 76q^2 - 243q^3 + 1188q^4 - 1384q^5 + \dots \tag{4.2.9}$$

This is a Hauptmodul for $\Gamma_0(3)$. In particular, the congruence subgroup associated to the dessin in this case is $\Gamma_0(9)$, which is a subgroup of $\Gamma_0(3)$.

Example 3: No. 5, 6 The Newton polynomials are $P = k - z - z^{-1}w^2 - z^{-1}w^{-1} - w^{-1} - 2w - 3z^{-1}w - 3z^{-1}$ for No.5 and $P = k - z - w - z^{-1}w - z^{-1}w^{-1} - zw^{-1} - 2z^{-1} - 2w^{-1}$ for No.6. This has actually been computed in [184, 185]:

$$u_0 = 1 + \frac{1}{2}\sum_{n=1}^{\infty}\left((3-\mathrm{i})\chi(n) + (3+\mathrm{i})\overline{\chi(n)}\right)\frac{q^n}{1-q^n},$$

$$e = 1 + \frac{1}{2}\sum_{n=1}^{\infty}\left((2-\mathrm{i})\chi(n) + (2+\mathrm{i})\overline{\chi(n)}\right)\frac{n^2q^n}{1-q^n}, \tag{4.2.10}$$

$$m(P) = -2\pi\mathrm{i}\tau - \frac{1}{2}\sum_{n=1}^{\infty}\sum_{d|n}\left((2-\mathrm{i})\chi(d) + (2+\mathrm{i})\overline{\chi(d)}\right)nq^n,$$

where $\chi(n) = \mathrm{i}^l$ when $n \equiv 2^l \pmod 5$. Moreover, we have

$$(k-3)^{-1} = q\prod_{n=1}^{\infty}(1-q^n)^{5\left(\frac{n}{5}\right)} = 3 + q - 5q^2 + 15q^3 - 30q^4 + 40q^5 - \dots, \tag{4.2.11}$$

where $\left(\frac{n}{5}\right) = (-1)^l$ when $n \equiv 2^l \pmod 5$. This is a Hauptmodul for $\Gamma_1(5)$. In particular, the congruence subgroup associated to the dessin in this case is $\Gamma_1(5)$.

Example 4: No.7, 8, 9, 10 This has actually been computed in [184, 185]:

$$u_0 = \frac{\eta(2\tau)\eta^6(3\tau)}{\eta^2(\tau)\eta^3(6\tau)},$$

$$e = 1 + \sum_{n=1}^{\infty} (-1)^n \chi_{-3}(n) \frac{n^2 q^n}{1 - q^n}, \qquad (4.2.12)$$

$$m(P) = -2\pi \mathrm{i}\tau - \sum_{n=1}^{\infty} \sum_{d|n} (-1)^d \chi_{-3}(d) n q^n,$$

where $\chi_{-3}(n)$ is the same as in Example 2. Moreover, we have

$$k - 2 = \frac{\eta^3(2\tau)\eta^9(3\tau)}{\eta^3(\tau)\eta^9(6\tau)} = \frac{1}{q} + 3 + 6q + 4q^2 - 3q^3 - 12q^4 - 8q^5 + \dots \qquad (4.2.13)$$

This is a Hauptmodul for $\Gamma_0(6)$. In particular, the congruence subgroup associated to the dessin in this case is $\Gamma_0(6)$.

As we can see, the k parameter is closely related to the Hauptmodul of certain congruence subgroup[6]. We may also conjecture that

Conjecture 4.2.6. *Let Γ^a be the congruence subgroup associated to the dessin for the reflexive polygons (with maximally tempered coefficients). Then k^n is a Hauptmodul for some congruence subgroup Γ^b, and $\Gamma^a \leq \Gamma^b$. Moreover, Γ^b is the monodromy group of the corresponding Picard-Fuchs equation.*

We may even give a stronger conjecture.

Conjecture 4.2.7. *If $\Gamma^a = \Gamma_{l_1}(r_1)$ and $\Gamma^b = \Gamma_{l_2}(r_2)$ (where $l_{1,2} = 0, 1$), then $l_1 = l_2$ and $r_1 = |n_2| r_2$.*

Here, we are focusing on the maximally tempered coefficients. Mathematically, we would also wonder whether the k parameters could be related to Hauptmoduln for certain congruence subgroups for any coefficients. In Appendix D.1, we give different types of examples for minimally tempered coefficients.

4.2.3 Mahler Measure and j-Invariant

As the Mahler measures and dessins are connected to each other, it should be possible to write $m(P)$ in terms of j. Let us first start with a rather general definition of periods introduced in [176]:

Definition 4.2.1. *A **period** is a complex number whose real and imaginary parts are values of absolutely convergent integrals of rational functions with rational coefficients, over domains in $\mathbb{R}$ given by polynomial inequalities with rational coefficients.*

As a matter of fact, the set of periods, which is countable, form an algebra under the usual sum and product operations. Famous constants such as π can be shown to be periods. In particular, when the Newton polynomial has rational coefficients, *the Mahler measure is a period* [176]. For those considered in this paper, i.e., $P(z, w) = k - p(z, w)$ with *any* tempered coefficients, this means $m(P)$ is a period when $k \in \mathbb{Q}$.

An important theorem in [176] says that

Theorem 4.2.8. *Consider $\mathrm{SL}(2, \mathbb{Z})$ or any of its subgroup of finite index. Let $f(z)$ be a modular form (either holomorphic or meromorphic) of some positive weight $\mathfrak{w}$ and let $t(z)$ be a modular function under the action of the group. Then $F(t(z)) \equiv f(z)$, which is multi-valued, satisfies a*

---

[6]Therefore, the Hauptmoduln, and hence the meromorphic functions on modular curves, should be related to the (sizes of) gas phases for dimer models and the Mahler flows [9, 139]

homogeneous linear differential equation of order $(\mathfrak{w} + 1)$, $\sum_{n=0}^{\mathfrak{w}+1} a_n F^n(t(z)) = 0$ *with* a_n *algebraic functions of* $t(z)$.

Since λ, u_0 and e are modular forms of weights 0, 1 and 3 respectively (though with singularities), and since $j(\tau)$ is a modular function, we have

Corollary 4.2.8.1. *The modular forms* $\lambda(j(\tau))$, $u_0(j(\tau))$ *and* $e(j(\tau))$ *satisfy linear differential equations (with respect to* j*) of order* 1, 2 *and* 4 *respectively.*

Recall that e generates the coefficients of $m(P)$ in q-series. It would therefore be reasonable to expect certain relations between Mahler measures and j-invariants.

Another crucial result in [176] says that

Theorem 4.2.9. *Let* $f(z)$ *be a modular form of positive weight* $\mathfrak{w}$ *and let* $t(z)$ *be a modular function, both defined over* $\overline{\mathbb{Q}}$. *Then* $\forall z_0 \in \mathfrak{h}$ *for which* $t(z_0)$ *is algebraic,* $\pi^{\mathfrak{w}} f(z_0)$ *is a period.*

We may now apply this theorem to the modular forms in our paper.

Corollary 4.2.9.1. *When* $j(\tau)$ *is algebraic,* $\lambda(j(\tau))$, $\pi u_0(j(\tau))$ *and* $\pi^3 e(j(\tau))$ *are periods.*

Moreover, when $j \in \overline{\mathbb{Q}}$, we also learn that q is transcendental following [186]. Since $m(P)$ is a period when $P \in \mathbb{Q}[z^{\pm 1}, w^{\pm 1}]$ and j is a rational function of k, we learn that $m(P)$ is a period if j is rational. In fact, we can extend this to j being algebraic. This is because $m(P)$ is a sum over λ^n/n with integer coefficients[7]. Now this follows from λ being a period and that periods form an algebra with countably many elements. Hence, we conclude that

Proposition 4.2.10. *The Mahler measure* $m(P)$ *is a period if* j *is algebraic.*

Since λ and u_0 satisfy certain differential equations, that is,

$$\lambda' = \alpha_0 \lambda, \quad u_0'' + \alpha_1 u_0' + \alpha_2 u_0 = 0, \tag{4.2.14}$$

where f' denotes the derivative with respect to j and $\alpha_{0,1,2}$ are differentiable algebraic functions of j, we can use the Mahler flow equation

$$\frac{\mathrm{d}m}{\mathrm{d}\log\lambda} = \lambda \frac{\mathrm{d}m}{\mathrm{d}\lambda} = -u_0 \tag{4.2.15}$$

to get

$$\lambda \frac{\mathrm{d}m}{\mathrm{d}j} \frac{1}{\lambda'} = \frac{1}{\alpha_0} m' = -u_0. \tag{4.2.16}$$

Plugging this into the Picard-Fuchs equation for u_0 (with respect to j) yields

$$m'''(j) + \left(\alpha_1 - \frac{2\alpha_0''}{\alpha_0}\right) m''(j) + \left(\alpha_2 - \frac{\alpha_1\alpha_0'}{\alpha_0} + \frac{2(\alpha_0')^2}{\alpha_0^2} - \frac{2\alpha_0'}{\alpha_0}\right) m'(j) = 0. \tag{4.2.17}$$

Tropical limit   Recall that $m \sim \log k$ in the tropical limit where $k \to \infty$. Likewise, we have $j \to \infty$ as $j(k)$ is a rational function $\frac{f_1(k)}{f_2(k)}$ with $\deg(f_1) > \deg(f_2)$. More precisely, $j \sim k^n$ in the tropical limit, where $n = \deg(f_1) - \deg(f_2)$ is the power for the external face in the passport of the corresponding dessin. Hence, in the tropical limit,

$$m \sim \frac{1}{n} \log j. \tag{4.2.18}$$

One may wonder whether for any j, $m(j)$ can be expressed by further adding a sum of $-c_l/j^l$ where $l \geq 2$ are integers and c_l are some coefficients. However, due to the multi-valuedness of k as a function of j, this would only be valid on one branch. Indeed, j could still diverge for some finite k while $m(j)$ would remain finite in this case.

---

[7]This can be seen from u_0 as its coefficients are integers that count F-term relations.

Remark 22. *Using the Mahler flow equation and the Picard-Fuchs equation* (4.1.6), *we may also write $m(P)$ as a differential equation with respect to λ as λ is of weight 0 (under the monodromy of Picard-Fuchs equation). Then the differential equation reads*

$$\lambda A \frac{\mathrm{d}^3 m(\lambda)}{\mathrm{d}\lambda^3} + (\lambda B + 2A) \frac{\mathrm{d}^2 m(\lambda)}{\mathrm{d}\lambda^2} + (\lambda C + B) \frac{\mathrm{d}m(\lambda)}{\mathrm{d}\lambda} = 0. \tag{4.2.19}$$

4.2.4 Mahler Flow and the $\tau_{R,G,B}$ Conjecture

There has been a long puzzle about the nature of brane tilings as bipartite graphs on $\mathbb{T}^2$ [8, 109, 173, 187, 188]. On the one hand, they could be interpreted as dessins[8] on $\mathbb{T}^2$, acquiring a complex structure called τ_B (the subscript B indicates its origin from Belyi) which is that of $\mathbb{T}^2$ as an elliptic curve.

On the other hand, the R-charges in the quiver theory obtained from the isoradial brane tiling correspond to angles of the faces in the tiling[9]. The R-charges would then determine the complex structure τ_R on the torus which supports the tiling. It would be natural to suspect that the two complex structures would coincide. However, as later discussed in [109, 187], counterexamples exist and this $\tau_B = \tau_R$ conjecture does not hold in general.

Furthermore, there is a third complex parameter called τ_G coming directly from the geometry of the CY3 singularity corresponding to the toric diagram. In particular, a $U(1)^2$ subgroup of the $\mathbb{T}^3$-action would leave the Kähler form and the holomorphic 3-form invariant. When the CY space is viewed as a special Lagrangian fibration, the $U(1)^2$ would then define an invariant part of such fibration, which turns out to be a torus. The metric on this torus, which is the pullback of the metric on the CY singularity, leads to the complex structure τ_G. As studied in [188], $\tau_{R,G,B}$ may sometimes be coincident with each other, but they do not always equal in general. Notice that when we say $\tau_{R,G,B}$ coincide, this is always up to $SL(2, \mathbb{Z})$ transformation. In practice, we would always compare $j(\tau_{R,G,B})$ as it is modular invariant. The $\tau_{R,G,B}$ conjecture is then to find when and how $j(\tau_{R,G,B})$ are all equal.

Since $j(k) = \frac{f_1(k)}{f_2(k)}$ where $f_{1,2}(k)$ are polynomials of k, the range of $j(k)$ is the whole $\mathbb{C} \sqcup \{\infty\}$. Therefore, no matter what value $j(\tau_{R,G,B})$ takes, there must be at least one k on $\mathbb{P}^1$ such that $j(\tau) = j(\tau_{R,G,B})$. Thus,

Proposition 4.2.11. *The Mahler flow extrapolates $\tau_{R,G,B}$.*

This is true in general, and not just restricted to the reflexive cases. Since we still have the freedom to choose the coefficients for the Newton polynomial even if the polygon is fixed, one may wonder which Mahler flow would be the appropriate choice. As τ_R originates from R-charges and R-charges are associated to angles in the isoradial (or even non-isoradial) tilings, instead of tempered coefficients, we shall always use the coefficients from the canonical edge weights on the tilings[10].

Example 18. *For (chiral) orbifolds of $\mathbb{C}^3$ and of the conifold ($\mathcal{C}$), the three complex structures coincide [109, 173, 187, 188], due to the hexagonal and square symmetries of the tiling. For instance, $j(k) = \frac{k^3(k^3-24)^3}{k^3-27}$ for dP_0, which is a $\mathbb{Z}/3$-orbifold of $\mathbb{C}^3$ and $j(\tau_{R,G,B}) = 0$. Solving $j(k) = j(k_{R,G,B})$, we find that the $\tau_{R,G,B}$ complex structure is located at*

$$k = 0, \ 2\sqrt[3]{3}, \ 2\sqrt[3]{3}e^{\pm 2\pi i/3} \tag{4.2.20}$$

on the sphere.

---

[8]They are embedded on $\mathbb{T}^2$ instead of $\mathbb{P}^1$ compared to the dessins discussed in this chapter so far.

[9]Recall from the previous chapter that we may also treat non-isoradial tilings as "isoradial" tilings in a similar manner if we allow zero or negative angles.

[10]Therefore, in $j(k) = \frac{f_1(k)}{f_2(k)}$, $f_{1,2}$ have algebraic coefficients.

As another example, $j(k) = \frac{(k^4 - 16k^2 + 16)^3}{k^2(k^2 - 16)}$ for F_0, a $\mathbb{Z}/2$-orbifold of $\mathcal{C}$ and $j(\tau_{R,G,B}) = 1728$. Solving $j(k) = j(k_{R,G,B})$, we find that the $\tau_{R,G,B}$ complex structure is located at

$$k = \pm 2\sqrt{2}, \ \pm\sqrt{2(4 + 3\sqrt{2})}, \ \pm i\sqrt{2(-4 + 3\sqrt{2})} \tag{4.2.21}$$

on the sphere.

Example 19. *Unlike the above example, the suspended pinch point (SPP) and its orbifolds have different $\tau_{R,G,B}$. For instance, $\mathrm{SPP}/\mathbb{Z}_2$ with action $(0,1,1,1)$ (No.8 in the list of reflexive polygons) has Newton polynomial*

$$P(z,w) = -2A^2 zw^2 - A^2 w^3 - A^2 z^2 w - 2ABw^2 - B^2 z - B^2 w + kzw \tag{4.2.22}$$

for canonical edge weights, where

$$A = \sin^2\left(\frac{\pi}{2\sqrt{3}}\right), \quad B = \sin\left(\left(1 - \frac{1}{\sqrt{3}}\right)\pi\right)\sin\left(\frac{1}{2}\left(1 - \frac{1}{\sqrt{3}}\right)\right). \tag{4.2.23}$$

Therefore,

$$j(k) = \frac{256C^3 k^3(-6 - 6Ck + C^3 k^3)^3}{(-3 + Ck)(1 + Ck)^3(3 + 2Ck)^2}, \tag{4.2.24}$$

where

$$C = \csc\left(\frac{\pi}{2\sqrt{3}}\right)\csc^2\left(\frac{\pi}{\sqrt{3}}\right). \tag{4.2.25}$$

As computed in [187],

$$j(\tau_B) = \frac{132304644}{5}, \quad j(\tau_R) = 287496. \tag{4.2.26}$$

Therefore, the τ_B complex structure is located at approximately

$$\begin{aligned}
k = &-1.112, \ 6.909, \ -2.898 \pm 5.439i, \ -6.157, \ -1.114, \ -0.752, \ 2.2260, \\
&-0.737 \pm 0.009i, \ 3.635 \pm 5.430i
\end{aligned} \tag{4.2.27}$$

while the τ_R complex structure is located at approximately

$$\begin{aligned}
k = &-1.107, \ 3.677, \ -1.285 \pm 2.392i, \ -2.892, \ -1.112, \ -0.785, \ 2.2261, \\
&-0.721 \pm 0.041, \ 2.006 \pm 2.351i
\end{aligned} \tag{4.2.28}$$

on the Mahler flow sphere.

Based on the known examples, it seems that the toric diagrams (e.g. $\mathbb{C}$ and $\mathcal{C}$) which satisfy the $\tau_B = \tau_R$ conjecture look more "symmetric" than those (e.g. SPP) do not satisfy the $\tau_B = \tau_R$ conjecture. It turns out that the coefficients from canonical weights for those more "symmetric" polygons coincide with the maximally tempered coefficients while those from canonical weights for the less "symmetric" ones do not agree with the maximally tempered coefficients. Based on the above examples, it is natural to conjecture that

Conjecture 4.2.12. *Up to* $\mathrm{SL}(2,\mathbb{Z})$*, the $\tau_B = \tau_R$ condition holds if and only if the maximally tempered coefficients of the Newton polynomial coincide with the coefficients from canonical edge weights on the tiling.*

Remark 23. *Our observation also agrees with the fact that those less "symmetric" cases have a more non-trivial a-maximization. In particular, it was shown in [9] that a-maximization is equivalent to maximization of Mahler measure with canonical weights. Therefore, the non-triviality of a-maximization can be interpreted as the discrepancy between maximally tempered and canonically weighted coefficients in terms of Mahler measure.*

4.3 Further Connections to String/F-Theory

In this section, we shall briefly discuss some relations with F-theory compactification and its BPS states/Gromov-Witten invariants. If we consider a sigma model whose target space is one of the non-compact CY 3-folds from the reflexive polygons, then its mirror is the Landau-Ginzburg theory with the W-plane $W = P(z, w)$. In particular, the BPS states from D-branes wrapping compact cycles can be studied via some F-theory background [157].

4.3.1 Dessins and 7-Branes

We recall that given an elliptic fibration over some complex base B with fibre $y^2 = x^3 + f(v)x + g(v)$ and $v \in B$, the F-theory compactified on it is equivalent to Type IIB compactification on B with complexified coupling τ. This coupling τ, which serves as the complex structure of the elliptic fibre, can be exactly identified as $\tau = \frac{1}{2\pi i} \frac{u_1}{u_0}$ in our modular Mahler measure discussions, and is defined up to $\mathrm{SL}(2, \mathbb{Z})$ transformations.

As mentioned before, the elliptic curve becomes singular and the fibre degenerates when the discriminant $\Delta = 4f^3 + 27g^2$ vanishes. These are the positions where (p, q) 7-branes are placed since τ is transformed by $\mathrm{SL}(2, \mathbb{Z})$ transformations under the monodromies around 7-branes in Type IIB. Here, let us consider the surface that corresponds to a toric diagram, which defines the CY singularity, or we can think of the geometry as a double fibration over the W-plane with a $\mathbb{C}^*$ fibre and a punctured Riemann surface $W = P(z, w)$. In particular, the surface is now over the base $\mathbb{P}^1$ parametrized by the k parameter with fibre $P(z, w)$.

From Table 4.2.1, we know that in our cases $f(k)$ and $g(k)$ are always of degrees 4 and 6 respectively. Therefore, one would expect Δ to be of degree 12. This would agree with the requirement of 12 7-branes in physics. However, it is possible for Δ to have degree less than 12. The reasons are that $4f^3 + 27g^2$ may have cancellations of terms. Nevertheless, as we shall now discuss, we are still able to recover the 12 7-branes, and we can actually put them on the dessin.

As the fibre degenerates at the n zeros of Δ (counted with multiplicity), there must be n 7-branes associated to them. It turns out that the remaining $(12 - n)$ 7-branes are compensated by $j \to \infty$ at the tropical limit, that is, $k \to \infty$. Indeed, by checking the degree of the numerator minus the degree of the denominator of j in Table 4.2.2, we find that they are precisely equal to 12 minus the degree of Δ. This actually makes sense since we are now considering the compact $\mathbb{P}^1$ as the space of k. Therefore, we should also take the singular curve at k tropical into account, which is just a usual point on the compact sphere.

As the corresponding dessin is parametrized by $\beta = j/1728$, one may consider to associate the 7-branes to the faces of the dessin. However, some 7-branes could still not correspond to the faces (both internal and external), i.e., $j \to \infty$. This is because the numerator and denominator of j may have some factors being cancelled. Suppose the j-invariant is

$$j = \frac{4 \times (24f)^3}{\Delta} = \frac{(k - k_*)^{n_1} f_1(k)}{(k - k_*)^{n_2} f_2(k)}, \tag{4.3.1}$$

where $n_1 > n_2$ and $f_{1,2}$ do not have any $(k - k_*)$ factor. As a result, $k = k_*$ is a zero of Δ which makes the curve singular, but this information is not encoded by $j \to \infty$ since such factors all get cancelled in the denominator. Nevertheless, as $n_1 > n_2$, we find that such 7-branes now correspond to a black node (pre-image of $j = 0$) in the dessin.

Notice that we have not considered the possibility of $n_1 = n_2$. If so, then such number of 7-branes would not correspond to a face or a black vertex in the dessin. We shall then write[11]

$$f = (k - k_*)^{2n} f_a, \quad g = (k - k_*)^{3n} g_b, \tag{4.3.2}$$

---

[11] Notice that we do not have any further restrictions on f_a and g_b, so they could still have common factors. However, (4.3.2) suffices to complete our argument as we only need to know whether 7-branes could be associated to places other than faces and black vertices.

where the subscripts a, b indicate the degree of f_a and g_b. This is because now the j-invariant looks like

$$j = 4 \times 24^3 \times \frac{(k - k_*)^{6n} f_a^3}{4(k - k_*)^{6n} f_a^3 + 27(k - k_*)^{6n} g_b^2}. \tag{4.3.3}$$

Since the degrees of f and g are 4 and 6 respectively, n can only be 1 or 2.

Let us first consider the case $n = 2$. Then $a = b = 0$. In other words, $f^3 \propto g^2$. In this case, the j-invariant is trivially a constant, and the dessin is empty. Equivalently, we can think of it as the external face where all the 7-branes live being the whole sphere with no other elements for the dessin.

If $n = 1$, then we can write the elliptic curve as

$$\frac{y^2}{(k - k_*)^3} = \frac{x^3}{(k - k_*)^3} + \frac{f_2 x}{(k - k_*)} + g_3. \tag{4.3.4}$$

Under the redefinition $x/(k - k_*) \to x$ and $y/(k - k_*)^{3/2} \to y$, we get the Weierstrass normal form

$$y^2 = x^3 + f_2 x + g_3, \tag{4.3.5}$$

where f_2 and g_3 are of degrees 2 and 3. Hence, no matter what value k_* is, we would only get the same curve, and we are only left with six 7-branes.

We have therefore shown that

Theorem 4.3.1. *On the dessin, all the faces (including both internal and external) and some of the black vertices (the pre-images $j = 0$) correspond to 7-branes. A black vertex at $k = k_*$ is associated to 7-branes if and only if $j(k_*) = 0$ and $\Delta(k_*) = 0$.*

Example 20. *Let us illustrate this with an example whose 7-branes are associated to both faces and a black vertex. The dessin for the reflexive polygon No.1 is given in Figure 4.2.1(a). Moreover,*

$$\Delta = (k + 6)^8 (k - 21), \quad j = \frac{(k - 18)^3 (k + 6)}{k - 21}. \tag{4.3.6}$$

Hence, there is a 7-brane located at the centre $k = 21$ of the internal face. Moreover, since there is a zero of order 8 for Δ at $k = -6$, this would give eight 7-branes on top of each other. As j is also zero in this case, we find that the eight 7-branes correspond to the leftmost black vertex in the dessin. So far, we have only found nine 7-branes. The remaining three are placed at the tropical k in the external face on the sphere. Indeed, we have $j \to k^3$ when $k \to \infty$.

It is worth noting that when j diverges at say $k = k_*$, near this point we have $j \sim \frac{1}{k - k_*}$. This yields $\tau \sim \frac{1}{2\pi i} \log(k - k_*)$. When $k \to k_*$, we get $\tau \to i\infty$. As $\tau = \frac{\theta}{2\pi} + \frac{i}{g_{\text{IIB}}}$, we have $g_{\text{IIB}} \to 0$. Notice that this weak coupling regime is only local due to the $\text{SL}(2, \mathbb{Z})$ transformation. In the special case when $f^3 \propto g^2$, j becomes a constant. In particular, when f^3/g^2 is $\frac{-3}{4^{1/3}}$, we have a global weak coupling [189, 190].

Brane monodromy and dessin monodromy   The non-trivial effect of passing the branch cut of a (p, q) 7-brane is often encoded by the monodromy matrix $M_{p,q} \in \text{SL}(2, \mathbb{Z})$ [191]. In fact, we can relate the monodromy group G of the dessin generated by $(\sigma_0, \sigma_1, \sigma_\infty)$ to the monodromies of the 7-branes.

The general strategy is as follows. First, we choose a reference point on the dessin, just like what one does for 7-branes. As the monodromy for a 7-brane is analyzed by a loop going around the branch cut connecting the brane and the reference point, we also go along the loops on the dessin surrounding the reference point and the internal faces/black vertices where the 7-branes are. Then these loops would correspond to some permutations $\sigma^i \in G$ which can be obtained from the generators (σ_0, σ_1). Finally, we can determine the permutation for the external face, namely the tropical limit $k \to \infty$, using $\prod \sigma^i = 1$ as $\prod M_{p,q} = 1$. Notice that this identity also guarantees that the permutation for the external face must be an element of G.

Example 21. *Let us illustrate this again with the reflexive polygon No.1. In Figure 4.3.1, we label the edges and plot the monodromies explicitly on the dessin. It is then easy to see that the*
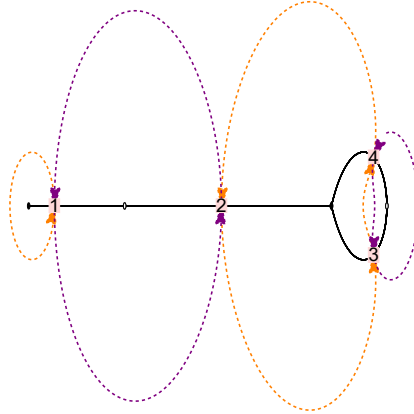
FIGURE 4.3.1: The dessin associated to $\Gamma_0(3)$ with passport $\{1^1 3^1, 2^2, 1^1 3^1\}$. Here, the numbers are the labels of the edges, and the orange (purple) cycles indicate the permutations around black (white) vertices.

monodromy group G is generated by $\sigma_0 = \{(1), (234)\}$ and $\sigma_1 = \{(12), (34)\}$. This is a subgroup of $\mathfrak{S}_4$ with $|G| = 12$. From $\sigma_\infty \circ \sigma_1 \circ \sigma_0 = 1$, we get $\sigma_\infty = \{(142)\}$.

Now for instance, let us choose a point on edge 2 as reference point. Then the monodromy for the 7-brane associated to the internal face can be chosen to correspond to the permutation $\sigma^a = (234)$ while the (total) monodromy associated to the leftmost black vertex can be chosen to correspond to $\sigma^b = (12)$. As a result, the (total) monodromy for the 7-branes associated to the external face is $\sigma^c = (2143)$ so that $\sigma^c \circ \sigma^b \circ \sigma^a = 1$. It is obvious that $\sigma^a \in \sigma_0$, $\sigma^b \in \sigma_1$ and $\sigma^c = (\sigma^b \circ \sigma^a)^{-1}$ all belong to G.

As the choice for (p, q) is not unique, alternatively we may also choose for example $\sigma^a = (234)(34) = (23)$ and $\sigma^b = (12)$. Then $\sigma^c = (213)$.

A comment on F-theory on elliptically fibred K3 It is well-known that the compactification of F-theory on an elliptically fibred K3 surface is dual to heterotic string theory compactified on $\mathbb{T}^2$. In this setting, the elliptic fibre is still $y^2 = x^3 + f(k)x + g(k)$ with $k \in \mathbb{P}^1$, but now the degrees of f and g become 8 and 12 respectively. Hence, the number of 7-branes is 24. Although the graph consisting of edges connecting black and white vertices may not be a dessin or even be bipartite any more, the above discussions should still apply following the similar methods.

4.3.2   Mahler Measure and Gromov-Witten Invariants

When the F-theory is compactified on one of our CY 3-folds, its effective theory is a closed subsector of the type II compactification. The BPS states of the F-theory compactification should then give a subsector of those in the full Type II theory. In [192, 193], such instanton expansions were computed. In particular, the GW invariants of local vanishing del Pezzo surfaces (independently of the global embedding in the CY spaces where F-theory compactifies) were observed to coincide with certain modular expansions of Mahler measures from the same toric diagrams later in [185]. It could also be possible that the GW invariants of any vanishing 4-cycles could be recovered from such modular expansions from the corresponding toric diagrams according to the dictionary of the two sides.

As an elliptic curve is topologically $\mathbb{T}^2$, the periods are given by $\tilde{\phi}$ and $\tilde{\phi}_D$ following the notations of [193]. Then we shall identify the gauge coupling $\partial\tilde{\phi}_D/\partial\tilde{\phi}$ with τ on the modular Mahler measure

side, that is,

$$\tau \sim \frac{\partial \tilde{\phi}_D}{\partial \tilde{\phi}}. \tag{4.3.7}$$

The instanton expansions in [193] are worked out at the large complex structure point $c = 0$, where $c = \mathrm{e}^{2\pi i \tilde{\phi}} + \ldots$ provides a coordinate on the moduli space. This corresponds to the tropical limit $k \to \infty$, or equivalently, $q \to 0$. A natural ansatz for the correspondence would then be

$$c \sim q^\nu \tag{4.3.8}$$

for some $\nu \in \mathbb{Z}^+$.

In order to have the correspondence consistent, our goal is to show that this leads to the correspondence between the Yukawa coupling $C_{\tilde{\phi}\tilde{\phi}\tilde{\phi}}$ in [193] and $\frac{\mathrm{d}\log q}{\mathrm{d}m}$ in [185]. In particular, they have the expansions

$$C_{\tilde{\phi}\tilde{\phi}\tilde{\phi}} = c_0 + \sum_{n=1}^{\infty} \frac{\mathfrak{a}_n n^3 q_{\tilde{\phi}}^n}{1 - q_{\tilde{\phi}}^n}, \quad \frac{\mathrm{d}\log q}{\mathrm{d}m} = -1 + \sum_{n=1}^{\infty} \frac{a_n n^3 (\mathrm{e}^{-\nu m})^n}{1 - (\mathrm{e}^{-\nu m})^n}, \tag{4.3.9}$$

where $q_{\tilde{\phi}} := \mathrm{e}^{2\pi i \tilde{\phi}}$ and ν, c_0 are some positive constants depending on different cases. Then a_n coincides with the GW invariants $\mathfrak{a}_n$ up to the constant c_0, that is, $\mathfrak{a}_n = -c_0 a_n$.

Following these two expansions, we should have

$$\mathrm{e}^{-\nu m} \sim q_{\tilde{\phi}} = \mathrm{e}^{2\pi i \tilde{\phi}}. \tag{4.3.10}$$

Indeed, the expansion for q^ν is $q^\nu = \mathrm{e}^{-\nu m} + \ldots$, which agrees with $c = \mathrm{e}^{2\pi i \tilde{\phi}} + \ldots$. Now, since $m = -2\pi i \tau - \ldots$, we have $m \sim -2\pi i \tau$. This would yield $\tilde{\phi} \sim \nu\tau$. As $u_0 \sim 1$, we shall further tune the constant factor to be

$$\tilde{\phi} \sim -c_0 \tau u_0. \tag{4.3.11}$$

The reason is that with

$$\tilde{\phi}_D \sim -\frac{1}{2\pi i} c_0 \tau u_1, \tag{4.3.12}$$

using $u_1 \sim u_0 \log \lambda \sim u_0 \log q = 2\pi i \tau u_0$, we can recover

$$\frac{\partial \tilde{\phi}_D}{\partial \tilde{\phi}} = \frac{\partial \tilde{\phi}_D / \partial \tau}{\partial \tilde{\phi} / \partial \tau} \sim \frac{1}{2\pi i} \frac{c_0 \partial u_1 / \partial \tau}{c_0 u_0} = \tau. \tag{4.3.13}$$

Now we are ready to show that

$$C_{\tilde{\phi}\tilde{\phi}\tilde{\phi}} \sim -c_0 \frac{\mathrm{d}\log q}{\mathrm{d}m}, \tag{4.3.14}$$

where

$$C_{\tilde{\phi}\tilde{\phi}\tilde{\phi}} = \frac{\partial^2 \tilde{\phi}_D}{\partial \tilde{\phi}^2} \sim \frac{\partial \tau}{\partial \tilde{\phi}}. \tag{4.3.15}$$

This can be seen as follows. Since $\lambda = q + \ldots$, we have

$$-\frac{\mathrm{d}m}{\mathrm{d}\log q} = -\frac{\mathrm{d}m}{\mathrm{d}\log \lambda} = u_0. \tag{4.3.16}$$

On the other hand,

$$\frac{\partial \tilde{\phi}}{\partial \tau} \sim \frac{\partial(-c_0 \tau u_0)}{\partial \tau} = -c_0 u_0. \tag{4.3.17}$$

Thus,

$$C_{\tilde{\phi}\tilde{\phi}\tilde{\phi}} \sim -\frac{1}{c_0 u_0} \sim -c_0 \frac{\mathrm{d}\log q}{\mathrm{d}m}. \tag{4.3.18}$$

Since we are working at the large complex structure point/tropical limit, "$\sim$" can be turned into "$=$". To summarize, the correspondence of quantities between Mahler measure and GW invariants is listed in Table 4.3.1. This generalizes the observations in [185].

Mahler	$-c_0\tau u_0$	$-\frac{1}{4\pi i}c_0\tau u_1$	τ	q^ν	$\mathrm{e}^{-\nu m}$	$-c_0\frac{\mathrm{d}\log q}{\mathrm{d}m}$
GW	$\tilde{\phi}$	$\tilde{\phi}_D$	$\partial\tilde{\phi}_D/\partial\tilde{\phi}$	c	$q_{\tilde{\phi}}$	$C_{\tilde{\phi}\tilde{\phi}\tilde{\phi}}$

TABLE 4.3.1: The correspondence between Mahler and GW (in the tropical limit).

Outlook   Regarding the dictionary in Table 4.3.1, it is natural to expect that the correspondence between Mahler measure and GW invariants holds for all 16 reflexive polygons. It would be interesting to have a precise proof of the correspondence. Incidentally, the partition function on S^2 for certain gauged linear sigma model was used to compute genus-0 GW invariants for a 3d CY variety[12] in [194] without the use of mirror symmetry. In particular, this linear sigma model flows an IR non-linear sigma model with the CY variety as the target space. It would be interesting to see whether the modular Mahler measures could have any relations to this. Moreover, the dictionary between Mahler measure and GW invariants can be potentially extended to the topological vertex formalism.

By virtue of the elliptic curves, the theories discussed in this section would have natural connections to Seiberg-Witten (SW) theories as pointed out in [157, 193]. It is also worth noting that dessins have also appeared in the study of SW curves as in [5, 168, 171] (see also Appendix C). It could be possible that the discussions on dessins and (modular) Mahler measures here would give some new insights to the study of SW theories and topological strings. From the perspective of (modular) Mahler measure, it would also be interesting to apply this to crystal melting, superconformal index, knot/quiver correspondence, black holes etc.

---

[12]Notice that the CY varieties studied are all compact, though some discussions are made in the large volume regime.

Chapter 5

BPS Algebras and Crystal Melting

Recently, the BPS algebras [195, 196] in Type IIA on the toric CY threefolds setting, dubbed quiver Yangians, were constructed in [57, 197, 198]. In this chapter, we shall study such algebras as well as their trigonometric and elliptic cousins [199–201]. We will start with the crystal representations. Then we will discuss their connections to integrability and VOAs.

Before we give the reviews on relevant topics, let us briefly summarize the results of this chapter. It was well-known that the crystal melting model can be used to count the BPS states of a toric quiver gauge theory. Such crystal models can be constructed as the 3d uplifts of the periodic quivers. In particular, the configurations of the molten crystals are in one-to-one correspondence with the BPS states. These BPS states are the bound states formed by Dp-branes wrapping compact cycles in the toric CY threefold in the Type IIA setup. We first discuss the construction of the crystal models for different (cyclic) chambers that are connected to non-commutative Donaldson-Thomas chamber (with known crystals) under (a series of) wall crossings. In particular, we find the crystal configurations from the core chamber to the PT chamber for $\mathbb{C} \times \mathbb{C}^2/\mathbb{Z}_2$, which together with the finite crystal configurations for the conifold could be served as possible building blocks of the crystals for more general geometries. Moreover, for the chambers with infinite crystals, we propose that wall crossing corresponds to "peeling off" the semi-infinite faces of the crystals.

The BPS algebras of the theories, which are known as the quiver Yangians, have the crystal configurations as their representations. We construct the $\mathcal{R}$-matrix formalism for these algebras. We give the expressions of the actions of the $\mathcal{R}$-matrices on the Fock modules labelled by (2d) crystals. We then discuss how one can derive the Bethe ansatz equations from the BPS algebras of the 4d gauge theories (for non-chiral quivers). This implements the Bethe/gauge correspondence, and these Bethe ansatz equations should describe certain Hitchin systems.

In the study of integrability, the coalgebra structure often plays an important role. We give the coproduct of the quiver Yangians for non-chiral quivers here. Moreover, we show that for toric dual quivers, their BPS algebras are isomorphic by explicitly giving the transformations.

As the BPS algebras for the 4d $\mathcal{N} = 1$ gauge theories, the quiver Yangians should also appear in the context of 2d/4d (aka BPS/CFT, AGT) correspondence. Indeed, for generalized conifolds, we show that the $\mathcal{W}$-algebras, which roughly speaking can be realized as the symmetry algebras arised at the interfaces of brane webs, are truncations of the quiver Yangians. In other words, we give the surjective homomorphisms from the BPS algebra to the vertex operator algebras.

One may also consider the trignometric and elliptic counterparts of the quiver Yangians, i.e., toroidal and elliptic quiver BPS algebras. In short, they can be realized by low energy effective theories on the worldvolume of the D-branes under dimensional reduction. We have a similar discussion for these two types of algebras as well. For non-chiral quivers, we give the isomorphic maps for toric dual algebras. We further show that such algebra for a higgsed theory is a subalgebra of the one for its parent theory in the case when the algebras have only one free parameter. For chiral quivers, it is still not clear how to obtain such transformations although it is natural to conjecture that we still the isomorphisms under Seiberg duality and the subalgebra structures

under higgsing. Nevertheless, we give a free field realization for the toroidal and elliptic algebras in the chiral case.

5.1 Crystal Melting Models

Given a quiver Q with superpotential W associated to a toric CY, let us denote the sets of nodes and arrows as Q_0 and Q_1 respectively. Such quiver theory can be used to describe the supersymmetric quantum mechanics on the D-branes, where the BPS states arise from the Dp-branes wrapping holomorphic p-cycles of the CY$_3$ in the type IIA compactification setting. The crystal melting model can then be thought of as the 3d uplift of the (periodic) quiver, where each atom in the crystal corresponds to a gauge node in the quiver while the bifundamental/adjoint arrows are chemical bonds. Moreover, the atoms associated to different gauge nodes have different "colours".

More concretely, we shall choose an initial atom $\mathfrak{o}$ in the periodic quiver. All the other atoms are placed at the nodes in the periodic quiver level by level along the arrows. As the paths connecting two fixed atoms should be equivalent in the crystal, we have the path algebra defined modulo the F-term relations, that is, $\mathbb{C}Q/\langle \partial W \rangle$.

The molten crystal configurations which correspond to the BPS states are obtained following the crystal melting rule. An atom $\mathfrak{a}$ is in the molten crystal $\mathfrak{C}$ if there exists an arrow $I \in Q_1$ such that $I \cdot \mathfrak{a} \in \mathfrak{C}$. This equivalently states that the complement of the molten crystal is an ideal of the path algebra. As we will review shortly, the generators of the quiver Yangian have natural actions on the molten crystal configurations.

5.1.1 Crystal Configurations and Wall Crossings

The crystal configuration for a given quiver in the non-commutative Donaldson-Thomas (NCDT) chamber is well-known. It could be possible that there are certain crystal models describing other chambers under wall crossings. In the case of the conifold $\mathcal{C}$, we know that the crystal in the chamber C_N the pyramid partition with a ridge of $(N + 1)$ atoms on the top row. The crystal partition function reads [202, 203]

$$Z_{\text{crystal}}\left(q_{0,N}, q_{1,N}\right) = M(q_{0,N}q_{1,N})^2 M\left(-q_{0,N}^{N-1}q_{1,N}^N, q_{0,N}q_{1,N}\right)^{-1} M_\wedge\left(-q_{0,N}^{-(N-1)}q_{1,N}^{-N}, q_{0,N}q_{1,N}; N\right)^{-1},$$
(5.1.1)

where $q_{i,N}$ is the variable for the atom of ith colour in the crystal for C_N. The definitions of the (generalized) MacMahon functions M, $M^\wedge$ and $M_\wedge$ can be found in Appendix F. Under $q_{0,N} = q_0^N q_1^{N-1}$ and $q_{1,N} = q_0^{-N+1}q_1^{-N+2}$, we obtain

$$Z_{\text{crystal}}(q_0, q_1) = M(q_0q_1)^2 M(-q_1, q_0q_1)^{-1} M_\wedge(-q_1, q_0q_1; N)^{-1}.$$
(5.1.2)

This is similar in the $\widetilde{C}_N$ chamber, where the crystal is finite and

$$Z_{\text{crystal}}\left(q_{0,N}, q_{1,N}\right) = M^\wedge\left(-q_{0,N}^{N+1}q_{1,N}^N, q_{0,N}^{-1}q_{1,N}^{-1}; N\right)^{-1}$$
(5.1.3)

with $q_{0,N} = q_0^N q_1^{N+1}$, $q_{1,N} = q_0^{-N-1}q_1^{-N-2}$ [204]. More examples on the BPS partition functions and relevant discussions can be found in Appendix F.

For a general CY, it is still not clear whether there is a crystal for every chamber. We conjecture that such crystal should exist, at least upon "artificial" constructions. For instance, the crystal for $\widetilde{C}_2$ for the conifold is shown in Figure 5.1.1(a). Together with another copy with different colours in Figure 5.1.1(b), we have a crystal with two disjoint parts as in Figure 5.1.1(c). In other words, they form a crystal whose white-black part and blue-red part have no chemical bonds between each other. More generally, for two copies for the chamber $\widetilde{C}_N$ of the conifold, this gives the partition
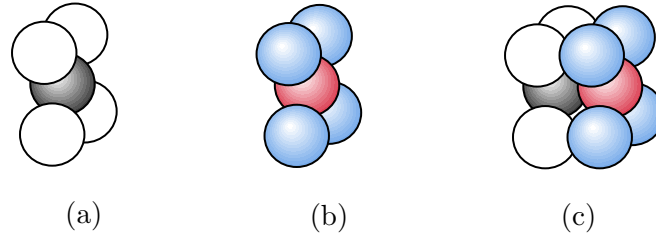
FIGURE 5.1.1: (a) The crystal for $\widetilde{C}_2$ for the conifold $\mathcal{C}$. (b) The same copy with different colours. (c) The crystal which is a disjoint union of (a) and (b).

function

$$
\begin{aligned}
Z_{\text{crystal}} &= M^\wedge \left(-q_{\text{white}}^{N+1} q_{\text{black}}^{N}, q_{\text{white}}^{-1} q_{\text{black}}^{-1}; N \right)^{-1} M^\wedge \left(-q_{\text{blue}}^{N+1} q_{\text{red}}^{N}, q_{\text{blue}}^{-1} q_{\text{red}}^{-1}; N \right)^{-1} \\
&= M^\wedge \left(-q_1, x; N \right)^{-1} M^\wedge \left(-q_3, x; N \right)^{-1},
\end{aligned}
\tag{5.1.4}
$$

where the second line is obtained under the substitutions

$$
q_{\text{white}} = q_0^N q_1^{N+1} q_2^N q_3^N,
\tag{5.1.5}
$$

$$
q_{\text{black}} = q_0^{-N-1} q_1^{-N-2} q_2^{-N-1} q_3^{-N-1},
\tag{5.1.6}
$$

$$
q_{\text{blue}} = q_0^N q_1^N q_2^N q_3^{N+1},
\tag{5.1.7}
$$

$$
q_{\text{red}} = q_0^{-N-1} q_1^{-N-1} q_2^{-N-1} q_3^{-N-2},
\tag{5.1.8}
$$

$$
x = q_0 q_1 q_2 q_3.
\tag{5.1.9}
$$

Notice that however, this partition function does not correspond to any chamber for $\mathcal{C}/\mathbb{Z}_2$ due to the constraints on $[B]$ discussed above. To recover the partition function of certain chamber, one should not only consider such crystal associated to $M^\wedge(\bullet, \bullet; N)^{-1}$, but also consider the crystal for $\widetilde{C}_N$ of $\mathbb{C} \times \mathbb{C}^2/\mathbb{Z}_2$. This is because in general we would also have $M^\wedge(\bullet, \bullet; N)$ in the partition function.

Here, we propose that the (natural) crystal for the chamber $\widetilde{C}_N$ for $\mathbb{C} \times \mathbb{C}^2/\mathbb{Z}_2$ has the shape of a tilted (semi-)infinite "triangular log store" as shown in Figure 5.1.2. The crystal partition function
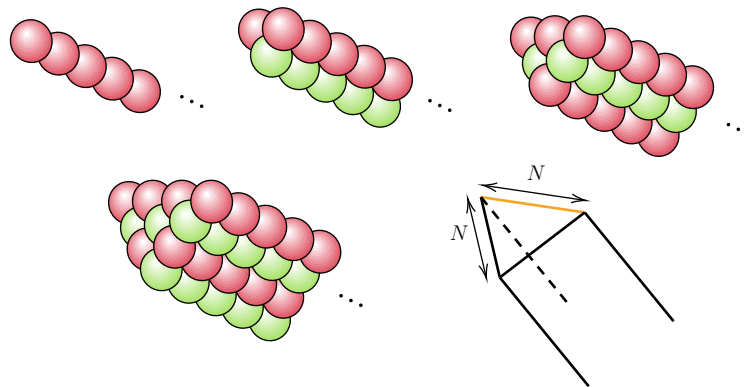
FIGURE 5.1.2: The crystal for chamber $\widetilde{C}_N$ for $\mathbb{C} \times \mathbb{C}^2/\mathbb{Z}_2$. Here we show the cases for $N = 1, 2, 3, 4$. We also give a sketch of general N with the orange line as the top row. The crystal is infinitely long.

is

$$
Z_{\text{crystal}}\left(q_{0,N}, q_{1,N} \right) = M^\wedge \left(q_{0,N}^{N+1} q_{1,N}^{N}, q_{0,N}^{-1} q_{1,N}^{-1}; N \right).
\tag{5.1.10}
$$

Under $q_{0,N} = q_0^N q_1^{N+1}$, $q_{1,N} = q_0^{-N-1} q_1^{-N-2}$, we recover $M^{\wedge}(q_1, q_0 q_1; N)$ as expected. As an illustration, we list the perturbative expansion of $Z_{\text{crystal}}(q_{0,N}, q_{1,N})$ for some small N:

$$
\begin{aligned}
N = 1 &: 1 + q_{0,1} + q_{0,1}^2 + q_{0,1}^3 + \ldots; \\
N = 2 &: 1 + 2q_{0,2} + (3 + q_{1,2})q_{0,2}^2 + (4 + 2q_{1,2})q_{0,2}^3 + \ldots; \\
N = 3 &: 1 + 3q_{0,3} + (6 + 2q_{1,3})q_{0,3}^2 + (10 + 6q_{1,3} + q_{1,3}^2)q_{0,3}^3 + \ldots; \\
N = 4 &: 1 + 4q_{0,4} + (10 + 3q_{1,3})q_{0,4}^2 + (20 + 12q_{1,4} + 2q_{1,4}^2)q_{0,4}^3 + \ldots.
\end{aligned}
\tag{5.1.11}
$$

Now, any chamber $\widetilde{C}$ for any toric CY without compact 4-cycles could be represented by a disjoint union of the crystals in Figure 5.1.1 and Figure 5.1.2. For instance, three copies of Figure 5.1.1 and two copies of Figure 5.1.2 (all with distinct colours) yield the chamber with

$$
Z_{\text{crystal}} = M^{\wedge}(-q_1, x; 1)^{-1} M^{\wedge}(-q_3, x; 1)^{-1} M^{\wedge}(q_1 q_2, x; 1) M^{\wedge}(q_2 q_3, x; 1) M^{\wedge}(-q_1 q_2 q_3, x; 2)^{-1}
\tag{5.1.12}
$$

for $\mathcal{C}/\mathbb{Z}_2$. The maps from $q_{i,N}$ to q_j should be straightforward from the above discussions[1].

In the case of $\mathbb{C} \times \mathbb{C}^2/\mathbb{Z}_n$ or $\mathcal{C}/\mathbb{Z}_n$, a more natural crystal could be the same as the one for $\mathbb{C} \times \mathbb{C}^2/\mathbb{Z}_2$ or $\mathcal{C}$ but with more colours. Nevertheless, this artificial method allows us to construct the crystal for arbitrary chamber $\widetilde{C}$ for any toric CY without compact 4-cycles.

One may consider a similar construction for a chamber C such that there is a crystal model for each $(M(\prod q_i, x) M_{\wedge}(\prod q_i, x; N))^{\pm 1}$ where ± 1 determines the crystal being either pyramid partition or bicoloured plane partition. Then the union of the crystals would give all the factors in the partition function. For such constructions, we need to point out the followings:

- There could be more colours $q_{i,\cup}$ of this union than the actual number of variables q_i. Therefore, the map from $\{q_{i,\cup}\}$ to $\{q_i\}$ should reduce such number. This is similar to the case for $\widetilde{C}$.

- Every (sub-)crystal in the union would introduce a factor of $M(x)^2$ in the product. To remove these extra factors, we need to make identifications of some atoms when gluing the crystals together. For each factor of $M(x)$, a pair of $\mathbb{C}^3$ sub-crystal in the union should "merge" into one. For some special/simpler cases, one may also consider merging a different sub-crystal. This is illustrated in Figure 5.1.3 where the CY geometry is not even changed but we have a different chamber[2].

- After merging, the truncations N in the (remaining) factors $M_{\wedge}(\bullet, \bullet; N)$ could change. Again, Figure 5.1.3 provides an example. It could be possible that cancelling the surplus colours in $\{q_{i,\cup}\}$ would simultaneously correct N in the remaining $M_{\wedge}(\bullet, \bullet; N)$.

It is not clear whether such construction would give a "natural" crystal description of the BPS states in different chambers. Nevertheless, if there does exist a natural crystal description, the 2d projection of the crystal shape should coincide with the web diagram of the toric CY. This is because the thickening of the web would give the 2d projection of the crystal melting in the thermodynamic limit[3]. Then the tops of the crystals would be the finite ridges in the webs with different numbers of coloured atoms for different chambers.

Let us take a closer look at the bicoloured crystals for $\mathbb{C} \times \mathbb{C}^2/\mathbb{Z}_2$ and the conifold in the chambers C_N. As shown in Figure 5.1.4, we can "peel" one semi-infinite face (in grey) off the crystal for the

---

[1]One may check that this indeed corresponds to some chamber. For example, the θ map (see Appendix F) can be chosen as $\theta(1/2) = -7/2$, $\theta(3/2) = 3/2$, $\theta(5/2) = 7/2$ and $\theta(7/2) = 9/2$.

[2]Of course, for general CY it would be easier to consider merging its own crystals rather than combining copies of bicoloured pyramid or plane partition and identifying $\mathbb{C}^3$ sub-crystals. However, the premise is to know the crystals for this general CY in different (or at least a few) chambers.

[3]The thickening of the web is known as the amoeba [22, 139]. As the (thermodynamic) limit shape of the crystal and the amoeba are general features for any CY, we expect the discussion here would also work for CYs with compact 4-cycles.
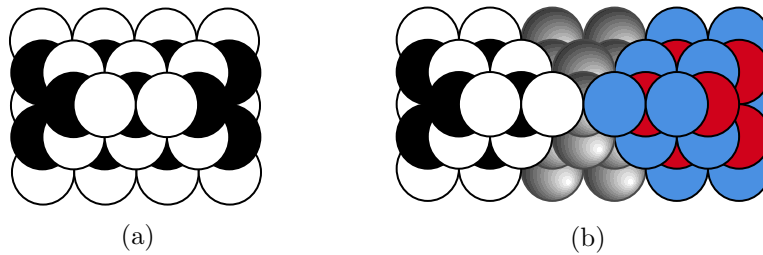
FIGURE 5.1.3: (a) The crystal for C_1 for the conifold $\mathcal{C}$. (b) "Merging" two such copies. Here, we still stay in the case $\mathcal{C}$, but with a different chamber. Each copy gives $M(x)^2 \widetilde{M}_\wedge(2)^{-1}$ where $\widetilde{M}_\wedge(2) := M(\prod q_i, x) M_\wedge(\prod q_i, x; 2)$. After merging the shaded pyramid (where the colours are ignored), we reach the chamber C_3 with partition function $M^2 \widetilde{M}_\wedge(4)^{-1}$ with the blue (red) colour identified with the white (black) colour.

conifold. This then leads to the crystal for chamber C_1. Keep peeling the semi-infinite face on the same side, and we can reach the crystal for any C_N. In the web diagram which corresponds to the
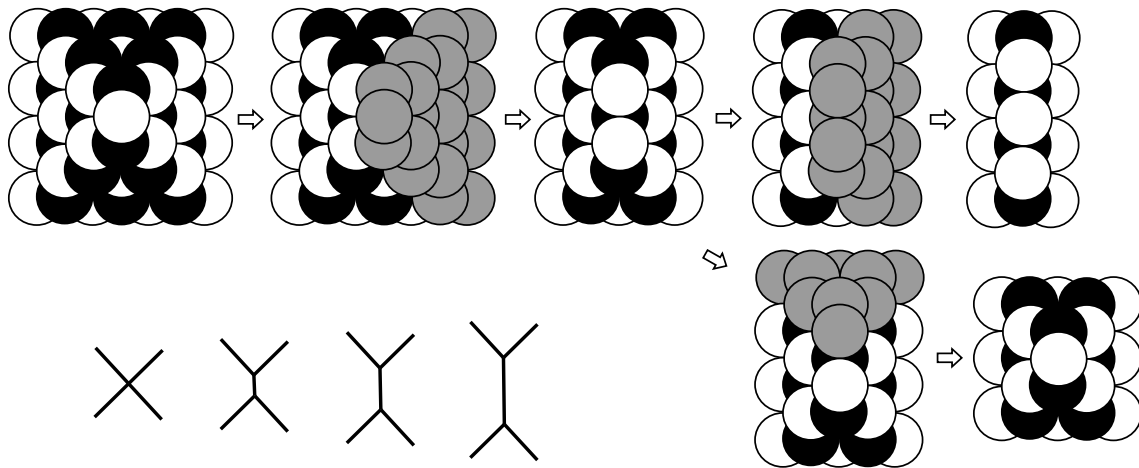
FIGURE 5.1.4: Peeling off the semi-infinite faces of the conifold crystal. This changes the length of the top row.

ridges of the crystal, peeling the semi-infinite face is actually changing the length of the internal line, that is, varying the Kähler moduli. This indicates that removing a factor of $(1 - x^k Q^{-1})^k$ in the partition function corresponds to peeling a semi-infinite face off the crystal. If we peel another semi-infinite face as in the second row in Figure 5.1.4, we can see that this is going the opposite direction in the moduli space, and we get back to the NCDT chamber C_0 from C_1.

Now we propose a similar construction for $\mathbb{C} \times \mathbb{C}^2/\mathbb{Z}_2$. In Figure 5.1.5, if we peel one semi-infinite ridge (in grey) off the crystal, we would reach the chamber C_1. Then keep peeling the semi-infinite face on the same side, and we can reach the crystal for any C_N. In the web diagram, this is again changing the length of the internal line, that is, varying the Kähler moduli. This corresponds to removing a factor of $(1 - x^k Q^{-1})^{-k}$ in the partition function. Similar to the conifold, the crystal partition function in this case should be given by

$$Z_{\text{crystal}}(q_{0,N}, q_{1,N}) = M(q_{0,N} q_{1,N})^2 M\left(q_{0,N}^{N-1} q_{1,N}^N, q_{0,N} q_{1,N}\right) M_\wedge\left(q_{0,N}^{-(N-1)} q_{1,N}^{-N}, q_{0,N} q_{1,N}; N\right),$$
(5.1.13)

with $q_{0,N} = q_0^N q_1^{N-1}$ and $q_{1,N} = q_0^{-N+1} q_1^{-N+2}$.

This peeling process can then be generalized to any toric CY. Every time we cross a wall, a semi-infinite face (with a ridge being a degenerate face) is peeled off the crystal. This corresponds to losing/obtaining a factor of $(1 - x^k \prod Q_i^{-1})^{\pm k}$, where the sign in the power is determined by the curve ($\mathcal{O}(-2,0)$ or $\mathcal{O}(-1,-1)$) for the internal line in the web, or equivalently, the signs in σ. As an example, we illustrate several different ways of peeling for $\mathbb{C} \times \mathbb{C}^2/\mathbb{Z}_3$ in Figure 5.1.6.
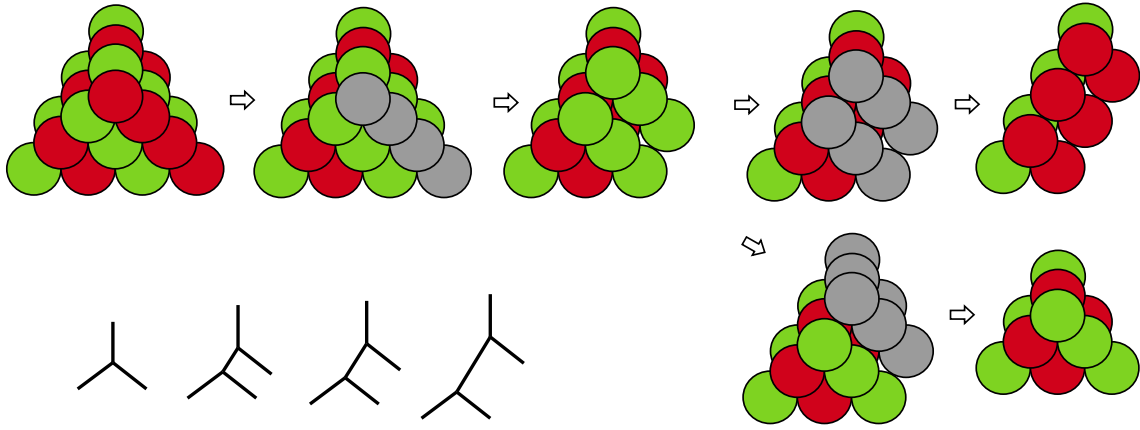
FIGURE 5.1.5: Peeling off the semi-infinite faces of the $\mathbb{C} \times \mathbb{C}^2/\mathbb{Z}_2$ crystal.
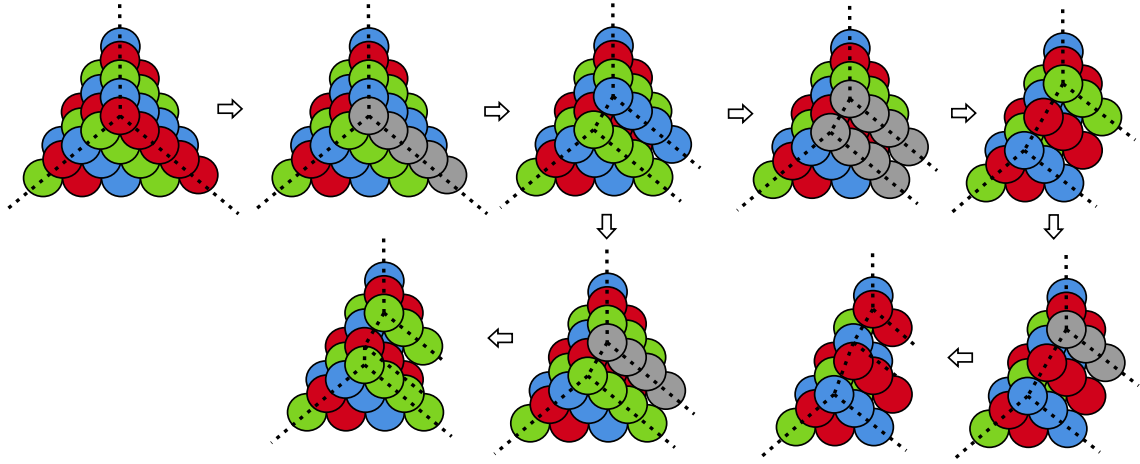
FIGURE 5.1.6: Peeling off the semi-infinite faces of the $\mathbb{C} \times \mathbb{C}^2/\mathbb{Z}_3$ crystal. The dashed brane webs is composed of the ridges.

In general, the initial atoms are at the intersections of (at least) two semi-infinite ridges. Moreover, these initial atoms do not have to lie at the same "height" in the crystal.

5.2   Quiver Yangians

Let us first briefly review the concept of the (rational) quiver Yangians as introduced in [57]. Given a quiver $Q = (Q_0, Q_1)$ with superpotential W, its quiver Yangian $\mathsf{Y}_{Q,W}$ is generated by the modes $e_i^{(a)}$, $f_i^{(a)}$ and $\psi_j^{(a)}$ ($a \in Q_0$, $i \in \mathbb{N}$, $j \in \mathbb{Z}$)[4] satisfying the relations

$$\left[\psi_n^{(a)}, \psi_m^{(b)} \right] = 0, \tag{5.2.1}$$

$$\left[e_n^{(a)}, f_m^{(b)} \right\} = \delta_{ab} \psi_{m+n}^{(a)}, \tag{5.2.2}$$

$$\sum_{k=0}^{|b \to a|} (-1)^{|b \to a| - k} \sigma_{|b \to a| - k}^{b \to a} \left[\psi_n^{(a)} e_m^{(b)} \right]_k = \sum_{k=0}^{|a \to b|} \sigma_{|a \to b| - k}^{a \to b} \left[e_m^{(b)} \psi_n^{(a)} \right]^k, \tag{5.2.3}$$

$$\sum_{k=0}^{|b \to a|} (-1)^{|b \to a| - k} \sigma_{|b \to a| - k}^{b \to a} \left[e_n^{(a)} e_m^{(b)} \right]_k = (-1)^{|(a)||(b)|} \sum_{k=0}^{|a \to b|} \sigma_{|a \to b| - k}^{a \to b} \left[e_m^{(b)} e_n^{(a)} \right]^k, \tag{5.2.4}$$

$$\sum_{k=0}^{|b \to a|} (-1)^{|b \to a| - k} \sigma_{|b \to a| - k}^{b \to a} \left[f_m^{(b)} \psi_n^{(a)} \right]^k = \sum_{k=0}^{|a \to b|} \sigma_{|a \to b| - k}^{a \to b} \left[\psi_n^{(a)} f_m^{(b)} \right]_k, \tag{5.2.5}$$

---

[4] In this thesis, we have the convention $\mathbb{N} = \mathbb{Z}_{\geq 0}$.

$$\sum_{k=0}^{|b\to a|}(-1)^{|b\to a|-k}\sigma_{|b\to a|-k}^{b\to a}\left[f_m^{(b)}f_n^{(a)}\right]^k = (-1)^{|(a)||(b)|}\sum_{k=0}^{|a\to b|}\sigma_{|a\to b|-k}^{a\to b}\left[f_n^{(a)}f_m^{(b)}\right]_k. \tag{5.2.6}$$

The notations require some explanation. The bracket $[\text{-},\text{-}\}$ is the super bracket, that is, anti-commutator for two fermionic modes and commutator otherwise. In a quiver, the nodes with (without) adjoint loops are bosonic (fermionic) such that $|(a)| = 0$ ($|(a)| = 1$). Then $e_i^{(a)}$ and $f_i^{(a)}$ have the $\mathbb{Z}_2$-grading same as the corresponding node a while $\psi_j^{(a)}$ is always bosonic. We use $a \to b$ to denote the set of arrows from a to b, and the total number is $|a \to b|$. For each edge $I \in Q_1$, we assign a weight/charge $\widetilde{\epsilon}_I$ to it, and $\sigma_k^{a\to b}$ is the kth symmetric sum of $\widetilde{\epsilon}_I$ for all $I \in a \to b$. Moreover, we have

$$[A_nB_m]_k := \sum_{l=0}^{k}(-1)^l\binom{k}{l}A_{n+k-l}B_{m+l}, \quad [B_mA_n]^k := \sum_{l=0}^{k}(-1)^l\binom{k}{l}B_{m+l}A_{n+k-l}. \tag{5.2.7}$$

The defining relations for generalized conifolds, along with the constructions of the quivers, are given in Appendix E. For toric CYs, as the superpotential can be unambiguously determined for a given quiver, we shall sometimes abbreviate $\mathtt{Y}_{Q,W}$ as $\mathtt{Y}_Q$ or even $\mathtt{Y}$ if it would not cause confusions.

To correctly recover the counting of crystal configurations/BPS states, we need to further mod out the Serre relations[5]. For generalized conifolds, the Serre relations read

$$\text{Sym}_{n_1,n_2}\left[e_{n_1}^{(a)},\left[e_{n_2}^{(a)},e_m^{(a\pm1)}\right]\right]=0, \quad \text{Sym}_{n_1,n_2}\left[f_{n_1}^{(a)},\left[f_{n_2}^{(a)},f_m^{(a\pm1)}\right]\right]=0, \tag{5.2.8}$$

for $|(a)| = 0$, and

$$\text{Sym}_{n_1,n_2}\left[e_{n_1}^{(a)},\left[e_{m_1}^{(a+1)},\left[e_{n_2}^{(a)},e_{m_2}^{(a-1)}\right\}\right\}\right\}=0, \quad \text{Sym}_{n_1,n_2}\left[f_{n_1}^{(a)},\left[f_{m_1}^{(a+1)},\left[f_{n_2}^{(a)},f_{m_2}^{(a-1)}\right\}\right\}\right\}=0 \tag{5.2.9}$$

for $|(a)| = 1$. The Yangian algebra after the quotient of the Serre relations is also called the reduced quiver Yangian. However, as we will mainly focus on the Yangian algebra with Serre relations included, we shall simply refer to it as the quiver Yangian $\mathtt{Y}$.

We can then introduce the currents

$$e^{(a)}(u) := \sum_{n=0}^{\infty}\frac{e_n^{(a)}}{u^{n+1}}, \quad f^{(a)}(u) := \sum_{n=0}^{\infty}\frac{f_n^{(a)}}{u^{n+1}}, \quad \psi^{(a)}(u) := \sum_{n\in\mathbb{Z}}\frac{\psi_n^{(a)}}{u^{n+1}}. \tag{5.2.10}$$

In the molten crystal, $e^{(a)}(u)$ ($e_n^{(a)}$) creates atoms in the configuration while $f^{(a)}(u)$ ($f_n^{(a)}$) annihilates atoms. Moreover, $\psi^{(a)}(u)$ contains all the Cartan modes $\psi_n^{(a)}$. It was shown in [57] that for toric CYs without compact divisors (or more generally, any symmetric quivers), $\psi_{n<-1}^{(a)} = 0$ and $\psi_{-1}^{(a)} = 1$.

We may then write the relations in terms of the currents as

$$\left[e^{(a)}(u),f^{(b)}(v)\right\} = \delta_{ab}\frac{\psi^{(a)}(u)-\psi^{(a)}(v)}{u-v}+\ldots, \tag{5.2.11}$$

$$\bar{g}_{ba}(u-v)\psi^{(a)}(u)e^{(b)}(v) = g_{ab}(u-v)e^{(b)}(v)\psi^{(a)}(u)+\ldots, \tag{5.2.12}$$

$$\bar{g}_{ba}(u-v)e^{(a)}(u)e^{(b)}(v) = (-1)^{|(a)||(b)|}g_{ab}(u-v)e^{(b)}(v)e^{(a)}(u)+\ldots, \tag{5.2.13}$$

$$\bar{g}_{ba}(u-v)f^{(b)}(v)\psi^{(a)}(u) = g_{ab}(u-v)\psi^{(a)}(u)f^{(b)}(v)+\ldots, \tag{5.2.14}$$

$$\bar{g}_{ba}(u-v)f^{(b)}(v)f^{(a)}(u) = (-1)^{|(a)||(b)|}g_{ab}(u-v)f^{(a)}(u)f^{(b)}(v)+\ldots, \tag{5.2.15}$$

$$\tag{5.2.16}$$

---

[5]Recently, the Serre relations for any quivers for the trigonometric versions were obtained in [205]. By taking the rational limit, we may get the Serre relations for the rational quiver Yangians. Nevertheless, we shall only consider the cases for generalized conifolds here.

where

$$g_{ab}(z) := \prod_{i=1}^{|a \to b|} (z + \widetilde{\epsilon}_{ab,i}), \quad \overline{g}_{ba}(z) := \prod_{i=1}^{|b \to a|} (z - \widetilde{\epsilon}_{ba,i}). \tag{5.2.17}$$

The ellipses indicate the local terms in the sense of [206] as they would not contribute when we compute the contour integrals to recover most of the mode relations[6]. For instance, when the toric CY does not have compact 4-cycles, we have the local terms for the ψe relation as

$$
\begin{aligned}
&\left(\sum_{k=0}^{|b \to a|} (-1)^{|b \to a|} \sigma_{|b \to a|-k}^{b \to a} \sum_{j=0}^{k} (-1)^j \binom{k}{j} u^{k-j} v^j \left(\psi^{(a)}(u) \left(\sum_{m=0}^{j-1} \frac{e_m^{(b)}}{v^{m+1}} \right) + \left(\sum_{n=-1}^{k-j-1} \frac{\psi_n^{(a)}}{u^{n+1}} \right) e^{(b)}(v) \right. \right. \\
&\left. - \sum_{m=0}^{j-1} \sum_{n=-1}^{k-j-1} \frac{\psi_n^{(a)}}{u^{n+1}} \frac{e_m^{(b)}}{v^{m+1}} \right) \right) - \left(\sum_{k=0}^{|a \to b|} \sigma_{|a \to b|-k}^{a \to b} \sum_{j=0}^{k} (-1)^j \binom{k}{j} u^{k-j} v^j \left(\left(e^{(b)}(v) \sum_{n=-1}^{k-j-1} \frac{\psi_n^{(a)}}{u^{n+1}} \right) \right. \right. \\
&\left. \left. + \left(\sum_{m=0}^{j-1} \frac{e_m^{(b)}}{v^{m+1}} \right) \psi^{(a)}(u) - \sum_{m=0}^{j-1} \sum_{n=-1}^{k-j-1} \frac{e_m^{(b)}}{v^{m+1}} \frac{\psi_n^{(a)}}{u^{n+1}} \right) \right).
\end{aligned}
\tag{5.2.18}
$$

By analyzing how the atoms in the molten crystal configuration can be added and removed, we can write down the action of the currents on any crystal state $|\mathfrak{C}\rangle$. Consider an atom $\mathfrak{a}$ of colour a that can be added to (removed from) the molten crystal according to the melting rule. Then we shall use the notation $\mathfrak{a} \in \mathfrak{C}_+$ ($\mathfrak{a} \in \mathfrak{C}_-$) such that $|\mathfrak{C}\rangle$ would become $|\mathfrak{C} + \mathfrak{a}\rangle$ ($|\mathfrak{C} - \mathfrak{a}\rangle$) after the corresponding action. Suppose the initial atom $\mathfrak{o}$ in the crystal has colour $o = 1$. We have [57]

$$\psi^{(a)}(u)|\mathfrak{C}\rangle = \Psi_{\mathfrak{C}}^{(a)}(u)|\mathfrak{C}\rangle, \tag{5.2.19}$$

$$e^{(a)}(u)|\mathfrak{C}\rangle = \sum_{\mathfrak{a} \in \mathfrak{C}_+} \frac{\pm \sqrt{-(-1)^{|(a)|} \mathrm{Res}_{\widetilde{\epsilon}(\mathfrak{a})} \Psi_{\mathfrak{C}}^{(a)}(u)}}{u - \widetilde{\epsilon}(\mathfrak{a})} |\mathfrak{C} + \mathfrak{a}\rangle, \tag{5.2.20}$$

$$f^{(a)}(u)|\mathfrak{C}\rangle = \sum_{\mathfrak{a} \in \mathfrak{C}_-} \frac{\pm \sqrt{\mathrm{Res}_{\widetilde{\epsilon}(\mathfrak{a})} \Psi_{\mathfrak{C}}^{(a)}(u)}}{u - \widetilde{\epsilon}(\mathfrak{a})} |\mathfrak{C} - \mathfrak{a}\rangle, \tag{5.2.21}$$

where

$$\Psi_{\mathfrak{C}}^{(a)}(u) := \left(\frac{u + C}{u} \right)^{\delta_{a,1}} \prod_{b \in Q_0} \prod_{\mathfrak{b} \in \mathfrak{C}} \phi^{b \Rightarrow a}(u - \widetilde{\epsilon}(\mathfrak{b})), \tag{5.2.22}$$

$$\phi^{b \Rightarrow a}(u) = \frac{\prod\limits_{I \in a \to b} (u + \widetilde{\epsilon}_I)}{\prod\limits_{I \in b \to a} (u - \widetilde{\epsilon}_I)}, \tag{5.2.23}$$

$$\widetilde{\epsilon}(\mathfrak{a}) = \sum_{I \in \mathrm{path}[\mathfrak{o} \to \mathfrak{a}]} \widetilde{\epsilon}_I. \tag{5.2.24}$$

Here, C is some numerical constant known as the vacuum charge[7]. The $\pm$ signs in the actions depend on the statistics of the algebra. Moreover, the charge assignment $\widetilde{\epsilon}_I$ should be compatible with the superpotential[8]. Therefore, the coordinate parameters $\widetilde{\epsilon}_I$ of the arrows should satify the

---

[6]More specifically, when applying the contour integral $\frac{1}{(2\pi i)^2} \oint u^n v^m \mathrm{d}u \mathrm{d}v$ with $m, n \geq 0$ (or taking the formal mode expansion), these terms do not contribute as they have zero residues. However, they would affect the results for relations such as $\left[\psi^{(a)}(u), e_0^{(b)} \right]$ which has $m = -1$. See for instance [206] for some explicit examples.

[7]For toric CY without compact 4-cycles, it can be identified as the central term $\sum\limits_{a \in Q_0} \psi_0^{(a)}$.

[8]This means that $\widetilde{\epsilon}_I$ can be viewed as charges under a global symmetry of the quiver quantum mechanics, and this charge constraint is the only role that the superpotential plays in the definition of Y.

loop constraint

$$\sum_{I \in L} \widetilde{\epsilon}_I = 0, \tag{5.2.25}$$

for any closed loop L in the periodic quiver. It turns out that the number of coordinate parameters is given by

$$|Q_1| - |Q_2| - 1 = |Q_0| + 1, \tag{5.2.26}$$

where Q_2 denotes the faces of the periodic quiver, or equivalently, the monomial terms in the superpotential.

Moreover, as pointed out in [57], there is redundancy associate to each node in the sense that certain shifts of $\widetilde{\epsilon}_I$ would give automorphisms of the algebra. One can then introduce a gauge fixing condition to get rid of this shift. This is known as the vertex constraint:

$$\sum_{I \in a} \mathrm{sgn}_a(I) \widetilde{\epsilon}_I = 0, \tag{5.2.27}$$

where the sign function $\mathrm{sgn}_a(I)$ is equal to $+1$ (-1) when the arrow I starts from (ends at) the node a, and 0 otherwise. As an overall U(1) symmetry decouples, the total number of the vertex constraints is $|Q_0| - 1$. Together with the $|Q_0| + 1$ loop constraints, we are then left with two independent parameters[9] denoted as $\epsilon_{1,2}$. It would also be convenient to introduce a third parameter ϵ_3 such that $\epsilon_1 + \epsilon_2 + \epsilon_3 = 0$.

5.3 Yang-Baxter Algebras and $\mathcal{R}$-Matrices

As the name suggests, the quiver Yangian should enjoy an $\mathcal{R}$-matrix formalism [59, 207]. The $\mathcal{R}$-matrix can be defined by considering a set of vector spaces $\mathcal{F}_i$ and the operator-valued functions $\mathcal{R}_{\mathcal{F}_i,\mathcal{F}_j}(u) \in \mathrm{End}(\mathcal{F}_i \otimes \mathcal{F}_j)(u)$. Here, u is the spectral parameter and the $\mathcal{R}$-matrix should satisfy the Yang-Baxter (YB) equation

$$\mathcal{R}_{12}(u)\mathcal{R}_{13}(u+v)\mathcal{R}_{23}(v) = \mathcal{R}_{23}(v)\mathcal{R}_{13}(u+v)\mathcal{R}_{12}(u), \tag{5.3.1}$$

where $\mathcal{R}_{12} := \mathcal{R}_{\mathcal{F}_1,\mathcal{F}_2} \otimes 1_{\mathcal{F}_3}$. Henceforth, we shall slightly abuse the notation and simply write $\mathcal{R}_{\mathcal{F}_i,\mathcal{F}_j}$ as $\mathcal{R}_{ij}$. Now, consider the tensor product of the Fock spaces, $\mathcal{F}_1(u_1) \otimes \cdots \otimes \mathcal{F}_n(u_n)$, and choose an auxiliary space $\mathcal{F}_0 \in \{\mathcal{F}_i\}$. We can define the operator

$$\mathcal{T}_0(u) = \mathcal{R}_{0n}(u - u_n) \ldots \mathcal{R}_{01}(u - u_1). \tag{5.3.2}$$

The YB equation then implies the $\mathcal{R}\mathcal{T}\mathcal{T}$ relation

$$\mathcal{R}_{ij}(u - v)\mathcal{T}_i(u)\mathcal{T}_j(v) = \mathcal{T}_j(v)\mathcal{T}_i(u)\mathcal{R}_{ij}(u - v). \tag{5.3.3}$$

More rigorously, following [59], we should start with an integral domain $\mathbb{K} \supset \mathbb{Q}$ with $\otimes = \otimes_{\mathbb{K}}$ and $\mathrm{End} = \mathrm{End}_{\mathbb{K}}$. Then the Maulik-Okounkov (MO) Yangian acts on $F_i(u_i) := F_i \otimes \mathbb{K}[u_i]$ for some free $\mathbb{K}$-module F_i, or more generally on the tensor product $\bigotimes_i F_i(u_i) = \bigotimes_i F_i \otimes \mathbb{K}[u_1, \ldots, u_n]$. Given a quiver Q, the modules F_i can be identified with certain equivariant cohomologies of the Nakajima quiver variety.

The precise relation between quiver Yangians and MO Yangians is still not clear, but they should be different for the same quiver Q. For $\mathbb{C} \times \mathbb{C}^2/\mathbb{Z}_n$ whose quiver Yangian is $\mathtt{Y}\left(\widehat{\mathfrak{gl}}_n\right)$, as it is the tripled quiver[10] $\widehat{Q}$ of the affine A-type quiver Q, we conjecture that its quiver Yangian $\mathtt{Y}_{\widehat{Q}}$ is isomorphic

---

[9]These two coordinate parameters, along with the R-symmetry, give the U(1)^3 isometry of the toric CY threefold.

[10]Given a quiver Q, its tripled quiver is defined as follows. We first construct its doubled quiver $\overline{Q} = (Q_0, Q_1 \sqcup Q_1^*)$ where an arrow I^* in the opposite direction is added for each $I \in Q_1$. Then the tripled quiver $\widehat{Q}$ is obtained by adding a self-loop ω_a to each node a. It has (super)potential $W = \sum \omega_a[X, X^*]$.

to the MO Yangian of Q. This is consistent with the conjecture in [208] regarding their positive parts.

In [206, 209], the MO $\mathcal{R}$-matrices were constructed using the $\mathcal{RTT}$ relation and some current algebras known as the Yang-Baxter algebras for $\widehat{\mathfrak{gl}}_1$ and $\widetilde{\mathfrak{gl}}_2$. In this section, we shall first define the YB algebras for general (non-chiral) quivers.

5.3.1 Yang-Baxter Algebras

Given a quiver Q, the YB algebra YB_Q is defined by the generators $h_i^{(a)}$, $e_i^{(a)}$, $f_i^{(a)}$ and $\psi_j^{(a)}$ ($a \in Q_0$, $i \in \mathbb{N}$, $j \in \mathbb{Z}$) subject to the relations

$$\left[h_n^{(a)}, h_m^{(b)} \right] = \left[h_n^{(a)}, \psi_m^{(b)} \right] = 0, \tag{5.3.4}$$

$$\left[h_n^{(a)}, e_m^{(b)} \right] = \delta_{ab} \epsilon_3 \sum_{k=0}^{n} h_{n-k-1}^{(a)} e_{m+k}^{(b)}, \tag{5.3.5}$$

$$\left[f_m^{(b)}, h_n^{(a)} \right] = \delta_{ab} \epsilon_3 \sum_{k=0}^{n} f_{m+k}^{(b)} h_{n-k-1}^{(a)}, \tag{5.3.6}$$

$$\left[\psi_n^{(a)}, \psi_m^{(b)} \right] = 0, \tag{5.3.7}$$

$$\left[e_n^{(a)}, f_m^{(b)} \right\} = -\delta_{ab} \psi_{m+n}^{(a)}, \tag{5.3.8}$$

$$\sum_{k=0}^{|b \to a|} (-1)^{|b \to a| - k} \sigma_{|b \to a| - k}^{b \to a} \left[\psi_n^{(a)} e_m^{(b)} \right]_k = \sum_{k=0}^{|a \to b|} \sigma_{|a \to b| - k}^{a \to b} \left[e_m^{(b)} \psi_n^{(a)} \right]^k, \tag{5.3.9}$$

$$\sum_{k=0}^{|b \to a|} (-1)^{|b \to a| - k} \sigma_{|b \to a| - k}^{b \to a} \left[e_n^{(a)} e_m^{(b)} \right]_k = (-1)^{|(a)||(b)|} \sum_{k=0}^{|a \to b|} \sigma_{|a \to b| - k}^{a \to b} \left[e_m^{(b)} e_n^{(a)} \right]^k, \tag{5.3.10}$$

$$\sum_{k=0}^{|b \to a|} (-1)^{|b \to a| - k} \sigma_{|b \to a| - k}^{b \to a} \left[f_m^{(b)} \psi_n^{(a)} \right]^k = \sum_{k=0}^{|a \to b|} \sigma_{|a \to b| - k}^{a \to b} \left[\psi_n^{(a)} f_m^{(b)} \right]_k, \tag{5.3.11}$$

$$\sum_{k=0}^{|b \to a|} (-1)^{|b \to a| - k} \sigma_{|b \to a| - k}^{b \to a} \left[f_m^{(b)} f_n^{(a)} \right]^k = (-1)^{|(a)||(b)|} \sum_{k=0}^{|a \to b|} \sigma_{|a \to b| - k}^{a \to b} \left[f_n^{(a)} f_m^{(b)} \right]_k, \tag{5.3.12}$$

Serre relations. $\tag{5.3.13}$

As we can see, the relations among $e_i^{(a)}$, $f_i^{(a)}$ and $\psi_j^{(a)}$ are exactly the same as the ones for their namesakes in the quiver Yangian Y_Q except the extra minus sign in the ef relation. Moreover, similar to $\psi_j^{(a)}$, the modes $h_i^{(a)}$ are Cartan modes and are always bosonic for any node a. Denoting the subalgebra of YB generated by $e_i^{(a)}$, $f_i^{(a)}$ and $\psi_j^{(a)}$ as YB_0, it is then straightforward to see that given a quiver Q, the map

$$\rho : \text{Y} \to \text{YB}_0, \quad e_i^{(a)} \mapsto e_i^{(a)}, \quad -f_i^{(a)} \mapsto f_i^{(a)}, \quad \psi_i^{(a)} \mapsto \psi_i^{(a)} \tag{5.3.14}$$

is an isomorphism[11]. In general, the YB algebra is strictly larger than the quiver Yangian. For instance, $\text{Y}\left(\widehat{\mathfrak{gl}}_1\right)$ is the factorization of the YB algebra for $\mathbb{C}^3$ over its centre as shown in [206]. In the remaining of this section (§5.3), we shall always refer to f as the generators for the YB algebra.

We may then write the currents

$$h^{(a)}(u) = 1 + \sum_{n=0}^{\infty} \frac{h_n^{(a)}}{u^{n+1}}, \quad e^{(a)}(u) = \sum_{n=0}^{\infty} \frac{e_n^{(a)}}{u^{n+1}}, \quad f^{(a)}(u) = \sum_{n=0}^{\infty} \frac{f_n^{(a)}}{u^{n+1}}, \quad \psi^{(a)}(u) = \sum_{n \in \mathbb{Z}} \frac{\psi_n^{(a)}}{u^{n+1}}. \tag{5.3.15}$$

---

[11] The case for $\mathbb{C}^3$ was proven in [210].

In particular, we can define $h^{(a)}_{-1} = 1$. In terms of currents, the relations read

$$\left[h^{(a)}(u), h^{(b)}(v) \right] = \left[h^{(a)}(u), \psi^{(b)}(v) \right] = 0, \tag{5.3.16}$$

$$(u - v - \delta_{ab}\epsilon_3) h^{(a)}(u) e^{(b)}(v) = (u - v) e^{(b)}(v) h^{(a)}(u) - \delta_{ab}\epsilon_3 h^{(a)}(u) e^{(b)}(u), \tag{5.3.17}$$

$$(u - v - \delta_{ab}\epsilon_3) f^{(b)}(v) h^{(a)}(u) = (u - v) h^{(a)}(u) f^{(b)}(v) - \delta_{ab}\epsilon_3 f^{(b)}(u) h^{(a)}(u), \tag{5.3.18}$$

as well as those for $e^{(a)}(u)$, $f^{(a)}(u)$ and $\psi^{(a)}(u)$ being the same as in quiver Yangians (with minus signs correspondingly added due to different conventions of f). Again, the terms involving only the parameter u are called local terms.

Remark 24. *Instead of introducing an $h^{(a)}(u)$ for each node a, we could also consider a single current $h(u)$ such that $h(u) := \prod\limits_{a \in Q_0} h^{(a)}(u)$ with mode expansion $h(u) = \sum\limits_{n=-1}^{\infty} \frac{h_n}{u^{n+1}}$ (where $h_{-1} = 1$). This would slightly alter the definition of* YB, *but the relations would still be very similar. We can simply remove the factors δ_{ab} (and of course also the superscripts in h) to get both the mode and current relations for h.*

More generally, especially for CY_3 *with compact 4-cycles, we may also introduce negative modes for $h^{(a)}(u)$ (or $h(u)$) in the definition of YB algebras just like $\psi^{(a)}(u)$. This might be more convenient when discussing the relations between* YB *and* Y. *However, for our purpose here (especially for symmetric quivers without negative $\psi^{(a)}_j$ modes), it suffices to consider $h^{(a)}(u)$ with modes $n \geq -1$.*

As the quiver Yangians have crystal representations, we may also find how YB, or more specifically $h^{(a)}(u)$, would act on the crystals. This can be done with the help of the actions of other generators. Write $h^{(a)}(u)|\mathfrak{C}\rangle = h^{(a)}_{\mathfrak{C}}|\mathfrak{C}\rangle$ for an arbitrary crystal configuration $\mathfrak{C}$. Using the he relation, we have

$$(u - v - \delta_{ab}\epsilon_3) h^{(a)}(u) e^{(b)}(v)|\mathfrak{C}\rangle = \Big((u - v) e^{(b)}(v) h^{(a)}(u) - \delta_{ab}\epsilon_3 h^{(a)}(u) e^{(b)}(u) \Big) |\mathfrak{C}\rangle. \tag{5.3.19}$$

Then

$$(u - v - \delta_{ab}\epsilon_3) h^{(a)}(u) \sum_{\mathfrak{b} \in \mathfrak{C}_+} \frac{\text{Num}(\mathfrak{b})}{v - \widetilde{\epsilon}(\mathfrak{b})}|\mathfrak{C} + \mathfrak{b}\rangle$$

$$= (u - v) e^{(b)}(v) h^{(a)}_{\mathfrak{C}}|\mathfrak{C}\rangle - \delta_{ab}\epsilon_3 h^{(a)}(u) \sum_{\mathfrak{b} \in \mathfrak{C}_+} \frac{\text{Num}(\mathfrak{b})}{u - \widetilde{\epsilon}(\mathfrak{b})}|\mathfrak{C} + \mathfrak{b}\rangle, \tag{5.3.20}$$

where the numerator in the action of $e^{(b)}$ is denoted as $\text{Num}(\mathfrak{b})$. The explicit expression can be found in §5.2, but it is not important here. This yields

$$(u - v - \delta_{ab}\epsilon_3) \sum_{\mathfrak{b} \in \mathfrak{C}_+} \frac{\text{Num}(\mathfrak{b})}{v - \widetilde{\epsilon}(\mathfrak{b})} h^{(a)}_{\mathfrak{C}+\mathfrak{b}}|\mathfrak{C} + \mathfrak{b}\rangle$$

$$= (u - v) \sum_{\mathfrak{b} \in \mathfrak{C}_+} \frac{\text{Num}(\mathfrak{b})}{v - \widetilde{\epsilon}(\mathfrak{b})} h^{(a)}_{\mathfrak{C}}|\mathfrak{C} + \mathfrak{b}\rangle - \delta_{ab}\epsilon_3 \sum_{\mathfrak{b} \in \mathfrak{C}_+} \frac{\text{Num}(\mathfrak{b})}{u - \widetilde{\epsilon}(\mathfrak{b})} h^{(a)}_{\mathfrak{C}+\mathfrak{b}}|\mathfrak{C} + \mathfrak{b}\rangle. \tag{5.3.21}$$

In other words,

$$(u - v - \delta_{ab}\epsilon_3) \frac{\text{Num}(\mathfrak{b})}{v - \widetilde{\epsilon}(\mathfrak{b})} h^{(a)}_{\mathfrak{C}+\mathfrak{b}} = (u - v) \frac{\text{Num}(\mathfrak{b})}{v - \widetilde{\epsilon}(\mathfrak{b})} h^{(a)}_{\mathfrak{C}} - \delta_{ab}\epsilon_3 \frac{\text{Num}(\mathfrak{b})}{u - \widetilde{\epsilon}(\mathfrak{b})} h^{(a)}_{\mathfrak{C}+\mathfrak{b}}. \tag{5.3.22}$$

By taking the contour integral $\oint_{v=\infty}$ (or equivalently, the large v expansion), we have

$$\frac{h^{(a)}_{\mathfrak{C}+\mathfrak{b}}}{h^{(a)}_{\mathfrak{C}}} = \frac{u - \widetilde{\epsilon}(\mathfrak{b})}{u - \widetilde{\epsilon}(\mathfrak{b}) - \delta_{ab}\epsilon_3}. \tag{5.3.23}$$

Let us choose the normalization $h^{(a)}(u)|\varnothing\rangle = |\varnothing\rangle$. Then we get

$$h^{(a)}(u)|\mathfrak{C}\rangle = \prod_{\mathfrak{a}\in\mathfrak{C}} \frac{u - \widetilde{\epsilon}(\mathfrak{a})}{u - \widetilde{\epsilon}(\mathfrak{a}) - \epsilon_3} |\mathfrak{C}\rangle \tag{5.3.24}$$

for any crystal configuration $\mathfrak{C}$. Thus, $h^{(a)}(u)$ only sees the atoms of colour a in the crystal[12].

By comparing the actions of $h^{(a)}(u)$ and $\psi^{(a)}(u)$ (with vertex constraints taken into account), we can write $\psi^{(a)}(u)$ in terms of $h^{(a)}(u)$. For instance, for generalized conifolds, we have the relation

$$\psi^{(a)}(u) = \left(\frac{u + \psi_0}{u}\right)^{\delta_{a1}} h^{(a-1)}(u + \sigma_a\epsilon_1)h^{(a-1)}(u + \sigma_a\epsilon_2)$$
$$h^{(a+1)}(u + \sigma_{a+1}\epsilon_1)h^{(a+1)}(u + \sigma_{a+1}\epsilon_2)\left(h^{(a)}(u)h^{(a)}(u + \epsilon_3)\right)^{\frac{\sigma_a+\sigma_{a+1}}{2}}, \tag{5.3.25}$$

where we have used $C = \sum_{a\in Q_0} \psi_0^{(a)} =: \psi_0$ for the vacuum charge as shown in [57] for generalized conifolds.

5.3.2 Crystal Melting and the $\mathcal{RTT}$ Relation

Given a quiver and its quiver Yangian, we shall construct the $\mathcal{R}$-matrices by acting the $\mathcal{RTT}$ relation on the Fock modules of the algebra. For any quiver, we propose that we can consider a particular representation whose states are labelled by molten crystal configurations at depth 0 in the crystal melting model. In other words, such representation is a 2d crystal which is a surface of the 3d crystal constructed from the periodic quiver. Indeed, the Fock representation would arise when one considers the D4-brane framing for the quiver. On the other hand, it was shown in [152] that the torus fixed points of the D4 moduli space are in one-to-one correspondence with the 2d molten crystal configurations. Moreover, the 2d crystal structure, that is, the specific surface in the 3d crystal, is determined by the correpsonding (non-compact) divisor in the toric diagram[13].

In fact, this agrees with the modules used in [206, 209], where the states are labelled by partitions and bi-coloured partitions for $\widehat{\mathfrak{gl}}_1$ and $\widehat{\mathfrak{gl}}_2$ respectively (see also [197]). Now, if we know how the currents of YB are connected to $\mathcal{T}$, the actions of the $\mathcal{R}$-matrix can then be found using the relations among these currents.

The strategy is to consider the matrix element obtained by sandwiching $\mathcal{T}$ between two states $|\mu_{1,2}\rangle \in \bigoplus_a \mathcal{F}_{(a),0}(u)$, viz, $\mathcal{T}_{\mu_1,\mu_2}(u) := \langle\mu_1|\mathcal{T}(u)|\mu_2\rangle$. Here, we have further labelled the auxiliary spaces $\mathcal{F}_{(a),0}(u)$ with the colours a as the 2d crystals can have different initial atoms of different colours. As the name of YB algebras suggests, we propose that the first matrix elements are related to our currents of YB by

$$h^{(a)}(u) = \mathcal{T}_{\varnothing_{(a)},\varnothing_{(a)}}(u), \quad h^{(a)}(u)e^{(a)}(u) = \mathcal{T}_{\varnothing_{(a)},\square_{(a)}}(u), \quad f^{(a)}(u)h^{(a)}(u) = \mathcal{T}_{\square_{(a)},\varnothing_{(a)}}(u),$$
$$\psi^{(a)}(u - \epsilon_3) = \left(\mathcal{T}_{\square_{(a)},\square_{(a)}}(u) - \mathcal{T}_{\varnothing_{(a)},\square_{(a)}}(u)h^{(a)}(u)^{-1}\mathcal{T}_{\square_{(a)},\varnothing_{(a)}}(u)\right)h^{(a)}(u)^{-1}, \tag{5.3.26}$$

---

[12]Hence, if we consider the action of $h(u) = \prod_{a\in Q_0} h^{(a)}(u)$, then we would get

$$h(u)|\mathfrak{C}\rangle = \prod_{a\in Q_0}\prod_{\mathfrak{a}\in\mathfrak{C}} \frac{u - \widetilde{\epsilon}(\mathfrak{a})}{u - \widetilde{\epsilon}(\mathfrak{a}) - \epsilon_3} |\mathfrak{C}\rangle.$$

[13]As studied in [57], the representation of Y constructed from cyrstal configurations would become reducible for some special values of $\widetilde{\epsilon}_I$. In terms of crystals, truncations would appear to stop the molten crystal growing at certain atoms. Therefore, some $\mathrm{Res}\Psi_{\mathfrak{C}}^{(a)}(u)$ would vanish in the actions of $e^{(a)}(u)$ and $f^{(a)}(u)$. The representation would then become irreducible in the truncated algebra. As the 2d crystal is essentially a surface of the 3d crystal, it could be possible to study this from the perspective of truncations. It would be interesting to see if there could be any new insights for the truncations by considering the relations between Y and YB.

where $\varnothing_{(a)}$ and $\square_{(a)}$ denote the empty 2d crystal and one single atom of colour a respectively. Intuitively, starting with the "empty" $h^{(a)}(u)$, we can create an atom by acting $f^{(a)}(u)$ ($e^{(a)}(u)$) on the empty bra (ket) vector. Nevertheless, the actual situation is more complicated (although we would have a conjectural expression for higher levels with a similar intuition involving integrals). Indeed, the expression for $\psi^{(a)}(u)$ in terms of the matrix elements already looks somewhat intricate.

Now we can try to find the actions of the $\mathcal{R}$-matrix on these states via the $\mathcal{R}\mathcal{T}\mathcal{T}$ relation. Let us take the normalization $\mathcal{R}_{12}(u-v)|\varnothing_{(a)}, \varnothing_{(b)}\rangle = |\varnothing_{(a)}, \varnothing_{(b)}\rangle$. Then

$$\langle \varnothing_{(a)}, \varnothing_{(b)}|\mathcal{R}_{12}(u-v)\mathcal{T}_1(u)\mathcal{T}_2(v)|\varnothing_{(a)}, \varnothing_{(b)}\rangle = \langle \varnothing_{(a)}, \varnothing_{(b)}|\mathcal{T}_2(v)\mathcal{T}_1(u)\mathcal{R}_{12}(u-v)|\varnothing_{(a)}, \varnothing_{(b)}\rangle \quad (5.3.27)$$

simply yields the hh relation

$$h^{(a)}(u)h^{(b)}(v) = h^{(b)}(v)h^{(a)}(u). \quad (5.3.28)$$

Next, we can consider

$$\langle \square_{(a)}, \varnothing_{(b)}|\mathcal{R}_{12}(u-v)\mathcal{T}_1(u)\mathcal{T}_2(v)|\varnothing_{(a)}, \varnothing_{(b)}\rangle = \langle \square_{(a)}, \varnothing_{(b)}|\mathcal{T}_2(v)\mathcal{T}_1(u)\mathcal{R}_{12}(u-v)|\varnothing_{(a)}, \varnothing_{(b)}\rangle. \quad (5.3.29)$$

The right hand side is actually

$$\mathcal{T}_{\varnothing_{(b)}, \varnothing_{(b)}}(v)\mathcal{T}_{\square_{(a)}, \varnothing_{(a)}}(u) = h^{(b)}(v)f^{(a)}(u)h^{(a)}(u). \quad (5.3.30)$$

By applying the hf and hh relations, we get

$$\begin{aligned}
&\langle \square_{(a)}, \varnothing_{(b)}|\mathcal{R}_{12}(u-v)\mathcal{T}_1(u)\mathcal{T}_2(v)|\varnothing_{(a)}, \varnothing_{(b)}\rangle \\
&= \frac{1}{v-u}\left((v-u-\delta_{ab}\epsilon_3)f^{(a)}(u)h^{(b)}(v)h^{(a)}(u) + \delta_{ab}\epsilon_3 f^{(a)}(v)h^{(b)}(v)h^{(a)}(u) \right) \\
&= \frac{1}{v-u}\left((v-u-\delta_{ab}\epsilon_3)f^{(a)}(u)h^{(a)}(u)h^{(b)}(v) + \delta_{ab}\epsilon_3 f^{(a)}(v)h^{(b)}(v)h^{(a)}(u) \right) \\
&= \frac{1}{v-u}(v-u-\delta_{ab}\epsilon_3)\mathcal{T}_{\square_{(a)}, \varnothing_{(a)}}(u)\mathcal{T}_{\varnothing_{(b)}, \varnothing_{(b)}}(v) + \frac{1}{v-u}\delta_{ab}\epsilon_3 \mathcal{T}_{\square_{(b)}, \varnothing_{(b)}}(v)\mathcal{T}_{\varnothing_{(a)}, \varnothing_{(a)}}(u).
\end{aligned} \quad (5.3.31)$$

Therefore, we find that

$$\langle \square_{(a)}, \varnothing_{(b)}|\mathcal{R}_{12}(u-v) = \langle \square_{(a)}, \varnothing_{(b)}|\frac{v-u-\delta_{ab}\epsilon_3}{v-u} + \langle \varnothing_{(a)}, \square_{(b)}|\frac{\delta_{ab}\epsilon_3}{v-u}. \quad (5.3.32)$$

Likewise, $\mathcal{R}_{12}(u-v)|\square_{(a)}, \varnothing_{(b)}\rangle$ can be obtained by using the he and ee relations.

One can then proceed to higher levels with more atoms. However, we do not know how general $\mathcal{T}_{\mu_1, \mu_2}$ correspond to the currents. A possible way is to look for currents at higher levels that appear in the local terms from ee and ff relations. These higher currents would then give rise to matrix elements of $\mathcal{T}$ at higher levels. However, the computations would get rather involved even at the levels with 2 atoms for a general quiver. In [206, 209], for $\widehat{\mathfrak{gl}}_1$ and $\widehat{\mathfrak{gl}}_2$, it was found that any such matrix element can be expressed as some contour integral in terms of the currents. Here, we conjecture that this remains true for any general quiver. Explicitly, we have

$$\mathcal{T}_{\mu_1, \mu_2}(u) = \frac{1}{(2\pi i)^n}\oint_{\mathcal{C}_1} dz_1 \cdots \oint_{\mathcal{C}_n} dz_n F(\boldsymbol{z})\left(\prod_{j=k+1}^{n} f^{(a_j)}(z_j)\right) h^{(a_0)}(u)\left(\prod_{j=1}^{k} e^{(a_j)}(z_j)\right), \quad (5.3.33)$$

where the rational function $F(\boldsymbol{z})$ has poles at $z_j = u$. The clockwise contour $\mathcal{C}_j$ goes around $z_j = u, \infty$ and can be deformed in a way such that the contributions from local terms would be cancelled when applying current relations to swap $e^{(a)}(z_j)$ or $f^{(a)}(z_j)$ with other currents. Moreover, the indices a_j (including a_0) should correspond to the colours of the atoms in μ_1 and μ_2.

This conjecture does not tell us how to compute $F(\boldsymbol{z})$, which is the key to get the exact results. Nevertheless, we may still verify this with the expression at level 1. Indeed,

$$
\begin{aligned}
\frac{1}{2\pi i} \oint_{\mathcal{C}} \frac{1}{u-z} f^{(a)}(z) h^{(a)}(u) \mathrm{d}z &= -\operatorname{Res}_u \left(\frac{f^{(a)}(z) h^{(a)}(u)}{u-z} \right) - \operatorname{Res}_\infty \left(\frac{f^{(a)}(z) h^{(a)}(u)}{u-z} \right) \\
&= f^{(a)}(u) h^{(a)}(u) + \operatorname{Res}_0 \left(\frac{1}{z^2} \frac{f^{(a)}(1/z) h^{(a)}(u)}{u-1/z} \right) \\
&= f^{(a)}(u) h^{(a)}(u)
\end{aligned}
\tag{5.3.34}
$$

recovers $\mathcal{T}_{\square_{(a)},\varnothing_{(a)}}(u)$ with $F(z) = 1/(u-z)$. We also give some examples for states at higher levels in Appendix G.

The motivation of this conjecture stems from the $\mathcal{R}$-matrix being the intertwiner between certain free field representations. For the $\mathbb{C}^3$ case, it was found in [206, 211] that we have the relations

$$
\begin{aligned}
[a_{-n}, \mathcal{T}_{\mu_1,\mu_2}] = \mathcal{T}_{\mu_1,\mu_2'}, \quad & [\mathcal{T}_{\mu_1,\mu_2}, a_n] = \mathcal{T}_{\mu_1',\mu_2}, \\
a_{-n} = \frac{1}{\epsilon_3^k (n-1)!} \mathrm{ad}_{e_1}^{n-1} e_0, \quad & a_n = \frac{1}{\epsilon_3^k (n-1)!} \mathrm{ad}_{f_1}^{n-1} f_0,
\end{aligned}
\tag{5.3.35}
$$

where $a_{-n}|\mu\rangle = |\mu'\rangle$ $(n > 0)$ creates boxes/atoms in the Young tableau. Therefore,

$$
\begin{aligned}
a_{-n} &= \frac{1}{(-\epsilon_3)^k (n-1)!} \frac{1}{(2\pi i)^n} \oint \mathrm{d}\boldsymbol{z} \left(\prod_{j=1}^n z_j \right) \left(\sum_{j=1}^n \frac{(-1)^{j-1} \binom{n-1}{j-1}}{z_j} \right) \prod_{j=1}^n e(z_j), \\
a_n &= \frac{1}{(-\epsilon_3)^k (n-1)!} \frac{1}{(2\pi i)^n} \oint \mathrm{d}\boldsymbol{z} \left(\prod_{j=1}^n z_j \right) \left(\sum_{j=1}^n \frac{(-1)^{j-1} \binom{n-1}{j-1}}{z_j} \right) \prod_{j=1}^n f(z_j).
\end{aligned}
\tag{5.3.36}
$$

The integral expression for matrix elements of $\mathcal{T}$ would then follow from their commutation relations with the modes. In general, such process is still not clear, and the explicit expression for the rational function $F(\boldsymbol{z})$ is desired. Nevertheless, we can still apply this to certain problems without the knowledge of its precise form. We will also further expound the contour integral conjecture in §5.4 for a certain class of quivers.

5.3.3 Bethe Ansatz

As an application of our previous results, let us now try to generalize the results in [206, 209] and obtain the Bethe ansatz equation for any quiver Q. Consider the quantum space which is the tensor product of n Fock spaces, $\mathcal{F}(u_1) \otimes \cdots \otimes \mathcal{F}(u_n)$. We can define the Knizhinik-Zamolodchikov (KZ) operator

$$
T_1 := t_1^{L_1} \dots t_G^{L_G} \mathcal{R}_{1,n}(u_1 - u_n) \dots \mathcal{R}_{1,2}(u_1 - u_2),
\tag{5.3.37}
$$

where $t_a \in [0,1)$ are the twist parameters and $G = |Q_0|$. The quantum space is graded under each level operator L_a via

$$
L_a := \sum_{j=1}^n L_{a,j} \quad \text{such that} \quad L_{a,j} |\boldsymbol{\mu}\rangle_u = N_{a,j} |\boldsymbol{\mu}\rangle_u
\tag{5.3.38}
$$

gives the number $N_{a,j}$ of atoms with colour a in the jth 2-dimensional crystal, where the subscript u indicates that the state belongs to $\bigotimes \mathcal{F}(u_j)$. By considering

$$
|\chi\rangle_x := |\square_1, \dots, \square_1, \dots, \square_G, \dots, \square_G\rangle_x \in \mathcal{F}_1(x_{1,1}) \otimes \cdots \otimes \mathcal{F}_1(x_{1,N_1}) \otimes \cdots \otimes \mathcal{F}_G(x_{G,1}) \otimes \cdots \otimes \mathcal{F}_G(x_{G,N_G}),
\tag{5.3.39}
$$

let us further introduce the off-shell Bethe vector

$$|B(x)\rangle_u := {}_x\langle\varnothing|\mathcal{R}_{x_{1,1},\, u_1}\ldots\mathcal{R}_{x_{1,1},\, u_n}\ldots\mathcal{R}_{x_{1,N_1},\, u_1}\ldots\mathcal{R}_{x_{1,N_1},\, u_n}$$
$$\ldots\mathcal{R}_{x_{G,1},\, u_1}\ldots\mathcal{R}_{x_{G,1},\, u_n}\ldots\mathcal{R}_{x_{G,N_G},\, u_1}\ldots\mathcal{R}_{x_{G,N_G},\, u_n}|\varnothing\rangle_u|\chi\rangle_x \tag{5.3.40}$$

in the quantum space, where ${}_x\langle\varnothing,\ldots,\varnothing|$ is abbreviated as ${}_x\langle\varnothing|$ for brevity. Notice that it was pointed out in [58] that due to the non-trivial coproduct of the algebra from soliton contributions, in general $|\chi\rangle_x$ should be a mixed state of the chains of crystals rather than simply being identified as a chain of single-atom states. See [58] for the modification of this subtlety. Nevertheless, we shall take this single-atom states for $|\chi\rangle_x$ as an illustration. In the following discussions, this would change the eigenvalue of the KZ operator with the results on Bethe ansatz equations unaffected.

Now, we would like to find the condition such that the off-shell Bethe vector is an eigenvector of the KZ operator, that is, $T_1|B(x)\rangle_u = \mathtt{t}|B(x)\rangle_u$. Pictorially, we have

$$(5.3.41)$$

and

$$(5.3.42)$$

following the $\mathcal{RTT}$ relations along with $\mathcal{R}_{1,j}|\varnothing,\varnothing\rangle = |\varnothing,\varnothing\rangle$.

If we project the eigenvalue equation onto some state ${}_u\langle\boldsymbol{\mu}|$ satisfying $\sum_{j=1}^{n} N_{a,j} = N_a$ for all a, then

$$\begin{aligned}
{}_u\langle\boldsymbol{\mu}|T_1|B(x)\rangle_u &= t_1^{N_{1,1}}\ldots t_n^{N_{G,1}}\, {}_x\langle\varnothing|\mathcal{T}_{\mu_2,\emptyset}(u_2)\ldots\mathcal{T}_{\mu_n,\varnothing}(u_n)\mathcal{T}_{\mu_1,\varnothing}(u_1)|\chi\rangle_x \\
&= \mathtt{t}\, {}_x\langle\varnothing|\mathcal{T}_{\mu_1,\varnothing}(u_1)\mathcal{T}_{\mu_2,\varnothing}(u_2)\ldots\mathcal{T}_{\mu_n,\varnothing}(u_n)|\chi\rangle_x.
\end{aligned} \tag{5.3.43}$$

By setting ${}_x\langle\boldsymbol{\mu}| = {}_x\langle\varnothing, \mu_2,\ldots|$, i.e., $\mu_1 = \varnothing$, this equation becomes

$$t_1^0\ldots t_G^0\, {}_x\langle\varnothing|\mathcal{T}_{\mu_2,\varnothing}(u_2)\ldots\mathcal{T}_{\mu_n,\varnothing}(u_n)h^{(a)}(u_1)|\chi\rangle_x = \mathtt{t}\, {}_x\langle\varnothing|h^{(a)}(u_1)\mathcal{T}_{\mu_2,\varnothing}(u_2)\ldots\mathcal{T}_{\mu_n,\varnothing}(u_n)|\chi\rangle_x. \tag{5.3.44}$$

The actions of the currents/modes in YB on the 2d crystal are completely analogous to the actions on the 3d crystal discussed above. Therefore[14],

$$h^{(a)}(u)|\chi\rangle_x = \prod_{j=1}^{N_a} \frac{u - x_{a,j}}{u - x_{a,j} + \epsilon}|\chi\rangle_x, \tag{5.3.45}$$

where we have used $\epsilon := \epsilon_1 + \epsilon_2 = -\epsilon_3$. As a result,

$$\mathtt{t} = \prod_{j=1}^{N_1} \frac{u_1 - x_{1,j}}{u_1 - x_{1,j} + \epsilon}. \tag{5.3.46}$$

---

[14]Notice that the coordinates are now given by $y + \tilde{\epsilon}(\mathfrak{a}) = y + \sum_I N_I\tilde{\epsilon}_I$ for an atom $\mathfrak{a}$ in $|\mu\rangle_y$ [206, 209].

Now let us consider the state $_x\langle\boldsymbol{\mu}|$ with $N_{a,1} = \delta_{aa'}$ for some colour a'. Using the contour integral form of $\mathcal{T}_{\mu_j,\varnothing}$, the eigenvalue equation reads

$$t_1 \left\langle\varnothing\right| \oint F(\boldsymbol{z}) \left(f^{(1)}\left(z_{1,1}^{(n)}\right)\dots f^{(1)}\left(z_{1,N_{1,n}}^{(n)}\right)\dots f^{(G)}\left(z_{G,1}^{(n)}\right)\dots f^{(G)}\left(z_{G,N_{G,n}}^{(n)}\right) h^{(1)}(u_n)\right)$$

$$\dots \left(f^{(1)}\left(z_{1,1}^{(2)}\right)\dots f^{(G)}\left(z_{G,N_{G,2}}^{(2)}\right) h^{(1)}(u_2)\right) f^{(1)}\left(z_{1,1}^{(1)}\right) h^{(1)}(u_1)\mathrm{d}\boldsymbol{z}\left|\chi\right\rangle_x$$

$$=\mathtt{t} \left\langle\varnothing\right| \oint F(\boldsymbol{z}) f^{(1)}\left(z_{1,1}^{(1)}\right) h^{(1)}(u_1) \left(f^{(1)}\left(z_{1,1}^{(n)}\right)\dots h^{(1)}(u_n)\right)\dots \left(f^{(1)}\left(z_{1,1}^{(2)}\right)\dots h^{(1)}(u_2)\right)\mathrm{d}\boldsymbol{z}\left|\chi\right\rangle_x .$$

$$(5.3.47)$$

Given the different variables with three indices, it would be better to clarify the notation here. For $z_{*,\star}^{(\circledast)}$ indicating the $\circledast^{\text{th}}$ state/2d crystal, $*$ denotes the colour of an atom (as in $f^{(*)}$), and $\star$ enumerates the number of the atoms of such colour. Recall that each Fock space in the quantum space is $\mathcal{F}_1$ whose initial atom is of colour 1 (as in $h^{(1)}$).

Using the hf and ff relations, we can get

$$t_1 \left(\prod_{i=2}^{n} \frac{u_i - x_{1,1} + \epsilon}{u_i - x_{1,1}}\right) (-1)^{|(1)|\sum_{a=1}^{G}|(a)|N_a} \left(\prod_{a=1}^{G} \prod_{\substack{j=1 \\ (a,j)\neq(1,1)}}^{N_a} \frac{g_{1a}(x_{1,1} - x_{a,j})}{\overline{g}_{a1}(x_{1,1} - x_{a.j})}\right) \left(\prod_{l=1}^{N_1} \frac{u_1 - x_{1,l}}{u_1 - x_{1,l} + \epsilon}\right) = \mathtt{t}.$$

$$(5.3.48)$$

Notice that the parameters $\widetilde{\epsilon}_{1a,i}$ and $\widetilde{\epsilon}_{a1,i}$ in g_{1a} and $\overline{g}_{a1}$ should be correspondingly changed to ϵ_j in terms of the loop and vertex constraints from the quiver Yangian. Plugging in the value of $\mathtt{t}$ yields the Bethe equation

$$\left(\prod_{i=2}^{n} \frac{u_i - x_{1,1}}{u_i - x_{1,1} + \epsilon}\right) \left(\prod_{a=1}^{G} \prod_{\substack{j=1 \\ (a,j)\neq(1,1)}}^{N_a} \frac{\overline{g}_{a1}(x_{1,1} - x_{a.j})}{g_{1a}(x_{1,1} - x_{a,j})}\right) = (-1)^{|(1)|\sum_{a=1}^{G}|(a)|N_a} t_1. \qquad (5.3.49)$$

One may then consider other states $_x\langle\boldsymbol{\mu}|$ with different 2d crystal configurations (whose initial atoms are still labelled by 1) so that the other twist parameters t_j would also appear in the Bethe equations. There should be a set of G independent such equations as the sufficient and necessary condition for the off-shell Bethe vector $|B(x)\rangle_u$ to be an eigenstate of the KZ operator T_1. These equations can then be labelled by $(\text{eqn})_{1,\dots,G}$ so that they are chosen by considering the state where the atom of colour a first appears in the 2d crystal for $(\text{eqn})_a$.

Examples Consider the Jordan quiver, that is, one node with one loop. Taking the quantum (auxiliary) space to be a tensor product of L (M) Fock space $\mathcal{F}$, we simply have

$$\prod_{l=1}^{L} \frac{x_j - u_l}{x_j - u_l + \epsilon} = t \prod_{k\neq j}^{M} \frac{x_j - x_k - \epsilon}{x_j - x_k + \epsilon}. \qquad (5.3.50)$$

This reduces to the familiar Bethe equation

$$\left(\frac{x_j + i}{x_j - i}\right)^{L} = t \prod_{k\neq j}^{M} \frac{x_j - x_k + 2i}{x_j - x_k - 2i} \qquad (5.3.51)$$

for the XXX spin chain under $u_l = -i$, $\epsilon = -2i$.

As the simplest toric CY example, consider $\mathbb{C}^3$ whose quiver Yangian is the affine Yangian $\mathrm{Y}\left(\widehat{\mathfrak{gl}}_1\right)$. Taking the quantum (auxiliary) space to be a tensor product of n (N) Fock space $\mathcal{F}$ (notice that

we only have one node in the quiver), we get the equation

$$\prod_{l=1}^{n} \frac{x_j - u_l}{x_j - u_l - \epsilon_3} = t \prod_{k \neq j}^{N} \prod_{\alpha=1}^{3} \frac{x_j - x_k + \epsilon_\alpha}{x_j - x_k - \epsilon_\alpha} \tag{5.3.52}$$

for any $j = 1, \ldots, N$, as obtained in [206].

The connection to Bethe ansatz equation would be of particular interest in the context of Bethe/gauge correspondence [212–214] (see [58] for a more recent discussion on this). For instance, the rapidities (denoted as x_j in the above examples) in the Bethe equations correspond to the supersymmetric vacua of the associated 2d $\mathcal{N} = (2,2)$ theory. In terms of the S-matrix, due to its factorized scattering property, we expect that each (2-magnon) S-matrix would correspond to a bond factor $\phi^{b \Rightarrow a}(x_j - x_k)$ as in (5.2.23) on the quiver side.

5.4 Generators of Quiver Yangians

For toric CYs without compact divisors whose quivers have more than two nodes[15], the quiver Yangians are actually generated by finitely many generators[16]. In this section, $f_n^{(a)}$ will be used to denote the generators in Y (instead of YB).

Recall that the generators are $e_i^{(a)}$, $f_i^{(a)}$ and $\psi_j^{(a)}$ with $a \in Q_0$, $i \in \mathbb{N}$ and $j \in \mathbb{Z}_{\geq -1}$. In particular, $\psi_{-1}^{(a)} = 1$. As $|a \to b| \leq 1$, we have the relations

$$\left[\psi_{n+1}^{(a)}, e_m^{(b)}\right] = \sigma_1 e_m^{(b)} \psi_n^{(a)} + \sigma_1' \psi_n^{(a)} e_m^{(b)} + \left[\psi_n^{(a)}, e_{m+1}^{(b)}\right],$$
$$\left[\psi_{n+1}^{(a)}, f_m^{(b)}\right] = -\sigma_1' f_m^{(b)} \psi_n^{(a)} - \sigma_1 \psi_n^{(a)} f_m^{(b)} + \left[\psi_n^{(a)}, f_{m+1}^{(b)}\right], \tag{5.4.1}$$

where $\sigma_1 := \sigma_1^{a \to b}$ and $\sigma_1' := \sigma_1^{b \to a}$. Then for $n = -1$, we have

$$\left[\psi_0^{(a)}, e_m^{(b)}\right] = \widetilde{\sigma}_1 e_m^{(b)}, \quad \left[\psi_0^{(a)}, f_m^{(b)}\right] = -\widetilde{\sigma}_1 f_m^{(b)}, \tag{5.4.2}$$

where $\widetilde{\sigma}_1 := \sigma_1 + \sigma_1'$. Notice that these were also used when discussing the relation of quiver Yangians and Ueda's affine super Yangians. Therefore, for $n = 0$, we get

$$\left[\psi_1^{(a)}, e_m^{(b)}\right] = \frac{\sigma_1}{\widetilde{\sigma}_1} \psi_0^{(a)} \left[\psi_0^{(a)}, e_m^{(b)}\right] + \frac{\sigma_1'}{\widetilde{\sigma}_1} \left[\psi_0^{(a)}, e_m^{(b)}\right] \psi_0^{(a)} + \widetilde{\sigma}_1 e_{m+1}^{(b)},$$
$$\left[\psi_1^{(a)}, f_m^{(b)}\right] = \frac{\sigma_1'}{\widetilde{\sigma}_1} \psi_0^{(a)} \left[\psi_0^{(a)}, f_m^{(b)}\right] + \frac{\sigma_1}{\widetilde{\sigma}_1} \left[\psi_0^{(a)}, f_m^{(b)}\right] \psi_0^{(a)} - \widetilde{\sigma}_1 f_{m+1}^{(b)}. \tag{5.4.3}$$

Notice that we have chosen a and b with arrows connecting them so that σ_1 and σ_1' are non-zero.

For $|(a)| = 0$, choosing $b = a$, we have

$$e_{m+1}^{(a)} = \frac{1}{2\sigma_1} \left[\psi_1^{(a)} - \frac{1}{2}\left(\psi_0^{(a)}\right)^2, e_m^{(a)}\right], \quad f_{m+1}^{(a)} = -\frac{1}{2\sigma_1} \left[\psi_1^{(a)} - \frac{1}{2}\left(\psi_0^{(a)}\right)^2, f_m^{(a)}\right]. \tag{5.4.4}$$

For $|(a)| = 1$, choosing $a = b + 1$, we have

$$e_{m+1}^{(b)} = \frac{1}{\widetilde{\sigma}_1} \left[\psi_1^{(b+1)} - \frac{\sigma_1}{\widetilde{\sigma}_1}\left(\psi_0^{(b+1)}\right)^2, e_m^{(b)}\right] - \frac{\sigma_1 - \sigma_1'}{\widetilde{\sigma}_1} e_m^{(b)} \psi_0^{(b+1)},$$
$$f_{m+1}^{(b)} = -\frac{1}{\widetilde{\sigma}_1} \left[\psi_1^{(b+1)} - \frac{\sigma_1}{\widetilde{\sigma}_1}\left(\psi_0^{(b+1)}\right)^2, f_m^{(b)}\right] + \frac{\sigma_1 - \sigma_1'}{\widetilde{\sigma}_1} \psi_0^{(b+1)} f_m^{(b)}. \tag{5.4.5}$$

---

[15]More generally, the discussions here should work for any symmetric quiver with at most one pair of arrows between any two nodes.

[16]In fact, as we will discuss later, they are not only finitely generated but also finitely presented. In other words, the defining relations for higher modes can be obtained from finitely many relations at lower orders.

Notice that we can always write σ_1 and σ_1' in terms of $\epsilon_{1,2,3}$ due to vertex constraints. For both bosonic and fermionic nodes, define

$$\widetilde{\psi}_1^{(a)} := \psi_1^{(a)} - \frac{\sigma_1^{a \to b}}{\sigma_1^{a \to b} + \sigma_1^{b \to a}} \left(\psi_0^{(a)} \right)^2. \tag{5.4.6}$$

We can then compactly write the relations as

$$
\begin{aligned}
e_{m+1}^{(a)} &= \frac{1}{\sigma_1^{b \to a} + \sigma_1^{a \to b}} \left[\widetilde{\psi}_1^{(b)}, e_m^{(a)} \right] - \frac{\sigma_1^{b \to a} - \sigma_1^{a \to b}}{\sigma_1^{b \to a} + \sigma_1^{a \to b}} e_m^{(a)} \psi_0^{(b)}, \\
f_{m+1}^{(a)} &= -\frac{1}{\sigma_1^{b \to a} + \sigma_1^{a \to b}} \left[\widetilde{\psi}_1^{(b)}, f_m^{(a)} \right] + \frac{\sigma_1^{b \to a} - \sigma_1^{a \to b}}{\sigma_1^{b \to a} + \sigma_1^{a \to b}} \psi_0^{(b)} f_m^{(a)},
\end{aligned}
\tag{5.4.7}
$$

where $b = a$ for $|(a)| = 0$ and $b = a + 1$ for $|(a)| = 1$. Moreover, we have

$$\psi_{m+1}^{(a)} = \left[e_{m+1}^{(a)}, f_0^{(a)} \right\}. \tag{5.4.8}$$

As a result, we have shown that the quiver Yangian in this case is generated by $e_0^{(a)}$, $f_0^{(a)}$ and $\psi_{0,1}^{(a)}$. The other modes can actually be inductively obtained using (5.4.7) and (5.4.8).

Moreover, we can now also get the matrix elements of $\mathcal{T}(u)$ at higher levels inductively. For instance,

$$\mathcal{T}_{\varnothing, \mu'}(u) = \langle \varnothing | \mathcal{T}(u) | \mu' \rangle = \langle \varnothing | \mathcal{T}(u) e_m^{(a)} | \mu \rangle. \tag{5.4.9}$$

Then using (5.4.7) and (5.4.8), we can express all $\mathcal{T}_{\mu_1, \mu_2}(u)$ in terms of $e_0^{(a)}$, $f_0^{(a)}$ and $\psi_{0,1}^{(a)}$. If we can write the contour integral expressions for all the states generated only by $e_0^{(a)}$ (and $f_0^{(a)}$), then we can write the contour integral expression for any $\mathcal{T}_{\mu_1, \mu_2}(u)$ and hence obtain the action of the $\mathcal{R}$-matrix (recall that we know the actions of ψ from §5.2 and §5.3.3).

In fact, analogous to the known cases, we conjecture that for $|\mu'\rangle = e_0^{(a)} |\mu\rangle$, where $|\mu\rangle$ is a state generated only from $e_0^{(a_i)}$, we have

$$
\begin{aligned}
\mathcal{T}_{\varnothing, \mu'}(u) &= \frac{1}{2\pi i} \oint_{\infty + u} \mathrm{d}z \frac{1}{\epsilon_3} \left(1 - \frac{u - z - \epsilon_3}{u - z} \prod_{i=1}^{k} \frac{\overline{g}_{a a_i}(u - z)}{g_{a_i a}(u - z)} \right) \mathcal{T}_{\varnothing, \mu}(u) e^{(a)}(z) \\
&= \frac{1}{2\pi i} \oint_{\infty + u} \mathrm{d}z \frac{1}{\epsilon_3} \left(1 - \frac{u - z - \epsilon_3}{u - z} \prod_{i=1}^{k} \frac{1}{\phi^{a \Rightarrow a_i}(u - z)} \right) \mathcal{T}_{\varnothing, \mu}(u) e^{(a)}(z),
\end{aligned}
\tag{5.4.10}
$$

where $\mathcal{T}_{\varnothing, \mu}(u) = \frac{1}{(2\pi i)^k} \oint \mathrm{d}\boldsymbol{z} F(\boldsymbol{z}) h^{(a_0)}(u) e^{(a_1)}(z_1) \dots e^{(a_k)}(z_k)$. Similarly,

$$
\begin{aligned}
\mathcal{T}_{\mu', \varnothing}(u) &= \frac{1}{2\pi i} \oint_{\infty + u} \mathrm{d}z \frac{1}{\epsilon_3} \left(1 - \frac{u - z - \epsilon_3}{u - z} \prod_{i=1}^{k} \frac{\overline{g}_{a a_i}(u - z)}{g_{a_i a}(u - z)} \right) \left(-f^{(a)}(z) \right) \mathcal{T}_{\mu, \varnothing}(u) \\
&= \frac{1}{2\pi i} \oint_{\infty + u} \mathrm{d}z \frac{1}{\epsilon_3} \left(1 - \frac{u - z - \epsilon_3}{u - z} \prod_{i=1}^{k} \frac{1}{\phi^{a \Rightarrow a_i}(u - z)} \right) \left(-f^{(a)}(z) \right) \mathcal{T}_{\mu, \varnothing}(u).
\end{aligned}
\tag{5.4.11}
$$

We can then get any $\mathcal{T}_{\mu_1, \mu_2}(u)$ inductively using the contour integral expressions. For instance, at level 1, we simply have

$$\mathcal{T}_{\varnothing, \square_{(a)}}(u) = \frac{1}{2\pi i} \oint_{\infty + u} \mathrm{d}z \frac{1}{\epsilon_3} \left(1 - \frac{u - z - \epsilon_3}{u - z} \right) \mathcal{T}_{\varnothing, \varnothing}(u) e^{(a)}(z) = \frac{1}{2\pi i} \oint_{\infty + u} \mathrm{d}z \frac{1}{u - z} h^{(a)}(u) e^{(a)}(z), \tag{5.4.12}$$

which agrees with our discussions in §5.3.2. More examples at higher levels can be found in Appendix G.

5.5 Coproduct of Quiver Yangians

For the remaining part of this chapter, we shall mainly focus on the generalized conifolds $xy = z^M w^N$ with $M + N > 2$. Moreover, in §5.5~5.7 (and Appendix E) only, we shall rescale the generators as $e_n^{(a)} \to (\epsilon_1+\epsilon_2)^{1/2} e_n^{(a)}$, $f_n^{(a)} \to (\epsilon_1+\epsilon_2)^{1/2} f_n^{(a)}$ and $\psi_n^{(a)} \to (\epsilon_1+\epsilon_2)\psi_n^{(a)}$ for convenience.

Following the strategy in [215, 216], a coproduct of the quiver Yangian can be obtained based on the underlying Kac-Moody superalgebra $\mathfrak{g} = A_{M-1,N-1}^{(1)}$. In the Chevalley basis, we have the generators with $\left[x_+^{(a)}, x_-^{(a)}\right] = h^{(a)}$ and $\left(x_+^{(a)}, x_-^{(a)}\right) = 1$, where (-,-) is an invariant inner product on the Kac-Moody superalgebra. Let $\Delta = \Delta_+ \cup \Delta_-$ be the set of roots composed of positive and negative roots. Denote the sets of real and imaginary roots as Δ^{re} and Δ^{im} respectively. Write $\mathfrak{g}_\alpha$ as the root space attached to the root α, and the simple roots will be labelled as $\alpha^{(a)}$. In particular, $\Delta_+^{\mathrm{re}} = \mathring{\Delta}_+ \cup \left\{n\delta + \alpha | n \in \mathbb{Z}_+, \alpha \in \mathring{\Delta}\right\}$ and $\Delta_+^{\mathrm{im}} = \{n\delta | n \in \mathbb{Z}_+\}$, where $\mathring{\Delta}$ is the set of roots of the underlying Lie superalgebra with the zeroth vertex removed in the Dynkin diagram of $\mathfrak{g}$ and $\delta = \sum_a \alpha^{(a)}$ is the minimal positive imaginary root of $\mathfrak{g} = A_{M-1,N-1}^{(1)}$. Notice that all the odd roots are isotropic (i.e., with vanishing inner product) in such case.

Following the Cartan matrix (with the first non-zero diagonal element being 2), our convention would be taken as $\sigma_1^{ab} + \sigma_1^{ba} = (\epsilon_1 + \epsilon_2)\left(\alpha^{(a)}, \alpha^{(b)}\right)$ for future convenience. In other words, we shall always choose $\varsigma_a = -1$ for the corresponding simplex in the toric diagram. Therefore, $\sigma_1^{aa} = -\frac{1}{2}\epsilon_3\left(\alpha^{(a)}, \alpha^{(a)}\right)$. Then it is straightforward to see that there is an algebra homomorphism ι from $U(\mathfrak{g})$ to $\mathtt{Y}$ with $h^{(a)} \mapsto \psi_0^{(a)}$, $x_+^{(a)} \mapsto e_0^{(a)}$ and $x_-^{(a)} \mapsto f_0^{(a)}$. For each positive root α, choose a basis $\left\{x_+^{(\alpha,k)}\right\}$ of $\mathfrak{g}_\alpha$ with a dual basis $\left\{x_-^{(\alpha,k)}\right\}$ of $\mathfrak{g}_{-\alpha}$ such that $\left(x_+^{(\alpha,k)}, x_-^{(\alpha,l)}\right) = \delta_{kl}$. We will also denote $e^{(\alpha,k)} = \iota\left(x_+^{(\alpha,k)}\right)$ and $f^{(\alpha,k)} = \iota\left(x_-^{(\alpha,k)}\right)$, where $k = 1,\dots,\dim \mathfrak{g}_\alpha$. When α is a real root, $\dim \mathfrak{g}_\alpha = 1$ and we shall simply write $e^{(\alpha)} = e^{(\alpha,1)}$, $f^{(\alpha)} = f^{(\alpha,1)}$. In particular, given a simple root $\alpha^{(a)}$, we have $e_0^{(a)} = e^{\left(\alpha^{(a)}\right)}$ and $f_0^{(a)} = f^{\left(\alpha^{(a)}\right)}$.

5.5.1 A Minimalistic Presentation

The definition of the quiver Yangian in §5.2 involves infinitely many generators. To write the coproduct, we first need to give a presentation with generators of a finite number.

Recall from the above discussions that all the generators can in fact be inductively obtained from $e_0^{(a)}$, $f_0^{(a)}$ and $\psi_{0,1}^{(a)}$ by

$$e_{m+1}^{(a)} = \frac{1}{\left(\alpha^{(a)}, \alpha^{(b)}\right)} \left[\widetilde{\psi}_1^{(b)}, e_m^{(a)}\right] - \frac{\sigma_1^{ab} - \sigma_1^{ba}}{2\left(\alpha^{(a)}, \alpha^{(b)}\right)} \left[\psi_0^{(b)}, e_m^{(a)}\right] = \frac{1}{\left(\alpha^{(a)}, \alpha^{(b)}\right)} \left[\widetilde{\psi}_1^{(b)}, e_m^{(a)}\right] - \frac{\sigma_1^{ab} - \sigma_1^{ba}}{2} e_m^{(a)},$$

$$f_{m+1}^{(a)} = -\frac{1}{\left(\alpha^{(a)}, \alpha^{(b)}\right)} \left[\widetilde{\psi}_1^{(b)}, f_m^{(a)}\right] + \frac{\sigma_1^{ab} - \sigma_1^{ba}}{2\left(\alpha^{(a)}, \alpha^{(b)}\right)} \left[\psi_0^{(b)}, f_m^{(a)}\right] = -\frac{1}{\left(\alpha^{(a)}, \alpha^{(b)}\right)} \left[\widetilde{\psi}_1^{(b)}, f_m^{(a)}\right] - \frac{\sigma_1^{ab} - \sigma_1^{ba}}{2} f_m^{(a)},$$

$$\psi_{m+1}^{(a)} = \left[e_{m+1}^{(a)}, f_0^{(a)}\right],$$

$$(5.5.1)$$

where $\widetilde{\psi}_1^{(b)} := \psi_1^{(b)} - \frac{\epsilon_1+\epsilon_2}{2}\left(\psi_0^{(b)}\right)^2$, and the node b can be taken as a (resp. $a+1$) when a is bosonic (resp. fermionic). Therefore, it is natural to expect that the quiver Yangian can be generated only by finitely many relations of the three sets of zero modes together with $\psi_1^{(a)}$ (or equivalently, $\widetilde{\psi}_1^{(a)}$). To confirm that this is the case, we need to show that they can recover all the defining relations of the quiver Yangian in §5.2.

For this minimalistic presentation of the (reduced) quiver Yangians, as discussed in [15], we also need to exclude two special cases: (1) $(M, N) = (2, 1), (1, 2)$; (2) $(M, N) = (2, 2)$ with only fermionic nodes[17]. Their quivers are depicted in Figure 5.5.1.

<div align="center">(a)   (b)</div>
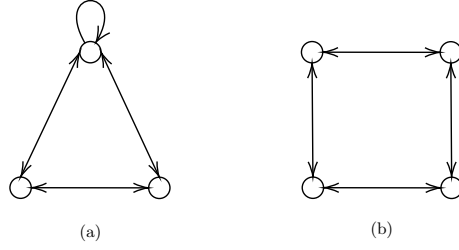
FIGURE 5.5.1: (a) The SPP quiver with $(M, N) = (2, 1), (1, 2)$. (b) The quiver for the $\mathbb{Z}_2$ orbifold of the conifold with $(M, N) = (2, 2)$ in one of the toric phases.

Theorem 5.5.1. *For generalized conifolds with $M + N > 2$, the non-reduced quiver Yangian is generated by the modes $e_r^{(a)}$, $f_r^{(a)}$ and $\psi_r^{(a)}$ $(a \in Q_0,\ r = 0, 1)$ satisfying the relations*

$$\left[\psi_r^{(a)}, \psi_s^{(b)}\right] = 0, \tag{5.5.2}$$

$$\left[e_0^{(a)}, f_0^{(b)}\right] = \delta_{ab}\psi_0^{(a)}, \quad \left[e_1^{(a)}, f_0^{(b)}\right] = \left[e_0^{(a)}, f_1^{(b)}\right] = \delta_{ab}\psi_1^{(a)}, \tag{5.5.3}$$

$$\left[\psi_0^{(a)}, e_r^{(b)}\right] = \left(\alpha^{(a)}, \alpha^{(b)}\right) e_r^{(b)}, \tag{5.5.4}$$

$$\left[\psi_1^{(a)}, e_0^{(b)}\right] = \left(\alpha^{(a)}, \alpha^{(b)}\right) e_1^{(b)} + \sigma_1^{ba}\psi_0^{(a)}e_0^{(b)} + \sigma_1^{ab}e_0^{(b)}\psi_0^{(a)}, \tag{5.5.5}$$

$$\left[\psi_0^{(a)}, f_r^{(b)}\right] = -\left(\alpha^{(a)}, \alpha^{(b)}\right) f_r^{(b)}, \tag{5.5.6}$$

$$\left[\psi_1^{(a)}, f_0^{(b)}\right] = -\left(\alpha^{(a)}, \alpha^{(b)}\right) f_1^{(b)} + \sigma_1^{ab}\psi_0^{(a)}f_0^{(b)} + \sigma_1^{ba}f_0^{(b)}\psi_0^{(a)}, \tag{5.5.7}$$

$$\left[e_0^{(a)}, e_0^{(b)}\right] = \left[f_0^{(a)}, f_0^{(b)}\right] = 0 \qquad (\sigma_1^{ab} = 0), \tag{5.5.8}$$

$$\left[e_1^{(a)}, e_0^{(b)}\right] - \left[e_0^{(a)}, e_1^{(b)}\right] = \sigma_1^{ba}e_0^{(a)}e_0^{(b)} + (-1)^{|a||b|}\sigma_1^{ab}e_0^{(b)}e_0^{(a)}, \tag{5.5.9}$$

$$\left[f_1^{(a)}, f_0^{(b)}\right] - \left[f_0^{(a)}, f_1^{(b)}\right] = -\sigma_1^{ab}f_0^{(a)}f_0^{(b)} - (-1)^{|a||b|}\sigma_1^{ba}f_0^{(b)}f_0^{(a)}. \tag{5.5.10}$$

Then the higher modes $\psi_n^{(a)}$, $e_m^{(a)}$ and $f_m^{(a)}$ $(n > 1, m > 0)$ are defined via (5.5.1). *Moreover, when the quiver does* not *belong to those in Figure* 5.5.1, *the quiver Yangian is generated by these relations together with*

$$\left[e_0^{(a)}, \left[e_0^{(a)}, e_0^{(a\pm1)}\right]\right] = \left[f_0^{(a)}, \left[f_0^{(a)}, f_0^{(a\pm1)}\right]\right] = 0 \qquad (|a| = 0), \tag{5.5.11}$$

$$\left[e_0^{(a)}, \left[e_0^{(a+1)}, \left[e_0^{(a)}, e_0^{(a-1)}\right]\right]\right] = \left[f_0^{(a)}, \left[f_0^{(a+1)}, \left[f_0^{(a)}, f_0^{(a-1)}\right]\right]\right] = 0 \qquad (|a| = 1). \tag{5.5.12}$$

In terms of $\widetilde{\psi}_1^{(a)}$, the $\psi_1 e_0$ and $\psi_1 f_0$ relations can be written as

$$\left[\widetilde{\psi}_1^{(a)}, e_0^{(b)}\right] = \left(\alpha^{(a)}, \alpha^{(b)}\right) e_1^{(b)} + \frac{\sigma_1^{ba} - \sigma_1^{ab}}{2}\left(\alpha^{(a)}, \alpha^{(b)}\right) e_0^{(b)},$$

$$\left[\widetilde{\psi}_1^{(a)}, f_0^{(b)}\right] = -\left(\alpha^{(a)}, \alpha^{(b)}\right) f_1^{(b)} - \frac{\sigma_1^{ba} - \sigma_1^{ab}}{2}\left(\alpha^{(a)}, \alpha^{(b)}\right) f_0^{(b)}. \tag{5.5.13}$$

It is worth noting that this resembles Drinfeld's realization in [217]. For simplicity, we shall denote all the relations (5.5.2)∼(5.5.10) as (R) and the relations (5.5.11), (5.5.12) as (S). A proof of this can be found in [15].

---

[17]Notice that the other toric phase for $(M, N) = (2, 2)$ is not excluded, where the quiver has four nodes being bosonic and fermionic alternatively, though all cases with $M = N$ will not be considered when we discuss coproducts later.

Although we omit the proof here, let us mention some useful identities used therein.

Lemma 5.5.2. *For $m \in \mathbb{N}$, we have*

$$\left[\psi_0^{(a)}, e_m^{(b)}\right] = \left(\alpha^{(a)}, \alpha^{(b)}\right) e_m^{(b)}, \tag{5.5.14}$$

$$\left[\psi_1^{(a)}, e_m^{(b)}\right] = \left(\alpha^{(a)}, \alpha^{(b)}\right) e_{m+1}^{(b)} + \sigma_1^{ba} \psi_0^{(a)} e_m^{(b)} + \sigma_1^{ab} e_m^{(b)} \psi_0^{(a)}, \tag{5.5.15}$$

and similar relations for $f_m^{(b)}$ from (R).

It would be helpful to also spell out these relations using $\widetilde{\psi}_1^{(a)}$:

$$\left[\widetilde{\psi}_1^{(a)}, e_m^{(b)}\right] = \left(\alpha^{(a)}, \alpha^{(b)}\right) e_{m+1}^{(b)} + \frac{\sigma_1^{ba} - \sigma_1^{ab}}{2} \left(\alpha^{(a)}, \alpha^{(b)}\right) e_m^{(b)},$$
$$\left[\widetilde{\psi}_1^{(a)}, f_m^{(b)}\right] = -\left(\alpha^{(a)}, \alpha^{(b)}\right) f_{m+1}^{(b)} - \frac{\sigma_1^{ba} - \sigma_1^{ab}}{2} \left(\alpha^{(a)}, \alpha^{(b)}\right) f_m^{(b)}. \tag{5.5.16}$$

5.5.2 Another Presentation and Coproduct

From now on, besides the restrictions $M + N > 2$ and $MN \neq 2$, we will mainly focus on the cases with $M \neq N$ due to the subtleties from the underlying simple Lie superalgebra $\mathfrak{psl}(M|M)$ (when $M = N$). Analogous to [215], we can write an algebra homomorphism $\Delta_{V_1, V_2} : \mathtt{Y} \to \mathrm{End}_{\mathbb{C}}(V_1 \otimes V_2)$ for any modules $V_{1,2}$ in the category $\mathcal{O}$. In particular, this can be promoted to a coproduct of the Yangian algebra by considering its completion $\widehat{\mathtt{Y}}$ following the argument in [215, §5]. Then any Δ_{V_1, V_2} can be recovered from $\Delta : \mathtt{Y} \to \mathtt{Y} \widehat{\otimes} \mathtt{Y}$, where $\mathtt{Y} \widehat{\otimes} \mathtt{Y}$ is the completion of $\mathtt{Y} \otimes \mathtt{Y}$ we are now going to discuss.

The quiver Yangian has the triangular decomposition $\mathtt{Y} \cong \mathtt{Y}^+ \otimes \mathtt{Y}^0 \otimes \mathtt{Y}^-$, where $\mathtt{Y}^+$ ($\mathtt{Y}^-$, resp. $\mathtt{Y}^0$) is generated by $e_n^{(a)}$ ($f_n^{(a)}$, resp. $\psi_n^{(a)}$) for all $a \in Q_0$ and $n \in \mathbb{N}$ [57]. We shall also assume that the positive (resp. negative) part $\mathtt{Y}^+$ (resp. $\mathtt{Y}^-$) is isomorphic to the free algebra on $e_n^{(a)}$ (resp. $f_n^{(a)}$) quotiented out by the ee (resp. ff) relations. We will denote the subalgebra generated by $e_n^{(a)}$ (resp. $f_n^{(a)}$) and $\psi_n^{(a)}$ as $\mathtt{Y}^{\geq 0}$ (resp. $\mathtt{Y}^{\leq 0}$).

We can set a degree as $\deg e_n^{(a)} = 1$ whose grading is compatible with the algebra structure. With respect to this grading, $\mathtt{Y}^+ = \bigoplus_{k=0}^{\infty} \mathtt{Y}_k^+$ with $\mathtt{Y}_k^+$ spanned by monomials of degree k in $\mathtt{Y}^+$. We also write $\mathtt{Y}_{\geq n}^+ := \bigoplus_{k \geq n}^{\infty} \mathtt{Y}_k^+$. Therefore, the quiver Yangian is a graded *vector space* as $\mathtt{Y} = \bigoplus_{k=0}^{\infty} \mathtt{Y}_k$, where $\mathtt{Y}_k = \mathtt{Y}^{\leq 0} \otimes \mathtt{Y}_k^+$. Now consider the pair (A_n, q_n) for $n \in \mathbb{N}$ with the left $\mathtt{Y}$-module $A_n := \mathtt{Y} / \left(\mathtt{Y} \cdot \mathtt{Y}_{\geq n}^+\right)$ and the natural quotient map q_n from $\mathtt{Y}$ to A_n. Then q_{n-1} factors through A_n, that is, $p_n \circ q_n = q_{n-1}$ with the homomorphism $p_n : A_n \to A_{n-1}$. The pairs (A_n, p_n) give rise to an inverse system of $\mathtt{Y}$-modules, and we can define the completion of the quiver Yangian as the projective limit [218, §10.1]:

$$\widehat{\mathtt{Y}} := \varprojlim_n A_n. \tag{5.5.17}$$

We will also write $\mathtt{Y} \widehat{\otimes} \mathtt{Y}$ as the completion of $\mathtt{Y} \otimes \mathtt{Y}$.

To write down the coproduct of the quiver Yangian, we need another presentation of the algebra. Drinfeld's J presentation is used for finite dimensional cases in [219], but can be appropriately extended to affine cases following the recipe of [215]. In this presentation, the quiver Yangian is generated by x and $J(x)$ for x elements of the underlying Kac-Moody superalgebra $\mathfrak{g}$. Together with the Chevalley generators of $\mathfrak{g}$ mapped to the zero modes of $\mathtt{Y}$ (recall the beginning of §5.5), the isomorphism is given by

$$J\left(\psi_0^{(a)}\right) = \psi_1^{(a)} + v^{(a)}, \quad J\left(e_0^{(a)}\right) = e_1^{(a)} + w_+^{(a)}, \quad J\left(f_0^{(a)}\right) = f_1^{(a)} + w_-^{(a)}, \tag{5.5.18}$$

where[18] [215]

$$v^{(a)} = \frac{1}{2}(\epsilon_1 + \epsilon_2) \sum_{\alpha \in \Delta_+} \left(\alpha, \alpha^{(a)} \right) \sum_{k=1}^{\dim \mathfrak{g}_\alpha} f^{(\alpha,k)} e^{(\alpha,k)} - \frac{1}{2}(\epsilon_1 + \epsilon_2) \left(\psi_0^{(a)} \right)^2. \tag{5.5.19}$$

Then $w_\pm^{(a)}$ can be obtained by requiring

$$J\left(\left[\psi_0^{(a)}, e_0^{(a)} \right] \right) = \left[J\left(\psi_0^{(a)} \right), e_0^{(a)} \right], \quad J\left(\left[\psi_0^{(a)}, f_0^{(a)} \right] \right) = \left[J\left(\psi_0^{(a)} \right), f_0^{(a)} \right]. \tag{5.5.20}$$

In general, a direct computation shows that

$$\left[J\left(\psi_0^{(a)} \right), e_0^{(b)} \right] - J\left(\left[\psi_0^{(a)}, e_0^{(b)} \right] \right)$$

$$= \frac{\epsilon_1 + \epsilon_2}{2} \left[\sum_{\alpha \in \Delta_+} \left(\alpha, \alpha^{(a)} \right) \sum_{k=1}^{\dim \mathfrak{g}_\alpha} f^{(\alpha,k)} e^{(\alpha,k)}, e_0^{(a)} \right] + \frac{\sigma_1^{ba} - \sigma_1^{ab}}{2} \left(\alpha^{(a)}, \alpha^{(b)} \right) e_0^{(b)} - \left(\alpha^{(a)}, \alpha^{(b)} \right) w_+^{(b)}. \tag{5.5.21}$$

As derived in [15], we have

$$w_+^{(a)} = \frac{\epsilon_1 + \epsilon_2}{2} \sum_{\alpha \in \Delta_+} \sum_{k=1}^{\dim \mathfrak{g}_\alpha} f^{(\alpha,k)} \left[e^{(\alpha,k)}, e_0^{(a)} \right] - \frac{\epsilon_1 + \epsilon_2}{2} \psi_0^{(a)} e_0^{(a)}. \tag{5.5.22}$$

Likewise,

$$w_-^{(a)} = -\frac{\epsilon_1 + \epsilon_2}{2} \sum_{\alpha \in \Delta_+} \sum_{k=1}^{\dim \mathfrak{g}_\alpha} \left[f_0^{(a)}, f^{(\alpha,k)} \right] e^{(\alpha,k)} - \frac{\epsilon_1 + \epsilon_2}{2} f_0^{(a)} \psi_0^{(a)}. \tag{5.5.23}$$

With the expressions for $v^{(a)}$ and $w_\pm^{(a)}$, we can write the commutation relations for the generators in the J presentation. For brevity, we shall also define

$$\widetilde{v}^{(a)} := v^{(a)} + \frac{\epsilon_1 + \epsilon_2}{2} \left(\psi_0^{(a)} \right)^2 = \frac{1}{2}(\epsilon_1 + \epsilon_2) \sum_{\alpha \in \Delta_+} \left(\alpha, \alpha^{(a)} \right) \sum_{k=1}^{\dim \mathfrak{g}_\alpha} f^{(\alpha,k)} e^{(\alpha,k)}. \tag{5.5.24}$$

It was then shown in [15] that

Lemma 5.5.3. *We have*

$$\left[\psi_0^{(a)}, v^{(b)} \right] = 0, \tag{5.5.25}$$

$$\left[\widetilde{v}^{(a)}, e_0^{(b)} \right] = \left(\alpha^{(a)}, \alpha^{(b)} \right) w_+^{(b)}, \tag{5.5.26}$$

$$\left[\widetilde{v}^{(a)}, f_0^{(b)} \right] = -\left(\alpha^{(a)}, \alpha^{(b)} \right) w_-^{(b)}, \tag{5.5.27}$$

$$\left[w_+^{(a)}, f_0^{(b)} \right] = \left[e_0^{(a)}, w_-^{(b)} \right] = \delta_{ab} v^{(a)}, \tag{5.5.28}$$

$$\left[w_+^{(a)}, e_0^{(b)} \right] - \left[e_0^{(a)}, w_+^{(b)} \right] = -\frac{\epsilon_1 + \epsilon_2}{2} \left(\alpha^{(a)}, \alpha^{(b)} \right) \left[e_0^{(a)}, e_0^{(b)} \right], \tag{5.5.29}$$

$$\left[w_-^{(a)}, f_0^{(b)} \right] - \left[f_0^{(a)}, w_-^{(b)} \right] = \frac{\epsilon_1 + \epsilon_2}{2} \left(\alpha^{(a)}, \alpha^{(b)} \right) \left[f_0^{(a)}, f_0^{(b)} \right]. \tag{5.5.30}$$

From these relations, it is straightforward to get the following corollary by definitions of $J\left(\psi_0^{(a)} \right)$, $J\left(e_0^{(a)} \right)$ and $J\left(f_0^{(a)} \right)$.

---

[18]Notice that this is a well-defined operator when acting on modules in the category $\mathcal{O}$ as $e^{(\alpha,k)}$ (i.e., $x_+^{(\alpha,k)}$) annihilates a vector for α with sufficiently large height.

Corollary 5.5.3.1. *We have*

$$\left[\psi_0^{(a)}, J\left(X_0^{(b)}\right)\right] = J\left(\left[\psi_0^{(a)}, X_0^{(b)}\right]\right) \qquad (X = \psi, e, f), \tag{5.5.31}$$

$$\left[J\left(\psi_0^{(a)}\right), e_0^{(b)}\right] = \left(\alpha^{(a)}, \alpha^{(b)}\right) J\left(e_0^{(b)}\right) + \frac{\sigma_1^{ba} - \sigma_1^{ab}}{2}\left(\alpha^{(a)}, \alpha^{(b)}\right) e_0^{(b)}, \tag{5.5.32}$$

$$\left[J\left(\psi_0^{(a)}\right), f_0^{(b)}\right] = -\left(\alpha^{(a)}, \alpha^{(b)}\right) J\left(f_0^{(b)}\right) - \frac{\sigma_1^{ba} - \sigma_1^{ab}}{2}\left(\alpha^{(a)}, \alpha^{(b)}\right) f_0^{(b)}, \tag{5.5.33}$$

$$\left[J\left(e_0^{(a)}\right), f_0^{(b)}\right] = \left[e_0^{(a)}, J\left(f_0^{(b)}\right)\right] = \delta_{ab} J\left(\psi_0^{(a)}\right), \tag{5.5.34}$$

$$\left[J\left(e_0^{(a)}\right), e_0^{(b)}\right] - \left[e_0^{(a)}, J\left(e_0^{(b)}\right)\right] = \frac{1}{2}\left(\sigma_1^{ba} - \sigma_1^{ab}\right)\left[e_0^{(a)}, e_0^{(b)}\right], \tag{5.5.35}$$

$$\left[J\left(f_0^{(a)}\right), f_0^{(b)}\right] - \left[f_0^{(a)}, J\left(f_0^{(b)}\right)\right] = -\frac{1}{2}\left(\sigma_1^{ba} - \sigma_1^{ab}\right)\left[f_0^{(a)}, f_0^{(b)}\right], \tag{5.5.36}$$

$$\left[J\left(e_0^{(a)}\right), e_0^{(b)}\right] = \left[J\left(f_0^{(a)}\right), f_0^{(b)}\right] = 0 \qquad (\sigma_1^{ab} = 0). \tag{5.5.37}$$

Notice that the last line follows from

$$J\left(e_0^{(a)}\right) = \frac{1}{\left(\alpha^{(c)}, \alpha^{(a)}\right)}\left[J\left(\psi_0^{(c)}\right), e_0^{(a)}\right] - \frac{\sigma_1^{ac} - \sigma_1^{ca}}{2} e_0^{(a)}, \tag{5.5.38}$$

and likewise for $f_0^{(a)}$. When a is bosonic, we can take $c = a$. When a is fermionic, c can be taken as one of $a \pm 1$ such that $\sigma_1^{cb} = 0$. It is straightforward to see that each relation in this corollary is equivalent to one of the relations (involving non-zero modes) in (R) in Theorem 5.5.1.

It is also possible to write J acting on any positive real roots besides the simple ones with the help of the Weyl group of the untwisted affine A-type superalgebra. Since $\dim \mathfrak{g}_\alpha = 1$ for $\alpha \in \Delta_+^{\mathrm{re}}$, we shall omit the label k in the corresponding elements. Due to the Serre relations, given an even simple root $\alpha^{(b)}$, the operator $\tau^{(b)} := \exp\left(\mathrm{ad}_{e_0^{(b)}}\right) \exp\left(-\mathrm{ad}_{f_0^{(b)}}\right) \exp\left(\mathrm{ad}_{e_0^{(b)}}\right)$ is well-defined and is an automorphism of the quiver Yangian (see for example [220, 221]). Following the same argument as in [215, Lemma 3.17], $\tau^{(b)}$ can be applied to $J\left(\psi_0^{(a)}\right)$, $J\left(e_0^{(a)}\right)$ and $J\left(f_0^{(a)}\right)$ for any simple root $\alpha^{(a)}$. Moreover, we find that

$$\tau^{(b)}\left(J\left(\psi_0^{(a)}\right)\right) = J\left(\psi_0^{(a)}\right) - \frac{2\left(\alpha^{(b)}, \alpha^{(a)}\right)}{\left(\alpha^{(b)}, \alpha^{(b)}\right)} J\left(\psi_0^{(b)}\right) - \left(\sigma_1^{ba} - \sigma_1^{ab}\right)\frac{\left(\alpha^{(b)}, \alpha^{(a)}\right)}{\left(\alpha^{(b)}, \alpha^{(b)}\right)} \psi_0^{(b)}. \tag{5.5.39}$$

Suppose a root α can be obtained from a simple root $\alpha^{(a)}$ under the even reflections $s^{(b)}$ via $\alpha = s^{(b_1)} \ldots s^{(b_p)}\left(\alpha^{(a)}\right)$. Then we may write $e^{(\alpha)} = \tau^{(b_1)} \ldots \tau^{(b_p)}\left(e^{(a)}\right)$ and define $J\left(e^{(\alpha)}\right) := \tau^{(b_1)} \ldots \tau^{(b_p)}\left(J\left(e^{(a)}\right)\right)$ (and likewise for f).

Proposition 5.5.4. *For any positive real root α and $a \in Q_0$, we have*

$$\begin{aligned}
\left[J\left(\psi_0^{(a)}\right), e^{(\alpha)}\right] &= \left[\psi_0^{(a)}, J\left(e^{(\alpha)}\right)\right] + c^{a\alpha} e^{(\alpha)} = \left(\alpha^{(a)}, \alpha\right) J\left(e^{(\alpha)}\right) + c^{a\alpha} e^{(\alpha)}, \\
\left[J\left(\psi_0^{(a)}\right), f^{(\alpha)}\right] &= \left[\psi_0^{(a)}, J\left(f^{(\alpha)}\right)\right] - c^{a\alpha} e^{(\alpha)} = -\left(\alpha^{(a)}, \alpha\right) J\left(f^{(\alpha)}\right) - c^{a\alpha} f^{(\alpha)},
\end{aligned} \tag{5.5.40}$$

where $c^{a\alpha} \in \frac{\epsilon_1 - \epsilon_2}{2}\mathbb{Z}$.

A proof of this can be found in [15]. As a result, $J\left(e^{(\alpha)}\right)$ and $J\left(f^{(\alpha)}\right)$ are independent of the choice of the sequence of $\tau^{(b)}$ up to a constant multiple. From this proposition, it is also straightforward to obtain the following corollary.

Corollary 5.5.4.1. *For any positive real root α and $a \in Q_0$, we have*

$$\begin{aligned}
\left(\alpha^{(b)}, \alpha\right)\left[J\left(\psi_0^{(a)}\right), e^{(\alpha)}\right] - \left(\alpha^{(a)}, \alpha\right)\left[J\left(\psi_0^{(b)}\right), e^{(\alpha)}\right] &= c_\alpha^{ab} e^{(\alpha)}, \\
\left(\alpha^{(b)}, \alpha\right)\left[J\left(\psi_0^{(a)}\right), e^{(\alpha)}\right] - \left(\alpha^{(a)}, \alpha\right)\left[J\left(\psi_0^{(b)}\right), e^{(\alpha)}\right] &= c_\alpha^{ab} e^{(\alpha)},
\end{aligned} \tag{5.5.41}$$

where $c_\alpha^{ab} = \left(\alpha^{(b)}, \alpha\right) c^{a\alpha} - \left(\alpha^{(a)}, \alpha\right) c^{b\alpha}$.

Now, we are prepared to write our coproduct of the quiver Yangians. Recall that in general, $(x \otimes y)(z \otimes w) = (-1)^{|y||z|}(xz) \otimes (yw)$. For brevity, let us write a linear operator $\square(x) := x \otimes 1 + 1 \otimes x$ and define a Casimir element

$$\Omega_- := \sum_{\alpha \in \Delta_+} \sum_{k=1}^{\dim \mathfrak{g}_\alpha} f^{(\alpha,k)} \otimes e^{(\alpha,k)}. \tag{5.5.42}$$

It is straightforward to get the following commutation relations:

Lemma 5.5.5. *We have*

$$\left[\square\left(\psi_r^{(a)}\right), \Omega_-\right] = 0, \quad \left[\square\left(e_0^{(a)}\right), \Omega_-\right] = \psi_0^{(a)} \otimes e_0^{(a)}, \quad \left[\square\left(f_0^{(a)}\right), \Omega_-\right] = -f_0^{(a)} \otimes \psi_0^{(a)}. \tag{5.5.43}$$

Let us also introduce another map Δ defined by

$$\Delta\left(\psi_0^{(a)}\right) = \square\left(\psi_0^{(a)}\right), \quad \Delta\left(e_0^{(a)}\right) = \square\left(e_0^{(a)}\right), \quad \Delta\left(f_0^{(a)}\right) = \square\left(f_0^{(a)}\right),$$
$$\Delta\left(\psi_1^{(a)}\right) = \square\left(\psi_1^{(a)}\right) + (\epsilon_1 + \epsilon_2)\psi_0^{(a)} \otimes \psi_0^{(a)} + (\epsilon_1 + \epsilon_2)\left[\psi_0^{(a)} \otimes 1, \Omega_-\right] \tag{5.5.44}$$
$$= \square\left(\psi_1^{(a)}\right) + (\epsilon_1 + \epsilon_2)\psi_0^{(a)} \otimes \psi_0^{(a)} - (\epsilon_1 + \epsilon_2) \sum_{\alpha \in \Delta_+^{\mathrm{re}}} \left(\alpha^{(a)}, \alpha\right) f^{(\alpha)} \otimes e^{(\alpha)}.$$

Notice that this uniquely determines Δ as the actions on all modes can be obtained following the discussions in §5.5.1. For instance,

$$\Delta\left(\widetilde{\psi}_1^{(a)}\right) = \square\left(\widetilde{\psi}_1^{(a)}\right) + (\epsilon_1 + \epsilon_2)\left[\psi_0^{(a)} \otimes 1, \Omega_-\right], \tag{5.5.45}$$

$$\Delta\left(e_1^{(a)}\right) = \square\left(e_1^{(a)}\right) - (\epsilon_1 + \epsilon_2)\left[\Omega_-, e_0^{(a)} \otimes 1\right], \tag{5.5.46}$$

$$\Delta\left(f_1^{(a)}\right) = \square\left(f_1^{(a)}\right) + (\epsilon_1 + \epsilon_2)\left[\Omega_-, 1 \otimes f_0^{(a)}\right]. \tag{5.5.47}$$

This operator in fact gives a coproduct of the quiver Yangian.

Theorem 5.5.6. *For $M + N > 2$, $MN \neq 2$ and $M \neq N$, the map $\Delta : \mathtt{Y} \to \mathtt{Y} \widehat{\otimes} \mathtt{Y}$ specified by* (5.5.44) *is a coassociative algebra homomorphism.*

This can be proven using the properties and identities for the minimalistic presentations and the J presentations mentioned above. A detailed proof can be found in [15].

5.6 Isomorphism of Quiver Yangians

Given *any* toric CY threefold, its quivers can be in different toric phases. Since these quivers are related by Seiberg/toric duality, it is natural to conjecture that their quiver Yangians are isomorphic. Here, we shall prove this for the generalized conifolds considered in this paper. As a result, different toric phases correspond to different triangulations of the toric diagram, i.e., different sequences ς.

A special feature for these generalized conifold is their underlying Kac-Moody superalgebras, which are of untwisted affine A-type. The zero modes of the quiver Yangians are actually different sets of Chevalley generators. For any two inequivalent sets of Chevalley generators, one can reach one from the other by odd reflections and Weyl groupoids [221–223]. We shall now extend this to isomorphisms of quiver Yangians. Recall that each quiver has an underlying Dynkin diagram

associated to $\widehat{\mathfrak{sl}}_{M|N}$. In such case, the odd reflection corresponding to an odd simple root $\alpha^{(F)}$ acts on any simple root $\alpha^{(a)}$ as[19]

$$\alpha'^{(a)} = r^{(F)}\left(\alpha^{(a)}\right) = \begin{cases} -\alpha^{(a)}, & a = F, \\ \alpha^{(a)} + \alpha^{(F)}, & a = F \pm 1, \\ \alpha^{(a)}, & \text{otherwise.} \end{cases} \tag{5.6.1}$$

The Cartan matrix $A = (A_{ab})$ where $A_{ab} = \left(\alpha^{(a)}, \alpha^{(b)}\right)$ is mapped to $A' = RAR^{\mathrm{T}}$ with $R = (R_{ab})$ given by

$$R_{ab} = \begin{cases} -1, & a = b = F, \\ 1, & a = b \neq F, \\ 1, & b = F, A_{aF} \neq 0, \\ 0, & \text{otherwise.} \end{cases} \tag{5.6.2}$$

In terms of Dynkin diagrams, this manipulation changes the $\mathbb{Z}_2$-grading of the nodes (and hence their e, f generators) connected to the node F (i.e., those with $A_{aF} \neq 0$) and leaves the remaining ones unchanged. The Chevalley generators are mapped to

$$\psi_0'^{(a)} = \sum_{b=1}^{M+N} R_{ab}\psi_0^{(b)} = \begin{cases} -\psi_0^{(a)}, & a = F, \\ \psi_0^{(a)} + \psi_0^{(F)}, & a = F \pm 1, \\ \psi^{(a)}, & \text{otherwise;} \end{cases}$$

$$e_0'^{(a)} = \begin{cases} f_0^{(a)}, & a = F, \\ \left[e_0^{(F)}, e_0^{(a)}\right], & a = F \pm 1, \\ e_0^{(a)}, & \text{otherwise;} \end{cases} \qquad f_0'^{(a)} = \begin{cases} -e_0^{(a)}, & a = F, \\ -\frac{1}{A_{aF}}\left[f_0^{(a)}, f_0^{(F)}\right], & a = F \pm 1, \\ f_0^{(a)}, & \text{otherwise.} \end{cases} \tag{5.6.3}$$

Notice that A_{aF} is simply ± 1.

It would also be useful to spell out the following lemmas.

Lemma 5.6.1. *We have*

$$\left(\alpha'^{(a)}, \alpha'^{(b)}\right) = \begin{cases} -\left(\alpha^{(a)}, \alpha^{(b)}\right), & (a,b) = (F \pm 1, F), (F, F \pm 1), \\ \left(\alpha^{(a)}, \alpha^{(a)}\right) + 2\left(\alpha^{(F)}, \alpha^{(a)}\right), & a = b = F \pm 1, \\ \left(\alpha^{(a)}, \alpha^{(b)}\right), & \text{otherwise.} \end{cases} \tag{5.6.4}$$

Lemma 5.6.2. *We have* $\sigma_1'^{F \pm 1, F} = -\sigma_1^{F, F \pm 1}$ *and* $\sigma_1'^{F, F \pm 1} = -\sigma_1^{F \pm 1, F}$ *while the other* σ_1^{ab} *are invariant. Therefore,* $\sigma_1'^{ab} - \sigma_1'^{ba} = \sigma_1^{ab} - \sigma_1^{ba}$.

It was then shown in [15] that

Theorem 5.6.3. *Given a generalized conifolds with $M \neq N$, the quiver Yangians in different toric phases are isomorphic algebras.*

---

[19]More generally (especially when the Kac-Moody superalgebra has non-isotropic odd roots), the odd reflection associated to an isotropic simple odd root has the same action with the second condition as $\alpha^{(a)} + \alpha^{(F)}$ being a root.

Although we will not write the detailed proof here, let us give the transformations for the generators. The transformations are given by (5.6.3) and

$$
J\left(\psi_0'^{(a)}\right) = \begin{cases} -J\left(\psi_0^{(a)}\right), & a = F, \\ J\left(\psi_0^{(a)}\right) + J\left(\psi_0^{(F)}\right) - \frac{1}{2}\left(\sigma_1^{aF} - \sigma_1^{Fa}\right)\psi_0^{(F)}, & a = F \pm 1, \\ J\left(\psi_0^{(a)}\right), & \text{otherwise;} \end{cases}
$$

$$
J\left(e_0'^{(a)}\right) = \begin{cases} J\left(f_0^{(a)}\right), & a = F, \\ \left[e_0^{(F)}, J\left(e_0^{(a)}\right)\right], & a = F \pm 1, \\ J\left(e_0^{(a)}\right), & \text{otherwise;} \end{cases} \tag{5.6.5}
$$

$$
J\left(f_0'^{(a)}\right) = \begin{cases} -J\left(e_0^{(a)}\right), & a = F, \\ -\frac{1}{A_{aF}}\left[J\left(f_0^{(a)}\right), f_0^{(F)}\right], & a = F \pm 1, \\ J\left(f_0^{(a)}\right), & \text{otherwise.} \end{cases}
$$

In terms of $\psi_1^{(a)}$, $e_1^{(a)}$ and $f_1^{(a)}$, we have

$$
\widetilde{\psi}_1'^{(a)} = \begin{cases} -\widetilde{\psi}_1^{(a)}, & a = F, \\ \widetilde{\psi}_1^{(a)} + \widetilde{\psi}_1^{(F)} - \sigma_1^{aF} e_0^{(F)} f_1^{(F)} + \sigma_1^{Fa} f_1^{(F)} e_0^{(F)}, & a = F \pm 1, \\ \widetilde{\psi}_1^{(a)}, & \text{otherwise;} \end{cases}
$$

$$
e_1'^{(a)} = \begin{cases} f_1^{(F)} - \frac{\sigma_1^{bF}}{\left(\alpha^{(F)}, \alpha^{(b)}\right)}\psi_0^{(F)} f_0^{(F)} - \frac{\sigma_1^{Fb}}{\left(\alpha^{(F)}, \alpha^{(b)}\right)} f_0^{(F)} \psi_0^{(F)}, & a = F, \\ \left[e_0^{(F)}, e_1^{(a)}\right], & a = F \pm 1, \\ e_1^{(a)}, & \text{otherwise;} \end{cases} \tag{5.6.6}
$$

$$
f_1'^{(a)} = \begin{cases} -e_1^{(F)} + \frac{\sigma_1^{bF}}{\left(\alpha^{(F)}, \alpha^{(b)}\right)} e_0^{(F)} \psi_0^{(F)} + \frac{\sigma_1^{Fb}}{\left(\alpha^{(F)}, \alpha^{(b)}\right)} \psi_0^{(F)} e_0^{(F)}, & a = F, \\ -\frac{1}{\left(\alpha^{(F)}, \alpha^{(a)}\right)}\left[f_1^{(a)}, f_0^{(F)}\right], & a = F \pm 1, \\ f_1^{(a)}, & \text{otherwise.} \end{cases}
$$

Here, b can be taken as either $F + 1$ or $F - 1$ which would give the same result. One may check that this satisfies the relations for quiver Yangians in Theorem 5.5.1. Notice that the coefficients σ_1^{bF}/A_{bF} and σ_1^{Fb}/A_{bF} are equal to $\epsilon_{1,2}$.

5.7 Connections to $\mathcal{W}$-Algebras

As mentioned before, the quiver Yangians and certain $\mathcal{W}$-algebras are expected to have intimate relations that implement the BPS/CFT correspondence. Indeed, as we are now going to see, the rectangular $\mathcal{W}$-algebras for the associated generalized conifolds can be viewed as truncations of the quiver Yangians.

5.7.1 From $\mathtt{Y}$ to $\mathcal{W}$

Here, we shall directly start with the commutation relations for the generators of rectangular $\mathcal{W}$-algebras for the generalized conifold $xy = z^M w^N$. A mathematical definition of rectangular $\mathcal{W}$-algebras $\mathcal{W}^k\left(\mathfrak{gl}(Ml|Nl), \left(l^{(M|N)}\right)\right)$ is given in Appendix H with the notations and conventions set up therein. For brevity, we shall abbreviate it as $\mathcal{W}_{M|N \times l}$.

The $\mathcal{W}$-algebras of interest in this paper can be generated by $U_{ij}^{(s)}$ with spin $s = 1, 2$ and $i, j \in \mathbb{Z}/(M+N)\mathbb{Z}$. Given a parity sequence $\varsigma = \{\varsigma_i\}$ as introduced in §5.2, the generator $U_{ij}^{(s)}$ has

the $\mathbb{Z}_2$-grading given by $(-1)^{p(i)+p(j)}$, where $(-1)^{p(i)} = \varsigma_i$ (see also (H.0.1))[20]. The OPEs of the currents $U_{ij}^{(s)}(z)$ were obtained in [69, 70]. The following commutation relations for their modes $U_{ij}^{(s)}[m]$ can then be computed directly using (H.0.22).

Lemma 5.7.1. *We have*

$$\left[U_{i_1j_1}^{(1)}[m], U_{i_2j_2}^{(1)}[n]\right\}$$
$$= \delta_{m,-n} ml \left(\delta_{j_1i_2}\delta_{i_1j_2}(-1)^{p(j_1)}\varkappa + \delta_{i_1j_1}\delta_{i_2j_2}\right)$$
$$+ (-1)^{p(i_1)p(j_1)+p(i_2)p(j_2)+p(j_1)p(i_2)}\delta_{i_1j_2}U_{i_2j_1}^{(1)}[m+n] - (-1)^{p(j_1)}\delta_{i_2j_1}U_{i_1j_2}^{(1)}[m+n], \qquad (5.7.1)$$

$$\left[U_{i_1j_1}^{(1)}[m], U_{i_2j_2}^{(2)}[n]\right\}$$
$$= \frac{1}{2}l(l-1)m(m-1)\varkappa\delta_{m,-n}\left((-1)^{p(j_1)}\varkappa\delta_{i_1j_2}\delta_{i_2j_1} + \delta_{i_1j_1}\delta_{i_2j_2}\right)$$
$$+ m(l-1)\left((-1)^{p(i_1)p(j_1)+p(i_2)p(j_2)+p(j_1)p(i_2)}\varkappa\delta_{i_1j_2}U_{i_2j_1}^{(1)}[m+n] + \delta_{i_1j_1}U_{i_2j_2}^{(1)}[m+n]\right)$$
$$+ (-1)^{p(i_1)p(j_1)+p(i_2)p(j_2)+p(j_1)p(i_2)}\delta_{i_1j_2}U_{i_2j_1}^{(2)}[m+n] - (-1)^{p(j_1)}\delta_{i_2j_1}U_{i_1j_2}^{(2)}[m+n], \qquad (5.7.2)$$

$$\left[U_{ii}^{(2)}[m], U_{jj}^{(2)}[n]\right\}$$
$$= \frac{1}{12}l(l-1)m(m-1)(m+1)\delta_{m,-n}\left(2\varkappa((1-2l)\alpha^2+1)(-1)^{p(i)}\delta_{ij} - (4l-3)\varkappa^2+1\right)$$
$$+ \frac{1}{2}m(m+1)\left((l-1)^2\varkappa\left(U_{ii}^{(1)}[m+n] - U_{jj}^{(1)}[m+n]\right)\right)$$
$$- (m+1)\left(U_{jj}^{(2)}[m+n] + U_{ii}^{(2)}[m+n] + 2\varkappa(-1)^{p(i)}\delta_{ij}U_{ii}^{(2)}[m+n]\right)$$
$$+ (m+1)(l-1)\left(\sum_{k<0}U_{ii}^{(1)}[k]U_{jj}^{(1)}[m+n-k] + \sum_{k\geq0}U_{jj}^{(1)}[m+n-k]U_{ii}^{(1)}[k]\right)$$
$$+ (m+1)(l-1)(-1)^{p(j)}\varkappa\left(\sum_{k<0}U_{ij}^{(1)}[k]U_{ji}^{(1)}[m+n-k] + (-1)^{p(i)+p(j)}\sum_{k\geq0}U_{ji}^{(1)}[m+n-k]U_{ij}^{(1)}[k]\right)$$
$$- (m+1)l(l-1)\varkappa(m+n+1)\left(1 + (-1)^{p(i)}\varkappa\delta_{ij}\right)U_{ii}^{(1)}[m+n]$$
$$- (m+n+2)\left(U_{jj}^{(2)}[m+n] - (-1)^{p(i)}\varkappa\delta_{ij}U_{ii}^{(2)}[m+n] - 2U_{ii}^{(2)}[m+n]\right)$$
$$+ (-1)^{p(i)}\left(\sum_{k<-1}U_{ji}^{(2)}[k]U_{ij}^{(1)}[m+n-k] + \sum_{k\geq-1}(-1)^{p(i)+p(j)}U_{ij}^{(1)}[m+n-k]U_{ji}^{(2)}[k]\right)$$
$$- (-1)^{p(j)}\left(\sum_{k<-1}U_{ij}^{(2)}[k]U_{ji}^{(1)}[m+n-k] + \sum_{k\geq-1}(-1)^{p(i)+p(j)}U_{ji}^{(1)}[m+n-k]U_{ij}^{(2)}[k]\right)$$
$$+ (l-1)\left(\sum_{k<0}(-k-1)U_{ii}^{(1)}[k]U_{jj}^{(1)}[m+n-k] + \sum_{k\geq0}(-k-1)U_{jj}^{(1)}[m+n-k]U_{ii}^{(1)}[k]\right)$$
$$+ (l-1)\varkappa(-1)^{p(j)}\left(\sum_{k<0}(-k-1)U_{ij}^{(1)}[k]U_{ji}^{(1)}[m+n-k]\right.$$
$$\left. + (-1)^{p(i)+p(j)}\sum_{k\geq0}(-k-1)U_{ji}^{(1)}[m+n-k]U_{ij}^{(1)}[k]\right)$$

---

[20]As we will see shortly, $|a|$ and $p(i)$ are indeed consistent in the sense of ς when relating $\mathbb{Y}$ and $\mathcal{W}$. In other words, $|a|$ is bosonic when $p(a) = p(a+1)$ and fermionic otherwise.

$$+ \frac{1}{2}(l-1)(m+n+1)(m+n+2)\left((l+1)\varkappa U_{ii}^{(1)}[m+n] - \varkappa U_{jj}^{(1)}[m+n]\right)$$

$$+ \frac{1}{2}(l-1)(m+n+1)(m+n+2)(-1)^{p(j)}l\varkappa^2\delta_{ij}U_{ii}^{(1)}[m+n]. \tag{5.7.3}$$

Notice that we only give the $U_{i_1i_2}^{(2)}U_{j_1j_2}^{(2)}$ relation when $i_1 = j_1$ and $i_2 = j_2$ as this is sufficient for the use here. It is also straightforward to get the more general case from the OPE. Here, we shall always assume $\varkappa \neq 0$.

The $\mathcal{W}$-algebra is often defined via the distinguished parity sequence, that is, only two fermionic $p(i)$ (the non-super case $M|0$ always has bosonic ones only). Here, we allow it to have different ς. Analogous to the quiver Yangians related by Seiberg dualities, we would expect the $\mathcal{W}$-algebras with different ς are essentially the same. In fact, the proof of this is much simpler than the quiver Yangian case in §5.6 by virtue of the matrix presentation here.

Proposition 5.7.2. *Given M, N and l, the rectangular $\mathcal{W}$-algebras $\mathcal{W}_{M|N\times l}$ are isomorphic for different ς.*

Proof. The isomorphism can be constructed from a sequence of the following isomorphic maps. Suppose ς and ς' are related by $\sigma \in \mathfrak{S}_{M+N}$ that permutes the ith and $(i+1)^{\text{th}}$ elements. Then the transformation is given by $U_{ij}^{(r)} \mapsto U_{\sigma(i)\sigma(j)}^{(r)}$. It is straightforward to see that this preserves the relations for the generators. $\qquad\square$

Therefore, when considering the map from the quiver Yangians to the (universal enveloping algebra of) $\mathcal{W}$-algebra below, we can simply take them to have the same ς. The isomorphic ones are related by the transformations in Theorem 5.6.3 and Proposition 5.7.2 respectively.

Let $\epsilon_\pm = \epsilon_1 \pm \epsilon_2$. Since

$$\varsigma_a(\epsilon_1 - \epsilon_2) = \begin{cases} \varsigma_{a+1}(\epsilon_1 - \epsilon_2), & \varsigma_a = \varsigma_{a+1} \\ \varsigma_{a+1}(\epsilon_2 - \epsilon_1), & \varsigma_a = -\varsigma_{a+1}, \end{cases} \tag{5.7.4}$$

we can take $\epsilon_- = \sigma_1^{a+1,a} - \sigma_1^{a,a+1}$ for any a based on Figure E.0.2 without loss of generality. This allows us to consider another presentation of the quiver Yangian which would be convenient for our discussions. Let us prepare the generators defined as

$$\begin{cases} \mathcal{H}_0^{(a)} = \psi_0^{(a)} \\ \mathcal{E}_0^{(a)} = e_0^{(a)} \\ \mathcal{F}_0^{(a)} = f_0^{(a)}, \end{cases} \qquad \begin{cases} \mathcal{H}_1^{(a)} = \psi_1^{(a)} + \frac{1}{2}\nu(a)\epsilon_-\psi_0^{(a)} \\ \mathcal{E}_1^{(a)} = e_1^{(a)} + \frac{1}{2}\nu(a)\epsilon_-e_0^{(a)} \\ \mathcal{F}_1^{(a)} = f_1^{(a)} + \frac{1}{2}\nu(a)\epsilon_-f_0^{(a)}, \end{cases} \tag{5.7.5}$$

where $\nu(a)$ can be any function satisfying $\nu(a\pm 1) = \nu(a)\pm 1$ for $0 \leq a \leq M+N-1$. In particular, this means that $\nu(-1) \neq \nu(M+N-1)$ and $\nu(0) \neq \nu(M+N)$. For instance, the simplest example would be $\nu(a) = a$ ($-1 \leq a \leq M+N$). We shall also pick a reference node labelled by $a = 0$.

Proposition 5.7.3. *The quiver Yangian is generated by $\mathcal{H}_r^{(a)}$, $\mathcal{E}_r^{(a)}$, $\mathcal{F}_r^{(a)}$ ($a \in Q_0$, $r = 0, 1$) subject to the relations*

$$\left[\mathcal{H}_r^{(a)}, \mathcal{H}_s^{(b)}\right] = 0, \tag{5.7.6}$$

$$\left[\mathcal{E}_r^{(a)}, \mathcal{F}_s^{(b)}\right\} = \delta_{ab}\mathcal{H}_{r+s}^{(a)}, \tag{5.7.7}$$

$$\left[\mathcal{H}_0^{(a)}, \mathcal{E}_r^{(a)}\right] = A_{ab}\mathcal{E}_r^{(a)}, \tag{5.7.8}$$

$$\left[\widetilde{\mathcal{H}}_1^{(a)}, \mathcal{E}_0^{(b)}\right] = \begin{cases} A_{ab}\mathcal{E}_1^{(b)} + \frac{1}{2}A_{ab}\nu(M+N)\epsilon_-\mathcal{E}_0^{(b)}, & (a,b) = (M+N-1, 0) \\ A_{ab}\mathcal{E}_1^{(b)} - \frac{1}{2}A_{ab}\nu(M+N)\epsilon_-\mathcal{E}_0^{(b)}, & (a,b) = (0, M+N-1) \\ A_{ab}\mathcal{E}_1^{(b)}, & \text{otherwise,} \end{cases} \tag{5.7.9}$$

$$\left[\mathcal{H}_0^{(a)}, \mathcal{F}_r^{(a)}\right] = -A_{ab}\mathcal{F}_r^{(a)}, \tag{5.7.10}$$

$$\left[\widetilde{\mathcal{H}}_1^{(a)}, \mathcal{F}_0^{(b)}\right] = \begin{cases} -A_{ab}\mathcal{E}_1^{(b)} - \frac{1}{2}A_{ab}\nu(M+N)\epsilon_-\mathcal{E}_0^{(b)}, & (a,b) = (M+N-1,0) \\ -A_{ab}\mathcal{E}_1^{(b)} + \frac{1}{2}A_{ab}\nu(M+N)\epsilon_-\mathcal{E}_0^{(b)}, & (a,b) = (0, M+N-1) \\ -A_{ab}\mathcal{E}_1^{(b)}, & \text{otherwise,} \end{cases} \tag{5.7.11}$$

$$\left[\mathcal{E}_0^{(a)}, \mathcal{E}_0^{(b)}\right\} = \left[\mathcal{F}_0^{(a)}, \mathcal{F}_0^{(b)}\right\} = 0 \qquad (\sigma_1^{ab} = 0), \tag{5.7.12}$$

$$\left[\mathcal{E}_1^{(a)}, \mathcal{E}_0^{(b)}\right\} - \left[\mathcal{E}_0^{(a)}, \mathcal{E}_1^{(b)}\right\}$$
$$= \begin{cases} \frac{1}{2}A_{ab}\epsilon_+ \left\{\mathcal{E}_0^{(a)}, \mathcal{E}_0^{(b)}\right] - \frac{1}{2}\nu(M+N)\epsilon_- \left[\mathcal{E}_0^{(a)}, \mathcal{E}_0^{(b)}\right\}, & (a,b) = (0, M+N-1) \\ \frac{1}{2}A_{ab}\epsilon_+ \left\{\mathcal{E}_0^{(a)}, \mathcal{E}_0^{(b)}\right], & \text{otherwise,} \end{cases} \tag{5.7.13}$$

$$\left[\mathcal{F}_1^{(a)}, \mathcal{F}_0^{(b)}\right\} - \left[\mathcal{F}_0^{(a)}, \mathcal{F}_1^{(b)}\right\}$$
$$= \begin{cases} -\frac{1}{2}A_{ab}\epsilon_+ \left\{\mathcal{F}_0^{(a)}, \mathcal{F}_0^{(b)}\right] - \frac{1}{2}\nu(M+N)\epsilon_- \left[\mathcal{F}_0^{(a)}, \mathcal{F}_0^{(b)}\right\}, & (a,b) = (0, M+N-1) \\ -\frac{1}{2}A_{ab}\epsilon_+ \left\{\mathcal{F}_0^{(a)}, \mathcal{F}_0^{(b)}\right], & \text{otherwise,} \end{cases} \tag{5.7.14}$$

Serre relations (S), $\qquad\qquad\qquad\qquad\qquad\qquad\qquad\qquad\qquad\qquad\qquad$ (5.7.15)

where $\widetilde{\mathcal{H}}_1^{(a)} := \mathcal{H}_1^{(a)} - \frac{1}{2}\epsilon_+ \left(\mathcal{H}_0^{(a)}\right)^2$. Here, for brevity, we have used $\{x, y]$ to denote $xy + (-1)^{|x||y|}yx$. The higher modes with $r \geq 2$ can be obtained in a way similar to the presentation using ψ, e, f.

This can be verified by straightforward calculations. Hence, we omit the explicit proof here. When checking these relations, it is also worth noting that

$$A_{ab} = \left(\alpha^{(a)}, \alpha^{(b)}\right) = \begin{cases} -(\varsigma_b + \varsigma_{b+1}), & a = b \\ \varsigma_{b+1}, & a = b+1 \\ \varsigma_b, & b = a+1 \\ 0, & \text{otherwise.} \end{cases} \tag{5.7.16}$$

Remark 25. *As pointed out in [14], the quiver Yangian is only isomorphic to Ueda's affine super Yangian introduced in [216] when $\epsilon_- = 0$. By comparing the presentation above with the similar presentation for Ueda's affine super Yangian in [224], it is straightforward to see that this difference is encoded by $\nu(a)$ here and the coefficients in the presentation in [224].*

Now, we are ready to bridge the quiver Yangians and $\mathcal{W}$-algebras. Again, let us only state the theorem here, and the proof can be found in [15].

Theorem 5.7.4. *Given a generalized conifold with $M + N > 2$, $MN \neq 2$ and $M \neq N$, when $\nu(M+N)\epsilon_- = (2\varkappa - M - N)\epsilon_+$, there is a surjective algebra homomorphism from the quiver Yangian to the universal enveloping algebra of $\mathcal{W}_{M|N\times l}$. Fixing a parity sequence ς, such map $\Phi : \mathtt{Y} \to U\left(\mathcal{W}_{M|N\times l}\right)$ can be uniquely determined by*

$$\Phi\left(X_0^{(a)}\right) = \Phi\left(Y_0^{(a)}\right), \qquad \Phi\left(X_1^{(a)}\right) = \Phi\left(Y_1^{(a)}\right) - \frac{1}{2}\nu(a)\epsilon_-\Phi\left(Y_0^{(a)}\right) \tag{5.7.17}$$

for $(X, Y) = (\psi, \mathcal{H}), (e, \mathcal{E}), (f, \mathcal{F})$, where

$$\Phi\left(\mathcal{H}_0^{(a)}\right) = \begin{cases} U_{M+N,M+N}^{(1)}[0] - U_{11}^{(1)}[0] + l\varkappa, & a = 0 \\ U_{aa}^{(1)}[0] - U_{a+1,a+1}^{(1)}[0], & a \neq 0, \end{cases} \tag{5.7.18}$$

$$\Phi\left(\mathcal{E}_0^{(a)}\right) = \begin{cases} -(-1)^{p(1)}U_{M+N,1}^{(1)}[-1], & a = 0 \\ -(-1)^{p(a+1)}U_{a,a+1}^{(1)}[0], & a \neq 0, \end{cases} \tag{5.7.19}$$

$$\Phi\left(\mathcal{F}_0^{(a)}\right) = \begin{cases} U_{1,M+N}^{(1)}[1], & a = 0 \\ U_{a+1,a}^{(1)}[0], & a \neq 0, \end{cases} \tag{5.7.20}$$

$$\Phi\left(\mathcal{H}_1^{(0)}\right) = \epsilon_+\Bigg(U_{M+N,M+N}^{(2)}[0] - U_{11}^{(2)}[0] - U_{M+N,M+N}^{(1)}[0]U_{11}^{(1)}[0]$$

$$- \sum_{c=1}^{M+N}\sum_{k\geq 0}(-1)^{p(c)+p(M+N)}U_{c,M+N}^{(1)}[-k]U_{M+N,c}^{(1)}[k]$$

$$+ \sum_{c=1}^{M+N}\sum_{k\geq 0}(-1)^{p(c)+p(1)}U_{c,1}^{(1)}[-k-1]U_{1,c}^{(1)}[k+1]$$

$$+ \left(\frac{1}{2}\nu(1) - \frac{1}{2} - l\varkappa\right)\left(U_{M+N,M+N}^{(1)}[0] - U_{11}^{(1)}[0] + l\varkappa\right) + \varkappa U_{M+N,M+N}^{(1)}[0]\Bigg), \tag{5.7.21}$$

$$\Phi\left(\mathcal{H}_1^{(a\neq 0)}\right) = \epsilon_+\Bigg(U_{aa}^{(2)}[0] - U_{a+1,a+1}^{(2)}[0] - U_{aa}^{(1)}[0]U_{a+1,a+1}^{(1)}[0] + \frac{1}{2}\nu(a)\left(U_{aa}^{(1)}[0] - U_{a+1,a+1}^{(1)}[0]\right)$$

$$- \sum_{c=1}^{a}\sum_{k\geq 0}(-1)^{p(c)+p(a)}U_{ca}^{(1)}[-k]U_{ac}^{(1)}[k]$$

$$+ \sum_{c=a+1}^{M+N}\sum_{k\geq 0}(-1)^{p(c)+p(a)}U_{ca}^{(1)}[-k-1]U_{ac}^{(1)}[k+1]$$

$$- \sum_{c=1}^{a}\sum_{k\geq 0}(-1)^{p(c)+p(a+1)}U_{c,a+1}^{(1)}[-k]U_{a+1,c}^{(1)}[k]$$

$$+ \sum_{c=a+1}^{M+N}\sum_{k\geq 0}(-1)^{p(c)+p(a+1)}U_{c,a+1}^{(1)}[-k-1]U_{a+1,c}^{(1)}[k+1]\Bigg), \tag{5.7.22}$$

$$\Phi\left(\mathcal{E}_1^{(0)}\right) = \epsilon_+\Bigg(-(-1)^{p(1)}U_{M+N,1}^{(2)}[-1] - (-1)^{p(1)}\left(\frac{1}{2}\nu(1) - \frac{1}{2} - l\varkappa\right)U_{M+N,1}^{(1)}[-1]$$

$$+ \sum_{c=1}^{M+N}\sum_{k\geq 0}(-1)^{p(c)+p(M+N)p(c)+p(1)p(c)+p(M+N)p(1)+p(M+N)}U_{c,1}^{(1)}[-k-1]U_{M+N,c}^{(1)}[k]\Bigg), \tag{5.7.23}$$

$$\Phi\left(\mathcal{E}_1^{(a\neq 0)}\right) = \epsilon_+\Bigg(-(-1)^{p(a+1)}U_{a,a+1}^{(2)}[0] - \frac{1}{2}\nu(a)(-1)^{p(a+1)}U_{a,a+1}^{(1)}[0]$$

$$- \sum_{c=1}^{a}\sum_{k\geq 0}(-1)^{p(c)+p(a)p(c)+p(a+1)p(c)+p(a)p(a+1)+p(a)}U_{c,a+1}^{(1)}[-k]U_{ac}^{(1)}[k]$$

$$+ \sum_{c=a+1}^{M+N}\sum_{k\geq 0}(-1)^{p(c)+p(a)p(c)+p(a+1)p(c)+p(a)p(a+1)+p(a)}U_{c,a+1}^{(1)}[-k-1]U_{ac}^{(1)}[k+1]\Bigg) \tag{5.7.24}$$

$$\Phi\left(\mathcal{F}_1^{(0)}\right) = \epsilon_+\Bigg(U_{1,M+N}^{(2)}[1] + \left(\frac{1}{2}\nu(1) - \frac{1}{2} + \varkappa\right)U_{1,M+N}^{(1)}[1]$$

$$- \sum_{c=1}^{M+N}\sum_{k\geq 0}(-1)^{p(c)+p(M+N)p(c)+p(1)p(c)+p(M+N)p(1)}U_{c,M+N}^{(1)}[-k]U_{1,c}^{(1)}[k+1]\Bigg), \tag{5.7.25}$$

$$\Phi\left(\mathcal{F}_1^{(a\neq 0)}\right) = \epsilon_+\Bigg(U_{a+1,a}^{(2)}[0] + \frac{1}{2}\nu(a)U_{a+1,a}^{(1)}[0]$$

$$- \sum_{c=1}^{a} \sum_{k \geq 0} (-1)^{p(c)+p(a)p(c)+p(a+1)p(c)+p(a)p(a+1)} U_{ca}^{(1)}[-k] U_{a+1,c}^{(1)}[k]$$

$$+ \sum_{c=a+1}^{M+N} \sum_{k \geq 0} (-1)^{p(c)+p(a)p(c)+p(a+1)p(c)+p(a)p(a+1)} U_{ca}^{(1)}[-k-1] U_{a+1,c}^{(1)}[k+1] \Bigg).$$

$$(5.7.26)$$

Remark 26. *From Theorem 5.7.4, we can see that the universal enveloping algebras of $\mathcal{W}_{M|N \times l}$ are essentially truncations of the quiver Yangians, that is,*

$$\mathbf{Y}/\ker(\Phi) \cong U(\mathcal{W}_{M|N \times l}). \tag{5.7.27}$$

Therefore, we may view the quiver Yangian as some sort of "$U(\mathcal{W}_{M|N \times \infty})$" algebra (cf. [69])[21]. This allows us to apply our knowledge in BPS algebras to VOAs and vice versa.

At first glance, one might wonder whether we could write such surjective homomorphism without choosing a reference $a = 0$ so that the map would become more "uniform". However, as we will see shortly, this is actually very natural on the quiver Yangian side (not just due to the presentation in Proposition 5.7.3), especially when discussing the crystal melting models.

Coproduct and parabolic induction As the coproduct for the quiver Yangians is obtained in §5.5, we can thence consider the parabolic induction for the $\mathcal{W}$-algebras. In other words, given representations $R_{1,2}$ of $U(\mathcal{W}_{M|N \times l_{1,2}})$, we have $R_1 \otimes R_2$ as a representation of $U(\mathcal{W}_{M|N \times (l_1+l_2)})$. In particular, the study in [225] (see also [226] for non-super cases including some cases of BCD types) answers Conjecture 2 in [69].

Consider $\widehat{\mathfrak{gl}}(M|N)_\varkappa = \widehat{\mathfrak{sl}}(M|N)_\varkappa \oplus \widehat{\mathfrak{z}}(M|N)_{\varkappa+M-N}$, where $\widehat{\mathfrak{z}}$ is the Heisenberg algebra at level $\varkappa + M - N = k + l(M - N)$. We have an algebra automorphism given by [225]

$$\eta_\beta (E_{ij}[m]) = E_{ij}[m] + \delta_{m,0} \delta_{ij} \beta \tag{5.7.28}$$

for some complex number β. This yields an algebra automorphism

$$\eta_\beta^{\otimes l} = \bigotimes_{l \text{ times}} \eta_\beta \in \mathrm{Aut}\left(U\left(\widehat{\mathfrak{gl}}(M|N)_\varkappa\right)^{\widehat{\otimes}l} \right). \tag{5.7.29}$$

Using (H.0.20), we have

$$\eta_\beta^{\otimes l}\left(U_{ij}^{(1)}[m] \right) = U_{ij}^{(1)}[m] + \delta_{m,0} \delta_{ij} l\beta,$$

$$\eta_\beta^{\otimes l}\left(U_{ij}^{(2)}[m] \right) = U_{ij}^{(2)}[m] + (l-1)\varkappa U_{ij}^{(1)}[m] + \frac{1}{2} \delta_{m,0} \delta_{ij} l(l-1)(\beta^2 - \varkappa\beta). \tag{5.7.30}$$

To relate the parabolic induction with the coproduct of quiver Yangians, let us take $l = l_1 + l_2$ and $k + l(M - N) = k_1 + l_1(M - N) = k_2 + l_2(M - N)$ such that $\varkappa$ remains the same for $\mathcal{W}_{M|N \times l}$ and $\mathcal{W}_{M|N \times l_{1,2}}$. Then there exists an inclusion map $\Delta_{l_1,l_2} : \mathcal{W}_{M|N \times l} \to \mathcal{W}_{M|N \times l_1} \otimes \mathcal{W}_{M|N \times l_2}$ that splits (H.0.18) into two pieces of sizes l_1 and l_2 (see also (5.5) in [69]). As computed in [69, 225], we have[22]

$$\Delta_{l_1,l_2}\left(U_{ij}^{(1)}[m] \right) = U_{ij}^{(1)}[m] \otimes 1 + 1 \otimes U_{ij}^{(1)}[m],$$

$$\Delta_{l_1,l_2}\left(U_{ij}^{(2)}[m] \right) = U_{ij}^{(2)}[m] \otimes 1 + 1 \otimes U_{ij}^{(2)}[m] + \sum_{c=1}^{M+N} \sum_{n \in \mathbb{Z}} U_{in}^{(1)}[k] \otimes U_{nj}^{(2)}[m-k] - (m+1)l_1\varkappa 1 \otimes U_{ij}^{(1)}[m].$$

$$(5.7.31)$$

---

[21]Notice that this is not claiming that Φ becomes an isomorphism when taking the limit $l \to \infty$. It still requires to show the injectivity. However, this map does not seem to be well-defined when l diverges, and the factors l cannot be fully absorbed under redefinitions of the generators in these expressions. One might think of taking $\varkappa \to 0$ as another possible way to bypass this divergence, but some properties of Φ, such as surjectivity, rely on $\varkappa \neq 0$.

[22]We are not adding extra labels l and $l_{1,2}$ to these $U_{ij}^{(s)}$ as it should be clear which elements belong to which parts.

Let us also define the map $\widetilde{\Delta}_{l_1,l_2} = \left(\mathrm{id}^{\otimes l_1} \otimes \eta_{-l_1\varkappa}^{\otimes l_2}\right) \circ \Delta_{l_1,l_2}$. Then following the same proof as in [225], we have the commutative diagram

$$
\begin{array}{ccc}
\mathtt{Y} & \xrightarrow{\ \ \Phi_l\ \ } & U(\mathcal{W}_{M|N\times l}) \\[2pt]
\Big\downarrow{\scriptstyle \Delta} & & \Big\downarrow{\scriptstyle \widetilde{\Delta}_{l_1,l_2}} \\[2pt]
\mathtt{Y}\widehat{\otimes}\mathtt{Y} & \xrightarrow{\ \Phi_{l_1}\otimes\Phi_{l_2}\ } & U(\mathcal{W}_{M|N\times l_1})\widehat{\otimes}U(\mathcal{W}_{M|N\times l_2})
\end{array}
\tag{5.7.32}
$$

where we have labelled Φ with subscripts l and $l_{1,2}$ for clarity.

More general truncations As studied in [65, 66, 88] for the $\mathbb{C}^3$ case and [69] for any generalized conifold, there exist larger families of truncations of the $\mathcal{W}$-algebras. These truncations, which are dictated by the functions $x^{l_3}y^{l_2}z^{l_4}w^{l_1} \in \mathbb{C}[x,y,z,w]/\langle xy = z^M w^N\rangle$, can be built from x-, y-, z- and w-algebras associated to different divisors in the CY_3. In particular, the x-algebra just corresponds to the Miura operator of form (H.0.18). More generally, these truncations have generalized Miura/pseudo-differential operators of different types.

In terms of (p,q)-brane webs, certain stacks of D3s are stretched in different regions, indicating the multiplicities of smooth components of these divisors. See for example Figure 6 in [69] for an illustration of the patterns of these elementary truncated algebras. The web diagram encodes the loci in the base where the T^2 part of the fibre degenerates to a circle in the (resolved) CY threefold. The complex coordinates that are used in the moment maps parametrizing the base can be grouped into variables x, y, z, w. This gives rise to the perspective of a 4d $\mathcal{N} = 4$ gauge theory which is divided into a junction of four interfaces (or three for the $\mathbb{C}^3$ case).

The generators for the elementary building blocks of truncations can be found in [69]. Here, we would just like to mention that with

$$
l = \frac{((N - M)\epsilon_1 - \epsilon_2)l_3 + \epsilon_2 l_2 - \epsilon_1 l_4 + \epsilon_1 l_1}{(N - M)\epsilon_1 - \epsilon_2},
\tag{5.7.33}
$$

the same argument as in Theorem 5.7.4 indicates that we have this surjective homomorphism from the quiver Yangian to the general $x^{l_3}y^{l_2}z^{l_4}w^{l_1}$-algebra, which reflects the feature of the VOAs as truncations. Notice that now the generators $U_{ij}^{(1)}$ and $U_{ab}^{(2)}$ are given in [69, (5.47)], satisfying the same OPEs as before.

5.7.2 Crystal Melting Representations

As argued in [57, 198], the truncations of quiver Yangians lead to truncated crystal configurations where the melting would stop at one or more atoms. Therefore, with the map Φ, we may consider the truncated crystals as modules of $U(\mathcal{W}_{M|N\times l})$.

To get the actions of $U_{ij}^{(s)}$ on the truncated crystals, we need to know how they can be expressed using the map Φ. Here, let us find such expressions for all the elements at spin $s = 1, 2$, which essentially gives the proof of the surjectivity of Φ.

First, let us consider $U_{ab}^{(1)}[m]$ for any $a, b = 1, \dots, M + N$ and $m \in \mathbb{Z}$. The zero modes of $\mathcal{H}, \mathcal{E}, \mathcal{F}$ already gives $U_{a,a+1}^{(1)}[0]$, $U_{a+1,a}^{(1)}[0]$ (with two exceptions) and $U_{aa}^{(1)}[0] - U_{a+1,a+1}^{(1)}[0]$. It is immediate to obtain $U_{aa}^{(1)}[0] - U_{bb}^{(1)}[0]$ for any a, b. Using the commutation relations

$$
\begin{cases}
-(-1)^{p(a+1)}\left[U_{a,a+1}^{(1)}[0], U_{a+1,a+2}^{(1)}[0]\right] = U_{a,a+2}^{(1)}[0], \\[6pt]
(-1)^{p(a)p(a+1)+p(a+1)p(a+2)+p(a)p(a+2)}\left[U_{a+1,a}^{(1)}[0], U_{a+2,a+1}^{(1)}[0]\right] = U_{a+2,a}^{(1)}[0]
\end{cases}
\tag{5.7.34}
$$

iteratively, we can get $U_{ab}^{(1)}[0]$ for any $a \neq b$ (including $U_{1,M+N}^{(1)}[0]$ and $U_{M+N,1}^{(1)}[0]$). This is consistent with the fact that $e_0^{(\alpha)}$ (and likewise for $f_0^{(\alpha)}$) is of form $\left[\ldots \left[\left[e_0^{(a_1)}, e_0^{(a_2)} \right], e_0^{(a_3)} \right] \ldots, e_0^{(a_n)} \right]$ when $\alpha = \alpha^{(a_1)} + \cdots + \alpha^{(a_n)}$. Now, using $\Phi\left(\mathcal{E}_0^{(a)} \right)$ and $\Phi\left(\mathcal{F}_0^{(a)} \right)$, we can write

$$\begin{cases} U_{M+N,a}^{(1)}[-1] = -(-1)^{p(1)} \left[U_{M+N,1}^{(1)}[-1], U_{1,a}^{(1)}[0] \right], \\ U_{a,M+N}^{(1)}[-1] = (-1)^{p(1)p(M+N)+p(a)p(1)+p(a)p(M+N)} \left[U_{1,M+N}^{(1)}[1], U_{a,1}^{(1)}[0] \right] \end{cases} \tag{5.7.35}$$

for $a \neq M + N$. Hence, via

$$\begin{cases} U_{ba}^{(1)}[-1] = (-1)^{p(M+N)p(a)+p(M+N)p(b)+p(a)p(b)} \left[U_{M+N,a}^{(1)}[-1], U_{b,M+N}^{(1)}[0] \right], \\ U_{ab}^{(1)}[1] = -(-1)^{p(M+N)} \left[U_{a,M+N}^{(1)}[1], U_{M+N,b}^{(1)}[0] \right], \end{cases} \tag{5.7.36}$$

we can get $U_{ab}^{(1)}[\pm 1]$ for any $a \neq b$. Keep this procedure, and we can obtain $U_{ab}^{(1)}[m]$ for any $a \neq b$ and $m \in \mathbb{Z}$.

For elements of spin 1, we are now left with $U_{aa}^{(1)}[m]$. Take

$$X_{ab}[m] := \left[U_{ab}^{(1)}[m], U_{bb}^{(2)}[0] - U_{b+1,b+1}^{(2)}[0] - U_{bb}^{(1)}[0]U_{b+1,b+1}^{(1)}[0] \right.$$
$$\left. - \sum_{k \geq 0} U_{bb}^{(1)}[-k]U_{bb}^{(1)}[k] + \sum_{k \geq 0} U_{b+1,b+1}^{(1)}[-k-1]U_{b+1,b+1}^{(1)}[k+1] \right] \tag{5.7.37}$$

for $a \neq b$. We are allowed to use this commutation relation because of $\Phi\left(\mathcal{H}_1^{(b)} \right)$. A straightforward computation yields

$$X_{ab}[m] = - (-1)^{p(b)} U_{ab}^{(2)}[m] + (-1)^{p(b)} U_{ab}^{(1)}[m]U_{b+1,b+1}^{(1)}[0]$$
$$+ \sum_{k \geq 0} (-1)^{p(b)} U_{ab}^{(1)}[m-k]U_{bb}^{(1)}[k] - \sum_{k \geq 0} (-1)^{p(b)} U_{bb}^{(1)}[-k]U_{ab}^{(1)}[m+k]. \tag{5.7.38}$$

Therefore,

$$\left[U_{ba}^{(1)}[0], (-1)^{p(b)} X_{ab}[m] \right] - \left[U_{ba}^{(1)}[1], (-1)^{p(b)} X_{ab}[m-1] \right]$$
$$= - (l-1)(-1)^{p(a)} \varkappa U_{bb}^{(1)}[m] - \delta_{m,0} l(-1)^{p(a)} \varkappa U_{b+1,b+1}^{(1)}[0] - \delta_{m \geq 0} l(-1)^{p(a)} \varkappa U_{bb}^{(1)}[m] \tag{5.7.39}$$
$$+ \delta_{m \leq 0} l(-1)^{p(a)} \varkappa U_{bb}^{(1)}[m] + (-1)^{p(b)} U_{ab}^{(1)}[m]U_{ba}^{(1)}[0] - (-1)^{p(b)} U_{ba}^{(1)}[0]U_{ab}^{(1)}[m].$$

Notice that most terms appeared in the calculation get cancelled since $0 + m = 1 + m - 1$. When $m > 0$, (5.7.39) is equal to

$$-(-1)^{p(a)} \varkappa U_{bb}^{(1)}[m] - l(-1)^{p(a)} \varkappa U_{bb}^{(1)}[m] + (-1)^{p(b)} U_{ab}^{(1)}[m]U_{ba}^{(1)}[0] - (-1)^{p(b)} U_{ba}^{(1)}[0]U_{ab}^{(1)}[m]. \tag{5.7.40}$$

As a result, we obtain $U_{bb}^{(1)}[m]$ for $m > 0$. This is likewise for $m < 0$. When $m = 0$, (5.7.39) is

$$-(-1)^{p(a)} \varkappa U_{bb}^{(1)}[0] - l(-1)^{p(a)} \varkappa U_{b+1,b+1}^{(1)}[0] + (-1)^{p(b)} U_{ab}^{(1)}[0]U_{ba}^{(1)}[0] - (-1)^{p(b)} U_{ba}^{(1)}[0]U_{ab}^{(1)}[m]. \tag{5.7.41}$$

This in particular gives $-(-1)^{p(a)} \varkappa U_{bb}^{(1)}[0] - l(-1)^{p(a)} \varkappa U_{b+1,b+1}^{(1)}[0]$. Together with $U_{bb}^{(1)}[0] - U_{b+1,b+1}^{(1)}[0]$, we can get $U_{bb}^{(1)}[0]$.

Now, we shall consider the elements of spin 2. From $\Phi\left(\mathcal{H}_1^{(a)} \right)$, $\Phi\left(\mathcal{E}_1^{(a)} \right)$ and $\Phi\left(\mathcal{F}_1^{(a)} \right)$, we get $U_{a,a+1}^{(2)}[0]$, $U_{(a+1,a)}^{(2)}[0]$ (with two exceptions) and $U_{aa}^{(2)}[0] - U_{a+1,a+1}^{(2)}[0]$. Similar to the case of $U_{ab}^{(1)}[m]$,

we can then obtain $U_{ab}^{(2)}[m]$, as well as $U_{aa}^{(2)}[m] - U_{bb}^{(2)}[m]$, for any $a \neq b$ and $m \in \mathbb{Z}$ using the $U^{(1)}U^{(2)}$ commutation relation.

To get the remaining elements $U_{aa}^{(2)}[m]$, let us compute

$$\left[U_{aa}^{(2)}[1] - U_{bb}^{(2)}[1], U_{aa}^{(2)}[m] - U_{bb}^{(2)}[m] \right] - \left[U_{aa}^{(2)}[1] - U_{bb}^{(2)}[1], U_{aa}^{(2)}[m+1] - U_{bb}^{(2)}[m+1] \right] \quad (5.7.42)$$

for $a \neq b$. This could be tedious due to all the $U^{(2)}U^{(2)}$ commutation relations, but we notice that most of the terms can be cancelled, and it becomes

$$- 2\varkappa(-1)^{p(a)}U_{aa}^{(2)}[m+1] - 2\varkappa(-1)^{p(b)}U_{bb}^{(2)}[m+1]$$

$$+ (l-1)\left((1+(-1)^{p(a)})\left(\sum_{k>0}U_{aa}^{(1)}[-k]U_{aa}^{(1)}[m+1+k] + \sum_{k\geq0}U_{aa}^{(1)}[m+1-k]U_{aa}^{(1)}[k] \right) \right.$$

$$+ (1+(-1)^{p(b)})\left(\sum_{k>0}U_{bb}^{(1)}[-k]U_{bb}^{(1)}[m+1+k] - \sum_{k\geq0}U_{bb}^{(1)}[m+1-k]U_{bb}^{(1)}[k] \right)$$

$$- \sum_{k>0}U_{aa}^{(1)}[-k]U_{bb}^{(1)}[m+1+k] - \sum_{k\geq0}U_{bb}^{(1)}[m+1-k]U_{aa}^{(1)}[k]$$

$$- \sum_{k>0}U_{bb}^{(1)}[-k]U_{aa}^{(1)}[m+1+k] - \sum_{k\geq0}U_{aa}^{(1)}[m+1-k]U_{bb}^{(1)}[k]$$

$$- (-1)^{p(b)}\varkappa\sum_{k>0}U_{ab}^{(1)}[-k]U_{ba}^{(1)}[m+1-k] - (-1)^{p(a)}\varkappa\sum_{k\geq0}U_{ba}^{(1)}[m+1-k]U_{ab}^{(1)}[k]$$

$$\left. - (-1)^{p(a)}\varkappa\sum_{k>0}U_{ba}^{(1)}[-k]U_{ab}^{(1)}[m+1-k] - (-1)^{p(b)}\varkappa\sum_{k\geq0}U_{ab}^{(1)}[m+1-k]U_{ba}^{(1)}[k] \right)$$

$$- l(l-1)(m+2)\varkappa^2\left((-1)^{p(a)}U_{aa}^{(1)}[m+1] + (-1)^{p(b)}U_{bb}^{(1)}[m+1] \right). \quad (5.7.43)$$

From this, we get $(-1)^{p(a)}U_{aa}^{(2)}[n] + (-1)^{p(b)}U_{bb}^{(2)}[n]$. Choose a, b such that $p(a) = p(b)$ (which is always possible for the cases we focus on in this paper). Together with $U_{aa}^{(2)}[n] - U_{bb}^{(2)}[n]$, we can obtain $U_{aa}^{(2)}[n]$ for any $a = 1, \ldots, M+N$ and $n \in \mathbb{Z}$.

Now, we can in principle write the actions of any $U_{ab}^{(s)}[m]$ on the (truncated) crystals. Since the crystal configuration always starts from the empty state $|\varnothing\rangle$ on which only the $e_0^{(0)}$ and $\psi_0^{(0)}$ modes would have non-trivial action. It is natural to wonder whether the truncated crystal can be a highest weight representation of $U(\mathcal{W}_{M|N\times l})$ with $|\varnothing\rangle$ being the highest weight vector. In particular, all the modes $U_{ab}^{(s)}[m]$ with $s \in \mathbb{Z}_+$, $a, b = 1, \ldots, M+N$ and $m > 0$ should annihilate the highest weight state. To make this state unique, we also need $U_{ab}^{(1)}[0]$ to act trivially on it for all $a > b$ in our convention here.

Corollary 5.7.4.1. *The truncated crystal is a highest weight representation of $U(\mathcal{W}_{M|N\times l})$ with the empty room configuration $|\varnothing\rangle$ as the highest weight state[23].*

Again, the proof can be found in [15].

When considering $\mathcal{H}_0^{(a\neq0)}|\varnothing\rangle = \psi_0^{(a)}|\varnothing\rangle = 0$, we can see that $U_{11}^{(1)}|\varnothing\rangle = U_{22}^{(1)}|\varnothing\rangle = \cdots = U_{M+N,M+N}^{(1)}|\varnothing\rangle$. On the other hand, $\left(U_{M+N,M+N}^{(1)}[0] - U_{11}^{(1)}[0] + l\varkappa \right)|\varnothing\rangle = \mathcal{H}_0^{(0)}|\varnothing\rangle = C|\varnothing\rangle$. This then relates the parameter on the $\mathcal{W}$-algebra side with the vacuum charge in the quiver Yangian:

Corollary 5.7.4.2. *We have $C = l\varkappa$, where C is the vacuum charge.*

---

[23]Notice that we are only considering the x-algebra here. For the other types of truncations, since $U^{(n>l)}$ do not vanish due to the pseudo-differential operators, one further needs to show that $U^{(n>l)}$ annihilates all the states in the truncated crystal.

Example Let us illustrate the above discussions with an example. The simplest case would be $\mathbb{C} \times \mathbb{C}^2/\mathbb{Z}_3$ whose quiver and crystal model are depicted in Figure 5.7.1. The possible configurations
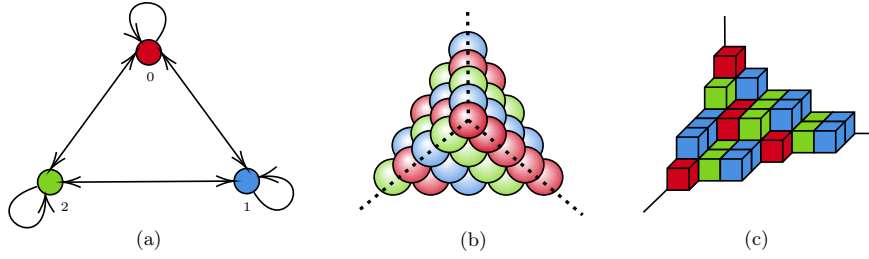
FIGURE 5.7.1: (a) The quiver for $\mathbb{C} \times \mathbb{C}^2/\mathbb{Z}_3$. (b) The corresponding crystal model with three colours. The dased lines are the ridges of the crystal. (c) The equivalent crystal model visualized using coloured plane partitions.

with the corresponding modes acting on $|\varnothing\rangle$ at low levels are listed in [57]. For instance, take $|\mathfrak{C}\rangle$ to be

$$|\mathfrak{C}\rangle = e_0^{(2)} e_0^{(0)} |\varnothing\rangle = \quad \text{}. \tag{5.7.44}$$

One possible way to add an atom is to act $\mathcal{E}_0^{(1)} = e_0^{(1)}$. Using the action of $e^{(1)}(z)$, we have

$$\Psi_{\mathfrak{C}}^{(1)} = \frac{(z + \widetilde{\epsilon}_{10})\,(z - \widetilde{\epsilon}_{02} + \widetilde{\epsilon}_{12})}{(z - \widetilde{\epsilon}_{01})\,(z - \widetilde{\epsilon}_{02} - \widetilde{\epsilon}_{21})}, \tag{5.7.45}$$

where we have kept the notation $\widetilde{\epsilon}_I$. Therefore,

$$\mathcal{E}_0^{(1)}|\mathfrak{C}\rangle = -\left(\frac{(\widetilde{\epsilon}_{10} + \widetilde{\epsilon}_{02} + \widetilde{\epsilon}_{21})\,(\widetilde{\epsilon}_{12} + \widetilde{\epsilon}_{21})}{\widetilde{\epsilon}_{01} - \widetilde{\epsilon}_{02} - \widetilde{\epsilon}_{21}}\right)^{1/2}|\mathfrak{C} + \mathbf{1}\rangle. \tag{5.7.46}$$

This gives

$$U_{12}^{(1)}[0]|\mathfrak{C}\rangle = \frac{3\epsilon_2(\epsilon_1 + \epsilon_2)}{\epsilon_1 - 2\epsilon_2}|\mathfrak{C} + \mathbf{1}\rangle, \tag{5.7.47}$$

where

$$|\mathfrak{C} + \mathbf{1}\rangle = \quad \text{}. \tag{5.7.48}$$

One may apply the procedure above used for constructing other elements and get their actions. Here, we list a few examples for $U_{ij}^{(1)}[m]$:

$|\mathfrak{C}\rangle$	$U_{23}^{(1)}[0]$	$U_{31}^{(1)}[-1]$	$U_{13}^{(1)}[0]$	$U_{21}^{(1)}[0]$	$U_{32}^{(1)}[0]$	$U_{13}^{(1)}[1]$	$U_{31}^{(1)}[0]$	$U_{32}^{(1)}[-1]$	$U_{21}^{(1)}[-1]$
$|\mathfrak{C}'\rangle$	0			0		0	0		

$$\tag{5.7.49}$$

where we omit the coefficients and only show the crystal configurations. By considering higher modes of the quiver Yangian generators, we can also get the actions of $U^{(s)}$ with higher spins.

Let us take a brief look at how the truncations of the crystal could happen. Here, we shall only discuss the simplest example which truncates the algebra at $l = 1$. In such case, we just have the universal enveloping algebra of the Kac-Moody algebra with only zero modes for the quiver Yangian, or equivalently, only spin 1 elements for the $\mathcal{W}$-algebra. It is straightforward to see that the truncated crystal has the shape

$$\tag{5.7.50}$$

of semi-infinite length. We simply have $U_{ab}^{(s \geq 2)}[m]|\mathfrak{C}\rangle = 0$ for any $a, b \in \{1, 2, 3\}$, $m \in \mathbb{Z}$ and any configuration $\mathfrak{C}$ as $U_{ab}^{(s)}[m]$ vanishes for $s > l$.

In general, for any quiver Yangian we focus on in this paper, the truncation at the very first level $l = 1$ can be desribed in this manner. For more general truncations of the crystal and larger l, this could be more involved, and we leave this to future work (see also §5.13).

5.8 Toroidal and Elliptic Cases

Let us now have a discussion on the trigonometric and elliptic counterparts of the rational quiver Yangians [199] (see also [200, 201]). Such algebras, dubbed rational (toroidal, resp. elliptic) quiver BPS algebras, can be realized by 3d $\mathcal{N} = 2$ (2d $\mathcal{N} = (2, 2)$, resp. 1d $\mathcal{N} = 4$) quantum field theories. These theories are low-energy effective theories on the D-branes that probe the CY threefolds. In particular, the three types of algebras can be uniformly described by some bond factors. For the elliptic algebras, the bond factor is composed of certain theta function $\Theta_q(u)$, where q is the square of the nome. In other words, it is related to the modulus τ of the torus by $q = \exp(2\pi i \tau)$. Under dimensional reduction, this gives the trigonometric version of the algebras whose bond factor is determined by $\mathrm{Sin}_\beta(u) := 2 \sinh(\beta u/2)$. In the limit where the radius β of the circle goes to 0, one reaches the rational case with the bond factor consisting of the rational function u. For future convenience, we shall use $h_{1,2}$ to denote the two parameters of the algebras in the remaining of this chapter.

To extend the above definition of the rational quiver Yangians, we need to consider three types of currents, $\psi_\pm^{(a)}(u)$, $e^{(a)}(u)$ and $f^{(a)}(u)$, where we now have $\psi_\pm$ instead of the single ψ. The currents have the following mode expansions[24]:

$$
x^{(a)}(u) = \begin{cases}
\sum\limits_{n \in \mathbb{Z}_+} \dfrac{x_n^{(a)}}{u^n}, & \text{rational} \\
\sum\limits_{n \in \mathbb{Z}} \dfrac{x_n^{(a)}}{U^n}, & \text{trigonometric} \\
\sum\limits_{n \in \mathbb{Z}} \dfrac{x_n^{(a)}}{U^n} = \sum\limits_{n \in \mathbb{Z}} \sum\limits_{\alpha \in \mathbb{Z}_{\geq 0}} \dfrac{x_{n,\alpha}^{(a)}}{U^n} q^\alpha, & \text{elliptic}
\end{cases}
\tag{5.8.1}
$$

where $x = e, f$. For non-chiral quivers,

$$
\psi_\pm^{(a)}(u) = \begin{cases}
\sum\limits_{n \in \mathbb{Z}_{\geq 0}} \dfrac{\psi_n^{(a)}}{u^n}, & \text{rational} \\
\sum\limits_{n \in \mathbb{Z}_{\geq 0}} \dfrac{\psi_{\pm,n}^{(a)}}{U^{\pm n}}, & \text{trigonometric} \\
\sum\limits_{n \in \mathbb{Z}} \dfrac{\psi_{\pm,n}^{(a)}}{U^{\pm n}} = \sum\limits_{n \in \mathbb{Z}} \sum\limits_{\alpha \in \mathbb{Z}_{\geq 0}} \dfrac{\psi_{\pm,n,\alpha}^{(a)}}{U^{\pm n}} q^\alpha, & \text{elliptic}
\end{cases}
\tag{5.8.2}
$$

with $\psi_{\pm,n<0,0}^{(a)} = 0$ in the elliptic case. For chiral quivers,

$$
\psi_\pm^{(a)}(u) = \begin{cases}
\sum\limits_{n \in \mathbb{Z}} \dfrac{\psi_n^{(a)}}{u^n}, & \text{rational} \\
\sum\limits_{n \in \mathbb{Z}} \dfrac{\psi_{\pm,n}^{(a)}}{U^{\pm n}}, & \text{trigonometric} \\
\sum\limits_{n \in \mathbb{Z}} \dfrac{\psi_{\pm,n}^{(a)}}{U^{\pm n}} = \sum\limits_{n \in \mathbb{Z}} \sum\limits_{\alpha \in \mathbb{Z}_{\geq 0}} \dfrac{\psi_{\pm,n,\alpha}^{(a)}}{U^{\pm n}} q^\alpha, & \text{elliptic}
\end{cases}
\tag{5.8.3}
$$

---

[24]One can also consider shifted quiver BPS algebras that would introduce an extra shift parameter to (some part of) the mode expansion of $\psi_\pm$ [199]. This is closely related to the crystal representations and the framings of the quivers [198, 201]. However, we shall not consider this here.

Notice that in the rational case, $\psi_+ = \psi_- = \psi$. Moreover, the expansions for trigonometric and elliptic cases are in terms of U rather than u. The letters in the upper case are related to those in the lower case by[25]

$$X = e^{\beta x}, \qquad (x, X) = (u, U), (v, V), (c, C), (\mathtt{h}_I, \mathtt{H}_I), \ldots \tag{5.8.4}$$

Henceforth, we will use the upper and lower cases interchangeably (such as $e^{(a)}(U) = e^{(a)}(u)$) in the arguments of the currents for trionometric and elliptic cases. For convenience, we may also write $e^{(a)}(U) = \sum_{\alpha \in \mathbb{Z}_{\geq 0}} e_\alpha^{(a)}(U) q^\alpha$ (and likewise for the other currents) in the elliptic case.

To write their relations, we first need to introduce some necessary concepts. To distinguish chiral and non-chiral quivers, we define the chirality parameter as

$$\chi_{ab} = |a \to b| - |b \to a| \tag{5.8.5}$$

for each pair of nodes a, b in the quiver, where $|a \to b|$ denotes the number of arrows from a to b. Moreover, we shall define the formal delta function as

$$\delta(u) = \begin{cases} 1/u, & \text{rational} \\ \sum_{n \in \mathbb{Z}} U^n, & \text{otherwise} \end{cases}. \tag{5.8.6}$$

Recall that the key factor in the definition of the algebras is the bond factor $\varphi^{a \Leftarrow b}(u)$. Here, we shall write it as[26]

$$\varphi^{a \Leftarrow b}(u) = \frac{\prod\limits_{a \to b} \zeta(\mathtt{h}_I + u)}{\prod\limits_{b \to a} \zeta(\mathtt{h}_I - u)}, \tag{5.8.7}$$

where $\mathtt{h}_I$ is the parameter/charge associated to the arrow I in the quiver, and

$$\zeta(u) = \begin{cases} u, & \text{rational} \\ \mathrm{Sin}_\beta(u) := 2 \sinh \frac{\beta u}{2} = U^{1/2} - U^{-1/2}, & \text{trigonometric} \\ \Theta_q(u) := -U^{-1/2} \theta_q(u) = \left(U^{1/2} - U^{-1/2}\right) \prod\limits_{k=0}^{\infty} \left(1 - U^{-1} q^k\right) \left(1 - U q^k\right), & \text{elliptic} \end{cases}. \tag{5.8.8}$$

Here, $\theta_q(u) = (U; q)_\infty \left(q U^{-1}; q\right)_\infty$ in terms of the q-Pochhammer symbols. From the expressions for ζ, we have

$$\zeta(u) = -\zeta(-u). \tag{5.8.9}$$

It is straightforward to see that in the rational limit $\beta \to 0$, the trigonometric case reduces to the rational one. Likewise, when $q \to 0$, the elliptic one reduces to the trigonometric one. This will also be the limits that relate the three types of quiver BPS algebras.

To get rid of the powers with half-integers, we will take the balanced bond factor

$$\phi^{a \Leftarrow b}(u, v) = (UV)^{\frac{\mathtt{t}}{2} \chi_{ab}} \varphi^{a \Leftarrow b}(u - v), \tag{5.8.10}$$

where $\mathtt{t}$ is 0 in the rational case and -1 otherwise[27]. Therefore, this balancing would only affect chiral quivers in the trigonometric and elliptic cases. As can be seen from its expression, the bond factor satisfies

$$\varphi^{a \Leftarrow b}(u) \varphi^{b \Leftarrow a}(-u) = 1. \tag{5.8.11}$$

---

[25]As a result, β can be absorbed under a redefinition of variables. Nevertheless, we shall keep it here due to its physical origin.

[26]This is slightly different from the notion in [199] when both $|a \to b|$ and $|b \to a|$ are odd. Nevertheless, the bond factor here should still be legitimate as it satisfies the reciprocity condition (5.8.11) below.

[27]Notice that this is slightly different from the original one in [199] where $\mathtt{t}$ was defined to be 1 for the trigonometric and elliptic cases. This is only a choice for our later discussions on mode expansions for chiral quivers. Since the balancing factor $(UV)^{\frac{1}{2} \chi_{ab}}$ is used to get rid of the half-integer powers in the Laurent expansions of the expressions, this should just be a matter of convention.

Therefore,

$$\phi^{a \Leftarrow b}(u, v)\phi^{b \Leftarrow a}(v, u) = 1. \tag{5.8.12}$$

Moreover, we have

$$\phi^{a \Leftarrow b}(u + s, v) = s^{\mathsf{t}\chi_{ab}}\phi^{a \Leftarrow b}(u, v - s). \tag{5.8.13}$$

With this (balanced) bond factor, the three types of quiver Yangians can be presented in a unified way as [57, 199]

$$\psi_{\pm}^{(a)}(u)\psi_{\pm}^{(b)}(v) \simeq C^{\pm \mathsf{t}\chi_{ab}}\psi_{\pm}^{(b)}(v)\psi_{\pm}^{(a)}(u), \tag{5.8.14}$$

$$\psi_{+}^{(a)}(u)\psi_{-}^{(b)}(v) \simeq \frac{\phi^{a \Leftarrow b}(u + c/2, v - c/2)}{\phi^{a \Leftarrow b}(u - c/2, v + c/2)}\psi_{-}^{(b)}(v)\psi_{+}^{(a)}(u), \tag{5.8.15}$$

$$\psi_{\pm}^{(a)}(u)e^{(b)}(v) \simeq \phi^{a \Leftarrow b}(u \pm c/2, v)e^{(b)}(v)\psi_{\pm}^{(a)}(u), \tag{5.8.16}$$

$$\psi_{\pm}^{(a)}(u)f^{(b)}(v) \simeq \phi^{a \Leftarrow b}(u \mp c/2, v)^{-1}f^{(b)}(v)\psi_{\pm}^{(a)}(u), \tag{5.8.17}$$

$$e^{(a)}(u)e^{(b)}(v) \simeq (-1)^{|a||b|}\phi^{a \Leftarrow b}(u, v)e^{(b)}(v)e^{(a)}(u), \tag{5.8.18}$$

$$f^{(a)}(u)f^{(b)}(v) \simeq (-1)^{|a||b|}\phi^{a \Leftarrow b}(u, v)^{-1}f^{(b)}(v)f^{(a)}(u), \tag{5.8.19}$$

$$\left[e^{(a)}(u), f^{(b)}(v)\right\} \simeq -\delta_{ab}\left(\delta(u - v - c)\psi_{+}^{(a)}(u - c/2) - \delta(u - v + c)\psi_{-}^{(a)}(v - c/2)\right). \tag{5.8.20}$$

Here, c is the central element of the algebra which is 0 for the rational case (while it can be non-trivial for the other two cases). In the last relation, we have used the supercommutator $[x, y] = xy - (-1)^{|x||y|}yx$. For the rational quiver Yangians, "$\simeq$" indicates that the equalities are up to some sporadic $u^m v^n$ terms as we have seen before. For the trigonometric and elliptic cases, it means that the Laurent expansion on the two sides should agree, and we shall henceforth simply write it as "$=$". As shown in [199], (5.8.14)~(5.8.17) can be derived from (5.8.18)~(5.8.20). Therefore, when discussing the current relations, it suffices to consider the ee, ff and ef relations.

Besides the above relations, we also need the Serre relations. We will mention the Serre relations for the generalized conifolds below. Remarkably, the Serre relations for the toroidal algebras associated to any quivers (including chiral ones) were found recently in [205]. By taking the rational limit, we can obtain the Serre relations for the raitional quiver Yangians. Moreover, following the process to be mentioned in §5.10, we can get the Serre relations for the elliptic algebras as well.

5.8.1 Coproducts

The coproducts of the quiver BPS algebras are of particular interest due to their crucial role in the construction of R-matrices and the study of Bethe/gauge correspondence [14, 58]. For rational quiver Yangians of certain non-chiral quivers, the coproduct was discussed in §5.5. In contrast, the coproducts for trigonometric and elliptic cases (for either chiral or non-chiral quivers) are more straightforward. One may verify that the following gives a coassociative homomorphism (cf. [200]):

$$\Delta\left(e^{(a)}(U)\right) = e^{(a)}(U) \otimes 1 + \psi^{(a)}\left(C_1^{1/2}U\right) \otimes e^{(a)}(C_1 U), \tag{5.8.21}$$

$$\Delta\left(f^{(a)}(U)\right) = 1 \otimes f^{(a)}(U) + f^{(a)}(C_2 U) \otimes f^{(a)}\left(C_2^{1/2}U\right), \tag{5.8.22}$$

$$\Delta\left(\psi_{+}^{(a)}(U)\right) = \psi_{+}^{(a)}(U) \otimes \psi_{+}^{(a)}\left(C_1^{-1}U\right), \tag{5.8.23}$$

$$\Delta\left(\psi_{-}^{(a)}(U)\right) = \psi_{-}^{(a)}\left(C_2^{-1}U\right) \otimes \psi_{-}^{(a)}(U), \tag{5.8.24}$$

$$\Delta(C) = C \otimes C. \tag{5.8.25}$$

Here, $C_1 = C \otimes 1$ and $C_2 = 1 \otimes C$ are the conventional notations that indicate where the C factors should be in the mode expressions. More explicitly, for the toroidal algebras associated to non-chiral quivers, we have

$$\Delta\left(e_n^{(a)}\right) = e_n^{(a)} \otimes 1 + \sum_{j=0}^{\infty} C^{-n-j/2}\psi_{-,j}^{(a)} \otimes e_{n+j}^{(a)}, \tag{5.8.26}$$

$$\Delta\left(f_n^{(a)}\right) = 1 \otimes f_n^{(a)} + \sum_{j=0}^{\infty} f_{n-j}^{(a)} \otimes C^{-n+j/2}\psi_{+,j}^{(a)}, \tag{5.8.27}$$

$$\Delta\left(\psi_{+,n}^{(a)}\right) = \sum_{j=0}^{n} C^{n-j}\psi_{+,j}^{(a)} \otimes \psi_{+,n-j}^{(a)}, \tag{5.8.28}$$

$$\Delta\left(\psi_{-,n}^{(a)}\right) = \sum_{j=0}^{n} \psi_{-,n-j}^{(a)} \otimes C^{-n+j}\psi_{-,j}^{(a)}. \tag{5.8.29}$$

For the elliptic algebras and the algebras for chiral quivers, we just need to replace all $\sum_{j=0}^{\infty}$ and $\sum_{j=0}^{n}$ with $\sum_{j\in\mathbb{Z}}$. In the elliptic case, it is also straightforward to write down this in terms of $x_{n,\alpha}^{(a)}$ ($x = e, f, \psi_{\pm}$). We simply replace $x_n \otimes 1$ (resp. $1 \otimes x_n$) with $x_{n,\alpha} \otimes 1$ (resp. $1 \otimes x_{n,\alpha}$) and $x_m \otimes y_n$ with $\sum_{\gamma=0}^{\alpha} x_{m,\gamma} \otimes y_{n,\alpha-\gamma}$.

Hopf algebras   Together with the above coproduct in terms of the currents, we can have a counit and an antipode such that the algebra is endowed with the Hopf (super)algebra structure. The counit reads

$$\epsilon\left(e^{(a)}(U)\right) = \epsilon\left(f^{(a)}(U)\right) = 0, \quad \epsilon\left(\psi_{\pm}^{(a)}(U)\right) = \epsilon(C) = 1. \tag{5.8.30}$$

The antipode is an anti-homomorphism, that is, $S(xy) = (-1)^{|x||y|}S(y)S(x)$. Assuming that $\psi_{\pm}^{(a)}(U)$ are invertible in the algebra, then

$$S\left(e^{(a)}(U)\right) = -\psi_{-}^{(a)}\left(C^{-3/2}U\right)^{-1}e^{(a)}(CU), \tag{5.8.31}$$

$$S\left(f^{(a)}(U)\right) = -f^{(a)}(CU)\psi_{+}^{(a)}\left(C^{-3/2}U\right)^{-1}, \tag{5.8.32}$$

$$S\left(\psi_{\pm}^{(a)}(U)\right) = \psi_{\pm}^{(a)}\left(C^{-1}U\right)^{-1}, \tag{5.8.33}$$

$$S(C) = C^{-1}. \tag{5.8.34}$$

It is also straightforward to write them in terms of the modes. One may check that they satisfy the properties of Hopf algebras, such as $\mathcal{M} \circ (S \times \mathrm{id}) \circ \Delta = \mathcal{M} \circ (\mathrm{id} \times S) \circ \Delta = \eta \circ \epsilon$, where $\mathcal{M}$ and η denote the multiplication and the unit map respectively.

5.8.2   Gradings

Similar to the discussions in [227, 228], we can assign different gradings to the quiver BPS algebras. The degree of an element x can be written as $\deg(x) = (\mathrm{pdeg}(x), \mathrm{hdeg}(x))$, where $\mathrm{pdeg}(x) = \left(\mathrm{pdeg}^{(a)}(x)\right)$ is a vector known as the principal degree and $\mathrm{hdeg}(x)$ is a number called the homogeneous degree. We can introduce some invertible elements $D^{(a)}$ and D such that $D^{(a)}x\left(D^{(a)}\right)^{-1} = \mathrm{e}^{\beta\mathrm{pdeg}^{(a)}(x)}x$ and $DxD^{-1} = \mathrm{e}^{-\beta\mathrm{hdeg}(x)}x$.

We have $\deg\left(e_n^{(a)}\right) = (0,\ldots,1,\ldots,0,n)$ and $\deg\left(f_n^{(a)}\right) = (0,\ldots,-1,\ldots,0,n)$, where ± 1 is at the ath entry. On the other hand, $\deg\left(\psi_{\pm,n}^{(a)}\right) = (\mathbf{0},\pm n)$ and $\deg(C) = \deg\left(D^{(a)}\right) = \deg(D) = (\mathbf{0},0)$. For elliptic algebras, we may further consider the degree with respect to q, as well as an operator D_q, such that the modes at order α would have q-deg equal to α.

5.9   Toroidal Algebras for Non-Chiral Quivers

The first examples we shall discuss are the toroidal algebras for non-chiral quivers. Here, we will mainly focus on the generalized conifolds $xy = z^M w^N$ with $M + N \geq 3$. In particular, it suffices to

consider these cases in the discussions of toric duality as the other cases all have one single toric phase[28].

We shall use the same convention as in [199] for the two parameters $h_{1,2}$ of the algebra. For the arrow pointing from a to b, its charge is

$$h_{ab} = A_{ab}h_1 + M_{ab}h_2 = \begin{cases} 2\varsigma_a h_1, & a = b \\ \varsigma_b(-h_1 - h_2), & a+1 = b \\ \varsigma_a(-h_1 + h_2), & a = b+1 \\ 0, & \text{otherwise} \end{cases} \tag{5.9.1}$$

Equivalently, we can write $H_{ab} = H_1^{A_{ab}} H_2^{M_{ab}}$. Here, A_{ab} is the Cartan matrix

$$A_{ab} = (\varsigma_a + \varsigma_{a+1})\delta_{ab} - \varsigma_a\delta_{a,b+1} - \varsigma_b\delta_{a+1,b}, \tag{5.9.2}$$

and M_{ab} is defined as

$$M_{ab} = \varsigma_a\delta_{a,b+1} - \varsigma_b\delta_{a+1,b}. \tag{5.9.3}$$

Therefore, A_{ab} is symmetric while M_{ab} is antisymmetric.

The relations for the toroidal quiver algebra $\mathtt{T}$ can then be explicitly written as

$$\psi_\pm^{(a)}(U)\psi_\pm^{(b)}(V) = \psi_\pm^{(b)}(V)\psi_\pm^{(a)}(U), \tag{5.9.4}$$

$$\frac{H_2^{M_{ab}} H_1^{A_{ab}} U - CV}{H_2^{M_{ab}} U - H_1^{A_{ab}} CV}\psi_\pm^{(a)}(U)\psi_\mp^{(b)}(V) = \frac{H_2^{M_{ab}} H_1^{A_{ab}} CU - V}{H_2^{M_{ab}} CU - H_1^{A_{ab}} V}\psi_\mp^{(b)}(V)\psi_\pm^{(a)}(U), \tag{5.9.5}$$

$$\left(H^{M_{ab}} C^{\pm 1/2} U - H_1^{A_{ab}} V\right)\psi_\pm^{(a)}(U)e^{(b)}(V) = \left(H_2^{M_{ab}} H_1^{A_{ab}} C^{\pm 1/2} U - V\right)e^{(b)}(V)\psi_\pm^{(a)}(U), \tag{5.9.6}$$

$$\left(H^{M_{ab}} C^{\mp 1/2} U - H_1^{-A_{ab}} V\right)\psi_\pm^{(a)}(U)f^{(b)}(V) = \left(H_2^{M_{ab}} H_1^{-A_{ab}} C^{\mp 1/2} U - V\right)f^{(b)}(V)\psi_\pm^{(a)}(U), \tag{5.9.7}$$

$$\left(H^{M_{ab}} U - H_1^{A_{ab}} V\right)e^{(a)}(U)e^{(b)}(V) = (-1)^{|a||b|}\left(H_2^{M_{ab}} H_1^{A_{ab}} U - V\right)e^{(b)}(V)e^{(a)}(U), \tag{5.9.8}$$

$$\left(H^{M_{ab}} U - H_1^{-A_{ab}} V\right)f^{(a)}(U)f^{(b)}(V) = (-1)^{|a||b|}\left(H_2^{M_{ab}} H_1^{-A_{ab}} U - V\right)f^{(b)}(V)f^{(a)}(U), \tag{5.9.9}$$

$$\left[e^{(a)}(U), f^{(b)}(V)\right\} = -\delta_{ab}\left(\delta\left(UV^{-1}C^{-1}\right)\psi_+^{(a)}\left(UC^{-1/2}\right) - \delta\left(UV^{-1}C\right)\psi_-^{(a)}\left(VC^{-1/2}\right)\right). \tag{5.9.10}$$

In particular, when the central charge is trivial, that is, when $C = 1$, ψ_+ would commute with the ψ_- as can be seen directly from their current relations. The Serre relations are

$$\underset{u_1,u_2}{\mathrm{Sym}}\left[\!\!\left[e^{(a)}(u_1), \left[\!\!\left[e^{(a)}(u_2), e^{(a\pm 1)}(v)\right]\!\!\right]_{H_1}\right]\!\!\right]_{H_1} = 0 \qquad (|a| = 0), \tag{5.9.11}$$

$$\underset{u_1,u_2}{\mathrm{Sym}}\left[\!\!\left[e^{(a)}(u_1), \left[\!\!\left[e^{(a+1)}(v_1)\left[\!\!\left[e^{(a)}(u_2), e^{(a-1)}(v_2)\right]\!\!\right]_{H_1}\right]\!\!\right]_{H_1}\right]\!\!\right]_{H_1} = 0 \qquad (|a| = 1), \tag{5.9.12}$$

$$\underset{u_1,u_2}{\mathrm{Sym}}\left[\!\!\left[f^{(a)}(u_1), \left[\!\!\left[f^{(a)}(u_2), f^{(a\pm 1)}(v)\right]\!\!\right]_{H_1^{-1}}\right]\!\!\right]_{H_1^{-1}} = 0 \qquad (|a| = 0), \tag{5.9.13}$$

$$\underset{u_1,u_2}{\mathrm{Sym}}\left[\!\!\left[f^{(a)}(u_1), \left[\!\!\left[f^{(a+1)}(v_1)\left[\!\!\left[f^{(a)}(u_2), f^{(a-1)}(v_2)\right]\!\!\right]_{H_1^{-1}}\right]\!\!\right]_{H_1^{-1}}\right]\!\!\right]_{H_1^{-1}} = 0 \qquad (|a| = 1). \tag{5.9.14}$$

Here, the $\mathfrak{q}$-graded bracket is given by $[\![x, y]\!]_{\mathfrak{q}} = xy - (-1)^{|x||y|}\mathfrak{q}^{(x,y)}yx$, where (x, y) is the root pairing stemmed from the underlying affine Lie superalgebra. For instance, the pairing of two simple roots gives the corresponding entry in the Cartan matrix.

---

[28]Of course, for $M + N \geq 3$, all the triangles (i.e., $MN = 0$) and the suspended pinch point (i.e., $(M, N) = (2, 1), (1, 2)$) have one single toric phase as well.

5.9.1 More on Mode Expansions

We can also express (5.9.4)~(5.9.10) in terms of modes:

$$\psi_{\pm,m}^{(a)}\psi_{\pm,n}^{(b)} = \psi_{\pm,n}^{(b)}\psi_{\pm,m}^{(a)}, \tag{5.9.15}$$

$$H_2^{2M_{ab}}H_1^{A_{ab}}C\psi_{+,m+2}^{(a)}\psi_{-,n}^{(b)} - H_2^{M_{ab}}\left(H_1^{2A_{ab}}+C^2\right)\psi_{+,m+1}^{(a)}\psi_{-,n-1}^{(b)} - H_1^{A_{ab}}C\psi_{+,m}^{(a)}\psi_{-,n-2}^{(b)}$$
$$= H_2^{2M_{ab}}H_1^{A_{ab}}C\psi_{-,n}^{(b)}\psi_{+,m+2}^{(a)} - H_2^{M_{ab}}\left(H_1^{2A_{ab}}C^2+1\right)\psi_{-,n-1}^{(b)}\psi_{+,m+1}^{(a)} - H_1^{A_{ab}}C\psi_{-,n-2}^{(b)}\psi_{+,m}^{(a)}, \tag{5.9.16}$$

$$H_2^{M_{ab}}C^{1/2}\psi_{+,m+1}^{(a)}e_n^{(b)} - H_1^{A_{ab}}\psi_{+,m}^{(a)}e_{n+1}^{(b)} = H_2^{M_{ab}}H_1^{A_{ab}}C^{1/2}e_n^{(b)}\psi_{+,m+1}^{(a)} - e_{n+1}^{(b)}\psi_{+,m}^{(a)}, \tag{5.9.17}$$

$$H_2^{M_{ab}}C^{-1/2}\psi_{-,m}^{(a)}e_n^{(b)} - H_1^{A_{ab}}\psi_{-,m+1}^{(a)}e_{n+1}^{(b)} = H_2^{M_{ab}}H_1^{A_{ab}}C^{-1/2}e_n^{(b)}\psi_{-,m}^{(a)} - e_{n+1}^{(b)}\psi_{-,m+1}^{(a)}, \tag{5.9.18}$$

$$H_2^{M_{ab}}C^{-1/2}\psi_{+,m+1}^{(a)}f_n^{(b)} - H_1^{-A_{ab}}\psi_{+,m}^{(a)}f_{n+1}^{(b)} = H_2^{M_{ab}}H_1^{-A_{ab}}C^{-1/2}f_n^{(b)}\psi_{+,m+1}^{(a)} - f_{n+1}^{(b)}\psi_{+,m}^{(a)}, \tag{5.9.19}$$

$$H_2^{M_{ab}}C^{1/2}\psi_{-,m}^{(a)}f_n^{(b)} - H_1^{-A_{ab}}\psi_{-,m+1}^{(a)}f_{n+1}^{(b)} = H_2^{M_{ab}}H_1^{-A_{ab}}C^{1/2}f_n^{(b)}\psi_{-,m}^{(a)} - f_{n+1}^{(b)}\psi_{-,m+1}^{(a)}, \tag{5.9.20}$$

$$H_2^{M_{ab}}e_{m+1}^{(a)}e_n^{(b)} - H_1^{A_{ab}}e_m^{(a)}e_{n+1}^{(b)} = (-1)^{|a||b|}\left(H_2^{M_{ab}}H_1^{A_{ab}}e_n^{(b)}e_{m+1}^{(a)} - e_{n+1}^{(b)}e_m^{(a)}\right), \tag{5.9.21}$$

$$H_2^{M_{ab}}f_{m+1}^{(a)}f_n^{(b)} - H_1^{-A_{ab}}f_m^{(a)}f_{n+1}^{(b)} = (-1)^{|a||b|}\left(H_2^{M_{ab}}H_1^{-A_{ab}}f_n^{(b)}f_{m+1}^{(a)} - f_{n+1}^{(b)}f_m^{(a)}\right), \tag{5.9.22}$$

$$\left[e_m^{(a)}, f_n^{(b)}\right\} = -\delta_{ab}\left(C^{(m-n)/2}\psi_{+,m+n}^{(a)} - C^{-(m-n)/2}\psi_{-,-m-n}^{(a)}\right). \tag{5.9.23}$$

Notice that $\psi_{\pm,l<0}$ simply vanishes such as in the ef relations. In particular, the ψe and ψf relations include

$$\psi_{\pm,0}^{(a)}e_n^{(b)} = H_1^{\pm A_{ab}}e_n^{(b)}\psi_{\pm,0}^{(a)}, \quad \psi_{\pm,0}^{(a)}f_n^{(b)} = H_1^{\mp A_{ab}}f_n^{(b)}\psi_{\pm,0}^{(a)} \tag{5.9.24}$$

by setting $m=-1$ and

$$H_2^{M_{ab}}C^{1/2}\psi_{+,1}^{(a)}e_n^{(b)} - H_1^{A_{ab}}\psi_{+,0}^{(a)}e_n^{(b)} = H_2^{M_{ab}}H_1^{A_{ab}}C^{1/2}e_n^{(b)}\psi_{+,1}^{(a)} - e_{n+1}^{(b)}\psi_{+,0}^{(a)},$$
$$H_2^{M_{ab}}C^{-1/2}\psi_{-,0}^{(a)}e_n^{(b)} - H_1^{A_{ab}}\psi_{-,1}^{(a)}e_{n+1}^{(b)} = H_2^{M_{ab}}H_1^{A_{ab}}C^{-1/2}e_n^{(b)}\psi_{-,0}^{(a)} - e_{n+1}^{(b)}\psi_{-,1}^{(a)},$$
$$H_2^{M_{ab}}C^{-1/2}\psi_{+,1}^{(a)}f_n^{(b)} - H_1^{-A_{ab}}\psi_{+,0}^{(a)}f_{n+1}^{(b)} = H_2^{M_{ab}}H_1^{-A_{ab}}C^{-1/2}f_n^{(b)}\psi_{+,1}^{(a)} - f_{n+1}^{(b)}\psi_{+,0}^{(a)},$$
$$H_2^{M_{ab}}C^{1/2}\psi_{-,0}^{(a)}f_n^{(b)} - H_1^{-A_{ab}}\psi_{-,1}^{(a)}f_{n+1}^{(b)} = H_2^{M_{ab}}H_1^{-A_{ab}}C^{1/2}f_n^{(b)}\psi_{-,0}^{(a)} - f_{n+1}^{(b)}\psi_{-,1}^{(a)}$$
$$\tag{5.9.25}$$

by setting $m=0$. Likewise, the $\psi_+\psi_-$ relation includes

$$\psi_{+,m}^{(a)}\psi_{-,0}^{(b)} = \psi_{-,0}^{(b)}\psi_{+,m}^{(a)}, \quad \psi_{+,0}^{(a)}\psi_{-,n}^{(b)} = \psi_{-,n}^{(b)}\psi_{+,0}^{(a)} \tag{5.9.26}$$

by taking $n=0$ and $m=-2$ respectively. Therefore, $\psi_{\pm,0}$ commute with all the modes of $\psi_\pm$. It is worth noting that given a fixed fermionic node F, the $\psi_\pm^{(F)}$ modes commute with all F modes, and the $e^{(F)}$ (resp. $f^{(F)}$) modes anticommute with the $e^{(F)}$ (resp. $f^{(F)}$) modes. In fact, from (5.9.24), it is not hard to see that $\psi_{+,0}^{(a)}\psi_{-,0}^{(a)}$ is central for any node a. Write these central elements as $\mathsf{C}^{(a)} = \psi_{+,0}^{(a)}\psi_{-,0}^{(a)}$. Then we can write $\psi_{\pm,0}^{(a)} = \mathsf{C}^{(a)}\left(\psi_{\mp,0}^{(a)}\right)^{-1}$ with a mild assumption that $\left(\psi_{\pm,0}^{(a)}\right)^{-1}$ are also in the algebra. For convenience, we shall rescale them to be 1, that is, $\psi_{+,0}^{(a)} = \left(\psi_{-,0}^{(a)}\right)^{-1}$, in the following discussions.

Like many toroidal algebras, it is instructive to write the $\psi_\pm^{(a)}(U)$ currents as

$$\psi_\pm^{(a)}(U) = \psi_{\pm,0}^{(a)}\exp\left(\sum_{n=1}^\infty k_{\pm n}^{(a)}U^{\mp n}\right). \tag{5.9.27}$$

Therefore,

$$\psi_{\pm,n}^{(a)} = \psi_{\pm,0}^{(a)} \sum_{m=1}^{n} \frac{1}{m!} \sum_{\substack{r_1,\dots,r_m>0 \\ r_1+\cdots+r_m=n}} k_{\pm r_1}^{(a)} k_{\pm,r_2}^{(a)} \dots k_{\pm,r_m}^{(a)}. \tag{5.9.28}$$

Similarly, we can write the zero modes as

$$\psi_{+,0}^{(a)} = \exp\left(-\beta h_1 k_0^{(a)}\right) = H_1^{-k_0^{(a)}}, \quad \psi_{-,0}^{(a)} = \exp\left(\beta h_1 k_0^{(a)}\right) = H_1^{k_0^{(a)}}. \tag{5.9.29}$$

We shall refer to the modes $k_r^{(a)}$ ($r \in \mathbb{Z}$) as Heisenberg modes. There could also be different conventions to define these modes as discussed in Appendix I.

In terms of the Heisenberg modes, we can rewrite the relations involving $\psi_\pm$ as

$$\left[k_0^{(a)}, k_s^{(b)}\right] = 0, \quad \left[k_{r\neq0}^{(a)}, k_s^{(b)}\right] = \delta_{r+s,0}\frac{1}{r}\left(C^{-r} - C^r\right) H_2^{-rM_{ab}}\left(H_1^{rA_{ab}} - H_1^{-rA_{ab}}\right), \tag{5.9.30}$$

$$\left[k_0^{(a)}, e_n^{(b)}\right] = -A_{ab}e_n^{(b)}, \quad \left[k_0^{(a)}, f_n^{(b)}\right] = A_{ab}f_n^{(b)}, \tag{5.9.31}$$

$$\left[k_{r\neq0}^{(a)}, e_n^{(b)}\right] = \frac{1}{r}C^{-|r|/2}H_2^{-rM_{ab}}\left(H_1^{rA_{ab}} - H_1^{-rA_{ab}}\right) e_{n+r}^{(b)}, \tag{5.9.32}$$

$$\left[k_{r\neq0}^{(a)}, f_n^{(b)}\right] = -\frac{1}{r}C^{|r|/2}H_2^{-rM_{ab}}\left(H_1^{rA_{ab}} - H_1^{-rA_{ab}}\right) f_{n+r}^{(b)}. \tag{5.9.33}$$

Moreover, we have

$$\left[e_n^{(a)}, f_{-n}^{(b)}\right\} = \delta_{ab}\left(H_1^{k_0^{(a)}} - H_1^{-k_0^{(a)}}\right). \tag{5.9.34}$$

It would also be helpful to notice that

$$\left[e_{\pm1}^{(a)}, f_0^{(b)}\right\} = \mp\delta_{ab}C^{1/2}H_1^{\mp k_0^{(a)}}k_{\pm1}^{(a)}, \quad \left[e_0^{(a)}, f_{\pm1}^{(b)}\right\} = \mp\delta_{ab}C^{-1/2}H_1^{\mp k_0^{(a)}}k_{\pm1}^{(a)}. \tag{5.9.35}$$

Coproduct We can also write the coproduct above using $k_r^{(a)}$:

$$\Delta\left(k_r^{(a)}\right) = \begin{cases} C^r \otimes k_r^{(a)} + k_r^{(a)} \otimes 1, & r \geq 0 \\ k_r^{(a)} \otimes C^r + 1 \otimes k_r^{(a)}, & r < 0 \end{cases}. \tag{5.9.36}$$

In particular, $\Delta\left(k_0^{(a)}\right) = 1 \otimes k_0^{(a)} + k_0^{(a)} \otimes 1$.

Grading Likewise, for the aforementioned grading, we have $\deg\left(k_r^{(a)}\right) = (\mathbf{0}, r)$. In [227, 228], such gradings were useful in the quantum double construction of the universal R-matrix for certain toroidal algebra associated to $\mathfrak{gl}_1$. For toroidal BPS algebras associated to any non-chiral quivers here, a naive generalization would be $R = R^{(0)}R^{(1)}R^{(2)}$ with

$$R^{(0)} = \left(C^{-1} \otimes D^{-1}\right)\left(D^{-1} \otimes C^{-1}\right)\prod_a\left(\psi_{+,0}^{(a)} \otimes \left(D^{(a)}\right)^{-1}\right)\left(\left(D^{(a)}\right)^{-1} \otimes \psi_{+,0}^{(a)}\right),$$

$$R^{(1)} = \exp\left(\sum_{r\geq1} r \sum_a k_r^{(a)} \otimes k_{-r}^{(a)}\right), \quad R^{(2)} = 1 \otimes 1 + \sum_{n\in\mathbb{Z}}\sum_a e_n^{(a)} \otimes f_{-n}^{(a)} + \dots, \tag{5.9.37}$$

where the ellipsis in $R^{(2)}$ indicates terms with hdeg ≥ 1, and pdeg $\left(R^{(2)}\right)$ should be $\mathbf{0}$. However, whether these naive expressions would work and/or what modifications (such as proper normalizations etc.) are needed would still require further investigations in future.

5.9.2 Toric Duality

Now let us try to construct the transformations of the generators under toric duality. As mentioned in Appendix E, only fermionic nodes can be dualized. If the node F is dualized, then we just need to add an adjoint loop to $F \pm 1$ if $|F \pm 1| = 0$ or remove the existing adjoint loop on $F \pm 1$ if $|F \pm 1| = 1$. As a result,

$$\varsigma'_a = \begin{cases} -\varsigma_a, & a = F, F+1 \\ \varsigma_a, & \text{otherwise} \end{cases}, \tag{5.9.38}$$

where the primed notation stands for the one after performing the duality. Therefore, we have

$$A'_{ab} = \begin{cases} -A_{ab}, & (a,b) = (F \pm 1, F), (F, F \pm 1) \\ A_{aa} + 2A_{aF}, & a = b = F \pm 1 \\ A_{ab}, & \text{otherwise} \end{cases} \tag{5.9.39}$$

and

$$M'_{ab} = \begin{cases} -M_{ab}, & a = F-1, F, b = a+1 \\ -M_{ab}, & a = F, F+1, b = a-1 \\ M_{ab}, & \text{otherwise} \end{cases}. \tag{5.9.40}$$

Analogous to the rational case, the ke and kf commutation relations can be used to express higher e, f using lower modes[29]. The higher modes of k can in turn be obtained using the ef relations. In fact, the relations involving higher modes can also be derived from those with lower modes. Therefore, the toroidal BPS algebras for non-chiral quivers are finitely presented with the relations involving e_0, $e_{\pm 1}$, f_0, $f_{\pm 1}$, k_0, $k_{\pm 1}$ (or equivalently, $\psi_{\pm,0}$, $\psi_{\pm,1}$). Hence, it suffices to find the transformations for these modes.

We would like to mimic the isomorphisms for the rational case in discussed above. As all but three of the nodes are unaffected, we would expect the modes to be invariant for $a \neq F, F \pm 1$. Therefore, from their relations, we have

$$C' = C. \tag{5.9.41}$$

Now, let us first consider the zero modes. For $a = F$, the k'_0 modes should be determined only by k_0 themselves, possibly with changes of minus signs (such as multiplication by -1), while the e_0 and f_0 modes should get swapped. In the rational case, the ψ'_0 mode is a sum of $\psi_0^{(a)}$ and $\psi_0^{(F)}$ for $a = F \pm 1$. Here, our ansatz for ψ_0 would still be a combination of $\psi_0^{(a)}$ and $\psi_0^{(F)}$, but we expect it to be a multiplication instead of addition as we are dealing with the trigonometric case (and hence addition for k_0). On the other hand, for $e_0'^{(a)}$, the ansatz would be a linear combination of $e_0^{(a)} e_0^{(F)}$ and $e_0^{(F)} e_0^{(a)}$ (and likewise for $f_0'^{(a)}$).

By computing the supercommutators $[x, y\}$ with

$$x = e_0^{(F)} e_0^{(a)}, e_0^{(a)} e_0^{(F)} \quad \text{and} \quad y = f_0^{(a)} f_0^{(F)}, f_0^{(F)} f_0^{(a)}, \tag{5.9.42}$$

we find that for $a = F \pm 1$,

$$\begin{aligned} \psi'^{(a)}_{\pm,0} &= \psi^{(a)}_{\pm,0} \psi^{(F)}_{\pm,0}, \quad k'^{(a)}_0 = k^{(a)}_0 + k^{(F)}_0, \\ e'^{(a)}_0 &= e^{(F)}_0 e^{(a)}_0 - (-1)^{|a|} H_1^{A_{aF}} e^{(a)}_0 e^{(F)}_0, \\ f'^{(a)}_0 &= \frac{1}{H_1^{A_{aF}} - H_1^{-A_{aF}}} \left(f^{(a)}_0 f^{(F)}_0 - (-1)^{|a|} H_1^{-A_{aF}} f^{(F)}_0 f^{(a)}_0 \right) \end{aligned} \tag{5.9.43}$$

would verify the corresponding ef relation. Likewise, checking the ef relation for $a = F$, we have

$$\psi'^{(F)}_{\pm,0} = \psi^{(F)}_{\mp,0}, \quad k'^{(F)}_0 = -k^{(F)}_0, \tag{5.9.44}$$

---

[29]Here, by higher (resp. lower) modes, we mean the modes with larger (resp. smaller) absolute values $|n|$.

and $e_0'^{(F)} = f_0^{(F)}$, $f_0'^{(F)} = -e_0^{(F)}$. However, to be compatible with the ee and ff relations that contain modes with $n = 0, \pm 1$, we need to multiply them by some extra factors:

$$e_0'^{(F)} = \psi_{+,0}^{(F)} f_0^{(F)} = H_1^{-k_0^{(F)}} f_0^{(F)}, \quad f_0'^{(F)} = -\psi_{-,0}^{(F)} e_0^{(F)} = -H_1^{k_0^{(F)}} e_0^{(F)}. \tag{5.9.45}$$

Notice that they would still recover the transformations of the Chevalley generators under odd reflections in the limit $\beta \to 0$. One may check that these transformations are consistent with all the other relations involving zero modes.

Next, let us consider the modes with $n = \pm 1$. By considering the commutator of $k_1'^{(b \neq F)}$ and $e_0'^{(a)}$ with $b = a \pm 1$ (which is always possible since there are at least four nodes in the quiver), we find that for $a = F \pm 1$,

$$e_1'^{(a)} = e_0^{(F)} e_1^{(a)} - (-1)^{|a|} H_1^{A_{aF}} e_1^{(a)} e_0^{(F)}. \tag{5.9.46}$$

Likewise,

$$f_1'^{(a)} = \frac{1}{H_1^{A_{aF}} - H_1^{-A_{aF}}} \left(f_1^{(a)} f_0^{(F)} - (-1)^{|a|} H_1^{-A_{aF}} f_0^{(F)} f_1^{(a)} \right). \tag{5.9.47}$$

Again, computing $[x, y\}$ with

$$x = e_0^{(F)} e_1^{(a)}, e_1^{(a)} e_0^{(F)} \text{ and } y = f_1^{(a)} f_0^{(F)}, f_0^{(F)} f_1^{(a)}, \tag{5.9.48}$$

we find that

$$\psi_{+,1}'^{(a)} = \psi_{+,0}^{(F)} \psi_{+,1}^{(a)} - C^{1/2} H_2^{-M_{aF}} \left(H_1^{A_{aF}} f_1^{(F)} e_0^{(F)} + H_1^{-A_{aF}} e_0^{(F)} f_1^{(F)} \right) \psi_{+,0}^{(a)}, \tag{5.9.49}$$

$$\psi_{-,1}'^{(a)} = \psi_{-,0}^{(F)} \psi_{-,1}^{(a)} - C^{-1/2} H_2^{M_{aF}} \left(H_1^{A_{aF}} e_{-1}^{(F)} f_0^{(F)} + H_1^{-A_{aF}} f_0^{(F)} e_{-1}^{(F)} \right) \psi_{-,0}^{(a)}. \tag{5.9.50}$$

In terms of the Heisenberg modes, we have

$$k_1'^{(a)} = k_1^{(a)} - C^{1/2} H_2^{-M_{aF}} \left(H_1^{A_{aF}} f_1^{(F)} e_0^{(F)} + H_1^{-A_{aF}} e_0^{(F)} f_1^{(F)} \right) H_1^{k_0^{(F)}}, \tag{5.9.51}$$

$$k_{-1}'^{(a)} = k_{-1}^{(a)} - C^{-1/2} H_2^{M_{aF}} \left(H_1^{A_{aF}} e_{-1}^{(F)} f_0^{(F)} + H_1^{-A_{aF}} f_0^{(F)} e_{-1}^{(F)} \right) H_1^{-k_0^{(F)}}. \tag{5.9.52}$$

By considering the commutation relations of $k_1'^{(F \pm 1)}$ and $e_0'^{(F)}$, we find that

$$e_1'^{(F)} = C H_2^{-2M_{aF}} H_1^{k_0^{(F)}} f_1^{(F)}, \tag{5.9.53}$$

where a can either be $F + 1$ or $F - 1$ as M_{aF} would be the same. Likewise,

$$f_1'^{(F)} = H_2^{-2M_{aF}} \left(-C^{-1} e_1^{(F)} + C^{-1/2} k_1^{(F)} e_0^{(F)} \right) H_1^{k_0^{(F)}}, \tag{5.9.54}$$

$$e_{-1}'^{(F)} = H_2^{2M_{aF}} \left(C f_{-1}^{(F)} - C^{1/2} k_{-1}^{(F)} f_0^{(F)} \right) H_1^{-k_0^{(F)}}, \tag{5.9.55}$$

$$f_{-1}'^{(F)} = -C^{-1} H_2^{2M_{aF}} H_1^{-k_0^{(F)}} e_{-1}^{(F)}. \tag{5.9.56}$$

Using the ef relations, we get

$$\psi_{\pm,1}'^{(F)} = -H_2^{\mp 2M_{aF}} \left(\psi_{\mp,0}^{(F)} \right)^2 \psi_{\pm,1}^{(F)}, \quad k_{\pm 1}'^{(F)} = -H_2^{\mp 2M_{aF}} k_{\pm 1}^{(F)}. \tag{5.9.57}$$

One may check that these transformations are consistent with all the other relations.

From the above discussions, we may also derive the transformations in terms of currents. By applying the $k_{\pm 1}$ modes successively, it is not hard to see that

$$e'^{(a)}(U) = e_0^{(F)} e^{(a)}(U) - (-1)^{|a|} H_1^{A_{aF}} e^{(a)}(U) e_0^{(F)}, \tag{5.9.58}$$

$$f'^{(a)}(U) = \frac{1}{H_1^{A_{aF}} - H_1^{-A_{aF}}} \left(f^{(a)}(U) f_0^{(F)} - (-1)^{|a|} H_1^{-A_{aF}} f_0^{(F)} f^{(a)}(U) \right) \tag{5.9.59}$$

for $a = F \pm 1$. Then by considering their supercommutator, we find that each term contains some formal delta function with other terms being cancelled. This yields

$$\begin{aligned} \psi_\pm'^{(a)}(U) = & e_0^{(F)} \psi_\pm^{(a)}(U) f_0^{(F)} - (-1)^{|a|} H_1^{A_{aF}} e_0^{(F)} f_0^{(F)} \psi_\pm^{(a)}(U) \\ & - H_1^{-A_{aF}} \psi_\pm^{(a)}(U) e_0^{(F)} f_0^{(F)} - f_0^{(F)} \psi_\pm^{(a)}(U) e_0^{(F)}. \end{aligned} \tag{5.9.60}$$

It is less straightforward to write down the currents for F. Nevertheless, we can write some conjectural expressions by computing a few more higher modes and then verify them using the current relations. The perturbative calculations show that

$$e_0'^{(F)}(U) = f_{>0}^{(F)} \left(C^{-1} U \right) \overline{\psi}_+^{(F)} \left(C^{-1/2} H_2^{2M_{aF}} U \right) + f_{\leq 0}^{(F)} (CU) \overline{\psi}_-^{(F)} \left(C^{1/2} H_2^{2M_{aF}} U \right), \tag{5.9.61}$$

$$f_0'^{(F)}(U) = -e_{\geq 0}^{(F)} (CU) \overline{\psi}_+^{(F)} \left(C^{1/2} H_2^{2M_{aF}} U \right) - e_{<0}^{(F)} \left(C^{-1} U \right) \overline{\psi}_-^{(F)} \left(C^{-1/2} H_2^{2M_{aF}} U \right), \tag{5.9.62}$$

where

$$\begin{aligned} f_{>0}^{(F)}(U) = \sum_{n>0} f_n^{(F)} U^{-n}, \quad f_{\leq 0}^{(F)}(U) = \sum_{n\leq 0} f_n^{(F)} U^{-n}, \\ e_{\geq 0}^{(F)}(U) = \sum_{n\geq 0} e_n^{(F)} U^{-n}, \quad e_{<0}^{(F)}(U) = \sum_{n<0} e_n^{(F)} U^{-n}, \end{aligned} \tag{5.9.63}$$

and

$$\begin{aligned} \overline{\psi}_+^{(F)}(U) = \left(\psi_{-,0}^{(F)} \right)^2 \left(\psi_{+,0}^{(F)} - \frac{\psi_{+,1}^{(F)}}{U} - \frac{\psi_{+,2}^{(F)} - \left(\psi_{+,1}^{(F)} \right)^2 \psi_{-,0}^{(F)}}{U^2} \right. \\ \left. - \frac{\psi_{+,3}^{(F)} + \left(\psi_{+,1}^{(F)} \right)^3 \left(\psi_{-,0}^{(F)} \right)^2}{U^3} - \cdots \right), \end{aligned} \tag{5.9.64}$$

$$\begin{aligned} \overline{\psi}_-^{(F)}(U) = \left(\psi_{+,0}^{(F)} \right)^2 \left(\psi_{-,0}^{(F)} - \psi_{-,1}^{(F)} U - \left(\psi_{-,2}^{(F)} - \left(\psi_{-,1}^{(F)} \right)^2 \psi_{+,0}^{(F)} \right) U^2 \right. \\ \left. - \left(\psi_{-,3}^{(F)} + \left(\psi_{-,1}^{(F)} \right)^3 \left(\psi_{+,0}^{(F)} \right)^2 \right) U^3 - \cdots \right). \end{aligned} \tag{5.9.65}$$

In fact, we find that the perturbative expressions here coincide with the "inverse currents", that is,

$$\overline{\psi}_\pm^{(F)}(U) = \psi_\pm^{(F)}(U)^{-1}. \tag{5.9.66}$$

Then we have

$$\psi_\pm'^{(F)}(U) = \psi_\pm^{(F)} \left(H_2^{2M_{aF}} U \right)^{-1}. \tag{5.9.67}$$

Indeed, one may verify these expressions using the current relations. It is also worth noting that

$$k_n'^{(F)} = -H_2^{2nM_{aF}} k_n^{(F)}. \tag{5.9.68}$$

5.9.3 Higgsing

Recall that the toric quiver gauge theories have nice features under the Higgs-Kibble mechanism. It is then natural to wonder if their BPS algebras are also connected via blowing up/down the

singularities, or more precisely, if there is a subalgebra structure for a higgsed theory from a parent theory.

As the higgsing process always merges the two neighbouring nodes, say a and $a+1$, in the quiver for any toric CY without compact divisors, we expect the generators associated with other nodes (and the central element C) to be invariant. Of course, there is a relabelling for $b > a+1$ as the number of nodes is reduced by one after higgsing.

For $x'^{(a)}$ $(x = e, f, \psi, k)$, where the primed letters indicate the generators for the higgsed theory, it should be a combination of $x^{(a)}$ and $x^{(a+1)}$. As discussed in Appendix E, the parity should satisfy $\left|x'^{(a)}\right| = \left|x^{(a)}\right| + \left|x^{(a+1)}\right|$. Therefore, for the zero modes, a natural candidate would be a combination of $e_0^{(a)} e_0^{(a+1)}$ and $e_0^{(a+1)} e_0^{(a)}$ (and likewise for f). Similar to the construction for toric duality, we find that

$$e_0'^{(a)} = e_0^{(a+1)} e_0^{(a)} - (-1)^{|a||a+1|} H_1^{A_{a,a+1}} e_0^{(a)} e_0^{(a+1)}, \tag{5.9.69}$$

$$f_0'^{(a)} = \frac{1}{H_1^{A_{a,a+1}} - H_1^{-A_{a,a+1}}} \left(f_0^{(a)} f_0^{(a+1)} - (-1)^{|a||a+1|} H_1^{-A_{a,a+1}} f_0^{(a+1)} f_0^{(a)} \right), \tag{5.9.70}$$

$$\psi_{\pm,0}'^{(a)} = \psi_{\pm,0}^{(a)} \psi_{\pm,0}^{(a+1)}, \quad k_0'^{(a)} = k_0^{(a)} + k_0^{(a+1)} \tag{5.9.71}$$

would give the expected subalgebra structure for the zero modes. This is precisely the transformation for $a = F \pm 1$ in the above discussions of toric duality with F replaced by $a+1$. In fact, in the rational limit $\beta \to 0$, this gives the surjection map of the Chevalley generators of the corresponding affine Lie superalgebras.

However, when we use $k_{\pm 1}'^{(a-1)} = k_{\pm 1}^{(a)}$ or $k_{\pm 1}'^{(a+1)} = k_{\pm 1}^{(a+2)}$ to get the higher modes from $e_0'^{(a)}$ (resp. $f_0'^{(a)}$), the expressions are not symmetric in $e^{(a)}$ and $e^{(a+1)}$ (resp. $f^{(a)}$ and $f^{(a+1)}$) any more. Indeed, for instance, $\left[k_1^{(a-1)}, e_0'^{(a)} \right]$ yields

$$e_1'^{(a)} = e_0^{(a+1)} e_1^{(a)} - (-1)^{|a||a+1|} H_1^{A_{a,a+1}} e_1^{(a)} e_0^{(a+1)} \tag{5.9.72}$$

while $\left[k_1^{(a+2)}, e_0'^{(a)} \right]$ leads to

$$e_1'^{(a)} = e_1^{(a+1)} e_0^{(a)} - (-1)^{|a||a+1|} H_1^{A_{a,a+1}} e_0^{(a)} e_1^{(a+1)}. \tag{5.9.73}$$

They are not equal to each other as can be seen from the ee relation. Explicitly,

$$e_1^{(a+1)} e_0^{(a)} - (-1)^{|a||a+1|} H_1^{A_{a,a+1}} e_0^{(a)} e_1^{(a+1)} = H_2^{M_{a,a+1}} \left(e_0^{(a+1)} e_1^{(a)} - (-1)^{|a||a+1|} H_1^{A_{a,a+1}} e_1^{(a)} e_0^{(a+1)} \right). \tag{5.9.74}$$

Due to the non-trivial factor $H_2^{M_{a,a+1}}$, this transformation does not give the subalgebra structure. Nevertheless, when $H_2 = 1$, the quiver BPS algebras reduce to a one-parameter algebra, and the above two expressions for $e_1'^{(a)}$ would coincide.

Therefore, at least when $h_2 = 0$, for non-chiral quivers[30], the toroidal BPS algebra contains the ones for the higgsed theories as its subalgebras. The surjection for the generators associated with a and $a+1$ are the same as the transformations for $a = F \pm 1$ under toric duality with F replaced by $a \mp 1$ [31]. Of course, $a+1$ (as well as a) can be either bosonic or fermionic. This is also the case for the rational quiver Yangians, where the surjection map is most conveniently expressed in the J presentation. See (4.5) in [15] (with conventions therein). It is not clear whether higgsing would still lead to the subalgebra structure for generic h_2, and if so, what the surjection map would be. Physically, the two parameters of the algebra are related to the Ω-background that is used to resolve the singular target space of the supersymmetric quantum mechanics. In particular, the scalars in the vector multiplets would also have non-zero VEVs. Therefore, the algebra structure under higgsing could be closely related to the localizations of the Higgs and Coulomb branches [197].

---

[30] For $\mathbb{C}^3/(\mathbb{Z}_2 \times \mathbb{Z}_2)$ which can be higgsed to the suspended pinch point, this should also be true. The discussions here do not cover $\mathbb{C}^3$, $\mathbb{C} \times \mathbb{C}^2/\mathbb{Z}_2$ and the conifold although we still expect this to hold.

[31] As a result, this gives two transformations, but they should essentially be the same up to a normalization factor.

5.10 Elliptic Algebras for Non-Chiral Quivers

Now, let us have a discussion on the elliptic algebras for non-chiral quivers. Unlike the rational and toroidal algebras for non-chiral quivers, it is more difficult to work with modes. This is due to the existence of q-Pochhammer symbols in the elliptic case.

Given a generalized conifold $xy = z^M w^N$ with $M + N \geq 3$, the elliptic quiver algebra $\texttt{E}$ has the relations

$$\psi_\pm^{(a)}(U)\psi_\pm^{(b)}(V) = \psi_\pm^{(b)}(V)\psi_\pm^{(a)}(U), \tag{5.10.1}$$

$$\psi_\pm^{(a)}(U)\psi_\mp^{(b)}(V) = \frac{\left(UCV^{-1}H_1^{A_{ab}}H_2^{M_{ab}};q\right)_\infty \left(qU^{-1}C^{-1}VH_1^{-A_{ab}}H_2^{-M_{ab}};q\right)_\infty}{\left(U^{-1}C^{-1}VH_1^{A_{ab}}H_2^{-M_{ab}};q\right)_\infty \left(qUCV^{-1}H_1^{-A_{ab}}H_2^{M_{ab}};q\right)_\infty}$$
$$\frac{\left(U^{-1}CVH_1^{A_{ab}}H_2^{-M_{ab}};q\right)_\infty \left(qUC^{-1}V^{-1}H_1^{-A_{ab}}H_2^{M_{ab}};q\right)_\infty}{\left(UC^{-1}V^{-1}H_1^{A_{ab}}H_2^{M_{ab}};q\right)_\infty \left(qU^{-1}CVH_1^{-A_{ab}}H_2^{-M_{ab}};q\right)_\infty}\psi_\mp^{(b)}(V)\psi_\pm^{(a)}(U) \tag{5.10.2}$$

$$\psi_\pm^{(a)}(U)e^{(b)}(V) = H_1^{A_{ab}}\frac{\left(U^{-1}C^{\mp\frac{1}{2}}VH_1^{-A_{ab}}H_2^{-M_{ab}};q\right)_\infty \left(qUC^{\pm\frac{1}{2}}V^{-1}H_1^{A_{ab}}H_2^{M_{ab}};q\right)_\infty}{\left(U^{-1}C^{\mp\frac{1}{2}}VH_1^{A_{ab}}H_2^{-M_{ab}};q\right)_\infty \left(qUC^{\pm\frac{1}{2}}V^{-1}H_1^{-A_{ab}}H_2^{M_{ab}};q\right)_\infty}e^{(b)}(V)\psi_\pm^{(a)}(U) \tag{5.10.3}$$

$$\psi_\pm^{(a)}(U)f^{(b)}(V) = H_1^{-A_{ab}}\frac{\left(U^{-1}C^{\pm\frac{1}{2}}VH_1^{A_{ab}}H_2^{-M_{ab}};q\right)_\infty \left(qUC^{\mp\frac{1}{2}}V^{-1}H_1^{-A_{ab}}H_2^{M_{ab}};q\right)_\infty}{\left(U^{-1}C^{\pm\frac{1}{2}}VH_1^{-A_{ab}}H_2^{-M_{ab}};q\right)_\infty \left(qUC^{\mp\frac{1}{2}}V^{-1}H_1^{A_{ab}}H_2^{M_{ab}};q\right)_\infty}f^{(b)}(V)\psi_\pm^{(a)}(U) \tag{5.10.4}$$

$$e^{(a)}(U)e^{(b)}(V) = (-1)^{|a||b|}H_1^{A_{ab}}\frac{\left(U^{-1}VH_1^{-A_{ab}}H_2^{-M_{ab}};q\right)_\infty \left(qUV^{-1}H_1^{A_{ab}}H_2^{M_{ab}};q\right)_\infty}{\left(U^{-1}VH_1^{A_{ab}}H_2^{-M_{ab}};q\right)_\infty \left(qUV^{-1}H_1^{-A_{ab}}H_2^{M_{ab}};q\right)_\infty}e^{(b)}(V)e^{(a)}(U) \tag{5.10.5}$$

$$f^{(a)}(U)f^{(b)}(V) = (-1)^{|a||b|}H_1^{-A_{ab}}\frac{\left(U^{-1}VH_1^{A_{ab}}H_2^{-M_{ab}};q\right)_\infty \left(qUV^{-1}H_1^{-A_{ab}}H_2^{M_{ab}};q\right)_\infty}{\left(U^{-1}VH_1^{-A_{ab}}H_2^{-M_{ab}};q\right)_\infty \left(qUV^{-1}H_1^{A_{ab}}H_2^{M_{ab}};q\right)_\infty}f^{(b)}(V)f^{(a)}(U) \tag{5.10.6}$$

$$\left[e^{(a)}(U),f^{(b)}(V)\right\} = -\delta_{ab}\left(\delta\left(UV^{-1}C^{-1}\right)\psi_+^{(a)}\left(UC^{-1/2}\right) - \delta\left(UV^{-1}C\right)\psi_-^{(a)}\left(VC^{-1/2}\right)\right). \tag{5.10.7}$$

Similar to the toroidal case, for any fermionic node F, we have $\psi_\pm^{(F)}(U)e^{(F)}(V) = e^{(F)}(V)\psi_\pm^{(F)}(U)$, $e^{(F)}(U)e^{(F)}(V) = -e^{(F)}(V)e^{(F)}(U)$ etc. Moreover, when the central charge is trivial, that is, $C = 1$, $\psi_+^{(a)}(U)$ commutes with $\psi_-^{(b)}(V)$.

To write down the Serre relations, let us first recall that both the rational and the toroidal algebras have their versions of the brackets. Therefore, we would also like to use an "elliptic bracket" to write the Serre relations for the elliptic cases. Let us introduce the operators $\chi_a(u)$ and $\xi_a(u)$ that commute with all e, f, $\psi_\pm$ generators in the elliptic algebras. They have the following correlators:

$$e^{\langle\chi_a(u)\chi_b(v)\rangle} = \frac{\left(qH_1^{A_{ab}}H_2^{-M_{ab}}U^{-1}V;q\right)_\infty}{\left(qH_1^{-A_{ab}}H_2^{-M_{ab}}U^{-1}V;q\right)_\infty}, \tag{5.10.8}$$

$$e^{\langle \xi_a(u)\xi_b(v)\rangle} = \frac{\left(qH_1^{-A_{ab}}H_2^{-M_{ab}}U^{-1}V;q\right)_\infty}{\left(qH_1^{A_{ab}}H_2^{-M_{ab}}U^{-1}V;q\right)_\infty}, \tag{5.10.9}$$

$$e^{\langle \chi_a(u)\xi_b(v)\rangle} = 1. \tag{5.10.10}$$

Then using the correlators of the "dressed" operators

$$E^{(a)}(u) = e^{\chi_a(u)}e^{(a)}(u), \quad F^{(a)}(u) = e^{\xi_a(u)}f^{(a)}(u), \quad \Psi_\pm^{(a)}(u) = e^{\chi_a(u\pm c/2)}e^{\xi_a(u\mp c/2)}\psi_\pm^{(a)}(u), \tag{5.10.11}$$

the relations of the elliptic algebras can be written in the same forms as those of the toroidal algebras. For instance, the *ee* relations of the elliptic algebras now become

$$\left(H_2^{M_{ab}}U - H_1^{A_{ab}}V\right)\left\langle E^{(a)}(u)E^{(b)}(v)\right\rangle = (-1)^{|a||b|}\left(H_1^{A_{ab}}H_2^{M_{ab}}U - V\right)\left\langle E^{(b)}(v)E^{(a)}(u)\right\rangle. \tag{5.10.12}$$

Therefore, the Serre relations of the elliptic algebras can simply be obtained by taking the ones of the toroidal algebras. Then we replace the toroidal generators with the dressed elliptic generators and take the correlators of the whole expressions. For brevity, we shall write them using the "elliptic brackets" as

$$\underset{u_1,u_2}{\mathrm{Sym}}\left[e^{(a)}(u_1), \left[e^{(a)}(u_2), e^{(a\pm1)}(v)\right\}_\chi\right\}_\chi = 0 \qquad (|a|=0), \tag{5.10.13}$$

$$\underset{u_1,u_2}{\mathrm{Sym}}\left[e^{(a)}(u_1), \left[e^{(a+1)}(v_1)\left[e^{(a)}(u_2), e^{(a-1)}(v_2)\right\}_\chi\right\}_\chi\right\}_\chi = 0 \qquad (|a|=1), \tag{5.10.14}$$

$$\underset{u_1,u_2}{\mathrm{Sym}}\left[f^{(a)}(u_1), \left[f^{(a)}(u_2), f^{(a\pm1)}(v)\right\}_\xi\right\}_\xi = 0 \qquad (|a|=0), \tag{5.10.15}$$

$$\underset{u_1,u_2}{\mathrm{Sym}}\left[f^{(a)}(u_1), \left[f^{(a+1)}(v_1)\left[f^{(a)}(u_2), f^{(a-1)}(v_2)\right\}_\xi\right\}_\xi\right\}_\xi = 0 \qquad (|a|=1). \tag{5.10.16}$$

5.10.1 More on Mode Expansions

Although we would like to work with the currents directly, it would still be helpful to have a look at their mode expansions. There are infinitely many groups of relations as α can be any non-negative integer, but there are finitely many terms in each relation at each order. At order q^0, for instance, the *ee* relations read

$$e_{m+1,0}^{(a)}e_{n,0}^{(b)} - H_1^{A_{ab}}H_2^{-M_{ab}}e_{m,0}^{(a)}e_{n+1,0}^{(b)} = (-1)^{|a||b|}\left(H_1^{A_{ab}}e_{n,0}^{(b)}e_{m+1,0}^{(a)} - H_2^{-M_{ab}}e_{n+1,0}^{(b)}e_{m,0}^{(a)}\right), \tag{5.10.17}$$

which coincide with the *ee* relations for the toroidal algebra. In fact, all the relations at q^0 are the same as those in the toroidal case. Therefore, the elliptic subalgebra $\mathtt{E}_0$ at order q^0 is isomorphic to the toroidal algebra $\mathtt{T}$. This is expected as the elliptic algebra $\mathtt{E}$ reduces to $\mathtt{T}$ in the limit $q \to 0$.

As another example, let us also write the ψe relations at order q^1 here:

$$\left(H_2^{M_{ab}}U - H_1^{A_{ab}}V\right)\left(\left(-H_1^{-A_{ab}}H_2^{M_{ab}}UV^{-1} - H_1^{A_{ab}}H_2^{-M_{ab}}VU^{-1}\right)\psi_{\pm,0}^{(a)}\left(C^{\mp1/2}U\right)e_0^{(b)}(V)\right.$$
$$\left.+\psi_{\pm,1}^{(a)}\left(C^{\mp1/2}U\right)e_0^{(b)}(V) + \psi_{\pm,0}^{(a)}\left(C^{\mp1/2}U\right)e_1^{(b)}(V)\right)$$
$$= \left(H_1^{A_{ab}}H_2^{M_{ab}}U - V\right)\left(\left(-H_1^{A_{ab}}H_2^{M_{ab}}UV^{-1} - H_1^{-A_{ab}}H_2^{-M_{ab}}VU^{-1}\right)\psi_{\pm,0}^{(a)}\left(C^{\mp1/2}U\right)e_0^{(b)}(V)\right.$$
$$\left.+\psi_{\pm,1}^{(a)}\left(C^{\mp1/2}U\right)e_0^{(b)}(V) + e_1^{(b)}(V)\psi_{\pm,0}^{(a)}\left(C^{\mp1/2}U\right)\right), \tag{5.10.18}$$

from which we can write the corresponding mode relations. The other relations can be obtained in a similar manner. For relations at higher orders of q, there would be more terms with larger ranges of modes in the coefficients. In general, at order q^α, the $\psi_\pm \left(C^{\mp 1/2} U \right) e(V)$ relations read

$$
\left(H_2^{M_{ab}} U - H_1^{A_{ab}} V \right) \sum_{\gamma=0}^{\alpha} \sum_{\substack{\alpha_1, \alpha_2 \\ \alpha_1 + \alpha_2 = \alpha - \gamma}} K_\gamma(A_{ab}) \psi_{\pm, \alpha_1}^{(a)} \left(C^{\mp 1/2} U \right) e_{\alpha_2}^{(b)}(V)
$$

$$
= \left(H_1^{A_{ab}} H_2^{M_{ab}} U - V \right) \sum_{\gamma=0}^{\alpha} \sum_{\substack{\alpha_1, \alpha_2 \\ \alpha_1 + \alpha_2 = \alpha - \gamma}} K_\gamma(-A_{ab}) e_{\alpha_2}^{(b)}(V) \psi_{\pm, \alpha_1}^{(a)} \left(C^{\mp 1/2} U \right)
$$

(5.10.19)

for some functions K_γ coming from the expansions of (the product of) the q-Pochhammer symbols. Here, we have suppressed the other indices and arguments in K_γ for brevity. In particular, $K_0 = 1$. The $e(U)e(V)$ relations have the same coefficients (with an extra sign factor $(-1)^{|a||b|}$) while for the $\psi_\pm \left(C^{\mp} U \right) f(V)$ and $f(U)f(V)$ relations, we simply have $A_{ab} \leftrightarrow -A_{ab}$ on both sides. We can then write the mode relations at each order of q from these current relations.

Heisenberg modes   Similar to the discussions on the toroidal algebras above, as well as some elliptic deformed algebras in [229], we may expand the $\psi_\pm$ modes as

$$
\psi_+^{(a)}(U) = H_1^{-k_0^{(a)}} \exp \left(\sum_{n \neq 0} k_n^{(a)} U^{-n} \right), \quad \psi_-^{(a)}(U) = H_1^{l_0^{(a)}} \exp \left(\sum_{n \neq 0} l_{-n}^{(a)} U^n \right).
$$

(5.10.20)

For convenience, we shall still refer to the k and l modes as Heisenberg modes. Notice that the sums are now over $\mathbb{Z} \backslash \{0\}$. Moreover,

$$
\psi_{+,n}^{(a)} = H_1^{-k_0^{(a)}} \left(\sum_{m=0}^{\infty} \frac{1}{m!} \sum_{\substack{r_i \neq 0 \\ r_1 + \cdots + r_m = n}} k_{r_1} k_{r_2} \ldots k_{r_m} \right),
$$

(5.10.21)

$$
\psi_{-,n}^{(a)} = H_1^{-l_0^{(a)}} \left(\sum_{m=0}^{\infty} \frac{1}{m!} \sum_{\substack{r_i \neq 0 \\ r_1 + \cdots + r_m = n}} l_{r_1} l_{r_2} \ldots l_{r_m} \right).
$$

(5.10.22)

In particular, $k_0^{(a)}$ and $l_0^{(a)}$ are not equal to $\psi_{\pm,0}^{(a)}$ (or $\psi_{\pm,0,0}^{(a)}$) here. Nevertheless, the Heisenberg modes may still play the role that raises or lowers the e, f modes. More explicitly,

$$
\left[k_r^{(a)}, k_s^{(b)} \right] = \left[l_r^{(a)}, l_s^{(b)} \right] = \left[k_0^{(a)}, l_s^{(b)} \right] = \left[k_r^{(a)}, l_0^{(b)} \right] = 0,
$$

(5.10.23)

$$
\left[k_{r \neq 0}^{(a)}, l_s^{(b)} \right] = \delta_{r+s,0} \frac{1}{r} \frac{1}{1-q^r} \left(C^{-r} - C^r \right) H_2^{-r M_{ab}} \left(H_1^{r A_{ab}} - q^r H_1^{-r A_{ab}} \right),
$$

(5.10.24)

$$
\left[k_0^{(a)}, e_n^{(b)} \right] = -A_{ab} e_n^{(b)}, \quad \left[k_0^{(a)}, f_n^{(b)} \right] = A_{ab} f_n^{(b)},
$$

(5.10.25)

$$
\left[l_0^{(a)}, e_n^{(b)} \right] = A_{ab} e_n^{(b)}, \quad \left[l_0^{(a)}, f_n^{(b)} \right] = -A_{ab} f_n^{(b)},
$$

(5.10.26)

$$
\left[k_{r \neq 0}^{(a)}, e_n^{(b)} \right] = \frac{1}{r} \frac{1}{1-q^r} C^{-r/2} H_2^{-r M_{ab}} \left(H_1^{r A_{ab}} - H_1^{-r A_{ab}} \right) e_{n+r}^{(b)},
$$

(5.10.27)

$$
\left[k_{r \neq 0}^{(a)}, f_n^{(b)} \right] = -\frac{1}{r} \frac{1}{1-q^r} C^{r/2} H_2^{-r M_{ab}} \left(H_1^{r A_{ab}} - H_1^{-r A_{ab}} \right) f_{n+r}^{(b)},
$$

(5.10.28)

$$
\left[l_{r \neq 0}^{(a)}, e_n^{(b)} \right] = \frac{1}{r} \frac{1}{1-q^r} C^{-r/2} H_2^{-r M_{ab}} \left(H_1^{r A_{ab}} - H_1^{-r A_{ab}} \right) e_{n-r}^{(b)},
$$

(5.10.29)

$$
\left[l_{r \neq 0}^{(a)}, f_n^{(b)} \right] = -\frac{1}{r} \frac{1}{1-q^r} C^{r/2} H_2^{-r M_{ab}} \left(H_1^{r A_{ab}} - H_1^{-r A_{ab}} \right) f_{n-r}^{(b)}.
$$

(5.10.30)

However, the ef relations in terms of k and l would be quite different from those of the toroidal cases. This is one of the difficulties when discussing toric duality for elliptic algebras.

5.10.2 Toric Duality

Let us have a brief discussion on toric duality for the elliptic cases. In fact, as discussed above, the dressed currents $E^{(a)}(u)$, $F^{(a)}(u)$ and $\Psi_\pm^{(a)}(u)$ introduced therein have the same relations as those of the toroidal cases. Therefore, the previous transformations should also apply to the elliptic cases using the dressed currents (with products replaced by correlators or normal orderings). Moreover, by comparing these relations with the ones using the "bare" generators at each order q^α, we may write the correlators $\langle XY \rangle_\alpha$ in the expansion of q. For instance, from (5.10.19), we have

$$\left\langle \Psi_\pm^{(a)} \left(C^{\mp 1/2} U \right) E^{(b)}(V) \right\rangle_\alpha = \sum_{\gamma=0}^{\alpha} \sum_{\substack{\alpha_1,\alpha_2 \\ \alpha_1+\alpha_2=\alpha-\gamma}} K_\gamma(A_{ab})\psi_{\pm,\alpha_1}^{(a)} \left(C^{\mp 1/2} U \right) e_{\alpha_2}^{(b)}(V), \tag{5.10.31}$$

$$\left\langle E^{(b)}(V) \Psi_\pm^{(a)} \left(C^{\mp 1/2} U \right) \right\rangle_\alpha = \sum_{\gamma=0}^{\alpha} \sum_{\substack{\alpha_1,\alpha_2 \\ \alpha_1+\alpha_2=\alpha-\gamma}} K_\gamma(-A_{ab})e_{\alpha_2}^{(b)}(V)\psi_{\pm,\alpha_1}^{(a)} \left(C^{\mp 1/2} U \right). \tag{5.10.32}$$

Nevertheless, let us still take a look at the original bare generators e, f, $\psi_\pm$ directly in the followings for completeness.

Suppose that the node F is dualized. Then the currents associated to $a \neq F, F \pm 1$ (and hence C) should remain invariant. For $a = F \pm 1$, we expect the currents to have a combination of a and F currents/modes similar to the ones in the toroidal cases. Let us recall that for the toroidal algebras, we have

$$e'^{(a)}(U) = \left[e_0^{(F)}, e^{(a)}(U) \right\}_{H_1^{A_{aF}}}, \tag{5.10.33}$$

where the deformed bracket is given by $[x, y\}_{\mathfrak{q}} = xy - (-1)^{|x||y|}\mathfrak{q}yx$. Likewise, for the rational algebras, we have

$$e'^{(a)}(U) = \left[e_0^{(F)}, e^{(a)}(U) \right\}. \tag{5.10.34}$$

As a result, each transformation is determined by its corresponding version of the bracket. Moreover, these are preciously the brackets that appear in their Serre relations. Therefore, we propose that the elliptic version of the bracket is used here:

$$e'^{(a)}(U) = \left[e^{(F)}(V), e^{(a)}(U) \right\}_\chi \Big|_{V^0}, \tag{5.10.35}$$

where χ represents the elliptic deformed bracket as mentioned before and V^0 indicates that we only take the terms of order V^0. More explicitly, using the q-binomial theorem, we have

$$e'^{(a)}(U) = \sum_{n=0}^{\infty} \frac{\left(H_1^{2A_{aF}} ; q \right)_n}{(q;q)_n} \left(qH_1^{-A_{aF}} H_2^{M_{aF}} U \right)^n \tag{5.10.36}$$
$$\left(e_{-n}^{(F)} e^{(a)}(U) - (-1)^{|a|} H_1^{A_{aF}} H_2^{-2nM_{aF}} U^{-2n} e^{(a)}(U) e_n^{(F)} \right).$$

Likewise,

$$f'^{(a)}(U) = \sum_{n=0}^{\infty} \frac{\left(H_1^{-2A_{aF}} ; q \right)_n}{(q;q)_n} \frac{\left(qH_1^{A_{aF}} H_2^{-M_{aF}} U^{-1} \right)^n}{H_1^{A_{aF}} - H_1^{-A_{aF}}} \tag{5.10.37}$$
$$\left(f^{(a)}(U) f_n^{(F)} - (-1)^{|a|} H_1^{-A_{aF}} H_2^{2nM_{aF}} U^{2n} f_{-n}^{(F)} f^{(a)}(U) \right).$$

For the node F, we expect that $\psi'_\pm$ are still given by the inverse currents, that is,

$$\psi_\pm'^{(F)}(U) = \psi_\pm^{(F)} \left(H_2^{2M_{aF}} U \right)^{-1}. \tag{5.10.38}$$

Analogously, it is natural to conjecture that $e'^{(F)}$ and $f'^{(F)}$ would have the same forms as in the toroidal algebras. In other words $e' = f_{>0}\psi_+^{-1} + f_{\leq 0}\psi_-^{-1}$, $f' = -e_{\geq 0}\psi_+^{-1} - e_{<0}\psi_-^{-1}$, where we have omitted the different arguments in different factors for brevity.

Indeed, the inverse currents are consistent with the relations under toric duality. For instance, the $e'^{(a)}e'^{(F)}$ relation contains

$$
e^{(a)}(U)\mathcal{E}^{(F)}\mathcal{F}_\pm^{(F)}\psi_\pm^{(F)}\left(C^{\mp 1/2}H_2^{2M_{aF}}V\right)^{-1}
$$

$$
=(-1)^{|a|}U^{-1}VH_2^{M_{aF}}\frac{\left(UV^{-1}H_1^{-A_{aF}}H_2^{-M_{aF}};q\right)_\infty}{\left(U^{-1}VH_1^{-A_{aF}}H_2^{M_{aF}};q\right)_\infty}\frac{\left(qU^{-1}VH_1^{A_{aF}}H_2^{M_{aF}};q\right)_\infty}{\left(qUV^{-1}H_1^{A_{aF}}H_2^{-M_{aF}};q\right)_\infty} \tag{5.10.39}
$$

$$
\mathcal{F}_\pm^{(F)}\psi_\pm^{(F)}\left(C^{\mp 1/2}H_2^{2M_{aF}}V\right)^{-1}e^{(a)}(U)\mathcal{E}^{(F)}+\dots,
$$

where $\mathcal{E}^{(F)}$ (resp. $\mathcal{F}_\pm^{(F)}$) sketchily indicates the factors containing only $e^{(F)}$ (resp. $f^{(F)}$) modes. The ellipsis stands for the extra terms coming from exchanging these factors which should be cancelled in the whole expression. Recall that $A'_{aF} = -A_{aF}$ and $M'_{aF} = -M_{aF}$. As we can see, this recovers the correct coefficient for the $e'^{(a)}e'^{(F)}$ relation.

Higgsing Similar to the rational and toroidal cases, the surjection (if it exists) induced from higgsing should leave the central element C and all but two (say, a and $a+1$) currents invariant (with a possible relabelling of nodes). However, due to the complication at higher orders of q, it is more difficult to write the currents associated to a' in terms of those for a and $a+1$. Nevertheless, we may still conjecture that higgsing would also give subalgebras in the elliptic case, at least in certain one-parameter degeneracy.

5.11 Heisenberg Modes for Chiral Cases

The transformations of the algebras for chiral quivers under toric duality are more difficult to find since there does not seem to have the underlying affine Lie algebras and their relations can vary case by case. A preliminary discussion can be found in [16, §4.2]. Here, we shall just make some comments on the mode expansions. Similar to the discussions for non-chiral quivers, we may also take the mode expansions as

$$
\psi_+^{(a)}(U) = \exp\left(\sum_{n\in\mathbb{Z}}k_n^{(a)}U^{-n}\right), \quad \psi_-^{(a)}(U) = \exp\left(\sum_{n\in\mathbb{Z}}l_{-n}^{(a)}U^{n}\right). \tag{5.11.1}
$$

We shall still refer to k and l as Heisenberg modes. Notice that the conventions when writing k_0 and l_0 are slightly different from before, and the sums are over $\mathbb{Z}$.

Consider two nodes a and b in any chiral quiver. Suppose that there are $|a \to b| = r$ and $|b \to a| = s$. Then

$$
\left[k_0^{(a)}, l_0^{(b)}\right] = \log\left(C^{-r-s}\right) = -(r+s)\beta c, \tag{5.11.2}
$$

$$
\left[k_0^{(a)}, k_0^{(b)}\right] = -\left[l_0^{(a)}, l_0^{(b)}\right] = \log\left(C^{r-s}\right) = (r-s)\beta c, \tag{5.11.3}
$$

$$
\left[k_{m\neq 0}^{(a)}, k_n^{(b)}\right] = \left[l_{m\neq 0}^{(a)}, l_n^{(b)}\right] = \left[k_0^{(a)}, l_{n\neq 0}^{(b)}\right] = \left[k_{m\neq 0}^{(a)}, l_0^{(b)}\right] = 0. \tag{5.11.4}
$$

Moreover, we have

$$
\left[k_0^{(a)}, e^{(b)}(V)\right] = \left[l_0^{(a)}, e^{(b)}(V)\right] = \begin{cases} \log\left(\mathcal{H}_{ab}V^{-(r-s)}\right)e^{(b)}(V), & r > s \\ \log\left(-\mathcal{H}_{ab}V^{-(r-s)}\right)e^{(b)}(V), & r < s \;, \\ \log\left((-1)^r\mathcal{H}_{ab}\right)e^{(b)}(V), & r = s \end{cases} \tag{5.11.5}
$$

$$\left[k_0^{(a)}, f^{(b)}(V)\right] = \left[l_0^{(a)}, f^{(b)}(V)\right] = \begin{cases} -\log\left(\mathcal{H}_{ab}V^{-(r-s)}\right)f^{(b)}(V), & r > s \\ -\log\left(-\mathcal{H}_{ab}V^{-(r-s)}\right)f^{(b)}(V), & r < s \ , \\ -\log\left((-1)^r\mathcal{H}_{ab}\right)f^{(b)}(V), & r = s \end{cases} \tag{5.11.6}$$

where $\mathcal{H}_{ab} = \prod_{i=1}^{r} H_{ab,i}^{1/2} \prod_{j=1}^{s} H_{ba,j}^{1/2}$. It would be more useful to write them as

$$e^{\pm\frac{1}{r-s}k_0^{(a)}} e_n^{(b)} e^{\mp\frac{1}{r-s}k_0^{(a)}} = \text{sgn}(r,s) H_{ab}^{\pm\frac{1}{r-s}} e_{n\mp1}^{(b)} \quad (r \neq s), \tag{5.11.7}$$

$$e^{\pm\frac{1}{r-s}k_0^{(a)}} f_n^{(b)} e^{\mp\frac{1}{r-s}k_0^{(a)}} = \text{sgn}(r,s) H_{ab}^{\mp\frac{1}{r-s}} f_{n\pm1}^{(b)} \quad (r \neq s), \tag{5.11.8}$$

$$e^{k_0^{(a)}} e_n^{(b)} e^{-k_0^{(a)}} = \text{sgn}(r,s) \mathcal{H}_{ab} e_n^{(b)} \quad (r = s), \tag{5.11.9}$$

$$e^{k_0^{(a)}} f_n^{(b)} e^{-k_0^{(a)}} = \text{sgn}(r,s) \mathcal{H}_{ab} f_n^{(b)} \quad (r = s), \tag{5.11.10}$$

$$\tag{5.11.11}$$

and likewise for $l_0^{(a)}$, where we have defined

$$\text{sgn}(r,s) = \begin{cases} 1, & r > s \\ (-1)^r, & r = s \ . \\ -1, & r < s \end{cases} \tag{5.11.12}$$

The remaining relations would be different for the toroidal and the elliptic cases. For the toroidal algebras, we have

$$\left[k_m^{(a)}, e_n^{(b)}\right] = \frac{1}{m} C^{-m/2} \left(\sum_j H_{ba,j}^m - \sum_i H_{ab,i}^{-m}\right) e_{n+m}^{(b)} \quad (m > 0), \tag{5.11.13}$$

$$\left[k_m^{(a)}, f_n^{(b)}\right] = -\frac{1}{m} C^{m/2} \left(\sum_j H_{ba,j}^m - \sum_i H_{ab,i}^{-m}\right) f_{n+m}^{(b)} \quad (m > 0), \tag{5.11.14}$$

$$\left[l_{-m}^{(a)}, e_n^{(b)}\right] = \frac{1}{m} C^{m/2} \left(\sum_j H_{ba,j}^m - \sum_i H_{ab,i}^{-m}\right) e_{n+m}^{(b)} \quad (m > 0), \tag{5.11.15}$$

$$\left[l_{-m}^{(a)}, f_n^{(b)}\right] = -\frac{1}{m} C^{-m/2} \left(\sum_j H_{ba,j}^m - \sum_i H_{ab,i}^{-m}\right) f_{n+m}^{(b)} \quad (m > 0), \tag{5.11.16}$$

$$\left[k_m^{(a)}, e_n^{(b)}\right] = \left[k_m^{(a)}, f_n^{(b)}\right] = \left[l_{-m}^{(a)}, e_n^{(b)}\right] = \left[l_{-m}^{(a)}, f_n^{(b)}\right] = 0 \quad (m < 0), \tag{5.11.17}$$

$$\left[k_m^{(a)}, l_n^{(b)}\right] = \delta_{m+n,0} \frac{1}{m} \left(C^{-m} - C^m\right) \left(\delta_{m>0} \sum_j H_{ba,j}^m + \delta_{m<0} \sum_i H_{ab,i}^{-m}\right) \quad (m \neq 0), \tag{5.11.18}$$

where $\delta_{\texttt{cond}}$ is 1 when the condition $\texttt{cond}$ is satisfied and 0 otherwise. Notice that we would only raise the e, f modes using the non-zero Heisenberg modes. If we take $\mathfrak{t} = 1$ in the balancing factor $(UV)^{\frac{\mathfrak{t}}{2}\chi_{ab}}$ for the toroidal algebras, then only k_m and l_{-m} with $m < 0$ would lower the e, f modes while the other non-zero Heisenberg modes would commute with them. This would also make certain changs in (5.11.7)~(5.11.10).

For the elliptic algebras, we have

$$\left[k_m^{(a)}, e_n^{(b)}\right] = \frac{1}{m} \frac{1}{1-q^m} C^{-m/2} \left(\sum_j H_{ba,j}^m - \sum_i H_{ab,i}^{-m}\right) e_{n+m}^{(b)}, \tag{5.11.19}$$

$$\left[k_m^{(a)}, f_n^{(b)}\right] = -\frac{1}{m}\frac{1}{1-q^m}C^{m/2}\left(\sum_j H_{ba,j}^m - \sum_i H_{ab,i}^{-m}\right)f_{n+m}^{(b)}, \tag{5.11.20}$$

$$\left[l_{-m}^{(a)}, e_n^{(b)}\right] = \frac{1}{m}\frac{1}{1-q^m}C^{m/2}\left(\sum_j H_{ba,j}^m - \sum_i H_{ab,i}^{-m}\right)e_{n+m}^{(b)}, \tag{5.11.21}$$

$$\left[l_{-m}^{(a)}, f_n^{(b)}\right] = -\frac{1}{m}\frac{1}{1-q^m}C^{-m/2}\left(\sum_j H_{ba,j}^m - \sum_i H_{ab,i}^{-m}\right)f_{n+m}^{(b)}, \tag{5.11.22}$$

$$\left[k_m^{(a)}, l_n^{(b)}\right] = \delta_{m+n,0}\frac{1}{m}\frac{1}{1-q^m}\left(C^{-m} - C^m\right)\left(\sum_i H_{ab,i}^{-m} - \sum_j H_{ba,j}^m\right), \tag{5.11.23}$$

where $m \neq 0$. If we take $\mathfrak{t} = 1$ in the balancing factor $(UV)^{\frac{\mathfrak{t}}{2}\chi_{ab}}$, then $1/(1-q^m)$ would be changed to $1/(q^{-m}-1)$.

5.12 Free Field Realizations

Let us now discuss the free field realizations of the toroidal and elliptic quiver BPS algebras. From the discussions of the dressed operators above, it suffices to consider the toroidal case. For non-chiral quivers, the level $(1,0)$ representation (when $c = h_1$) was given in [?] with notations and conventions therein. Therefore, we shall only mention the cases for chiral quivers here.

Let us rewrite the balancing factor in (5.8.10) as $\left(\prod H_{ab,i}\right)^{1/2}\left(\prod H_{ba,i}\right)^{-1/2}(UV)^{\chi_{ab}/2}$ for convenience. We have essentially made two changes here. First, we use the convention $\mathfrak{t} = 1$ instead of -1. Moreover, the extra factors with $H_{ab,i}$ (and $H_{ba,i}$) are included so as to remove the half integer powers of these parameters (just like what (5.8.10) does for the spectral parameters). Of course, these extra factors can always be re-absorbed into the OPEs of the free fields that will be introduced below.

In the remaining part of this section, we shall write $\mathfrak{q} = C$. It would also be convenient to use the standard notation $[n]_\mathfrak{q} = \frac{\mathfrak{q}^n - \mathfrak{q}^{-n}}{\mathfrak{q} - \mathfrak{q}^{-1}}$. Let us write the OPE of two vertex operators as

$$\mathcal{V}_1(Z)\mathcal{V}_2(W) = \langle\mathcal{V}_1(Z)\mathcal{V}_2(W)\rangle(\mathcal{V}_1(Z)\mathcal{V}_2(W)), \tag{5.12.1}$$

where we have used $(\dots)$ to denote the normal ordering and $\langle\dots\rangle$ is the contraction. In particular, $(\mathcal{V}_1(Z)\mathcal{V}_2(W)) = (\mathcal{V}_2(W)\mathcal{V}_1(Z))$. Notice that here, the contraction $\langle\mathcal{V}_1(z)\mathcal{V}_2(w)\rangle$ which is a rational function should be understood as a Laurent series that converges in the region $|Z| \gg |W|$. Therefore, it would be helpful to recall that for any rational function $F(Z)$, we have

$$[F(Z)]_{|Z|\gg 1} - [F(Z)]_{|Z|\ll 1} = -\sum_i \delta\left(\frac{Z}{\mathbf{r}_i}\right)\mathrm{Res}_{\mathbf{r}_i}\frac{F(Z)}{Z}, \tag{5.12.2}$$

where $[\dots]_\mathcal{A}$ denotes the Laurent expansion in the region $\mathcal{A}$ and the sum is over all the poles $\mathbf{r}_i$ of F other than 0 and ∞. As we are actually considering the $\mathfrak{q}$-deformed algebras, we shall also use the difference operator ∂ such that

$$\partial\mathcal{V}(Z) = \frac{\mathcal{V}\left(\mathfrak{q}Z\right) - \mathcal{V}\left(\mathfrak{q}^{-1}Z\right)}{\left(\mathfrak{q} - \mathfrak{q}^{-1}\right)Z}. \tag{5.12.3}$$

Let us introduce the generators satisfying

$$\left[x_r^{(a)}, x_s^{(b)} \right] = \delta_{r+s,0} \frac{[r]_{\mathfrak{q}}^2}{r} \sum_i \mathfrak{q} H_{ba,i},$$

$$\left[y_r^{(b)}, y_s^{(a)} \right] = \delta_{r+s,0} \frac{[r]_{\mathfrak{q}}^2}{r} \sum_i \mathfrak{q} H_{ab,i}, \tag{5.12.4}$$

$$\left[\gamma_r^{(a)}, \gamma_s^{(b)} \right] = \delta_{ab} \delta_{r+s,0} \frac{[r]_{\mathfrak{q}}^2}{r},$$

with the other commutators vanishing. Consider the currents

$$X^{(a)}(U) = \log(U) + x_-^{(a)}\left(\mathfrak{q}^{-1} U \right) - x_+^{(a)}(U) + x_0^{(a)} \log(U) + \alpha_x^{(a)},$$

$$Y^{(a)}(U) = \log(U) + y_-^{(a)}(\mathfrak{q}^{-1} U) - y_+^{(a)}(U) - y_0^{(a)} \log(V) - \alpha_y^{(a)}, \tag{5.12.5}$$

$$\Gamma_\pm^{(a)}(U) = \pm \gamma_-^{(a)}(U) \mp \gamma_+^{(a)}(U) \pm \widetilde{\gamma}^{(a)} \pm \gamma_0^{(a)} \log(U),$$

where

$$x_\pm^{(a)}(U) = \sum_{r>0} \frac{x_r^{(a)}}{[r]_{\mathfrak{q}}} U^{\mp r} \tag{5.12.6}$$

and likewise for $y_\pm^{(a)}(U), \gamma_\pm^{(a)}(U)$. We have also introduced the elements $\alpha_{x,y}^{(a)}, \widetilde{\gamma}^{(a)}$ such that

$$\left\langle \exp\left(\alpha_x^{(a)} \right) U^{x_0^{(a)}} \right\rangle = U^{|a \to b|}, \quad \left\langle \exp\left(\alpha_y^{(a)} \right) U^{y_0^{(a)}} \right\rangle = U^{-|a \to b|},$$

$$\left(\exp\left(\alpha_i^{(a)} \right) \exp\left(\alpha_i^{(b)} \right) \right) = \epsilon(a,b)^{\delta_{a \neq b}} \left(\exp\left(\alpha_i^{(a)} + \alpha_i^{(b)} \right) \right) \quad (i = x, y),$$

$$\left(\exp\left(\alpha_i^{(a)} \right) \exp\left(\alpha_j^{(b)} \right) \right) = \varepsilon(a,b)^{\delta_{a \neq b}} \left(\exp\left(\alpha_x^{(a)} + \alpha_y^{(b)} \right) \right), \quad (i \neq j) \tag{5.12.7}$$

$$\left\langle U^{\gamma_0^{(a)}} \exp\left(\widetilde{\gamma}^{(b)} \right) \right\rangle = U^{\delta_{ab}}.$$

Here, $\epsilon(a,b)$ and $\varepsilon(a,b)$ can be any non-zero numbers satisfying $\frac{\epsilon(a,b)}{\epsilon(b,a)} = (-1)^{\chi_{ab}+1}$ and $\frac{\varepsilon(a,b)}{\varepsilon(b,a)} = -1$ (for $a \neq b$). We can then obtain the OPEs for $X^{(a)}, Y^{(a)}, \Gamma_\pm^{(a)}$ from

$$\left\langle \exp\left(x_+^{(a)}(U) \right) \exp\left(x_-^{(b)}(V) \right) \right\rangle = \prod_i \left(1 - \mathfrak{q} H_{ba,i} \frac{V}{U} \right),$$

$$\left\langle \exp\left(y_+^{(b)}(U) \right) \exp\left(y_-^{(a)}(V) \right) \right\rangle = \prod_i \left(1 - \mathfrak{q} H_{ab,i} \frac{V}{U} \right)^{-1}, \tag{5.12.8}$$

$$\left\langle \exp\left(\gamma_+^{(a)}(U) \right) \exp\left(\gamma_-^{(b)}(V) \right) \right\rangle = \left(1 - \frac{V}{U} \right)^{-\delta_{ab}}.$$

With these currents, we have

$$\psi_+^{(a)}(U) = \frac{1}{\mathfrak{q}^{-1} - \mathfrak{q}} \left(\exp\left(x_-^{(a)}\left(\mathfrak{q}^{-1/2} U \right) - x_+^{(a)}\left(\mathfrak{q}^{1/2} U \right) - y_+^{(a)}\left(\mathfrak{q}^{-1/2} U \right) + y_-^{(a)}\left(\mathfrak{q}^{-3/2} U \right) \right) \right),$$

$$\psi_-^{(a)}(U) = \frac{1}{\mathfrak{q}^{-1} - \mathfrak{q}} \left(\exp\left(x_-^{(a)}\left(\mathfrak{q}^{-3/2} U \right) - x_+^{(a)}\left(\mathfrak{q}^{-1/2} U \right) - y_+^{(a)}\left(\mathfrak{q}^{1/2} U \right) + y_-^{(a)}\left(\mathfrak{q}^{-1/2} U \right) \right) \right),$$

$$e^{(a)}(U) = \left(\exp\left(X^{(a)}(U) \right) \partial \exp\left(\Gamma_-^{(a)}(U) \right) \right),$$

$$f^{(a)}(U) = \left(\exp\left(Y^{(a)}(U) \right) \exp\left(\Gamma_+^{(a)}(U) \right) \right). \tag{5.12.9}$$

This follows from a straightforward check with the use of the property $\delta(Z/W)f(Z) = \delta(Z/W)f(W)$ of the formal delta function for any Laurent series $f(Z)$.

From the above discussions, we can also obtain the free field realization for the elliptic algebras using the dressed operators[32]. In other words, $\Psi_{\pm}^{(a)}(U), E^{(a)}(U), F^{(a)}(U)$ have the same expressions as the right hand sides in (5.12.9).

5.13 Outlook

The shallow discussion here is just the tip of the iceberg, and there are still many open problems left. For instance, it could be useful to consider the free fermion representations [230] in the discussions of $\mathcal{R}$-matrices. As such formalism is intimately related to crystal melting [41, 231], it could then be possible to give a full description of the contour integral forms in the $\mathcal{RTT}$ relation.

One may also use the Wakimoto representations [232, 233]. For the conifold case, this was analyzed very recently in [234]. It was shown that one can correctly recover the corresponding quiver Yangian starting from the $\mathcal{N} = 2$ superconformal $\mathcal{W}$ algebra. In general, a notable feature of $\mathcal{R}$-matrices constructed from Wakimoto realizations is that they would depend not only on $u - v$ but also on other more spectral parameters.

In the constructions of $\mathcal{R}$-matrices for various representations to reproduce the quiver Yangian relations, the screening operator is always a useful tool. For instance, a free field realization for the (truncations of) $\mathcal{W}$ algebra was constructed in [235] as the kernel of some screening fields acting on the tensor product of current algebras. This was shown to be equivalent to the free field realization from Miura operators in [66]. It would be interesting to investigate this in the context of matrix extended $\mathcal{W}$ algebras (some relevant discussions can be found in [14, §5]).

When starting from certain algebra/theory to construct the $\mathcal{R}$-matrix and reproduce the quiver Yangian relations, one often benefits from the underlying Kac-Moody (super)algebra. Therefore, it would be helpful to see if there is any similar approach for any CY_3/quivers that extends the cases of generalized conifolds. Moreover, the study of $\mathcal{R}$-matrices for quiver Yangians might lead to further applications to the Bethe/gauge correspondence [212–214]. Recently, it was later found in [58] that a consistent construction of $\mathcal{R}$-matrices is restricted to symmetric quivers (for unshifted quiver Yangians) and hence rules out those associated to CY_3 with compact divisors. Therefore, any further generalization would require a more delicate treatment.

As both the quiver Yangians and MO Yangians are constructed from quivers, it is natural to expect some connections of the two Yangian algebras. However, the precise relation between them is still not known in general. A possible direction could be the notion of tripled quivers. Further explorations of these quantum algebras might give us a deeper understanding of various physical and mathematical problems.

The coproduct plays an important role when studying the Bethe/gauge correspondence from the BPS quiver algebra [14,58]. Similar to the map from the quiver Yangian to the $\mathcal{W}$-algebra, it would be natural to wonder whether we can write some $\mathcal{RTT}$-like presentation of the quiver Yangian, which might in turn shed light on the Bethe/gauge correspondence. The construction of the co-product we have benefits from the untwisted affine Lie superalgebra of A-type. A natural extension would be a more thorough study on quiver Yangians for the remaining generalized conifolds (i.e., $(M, N) = (2, 0)$, $M = N$), as well as $\mathbb{C}^3/(\mathbb{Z}_2 \times \mathbb{Z}_2)$. All of them have underlying Kac-Moody algebras. It is worth noting that a method of computing the coproduct perturbatively is given in [58, Appendix C] for generalized conifolds. For the cases with $M = N$, due to the vanishing Killing forms[33], we would probably need to consider the algebra $\mathfrak{gl}(M|M)$. This could be similar to the Khoroshkin-Tolstoy approach [236, 237]. More generally, for toric CYs with compact

---

[32]Notice that the dressed operators discussed above are for non-chiral quivers. However, the construction is similar for the chiral cases.

[33]This is also the situation for $D(2, 1; \alpha)$ and $\mathfrak{osp}(2N + 2|2N)$. The former is associated to the quiver Yangian for $\mathbb{C}^3/(\mathbb{Z}_2 \times \mathbb{Z}_2)$. For the latter case, we do not have associated quiver Yangians so far. It would also be interesting to see whether there can be similar (BPS) algebras for the orthosymplectic cases.

4-cycles, the quiver Yangians do not seem to have such underlying Kac-Moody algebras. It would be desirable to find the coproduct of the rational algebra associated to any quiver.

Apart from the above perspectives, the study of quiver BPS algebras and $\mathcal{W}$-algebras could give new insights in the study of BPS/CFT correspondence [79, 80]. In particular, it is believed that both the quiver Yangians and the $\mathcal{W}_{M|N\times\infty}$ algebras should play the role as the double of the corresponding cohomological Hall algebras [57, 69]. This would also be intimately related to the wall crossing phenomenon.

Regarding the truncations and VOAs, we have only explicitly discussed the crystal configurations here for $l = 1$. As analyzed in [57], when the crystal is truncated at some atom, this leads to some extra conditions that $\widetilde{\epsilon}_I$ should satisfy on the quiver Yangian side. On the other hand, recall that we also have certain condition on ϵ_i for Φ to be homomorphic, and the truncation comes from the parameter l on the $\mathcal{W}$-algebra side. We expect that the cut at l would not provide all the possible truncations of the crystal. It is very likely that the coefficients in the actions of some U-modes become zero due to the truncation conditions on $\widetilde{\epsilon}_I$ from the quiver Yangians. Besides, there are more general truncations, namely the $x^{l_3}y^{l_2}z^{l_4}w^{l_1}$-algebras, as mentioned above. They might also give possible truncations on the crystal. Moreover, it would be interesting to see whether other crystal configurations, such as crystals in other chambers [12, 44, 151] and 2d crystals [14, 58, 152], could give similar relations.

It still remains an open question whether the quiver Yangians for more general geometry, especially those associated to toric CYs with compact divisors, could have some $\mathcal{W}$-algebras as their truncations. It might be possible to construct the VOAs from the quiver Yangians in this setting and compare them with other constructions.

We may also consider the truncations of the toroidal and even elliptic quiver BPS algebras. It could be possible that they would lead to deformations of the rational VOAs. In particular, the toroidal algebra for $\mathbb{C}^3$ is shown to be a q-deformation of the $\mathcal{W}_{1+\infty}$-algebra in [238]. We conjecture that there exist certain q-deformations of the $\mathcal{W}_{M|N\times\infty}$-algebras such that for toroidal BPS algebras T associated to the generalized conifolds, we have the following commutative diagram which would give the 5d AGT correspondence:

$$
\begin{array}{ccc}
\texttt{T} & \xrightarrow{\ \ \Phi_l\ \ } & U(_{\texttt{q}}\mathcal{W}_{M|N\times l}) \\[2pt]
{\scriptstyle\Delta}\downarrow & & \downarrow{\scriptstyle\widetilde{\Delta}_{l_1,l_2}} \\[2pt]
\texttt{T}\widehat{\otimes}\texttt{T} & \xrightarrow{\ \Phi_{l_1}\otimes\Phi_{l_2}\ } & U(_{\texttt{q}}\mathcal{W}_{M|N\times l_1})\widehat{\otimes}U(_{\texttt{q}}\mathcal{W}_{M|N\times l_2})
\end{array}
\tag{5.13.1}
$$

where Φ_l are some surjections and the hats denote the completions of the algebras. On the BPS algebra side, this would require a detailed study on the so-called horizontal representations of the algebras with non-trivial central element C so that we can get vertex operators from the generators. On the VOA side, we need to find some suitable deformations of the $\mathcal{W}_{M|N\times\infty}$-algebras studied in [69, 70].

Recall that there is another duality for toric quiver gauge theories known as the specular duality, and we have seen that many concepts and quantities enjoy nice properties under such duality. As specular duality does not preserve the mesonic moduli space (except self-dual cases) although the Hilbert series would agree up to some fugacity maps, we do not expect the quiver BPS algebras to be isomorphic under specular duality. However, it exchanges the internal and external perfect matchings, which are associated to the internal and external points of the toric diagram respectively, of the dual brane tilings.

As each arrow in the quiver can be written in terms of a product of some perfect matchings, the arrows also have a one-to-one correspondence for specular dual theories. It is then natural to wonder if the charge assignments would also follow this correspondence of the arrows. However,

we have checked several examples and this is not the case, even for self-dual ones[34]. Nevertheless, as argued in [57], the perfect matchings can be used to determine certain truncations of the quiver Yangian. This is because such truncations come from adding D4-branes to the divisors of the toric CY threefold, which correspond to the lattice points of the toric diagram. In [57], such truncations were only identified for external (or more precisely, corner) perfect matchings. It could be possible that the truncations from D4-branes associated to internal points can be studied from the specular dual case, where the internal perfect matchings are mapped to the external ones[35].

---

[34]For a self-dual quiver, an arrow would often be mapped to a different arrow in the quiver.

[35]Of course, there can also be external lattice points that are not at the corners. Moreover, for non-reflexive polygons, specular duality can relate brane tilings on Riemann surfaces with higher genus [239].

Chapter 6

Chiral Rings and K-Stability

So far, most of our discussions are restricted to the toric varieties. Although extending the study to more general settings could be difficult, in this chapter, we shall consider the chiral rings with the tools of K-stability that in principle can be applied to any geometry.

It is known mathematically that the K-stability of a ring can be determined by considering the so-called test symmetries that "perturb" the Hilbert series of the associated variety. However, explicit calculations have only been performed for the simplest cases before. Here, we consider more non-trivial examples, and discuss various ways to find the test symmetries. In particular, we give the first examples to our best knowledge whose test symmetries would also "perturb" the numerators of the Hilbert series. Moreover, we will also mention some subtleties previously overlooked in the calculations that are worth more careful study in future. Physically, it is conjectured that a chiral ring is a ring of some CFT if and only if it is K-stable. After illustrating the K-stability calculations with various examples, ranging from instanton moduli spaces to phenomenological models, we find some counterexamples of the conjecture. Nevertheless, this does not rule out the possibility that being K-stable still serves as a necessary condition.

Before we discuss these results in more detail, let us first review some preliminaries of the chiral rings, as well as the concept of K-stability. For supersymmetric gauge theories in 4d with $\mathcal{N} = 1$, the chiral rings are important in the study of their dynamics; this is the set of operators annihilated by $\widehat{Q}_{\dot{\alpha}}$, defined modulo $\{\widehat{Q}_{\dot{\alpha}}, \_\}$, closed under addition and multiplication, whereby forming a ring structure. In [89], the interesting question of when a polynomial ring is the chiral ring of a superconformal field theory (SCFT) was posed. Since many new symmetries might emerge when a theory flows to IR (e.g. some free operators in the IR have these new symmetries acting on them), the idea of chiral ring *stability* was introduced in [89] to determine whether there could be some new ring that would destabilize the original ring in the sense that the destabilizing ring would have a larger symmetry and would give no less central charge compared to the original ring[1]. It was argued in [89] that this is equivalent to the concept of *K-stability*[2]. In [160, 240], for a polarized ring with symmetry/Reeb vector field ζ, K-stability is determined via perturbing the ring by a test symmetry $\epsilon\eta$ for some symmetry η and small ϵ.

The *(Donaldson-)Futaki invariant*, which constitutes the criterion for K-stability, was originally defined in [241] and then generalized in [242] and [243] as an obstruction to constructing metrics: its vanishing is a necessary condition of the existence of Kähler-Einstein metrics on Fano varieties. For general compact complex manifolds, it is conjectured that K-stability is equivalent to the existence of constant scalar curvature Kähler (cscK) metric.

In [160, 240], the notion of K-stability was extended to any Sasakian manifold, including irregular ones. It was shown that if a Sasakian manifold S with Reeb vector field ζ has a constant scalar curvature metric, then its cone $(\mathrm{Cone}(S), \zeta)$ is K-semistable (see Definition 6.1.2). In particular, we can use Hilbert series (HS) to compute Futaki invariants. For an affine variety $X \subset \mathbb{C}^n$ cut out by

---

[1]Notice that this does not violate the a-theorem which requires the central charge to decrease under RG flow since the original ring is not a ring of an SCFT.

[2]Therefore, we will use the words "stability" and "K-stability" interchangeably throughout.

some $I \subset \mathbb{C}[x_1, \ldots, x_N]$ such that $X = \mathrm{Spec}(R)$, where $R = \mathbb{C}[x_1, \ldots, x_N]/I$, the symmetry/Reeb field $\zeta \in \mathfrak{t}$ acts on the functions on X with positive weights, where $\mathfrak{t}$ is the Lie algebra of the torus action $T \subset \mathrm{Aut}(X)$. Then we can write the HS with respect to the weighting of ζ (strictly, we should think of the HS as being associated to the weighted projective variety obtained from the projectivization of the affine variety, keeping the weights as multi-degrees). To see if there exists a destabilizing ring which has a larger symmetry, we perturb the HS with a test symmetry η by considering $(\zeta + \epsilon\eta)$. The information of the grading induced by η is reflected by the coefficients (and derivatives thereof) in the Laurent expansion for the perturbed HS. With this data, we may follow the standard algebro-geometric set-up to compute the Futaki invariant.

Such idea can then be applied to various aspects in physics. It was shown that the Lichnerowicz obstruction in [244] is in fact the problem of K-semistability for deformations arising from Rees algebras of principal ideals. Moreover, K-(semi)stability for product test configurations is equivalent to volume minimization. In light of AdS/CFT, this is then related to a-maximization [113]. For a general test configuration induced by η, if we find some destabilizing ring at the central fibre (i.e., the flat limit of the test configuration) whose symmetry is $\zeta(\epsilon)$ parameterized by ϵ, then following [89], the Futaki invariant is equal to the derivative of $a_0(\zeta(\epsilon))$ with respect to ϵ, where $a_0(\zeta(\epsilon))$ is the leading coefficient in the Laurent expansion for the HS of the destabilizing ring weighted by $\zeta(\epsilon)$. It turns out that this $a_0(\zeta(\epsilon))$ is inversely proportional to the central charge of the destabilizing chiral ring. Hence, K-stability, serving as some generalized a-maximization, is naturally related to the conformality of supersymmetric gauge theories.

6.1 Chiral Rings of Supersymmetric Gauge Theories

We shall focus on the chiral rings of (3+1)-dimensional SCFT [245–247] for whose supersymmetry we will write in $\mathcal{N} = 1$ language. In short, this is simply the set of operators $\mathcal{O}_i$ which are "holomorphic" in that they are annihilated by the supercharges $\bar{Q}_{\dot{\alpha}}$ so that they are defined modulo the cohomolgy thereof; hence there exists an operator χ such that

$$\mathcal{O}_i \sim \mathcal{O}_i + \left[\bar{Q}_{\dot{\alpha}}, \chi\right] \ . \tag{6.1.1}$$

The ring structure follows from the fact that (1) there is an identity operator $\mathcal{O} = \mathbb{I}$, (2) the sum and product of two chiral operators remain chiral, and (3) the structure constant is that for the (spacetime independent) OPE for the VEVs: $\mathcal{O}_i\mathcal{O}_j = \sum_k C_{ij}^k \mathcal{O}_k$. In fact, this ring is a (finite) commutative ring with identity.

Computationally, the *classical* chiral ring can be determined as follows. We have a superpotential W, which is a holomorphic polynomial in $\mathcal{O}_i$, each of which can be thought of as a matrix operator in an appropriate representation of the gauge group, with over-all trace. Consider all (complex) components ϕ_i of all the $\mathcal{O}_i$, and work over the polynomial ring $R = \mathbb{C}[\phi_i]$. The F-terms, constituted by the partial derivatives of W with respective to ϕ_i, can be thought of as the Jacobian ideal $J = \langle \partial_{\phi_i} W \rangle \subset R$. The chiral ring can then be thought of as the quotient ring R/J (giving us the "master space" [28]), and then quotiented further by any polynomial relations which arise from the traces, such as those obeyed by Newton relations. For example, for $SU(N)$ theory with a chiral field Φ in the adjoint, the chiral ring is freely generated by the single-trace operators $\mathrm{tr}(\Phi^i)$ for $i = 0, 1, 2, \ldots, N-1$ because any $\mathrm{tr}\left(\Phi^{i>N}\right)$ can be written as Newton polynomials of the former and any multi-trace operator is just products of these single-traces.

The above should be compared and contrasted with the calculation of the *classical* vacuum moduli space (VMS), which is the GIT quotient of J by the complexified gauge group [248]. Computationally, this is done by considering the minimal set of gauge invariant operators (GIOs) G_j in the theory, each being a single-trace operator, and thus a polynomial in the ϕ_i. Then the classical VMS is the image of quotient ring R/J under the map $\{D_j\}$ into $S = \mathbb{C}[D_j]$ [34,36,249]. Importantly, in AdS/CFT, this VMS is nothing more than the Calabi-Yau variety X which a single brane probes

and whose world-volume gauge theory is the SCFT; for N parallel stack of D-branes, the VMS is the Nth symmetric product of X.

It should be emphasized that the classical chiral ring and the VMS both receive quantum corrections due to strongly coupled effects such as instantons. Algebro-geometrically, the correction often corresponds to a complex structure deformation. For example, in $\mathcal{N} = 1$ SQCD, the classical chiral operators are the mesons $M_j^i = Q_a^i \tilde{Q}_j^a$ and baryons $B^{i_1 \cdots i_N} = \epsilon_{a_1 \ldots a_N} Q_{i_1}^{a_1} \ldots Q_{i_N}^{a_N}$, $\tilde{B} = \epsilon_{a_1 \ldots a_N} \tilde{Q}_{i_1}^{a_1} \ldots \tilde{Q}_{i_N}^{a_N}$ in terms of the quarks Q_i and $\tilde{Q}_i$, with the famous relation for the VMS: $B^{i_1 \cdots i_N} \tilde{B}_{j_1 \ldots j_N} = M_{j_1}^{[i_1} \ldots M_{j_N}^{i_N]}$. Interestingly, in [27], it was shown that all the classical VMSs are affine Calabi-Yau (Gorenstein) singularities.

6.1.1   Hilbert Series

One of the most important quantities which characterize an algebraic variety X is the Hilbert series. We have mentioned Hilber series in our previous discussions. For completeness, let us have a more detailed discussion here. The relevance of computing the HS in relation to the volume of the Sasaki-Einstein base in toric AdS/CFT has been the beautiful work of [113, 114, 250]. In parallel, a plethystic programme was established [25, 26] addressing the key problem of counting GIOs in gauge theory (q.v. [27–32]). Moreover, its properties have also been exploited to study the phenomenology of the standard model, ranging from question of vacuum structure to operator selection [33–40].

We recall that for a variety X in $\mathbb{C}[x_1, ..., x_k]$, the HS is the generating function for the dimension of the graded pieces:

$$\text{HS}(t; X) = \sum_{i=0}^{\infty} (\dim_{\mathbb{C}} X_i) \, t^i, \tag{6.1.2}$$

where X_i, the ith graded piece of X can be thought of as the number of independent degree i (Laurent) polynomials on the variety X. The most useful property of HS is that it is a rational function in t and can be written in 2 ways:

$$\text{HS}(t; X) = \begin{cases} \frac{Q(t)}{(1-t)^k} \, , & \text{HS of first kind ;} \\ \frac{P(t)}{(1-t)^{\dim(X)}} \, , & \text{HS of second kind .} \end{cases} \tag{6.1.3}$$

Importantly, both $P(t)$ and $Q(t)$ are polynomials with *integer* coefficients and the powers of the denominators are such that the order of the pole captures the dimension of the variety and the embedding space $\mathbb{C}^k$ within which X is an algebraic variety, respectively for the first and second kind.

Let us summarize a few key properties of the HS which we will need:

- It is *not* a topological invariant and does depend on embedding and choice of grading/weighting for the coordinate ring for X. The weight comes from a choice of a symmetry/Reeb vector field ζ of the theory. Typically, we choose the $\text{U}(1)_R$ symmetry of the SCFT to weight the fields, and, thence the GIO variables of X;

- Written in the second kind, $P(1)$ equals to the degree of the variety;

- Also in the second kind, if $P(t)$ is *palindromic*, then Stanley's theorem says this is equivalent to X being Gorenstein [251], which for our purposes can be taken to mean affine Calabi-Yau;

- A Laurent expansion for the Hilbert series of second kind in (6.1.3) can be developed, as a partial fraction expansion:

$$\text{HS}(t; X) = \frac{V_n}{(1-t)^n} + \cdots \frac{V_3}{(1-t)^3} + \frac{V_2}{(1-t)^2} + \frac{V_1}{1-t} + V_0 + \mathcal{O}(1-t) \, , \tag{6.1.4}$$

where we see explicitly that the Hilbert series is a rational function and the degree of its most singular pole is the dimension of X.

In the case of X being a toric Calabi-Yau variety of dimension 3 (such as in the vast majority of known cases of $\text{AdS}_5/\text{CFT}_4$), the coefficients $V_{0,1,2,3}$ are related directly to the Reeb vector of X so that V_3 is the volume of the spherical Sasaki-Einstein horizon[3].

- In the notation of [89], suppose the underlying (Calabi-Yau) geometry (VMS) is X, of complex dimension $n = 3$, we have a $\text{U}(1)_R$ symmetry ζ with the associated trial central charge $a(\zeta)$, we perform the Laurent expansion of the Hilbert series as

$$\text{HS}(t = e^{-s}, \zeta; X) = \frac{a_0(\zeta)}{s^3} + \frac{a_1(\zeta)}{s^2} + \dots \tag{6.1.5}$$

Then, we have that

- the coefficient a_0 is proportional to the (normalized) volume of the base over which X is a cone (for example, $X = \mathbb{C}^3 = \text{Cone}(S^5)$);

- the trial a-charge (of order N^2) is given by

$$a(\zeta) = \frac{27N^2}{32} \frac{1}{a_0(\zeta)}; \tag{6.1.6}$$

- the holomorphic volume $(3,0)$-form Ω (from the Calabi-Yau condition of X) will be chosen to have charge 2, which implies that $a_0 = a_1$;

- the coefficient $a_0(\zeta)$ is a convex function in the symmetry generators [113].

- For *complete intersection* varieties, i.e., the codimension of X being exactly equal to the number of defining polynomials, the HS is relatively easy to construct [25, 26]. In particular, the simplest case of a complete intersection is that of a single defining equation and X being codimension 1, viz., a hypersurface. For example, consider the quadric hypersurface $Q = \{x^2 + y^2 + z^2 + w^2 = 0\}$ in $\mathbb{C}^4$, otherwise known as the conifold singularity as a local Calabi-Yau threefold. Suppose we weigh the variables as $W(x, y, z, w) = (1, 1, 1, 1)$, then we have 4 generators (variables), each of degree 1, obeying the one quadratic defining relation, of degree 2. For each generator we place a factor of $(1 - t^W)$ in the denominator, and for each relation of degree d, we place a factor of $(1 - t^d)$ in the numerator. Therefore, the HS here is simply $\text{HS}(t; Q) = \frac{1 - t^2}{(1 - t)^4}$.

In fact, one can define a pair of inverse functions [26], the *plethystic exponential* $\text{PE}[f(t)]$ and the *plethystic logarithm* $\text{PL}[f(t)]$ for any analytic function $f(t)$ affording Taylor series about 0:

$$f(t) = \sum_{n=0}^{\infty} a_n t^n \quad \Rightarrow \quad \begin{cases} \text{PE}[f(t)] = \exp\left(\sum_{n=1}^{\infty} \frac{f(t^n) - f(0)}{n} \right) = \prod_{n=1}^{\infty} (1 - t^n)^{-a_n} \\ \text{PL}[f(t)] = \sum_{k=1}^{\infty} \frac{\mu(k)}{k} \log(f(t^k)) \end{cases} \tag{6.1.7}$$

where $\mu(k)$ is the Möbius function, which for an integer k is equal to 0 if k has repeated prime factors, equal to 1 if $k = 1$ and equal to $(-1)^n$ if k is a product of n distinct primes. That the above pair are indeed inverses of each other is non-trivial and involves the arithmetic properties of μ.

---

[3]The relation to the Reeb vector, at least for toric X, is as follows [114]. Refine the generating function into tri-variate (this can always be done for toric X), in terms of $t_{i=1,2,3}$ and set $t_i := \exp(-b_i q)$ where $\vec{b} = (b_1, b_2, b_3)$ is the Reeb vector for the 3 isometries of X as a toric variety. Then Laurent expand $f(t_1, t_2, t_3)$ near $q \to 0$ to compare with (6.1.4).

The remarkable fact is that (though it has poles at $t = 1$) the HS is analytic about $t = 0$ and can be used as the functional argument of PE and PL. Indeed, $\mathrm{HS}(t; X)$ for X being the supersymmetric vacuum moduli space of the SCFT is the generating function for the single-trace operators in the chiral ring and $\mathrm{PE}[\mathrm{HS}(t; X)]$ counts the multi-trace operators. Moreover, $\mathrm{PL}[\mathrm{HS}(t; X)]$ is a polynomial for complete intersections and explicitly counts the generators (the first positive terms) and relations (the first negative terms) for X of each degree[4]. For our above conifold example, $\mathrm{PL}[\mathrm{HS}(t; Q)] = 4t - t^2$, signifying 4 degree-one generators obeying 1 quadratic relation.

- It should be emphasized that the generic variety, and chiral ring, is *not* complete intersection and the presentation of the generators and relations could be rather complicated. In such situations, the most standard method is to compute the *Gröbner basis* of X. The advantage of the Gröbner basis method is that it is algebraic and algorithmic. We describe this in more detail in Appendix J. On the other hand, as we are considering the Higgs branch, we can also use another method, namely the *Molien-Weyl integral*, to compute HS. For a detailed treatment, readers are referred to [25].

6.1.2   Flat Limits and Central Fibres

As mentioned above, (K-)stability and the Futaki invariant are related to the existence of a destabilizing ring for X. We start with some *test configuration* X_t, that is, X with a one-parameter subgroup $\eta(t) : \mathbb{C}^* \hookrightarrow \mathrm{GL}(m, \mathbb{C})$. For any polynomial f, in our convention, we have $(\eta(t) \cdot f)(x_0, \ldots, x_m) = f(\eta(t)x_0, \ldots, \eta(t)x_m)$. We will always assume that $\eta(t)$ is *diagonal* under a unitary change of basis. The test configuration now has the ring $\mathbb{C}[x_0, \ldots, x_m]/I_t$ with $I_t = \{\eta(t) \cdot f | f \in I\}$, where I is the ideal defining the ring of X. Then to get the *central fibre*, we need to take the *flat limit* defined as follows (see Appendix J for details on initial ideals and polynomial ordering).

Definition 6.1.1. *For any $f \in I$, we find the initial polynomial $\mathrm{in}(f)$ with respect to the ordering defined by $\eta(t)$ such that $\mathrm{in}(f)$ is the lowest weight polynomial. Then the flat limit of I_t is $I_0 = \lim_{t \to 0} I_t = \{\mathrm{in}(f) | f \in I\}$.*

Notice that, however, following [89, 240], it should be a *partial* ordering rather than a total ordering. For instance, consider the conifold $w^2 + x^2 + y^2 + z^2 = 0$. If we have $\eta(t) \cdot (w, x, y, z) = (tw, x, y, z)$, then the test configuration is $t^2w^2 + x^2 + y^2 + z^2 = 0$. Taking the flat limit gives the central fibre $x^2 + y^2 + z^2 = 0$, rather than a single monomial. On the other hand, if we consider $\eta(t) \cdot (w, x, y, z) = (t^{-1}w, x, y, z)$, i.e., the test symmetry η with charges $(-1, 0, 0, 0)$, we would get $w^2 = 0$.

It is also worthing noting that for more general cases, if we simply take the initial polynomials of the generators of the ideal, we may get a smaller ideal than the flat limit [252][5]. To get the exact flat limit, the strategy is to compute the Gröbner basis. Let us consider the twisted cubic curve example in [253], where $I = \langle f_1, f_2, f_3 \rangle$ for $f_1 = w^2 - xy$, $f_2 = wy - xz$, $f_3 = wz - y^2$, and the action is $\eta(t) = (t^{-16}, t^{-4}, t^{-1}, 1)$. The test configuration is

$$\eta f_1 = t^{-32}w^2 - t^{-5}xy, \ \eta f_2 = t^{-17}wy - t^{-4}xz, \ \eta f_3 = t^{-16}wz - t^{-2}y^2. \tag{6.1.8}$$

Naively, the flat limit is generated by w^2, wy, wz. However, if we consider the Gröbner basis for f_i, we have

$$w^2 - xy, \ wy - xz, \ wz - y^2, \ xz^2 - y^3. \tag{6.1.9}$$

Hence, the flat limit should really be generated by w^2, wy, wz, xz^2.

---

[4]For non-complete intersections, there are terms of higher orders known as *syzygies* that enumerates relations among basic relations and generators.

[5]The reason behind it is actually related to the syzygies. For more details, see [253, 254].

6.1.3 Futaki Invariant and K-Stability

Let us start with the (polarized) ring (X, ζ) with symmetry ζ. Throughout, by "polarized" we mean that the ring is also equipped with a Reeb symmetry. Also note, by slight abuse of notation, that we will use X for varieties and associated coordinate rings interchangeably. Then to find out whether there would be a ring destabilizing X, we need to consider some test symmetry η. As aforementioned, this is done by considering some test configuration $X_t = \mathbb{C}[x_i]/I_t$ induced by the test symmetry, and then taking the flat limit $t \to 0$ to get the central fibre $X_0 = \mathbb{C}[x_i]/I_0$. For general t, X_t would be isometric to X while X_0 may or may not be trivial.

From [252], we know that the total weight w_k of the action on the (sufficiently high) degree k piece of our graded ring can be written as a polynomial

$$w_k = b_0 k^n + b_1 k^{n-1} + \dots \ , \tag{6.1.10}$$

where from [160], we learn that (up to a positive constant dependent only on the dimension n)[6]

$$b_i = -\frac{1}{n-i} \mathrm{D}_\epsilon a_i(\zeta + \epsilon \eta) \Big|_{\epsilon=0} \ . \tag{6.1.11}$$

The Futaki invariant is then defined as[7] [252]

$$F(X; \zeta, \eta) = \frac{a_1}{a_0} b_0 - b_1 \ . \tag{6.1.12}$$

There is also an equivalent definition in [160, 240][8]:

$$F(X; \zeta, \eta) = \mathrm{D}_\epsilon a_0(\zeta + \epsilon \eta) + n a_0 \mathrm{D}_\epsilon \frac{a_1(\zeta + \epsilon \eta)}{a_0(\zeta + \epsilon \eta)} \Big|_{\epsilon=0} \ , \tag{6.1.13}$$

where D_ϵ is defined in (6.1.16) below. We remark that the Futaki invariant in its original context, was in terms of a integral as detailed in the footnote, due to the purely algebraic recasting above, it is sometimes referred to as the Futaki-Donaldson invariant.

Algorithmically, our Futaki invariant can be determined as follows [89]:

- For a symmetry/weighting ζ of the variables of X such that the holomorphic top form has charge/weight 2, compute the HS (thus in particular $a_0(\zeta) = a_1(\zeta)$ in our convention);

- Find a test symmetry η of X, expressed as a vector of weights[9], as ζ;

- Consider the possible $U(1)_R$ symmetry, for some small $\epsilon > 0$ (so that the central fibre from the test symmetry $\epsilon(\eta - a\zeta)$ is the same as the one from η),

$$\zeta(\epsilon) = \zeta + \epsilon(\eta - a\zeta) = (1 - a\epsilon)\zeta + \epsilon\eta, \tag{6.1.14}$$

  where a can be obtained from

$$a = \frac{1}{a_0(\zeta)} \left(\frac{\mathrm{d}a_1(\zeta + \epsilon\eta)}{\mathrm{d}\epsilon} - \frac{\mathrm{d}a_0(\zeta + \epsilon\eta)}{\mathrm{d}\epsilon} \right) \Big|_{\epsilon=0}. \tag{6.1.15}$$

---

[6]In fact, up to some convention, the a_i's also act as leading and subleading coefficients of a polynomial, namely the dimension d_k of the degree k piece of the graded ring: $d_k = a_0 k^n + a_1 k^{n-1} + \dots$, which is nothing but the Hilbert function of X.

[7]There is also a differential geometric definition of Futaki invariant. Specifically, for a smooth n-dimensional normal variety X (the generalizations allow X to be singular) with Kähler form $\omega \in [c_1(T_X)]$ and Ricci potential h_ω so that $\mathrm{Ric}(\omega) - \omega = \frac{i}{2\pi} \partial\bar{\partial}h_\omega$ where $\mathrm{Ric}(\omega)$ is the Ricci form. Then the Futaki invariant, for some holomorphic vetor field v on X, is $F_{c_1(T_X)}(v) = \int_X v(h_\omega)\omega^n$. Since it is a character on the Lie algebra of v and independent of the choice of ω, this is an holomorphic invariant [255]. One can show that if X is smooth and the $\mathbb{C}^*$-action is induced by a holomorphic vector field, then (6.1.12) is the sames as the differential geometric Futaki invariant [252].

[8]Notice that due to different conventions of a_0 and a_1, our definition here should agree with the definition in [160, 240, 252] up to some positive constant depending only on dimension.

[9]Technically, η is a square matrix, but as we will see, it is always assumed to be diagnolizable.

- With respect to this new weighting, compute the HS and perform the usual Laurent expansion (6.1.5) to extract the coefficients $a_0(\zeta(\epsilon)) = a_1(\zeta(\epsilon))$;

- The Futaki invariant is obtained by

$$F(X;\zeta,\eta) = \left.\frac{\partial}{\partial\epsilon}a_0\left(\zeta(\epsilon)\right)\right|_{\epsilon=0} =: \mathrm{D}_\epsilon a_0(\zeta(\epsilon))|_{\epsilon=0}. \tag{6.1.16}$$

As argued in [89], (6.1.16) is equivalent to the original definition of Futaki invariant in [243] by considering

$$
\begin{aligned}
F &= \left.\mathrm{D}_\epsilon a_0\Big(\zeta(\epsilon) = \zeta + \epsilon(\eta - a\zeta)\Big)\right|_{\epsilon=0} \\
&= (\eta - a\zeta)\cdot a_0'|_{\epsilon=0} \\
&= \eta\cdot a_0' - a\zeta\cdot a_0'|_{\epsilon=0} \\
&= \mathrm{D}_\epsilon a_0(\zeta + \epsilon\eta) + \frac{1}{a_0}\left.\left(\frac{\mathrm{d}a_1(\zeta+\epsilon\eta)}{\mathrm{d}\epsilon} - \frac{\mathrm{d}a_0(\zeta+\epsilon\eta)}{\mathrm{d}\epsilon}\right)na_0\right|_{\epsilon=0} \\
&= \mathrm{D}_\epsilon a_0(\zeta + \epsilon\eta) + na_0\mathrm{D}_\epsilon\left.\frac{a_1(\zeta+\epsilon\eta)}{a_0(\zeta+\epsilon\eta)}\right|_{\epsilon=0}, \tag{6.1.17}
\end{aligned}
$$

where we have used $\zeta\cdot a_i' = \mathrm{D}_\epsilon a_i(\zeta+\epsilon\zeta) = -(n-i)a_i(\zeta)$ to get the fourth line, and the last equality is the quotient rule of derivatives with $\eta\cdot a_0|_{\epsilon=0} = \eta\cdot a_1|_{\epsilon=0} = a_0$. As we can see, the result obtained in (6.1.17) is exactly (6.1.13).

Following the third line in (6.1.17), it is straightforward that F is linear with respect to the test symmetry. For the first term, we have $(s\eta_1+\eta_2)\cdot a_0' = s\eta_1\cdot a_0'+\eta_2\cdot a_0'$ $(s>0)$. Hence, it is equivalent to showing that a is linear with respect to the test symmetry, which is then equivalent to showing that $\mathrm{D}_\epsilon a_i(\zeta+\epsilon\eta)$ is linear. This is certainly true as $\mathrm{D}_\epsilon a_i(\zeta+\epsilon(s\eta_1+\eta_2)) = (s\eta_1+\eta_2)\cdot a_i' = s\eta_1\cdot a_i'+\eta_2\cdot a_i'$.

Moreover, from the fourth line in (6.1.17), we also have

$$F = n\mathrm{D}_\epsilon a_1(\zeta + \epsilon\eta) - (n-1)\mathrm{D}_\epsilon a_0(\zeta + \epsilon\eta)|_{\epsilon=0}. \tag{6.1.18}$$

Inserting (6.1.11), we find that this is the same as definition (6.1.12) (up to some positive coefficient). Therefore, (6.1.16)$\sim$(6.1.18) all give the same answer and we can use them interchangeably.

As K-stability depends on the sign of Futaki invariant, we can almost introduce its definition. However, whether a test configuration is trivial still needs to be determined especially when $F = 0$. A test configuration was initially defined to be trivial when the central fibre is biholomorphic to X. However, as shown in [256], there exist non-trivial test configurations (which are trivial in codimension 1) satisfying biholomorphicity. To avoid such pathological cases, one has to restrict to normal (or S_2) test configurations when X is normal (or S_2). Here, following [252], we will use an alternative way to determine the K-stability when F vanishes without the normality condition. In particular, one can introduce the norm $||\eta||$ by considering the infinitesimal generator A_k of the $\mathbb{C}^*$-action on the degree k piece of the ring. It is not hard to see that $\mathrm{tr}(A_k) = w_k$. We can also define c_0, which is also a constant with respect to degree k, by

$$\mathrm{tr}(A_k^2) = c_0k^{n+1} + \ldots, \tag{6.1.19}$$

and it is shown in [160] that (up to a positive constant same as in b_0)

$$c_0 = \frac{1}{n(n+1)}\mathrm{D}_\epsilon^2 a_0(\zeta + \epsilon\eta)|_{\epsilon=0}. \tag{6.1.20}$$

Then we can define the norm as

$$||\eta||^2 = \begin{cases} 0, & I_0 \cong I_{t\neq 0}; \\ c_0 - \frac{b_0^2}{a_0}, & \text{otherwise.} \end{cases} \tag{6.1.21}$$

Thus defined, the notion of K-stability is clear:

Definition 6.1.2. *The ring (X, ζ) is K-semistable if for any test symmetry η, we have $F(X; \zeta, \eta) \geq 0$. If in addition $F = 0$ only when the norm vanishes, then the ring is K-stable.*

Let us have a closer look at the case with $F = 0$. A trivial test configuration (which leads to $F = 0$) for a K-stable ring should always have a vanishing norm. In the usual K-stability context, a well-defined triviality should be the equivalent to the norm being zero. However, as we will see below, besides the second line in (6.1.21), the first line is also necessary since there could be trivial configurations with non-zero values for the second line[10].

It is then the conjecture of [89] saying that

Conjecture 6.1.1. *The ring (X, ζ) is the chiral ring of an SCFT iff X is K-stable.*

As we will see, there seems to exist a counterexample where this K-stability criterion would not work. However, this is still possible to be true for a sub-class of supersymmetric theories such as the worldvolume theories of D3-branes probing CY_3.

6.1.4 Futaki Invariants for Non-Complete Intersections

For complete intersections, the denominators of the HS encode the charges of the coordinates/generators. With the aforementioned method, the Futaki invariants can then be quickly computed as in [89] since we can directly add the test charges to the corresponding terms in the denominator of HS. Here, we propose a method allowing us to obtain the Futaki invariants with Hilbert series which also works for general varieties.

We would like to know which factor in the HS our test symmetry can act on, but for non-complete intersections this piece of information is hidden (especially when we derive the HS from quivers in physics). The denominator simply encodes the dimension of the variety while the numerator contains other complicated data. Therefore, we can naturally use the plethystic logarithm to reveal the information we need.

We start with a general HS and take its PL whose first positive terms tell us all the generators at different degrees. For instance, if we have a generator of order k (and hence with weight/charge k), then we multiply the HS with $(1 - t^k)$ on its denominator and numerator:

$$\text{HS}_\zeta = \frac{1 - t^k}{1 - t^k} \text{HS} = \frac{1 - t^k}{1 - t^k} \times \frac{P(t)}{(1 - t^m)^{\dim(X)}}. \tag{6.1.22}$$

As we write out the specific generator explicitly in the denominator, as in the complete intersection case, we can easily get the HS for test symmetry η where only the generator at order k has non-vanishing charge:

$$\text{HS}_{\zeta + \epsilon \eta} = \frac{1}{1 - t^{k + \epsilon \eta}} \times \frac{\left(1 - t^k\right) P(t)}{(1 - t^m)^{\dim(X)}}. \tag{6.1.23}$$

Now we can immediately get $a_0(\zeta + \eta \epsilon)$ and $a_1(\zeta + \eta \epsilon)$ as usual. Then the Futaki invariant directly follows from (6.1.16)~(6.1.18). If we use (6.1.16), the Hilbert series for $\zeta(\epsilon)$ reads

$$\text{HS}_{\zeta(\epsilon)} = \frac{\left(1 - t^{k(1 - a\epsilon)}\right) P\left(t^{(1 - a\epsilon)}\right)}{\left(1 - t^{k(1 - a\epsilon) + \epsilon \eta}\right) \left(1 - t^{m(1 - a\epsilon)}\right)^{\dim(X)}}. \tag{6.1.24}$$

One may also check that for complete intersections, this approach reduces to the usual method before. We will see an example validating this approach on complete intersections in §6.2.2.

---

[10]In fact, there are various conventions to define K-stability in various literature. In some texts dealing with Fano manifolds, the "K-stability" we are considering here would be called "K-polystability" which could be subtlely different. Here, we will adopt the convention so that the trivial test configurations arise from automorphisms will automatimatically have norm zero.

To determine the stability, usually we need to consider quite a few test symmmetries. By the linearity discussed in §6.1.3, it suffices to compute the test symmetries η_i with charge δ_{ij} for the jth generator. Any test symmetry and hence F can be written as a linear combination of η_i's (though crucially it still requires some work to figure out what kinds of linear combinations we want). In fact, we can use this to get Futaki invariants in a quicker way as follows.

Suppose we have a generator of order/charge k under ζ. Let us show that for the test symmetry with charge $(0, \ldots, 0, 1, 0, \ldots, 0)$, where only this generator of order k has a non-vanishing charge, the Futaki invariant would have a simple expression. As usual, the HS has coefficient a_i for the $s^{-(n-i)}$ term under expansion around $s = 0$. Then with the test symmetry, we have

$$
\begin{aligned}
\text{HS}_{\zeta+\epsilon\eta} &= \frac{\text{HS}_\zeta \times \left(1 - e^{-ks}\right)}{1 - e^{-(k+\epsilon)s}} \\
&= \frac{a_0 k}{(k+\epsilon)s^n} + \frac{k(\epsilon a_0 + 2a_1)}{2(k+\epsilon)s^{n-1}} + \ldots
\end{aligned}
\tag{6.1.25}
$$

Since $a_0 = a_1$, we have

$$
a_0(\zeta + \epsilon\eta) = \frac{a_0 k}{k+\epsilon}, \ \ a_1(\zeta + \epsilon\eta) = \frac{a_0 k(\epsilon + 2)}{2(k+\epsilon)}.
\tag{6.1.26}
$$

Now using (the second line in) (6.1.18), we get

$$
F = n\frac{\text{d}}{\text{d}\epsilon}\frac{a_0 k(\epsilon+2)}{2(k+\epsilon)} - (n-1)\frac{\text{d}}{\text{d}\epsilon}\frac{a_0 k}{k+\epsilon}\bigg|_{\epsilon=0} = \frac{nk-2}{2k}a_0.
\tag{6.1.27}
$$

Likewise, using (6.1.21),

$$
||\eta||^2 = \frac{(n-1)a_0}{n^2(n+1)k^2}.
\tag{6.1.28}
$$

Incidentally, we can find that

$$
a = \frac{1}{a_0}\left(\frac{\text{d}}{\text{d}\epsilon}\frac{a_0 k(\epsilon+2)}{2(k+\epsilon)} - \frac{\text{d}}{\text{d}\epsilon}\frac{a_0 k}{k+\epsilon}\right)\bigg|_{\epsilon=0} = \frac{1}{2}.
\tag{6.1.29}
$$

We can also write a general expression for general test symmetries. Suppose we have a test symmetry η with charge v_i for the ith generator which has order k_i, then

$$
a_0(\zeta + \epsilon\eta) = a_0 \prod_i \frac{k_i}{k_i + v_i\epsilon}, \ \ a_1(\zeta + \epsilon\eta) = a_0 \prod_i \frac{k_i(v_i\epsilon + 2)}{2(k_i + v_i\epsilon)},
\tag{6.1.30}
$$

and

$$
a = \frac{1}{a_0} \times \frac{a_0}{2}\sum_i v_i = \frac{1}{2}\sum_i v_i.
\tag{6.1.31}
$$

The Futaki invariant is

$$
F = \sum_i v_i \frac{nk_i - 2}{2k_i}a_0,
\tag{6.1.32}
$$

and the norm is

$$
||\eta||^2 = \begin{cases} 0, & I_0 \cong I_{t\neq0}; \\ \frac{(n-1)a_0}{n^2(n+1)}\left(\sum_i \frac{v_i^2}{k_i^2} - \frac{2}{n-1}\sum_{j<l}\frac{v_j v_l}{k_j k_l}\right), & \text{otherwise.} \end{cases}
\tag{6.1.33}
$$

As an example, consider the orbifold $\mathbb{C}^3/\mathbb{Z}_5$ (1,2,2) studied in [2, 25] with

$$
\text{HS} = \frac{1 - t^{2/3} + 3t^2 - t^{8/3} + 3t^{10/3} - t^{14/3} + t^{16/3}}{\left(1 - t^{2/3}\right)^3\left(1 + t^{2/3} + t^{4/3} + t^2 + t^{8/3}\right)^2}.
\tag{6.1.34}
$$

Under Laurent expansion around $s = 0$, we have $a_0 = a_1 = 27/40$. Notice that here the *fractional powers* in the HS is just a consequence of our convention $a_0 = a_1$. Hence, they do not have to equal the corresponding R-charges numerically.

The PL of HS reads

$$\text{PL(HS)} = 3t^2 + 2t^{8/3} + 7t^{10/3} - t^4 - \dots, \tag{6.1.35}$$

where we see that there are 3 generators of order 2, 2 generators of order 8/3 and 7 generators of order 10/3. Therefore, we can quickly get a general expression for Futaki invariant using (6.1.32):

$$F = \frac{27}{40}(v_1 + v_2 + v_3) + \frac{243}{320}(v_4 + v_5) + \frac{81}{100}(v_6 + \dots + v_{12}), \tag{6.1.36}$$

for test symmetry η with charges $(v_1, v_2, \dots, v_{12})$. However, notice that this example is just for a pure calculation purpose: the orbifold here is actually a toric variety. As briefly aforementioned, for any toric singularity, there is no non-trivial test configuration because the number of $\mathbb{C}^*$-actions is already maximal [89, 257], or in other words, it has complexity zero. As a result, we should always expect the rings to be stable. We can also think of the quiver gauge theories which stay in the toric phase. Hence, there is no fractional brane that would prevent our theory from being conformal. On the other hand, for non-toric cases, we still need to find appropriate test symmetries to determine the stability.

6.1.5 Test Symmetries

In practice, there could be a lot of possible test symmetries for us to consider. To guarantee stability, we need to exhaustively check all these Futaki invariants, which can be difficult. However, we could try to reduce the number of test symmetries we need to check. As argued in [257], for hypersurface singularities, especially for those with complexity one (i.e. having isometry $U(1)^{n-1}$) whose degeneration is toric, we can consider X as a fibration over some Riemann surface, with the torus action acting on the fibre. Then the integer slopes of some piecewise-linear functions would help us find the correct test symmetries we want. See [257, 258] for more details. In general, from the perspective of field theory by viewing X_t as a deformation of X_0, it is also conjectured in [259] that it should suffice to only consider the test configurations that remove one of the monomials for (isolated) hypersurface singularities.

For non-hypersurface singularities or even non-complete intersections, the above methods are not applicable (except that the toric varieties still have no non-trivial test configurations). First of all, we need to get the relations on which we can act with the one-parameter $\mathbb{C}^*$-subgroup and take the flat limit. This can again be found by taking the PL of HS, where the relations are given by the first negative terms, but we need the refined HS to get the exact relations. For instance, if we have [25]

$$\text{PL}\left(\frac{xy(1/q^2 - 1)}{(1-qx)(1-qy)(1-x/q)(1-y/q)}\right) = \frac{q}{x} + qx + \frac{q}{y} + qy - q^2, \tag{6.1.37}$$

where x, y, q are the fugacities. The defining equation is then given by $(q/x)(qx) = (q/y)(qy) = q^2$, viz, $uv = wz$, which is exactly the conifold.

As detailed in §6.1.2, we should take the Gröbner basis of the relations to avoid generating a set smaller than the flat limit. Now when taking a test configuration, we always have some action $\eta(t)$ acting on these equations[11]. Then we will only keep the term(s) with lowest weight in each equation under the flat limit. In principle, there could be infinitely many η's. However, there might be fewer cases due to the symmetries of the variables in the equation(s).

Moreover, as checking stability is equivalent to checking the positivity of Futaki invariants, and the sign of (6.1.32) is determined by v_i's, the v_i-space would be divided into different areas which

---

[11] Notice that for hypersurfaces, there is no need to find the Gröbner basis, and the coefficients in front of the terms in the equations do not matter.

correspond to positive or negative Futaki invariants (recall that if $F = 0$, we can check the norm). In the v_i-space, each choice of η would be a point which lies in certain positive or negative region. To determine stability, it is equivalent to checking whether there are any points in the negative regions.

For example, consider the Futaki invariant for the hypersurface $w^2 + x^2 + y^2 + z^{n+1} = 0$ and test symmetry η with charges (v_1, v_2, v_3, v_4). Its Futaki invariant is given in (6.2.2). It is often difficult to visualize the v_i-space, but here since the coordinates w, x, y are symmetric, we can solely consider v_1 and v_4 (i.e. two ways of dropping terms, although we can use some specific method to reduce the number of test symmetries in this case). We depict some v_1-v_4 planes for small n's in Figure 6.1.1. Indeed, we see that the ring is only stable for $n = 1, 2$ as there is no red point inside
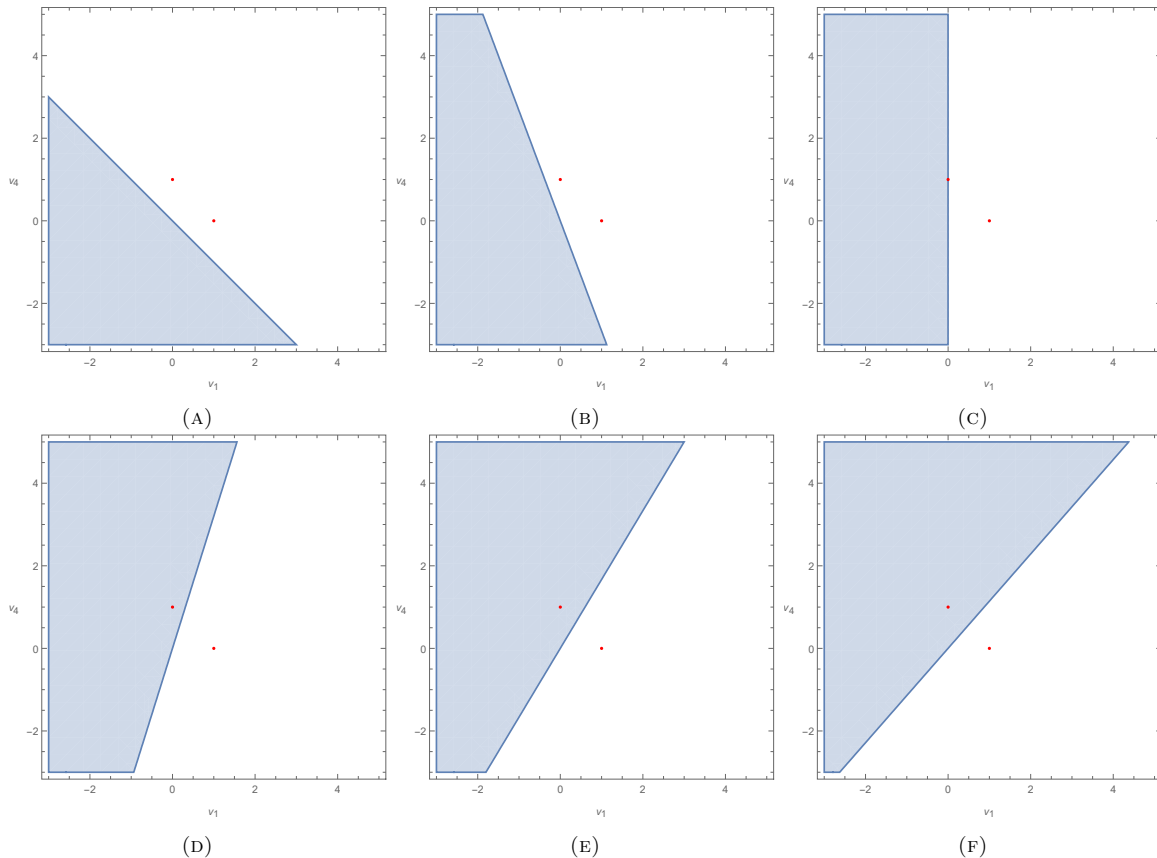
FIGURE 6.1.1: The region plot in v_i-space for $w^2 + x^2 + y^2 + z^{n+1} = 0$ at $n = 1, \ldots, 6$ shown in (a)∼(f) respectively. The red points correspond to the two test symmetries and the blue area is the region where $F < 0$ in each picture. A red point inside the blue region indicates that the ring is unstable.

the negative region which agrees with the result in [89]. We should be careful with $n = 3$ where a red point lives on the boundary of the blue region, showing that $F = 0$. The test configuration is certainly not trivial, and by computing the norm for this test symmetry with charges $(0,0,0,1)$, we get $||\eta||^2 = 27/128 \neq 0$. Hence, the ring is unstable for $n = 3$.

Some simplifications can be made to reduce the number of necessary test symmetries. In [89, 240], η is required to be normal and commuting with the automorphism group of X. For $X \subset \mathbb{C}^n$, the torus action and η are induced by the subgroups of $\mathrm{GL}(n, \mathbb{C})$. The commutation condition then implies that we can diagonlize the T- and $\mathbb{C}^*$-subgroups simultaneously. Hence, we will always assume that the test symmetries are diagonal under some unitary changes of basis. Normality could be boiled down to two conditions called Serre's criterion: S_2 and R_1. It is often not easy to check the former, but as we are always dealing with Cohen-Macaulay rings, S_2 is always guaranteed. Therefore, only R_1, namely being regular in codimension one, is left. This means that the singular locus has codimension no less than two, which can be checked via the Jacobian. We may also use `Macaulay2`

and the package `FastLinAlg` to tell this. In fact, we are also allowed to consider more general test configurations that are not normal or even those who have test symmetry not commuting with the T-action, but they will not give any additional information[12]. For simplicity, we will therefore not require the normality condition as this should not affect our results.

"Problematic" Test Symmetries Following the above procedure to compute the Futaki invariant, especially using (6.1.32), one can easily find some inconsistencies that seems to give "sick" test symmetries[13].

The non-zero norm problem The first problem is actually already resolved when defining the norm. Usually, a norm is defined only with the second line in (6.1.21), but we have to add the first line which makes the definition seemingly weird. For instance, for $\mathbb{C}^3 = \text{Cone}\left(S^5\right)$ (or more generally, $\mathbb{C}^n = \text{Cone}\left(S^{2n-1}\right)$), there would be no non-trivial test configurations as this is toric with a maximal number of torus action. Indeed, we always have a vanishing Futaki invariant. Its stability is for sure expected as physically this corresponds to the $\mathcal{N} = 4$ SYM in 4d which is superconformal. However, all the test symmetries, except the one with charge $(1, 1, 1)$, would yield non-zero norms. Another less "trivial" example is the conifold $uv + y^2 + z^2 = 0$ and the test symmetry with charges $(1, -1, 0, 0)$ (though we would not have this if we make a linear holomorphic change to $w^2 + x^2 + y^2 + z^2 = 0$), which leads to $F = 0$. Such test configuration is certainly trivial, but $(c_0 - b_0^2/a_0) = 1/3 \neq 0$. However, the conifold is undoubtedly stable as it admits a Ricci-flat cone metric.

The ϵ-region problem Recall that physically we are only focusing on the $\epsilon > 0$ region for $a_0(\zeta(\epsilon))$ to find whether there is a minimum because we want $\epsilon(\eta - a\zeta)$ to give the same central fibre as the test symmetry η does. However, if we consider $w^2 + x^2 + y^2 + z^5 = 0$ and η with $(-1, -1, -1, 0)$, we find that $(\eta - a\zeta)$ would give rise to $a = -3/2$ and weights $(8/7, 8/7, 8/7, 6/7)$, which has an opposite central fibre. This seems to indicate that we should look at the region with $\epsilon < 0$ in this case. Consequently, $F < 0$ here would not destabilize the ring. However, we know from Figure 6.1.1 and also §6.2.1 that $(0, 0, 0, 1)$, which has an equivalent test configuration as $(-1, -1, -1, 0)$, is the right test symmetry that destabilizes the ring. This becomes a bigger issue if we consider stable rings or even non-complete intersections. For instance, consider the orbifold $\mathbb{C}^3/(\mathbb{Z}_4 \times \mathbb{Z}_2)$ $(1, 0, 3)(0, 1, 1)$ whose relations are given in [105]:

$$x_1 x_3 = x_2^2, \ y_1 y_2 = x_3^2, \tag{6.1.38}$$

where x_1 has order $4/3$ and x_2 has order 2 with the remaining three having order $8/3$. Its Gröbner basis is

$$x_3^2 - y_1 y_2, \ x_1 y_1 y_2 - x_2^2 x_3, \ x_1 x_3 - x_2^2. \tag{6.1.39}$$

Since this is a toric variety, it should be K-stable. Let the test symmetry have charges $(0, 0, -1, 0, 0)$. Then the test configuration reads

$$t^{-2} x_3^2 - y_1 y_2, \ x_1 y_1 y_2 - t^{-1} x_2^2 x_3, \ t^{-1} x_1 x_3 - x_2^2. \tag{6.1.40}$$

However, with $a = -1/2$, $\epsilon(\eta - a\zeta)$ has charges $\epsilon(2/3, 1, 1/3, 4/3, 4/3)$. The test configuration is

$$t^{2\epsilon/3} x_3^2 - t^{8\epsilon/3} y_1 y_2, \ t^{10\epsilon/3} x_1 y_1 y_2 - t^{7\epsilon/3} x_2^2 x_3, \ t^{2\epsilon} x_1 x_3 - t^{2\epsilon} x_2^2. \tag{6.1.41}$$

Now, no matter what value ϵ takes, the two central fibres will never be the same. We do not even know which region of ϵ to consider.

---

[12]The condition of being normal is related to the triviality of the central fibre. It was discussed in [256] that normality could avoid some pathological test configurations. However, as pointed out in [252], we can instead use an alternative definition by introducing the norm whose vanishing is sufficient to give K-stability (when F is zero). Regarding the norm, there could also be different conventions as aforementioned, and here we take the definition as in (6.1.21).

[13]As we will see, these η's are not really "problematic" or "sick". We are just not using the correct way to do the computation.

The $F < 0$ problem   Even if a test symmetry does not cause the ϵ-region problem, the Futaki invariant we get could also be problematic. For example, let us consider the conifold $w^2 + x^2 + y^2 + z^2 = 0$ and the test symmetry with charges $(-1, -1, -1, 0)$. Now $a = -3/2$ and $(\eta - \epsilon\zeta)$ gives charges $(-5/2, -5/2, -5/2, -3/2)$. Therefore, we should still focus on the region of positive ϵ. Following (6.1.32), it is straightforward that $F = -3 < 0$. However, we already know that the conifold is stable. Under such construction, this contradiction can happen for any stable case. Another example is given in Figure 6.1.2(b).

In the next subsection, we will see a method to resolve this, but if we insist on the results from (6.1.32), we could physically understand the problem for a subset of these test symmetries. This can be explained if we contemplate the plots of $a_0(\zeta(\epsilon))$ against ϵ as in Figure 6.1.2. To destabilize
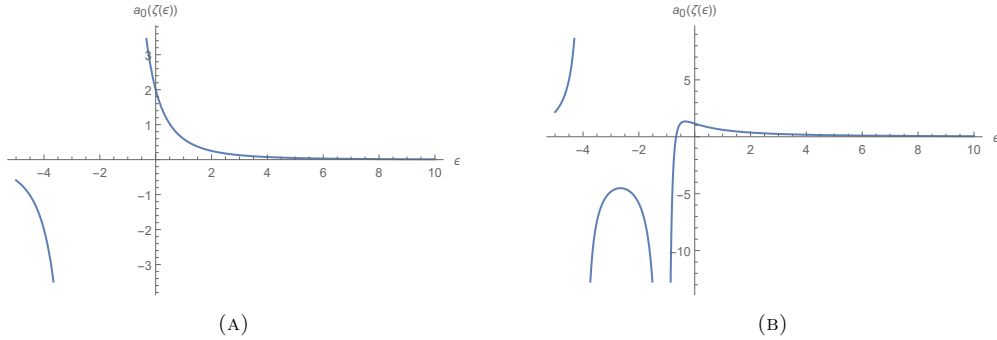
FIGURE 6.1.2: (a) The conifold $w^2 + x^2 + y^2 + z^2 = 0$ and η with charges $(0, -1, -1, -1)$, and $a_0(\zeta(\epsilon)) = \frac{16}{(\epsilon+2)^3}$. (b) The E_7 threefold $w^2 + x^2 + y^3 + yz^3 = 0$ and η with charges $(-1, -1, 0, -1)$, and $a_0(\zeta(\epsilon)) = \frac{750(3\epsilon+2)}{(\epsilon+4)(17\epsilon+18)^2}$.

the original ring, (the piece around some neighbourhood of $\epsilon = 0$ of) the curve should have a local minimum at some positive ϵ. However, the cases in Figure 6.1.2 do not have such local minima. In other words, $a_0(\zeta(\epsilon))$ keeps decreasing as $\epsilon \to \infty$, so if we consider the new R-symmetry parameterized by $\zeta(\epsilon) = \zeta + \epsilon(\eta - a\zeta)$, viz, $\zeta(\epsilon)/\epsilon = \zeta/\epsilon + (\eta - a\zeta)$ with $\epsilon \to \infty$, we would get $\eta = a\zeta$, which does not make sense. We should again emphasize that this could not account for all the "sick" η's. For example, if we consider the test symmetry with $(-1, -1, -1, 2)$ for the stable A_2 threefold $w^2 + x^2 + y^2 + z^3 = 0$, then $a_0(\zeta(\epsilon)) = \frac{375(\epsilon+2)}{16(3-\epsilon)^3(1+3\epsilon)}$. On the smooth piece around the neighbourhood of $\epsilon = 0$, it has a local minimum at $\epsilon = (5\sqrt{10} - 13)/9 > 0$.

Regularizations of Numerators   To find out what really goes wrong, it is always useful to start from the original definitions and derivations of K-stability. Recall that algebro-geometrically the Futaki invariant is defined as $F = B_0 A_1/A_0 - B_1$, where A_i's and B_i's are the leading and subleading coefficients of d_k and w_k respectively[14]. Therefore, we can compute A_i's and B_i's using their definitions and compare with the results from HS.

Let us again consider the conifold $w^2 + x^2 + y^2 + z^2 = 0$. For the usual test symmetry $\eta(t) \cdot (w, x, y, z) = (w, x, y, tz)$, the central fibre is $w^2 + x^2 + y^2 = 0$, and the HS gives

$$\text{HS} = \frac{1 - t^2}{(1 - t)^3 (1 - t^{1+\epsilon})} = \frac{2}{(1 + \epsilon)s^3} + \frac{2 + \epsilon}{(1 + \epsilon)s^2} + \dots \tag{6.1.42}$$

Taking $\epsilon = 0$, we have (in the convention of [160])

$$A_0(n - 1)! = 2A_0 = 2, \ A_1(n - 2)! = A_1 = 2. \tag{6.1.43}$$

Likewise,

$$B_0 = -\frac{1}{n}\mathrm{D}_\epsilon A_0(\epsilon)|_{\epsilon=0} = -\frac{1}{3}\mathrm{D}_\epsilon\left(\frac{1}{1+\epsilon}\right)\bigg|_{\epsilon=0} = \frac{1}{3},$$

---

[14]Since the a_i's have a different convention here, we will use capital letters for the traditional conventions in mathematics literature such as [160, 252] to distinguish them.

$$B_1 \;=\; -\frac{1}{n-1}\mathrm{D}_\epsilon A_1(\epsilon)|_{\epsilon=0} = -\frac{1}{2}\mathrm{D}_\epsilon \left(\frac{2+\epsilon}{1+\epsilon}\right)\Big|_{\epsilon=0} = \frac{1}{2}. \qquad (6.1.44)$$

By definition, the dimension of the degree k piece R_k of the ring is

$$d_k = \binom{k+3-1}{k} + \binom{k-1+3-1}{k-1} = k^2 + 2k + 1, \qquad (6.1.45)$$

where we have used that the number of independent monomials of degree k with m variables is $\binom{k+m-1}{k}$. In particular, the first term in (6.1.45) counts the number of independent monomials of the form $x^l y^m z^p$ with $l+m+p = k$, while the second term counts the monomials of the form $wx^l y^m z^p$ with $l+m+p = k-1$. Likewise, by definition, the total weight of R_k is

$$w_k = \sum_{i=0}^{k} \binom{k-i+2-1}{k-i} i + \sum_{i=0}^{k-1} \binom{k-i-1+2-1}{k-i-1} i = \frac{1}{3}k^3 + \frac{1}{2}k^2 + \frac{1}{6}k. \qquad (6.1.46)$$

Here, we see that the first term sums up the different choices for monomials weighted i of the form $x^l y^m z^i$ with $l+m = k-i$, while the second term sums for monomials of the form $wx^l y^m z^i$ with $l+m = k-i-1$. As we can see, the result from HS agrees with the one from definition for this test symmetry.

However, if we consider $\eta(t)\cdot(w,x,y,z) = \left(t^{-1}w, t^{-1}x, t^{-1}y, z\right)$, which yields $F < 0$, the A_i's remain the same while from

$$\mathrm{HS} = \frac{1-t^2}{(1-t)\left(1-t^{1-\epsilon}\right)^3} = -\frac{2}{(-1+\epsilon)^3 s^3} + \frac{-2+3\epsilon}{(-1+\epsilon)^3 s^2} + \dots, \qquad (6.1.47)$$

we get $B_0 = -1$ and $B_1 = -3/2$. On the other hand, by definition of w_k, $B_0 = -2/3$ and $B_1 = -3/2$. We see that the results are different.

Even for some non-negative F's, we would still have this issue. Consider the test symmetry $\eta(t)\cdot (w,x,y,z) = (tw,tx,ty,tz)$. Then from HS, we have

$$A_0 = 1, \;\; A_1 = 2, \;\; B_0 = \frac{4}{3}, \;\; B_1 = 2, \;\; F = \frac{2}{3}. \qquad (6.1.48)$$

In contrast, from definition, as w_k is simply kd_k here, we can easily get

$$A_0 = 1, \;\; A_1 = 2, \;\; B_0 = 1, \;\; B_1 = 2, \;\; F = 0. \qquad (6.1.49)$$

In fact, we expect the Futaki invariant to vanish for this test symmetry not only because this is the result from the computation using definition, but also because the test configuration $t^2\left(w^2 + x^2 + y^2 + z^2\right)$ is trivial.

One may wonder if this is a matter of convention. In other words, it might be possible that we have not found the right convention that makes all the parameters agree. After all, the precise values can differ by a positive numerical factor in different conventions. This possibility can be excluded by the example $xz - y^2 = 0$ with $\eta(t) \cdot (x,y,z) = \left(t^{-1}x, ty, z\right)$. The HS is

$$\mathrm{HS} = \frac{1-t^{2p}}{\left(1-t^{p+\epsilon}\right)\left(1-t^{p-\epsilon}\right)\left(1-t^p\right)}, \qquad (6.1.50)$$

where the convention is arbitrary with some power p. From this HS, we find that

$$B_0 = B_1 = 0. \qquad (6.1.51)$$

However, the correct answers are already obtained in [252] by definition:

$$B_0 = B_1 = \frac{1}{2}. \qquad (6.1.52)$$

Hence, no matter what positive constant we multiply, the two would never agree. This shows that the problem is from the steps in the HS method we use.

In [160], the index character is defined to be

$$G(\zeta) = \sum_{\alpha \in \mathfrak{t}^*} \mathrm{e}^{-s\alpha(\zeta)} \dim R_\alpha, \tag{6.1.53}$$

where $\mathfrak{t}$ is the Lie algebra of the torus action and R_α is the associated root space with root α in the root space decomposition of R. Since $\zeta \in \mathfrak{t}$ is a symmetry acting with positive weights, viz, a *Reeb vector field*, the sum converges for $\mathrm{Re}(s) > 0$ and has a meromorphic extension at $s = 0$. It is proven that the index character has a Laurent expansion

$$G = \frac{A_0(n-1)!}{s^n} + \frac{A_1(n-2)!}{s^{n-1}} + \ldots \tag{6.1.54}$$

at $s = 0$, which is exactly the HS. Similarly, to show that b_i's (and also c_0) are certain derivatives of a_i's, the weight character is defined to be

$$C_\eta = \sum_{\alpha \in \mathfrak{t}^*} \mathrm{e}^{-s\alpha(\zeta)}\alpha(\eta) \dim R_\alpha. \tag{6.1.55}$$

Then one can show that

$$-tC_\eta = \frac{\partial}{\partial \epsilon}G(\zeta + \epsilon\eta)\Big|_{\epsilon=0}. \tag{6.1.56}$$

Importantly, this expression is true because for sufficiently small ϵ, $(\zeta+\epsilon\eta)$ is a Reeb field, and hence the sum for $G(\zeta + \epsilon\eta)$ converges uniformly for $s > 0$. Therefore, since the Reeb field determines the weights of the relations and the information of these relations are contained in the numerator of HS, we should modify the HS with ϵ. In other words, we should also write the numerator with respect to the Reeb field $(\zeta + \epsilon\eta)$, rather than just ζ.

When we write HS, we still need to consider $(\zeta + \epsilon\eta)$ as two degrees for the grading: one variable t_0 for ζ and one variable t_1 for η. Only after this step, we can assign small ϵ to the powers of t_1. However, in the first step, η in fact is not a Reeb field and it would make the equations in the ideal inhomogenous. Therefore, we cannot simply write down the HS. One may try some homogenization of the equations, but it would not yield correct results for K-stability.

Here, we discuss a method to modify the numerator with the help of Gröbner basis[15]. As discussed in Appendix J.0.1, when writing HS, it suffices to consider the initial terms of the equations in the Gröbner basis. In particular, the initial terms are obtained from some ordering of the variables, and likewise, the initial terms for the flat limit are also obtained from a specific ordering, that is, the (lowest) powers/weights of t in the relations[16].

Therefore, to write the HS with respect to $(\zeta + \epsilon\eta)$, especially the t_1 for η, we also take the initial terms induced by the same ordering when taking flat limits. If the initial term has a factor t^p (regardless of the sign of p), then we should include the corresponding power of t_1 in the numerator. If the initial term has no t, then the numerator is free of t_1. In particular, the power of t_1 is determined by the power of initial terms of the ideal.

For instance, for the conifold example above, $(0, 0, 0, 1)$ would still give the same HS as in (6.1.42). For $(-1, -1, -1, 0)$, the initial term would have t^{-1}, and therefore we should add some power of ϵ

---

[15]To the authors' best knowledge, such method has never been mentioned in literature. Modifying the numerators might be known to mathematics society, but mathematicians mainly focus on the aforementioned complexity one varieties (such as those in §6.2.1 below), where one only needs to check several test symmetries using the method in [258]. It turns out that the remaining possible test symmetries are simple enough so that no modifications of numerators are required. The authors also consulted some mathematicians, but modifying the numerators was never mentioned. Therefore, it is worth spelling out such method here.

[16]We are using t both in the HS and in the test configuration, but it should be clear which t we are referring to in the context.

in the numerator. We see that the ideal of conifold is quadratic, so we add a factor of $t_1^{-2\epsilon}$ to the numerator. Let t_0 and t_1 denote the variables for ζ and $\epsilon\eta$ respectively. The multivariate (refined) HS reads

$$\text{HS} = \frac{1 - t_0^2 t_1^{-2\epsilon}}{(1 - t_0)\left(1 - t_0 t_1^{-\epsilon}\right)^3}. \tag{6.1.57}$$

Unrefining the HS by $t_0 = t_1 = t$, we get

$$\text{HS} = \frac{1 - t^{2(1-\epsilon)}}{(1 - t)\left(1 - t^{1-\epsilon}\right)^3}. \tag{6.1.58}$$

From this HS, following the usual steps of taking Laurent series and derivatives, we find that

$$A_0 = 1, \; A_1 = 2, \; B_0 = -\frac{2}{3}, \; B_1 = -\frac{3}{2}, \tag{6.1.59}$$

which is exactly the same result obtained from definition. Indeed, this yields $F = 1/6 > 0$, which equals to the Futaki invariant for $(0, 0, 0, 1)$. This agrees with the fact that the two test symmetries give rise to equivalent test configurations[17].

We may also check that for $(1, 1, 1, 0)$,

$$\text{HS} = \frac{1 - t^2}{(1 - t)\left(1 - t^{1+\epsilon}\right)^3} \tag{6.1.60}$$

since the initial term is z^2 which has weight t^0, and that for $(0, 0, 0, -1)$,

$$\text{HS} = \frac{1 - t^{2(1-\epsilon)}}{\left(1 - t^{1-\epsilon}\right)(1 - t)^3} \tag{6.1.61}$$

since the initial term is $t^{-2}z^2$. Again, we can verify that both of them yield the same correct A_i's and B_i's as those from definition, as well as a positive Futaki invariant. Likewise, one can also check that the $xz - y^2$ example gives the correct $B_0 = B_1 = 1/2$.

We can also verify that by modifying the numerators, for the aforementioned problems, we would not have the ϵ-region issue or negative F for stable rings any more. We will omit the detailed calculations here. Nevertheless, it is worth noting that some trivial test configurations will thence automatically have $F = 0$ and even a vanishing norm. Recall that without the modification of numerators, $(1, 1, 1, 1)$ yields a positive F, as well as a non-zero norm. After regularizing the numerator,

$$\text{HS} = \frac{1 - t^{2(1+\epsilon)}}{\left(1 - t^{1+\epsilon}\right)^4}. \tag{6.1.62}$$

This gives the correct $A_0 = B_0 = C_0 = 1$ and $A_1 = B_1 = 2$. Thus, $F = A_1 B_0 / A_0 - B_1 = 0$ and $||\eta||^2 = C_0 - B_0^2 / A_0 = 0$ as expected.

However, we still need the first line in the definition (6.1.21) of the norm. For example, when we write the conifold as $uv = xy$, and consider $(1, -1, 0, 0)$, the numerator still remains the same. Hence, $C_0 - B_0^2 / A_0$ is still not zero. However, such test symmetry is a bit special and we can still force the norm to vanish via definition. Incidentally, we find that if the HS is written as

$$\text{HS} = \frac{1 - t^{2\left(1-\epsilon^2\right)}}{\left(1 - t^{1-\epsilon}\right)\left(1 - t^{1+\epsilon}\right)(1 - t)^2}, \tag{6.1.63}$$

then $C_0 - B_0^2 / A_0 = 0$. Similarly, for $(1, -1, 1, -1)$, if we write the HS as

$$\text{HS} = \frac{1 - t^{2\left(1-\epsilon^2\right)}}{\left(1 - t^{1-\epsilon}\right)^2\left(1 - t^{1+\epsilon}\right)^2}, \tag{6.1.64}$$

---

[17]Notice that in our convention where $a_0 = a_1$, the value of Futaki invariant has an extra dimensional factor $n(n-1)$. For example, here we have $a_1 b_0 / a_0 - a_1 = 3 \times (3 - 1) \times 1/6 = 1$.

then $C_0 - B_0^2/A_0 = 0$ as well. So far it is still not clear why this happens. It might be possible that it requires higher order of corrections in the numerator for such special test symmetries, or maybe this is just a coincidence.

Now in our convention with a_i and b_i, although they take values different from those obtained by definition. They would always differ by a positive constant depending only on dimension, viz,

$$\frac{a_1}{a_0} b_0 - b_1 = n(n-1) \left(\frac{A_1}{A_0} B_0 - B_1 \right). \tag{6.1.65}$$

The norms (squared) agree up to the same positive constant as well. Therefore, this method can certainly be applied in any convention.

The Rescaling Method   We now have seen how to write the HS and get the Futaki invariants correctly by some modifications in the numerators. However, in principle, there could be a large number of possible test symmetries to determine K-stability and such method does not reduce this number. Here, by considering the central fibres, we propose a method that potentially simplifies the process of checking test symmetries.

In general, if the test symmetry has charge $(v_1, \ldots, v_m)$, then the test configuration for $I = \langle f_1, \ldots, f_l \rangle$ is generated by $f_1(t^{v_1}x_1, \ldots, t^{v_m}x_m), \ldots, f_l(t^{v_1}x_1, \ldots, t^{v_m}x_m)$. When taking the flat limit, only the initial terms would survive as discussed in §6.1.2. Another way to view the flat limit is by considering a rescaling of the f_i's [253]. Under the rescaling, we write $g_1 = t^{w_1}f_1(t^{v_1}x_1, \ldots, t^{v_m}x_m), \ldots, g_l = t^{w_l}f_l(t^{v_1}x_1, \ldots, t^{v_m}x_m)$ such that the initial terms in each f_i has weight zero with respect to t. Then at $t = 1$, we recover $I = \langle g_1, \ldots, g_l \rangle|_{t=1}$, and at $t = 0$, we recover the flat limit $I_0 = \langle g_1, \ldots, g_l \rangle|_{t=0}$. For example, $(0, -1, -1, -1)$, which has $F < 0$ by (6.1.32) without regularizing the numerator, gives $f = w^2 + t^{-2}x^2 + t^{-2}y^2 + t^{-2}z^2$ for the conifold, and we can rescale it to $g = t^2 f = t^2 w^2 + x^2 + y^2 + z^2$. It is worth noting that this g is what we get directly from $(1, 0, 0, 0)$ without rescaling. We may also consider $(-1, -1, -1, -1)$ which gives negative Futaki invariant if we naively use (6.1.32) to do the calculation. However, $t^{-2}w^2 + t^{-2}x^2 + t^{-2}y^2 + t^{-2}z^2$ is simply a trivial test configuration and can be rescaled to $w^2 + x^2 + y^2 + z^2$. Indeed, we would just get the trivial $\eta' = 0$.

Inspired by this, suppose we pick a test symmetry η with a random charge, then we may follow these steps to only compute F for η':

- We rescale the f_i's to g_i's such that the terms with lowest t-weights would have weight 0. This would lead to some new test symmetry η' that directly yields g_i's without any rescaling. Since all the initial terms have no t's and no regularization in the numerator is required, we can simply use (6.1.32) to compute the Futaki invariant.

- When dealing with non-hypersurfaces, it is possible to have some η whose rescaling (though we can always do such rescaling) does not correpsond to any η'. In other words, such configuration cannot have a test symmetry with all the initial terms having weight 0 for all the equations. In this case, we should find a "minimal" η' in the sense that the number of $g_i's$ with non-zero lowest weights is minimized. Moreover, these non-zero lowest weights should be positive. In this situation, there is at least one initial term having a positive t-weight. Therefore, we should apply the modification of the numerator to compute F.

At the first step, we have already seen such examples as those for the conifold. It is easy to check that this also works for positive Futaki invariants. For instance, $(1, 1, 1, 1)$ for the conifold can be rescaled to $(0, 0, 0, 0)$ as well, both of which have trivial test configuration. Moreover, for those like $(1, -1, 0, 0)$ for $uv = xy$ which does not receive regularization in the numerator but with $c_0 - b_0^2/a_0 \neq 0$, we can also rescale it to the trivial test configuration. Let us now contemplate some less non-trivial example whose K-stability is known to validate this. Consider the aforementioned orbifold $\mathbb{C}^3/(\mathbb{Z}_4 \times \mathbb{Z}_2)$ $(1,0,3)(0,1,1)$ with η-charges $(1, 1/2, -1/2, -1, 0)$ whose test configuration is

$$t^{-1}x_3^2 - t^{-1}y_1y_2, \; x_1y_1y_2 - t^{1/2}x_2^2x_3, \; t^{1/2}x_1x_3 - tx_2^2, \tag{6.1.66}$$

which should be rescaled according to the above steps. Indeed, a naive computation for this yields a negative F. Then the test configuration can be written as

$$x_3^2 - y_1 y_2, \ x_1 y_1 y_2 - t^2 x_2^2 x_3, \ x_1 x_3 - t^2 x_2^2 \tag{6.1.67}$$

with η' giving charges $(0, 1, 0, 0, 0)$. We can then simply apply (6.1.32) which yields a positive F.

For the second step, let us consider the same orbifold with test charges $(0, -1, 0, -1, -1)$ whose test configuration is

$$x_3^2 - t^{-2} y_1 y_2, \ t^{-2} x_1 y_1 y_2 - t^{-2} x_2^2 x_3, \ x_1 x_3 - t^{-2} x_2^2. \tag{6.1.68}$$

Under the rescaling, the test configuration can be written as

$$t^2 x_3^2 - y_1 y_2, \ t x_1 y_1 y_2 - t x_2^2 x_3, \ t^2 x_1 x_3 - x_2^2 \tag{6.1.69}$$

with η' giving charges $(1, 0, 1, 0, 0)$. Note that we can not simply rescale every relation in the ideal such that the initial term has weight 0 in t. For example, the first and third relations in (6.1.68) show that x_3 should have non-trivial weight and x_2 should have weight 0. This then fixes the form of the second relation to be that shown in (6.1.69). It turns out that for η'

$$\mathrm{HS} = \frac{1 - t^4 - t^{16/3} + t^{28/3}}{\left(1 - t^{4/3+\epsilon}\right)\left(1 - t^2\right)\left(1 - t^{8/3+\epsilon}\right)\left(1 - t^{8/3}\right)^2}, \tag{6.1.70}$$

where it has no ϵ's in the numerator, and we can therefore use (6.1.32) to get $F > 0$. However, as we will see later, in general there could be modifications in the numerator for η' in the second step.

It is also possible that for η_1 and η_2 with different η_1' and η_2' have the same central fibre, but they are not related by a simple rescaling. For hypersurfaces, these are often equivalent as $\eta_2' = s\eta_1'$ for $s > 0$ such as $(1, 0, 0, 0)$ and $(2, 0, 0, 0)$ for the aforementioned conifold example. Therefore, it suffices to consider only one of them. More generally, including non-hypersurfaces, it would be natural to speculate that η_1' and η_2' also give the same result as they lead to the same central fibre. Suppose we have m monomials in all the equations, then there would be at most $(2^m - 2)$ ways to drop terms (excluding dropping all terms or dropping no terms). This gives finitely many test symmetries although the number increases drastically when m increases and this does not tell us the exact (minimal) number of test symmetries or exactly which test symmetries we need to check (compared to complexity one varieties in [258]). The above steps are based on the following point, which is yet to manifest. Using rescaling, we are actually choosing a representative for each central fibre, so either the representative test symmetry should be able to correctly indicate whether the variety can be destabilized to the central fibre, or maybe every test symmetry with the same central fibre should give the same sign of F.

In fact, a consequence of such rescaling is that there are only two ways to get a negative F. One possibility is that the ζ-weight k of a generator is small enough so that $nk - 2 < 0$ in (6.1.32), such as the A-type threefolds in §6.2.1 below. The other possibility is that we have some negative weight in η, but this negative power of t gets cancelled by other positive powers in the monomials in the relations. Then if the generator with this negative η-weight has a large enough k, the Futaki invariant could become negative. Such example includes the D-type threefolds in §6.2.1 below.

These two ways of destabilizing the chiral ring should have explanations in terms of the dynamics of physics. The first way could be caused by the violation of unitarity bound. In particular, if a generator violates the unitarity bound, we would have $k < 2/3$, which is exactly $3k - 2 < 0$ from (6.1.32) for a three dimensional moduli space, such as the case for D3-branes probing CY_3. For higher dimensional moduli spaces, as we will see in §F.1, the orders k are not necessarily equal to R-charges numerically in the convention of $a_0 = a_1$, and more importantly, it could be possible that (violation of) the unitarity bound "leaks" out of the $nk - 2 < 0$ region. For the first way, being unstable could also be caused by irrelevance of superpotential terms or some unknown dynamical reasons. For the second way, as shown in [89], there could also be some unknown dynamical effects to prevent the ring from being a ring for an SCFT, such as the D-type threefolds.

6.2 Illustrative Examples

Now let us contemplate various examples to illustrate the above discussion. We will see (6.1.32) and the modification of numerator applied to different cases including non-complete intersections, and also how the rescaling method might reduce the number of possible test symmetries for equations whose variables have certain symmetries.

6.2.1 ADE Threefolds

The Kleinian singularities can be obtained by orbifolding $\mathbb{C}^2$ with some subgroups Γ of $SU(2)$, which are related to (affine) ADE Dynkin diagrams by McKay correspondence [260]. We may require $a_0 = a_1$ so that the canonical (2,0)-form has charge 2. However, they should always be stable as there would be no normal central fibres (and non-normal ones would not give any extra information). Hence, we can lift the ADE singularities to "ADE threefolds" [257] by adding another squared term of a new coordinate to the defining equation[18]. As one may check, the stabilities should be consistent with the results in [240, 257].

Cyclic group $\mathbb{Z}_{n+1}$: $\hat{A}_n$ The defining equation is $w^2 + x^2 + y^2 + z^{n+1} = 0$. This belongs to the family of Brieskorn-Pham (BP) singularity, also known as the Yau-Yu singularity of type I (YY-I) [160]. This ring X has a symmetry ζ with charges $\left(\frac{2n+2}{n+3}, \frac{2n+2}{n+3}, \frac{2n+2}{n+3}, \frac{4}{n+3}\right)$. Hence, we write the HS as

$$\text{HS} = \frac{1 - t^{(4n+4)/(n+3)}}{\left(1 - t^{4/(n+3)}\right)\left(1 - t^{(2n+2)/(n+3)}\right)^3}. \tag{6.2.1}$$

Under Laurent expansion around $s = 0$, we obtain $a_0(\zeta) = a_1(\zeta) = \frac{(n+3)^3}{8(n+1)^2}$. By (6.1.32),

$$F = (v_1 + v_2 + v_3)\frac{n(n+3)^3}{8(n+1)^3} + v_4\frac{(3-n)(n+3)^3}{32(n+1)^2} \tag{6.2.2}$$

for test symmetry with charges (v_1, v_2, v_3, v_4). It suffices to check the test symmetries η_i with charge δ_{ij} on the jth coordinate. In particular, $(0,0,0,1)$ gives us the non-trivial result: $0 < n < 3$ [19] for K-stability.

Dicyclic group Dic_{n-1}: $\hat{D}_{n+1}$ ($n \geq 3$) The defining equation is $w^2 + x^2 + y^2z + z^n = 0$. This belongs to the singularity of type YY-II. The ring X has a symmetry ζ with charges $\left(\frac{2n}{n+1}, \frac{2n}{n+1}, \frac{2n-2}{n+1}, \frac{4}{n+1}\right)$. Hence, we write the HS as

$$\text{HS} = \frac{1 - t^{4n/(n+1)}}{\left(1 - t^{4/(n+1)}\right)\left(1 - t^{(2n-2)/(n+1)}\right)\left(1 - t^{2n/(n+1)}\right)^2}. \tag{6.2.3}$$

Under Laurent expansion around $s = 0$, we obtain $a_0(\zeta) = a_1(\zeta) = \frac{(n+1)^3}{8n(n-1)}$. By (6.1.32),

$$F = (v_1 + v_2)\frac{(n+1)^3(2n-1)}{16n^2(n-1)} + v_3\frac{(n+1)^3(n-2)}{8n(n-1)^2} + v_4\frac{(n+1)^3(5-n)}{32n(n-1)} \tag{6.2.4}$$

for test symmetry with charges (v_1, v_2, v_3, v_4). It suffices to check test symmetries $(0, 0, -1/2, 1)$, which yields

$$F = -\frac{(n+1)^3(n-2)}{16n(n-1)^2} + \frac{(n+1)^3(5-n)}{32n(n-1)} = -\frac{(n+1)^3(n^2 - 4n + 1)}{32n(n-1)^2}. \tag{6.2.5}$$

---

[18]Note that these ADE threefolds are not to be confused with $\mathbb{C} \times \mathbb{C}^2/\Gamma$ which are extensively used in D-brane quiver gauge theories, whose chiral rings are all stable.

[19]As aforementioned in Figure 6.1.1, when $n = 3$, the Futaki invariant is zero, but it is unstable since $||\eta|| \neq 0$. Also, if the v_i's are complicated, we should modify the numerator to get the correct Futaki invariant rather than directly apply (6.1.32). However, for hypersurfaces, they can all be rescaled such that the lowest t-weights are 0 in the equation. We will not restate these two points for similar situations below.

In addition, for test symmetries $(1, 0, 0, 0)$ and $(0, 0, 1, 0)$, we see that $F > 0$ for $n > 3$. Hence, the ring is stable when $n^2 - 4n + 1 < 0$. Therefore, only the ring of $\hat{D}_4$ with $n = 3$ is stable.

Binary tetrahedral/icosahedral group $\mathbb{BT}, \mathbb{BI}$: $\hat{E}_{6,8}$ The defining equation is $w^2 + x^2 + y^3 + z^n = 0$, where $n = 4$ for $\mathbb{BT}$ and $n = 5$ for $\mathbb{BI}$. This belongs to the singularity of type YY-I. The ring has a symmetry ζ with charges $\left(\frac{3n}{3+n}, \frac{3n}{3+n}, \frac{2n}{3+n}, \frac{6}{3+n} \right)$. Hence, we write the HS as

$$\text{HS} = \frac{1 - t^{6n/(3+n)}}{\left(1 - t^{3n/(3+n)}\right)^2 \left(1 - t^{2n/(3+n)}\right) \left(1 - t^{6/(3+n)}\right)}. \tag{6.2.6}$$

Under Laurent expansion around $s = 0$, we obtain $a_0(\zeta) = a_1(\zeta) = \frac{(n+3)^3}{18n^2}$. By (6.1.32),

$$F = (v_1 + v_2)\frac{(n + 3)^3(7n - 6)}{108n^3} + v_3\frac{(n + 3)^3(2n - 3)}{36n^3} + v_4\frac{(n + 3)^3(6 - n)}{108n^2} \tag{6.2.7}$$

for test symmetry with charges (v_1, v_2, v_3, v_4). It suffices to check test symmetry $(0, 0, 0, 1)$, and hence the ring is stable when $2 \le n < 6$, in particular for $n = 4, 5$ here. For other test symmetries, $(1, 0, 0, 0)$ and $(0, 0, 1, 0)$, we see that $F > 0$ since $n \ge 2$.

Binary octahedral group $\mathbb{BO}$: $\hat{E}_7$ The defining equation is $w^2 + x^2 + y^3 + yz^3 = 0$. This belongs to the singularity of type YY-II. The ring has a symmetry ζ with charges $\left(\frac{9}{5}, \frac{9}{5}, \frac{6}{5}, \frac{4}{5}\right)$. Hence, we write the HS as

$$\text{HS} = \frac{1 - t^{18/5}}{\left(1 - t^{9/5}\right)^2 \left(1 - t^{6/5}\right) \left(1 - t^{4/5}\right)}. \tag{6.2.8}$$

Under Laurent expansion around $s = 0$, we obtain $a_0(\zeta) = a_1(\zeta) = \frac{125}{108}$. By (6.1.32),

$$F = \frac{2155}{1944}(v_1 + v_2) + \frac{125}{162}v_3 + \frac{125}{432}v_4 \tag{6.2.9}$$

for test symmetry with charges (v_1, v_2, v_3, v_4). It suffices to check test symmetries $(1, 0, 0, 0)$, $(0, 0, 1, -1/3)$ and $(0, 0, 0, 1)$, and hence the ring is stable. In [257], it was shown that the E_7 threefold does not admit a *non-commutative crepant resolution* (NCCR). Therefore, it is still possible to be an SCFT, but it could not have a string embedding. In other words, in light of Conjecture 6.1.1, this could be an SCFT without a D-brane system picture[20].

6.2.2   del Pezzo Spaces

Let us consider the del Pezzo family dP_n where $0 \le n \le 8$. The HS is [25]

$$\text{HS} = \frac{1 + (7 - n)t^2 + t^4}{(1 - t^2)^3}. \tag{6.2.10}$$

Under Laurent expansion around $s = 0$, we obtain $a_0(\zeta) = a_1(\zeta) = (9 - n)/8$. Notice that the singularities are toric for $n = 0, \ldots, 3$. Therefore, these four rings are all stable as the symmetries are already maximal, and we will now only focus on $n \ge 4$.

Case 1: dP$_4$ The PL of HS reads

$$\text{PL(HS)} = 6t^2 - 5t^4 + 5t^6 - \ldots . \tag{6.2.11}$$

There are 6 generators satifying 5 relations which can be written as [261]

$$x_2x_6 - x_3x_5 + x_4^2, \; x_2x_5 - x_3x_4 - x_6^2, \; x_1x_6 + x_2x_4 - x_3^2 - 2x_5x_6,$$

---

[20]It is also suggested that this could be a non-Lagrangian theory.

$$x_1x_5 - x_2x_3 + x_4x_6 - 2x_5^2, \ x_1x_4 - x_2^2 + x_3x_6 - 2x_4x_5. \tag{6.2.12}$$

It turns out that the Gröbner basis consists of 6 equations:

$$x_4^2x_5 - x_3x_5^2 + x_3x_4x_6 + x_6^3, \ x_4^2 - x_3x_5 + x_2x_6, \ x_1x_4 - x_2^2 - 2x_4x_5 + x_3x_6,$$
$$x_2x_4 + x_1x_6 - x_3^2 - 2x_5x_6, \ x_1x_5 - x_2x_3 - 2x_5^2 + x_4x_6, \ x_2x_5 - x_3x_4 - x_6^2. \tag{6.2.13}$$

Let us first consider η's that can be rescaled to some η' that simultaneously make the initial terms to have t-weight zero. Then by (6.1.32),

$$\frac{8}{5}F = (v_1 + v_2 + v_3 + v_4 + v_5 + v_6)\frac{3 \times 2 - 2}{2 \times 2} = v_1 + v_2 + v_3 + v_4 + v_5 + v_6 \tag{6.2.14}$$

(where we have put a_0 on the left hand side). From the Gröbner basis, we see that there are monomials of various powers solely containing one x_i without mixing for all $i \neq 1$, so we only need to consider whether there is a test symmetry with charges $(-1, \dots)$ that destabilizes the ring in terms of the rescaling method. However, it has to be compensated by positive charges from more generators in the 6 equations as there are several mixing terms of form $x_1^p x_{i \neq 1}^q$ and they all have $p = q = 1$. Alternatively, as it is sufficient to find one instance giving negative F to destabilize the ring, we can also solve a system of inequalities: $2v_4 + v_5 \geq 0$, $v_3 + 2v_5 \geq 0, \dots$, together with $F \leq 0$. It turns out there is no solution except $x_i = 0$ to the inequalities[21].

As an example, for the test symmetry η with charges $(0, -1, -1, -1, -1, -1)$ (which would certainly lead to negative Futaki invariant if we do not modify the numerator or rescale it), the central fibre is

$$x_4^2x_5 - x_3x_5^2 + x_3x_4x_6 + x_6^3, \ x_4^2 - x_3x_5 + x_2x_6, \ -x_2^2 - 2x_4x_5 + x_3x_6,$$
$$x_2x_4 + x_1x_6 - x_3^2 - 2x_5x_6, \ -x_2x_3 - 2x_5^2 + x_4x_6, \ x_2x_5 - x_3x_4 - x_6^2. \tag{6.2.15}$$

Consider $(\zeta + \epsilon\eta)$ as a Reeb field for small ϵ, then the HS for (6.2.12) (or equivalently (6.2.13)) is

$$\text{HS} = \frac{1 - 5t^{4-2\epsilon} + 5t^{6-3\epsilon} - t^{10-5\epsilon}}{(1 - t^{2-\epsilon})^5 (1 - t^2)}. \tag{6.2.16}$$

We find $a_0(\zeta) = a_1(\zeta) = \frac{5}{2(\epsilon-2)^2}$. Thus, in our convention,

$$F = n\text{D}_\epsilon a_1(\zeta + \epsilon\eta) - (n - 1)\text{D}_\epsilon a_0(\zeta + \epsilon\eta)|_{\epsilon=0} = \frac{5}{8}, \tag{6.2.17}$$

which is positive as expected. More importantly, if we consider the test symmetry with $(1, 0, 0, 0, 0)$, this is the rescaled η' we get from the above η with equivalent test configuration. It does not receive any modifications in the numerator. Hence, we can use (6.2.14) to compute the Futaki invariant, and indeed we get the same result $F = 5/8$.

For η's that cannot give zero t-weights to all the initial terms after rescaling, it is exhaustive to check all the cases. However, according to [262], we expect this ring to be stable.

Case 2: dP$_5$ The PL of HS reads

$$\text{PL(HS)} = 5t^2 - 2t^4 \ ; \tag{6.2.18}$$

the termination of the PL says that dP$_5$ is a complete intersection and it indeed is: the base Fano surface is a well-known degree 4 double-quadric in $\mathbb{P}^4$. There are 5 generators satifying 2 relations which following theorem 115 in [263] can be written as

$$\sum_{i=1}^{5} x_i^2 = \sum_{i=1}^{5} a_i x_i^2 = 0 \tag{6.2.19}$$

---

[21]Notice this is a necessary but not sufficient condition for all the initial terms having a vanishing t-weight, but as it has no solutions, this certainly shows that there is no such η' destabilizing the ring.

in $\mathbb{P}^4_\mathbb{C}$, where $a_i \neq a_j$ for $i \neq j$ and the subscript "$\mathbb{C}$" is explicit here just to emphasize that the field is algebraically closed as required by the theorem. By (6.1.32),

$$2F = (v_1 + v_2 + v_3 + v_4 + v_5)\frac{3 \times 2 - 2}{2 \times 2} = v_1 + v_2 + v_3 + v_4 + v_5. \tag{6.2.20}$$

It suffices to check the test symmetry with charges $(1,0,0,0,0)$ due to the fact that all generators are symmetric within the relation. This symmetry indeed gives $F > 0$. Hence, the ring is stable for $n = 5$.

Case 3: dP$_6$ The PL of HS reads

$$\mathrm{PL(HS)} = 4t^2 - t^6. \tag{6.2.21}$$

Again, this is a complete intersection: it is famous cubic surface in $\mathbb{P}^3$ with the 27 lines (in the PL, we have $-t^6$ because the generators are weighted by 2). There are 4 generators satisfying 1 relation which can be written as

$$x_1^3 + x_2^3 + x_3^3 + x_4^3 = 0. \tag{6.2.22}$$

By (6.1.32),

$$\frac{8}{3}F = (v_1 + v_2 + v_3 + v_4)\frac{3 \times 2 - 2}{2 \times 2} = v_1 + v_2 + v_3 + v_4. \tag{6.2.23}$$

It suffices to check the test symmetry with charges $(1,0,0,0,0)$ due to the fact that all generators are symmetric within the relation. This symmetry indeed gives $F > 0$. Hence, the ring is stable for $n = 6$.

Case 4: dP$_7$ The PL of HS reads

$$\mathrm{PL(HS)} = 3t^2 + t^4 - t^8. \tag{6.2.24}$$

There are 4 generators satifying 1 relation which can be written as

$$x_1^4 + x_2^4 + x_3^4 + x_4^2 = 0. \tag{6.2.25}$$

By (6.1.32),

$$4F = (v_1 + v_2 + v_3)\frac{3 \times 2 - 2}{2 \times 2} + v_4\frac{3 \times 4 - 2}{2 \times 4} = v_1 + v_2 + v_3 + \frac{5}{4}v_4. \tag{6.2.26}$$

It suffices to check the test symmetries with charges $(1,0,0,0)$ and $(0,0,0,1)$ which both give $F > 0$. Note here the generators x_1, x_2 and x_3 are symmetric in the relation. Hence, the ring is stable for $n = 7$.

Case 5: dP$_8$ The PL of HS reads

$$\mathrm{PL(HS)} = 2t^2 + t^4 + t^6 - t^{12}. \tag{6.2.27}$$

There are 4 generators satifying 1 relation which can be written as

$$x_1^6 + x_2^6 + x_3^3 + x_4^2 = 0. \tag{6.2.28}$$

By (6.1.32),

$$8F = (v_1 + v_2)\frac{3 \times 2 - 2}{2 \times 2} + v_3\frac{3 \times 4 - 2}{2 \times 4} + v_4\frac{3 \times 6 - 2}{2 \times 6} = v_1 + v_2 + \frac{5}{4}v_3 + \frac{4}{3}v_4. \tag{6.2.29}$$

It suffices to check the test symmetries with charges $(1,0,0,0)$, $(0,0,1,0)$ and $(0,0,0,1)$ which all give $F > 0$. Note here the generators x_1 and x_2 are symmetric in the relation. Hence, the ring is stable for $n = 8$.

As we can see, not all of the dPs are non-complete intersections (in fact, only dP_4 is a non-complete intersection). For instance, dP_8 is a complete intersection with

$$\mathrm{HS} = \frac{1 - t^{12}}{(1 - t^2)^2 \left(1 - t^4\right)\left(1 - t^6\right)}. \tag{6.2.30}$$

Therefore, we can also use the standard steps for complete intersections to compute the Futaki invariant. One may check that this yields the same result as above. In fact, when writing the HS for test symmetry using PL, this recovers to the HS from complete intersection relation. Indeed, the degrees of the generators in PL(HS)$= 2t^2 + t^4 + t^6 - t^{12}$ agree with those in (6.2.30). For instance, when we pick the test symmetry with non-vanishing charge on the generator at order 4, the HS becomes

$$\mathrm{HS} = \frac{\left(1 - t^2 + t^4\right)\left(1 - t^4\right)}{(1 - t^2)(1 - t^2)^2 \left(1 - t^{4+\epsilon}\right)}. \tag{6.2.31}$$

In particular,

$$\frac{\left(1 - t^2 + t^4\right)\left(1 - t^4\right)}{(1 - t^2)} = \frac{1 - t^{12}}{1 - t^6}. \tag{6.2.32}$$

Hence, we recover the HS in (6.2.30) with an explicit $1/(1 - t^4)$ factor. As a result, the method for non-complete intersections is consistent with the method for complete intersections. Importantly, our method is general and applies to arbitrary varieties.

6.2.3 One SU(N) Instanton Moduli Spaces on $\mathbb{C}^2$

The Higgs branch of D$(p-4)$-Dp brane systems, which is the moduli space of instantons, is studied in [264]. Here, we consider the worldvolume theory of a D3 brane in the background of stack of N D7 branes, whose $\mathcal{N} = 1$ quiver is given in Figure 7 (with $k = 1$) of [264]. The U(1) factor of the global U(N) global symmetry is absorbed into the gauge group U(1) in the quiver diagram. The superpotential is $W = q\Phi\tilde{q}$, where q and $\tilde{q}$ are the fundamentals and Φ is a U(1) adjoint. Notice that there are two other U(1) adjoints ϕ_1 and ϕ_2 with superpotential term $\epsilon^{\alpha\beta}\phi_\alpha\Phi\phi_\beta$, but since the adjoints are just complex numbers for U(1), it vanishes in the superpotential. The HS is[22]

$$\mathrm{HS} = \frac{\sum_{i=0}^{N-1} \binom{N-1}{i} t^{2i/N}}{\left(1 - t^{1/N}\right)^2 \left(1 - t^{2/N}\right)^{2(N-1)}}. \tag{6.2.33}$$

The dimension of the moduli space is $n = 2N$. Let us first consider the case with $N = 2$. Under Laurent expansion around $s = 0$, we have $a_0 = a_1 = 8$. The PL of HS reads

$$\mathrm{PL}(\mathrm{HS}) = 2t^{1/2} + 3t - t^2. \tag{6.2.34}$$

Algebro-geometrically, we can write the equation as

$$x_1^2 + x_2^2 + x_3^2 + x_4^4 + x_5^4 = 0. \tag{6.2.35}$$

If we consider the test symmetry with charges $(0, 0, 0, 0, 1)$, then we find that

$$F = 8 \times \frac{4 \times 1/2 - 2}{2 \times 1/2} = 0 \tag{6.2.36}$$

and

$$||\eta||^2 = \frac{(4 - 1) \times 8}{4^2 \times (4 + 1) \times (1/2)^2} = \frac{6}{5} \neq 0. \tag{6.2.37}$$

---

[22]Again, the fractional powers are always just computationally a result of our convention.

Hence, the ring is unstable. Interestingly, we can see that the central fibre is $x_1^2 + x_2^2 + x_3^2 + x_4^4 = 0$, which is also known to be unstable from §6.2.1. Therefore, the destabilizing ring in general may not necessarily be stable as well.

If we further destabilize this A_3 threefold singularity with $(0, 0, 0, 1, 0)$, we would get the stable[23] $x_1^2 + x_2^2 + x_3^2 = 0$, which is $\mathbb{C}^2/\mathbb{Z}_2$. In fact, if we remove the two ϕ_α's in the quiver diagram, we would get the same superpotential and

$$\text{HS} = \frac{1 - t^2}{(1 - t)^3}, \tag{6.2.38}$$

which in the IR fixed point should be the same as SQED with 2 flavours [265].

For general N, the varieties are not complete intersections. Even if we do not write the relations explicitly, we can still consider the test symmetry where only one generator of order $1/N$ has a charge 1 with other test charges vanishing. The Futaki invariant is then

$$\frac{F}{a_0} = \frac{2N \times 1/N - 2}{2 \times 1/N} = 0 \tag{6.2.39}$$

with

$$\frac{||\eta||^2}{a_0} = \frac{2N - 1}{(2N)^2 \times (2N + 1) \times (1/N)^2} = \frac{2N - 1}{4(2N + 1)} \neq 0. \tag{6.2.40}$$

Hence, the rings for one $\text{SU}(N)$ instanton moduli spaces are (K-)unstable.

6.2.4 Phenomenological Theories

Now, let us consider the VMS of some phenomenologically interesting SUSY gauge theories.

SQCD We can use the HS obtained in [27] to study the ring stabilities for SQCDs with $\text{SU}(N_c)$ gauge groups. The generators follow the standard relations between mesons and baryons: $B^{i_1 \cdots i_{N_c}} \tilde{B}_{j_1 \ldots j_{N_c}} = M^{[i_1}_{j_1} \ldots M^{i_{N_c}]}_{j_{N_c}}$ and $M^{[i_1}_j B^{ji_2 \ldots i_{N_c}]} = M^j_{[i_1} \tilde{B}_{ji_2 \ldots i_{N_c}]} = 0$.

Example 0: $N_f < N_c$ In such cases, the moduli spaces are freely generated, and the moduli spaces are simply $\mathbb{C}^{N_f^2}$ [27]. Hence, the HS is

$$\text{HS} = \frac{1}{\left(1 - t^{2/N_f^2}\right)^{N_f^2}}. \tag{6.2.41}$$

As aforementioned, there are no non-trivial test configurations for $\mathbb{C}^{N_f^2}$. Hence, the rings for $N_f < N_c$ are stable. Notice, however, the discussion here is semi-classical. When we take quantum corrections into account, there is no stable[24] ground state, and such vacuum variety is just an auxiliary space that helps us study the GIOs. For more details, see, for example, [27, 266].

Example 1: $N_f = 2$, $N_c = 2$ For $N_c = 2$, the refined HS is

$$\text{HS} = \sum_{k=0}^{\infty} \dim[0, k, 0, \ldots, 0] t^{k/N_f} = {}_2F_1\left(2N_f - 1, 2N_f; 2; t^{1/N_f}\right), \tag{6.2.42}$$

where $[n_1, \ldots, n_{N_f-1}]$ is the highest weight notation of $\text{SU}(N_f)$ irrep, and ${}_2F_1$ is the hypergeometric function. In particular, for $\text{SU}(2)$ gauge group, since the fundamentals are pseudoreal, there is no distinction between quarks and antiquarks. Moreover, as the fundamentals only have two colour

---

[23]Equivalently, we can consider $(0, 0, 0, 1, 1)$ for (6.2.35) to directly get this central fibre.

[24]Here, this "stable" should not be confused with "K-stable".

indices, the antisymmetrized product on three or more flavour indices vanish. Hence, the relation becomes $\epsilon_{i_1 \ldots i_{2N_f}} M^{i_1 i_2} M^{i_3 i_4} = 0$, where $i_1, \ldots, i_{2N_f} = 1, \ldots, 2N_f$.

Let us start with $SU(2)$ with 2 flavours. The (unrefined) HS is

$$\text{HS} = \frac{1-t}{\left(1-t^{1/2}\right)^6}. \tag{6.2.43}$$

Under Laurent expansion around $s = 0$, we have $a_0 = a_1 = 64$. The PL of HS reads

$$\text{PL(HS)} = 6t^{1/2} - t, \tag{6.2.44}$$

which is in fact a hypersurface. The defining equation is $x_1 x_2 + x_3 x_4 + x_5 x_6 = 0$, or under a holomorphic change of coordinates, $u^2 + v^2 + w^2 + x^2 + y^2 + z^2 = 0$. By (6.1.32),

$$F = \sum_{i=1}^{6} v_i \frac{5 \times 1/2 - 2}{2 \times 1/2} a_0 = 32 \sum_{i=1}^{6} v_i. \tag{6.2.45}$$

It suffices to check test symmetry with charges (1,0,0,0,0,0) due to the symmetry of generators in the relation. We then have $F > 0$. Hence, we conclude that the ring for SU(2) with $N_f = 2$ is stable.

Example 2: $N_f = 3$, $N_c = 3$ The HS for SU(3) with 3 flavours is

$$\text{HS} = \frac{1 - t^{2/3}}{\left(1 - t^{1/3}\right)^2 \left(1 - t^{2/9}\right)^9}. \tag{6.2.46}$$

Under Laurent expansion around $s = 0$, we have $a_0 = a_1 = 1162261467/256$. The PL of HS reads

$$\text{PL(HS)} = 9t^{2/9} + 2t^{1/3} - t^{2/3}. \tag{6.2.47}$$

There are 11 generators satisfying 1 relation which can be written as

$$x_{11}x_{22}x_{33} + x_{21}x_{12}x_{33} + x_{11}x_{32}x_{23} + x_{21}x_{32}x_{13} + x_{31}x_{22}x_{13} + x_{31}x_{12}x_{23} + y_1 y_2 = 0. \tag{6.2.48}$$

By (6.1.32),

$$F = \frac{1162261467}{256} \left(\frac{1}{2}(v_1 + \cdots + v_9) + 2(v_{10} + v_{11}) \right). \tag{6.2.49}$$

As the mesons and baryons are symmetric in the single equation respectively and there are no mixing terms of mesons and baryons, the ring for SU(3) with 3 flavours is expected to be stable.

A speculation for $N_f = N_c$ More generally, as observed in [27], the moduli space of $N_f = N_c$ is a hypersurface in $\mathbb{C}^{N_c^2 + 2}$ with

$$\text{HS} = \frac{1 - t^{2/N_c}}{\left(1 - t^{2/N_c^2}\right)^{N_c^2} \left(1 - t^{1/N_c}\right)^2}. \tag{6.2.50}$$

Since a hypersurface can always have the initial terms with t^0 under rescaling, we can apply (6.1.32) which yields

$$\frac{F}{a_0} = \frac{1}{2}(v_1 + \cdots + v_{N_c^2}) + \frac{(N_c - 1)^2}{2}(w_1 + w_2) \tag{6.2.51}$$

for test symmetry with charges $(v_1, \ldots, v_{N_c^2}, w_1, w_2)$. In particular, we have $F/a_0 = 1/2$ and $F/a_0 = (N_c - 1)^2/2$ for $(1, 0, 0, \ldots, 0)$ and $(0, 0, \ldots, 0, 1, 0)$ respectively. The mesons and baryons are symmetric in the hypersurface algebraic equation with same ζ-weights respectively, so in terms of the rescaling method it is natural to speculate that a negative η-charge of a generator would

require other generators to have positive η-charges to compensate this in the test configuration. Moreover, there are no monomials having both mesons and baryons in the relation. Hence, it is natural to expect that the rings for $N_f = N_c$ are stable.

However, as we learn from [267] that the ring is expected to be (K-)unstable for $N_f < 3N_c/2$. The (anti-)quarks have R-charges $(1 - N_c/N_f)$, and therefore equal to zero for $N_f = N_c$. However, to have a conformal fixed point, we require the R-charges (of GIOs) to be no less than $2/3$, i.e., $N_f \geq 3N_c/2$ here from the mesons. Thus, it seems that the K-stability criterion for conformality fails in this case.

Example 3: $N_f = 4$, $N_c = 3$ Even for non-zero R-charges, violation of unitarity bound might also "leak" out of the bound $nk - 2 < 0$ from stability. For instance, the HS for SU(3) with 4 flavours reads

$$\text{HS} = \frac{P(t)}{\left(1 - t^{1/6}\right)^{16} \left(1 - t^{1/4}\right)^{2}}, \tag{6.2.52}$$

where $P(t)$ is polynomial with palindromic coefficients whose exact expression can be found in [27] (up to some rescaling of t). Under Laurent expression, we learn that $n = 16$. In fact, we can see that $N_f = 4 < 3N_c/2 = 9/2$, and hence the mesons violate the unitarity bound. On the other hand, we have $nk - 2 = 16/6 - 2 = 2/3 > 0$ for the mesons. Therefore, the unitarity bound could live above the stability bound.

Electro-Weak MSSM   The electroweak sectors of minimal supersymmetric standard model (MSSM) with renormalizable superpotentials are classified in [37]. The simplest case is generated by LH and $H\bar{H}$ where L stands for the lepton doublets and H, $\bar{H}$ stand for the up and down types of Higgs doublets. Notice that we have suppressed the indices and Levi-Civita symbols in the generators. It turns out that geometrically this is just $\mathbb{C}^4$, and hence is trivially stable.

The next simplest case is generated by LLe and $L\bar{H}e$ where e stands for the lepton singlet. From [37], the HS is

$$\text{HS} = \frac{1 + 4t + t^2}{(1 - t)^5}. \tag{6.2.53}$$

Under Laurent expansion around $s = 0$, we have $a_0 = a_1 = 729/16$. The PL of HS reads

$$\text{PL(HS)} = 9t - 9t^2 + 16t^3 - \dots \tag{6.2.54}$$

There are 9 generators satifying 9 relations which can be written as

$$y_6 y_8 - y_5 y_9, \ y_3 y_8 - y_2 y_9, \ y_6 y_7 - y_4 y_9,$$
$$y_5 y_7 - y_4 y_8, \ y_3 y_7 - y_1 y_9, \ y_2 y_7 - y_1 y_8,$$
$$y_3 y_5 - y_2 y_6, \ y_3 y_4 - y_1 y_6, \ y_2 y_4 - y_1 y_5, \tag{6.2.55}$$

which already forms a Göbner basis. For those $(v_1, v_2, \dots, v_9)$ that can be rescaled such that all the 9 equations have initial terms with 0 t-weights, we can simply apply (6.1.32) which yields

$$F = \frac{729}{16} \times \frac{3}{2} \sum_{i=1}^{9} v_i = \frac{2187}{38} \sum_{i=1}^{9} v_i. \tag{6.2.56}$$

Due to the symmetry of the 9 variables, if there is a negative test charge, then it should be compensated by more positive test charges in order to satisfy the condition for a rescaled configuration. Hence, (6.2.56) should always give a positive F.

However, for the test symmetries that cannot be rescaled to one where (6.2.56) applies, it is exhaustive to check all of them. As an example, let us consider η with charges $(-1, -2, 0, 0, \dots, 0)$. The test configuration is then

$$y_6 y_8 - y_5 y_9, \ y_3 y_8 - t^{-2} y_2 y_9, \ y_6 y_7 - y_4 y_9,$$

$$y_5 y_7 - y_4 y_8, \ y_3 y_7 - t^{-1} y_1 y_9, \ t^{-2} y_2 y_7 - t^{-1} y_1 y_8,$$
$$y_3 y_5 - t^{-2} y_2 y_6, \ y_3 y_4 - t^{-1} y_1 y_6, \ t^{-2} y_2 y_4 - t^{-1} y_1 y_5. \tag{6.2.57}$$

With the help of `Macaulay2`, a direct computation with regularization in the numerator yields

$$\begin{aligned}
\text{HS} \ &= \ \frac{1}{(1-t)^7 \, (1 - t^{1-2\epsilon}) \, (1 - t^{1-\epsilon})} \times \big(1 - 3t^2 - 4t^{2-2\epsilon} - 2t^{2-\epsilon} \\
&+ 2t^{3-3\epsilon} + 9t^{3-2\epsilon} + 3t^{3-\epsilon} + 2t^3 - 3t^{4-3\epsilon} - 6t^{4-2\epsilon} + t^{5-2\epsilon} - t^{5-\epsilon} + t^{6-3\epsilon}\big).
\end{aligned} \tag{6.2.58}$$

Thus,

$$F = n \mathrm{D}_\epsilon a_1(\zeta + \epsilon\eta) - (n-1)\mathrm{D}_\epsilon a_0(\zeta + \epsilon\eta)|_{\epsilon=0} = \frac{1}{2}. \tag{6.2.59}$$

We also notice that this η can be rescaled to the "minimal" η' with charges $(1, 0, 2, 0, 0, \ldots, 0)$. The test configuration is then

$$y_6 y_8 - y_5 y_9, \ t^2 y_3 y_8 - y_2 y_9, \ y_6 y_7 - y_4 y_9,$$
$$y_5 y_7 - y_4 y_8, \ t^2 y_3 y_7 - t y_1 y_9, \ y_2 y_7 - t y_1 y_8,$$
$$t^2 y_3 y_5 - y_2 y_6, \ t^2 y_3 y_4 - t y_1 y_6, \ y_2 y_4 - t y_1 y_5. \tag{6.2.60}$$

Regularization in the numerator yields

$$\text{HS} = \frac{1 - 2t^{2+\epsilon} - 7t^2 + 5t^{3+\epsilon} + 11t^3 - 3t^{4+\epsilon} - 6t^4 - t^{5+\epsilon} + t^5 + t^{6+\epsilon}}{(1-t)^7 \, (1 - t^{1+\epsilon}) \, (1 - t^{1+2\epsilon})}. \tag{6.2.61}$$

Therefore, we find that

$$F = n \mathrm{D}_\epsilon a_1(\zeta + \epsilon\eta) - (n-1)\mathrm{D}_\epsilon a_0(\zeta + \epsilon\eta)|_{\epsilon=0} = \frac{1}{2}. \tag{6.2.62}$$

We have checked quite a few test symmetries with low values of v_i, all of which give positive Futaki invariants. It is natural to speculate that this ring is stable.

Outlook K-stability is naturally related to the chiral rings of SCFTs as some "generalized a-maximization". However, when an AdS/CFT picture is not present, the connection between K-stability and conformality becomes more subtle. However, as an example, we show that SQCD does not seem to follow the K-stability criterion for conformality. Furthermore, the unitarity bound is possible to live above the stability bound $nk - 2 \geq 0$, so some operators which violate the unitarity bound could have positive $nk - 2$. Nevertheless, K-stability should still play a crucial role in studying chiral rings and SCFTs since on the (emergent) gravity side, there usually involves many symmetries, and this is exactly what K-stability and destabilizing rings concern. We speculate that K-stability could be a *necessary* (but not sufficient) condition for the ring being a ring of SCFT. This condition might become sufficient as well in some special classes of theories, such as the gauge theories from D-branes probing CYs.

In [268], chiral ring stability is introduced when one drops certain superpotential terms. Its relation to K-stability still requires further study. It is also worth noting that in [257], non-commutative crepant resolution (NCCR) is applied to finding the quivers for various theories. However, the existence of NCCR and being K-stable are not necessary to each other. It would be interesting to further study their connections and also extend the discussions to supersymmetric theories in other dimensions.

Chapter 7

AI as a Witness?

In the past few years, machine learning has been introduced to the study of theoretical and mathematical physics [269, 270]. Instead of talking about some rudiments of machine learning and AI, we shall briefly discuss what we should expect from machine learning or how we should properly use machine learning in our study. Then we will use some examples to illustrate the recent progress.

The most straightforward way to apply machine learning is to feed the machine some known data and perform the training to see how well the algorithm behaves when making predictions. Here, by "how well", we mean that we use various measures to check how accurate the predictions the machine gives after training. However, such way, known as the supervised learning, is not really helpful. Of course, this shows the performance of machine learning in a specific research field and gives one some hint on how much it could be relied on. In many cases, espcially in algebraic geometry, we have seen many good performances such as in [3, 6, 7, 10, 13]. Nevertheless, this would not produce new physics or mathematics.

Therefore, it could be more helpful to consider methods such as unsupervised learning and reinforcement learning. It could be possible that with machine learning and AI, some hidden structures and patterns of certain objects can be revealed. In other words, instead of simply measuring how much one can trust on the predictions by the machine, it would be more instructive to see whether the machine can help one find plausible directions for investigations or even formulate any unknown conjectures, which could then be beneficial for our analytical study.

Since machine learning often only gives linear approximations, it is still difficult to find patterns or formulae that can be used practically. Nevertheless, this modern technique might still help us in numerical analysis and in the string landscape with huge data in future. Here, we shall give some preliminary examples where one can see some analytical results from the analysis of the machine learning results although these results are particularly simple and are known previously. In the first example, we show how a simple linear regressor can reproduce the volumes of the lattice polytopes in different dimensions from their Ehrhart series. In the second example, we illustrate how one can recover the conditions that determine the genus of the (lopsided) amoebae using data projections and unsupervised learning.

7.1 Ehrhart Series and Volumes of Polytopes

Our first example would be using the Ehrhart series to predict the volumes of the lattice polytopes in different dimensions associated to canonical Fano varieties. Let us start with some backgrounds on polytopes and Ehrhar series. More details can be found for example in [271].

The Ehrhart series is the key to enumerating interior lattice points of a polytope. As with Hilbert series in algebraic geometry, we have

Definition 7.1.1. *Given a polytope P in the lattice M, the Ehrhart polynomial is*

$$\mathrm{ehr}_P(k) := |kP \cap M| \, , \tag{7.1.1}$$

which counts the number of lattice points within the k-dilation of P. Then, the generating function is the **Ehrhart series***:*

$$\text{Ehr}_P(t) = \sum_{k \geq 0} \text{ehr}_P(k) t^k, \tag{7.1.2}$$

for a formal variable t.

Indeed, we expect that the number of lattice points, as with volume, grows polynomially with k in a fixed dimension, d. That is, ehr_P is a polynomial [272] in k. It is hence of the form

$$\text{ehr}_P(k) = c_d k^d + \cdots + c_1 k + c_0, \tag{7.1.3}$$

where $d!c_d$ is the (normalized) volume[1] of the P, called as $\text{Vol}(P)$ henceforth. In this case, the Ehrhart polynomial/series coincides with the Hilbert polynomial/series of the variety. The Ehrhart series can then be written as

$$\text{Ehr}_P(t) = \frac{g(t)}{(1-t)^{d+1}} = \frac{g_0 + g_1 t + \cdots + g_d t^d}{(1-t)^{d+1}}. \tag{7.1.4}$$

In particular, $g(1) = g_0 + g_1 + \cdots + g_d = d!c_d = \text{Vol}(P)$.

Example 22. *The Ehrhart polynomial for the polygon associated to dP_2 (No.12 in Figure 4.0.1) is $\text{ehr}_P(k) = \frac{5}{2}k^2 + \frac{5}{2}k + 1$. Therefore, the Ehrhart series reads*

$$\text{Ehr}_P(t) = \sum_{k=0}^{\infty} \left(\frac{5}{2}k^2 + \frac{5}{2}k + 1 \right) t^k = \frac{1 + 3t + t^2}{(1-t)^3}. \tag{7.1.5}$$

As one may check, $g_0 + g_1 + g_2 = 5$ gives the volume of P.

Now, let us use the regressors to predict the volumes of the polytopes of dimensions from 1 to 6. We use the coefficients in the Taylor expansions of the Ehrhart series up to order 30 as input. After training a few data, we find that the coefficients of the regressors can be extracted as follows:

$$\begin{aligned}
\dim &= 1 : [-1, 1]; \\
\dim &= 2 : [1, -2, 1]; \\
\dim &= 3 : [-1, 3, -3, 1]; \\
\dim &= 4 : [1, -4, 6, -4, 1]; \\
\dim &= 5 : [-1, 5, -10, 10, -5, 1]; \\
\dim &= 6 : [1, -6, 15, -20, 15, -6, 1].
\end{aligned} \tag{7.1.6}$$

As we can see, for dimension d, this is precisely

$$\sum_{i=0}^{d} \binom{d}{i} (-1)^i \text{ehr}_P(d-i). \tag{7.1.7}$$

Recall that the Ehrhart polynomial can be written as $\sum_{i=0}^{d} c_i k^i$, then

$$\sum_{i=0}^{d} \binom{d}{i} (-1)^i \text{ehr}_P(d-i) = \sum_{i=0}^{d} \binom{d}{i} (-1)^i (c_d(d-i)^d + \cdots + c_1(d-i) + c_0). \tag{7.1.8}$$

For $k < d$, $\sum_{i=0}^{d} \binom{d}{i} (-1)^i (d-i)^k$ vanishes. To see this, consider

$$\left(x \frac{\text{d}}{\text{d}x} \right)^k (x-1)^d = \left(x \frac{\text{d}}{\text{d}x} \right)^k \left(\sum_{i=1}^{d} \binom{d}{i} (-1)^i x^{d-i} \right) = \sum_{i=0}^{d} \binom{d}{i} (-1)^i (d-i)^k x^{d-i}. \tag{7.1.9}$$

---

[1]In the corresponding toric variety, this volume equals the degree of the toric variety polarized by the Cartier divisor D_P.

Taking $x = 1$, we see that this is indeed zero. Therefore,

$$\sum_{i=0}^{d} \binom{d}{i}(-1)^i \mathrm{ehr}_P(d-i) = c_d \sum_{i=0}^{d} \binom{d}{i}(-1)^i(d-i)^d = d!c_d, \tag{7.1.10}$$

where the last equality can again be obtained by acting $(x\mathrm{d}x/x)^k$ with $k = d$. This is exactly the volume of P. As we can see, such example works with the linear regressors as the formulae for the volumes are linear.

7.2 Amoebae and Genus

We shall now consider a slightly more complicated example. Let us take the amoebae and predict their genus, that is, the numbers of holes/gas phases. First, we need to introduce the lopsidedness of the amoebae [273].

Definition 7.2.1. *Let $f \in \mathbb{C}\left[z_1, z_1^{-1}, \ldots, z_r, z_r^{-1}\right]$ be a sum of (Laurent) monomials m_i as $f(\boldsymbol{z}) = m_1(\boldsymbol{z}) + \cdots + m_k(\boldsymbol{z})$. For $\boldsymbol{x} \in \mathbb{R}^r$, define the list of positive numbers*

$$f\{\boldsymbol{x}\} := \left\{\left|m_1(\mathrm{Log}^{-1}(\boldsymbol{x}))\right|, \ldots, \left|m_k(\mathrm{Log}^{-1}(\boldsymbol{x}))\right|\right\}. \tag{7.2.1}$$

We say a list of positive numbers is lopsided if one of the numbers is greater than the sum of all the others. This definition can then be applied to $f\{\boldsymbol{x}\}$.

It is then natural to define the following [274]:

Definition 7.2.2. *Given a Newton polynomial P, the lopsided amoeba is*

$$\mathcal{LA}_P := \{\boldsymbol{x} \in \mathbb{R}^r | \ P\{\boldsymbol{x}\} \text{ is not lopsided}\}. \tag{7.2.2}$$

For some cases, such as $P = z_1 + z_2 + 1$, $\mathcal{LA}_P = \mathcal{A}_P$. However, in general, they do not need to coincide. Nevertheless,

$$\mathcal{A}_P \subseteq \mathcal{LA}_P, \tag{7.2.3}$$

so that $\mathcal{LA}_P$ can be constructed as a crude approximation to $\mathcal{A}_P$. This can be made precise as follows.

Let n be a positive integer, $\boldsymbol{x} \in \mathbb{R}^r$, and $P(\boldsymbol{x})$ a (Newton) polynomial, define $\tilde{P}_n$ to be [2]

$$\tilde{P}_n(\boldsymbol{x}) := \prod_{k_1=0}^{n-1} \cdots \prod_{k_r=0}^{n-1} P\left(\mathrm{e}^{2\pi i k_1/n}x_1, \ldots, \mathrm{e}^{2\pi i k_r/n}x_r\right). \tag{7.2.4}$$

Clearly, $\tilde{P}_1 = P$. Such $\tilde{P}_n$ is in fact a *cyclic resultant*

$$\tilde{P}_n = \mathrm{res}_{u_r}\left(\mathrm{res}_{u_{r-1}}\left(\ldots \mathrm{res}_{u_1}\left(P(u_1 x_1, \ldots, u_r x_r), u_1^n - 1\right) \ldots, u_{r-1}^n - 1\right), u_r^n - 1\right) \tag{7.2.5}$$

where $\mathrm{res}_u(f, g)$ is the resultant of f, g with respect to the variable u.

The lopsided amoeba $\mathcal{LA}_{\tilde{P}_n}$ for $\tilde{P}_n$ approximates $\mathcal{A}_P$ itself [273]:

Theorem 7.2.1. *For an r-dimensional Newton polytope $\Delta(P)$, with polytope coordinates p_i for each ith direction in the $\mathbb{Z}^r$ lattice which the polytope is defined in, one defines $c_i := \max(p_i) - \min(p_i)$ over the polytope vertices; then $c = \max(c_i)$. Suppose $\boldsymbol{x} \in \mathbb{R}^r \setminus \mathcal{A}_P$ is a point in the amoeba complement whose distance from $\mathcal{A}_P$ is at least $\epsilon > 0$. If n is large enough so that*

$$n\epsilon \geq (r-1)\log n + \log((r+3)2^{r+1}c), \tag{7.2.6}$$

then $\tilde{P}_n\{\boldsymbol{x}\}$ is lopsided[3] and $\mathcal{LA}_{\tilde{P}_n}$ converges uniformly to $\mathcal{A}_P$ as $n \to \infty$.

---

[2] In [274], a faster algorithm was proposed to compute $\mathcal{LA}_{\tilde{P}_n}$ at level k where $n = 2^k$ using the properties of cyclic resultants. The time complexity is $\mathcal{O}(kd^2)$ with d being the degree of $P(z_1, z_2)$.

[3] In this paper, as r is always 2, we have $n\epsilon \geq \log n + \log(8c)$.

A consequence of this is one way to solve the membership problem:

Theorem 7.2.2. *Let $I \subset \mathbb{C}\left[z_1, z_1^{-1}, \ldots, z_r, z_r^{-1}\right]$ be an ideal. The point $\boldsymbol{x} \in \mathbb{R}^r$ is in the amoeba $\mathcal{A}_I$ if and only if $f\{\boldsymbol{x}\}$ is not lopsided for every $f \in I$.*

Therefore, to fully determine the boundary of an amoeba, we need to consider all the Laurent polynomials in the ideal generated by our Newton polynomial. Equivalently, we need to take $n \to \infty$ for the cyclic resultant. As a result, we often approximate the boundary with some finite large n in practice. This would also be our basic strategy to study the genus using neural networks later, although unlike finding the boundary, sometimes we can count the genus in other ways, as we will see.

Example For instance, consider the Newton polynomial $P = z^3 + w^3 + 2zw + 1$ whose amoeba is plotted red in Figure 7.2.1. The dark blue points (plus the red ones) form the lopsided amoeba $\mathcal{LA}_{\tilde{P}_{16}}$ while the chartreuse points (plus the red and dark blue ones) give the region of $\mathcal{LA}_{\tilde{P}_8}$.

FIGURE 7.2.1: It is clear from this example that the lopsided amoeba contains the amoeba as a subset. Figure taken from [274, Figure 1].

7.2.1 Lopsided Amoebae: $n = 1$

As discussed above, we will use lopsided amoebae since they are more amenable to computation. We begin with the simplest case of $n = 1$ where $\tilde{P}_1 = P$ by definition, so that $\mathcal{LA}_{\tilde{P}_1} = \mathcal{LA}_P$.

For a fixed Newton polynomial $P(z, w) = \sum c_k z^i w^j$, the input is the vector composed of the coefficients, i.e., $\{c_1, c_2, \ldots, c_n\}$, and the output is the genus. In other words, we have labelled data of the form

$$\{c_1, c_2, \ldots, c_n\} \longrightarrow g . \tag{7.2.7}$$

Example 1: F_0 We start with our simple running example F_0 whose toric diagram is No.15 in Figure 4.0.1. Some plots of the amoebae can be found in Appendix B. As the Newton polynomial is

$$P(z, w) = c_1 z + c_2 w + c_3 z^{-1} + c_4 w^{-1} + c_5. \tag{7.2.8}$$

our input is $\{c_1, c_2, c_3, c_4, c_5\}$. Since the resulting lopsided amoeba could have at most one genus (corresponding to its single interior point), this is a binary classification where the output is either $g = 0$ or $g = 1$. For this simple example, one can analytically derive (see Appendix K) the genus g as a function of the coefficients:

$$g = \begin{cases} 0, & |c_5| \leq 2|c_1 c_3|^{1/2} + 2|c_2 c_4|^{1/2} \\ 1, & |c_5| > 2|c_1 c_3|^{1/2} + 2|c_2 c_4|^{1/2} \end{cases}. \tag{7.2.9}$$

Now, the actual accuracy of classifying g, albeit very high, is not important here. Our purpose is to see whether we can recover these conditions from unsupervised learning.

To see how well the neural network (NN) is learning the above equation for g, we can a perform principal component analysis (PCA) projections, as visualized in Figure 7.2.2(a). With the help of the `Yellowbrick` package, we can use multi-dimensional scaling (MDS) manifold projection to make the two types of data points further separated as in Figure 7.2.2(b). For a brief introduction to different methods of manifold learning, see [7, Appendix B] and references therein.

(A)

MDS…Manifold…(fit…in…169.23…seconds)

Using…5…features

(B)

(C)
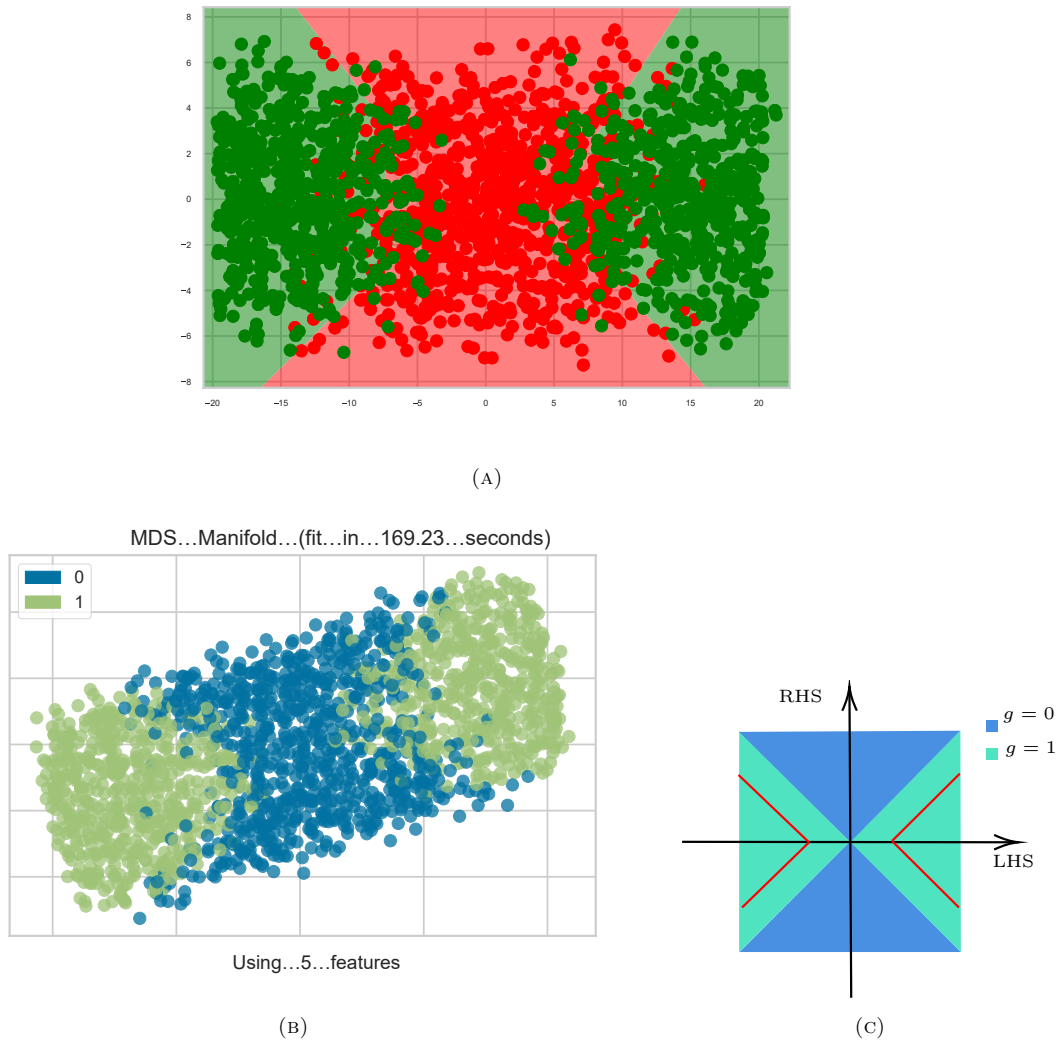
FIGURE 7.2.2: (a) The kernel PCA projection for an NN. (b) The MDS manifold projection which gives a better separation of the two classes of points. (c) Ideally, the blue and green regions would be separated by $y = \pm x$. In practice, due to the complication of square roots, the NN would get shifted. This shift, i.e., the actual separation of the blue and green points, is indicated by the red lines here.

To get an idea about how these data points are distributed in the projection, let us define[4] $x \equiv c_5$ and $|y| \equiv 2|c_1c_3|^{1/2} + 2|c_2c_4|^{1/2}$. Then the inequalities in (7.2.9) has the boundary lines $y = \pm x$. As depicted in Figure 7.2.2(c), the two lines divide the projection plane into different regions, where in the blue region we have genus zero while in the green region we have genus one. The equivalent separation coming from our NN in Figure 7.2.2(a,b) is represented by the red lines in (c), although we can see that they do not intersect at the origin and the $g = 0$ region would occupy some of the $g = 1$ parts.

Why is there a shift of the boundary lines? We believe that this is due to the non-trivial expression of y (especially the square roots therein). Although it is possible for an NN to learn such expression in principle, it could still be too complicated for a simple NN to fully simulate this.

There is another useful projection in this example, that is, the spectral embedding visualization as shown in Figure 7.2.3(a). As we can see, this gives a distribution in a parabola shape. We argue
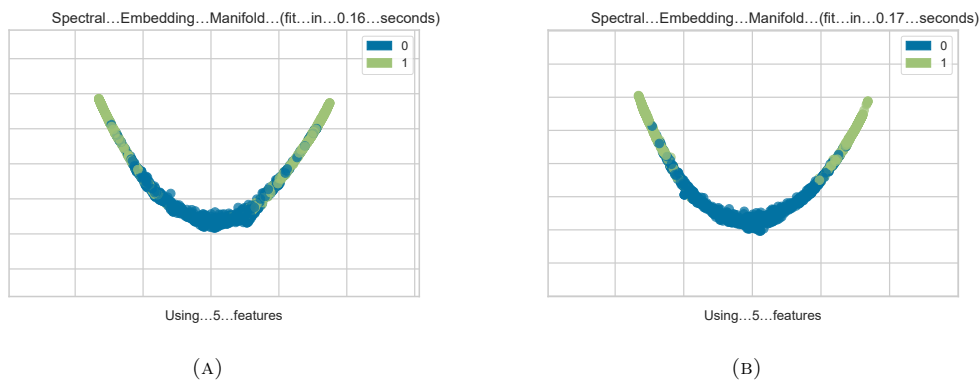
FIGURE 7.2.3: (a) The spectral embedding manifold projection of the dataset for F_0. For the input vectors, $c_{1,2,3,4}$ range from -5 to 5 while c_5 ranges from -20 to 20. (b) To verify our explanation for (a), we generate a dataset whose two classes are separated by $c_5'^2 = 4|c_1'c_3'| + 4|c_2'c_4'| + c_0$ (with c_i' the same range as c_i), where $c_0 = 4 \times 2 \times 2.5^2$ as 2.5 is the average of the possible values for $c_{1,2,3,4}$.

that this comes from squaring $y = \pm x$, i.e., $Y(\equiv y^2) = x^2$. However, again due to the complicated expression, it would be very hard for a simple NN to fully recover Y. Hence, there could still be some mixing at the boundary parts. As a validation, we generate a dataset whose binary classes are separated by the bound $c_5'^2 = 4|c_1'c_3'| + 4|c_2'c_4'| + 50$ and plot its spectral embedding as in Figure 7.2.3(b). Indeed, we obtain a similar parabola-shaped projection.

Example 2: $L^{3,3,2}$ Let us consider a non-reflexive example with two interior points, viz., $L^{3,3,2}$ whose toric diagram is

$$\tag{7.2.10}$$

The Newton Polynomial is

$$P(z, w) = c_1 z + c_2 w + c_3 z^{-1} + c_4 w^{-1} + c_5 z^2 + c_6. \tag{7.2.11}$$

Hence, our input is $\{c_1, c_2, c_3, c_4, c_5, c_6\}$. Since the resulting lopsided amoeba could have at most two holes (corresponding to its two interior points), this is a ternary classification where the output can be $g = 0, 1, 2$.

---

[4]As discussed in Appendix K, (7.2.9) works for all complex coefficients. However, we are only using real input vectors here, and more importantly, only the absolute values would matter in the condition. Hence, we can set $c_5 = x \in \mathbb{R}$ in the projection.

As with F_0, we can analytically find the boundary decisions, though the expressions are much more complicated. The details are presented in Appendix K, and we summarize them here:

$$g = \begin{cases} 0, & |c_1| \leq a_1 \text{ and } |c_6| \leq a_2 \\ 1, & (|c_1| > a_1 \text{ and } |c_6| \leq a_2) \text{ or } (|c_1| \leq a_1 \text{ and } |c_6| > a_2) \,, \\ 2, & |c_1| > a_1 \text{ and } |c_6| > a_2 \end{cases} \qquad (7.2.12)$$

where $a_1 := |c_2|w_0/z_0 + |c_3|/z_0^2 + |c_4|/(z_0 w_0) + |c_5|z_0 + |c_6|/z_0$ and $a_2 := |c_1|z_0' + |c_2|w_0 + |c_3|/z_0' + |c_4|/w_0 + |c_5|z_0'^2$ such that $z_0 := \sqrt[3]{-\frac{q}{2} + \sqrt{\Delta}} + \sqrt[3]{-\frac{q}{2} - \sqrt{\Delta}}$, with $\Delta := \left| \frac{c_3}{c_5} \right|^2 - \frac{(2|c_2 c_3|^{1/2} + |c_6|)^3}{27|c_5|^3}$, and z_0' is the positive root of $2|c_5|z_0'^3 + |c_1|z_0'^2 - |c_3| = 0$. Again, let us see to what extent the unsupervised learning can recover this.

Again, we can plot different manifold projections to visualize how the NN is simulating the above condition as shown in Figure 7.2.4(a,b,c). We can see that different projections give similar data

(A)

(B)

(C)

(D)
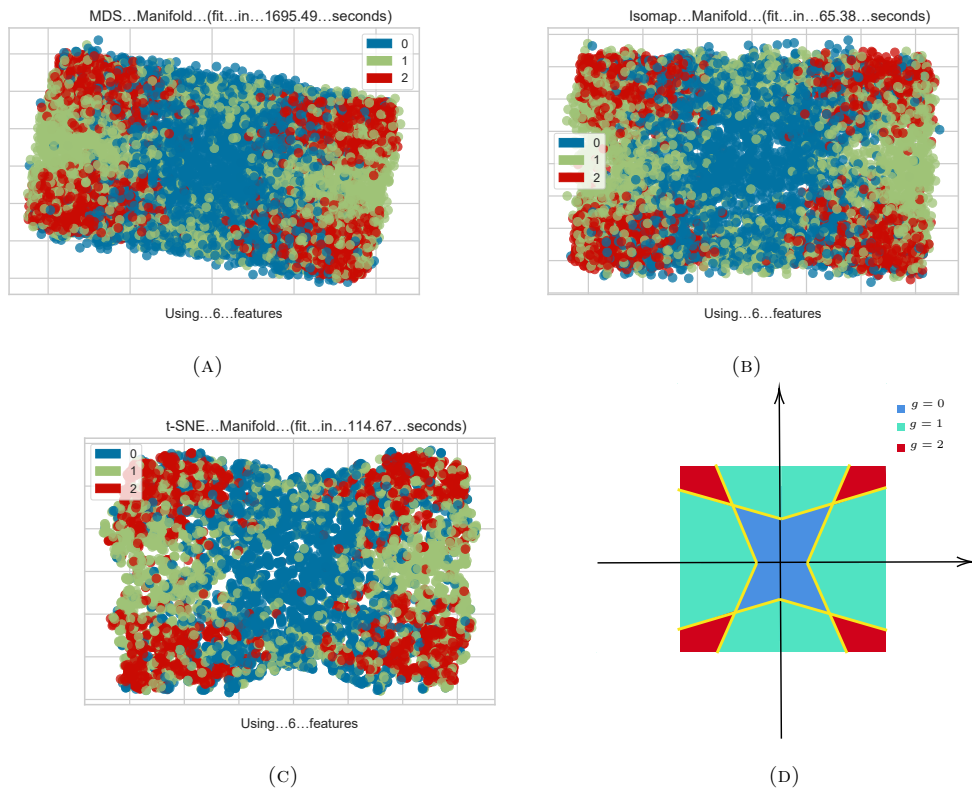
FIGURE 7.2.4: (a) The MDS embedding manifold projection of the dataset for $L^{3,3,2}$. (b) The Isomap embedding manifold projection. (c) The t-SNE embedding manifold projection. For instructions on these manifold projections, one is referred to [275]. (d) The sketch of an ideal separation of the data points.

separations. To understand such decision regions, let us first write the two bounds as

$$\begin{aligned} |c_1| = a_1 &\equiv |c_6|/z_0 + b_1, \\ |c_6| = a_2 &\equiv |c_1|z_0' + b_2, \end{aligned} \qquad (7.2.13)$$

where $b_i > 0$. In other words, when $g = 2$, the region is bounded by $|c_6|/z_0 + b_1 < |c_1| < |c_6|/z_0' - b_2$. This corresponds to the red region in Figure 7.2.4(d) whose horizontal and vertical axes are $x \equiv \pm|c_6|$ and $y \equiv \pm|c_1|$ respectively. Notice that z_0, z_0', b_i are not constants, but we can always draw

some boundary lines (in yellow) as a sketch (assuming that the changes of the boundary lines are small compared to different coloured regions[5]).

Likewise, it is straightforward to find the regions for $g = 0$ (in blue) and $g = 1$ (in green). Indeed, this is the decision regions we get from those different projections. As z_0, z_0' and b_i are not really constants and have some complicated expressions, it is natural to see some mixings in the projections.

7.2.2 Genus From Data Projections

One may also consider other toric diagrams. We may also consider lopsided amoebae for $n > 1$ (including $n \to \infty$ where one recovers the orignial amoebae). Such analysis with more examples can be found in [7]. Of course, the analysis would be more difficult for larger polygons as can be seen from the theorem on lopsidedness. Here, let us use data projections to see if we can also recover the conditions for the genus. For simplicity, we shall only consider the F_0 example as an illustration.

For instance, let us take Figure 7.2.2(b) for F_0 where MDS manifold projection was applied. Each point (x, y) in the plane represents one input vector as $(c_1, c_2, c_3, c_4, c_5) \mapsto (x, y)$. By checking the coordinates of (x, y), it is possible to recover the conditions in (7.2.9), i.e.,

$$g = \begin{cases} 0, & |c_5| \leq a \\ 1, & |c_5| > a \end{cases} \text{ with } a := |c_1 c_3|^{1/2} + 2|c_2 c_4|^{1/2}, \text{ as follows.}$$
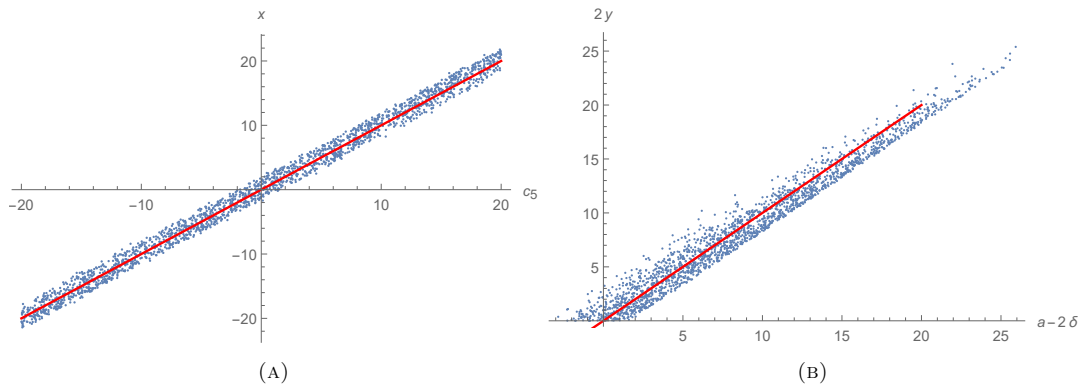
FIGURE 7.2.5: For the projection $(c_1, c_2, c_3, c_4, c_5) \mapsto (x, y)$ for F_0, we plot (a) x versus c_5 and (b) $2|y|$ versus $a - 2\delta$.

We plot x against c_5 in Figure 7.2.5(a) and find that the average of $(c_5 - x)$ is -0.172 ± 1.054. We also draw the line $x = c_5$ is in red to show a good fit. Indeed, we see that x is essentially recovering the left hand side of the above inequalities. For y, it is more complicated and we find that there is a nice fit with $|c_{1,2,3,4}|$:

$$|y_{\text{fit}}| = 0.141|c_1 c_3| + 0.166|c_2 c_4| + 2.411. \tag{7.2.14}$$

In fact, this fit actually contains a typical linear approximation of square roots, $\sqrt{m} \approx (0.1k + 1.2) \times 10^n$ for any real $k \in [1, 100)$ and $n \in \mathbb{Z}$ such that $m = k \times 10^{2n}$. Here, $c_{1,2,3,4}$ are random reals generated in the range $[-5, 5]$ and the right hand side is approximately $(0.1|c_1 c_3| + 1.2 + 0.1|c_2 c_4| + 1.2)$. This agrees with the linear approximation for square roots when $m = k$ and $n = 0$. In other words,

$$|y| \approx \sqrt{|c_1 c_3|} + \sqrt{|c_2 c_4|} = a/2. \tag{7.2.15}$$

---

[5]For instance, here $c_{1,6}$ are generated in the range $[-20, 20]$, and the means are $\mu(1/z_0) = 0.31, \mu(1/z_0') = 2.01, \mu(b_1) = 6.48, \mu(b_2) = 9.18$ with standard deviations $\sigma(1/z_0) = 0.18, \sigma(1/z_0') = 0.77, \sigma(b_1) = 3.72, \sigma(b_2) = 3.07$. We will not restate this explicitly for the examples discussed below. The complicated expressions for b_i and the standard deviations could account for the mis-classifications in machine learning.

We show this in Fig. 7.2.5(b). The blue points are the pairs $(a - 2\delta, 2|y|)$ and the line $2|y| = a - 2\delta$ is in red, where we have defined $\delta := |y_{\text{fit}}| - |y|$. Comparing the fitted results of (x, y) and Figure 7.2.2, we find that this indeed gives the bound $|c_5| = a$ for F_0.

Appendix A

The 45 Lattice Polygons with Two Interior Points

Below is the list of all inequivalent lattice polygons with two interior points as classified in [123]:

5 Triangles:

;
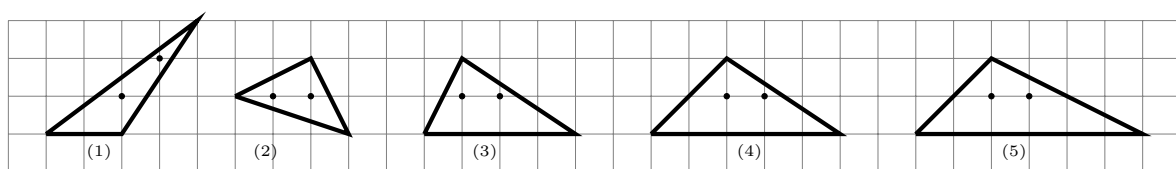
19 Quadrilaterals:

;
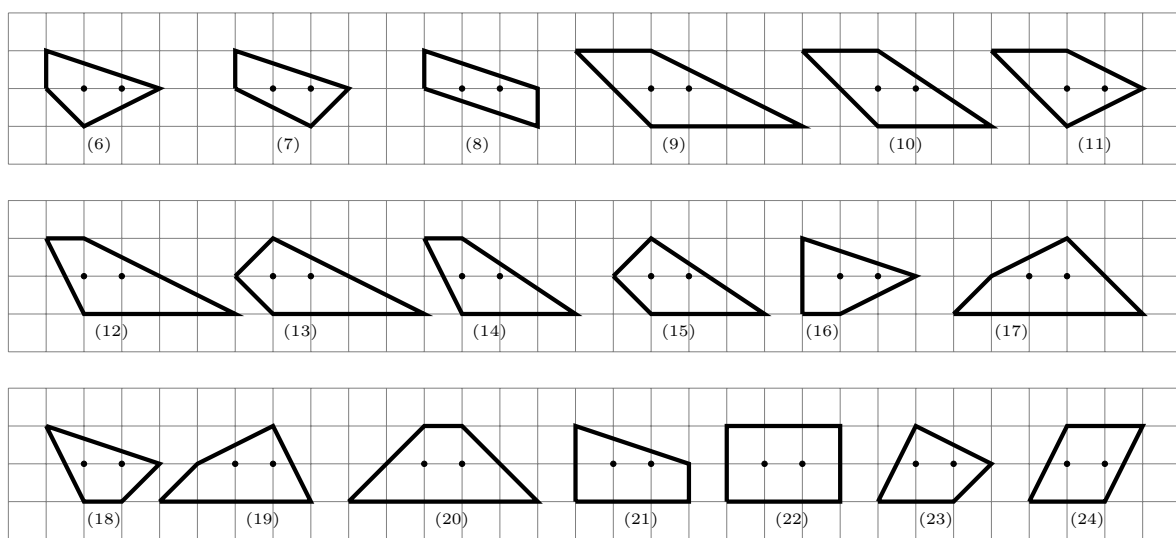
16 Pentagons:
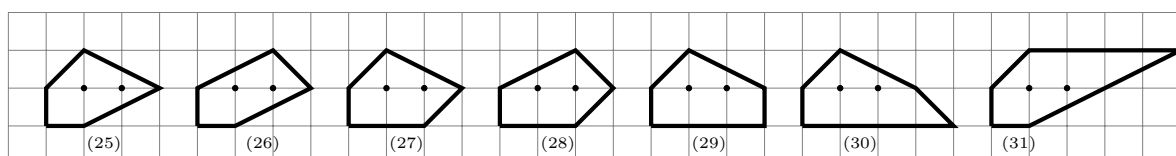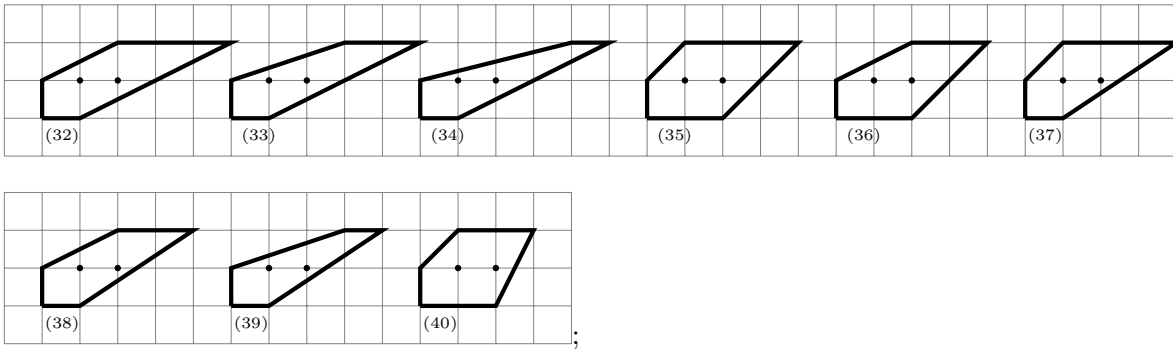
5 Hexagons:
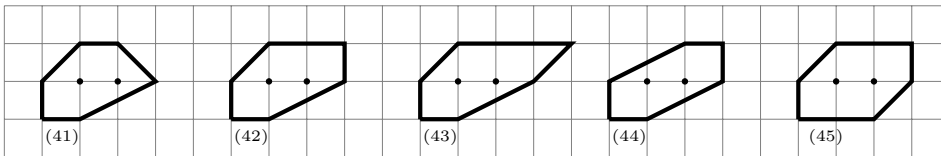
A.1 Volume Functions

For reference, we list all the 45 volume functions and their minima in Table A.1.1.

#	V	b_1^*	b_2^*	$V_{\min}$	$[L:\mathbb{Q}]$
(1)	$-\dfrac{18}{(b_2+3)(-3b_1+2b_2+6)(-3b_1+4b_2-6)}$	0	0	$\frac{1}{6}$	1
(2)	$-\dfrac{25}{(b_1-2b_2+3)(2b_1+b_2-9)(b_1+3b_2+3)}$	2	0	$\frac{1}{5}$	1
(3)	$\dfrac{16}{(b_2+3)(-2b_1+b_2-3)(2b_1+3b_2-9)}$	2	-1	$\frac{1}{8}$	1
(4)	$\dfrac{10}{(b_2+3)(-b_1+b_2-3)(2b_1+3b_2-9)}$	1	-1	$\frac{1}{10}$	1
(5)	$\dfrac{6}{(b_2+3)(-b_1+b_2-3)(b_1+2b_2-6)}$	2	-1	$\frac{1}{12}$	1
(6)	$\dfrac{3(4b_1+2b_2+21)}{(b_1+3)(b_1+b_2+3)(b_1+3b_2-6)(b_1-2(b_2+3))}$	$\frac{1}{2}(-6+3\sqrt{6})$	0	$\frac{4}{405}(9+4\sqrt{6})$	2
(7)	$\dfrac{6(b_1+b_2+12)}{(b_1+3)(b_1-b_2-6)(b_1+2b_2+3)(b_1+3b_2-6)}$	$\frac{3}{2}\left(\sqrt{33}-5\right)$	0	$\frac{1}{648}\left(63+11\sqrt{33}\right)$	2
(8)	$\dfrac{81}{(b_1-6)(b_1+3)(b_1+3b_2-6)(b_1+3b_2+3)}$	$\frac{3}{2}$	0	$\frac{16}{81}$	1
(9)	$-\dfrac{2(b_2-9)}{(b_2-3)(b_2+3)(b_1+b_2+3)(b_1+2b_2-6)}$	$3\left(\sqrt{3}-1\right)$	$3-2\sqrt{3}$	$\frac{\sqrt{3}}{18}$	2
(10)	$-\dfrac{2(b_2-15)}{(b_2-3)(b_2+3)(b_1+b_2+3)(2b_1+3b_2-9)}$	$\frac{1}{2}\left(5\sqrt{7}-11\right)$	$5+2\sqrt{7}$	$\frac{1}{243}(10+7\sqrt{7})$	2
(11)	$\dfrac{2(b_1+4(b_2-6))}{(b_2-3)(b_1+b_2+3)(b_1+2b_2-6)(b_1-2(b_2+3))}$	0	$4-\sqrt{13}$	$\frac{1}{648}(46+13\sqrt{13})$	2
(12)	$\dfrac{6(b_2-5)}{(b_2-3)(b_2+3)(2b_1+b_2+3)(b_1+2b_2-6)}$	$\frac{1}{6}\left(1+5\sqrt{13}\right)$	$\frac{1}{3}\left(5-2\sqrt{13}\right)$	$-\frac{1}{108}(35-13\sqrt{13})$	2
(13)	$\dfrac{2(2b_1+b_2+15)}{(b_2+3)(-b_1+b_2-3)(b_1+b_2+3)(b_1+2b_2-6)}$	3.27464	-0.831239	0.112571	4
(14)	$-\dfrac{8(b_2-6)}{(b_2-3)(b_2+3)(b_1+b_2+3)(2b_1+3b_2-9)}$	$\frac{1}{2}\left(2\sqrt{7}-1\right)$	$2-\sqrt{7}$	$\frac{4}{243}(-10+7\sqrt{7})$	2
(15)	$\dfrac{2(3b_1+2b_2+24)}{(b_2+3)(-b_1+b_2-3)(b_1+b_2+3)(2b_1+3b_2-9)}$	2.19488194	-0.760489	0.142613	4
(16)	$-\dfrac{b_1-12(b_2+4)}{(b_1+6)(b_2+3)(b_1-2b_2-3)(b_1+3b_2-3)}$	-2.8546585	-0.17276	0.156243	4
(17)	$-\dfrac{5b_1-7b_2+24}{(b_2+3)(b_1-2b_2+3)(b_1-b_2+3)(b_1+b_2-6)}$	1.8379935	-0.95469	0.0974795	4
(18)	$-\dfrac{2(b_1-7b_2-36)}{(b_2+3)(b_1-b_2-6)(2b_1+b_2+3)(b_1+3b_2-6)}$	1.2608787	-0.21349	0.184633	4
(19)	$-\dfrac{8b_1-11b_2+39}{(b_2+3)(b_1-2b_2+3)(b_1-b_2+3)(2b_1+b_2-9)}$	0.8345102	-0.93610217	0.120498	4
(20)	$-\dfrac{18-4b_2}{(b_2-3)(b_2+3)(-b_1+b_2-3)(b_1+b_2-6)}$	$\frac{3}{2}$	$\frac{1}{2}\left(3-\sqrt{21}\right)$	$\frac{4}{225}(-27+7\sqrt{21})$	2
(21)	$-\dfrac{3(b_1-15)}{(b_1-6)(b_1+3)(b_2+3)(b_1+3b_2-6)}$	$3(2-\sqrt{3})$	$\frac{1}{2}\left(\sqrt{3}-3\right)$	$\frac{2}{9\sqrt{3}}$	2
(22)	$\dfrac{18}{(b_1-6)(b_1+3)(b_2-3)(b_2+3)}$	$\frac{3}{2}$	0	$\frac{8}{81}$	1
(23)	$-\dfrac{4b_1-7b_2-69}{(b_2+3)(-2b_1+b_2-3)(-b_1+b_2+6)(b_1+2b_2-6)}$	1.20148202	-0.4914321	0.165004	4
(24)	$\dfrac{48}{(b_2-3)(b_2+3)(-2b_1+b_2-3)(-2b_1+b_2+9)}$	$\frac{3}{2}$	0	$\frac{4}{27}$	1
(25)	$-\dfrac{b_1{}^2-2b_1(4b_2+15)+4\left(b_2{}^2-6b_2-45\right)}{(b_1+3)(b_2+3)(b_1-b_2-6)(b_1+2b_2-6)(b_1-2(b_2+3))}$	0.746501345	-0.1982794	0.17226	11
(26)	$-\dfrac{b_1{}^2-4b_1(b_2+3)+4b_2{}^2-30b_2-207}{(b_1+3)(b_2+3)(b_1-2b_2+3)(b_1+b_2-6)(b_1-2(b_2+3))}$	1.11941442	-0.21197378	0.178752	8
(27)	$-\dfrac{2b_1{}^2-4b_1(b_2+6)+2b_2{}^2-3b_2-171}{(b_1+3)(b_2+3)(b_1-b_2-6)(b_1-b_2+3)(b_1+2b_2-6)}$	0.9337514	-0.449691462	0.15542	8
(28)	$-\dfrac{2\left(b_1{}^2-b_1(b_2+3)+b_2{}^2-3b_2-99\right)}{(b_1+3)(b_2+3)(b_1-2b_2+3)(b_1-b_2-6)(b_1+b_2-6)}$	1.26614895	-0.4677020986	0.158756	3
(29)	$-\dfrac{3\left(b_1{}^2-6b_1+6(b_2-9)\right)}{(b_1-6)(b_1+3)(b_2+3)(b_1-b_2+3)(b_1+2b_2-6)}$	1.32269853	-0.70067002	0.136079	8
(30)	$\dfrac{4b_1{}^2+4b_1(b_2-3)-2b_2{}^2+39b_2-153}{(b_1+3)(b_2+3)(b_1-b_2+3)(b_1+b_2-6)(b_1+2b_2-6)}$	1.939465	-0.8789301	0.116367	3

	V	b_1^*	b_2^*	$V_{\min}$	deg
(31)	$-\dfrac{2(b_2{}^2-3b_2-36)-3b_1(b_2+5)}{(b_1+3)(b_2-3)(b_2+3)(b_1-b_2+3)(b_1-2(b_2+3))}$	2.9071583	0.6850367	0.106224	9
(32)	$-\dfrac{-2b_1(b_2+6)+4b_2{}^2-90}{(b_1+3)(b_2-3)(b_2+3)(b_1-2b_2+3)(b_1-2(b_2+3))}$	3.0926707	0.479773042	0.121782	7
(33)	$-\dfrac{6(b_2{}^2+b_2-18)-b_1(b_2+9)}{(b_1+3)(b_2-3)(b_2+3)(b_1-3b_2+3)(b_1-2(b_2+3))}$	2.97485275	0.22750743	0.135851	9
(34)	$-\dfrac{2(3b_1-4b_2{}^2-6b_2+63)}{(b_1+3)(b_2-3)(b-2+3)(b_1-4b_2+3)(b_1-2(b_2+3))}$	$\frac{1}{4}\left(9\sqrt{57}-57\right)$	0	$\frac{143+19\sqrt{57}}{1944}$	2
(35)	$-\dfrac{-b_1(b_2+15)+b_2{}^2+3b_2-72}{(b_1+3)(b_2-3)(b_2+3)(b_1-b_2-6)(b_1-b_2+3)}$	2.2242667	0.26148655	0.112411	7
(36)	$-\dfrac{2(-6b_1+b_2{}^2+6b_2-45)}{(b_1+3)(b_2-3)(b_2+3)(b_1-2b_2+3)(b_1-b_2-6)}$	$\frac{1}{8}\left(9\sqrt{33}-33\right)$	0	$\frac{1}{972}\left(59+11\sqrt{33}\right)$	2
(37)	$-\dfrac{3(b_2{}^2-2b_2-39)-4b_1(b_2+6)}{(b_1+3)(b_2-3)(b_2+3)(b_1-b_2+3)(b_1-3(b_2+3))}$	1.84403082	0.57573193	0.133134	9
(38)	$-\dfrac{6(b_2{}^2+b_2-24)-2b_1(b_2+9)}{(b_1+3)(b_2-3)(b_2+3)(b_1-2b_2+3)(2b_1-3(b_2+3))}$	1.9049613	0.28929897	0.154554	9
(39)	$\dfrac{3(4b_1-3b_2{}^2-6b_2+57)}{(b_1+3)(b_2-3)(b_2+3)(b_1-3b_2+3)(2b_1-3(b_2+3))}$	$\frac{1}{16}\left(15\sqrt{145}-153\right)$	0	$\frac{347+29\sqrt{145}}{4050}$	2
(40)	$-\dfrac{-24b_1+b_2{}^2+12b_2-117}{(b_1+3)(b_2-3)(b_2+3)(b_1-b_2+3)(2b_1-b_2-9)}$	$\frac{1}{32}\left(15\sqrt{65}-81\right)$	0	$\frac{83+13\sqrt{65}}{1350}$	2
(41)	$\dfrac{6b_1{}^2-b_1(-4b_2{}^2+6b_2+72)-2b_2{}^3+27b_2{}^2+36b_2-513}{(b_1+3)(b_2-3)(b_2+3)(b_1+b_2-6)(b_1-2(b_2+3))}$	0.97912771	0	0.160827	3
(42)	$\dfrac{b_1{}^2((b_2+9))-18b_1(b_2+3)+18(b_2{}^2-2b_2-27)}{(b_1-6)(b_1+3)(b_2-3)(b_2+3)(b_1-b_2+3)(b_1-2(b_2+3))}$	1.3830544	0.2588732	0.145643	17
(43)	$\dfrac{2b_1{}^2(b_2+6)-2b_1(2b_2{}^2+15b_2+18)+2b_2{}^3+9b_2{}^2-108b_2-459}{(b_1+3)(b_2-3)(b_2+3)(b_1-b_2-6)(b_1-b_2+3)(b_1-2(b_2+3))}$	2.02070885	0.52070885	0.126977	3
(44)	$\dfrac{6(b_1{}^2-2b_1b_2-3b_1+6b_2{}^2+3b_2-99)}{(b_1-6)(b_1+3)(b_2-3)(b_2+3)(b_1-2b_2+3)(b_1-2(b_2+3))}$	$\frac{3}{2}$	0	$\frac{40}{243}$	1
(45)	$\dfrac{3(4b_1{}^2-4b_1(b_2+3)+3(b_2{}^2+2b_2-51))}{(b_1-6)(b_1+3)(b_2-3)(b_2+3)(b_1-b_2-6)(b_1-b_2+3)}$	$\frac{3}{2}$	0	$\frac{32}{243}$	1

TABLE A.1.1: Volume functions V, critical Reeb vectors b_i^* and their corresponding volume minima $V_{\min}$, with $b_3 = 3$. In the last column, we list the degree of the extension L (of $\mathbb{Q}$), where $L = \mathbb{Q}(b_1^*, b_2^*) = \mathbb{Q}(b_1^*)$.

As a matter of fact, all the minimized volume functions of Sasaki-Einstein manifolds Y are algebraic. When $V_{\min} \in \mathbb{Q}$, Y is said to be regular. If $V_{\min} \in \mathbb{Q}(\sqrt{c})$ ($c \in \mathbb{N}$), viz, quadratic irrationals, then Y is quasi-regular. In Fig. A.1.1, we plot the $1/V_{\min}$ against χ, with regular and quasi-regular Y's highlighted.
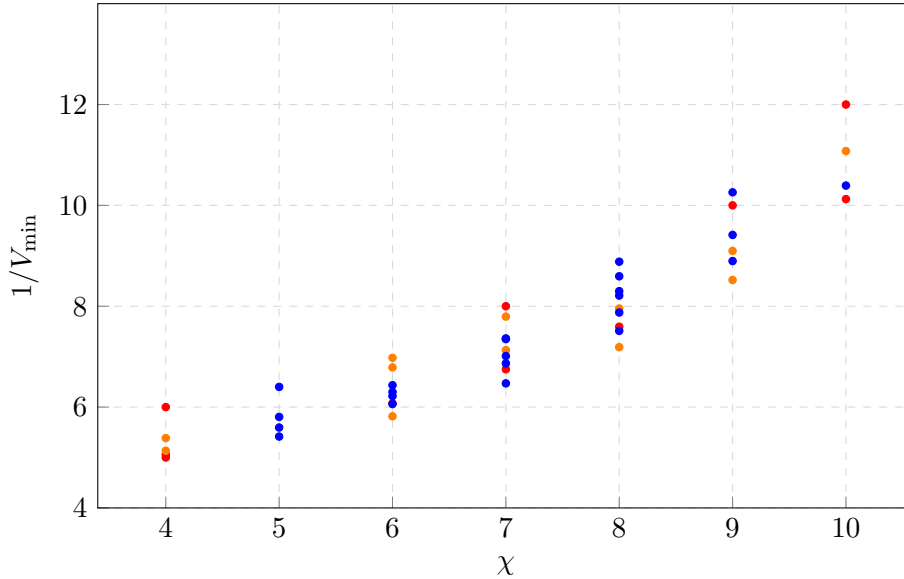
FIGURE A.1.1: The red points correspond to regular Sasaki-Einstein manifolds while the quasi-regular ones are in orange. We omit the first-grade points in the plot.

A.2   Higgsing the Parent Theory

The Higgs-Kibble mechanism states that by turning on a non-zero vev of a bifundamental and integrating out the quadratic mass terms in superpotential, we would get a theory with a different moduli space. This corresponds to removal of an edge in the brane tiling and merger of two gauge nodes in the quiver. In terms of toric diagrams, it is easy to identify the parent theories by blowing

up/down points. For instance, No.5 is the parent of all the triangles and the pentagon No.35 is the parent of all the hexagons here. As a simple example, we consider higgsing (2.2.1) to the theory of dP_0:
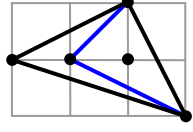
$$(A.2.1)$$

The superpotential of the parent theory is

$$
\begin{aligned}
W =& X_{12}^1 X_{25} X_{51}^2 + X_{12}^2 X_{23}^1 X_{31} + X_{23}^2 X_{34}^1 X_{42} + X_{34}^2 X_{45}^1 X_{53} + X_{45}^2 X_{51}^1 X_{14} \\
&- X_{12}^2 X_{25} X_{51}^1 - X_{12}^1 X_{23}^2 X_{31} - X_{23}^1 X_{34}^2 X_{42} - X_{34}^1 X_{45}^2 X_{53} - X_{45}^1 X_{51}^2 X_{14}.
\end{aligned}
$$

$$(A.2.2)$$

We first give a non-zero vev to X_{53}, viz, $\langle X_{53}\rangle = 1$:

$$
\begin{aligned}
W =& X_{12}^1 X_{25} X_{51}^2 + X_{12}^2 X_{23}^1 X_{31} + X_{23}^2 X_{34}^1 X_{42} + X_{34}^2 X_{45}^1 + X_{45}^2 X_{51}^1 X_{14} \\
&- X_{12}^2 X_{25} X_{51}^1 - X_{12}^1 X_{23}^2 X_{31} - X_{23}^1 X_{34}^2 X_{42} - X_{34}^1 X_{45}^2 - X_{45}^1 X_{51}^2 X_{14}.
\end{aligned}
$$

$$(A.2.3)$$

Integrating our the quadratic terms yields

$$
\begin{aligned}
W =& X_{12}^1 X_{23}^3 X_{31}^2 + X_{12}^2 X_{23}^1 X_{31}^3 + X_{42} X_{23}^2 X_{31}^1 X_{14} \\
&- X_{12}^2 X_{23}^3 X_{31}^1 - X_{12}^1 X_{23}^2 X_{31}^3 - X_{42} X_{23}^1 X_{31}^2 X_{14}.
\end{aligned}
$$

$$(A.2.4)$$

Finally, by turning on a vev of X_{42} such that $\langle X_{42}\rangle = 1$, the superpotential becomes

$$
\begin{aligned}
W =& X_{12}^1 X_{23}^3 X_{31}^2 + X_{12}^2 X_{23}^1 X_{31}^3 + X_{23}^2 X_{31}^1 X_{12}^3 \\
&- X_{12}^2 X_{23}^3 X_{31}^1 - X_{12}^1 X_{23}^2 X_{31}^3 - X_{23}^1 X_{31}^2 X_{12}^3,
\end{aligned}
$$

$$(A.2.5)$$

which is exactly the superpotential of the dP_0 theory. In terms of quivers, we have
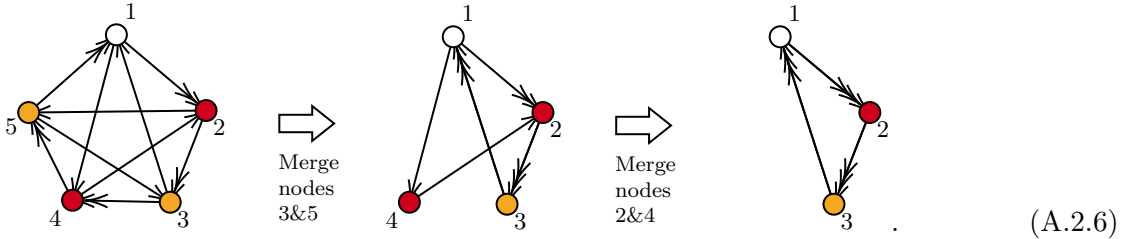
$$(A.2.6)$$

As a matter of fact, the 45 polygons can be higgsed from a same parent theory. This theory can be $\mathbb{C}^3/(\mathbb{Z}_6 \times \mathbb{Z}_6)$ $(1,0,5)(0,1,5)$ such that there is only one corresponding quiver in the toric phase. It is a huge quiver with 36 nodes and 108 bifundamentals. The R-charges of the bifundamentals are all $2/3$, and hence the three GLSM fields corresponding to the extremal points all have R-charge $2/3$, with others vanishing. If we only want the minimal parent toric diagram, then we would have $\mathcal{C}/(\mathbb{Z}_6 \times \mathbb{Z}_2)$ $(1,0,0,5)(0,1,1,0)$.

Appendix B

Example: Mahler Measure and Amoeba for F_0

We can compute the Mahler measure for any Newton polygon/polynomial directly from the definition. Let us use (3.1.6) to perform the integration. As an example, let us consider the familiar $\mathbb{F}_0$ whose Newton polynomial is $P(z, w) = -z - z^{-1} - w - w^{-1} + k$. Then its Mahler measure is

$$
\begin{aligned}
m(P) &= \frac{1}{(2\pi i)^2} \int_{|z|=|w|=1} \log|k - (z + z^{-1} + w + w^{-1})| \frac{dz}{z} \frac{dw}{w} \\
&= \mathrm{Re}\left(\frac{1}{(2\pi i)^2} \int_{|z|=|w|=1} \log(k - (z + z^{-1} + w + w^{-1})) \frac{dz}{z} \frac{dw}{w} \right).
\end{aligned}
\tag{B.0.1}
$$

The log part can be expanded as

$$
\log(k - (z + z^{-1} + w + w^{-1})) = \log k - \sum_{n=1}^{\infty} \frac{(z + z^{-1} + w + w^{-1})^n}{n} k^{-n},
\tag{B.0.2}
$$

where $|k| > 4$ or $k = 4$ as $\max_{|z|=|w|=1} |p(z, w)| = 4$.

For each summand in the above sum, they can be further expanded as

$$
\begin{aligned}
(z + z^{-1} + w + w^{-1})^n &= \sum_{i=0}^{n} \binom{n}{i} (z + z^{-1})^i (w + w^{-1})^{n-i} \\
&= \sum_{i=0}^{n} \binom{n}{i} \left(\sum_{j=0}^{i} \binom{i}{j} z^{2j-i} \right) \left(\sum_{l=0}^{n-i} \binom{n-i}{l} w^{2l-n+i} \right).
\end{aligned}
\tag{B.0.3}
$$

As the only contribution to the integral, its constant term satisfies $i = 2j, n - i = 2l$. Therefore, we can write the constant term as

$$
[(z + z^{-1} + w + w^{-1})^n]_0 = \sum_{\substack{i=0 \\ i \text{ even}}}^{n} \binom{n}{i} \binom{i}{i/2} \binom{n-i}{(n-i)/2},
\tag{B.0.4}
$$

where $[Q]_0$ denotes the constant term of Q. Equivalently, this can written as

$$
\begin{aligned}
[(z + z^{-1} + w + w^{-1})^{2n}]_0 &= \sum_{i=0}^{n} \binom{2n}{2i} \binom{2i}{i} \binom{2n-2i}{n-i} \\
&= \frac{4^{2n} \left(\frac{2n-1}{2} \right)!^2}{\pi n!^2} = \frac{16^n \Gamma^2 \left(\frac{2n+1}{2} \right)}{\pi n!^2}.
\end{aligned}
\tag{B.0.5}
$$

while $[(z + z^{-1} + w + w^{-1})^{2n-1}]_0$ vanishes. Hence,

$$\left[\sum_{n=1}^{\infty} \frac{(z + z^{-1} + w + w^{-1})^n}{n} k^{-n}\right]_0 = \left[\sum_{n=1}^{\infty} \frac{(z + z^{-1} + w + w^{-1})^{2n}}{2n} k^{-2n}\right]_0$$

$$= \sum_{n=1}^{\infty} \frac{16^n \Gamma^2\left(\frac{2n+1}{2}\right) k^{-2n}}{\pi n!^2} \frac{k^{-2n}}{2n} \qquad \text{(B.0.6)}$$

$$= 2k^{-2} {}_4F_3\left(1, 1, \frac{3}{2}, \frac{3}{2}; 2, 2, 2; 16k^{-2}\right),$$

where ${}_pF_q$ is the (generalized) hypergeometric function. Therefore, we get

$$m(P) = \text{Re}\left(\log k - 2k^{-2} {}_4F_3\left(1, 1, \frac{3}{2}, \frac{3}{2}; 2, 2, 2; 16k^{-2}\right)\right), \quad |k| > 4 \text{ or } k = 4. \qquad \text{(B.0.7)}$$

In this paper, we are mainly interested in the case $k \geq 4$. Therefore,

$$m(P) = \log k - 2k^{-2} {}_4F_3\left(1, 1, \frac{3}{2}, \frac{3}{2}; 2, 2, 2; 16k^{-2}\right), \quad k \geq 4. \qquad \text{(B.0.8)}$$

We may as well calculate the period $u_0(k)$ following the same manner. Recall that $u_0(k)$ can be written as the integral

$$u_0(k) = \frac{1}{(2\pi i)^2} \int_{|z|=|w|=1} \frac{1}{1 - k^{-1}(z + z^{-1} + w + w^{-1})} \frac{dz}{z} \frac{dw}{w}. \qquad \text{(B.0.9)}$$

Then we have the series expansion

$$\frac{1}{1 - k^{-1}(z + z^{-1} + w + w^{-1})} = \sum_{n=0}^{\infty} k^{-n}(z + z^{-1} + w + w^{-1})^n, \quad |k| > 4. \qquad \text{(B.0.10)}$$

Since we are still dealing with $(z + z^{-1} + w + w^{-1})^n$, the constant terms are still the same as (B.0.5). Hence,

$$u_0(k) = \sum_{n=0}^{\infty} \frac{16^n \Gamma^2\left(\frac{2n+1}{2}\right)}{\pi n!^2} k^{-2n} = \frac{2}{\pi} K(4k^{-1}) = {}_2F_1\left(\frac{1}{2}, \frac{1}{2}; 1; 16k^{-2}\right), \quad |k| > 4, \qquad \text{(B.0.11)}$$

where $K(x) = \int_0^1 \frac{dt}{\sqrt{(1-t^2)(1-x^2t^2)}}$ is the elliptic integral of the first kind. As we can see, $u_0(k)$ is simply a hypergeometric function and $m(P)$ can also be expressed concisely using some hypergeometric function. In general, there may not be such compact expressions for $m(P)$ and $u_0(k)$. We will then compute them perturbatively in terms of their series expansions as

$$m(P) = \log k - \sum_{n=2}^{\infty} \frac{f_n}{nk^n}, \quad u_0(k) = 1 + \sum_{n=2}^{\infty} \frac{f_n}{k^n}. \qquad \text{(B.0.12)}$$

In Figure B.0.1, we plot $m(P)$ along the Mahler flow. We also plot several amoebae using Monte-Carlo for different k to illustrate how the amoebae would change along the Mahler flow.

Incidentally, we also plot the Mahler measures for negative k in Figure B.0.1(a) which give the mirror shape of the positive Mahler flow. This shows a non-differentiable point at $k = 0$. If we plot the amoeba for $k = 0$ as in Figure B.0.1(b), we can see that it degenerates to two lines. In other words, the amoeba retracts to its spine in this case. By definition, $k = 0$ gives another tropical limit.
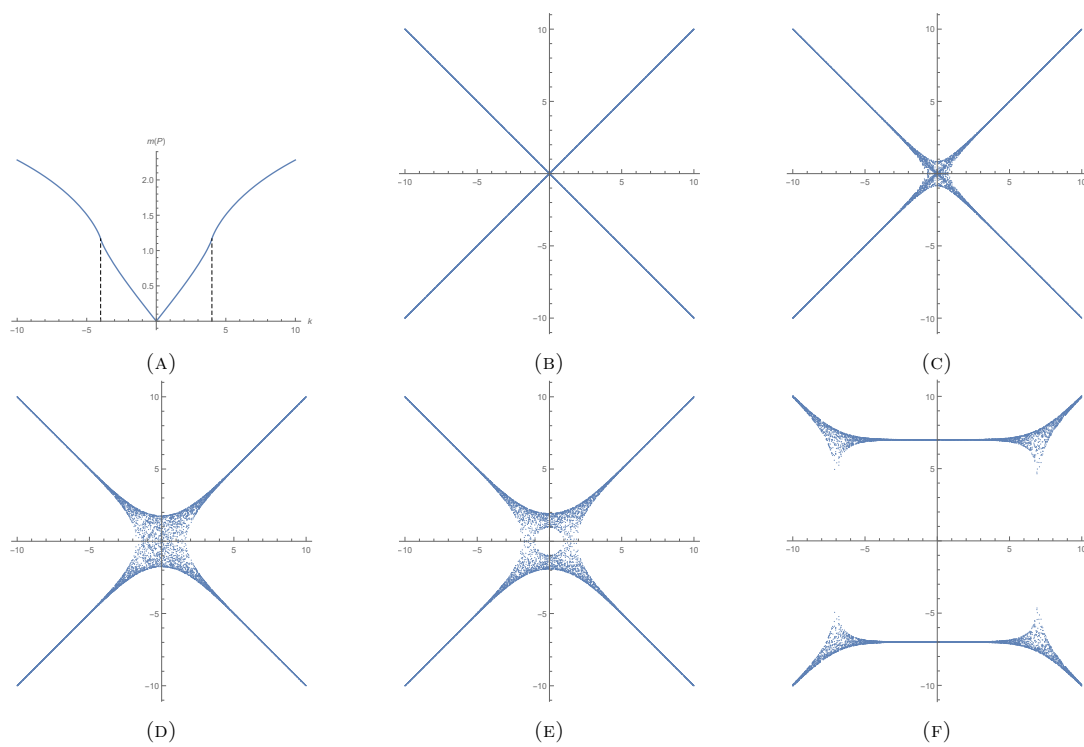
FIGURE B.0.1: The numerical $m(P)$ along the Mahler flow in (a). The amoeba for $P(z, w)$ when (b) $k = 0$, (c) $k = 3/4$, (d) $k = k_{\text{iso}} = 4$, (e) $k = 5$ and (f) $k = \mathrm{e}^7$.

Appendix C

Dessins, Seiberg-Witten Curves and Conformal Blocks

In this appendix, we discuss another aspect of dessins involving the connections to SW theories and conformal blocks (CBs). We shall focus on six specific trivalent dessins with 4 punctures on the sphere.

From these dessins, we obtain algebraic curves that we interpret as SW curves of 4d SU(2) $\mathcal{N} = 2$ $N_f = 4$, SYM theories. These curves are given in terms of six parameters, four mass parameters $(\mu_1, \mu_2, \mu_3, \mu_4)$, a parameter ζ and a modulus U. We write these curves in the form that appears in [276, 277], and use their mirror map to translate the above parameters to those characterizing the 4d instanton partition function of a 4d $\mathcal{N} = 2$ gauge theory. In particular, we map the modulus U to the Coulomb parameter a. Following that, we use the AGT dictionary [79, 80] to interpret the result in 2d CFT terms.

Let us take a closer look at the six parameters for the SU(2) gauge theory. With $N_f = 4$, the theory has an $SO(8) \supset SU(2)^4$ flavour symmetry. Then the mass parameters of the four hypers could be indentified as the charges of the primaries in Liouville theory under AGT correspondence. Following [278, 279], the AGT map could also lead to diagonal minimal models by further restrictions on the partition pairs. As usual, we would arrange the poles of the SW curves at $z = 0, 1, \infty$ and ζ. This ζ is nothing but the UV gauge coupling τ via $\zeta = e^{2\pi i \tau}$. For each dessin, we find that ζ could have several different values but these values enjoy certain triality.

Recall that the Coulomb parameter a denotes the vev of the adjoint scalar ϕ, or equivalently, a could be obtained by integrating the SW differential along the so-called A-cycle on SW curve. Such supersymmetric vacua can be gauge invariantly parametrized by $u = \langle \mathrm{tr} \phi^2 \rangle / 2 = a^2$ up to quantum corrections. As we will discuss, the parameter U, which will appear in the parametrization of the curve, is linear in the Coulomb moduli u. In fact, as we will see, each dessin gives a family of solutions for the gauge theory parameters, and indeed, we would have the same corresponding dessin under the change $m_i \to k m_i$, $a \to k a$, $U \to k^2 U$ for $k^2 \in \mathbb{R}$. This is consistent with their mass dimensions.

The above discussions can go the other way as well. Starting from the CBs in CFTs, we can write down the Nekrasov partition functions under the AGT dictionary. This 4d partition function can also be lifted to 5d, which leads to topological string partition functions and SW curves. As the SW differential and the Strebel differential from the dessin side are both quadratic, the gauge theories are naturally related to dessins.

Since the instanton partition functions with extra conditions on the Young tableaux pairs could be mapped to conformal blocks in minimal models [278, 279], we can then check whether (the parametrizations from) the dessins could correspond to such CBs in minimal models. As we will see, such map is not one-to-one. A dessin could correspond to one or more possible CBs in multiple minimal models. These CBs, albeit in different minimal models, would satisfy certain (fixed) rules for the dessin. There might also exist dessins that do not give rise to minimal models. On the

minimal model side, it is still not determined whether this subset of dessins could recover all the CBs or just part of them.

C.1 From Seiberg-Witten Curves to Dessins d'Enfants

Here, we shall only mention how dessins can arise from SW curves via the identification of the quadratic differentials. The details on obtaining Nekrasov partition functions as well as 5d and 4d topological string partition functions from conformal blocks can be found for example in [5, §2].

From Belyi maps to dessins Recall that we can associate a Belyi map $\beta(x)$ to a dessin via its *ramification indices*: the order of vanishing of the Taylor series for $\beta(x)$ at $\tilde{x}$ is the ramification index $r_{\beta(\tilde{x}) \in \{0,1,\infty\}}(i)$ at that i^{th} point. By convention, we mark one white node for the ith pre-image of 0 with $r_0(i)$ edges emanating therefrom. Similarly, we mark one black node for the jth pre-image of 1 with $r_1(j)$ edges. We then connect the nodes with the edges, joining only black with white, such that each face is a polygon with $2r_\infty(k)$ sides. In other words, there is one pre-image of ∞ corresponding to each polygon of $\mathcal{D}$. Moreover, there is a cyclic ordering arising from local monodromy winding around vertices, i.e., around local covering sheets that contain a common point.

Following Belyi's theorem, the existence of a dessin on X is equivalent to X admitting an algebraic equation over the algebraic numbers. Moreover, the Galois group $\text{Gal}(\bar{\mathbb{Q}} : \mathbb{Q})$ acts faithfully on the space of dessins.

Quadratic Differentials A *(holomorphic) quadratic differential q* on a Riemann surface X is a holomorphic section of the symmetric square of the contangent bundle. In terms of local coordinates z, $q = f(z)\mathrm{d}z \otimes \mathrm{d}z$, for some holomorphic function $f(z)$.

A curve $\gamma(t) \subset X$ can be classified by q as

- Horizontal trajectory: $f(\gamma(t))\dot{\gamma}(t)^2 > 0$;

- Vertical trajectory: $f(\gamma(t))\dot{\gamma}(t)^2 < 0$.

Locally, one can find coordinates so that horizontal tracjectories look like concentric circles while vertical trajectories look like rays emanating from a single point.

Then we can define the *Strebel differential*:

Definition C.1.1. *For a Riemann surface X of genus $g \geq 0$ with $n \geq 1$ marked points $\{p_1, \ldots, p_n\}$ such that $2 - 2g < n$, and a given n-tuple $a_{i=1,\ldots,n} \in \mathbb{R}^+$, a Strebel differential $q = f(z)\mathrm{d}z^2$ is a quadratic differential such that*

- *f is holomorphic on $X \backslash \{p_1, \ldots, p_n\}$;*

- *f has a second-order pole at each p_i;*

- *the union of all non-compact horizontal trajectories of q is a closed subset of X of measure 0;*

- *every compact horizontal of q is a simple loop A_i centered at p_i such that $a_i = \oint_{A_i} \sqrt{q}$. (Here the branch of the square root is chosen so that the integral has a positive value with respect to the positive orientation of A_i that is determined by the complex structure of X.)*

The upshot is that [280]

Theorem C.1.1. *The Strebel differential is the pull-back, by a Belyi map $\beta : X \to \mathbb{P}^1$, of a quadratic differential on $\mathbb{P}^1$ with 3 punctures,*

$$q = \beta^* \left(\frac{\mathrm{d}\zeta^2}{4\pi^2 \zeta(1-\zeta)} \right) = \frac{(\mathrm{d}\beta)^2}{4\pi^2 \beta(1-\beta)} = \frac{(\beta')^2}{4\pi^2 \beta(1-\beta)} \mathrm{d}z^2, \tag{C.1.1}$$

where z and ζ are coordinates on X and $\mathbb{P}^1$ respectively.

Recall the definition of the SW differential

$$\lambda = v\frac{\mathrm{d}z}{z}. \tag{C.1.2}$$

Then

$$q = \lambda^2 = v^2\frac{\mathrm{d}z^2}{z^2} =: \phi(z)\mathrm{d}z^2 \tag{C.1.3}$$

is the quadratic differential on $\mathcal{C}$.

SW curves and Dessins As mentioned above, the SW curve Σ is related to the quadratic differential q. Moving in the moduli space of the theory in question will alter the parameters in the SW curve, thereby altering the parameters in q [168]. Following [280], it was found in [168] that at certain isolated points in the Coulomb branch $\mathcal{U}_{g,n}$, where g is the genus of the Gaiotto curve $\mathcal{C}$ with n marked points, q is completely fixed and becomes a Strebel differential $q = \phi(t)\mathrm{d}t^2 = \frac{\mathrm{d}\beta^2}{4\pi^2\beta(t)(1-\beta(t))}$.

As examples for SU(2) with $N_f = 4$, we will discuss 6 Strebel points in $\mathcal{U}_{g,n} \times \mathbb{R}^n$, for which the Belyi maps are presented in Table C.1.1. These six Belyi maps are those found in [166, 281]

Graph	$\beta(t)$	Ramification	Strebel q
$\Gamma(3)$	$\frac{t^3(t+6)^3(t^2-6t+36)^3}{1728(t-3)^3(t^2+3t+9)^3}$	$[3^4|2^6|3^4]$	$-\frac{9t(t^3+216)}{4\pi^2(t^3-27)^2}$
$\Gamma_0(4) \cap \Gamma(2)$	$\frac{(t^4+224t^2+256)^3}{1728t^2(t-4)^4(t+4)^4}$	$[3^4|2^6|4^2,2^2]$	$-\frac{4t^4+896t^2+1024}{4\pi^2t^2(t^2-16)^2}$
$\Gamma_1(5)$	$\frac{(t^4+248t^3+4064t^2+22312t+40336)^3}{1728(t+5)(t^3-t-31)^5}$	$[3^4|2^6|5^2,1^2]$	$-\frac{t^4+248t^3+4064t^2+22312t+40336}{4\pi^2(t+5)^2(t^2-t-31)^2}$
$\Gamma_0(6)$	$\frac{(t+7)^3(t^3+237t^2+1443t+2287)^3}{1728(t+3)^2(t+4)^3(t-5)^6}$	$[3^4|2^6|6,3,2,1]$	$-\frac{(t+7)(t^3+237t^2+1443t+2287)}{4\pi^2(t+5)^2(t+3)^2(t+4)^2}$
$\Gamma_0(8)$	$\frac{(t^4+240t^3+2144t^2+3840t+256)^3}{1728t(t+4)^2(t-4)^8}$	$[3^4|2^6|8,2,1^2]$	$-\frac{t^4+240t^3+2144t^2+3840t+256}{4\pi^2t^2(t^2-16)^2}$
$\Gamma_0(9)$	$\frac{(t+6)^3(t^3+234t^2+756t+2160)^3}{1728(t^2+3t+9)(t-3)^9}$	$[3^4|2^6|9,1^3]$	$-\frac{(t+6)(t^3+234t^2+756t+2160)}{4\pi^2(t^3-27)^2}$

TABLE C.1.1: The list of the six genus-zero, torsion-free, congruence subgroups of the modular group Γ, of index 12. The corresponding Belyi maps $\beta(t)$ and their ramification indices, as well as the Strebel differentials are also shown. Note that the ramification indices for all 6 are such that there are 4 pre-images of 0 of order 3 and 6 pre-images of 1 of order 2. The pre-images of ∞ (aka the *cusp widths*) all add to 12, as do the ramification indices for 0 and 1. This is required by the fact that all the subgroups are of index 12 within Γ.

to be associated to the six *genus zero*, *torsion-free*, *congruence* subgroups of the modular group $\Gamma = \mathrm{PSL}(2, \mathbb{Z}) \cong \mathbb{Z}_2 * \mathbb{Z}_3$, where $*$ denotes the free product[1].

From the Belyi maps in Table C.1.1, we can compute the associated dessins as displayed in Figure C.1.1. The dessins d'enfants associated to each Strebel point of the generalised quiver theory in question turn out to have an interpretation as so-called *ribbon graphs* on the Gaiotto curve $\mathcal{C}$. For details, the readers are referred to [168, 280].

C.2 From Dessins to Conformal Blocks

Let us now complete the cycle of the route map above by considering what gauge theory and CFT data we can obtain starting from these 6 dessins.

---

[1]It remains an open question whether dessins associated to other subgroups of the modular group, perhaps of higher index, arise for other $\mathcal{N} = 2$ generalised quiver theories in a parallel manner.

$$\Gamma(3) \qquad \Gamma_0(4) \cap \Gamma(2) \qquad \Gamma_1(5)$$

$$\Gamma_0(6) \qquad \Gamma_0(8) \qquad \Gamma_0(9)$$
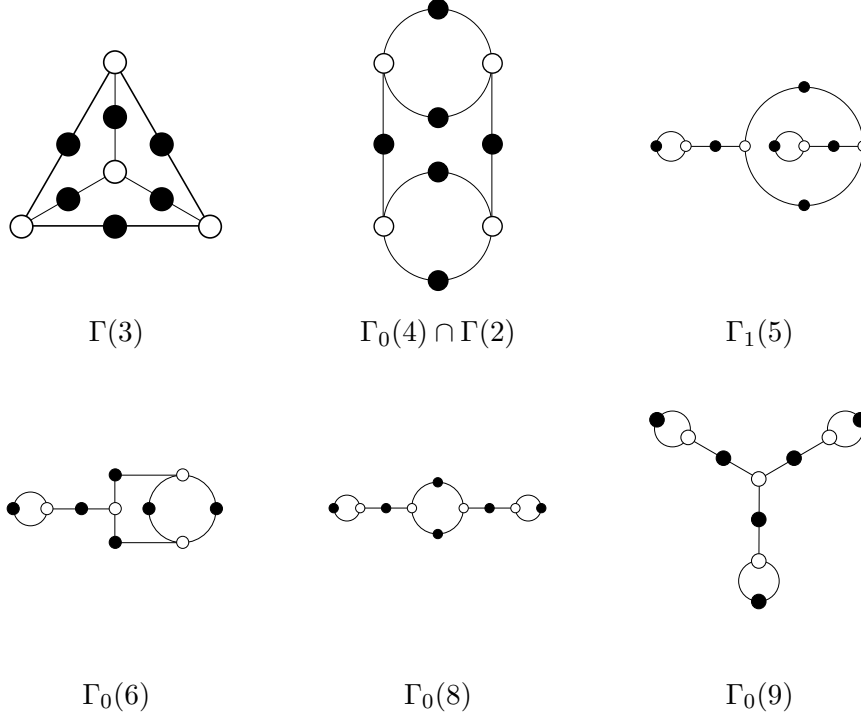
FIGURE C.1.1: The dessins d'enfants associated to the six Strebel points of the SU(2), $N_f = 4$ theory.

C.2.1 The SU(2) with 4 Flavours

Given that all our graphs in Figure C.1.1 are drawn on the Riemann surface (genus zero) with 4 marked points (one for each face), we can naturally interpret these as Gaiotto curves [168, 178], and thence $\mathcal{N} = 2$ gauge theories.

To begin, the Seiberg-Witten curve Σ for the SU(2) $N_f = 4$ theory in algebraic form is standard [282]. For future convenience, we write the SW differential as [276, 277]

$$\lambda_{\mathrm{SW}} = \frac{\sqrt{P_4(z)}}{z(z-1)(z-\zeta)}\mathrm{d}z, \qquad P_4(z) = m_0^2 \prod_{i=1}^{4}(z-\lambda_i) = m_0^2 \sum_{i=0}^{4} z^{4-i}S_i, \tag{C.2.1}$$

under the substitution

$$\lambda_{\mathrm{SW}} = v\mathrm{d}z/z, \; t = z,$$
$$\mu_1 = m_2 + m_0, \; \mu_2 = m_2 - m_0, \; \mu_3 = m_3 + m_1, \; \mu_4 = m_3 - m_1, \tag{C.2.2}$$

The parameters S_i are given in terms of the flavour mass and coupling parameters $m_{0,1,2,3}, \zeta, U \in \mathbb{C}$ so that $S_0 = 1$ for the top coefficient and

$$m_0^2 S_1 = -\left(m_0^2 + m_2^2(\zeta - 1) + m_0^2\zeta + 2m_2 m_3\zeta + (1+\zeta)U\right),$$
$$m_0^2 S_2 = (m_0^2 + m_1^2 - m_3^2 + 2m_2 m_3)\zeta + m_2^2(\zeta - 1)\zeta + 2m_2 m_3\zeta^2 + m_3^2\zeta^2 + (1+\zeta)^2 U,$$
$$m_0^2 S_3 = -\left((m_1^2 - m_3^2)\zeta + (m_1^2 + 2m_2 m_3 + m_3^2)\zeta^2 + \zeta(1+\zeta)U\right),$$
$$m_0^2 S_4 = m_1^2\zeta^2 . \tag{C.2.3}$$

Now the SW curve is of the form

$$z^2(v - (m_0 + m_2))(v - (m_2 - m_0)) + z(1+\zeta)\left(-v^2 + \frac{2\zeta}{(1+\zeta)}(m_2 + m_3)v + U\right)$$
$$+\zeta(v - (m_1 + m_3))(v - (m_3 - m_1)) = 0. \tag{C.2.4}$$

Now the SW curve is of the form

$$z^2(v - (m_0 + m_2))(v - (m_2 - m_0)) + z(1 + \zeta)\left(-v^2 + \frac{2\zeta}{(1+\zeta)}(m_2 + m_3)v + U\right)$$
$$+ \zeta(v - (m_1 + m_3))(v - (m_3 - m_1)) = 0. \tag{C.2.5}$$

On the other hand, the S-parameters can be written in terms of the λ_i as standard symmetric polynomials,

$$S_k = \sum_{1 \leq j_1 \leq \ldots \leq j_k \leq 4} \lambda_{j_1} \ldots \lambda_{j_k}. \tag{C.2.6}$$

As derived in [5, Appendix E.1], we can then write

$$\frac{\mathrm{d}a(U)}{\mathrm{d}U} = -\frac{1}{\pi \mathrm{i}}\frac{1 + \zeta}{m_0\sqrt{(\lambda_2 - \lambda_3)(\lambda_4 - \lambda_1)}}K(r), \tag{C.2.7}$$

where

$$r^2 = \frac{(\lambda_1 - \lambda_2)(\lambda_3 - \lambda_4)}{(\lambda_2 - \lambda_3)(\lambda_4 - \lambda_1)}, \tag{C.2.8}$$

and $K(r)$ is the elliptic integral of the first kind. The right hand side of (C.2.7) implicitly depends on U, through λ_i and thence S_i, thus we only need to integrate it to obtain $a(U)$ as a function of U, which could be a daunting task analytically.

Let us nevertheless attempt at some simplifications. First, we see that the right hand side depends only on the cross-terms in the four λ_i, which we will denote as $\lambda_{(ij)(kl)} = (\lambda_i - \lambda_j)(\lambda_k - \lambda_l)$. Combining with (C.2.6), let us see whether these can be directly expressed in terms of S_i, and thence, in terms of U. This is a standard algebraic elimination problem and we readily find the following:

Lemma C.2.1. *Consider the monic cubic polynomial,*

$$x^3 + \left(-2S_2^2 + 6S_1S_3 - 24S_4\right)x^2 + \left(S_2^4 - 6S_1S_3S_2^2 + 24S_4S_2^2 + 9S_1^2S_3^2 + 144S_4^2 - 72S_1S_3S_4\right)x$$
$$+ 27S_4^2S_1^4 + 4S_3^3S_1^3 - 18S_2S_3S_4S_1^3 - 144S_2S_4^2S_1^2 + 4S_2^3S_4S_1^2 + 6S_3^2S_4S_1^2 - 18S_2S_3^3S_1 + 192S_3S_4^2S_1$$
$$+ 80S_2^2S_3S_4S_1 + 27S_3^4 - 256S_4^3 + 4S_2^3S_3^2 - S_1^2S_2^2S_3^2 + 128S_2^2S_4^2 - 16S_2^4S_4 - 144S_2S_3^2S_4. \tag{C.2.9}$$

Then the squares of the 3 cross-products

$$x_1 = \lambda_{(12)(34)}^2, \quad x_2 = \lambda_{(23)(41)}^2, \quad x_3 = \lambda_{(13)(24)}^2 \tag{C.2.10}$$

are the three roots of it.

Of course, we can substitute the S_i parameters in terms of the m_i, ζ, U parameters from (C.2.1), though the expression become too long to present here. Now, we have

$$a(U_0) - a(U) = -\frac{1 + \zeta}{m_0\pi \mathrm{i}}\int_U^{U_0}\frac{\mathrm{d}U'}{\sqrt[4]{x_2(U')}}K\left(\frac{\sqrt[4]{x_1(U')}}{\sqrt[4]{x_2(U')}}\right). \tag{C.2.11}$$

To determine the integral constant, we choose U_0 such that $a(U_0) = 0$. We can find such U_0 by solving the discriminant of $P_4(z)$ where two branch points coincide and the A-cycle shrinks[2]. Hence,

$$a(U) = \frac{1 + \zeta}{m_0\pi \mathrm{i}}\int_U^{U_0}\frac{\mathrm{d}U'}{\sqrt[4]{x_2(U')}}K\left(\frac{\sqrt[4]{x_1(U')}}{\sqrt[4]{x_2(U')}}\right). \tag{C.2.12}$$

---

[2]Alternatively, we may also integrate from U to ∞ as the large U behaviour can be determined as in [5, Appendix E.2].

In general, when we integrate from some U to U_0, the positions of branch points and cuts might change. Therefore, this is really a sum of integrals:

$$\int_U^{U_0} = \int_U^{U_1} + \int_{U_1}^{U_2} + \cdots + \int_{U_{n-1}}^{U_n=U_0} \tag{C.2.13}$$

such that x_i does not change its expression for each integral on the right hand side.

Recall the definition of the Seiberg-Witten differential from (C.1.3), we have that

$$\lambda_{\mathrm{SW}}^2 = \phi_{\mathrm{SW}}(z)\mathrm{d}z^2 \tag{C.2.14}$$

is a quadratic differential. This is the above mentioned meromorphic quadratic differential on $\mathcal{C}$. Moving in the moduli space of the theory in question will alter the parameters in the Seiberg-Witten curve, thereby altering the parameters in q (cf. [168]). Following [280], it was found in [168] that at certain isolated points in the Coulomb branch of the moduli space $\mathcal{U}_{g,n}$ of the gauge theory in question, where g is the genus of the Gaiotto curve $\mathcal{C}$ with n marked points, q is completely fixed, which becomes a Strebel differential.

We therefore have two forms of the Strebel differentials, $\phi_\beta(t)$ coming from the dessin and $\phi_{\mathrm{SW}}(z)$ coming from the physics. Now, because dessins are *rigid*, they have no parameters. The insight of Belyi and Grothendieck is precisely that the maps β have parameters fixed at very special algebraic points in moduli space. Thus, $\phi_\beta(t)$ is of a particular form, as a rational function in t with fixed algebraic coefficients.

On the other hand $\phi_{\mathrm{SW}}(z)$ from the gauge theory has parameters which we saw earlier, corresponding to masses, couplings etc. Therefore, up to redefinition of the variables (t, z) and identifying $\phi_{\mathrm{SW}}(z)$ and $\phi_\beta(t)$ it is natural to ask how the special values of the parameters from the dessin perspective *fix* the physical parameters in the gauge theory and if a dessin implicates any interesting physical theory.

We have now introduced all the necessary dramatis personae of our tale and our strategy is thus clear. There are also some further details that we should be careful about in the calculations. We will work through an example in detail to illustrate them in the following subsection.

C.2.2 Example: $\Gamma(3)$

Let us take the dessin for $\Gamma(3)$, whose Belyi map is

$$\beta(t) = \frac{t^3(t+6)^3(t^2-6t+36)^3}{1728(t-3)^3(t^2+3t+9)^3}. \tag{C.2.15}$$

We can readily get the pre-images of 0, 1 and ∞:

	Pre-image	Ramification
$\beta^{-1}(0)$	-6	3
	0	3
	$3 - 3i\sqrt{3}$	3
	$3 + 3i\sqrt{3}$	3
$\beta^{-1}(1)$	$3(1 - \sqrt{3})$	2
	$3(1 + \sqrt{3})$	2
	$\left(\frac{3}{2} + \frac{3i}{2}\right)\left(\sqrt{3} + (-2 - i)\right)$	2
	$\left(-\frac{3}{2} - \frac{3i}{2}\right)\left(\sqrt{3} + (2 + i)\right)$	2
	$\frac{1}{2}\left((-3 + 9i) - (3 - 3i)\sqrt{3}\right)$	2
	$\frac{1}{2}\left((-3 + 9i) + (3 - 3i)\sqrt{3}\right)$	2
$\beta^{-1}(\infty)$	∞	3
	3	3
	$-\frac{3}{2}i\left(\sqrt{3} - i\right)$	3
	$\frac{3}{2}i\left(\sqrt{3} + i\right)$	3

$$\tag{C.2.16}$$

We can construct the corresponding dessin as in Figure C.1.1. Subsequently, using (C.1.1), we see that the Strebel differential is $q = \phi_\beta(t)\mathrm{d}t^2$, where

$$\phi_\beta(t) = -\frac{9t(t^3 + 216)}{4\pi^2(t^3 - 27)^2}. \tag{C.2.17}$$

We have marked ϕ with a subscript β to emphasize its dessin origin. On the other side, we have the Seiberg-Witten curve and quadratic differential for SU(2) with $N_f = 4$ from (C.2.1) and (C.2.14), to be

$$\phi_{\mathrm{SW}}(z) = \frac{P_4(z)}{(z(z-1)(z-\zeta))^2} \ , \quad \text{where}$$
$$\begin{aligned} P_4(z) = {}&z^4 m_0^2 - z^3 \left(m_0^2 + m_2^2(\zeta - 1) + m_0^2\zeta + 2m_2 m_3\zeta + (1+\zeta)U\right) \\ &+ z^2 \left((m_0^2 + m_1^2 - m_3^2 + 2m_2 m_3)\zeta + m_2^2(\zeta - 1)\zeta + 2m_2 m_3\zeta^2 + m_3^2\zeta^2 + (1+\zeta)^2 U\right) \\ &- z \left((m_1^2 - m_3^2)\zeta + (m_1^2 + 2m_2 m_3 + m_3^2)\zeta^2 + \zeta(1+\zeta)U\right) + m_1^2\zeta^2. \end{aligned} \tag{C.2.18}$$

Here, likewise we have marked ϕ with a subscript "SW" to emphasize its Seiberg-Witten origin. We have also explicitly written the differential coming from the Seiberg-Witten side in terms of the parameters $m_{0,1,2,3}, \zeta, U$.

We need to match (C.2.17) with (C.2.18), up to an PGL$(2,\mathbb{C})$ transformation on the complex variable z. The reason for this is that we are dealing in this example with a quadratic differential on the *sphere*. For curves of higher genus, such PGL$(2,\mathbb{C})$ transformations are generically not permitted, as they will not preserve the structure of the poles and zeros of the quadratic differential.

We can therefore write

$$z = \frac{at + b}{ct + d}, \qquad a, b, c, d \in \mathbb{C} \tag{C.2.19}$$

and solve for complex coefficients a, b, c, d as well as the parameters $m_{0,1,2,3}, \zeta, U$ so that we have identically for all t that

$$\phi_\beta(t) = \phi_{\mathrm{SW}}\left(\frac{at + b}{ct + d}\right). \tag{C.2.20}$$

There are actually continuous families of 2×2 matrices solving this equation for a given dessin. As the elliptic curve is the same up to an overall factor, it turns out that each continuous family would simply scale the SW differential by $\phi_{\mathrm{SW}} \to k^2\phi_{\mathrm{SW}}$ with $k^2 \in \mathbb{R}$, where the square comes from the λ_{SW}^2 in the differential. Obviously, equating the numerators of ϕ_β and ϕ_{SW} as well as equating their denominators would give a solution. For future convenience, such solution will be referred to as the "basic" values of the parametrization. Then other parametrizations would simply follow

$$\phi_{\mathrm{SW}} = k^2 \phi_{\mathrm{SW,basic}}. \tag{C.2.21}$$

There are two points we should pay attention to:

- As we will try to relate this to minimal models, due to modular invariance, we can only allow primary states with pure imaginary charges [283]. The AGT relation in terms of m_i is

$$\frac{m_0}{\sqrt{\epsilon_1\epsilon_2}} + \frac{Q}{2} = \alpha_4, \ \frac{m_1}{\sqrt{\epsilon_1\epsilon_2}} + \frac{Q}{2} = \alpha_1, \ \frac{m_2}{\sqrt{\epsilon_1\epsilon_2}} = \alpha_3, \ \frac{m_3}{\sqrt{\epsilon_1\epsilon_2}} = \alpha_2, \ \frac{a}{\sqrt{\epsilon_1\epsilon_2}} + \frac{Q}{2} = \alpha_{\mathrm{int}}. \tag{C.2.22}$$

  In fact, $\epsilon_{1,2}$ are not completely free once $Q = (\epsilon_1 + \epsilon_2)/\sqrt{\epsilon_1\epsilon_2}$ is chosen. Moreover, to have real conformal dimensions, m_i's and a should only be real or pure imaginary (depending on $\epsilon_{1,2}$). This is also the reason why k^2 should be real.

- One may easily check that an SW differential/elliptic curve would have the same j-invariant under $\phi \to k^2\phi$. As a result, the parameters, based on their mass dimensions or by looking at $P_4(z)$ and $a(U)$, would follow

$$m_i \to km_i, \ a \to ka, \ \epsilon_i \to k\epsilon_i, \ U \to k^2 U;$$

$$\zeta \to \zeta, \ \alpha_{i,\text{int}} \to \alpha_{i,\text{int}}, \ Q \to Q. \tag{C.2.23}$$

Therefore, rather than discrete parameters, we would have *families* of differentials. Importantly, we can see that the coupling ζ is *invariant*. Following the AGT map, the dimensionless CFT parameters, $\alpha_{i,\text{int}}$ and Q, are also invariant under the scaling though we still have the freedom to choose $\sqrt{\epsilon_1 \epsilon_2}$.

Now expanding the above and setting all the coefficients of t to vanish identically gives a complicated polynomial system in $(a, b, c, d, m_{0,1,2,3}, \zeta, U)$ for which one can find many solutions. For example, the following constitutes a solution (with $k^2 = 1$),

$$m_0 = -m_1 = m_2 = -m_3 = \frac{1}{2\sqrt{3}\pi}, \quad \zeta = \frac{1}{2} + \frac{\text{i}\sqrt{3}}{2}, \quad U = \frac{1}{9\pi^2} \tag{C.2.24}$$

with $(a, b, c, d) = \left(\frac{1+\text{i}}{\sqrt{2}3^{3/4}}, \ \text{i} \left(\frac{\sqrt[4]{3}}{2\sqrt{2}} - \frac{3^{3/4}}{2\sqrt{2}} \right) + \frac{\sqrt[4]{3}}{2\sqrt{2}} + \frac{3^{3/4}}{2\sqrt{2}}, \ 0, \ \frac{(1-\text{i})3^{3/4}}{\sqrt{2}} \right)$. The numerator of the SW differential takes the form

$$P_4(z) = -\frac{6z^4 - 4\text{i}\left(\sqrt{3} - 3\text{i}\right)z^3 + \left(6 + 6\text{i}\sqrt{3}\right)z^2 - 8\text{i}\sqrt{3}z + 3\text{i}\sqrt{3} - 3}{72\pi^2}. \tag{C.2.25}$$

We now need the roots λ_i of $P_4(z)$ as given in (C.2.1):

$$z^4 + \left(-2 - \frac{2\text{i}}{\sqrt{3}}\right)z^3 + \left(1 + \text{i}\sqrt{3}\right)z^2 - \frac{4\text{i}}{\sqrt{3}}z + \frac{1}{2}\text{i}\left(\sqrt{3} + \text{i}\right) = \prod_{i=1}^{4}(z - \lambda_i). \tag{C.2.26}$$

The SW curve itself is genus 1 and is in fact an elliptic curve. We can recast (C.2.18) as

$$\begin{aligned}
y^2 = \ & z^4 m_0^2 - z^3 \left(m_0^2 + m_2^2(\zeta - 1) + m_0^2 \zeta + 2m_2 m_3 \zeta + (1 + \zeta)U\right) \\
& + z^2 \left((m_0^2 + m_1^2 - m_3^2 + 2m_2 m_3)\zeta + m_2^2(\zeta - 1)\zeta + 2m_2 m_3 \zeta^2 + m_3^2 \zeta^2 + (1 + \zeta)^2 U\right) \\
& - z \left((m_1^2 - m_3^2)\zeta + (m_1^2 + 2m_2 m_3 + m_3^2)\zeta^2 + \zeta(1 + \zeta)U\right) + m_1^2 \zeta^2,
\end{aligned} \tag{C.2.27}$$

where the redefinition $y^2 = (z(z-1)(z-\zeta))^2 \phi_{\text{SW}}(z) = P_4(z)$ is used. Using the formula derived in [5, Appendix D], one may check that the j-invariant we get from the parameterization (C.2.24) agrees with the one directly from the Strebel differential (C.2.17):

$$j = 0. \tag{C.2.28}$$

Indeed, $j = 0$ corresponds to a special elliptic curve with $\mathbb{Z}/3\mathbb{Z}$-symmetry, much like the dessin for $\Gamma(3)$ itself.

In this case, we can integrate (C.2.12) numerically to obtain $a(U) = \frac{1}{3\sqrt{3}\pi}$ [3]. Now we can use the AGT relation (C.2.22) to get the parametrizations for CBs. If we take $Q = 0$, we have

$$\alpha_1 = \alpha_2 = -\alpha_3 = -\alpha_4 = \frac{\text{i}}{2\sqrt{3}\pi}, \ \alpha_{\text{int}} = \frac{\text{i}}{3\sqrt{3}\pi}, \tag{C.2.29}$$

where we have chosen $-\epsilon_1 = \epsilon_2 = 1$ as an example.

We can also have pure imaginary m_i's and a for the above example such as

$$m_0 = -m_1 = m_2 = -m_3 = \frac{\text{i}}{2\sqrt{3}\pi}, \ \zeta = \frac{1}{2} + \frac{\text{i}\sqrt{3}}{2}, \ U = -\frac{1}{9\pi^2}, \ a = \frac{\text{i}}{3\sqrt{3}\pi}. \tag{C.2.30}$$

Then we can still get the same CFT parameters for $Q = 0$ as in (C.2.29) with the choice $-\epsilon_1 = \epsilon_2 = \text{i}$.

---

[3] Numerical integration would often give decimals rather than precise values. For instance, here we get $a \approx 0.06125877$. In some cases like here, we give exact values for a with the help of minimal models. This can be done by checking multiple minimal models and finding certain $\epsilon_{1,2}$ so that Δ_i would fit into their Kac tables. Then the correct closed form of a can be obtained if Δ_{int} also lives in these Kac tables for *all these* minimal models. (To get the correct CBs under AGT map, we further need the fusion rule, but even if the corresponding Δ_{int} does not satisfy the fusion rule for some CB, this could still be regarded as a verfication of fine-tuning a as long as Δ_{int}, along with Δ_i, belongs to the Kac table.)

C.2.3 Matching Parameters

Here, we report all parameters from the six dessins in Table C.2.1~C.2.6. Notice that we are only giving solutions coming from $(\pm)\phi_{\text{SW,basic}}$ with pure imaginary m_i's and a. There is actually a family for each parametrization following (C.2.23).

$\zeta = e^{2\pi i\tau}$	m_0	m_1	m_2	m_3	U	$\sum_i m_i$	$a = \frac{\alpha_{\text{int}}}{\sqrt{\epsilon_1\epsilon_2}} + \frac{Q}{2}$
	$-\frac{i}{2\sqrt{3}\pi}$	$-\frac{i}{2\sqrt{3}\pi}$	$\frac{i}{2\sqrt{3}\pi}$	$-\frac{i}{2\sqrt{3}\pi}$	$-\frac{1}{9\pi^2}$	$\frac{i}{\sqrt{3}\pi}$	$-\frac{i}{3\sqrt{3}\pi}$
$\frac{1}{2}(1-i\sqrt{3})$	$-\frac{i}{2\sqrt{3}\pi}$	$\frac{i}{2\sqrt{3}\pi}$	$-\frac{i}{2\sqrt{3}\pi}$	$\frac{i}{2\sqrt{3}\pi}$	$-\frac{1}{9\pi^2}$	0	$-\frac{i}{3\sqrt{3}\pi}$
	$\frac{i}{2\sqrt{3}\pi}$	$-\frac{i}{2\sqrt{3}\pi}$	$\frac{i}{2\sqrt{3}\pi}$	$-\frac{i}{2\sqrt{3}\pi}$	$-\frac{1}{9\pi^2}$	0	$\frac{i}{3\sqrt{3}\pi}$
	$\frac{i}{2\sqrt{3}\pi}$	$\frac{i}{2\sqrt{3}\pi}$	$-\frac{i}{2\sqrt{3}\pi}$	$\frac{i}{2\sqrt{3}\pi}$	$-\frac{1}{9\pi^2}$	$-\frac{i}{\sqrt{3}\pi}$	$\frac{i}{3\sqrt{3}\pi}$
	$-\frac{i}{2\sqrt{3}\pi}$	$-\frac{i}{2\sqrt{3}\pi}$	$\frac{i}{2\sqrt{3}\pi}$	$-\frac{i}{2\sqrt{3}\pi}$	$\frac{1}{9\pi^2}$	$\frac{i}{\sqrt{3}\pi}$	$\frac{i}{3\sqrt{3}\pi}$
$\frac{1}{2}(1+i\sqrt{3})$	$-\frac{i}{2\sqrt{3}\pi}$	$\frac{i}{2\sqrt{3}\pi}$	$-\frac{i}{2\sqrt{3}\pi}$	$\frac{i}{2\sqrt{3}\pi}$	$-\frac{1}{9\pi^2}$	0	$\frac{i}{3\sqrt{3}\pi}$
	$\frac{i}{2\sqrt{3}\pi}$	$-\frac{i}{2\sqrt{3}\pi}$	$\frac{i}{2\sqrt{3}\pi}$	$-\frac{i}{2\sqrt{3}\pi}$	$-\frac{1}{9\pi^2}$	0	$-\frac{i}{3\sqrt{3}\pi}$
	$\frac{i}{2\sqrt{3}\pi}$	$\frac{i}{2\sqrt{3}\pi}$	$-\frac{i}{2\sqrt{3}\pi}$	$\frac{i}{2\sqrt{3}\pi}$	$\frac{1}{9\pi^2}$	$-\frac{i}{\sqrt{3}\pi}$	$-\frac{i}{3\sqrt{3}\pi}$

TABLE C.2.1: The parameters obtained from $\Gamma(3)$. Using (C.2.22), we can get the values for α_i's.

$\zeta = e^{2\pi i\tau}$	m_0	m_1	m_2	m_3	U	$\sum_i m_i$	a
	$-\frac{i}{8\pi}$	$-\frac{i}{4\pi}$	$-\frac{i}{4\pi}$	$-\frac{i}{8\pi}$	$-\frac{1}{192\pi^2}$	$\frac{3i}{4\pi}$	$\frac{i}{8\pi}$
	$\frac{i}{8\pi}$	$-\frac{i}{4\pi}$	$-\frac{i}{4\pi}$	$\frac{i}{8\pi}$	$-\frac{1}{192\pi^2}$	$\frac{i}{2\pi}$	$-\frac{i}{8\pi}$
	$-\frac{i}{8\pi}$	$-\frac{i}{4\pi}$	$-\frac{i}{4\pi}$	$\frac{i}{8\pi}$	$-\frac{3}{64\pi^2}$	$\frac{i}{2\pi}$	$\frac{i}{8\pi}$
	$\frac{i}{8\pi}$	$\frac{i}{4\pi}$	$-\frac{i}{4\pi}$	$\frac{i}{8\pi}$	$-\frac{1}{192\pi^2}$	$\frac{i}{4\pi}$	$\frac{i}{8\pi}$
	$\frac{i}{8\pi}$	$-\frac{i}{4\pi}$	$-\frac{i}{4\pi}$	$\frac{i}{8\pi}$	$-\frac{3}{64\pi^2}$	$\frac{i}{4\pi}$	$-\frac{i}{8\pi}$
	$-\frac{i}{8\pi}$	$\frac{i}{4\pi}$	$\frac{i}{4\pi}$	$\frac{i}{8\pi}$	$-\frac{3}{64\pi^2}$	$\frac{i}{4\pi}$	$\frac{i}{8\pi}$
	$\frac{i}{8\pi}$	$\frac{i}{4\pi}$	$-\frac{i}{4\pi}$	$-\frac{i}{8\pi}$	$-\frac{1}{192\pi^2}$	0	$-\frac{i}{8\pi}$
$\frac{1}{2}$	$-\frac{i}{8\pi}$	$\frac{i}{4\pi}$	$-\frac{i}{4\pi}$	$\frac{i}{8\pi}$	$-\frac{3}{64\pi^2}$	0	$\frac{i}{8\pi}$
	$\frac{i}{8\pi}$	$-\frac{i}{4\pi}$	$\frac{i}{4\pi}$	$-\frac{i}{8\pi}$	$-\frac{3}{64\pi^2}$	0	$-\frac{i}{8\pi}$
	$-\frac{i}{8\pi}$	$-\frac{i}{4\pi}$	$\frac{i}{4\pi}$	$\frac{i}{8\pi}$	$-\frac{1}{192\pi^2}$	0	$\frac{i}{8\pi}$
	$\frac{i}{8\pi}$	$\frac{i}{4\pi}$	$-\frac{i}{4\pi}$	$\frac{i}{8\pi}$	$-\frac{3}{64\pi^2}$	$-\frac{i}{4\pi}$	$-\frac{i}{8\pi}$
	$-\frac{i}{8\pi}$	$\frac{i}{4\pi}$	$\frac{i}{4\pi}$	$-\frac{i}{8\pi}$	$-\frac{3}{64\pi^2}$	$\frac{i}{4\pi}$	$\frac{i}{8\pi}$
	$\frac{i}{8\pi}$	$-\frac{i}{4\pi}$	$\frac{i}{4\pi}$	$\frac{i}{8\pi}$	$-\frac{1}{192\pi^2}$	$-\frac{i}{4\pi}$	$-\frac{i}{8\pi}$
	$\frac{i}{8\pi}$	$\frac{i}{4\pi}$	$-\frac{i}{4\pi}$	$-\frac{i}{8\pi}$	$-\frac{3}{64\pi^2}$	$-\frac{i}{2\pi}$	$-\frac{i}{8\pi}$
	$-\frac{i}{8\pi}$	$\frac{i}{4\pi}$	$\frac{i}{4\pi}$	$\frac{i}{8\pi}$	$-\frac{1}{192\pi^2}$	$-\frac{i}{2\pi}$	$\frac{i}{8\pi}$
	$\frac{i}{8\pi}$	$\frac{i}{4\pi}$	$\frac{i}{4\pi}$	$\frac{i}{8\pi}$	$-\frac{1}{192\pi^2}$	$-\frac{3i}{4\pi}$	$\frac{i}{8\pi}$
	$-\frac{i}{4\pi}$	$-\frac{i}{2\pi}$	$-\frac{i}{4\pi}$	$-\frac{i}{2\pi}$	$\frac{1}{6\pi^2}$	$\frac{3i}{2\pi}$	$\frac{i}{2\pi}$
	$\frac{i}{4\pi}$	$-\frac{i}{2\pi}$	$-\frac{i}{4\pi}$	$-\frac{i}{2\pi}$	$\frac{1}{6\pi^2}$	$\frac{i}{\pi}$	$-\frac{i}{2\pi}$
	$-\frac{i}{4\pi}$	$-\frac{i}{2\pi}$	$\frac{i}{4\pi}$	$-\frac{i}{2\pi}$	$-\frac{1}{6\pi^2}$	$\frac{i}{\pi}$	$\frac{i}{2\pi}$
	$\frac{i}{4\pi}$	$-\frac{i}{2\pi}$	$\frac{i}{4\pi}$	$-\frac{i}{2\pi}$	$-\frac{1}{6\pi^2}$	$\frac{i}{2\pi}$	$-\frac{i}{2\pi}$
	$-\frac{i}{4\pi}$	$-\frac{i}{2\pi}$	$-\frac{i}{4\pi}$	$\frac{i}{2\pi}$	$-\frac{1}{6\pi^2}$	$\frac{i}{2\pi}$	$\frac{i}{2\pi}$
	$-\frac{i}{4\pi}$	$\frac{i}{2\pi}$	$-\frac{i}{4\pi}$	$-\frac{i}{2\pi}$	$\frac{1}{6\pi^2}$	$\frac{i}{2\pi}$	$\frac{i}{2\pi}$
	$\frac{i}{4\pi}$	$\frac{i}{2\pi}$	$-\frac{i}{4\pi}$	$-\frac{i}{2\pi}$	$\frac{1}{6\pi^2}$	0	$-\frac{i}{2\pi}$

2	$-\frac{i}{4\pi}$	$\frac{i}{2\pi}$	$\frac{i}{4\pi}$	$-\frac{i}{2\pi}$	$-\frac{1}{6\pi^2}$	0	$\frac{i}{2\pi}$
	$\frac{i}{4\pi}$	$-\frac{i}{2\pi}$	$-\frac{i}{4\pi}$	$\frac{i}{2\pi}$	$-\frac{1}{6\pi^2}$	0	$-\frac{i}{2\pi}$
	$-\frac{i}{4\pi}$	$-\frac{i}{2\pi}$	$\frac{i}{4\pi}$	$\frac{i}{2\pi}$	$\frac{1}{6\pi^2}$	0	$\frac{i}{2\pi}$
	$\frac{i}{4\pi}$	$-\frac{i}{2\pi}$	$\frac{i}{4\pi}$	$\frac{i}{2\pi}$	$\frac{1}{6\pi^2}$	$-\frac{i}{2\pi}$	$-\frac{i}{2\pi}$
	$\frac{i}{4\pi}$	$\frac{i}{2\pi}$	$\frac{i}{4\pi}$	$-\frac{i}{2\pi}$	$-\frac{1}{6\pi^2}$	$-\frac{i}{2\pi}$	$-\frac{i}{2\pi}$
	$-\frac{i}{4\pi}$	$\frac{i}{2\pi}$	$-\frac{i}{4\pi}$	$\frac{i}{2\pi}$	$-\frac{1}{6\pi^2}$	$\frac{i}{2\pi}$	$\frac{i}{2\pi}$
	$\frac{i}{4\pi}$	$\frac{i}{2\pi}$	$-\frac{i}{4\pi}$	$\frac{i}{2\pi}$	$-\frac{1}{6\pi^2}$	$-\frac{i}{\pi}$	$-\frac{i}{2\pi}$
	$-\frac{i}{4\pi}$	$\frac{i}{2\pi}$	$\frac{i}{4\pi}$	$\frac{i}{2\pi}$	$\frac{1}{6\pi^2}$	$-\frac{i}{\pi}$	$\frac{i}{2\pi}$
	$\frac{i}{4\pi}$	$\frac{i}{2\pi}$	$\frac{i}{4\pi}$	$\frac{i}{2\pi}$	$\frac{1}{6\pi^2}$	$-\frac{3i}{2\pi}$	$-\frac{i}{2\pi}$
−1	$-\frac{i}{4\pi}$	$-\frac{i}{4\pi}$	$-\frac{i}{2\pi}$	$\frac{i}{2\pi}$	Any value[4]	$\frac{i}{2\pi}$	0
	$-\frac{i}{4\pi}$	$-\frac{i}{4\pi}$	$\frac{i}{2\pi}$	$-\frac{i}{2\pi}$		$\frac{i}{2\pi}$	
	$\frac{i}{4\pi}$	$-\frac{i}{4\pi}$	$-\frac{i}{2\pi}$	$\frac{i}{2\pi}$		0	
	$\frac{i}{4\pi}$	$-\frac{i}{4\pi}$	$\frac{i}{2\pi}$	$-\frac{i}{2\pi}$		0	
	$-\frac{i}{4\pi}$	$\frac{i}{4\pi}$	$-\frac{i}{2\pi}$	$\frac{i}{2\pi}$		0	
	$-\frac{i}{4\pi}$	$\frac{i}{4\pi}$	$\frac{i}{2\pi}$	$-\frac{i}{2\pi}$		0	
	$\frac{i}{4\pi}$	$\frac{i}{4\pi}$	$-\frac{i}{2\pi}$	$\frac{i}{2\pi}$		$-\frac{i}{2\pi}$	
	$\frac{i}{4\pi}$	$\frac{i}{4\pi}$	$\frac{i}{2\pi}$	$-\frac{i}{2\pi}$		$-\frac{i}{2\pi}$	

TABLE C.2.2: The parameters obtained from $\Gamma_0(4) \cap \Gamma(2)$. Using (C.2.22), we can get the values for α_i's.

As the size of the table increases, we will give a more compact version for the remaining cases below. For each ζ, there are usually $2^4 = 16$ possibilities. For a, as the sign of a only depends on the sign of m_0 (in the following sense), "$\pm$" in a means that a has the same sign as m_0 while "$\mp$" in a indicates that m_0 and a have opposite signs.

$\zeta = \mathrm{e}^{2\pi\mathrm{i}\tau}$	m_0	m_1	m_2	m_3	U	a
$\frac{1}{2} - \frac{11}{50}\sqrt{5}$	$\pm\frac{i\sqrt{5}}{50\pi}$	$\pm\frac{i\sqrt{5}}{10\pi}$	$\frac{i\sqrt{5}}{10\pi}$ $-\frac{i\sqrt{5}}{10\pi}$	$\frac{i\sqrt{5}}{50\pi}$ $-\frac{i\sqrt{5}}{50\pi}$	$\frac{(-607+85\sqrt{5})}{62750\pi^2}$	$\pm\frac{i\sqrt{5}}{25\pi}$
	$\pm\frac{i\sqrt{5}}{50\pi}$	$\pm\frac{i\sqrt{5}}{10\pi}$	$\frac{i\sqrt{5}}{10\pi}$ $-\frac{i\sqrt{5}}{10\pi}$	$-\frac{i\sqrt{5}}{50\pi}$ $\frac{i\sqrt{5}}{50\pi}$	$\frac{9(-69+20\sqrt{5})}{31375\pi^2}$	$\mp\frac{i\sqrt{5}}{25\pi}$
$\frac{1}{2} + \frac{11}{50}\sqrt{5}$	$\pm\frac{i\sqrt{5}}{50\pi}$	$\pm\frac{i\sqrt{5}}{10\pi}$	$\frac{i\sqrt{5}}{10\pi}$ $-\frac{i\sqrt{5}}{10\pi}$	$\frac{i\sqrt{5}}{50\pi}$ $-\frac{i\sqrt{5}}{50\pi}$	$\frac{(-607-85\sqrt{5})}{62750\pi^2}$	$\mp\frac{i\sqrt{5}}{25\pi}$
	$\pm\frac{i\sqrt{5}}{50\pi}$	$\pm\frac{i\sqrt{5}}{10\pi}$	$\frac{i\sqrt{5}}{10\pi}$ $-\frac{i\sqrt{5}}{10\pi}$	$-\frac{i\sqrt{5}}{50\pi}$ $\frac{i\sqrt{5}}{50\pi}$	$\frac{9(-69-20\sqrt{5})}{31375\pi^2}$	$\mp\frac{i\sqrt{5}}{25\pi}$
$\frac{125}{2} + \frac{55}{2}\sqrt{5}$	$\pm\frac{i(5\sqrt{5}+11)}{4\pi}$	$\pm\frac{i5(5\sqrt{5}+11)}{4\pi}$	$\frac{i(5\sqrt{5}+11)}{4\pi}$ $-\frac{i(5\sqrt{5}+11)}{4\pi}$	$\frac{i5(5\sqrt{5}+11)}{4\pi}$ $-\frac{i5(5\sqrt{5}+11)}{4\pi}$	100.010534	$\pm\frac{i2(5\sqrt{5}+11)}{4\pi}$
	$\pm\frac{i(5\sqrt{5}+11)}{4\pi}$	$\pm\frac{i5(5\sqrt{5}+11)}{4\pi}$	$\frac{i(5\sqrt{5}+11)}{4\pi}$ $-\frac{i(5\sqrt{5}+11)}{4\pi}$	$-\frac{i5(5\sqrt{5}+11)}{4\pi}$ $\frac{i5(5\sqrt{5}+11)}{4\pi}$	38.200625	$\pm\frac{i2(5\sqrt{5}+11)}{4\pi}$
$-\frac{123}{2} + \frac{55}{2}\sqrt{5}$	$\pm\frac{i\sqrt{5}}{50\pi}$	$\pm\frac{i\sqrt{5}}{50\pi}$	$\frac{i\sqrt{5}}{10\pi}$ $-\frac{i\sqrt{5}}{10\pi}$	$\frac{i\sqrt{5}}{10\pi}$ $-\frac{i\sqrt{5}}{10\pi}$	-0.000843	$\pm\frac{i\sqrt{5}}{25\pi}$

[4]Here, any complex number can be a basic value for U since all the terms of U in $P_4(z)$ contain $(1 + \zeta)$ as well. Moreover, the integral for a always vanishes.

	m_0	m_1	m_2	m_3	U	a
	$\pm\frac{i\sqrt{5}}{50\pi}$	$\pm\frac{i\sqrt{5}}{50\pi}$	$\frac{i\sqrt{5}}{10\pi}$ $-\frac{i\sqrt{5}}{10\pi}$	$-\frac{i\sqrt{5}}{10\pi}$ $\frac{i\sqrt{5}}{10\pi}$	-0.000674	$\mp\frac{i\sqrt{5}}{25\pi}$
$\frac{125}{2}-\frac{55}{2}\sqrt{5}$	$\pm\frac{i\sqrt{5}}{50\pi}$	$\pm\frac{i\sqrt{5}}{10\pi}$	$\frac{i\sqrt{5}}{50\pi}$ $-\frac{i\sqrt{5}}{50\pi}$	$\frac{i\sqrt{5}}{10\pi}$ $-\frac{i\sqrt{5}}{10\pi}$	-0.001278	$\mp\frac{i\sqrt{5}}{25\pi}$
	$\pm\frac{i\sqrt{5}}{50\pi}$	$\pm\frac{i\sqrt{5}}{10\pi}$	$\frac{i\sqrt{5}}{50\pi}$ $-\frac{i\sqrt{5}}{50\pi}$	$-\frac{i\sqrt{5}}{10\pi}$ $\frac{i\sqrt{5}}{10\pi}$	-0.003346	$\pm\frac{i\sqrt{5}}{25\pi}$
$-\frac{123}{2}-\frac{55}{2}\sqrt{5}$	$\pm\frac{i(5\sqrt{5}+11)}{4\pi}$	$\pm\frac{i(5\sqrt{5}+11)}{4\pi}$	$\frac{i5(5\sqrt{5}+11)}{4\pi}$ $-\frac{i5(5\sqrt{5}+11)}{4\pi}$	$\frac{i5(5\sqrt{5}+11)}{4\pi}$ $-\frac{i5(5\sqrt{5}+11)}{4\pi}$	303.899917	$\pm\frac{i2(5\sqrt{5}+11)}{4\pi}$
	$\pm\frac{i(5\sqrt{5}+11)}{4\pi}$	$\pm\frac{i(5\sqrt{5}+11)}{4\pi}$	$\frac{i5(5\sqrt{5}+11)}{4\pi}$ $-\frac{i5(5\sqrt{5}+11)}{4\pi}$	$-\frac{i5(5\sqrt{5}+11)}{4\pi}$ $\frac{i5(5\sqrt{5}+11)}{4\pi}$	-10.195921	$\pm\frac{i2(5\sqrt{5}+11)}{4\pi}$

TABLE C.2.3: The parameters obtained from $\Gamma_1(5)$. Using (C.2.22), we can get the values for α_i's and Q.

$\zeta=\mathrm{e}^{2\pi\mathrm{i}\tau}$	m_0	m_1	m_2	m_3	U	a
$\frac{1}{2}$	$\pm\frac{i}{4\pi}$	$\pm\frac{i\sqrt{109}}{2\pi}$	$\frac{2i}{\pi}$ $-\frac{2i}{\pi}$	$\frac{27i}{4\pi}$ $-\frac{27i}{4\pi}$	$\frac{595}{48\pi^2}$	$\pm0.30258i$
	$\pm\frac{i}{4\pi}$	$\pm\frac{i\sqrt{109}}{2\pi}$	$\frac{2i}{\pi}$ $-\frac{2i}{\pi}$	$-\frac{27i}{4\pi}$ $\frac{27i}{4\pi}$	$-\frac{269}{48\pi^2}$	$\pm0.30258i$
$\frac{1}{2}$	$\pm\frac{i}{4\pi}$	$\pm\frac{2i}{\pi}$	$\frac{i\sqrt{109}}{2\pi}$ $-\frac{i\sqrt{109}}{2\pi}$	$\frac{27i}{4\pi}$ $-\frac{2i}{\pi}$	$\frac{-665+108\sqrt{109}}{48\pi^2}$	$\pm0.741431i$
	$\pm\frac{i}{4\pi}$	$\pm\frac{2i}{\pi}$	$\frac{i\sqrt{109}}{2\pi}$ $-\frac{i\sqrt{109}}{2\pi}$	$-\frac{27i}{4\pi}$ $\frac{27i}{4\pi}$	$\frac{-665-108\sqrt{109}}{48\pi^2}$	$\pm0.741431i$
2	$\pm\frac{i}{2\pi}$	$\pm\frac{i\sqrt{109}}{\pi}$	$\frac{27i}{2\pi}$ $-\frac{27i}{2\pi}$	$\frac{4i}{\pi}$ $-\frac{4i}{\pi}$	$\frac{455}{3\pi^2}$	$\pm0.6051525i$
	$\pm\frac{i}{2\pi}$	$\pm\frac{i\sqrt{109}}{\pi}$	$\frac{27i}{2\pi}$ $-\frac{27i}{2\pi}$	$-\frac{4i}{\pi}$ $\frac{4i}{\pi}$	$\frac{23}{3\pi^2}$	$\pm0.6051525i$
2	$\pm\frac{i}{2\pi}$	$\pm\frac{4i}{\pi}$	$\frac{27i}{2\pi}$ $-\frac{27i}{2\pi}$	$\frac{i\sqrt{109}}{\pi}$ $-\frac{i\sqrt{109}}{\pi}$	$\frac{125+54\sqrt{109}}{3\pi^2}$	$\pm1.4828632i$
	$\pm\frac{i}{2\pi}$	$\pm\frac{4i}{\pi}$	$\frac{27i}{2\pi}$ $-\frac{27i}{2\pi}$	$-\frac{i\sqrt{109}}{\pi}$ $\frac{i\sqrt{109}}{\pi}$	$\frac{125-54\sqrt{109}}{3\pi^2}$	$\pm1.4828632i$

TABLE C.2.4: The parameters obtained from $\Gamma_0(6)$. Using (C.2.22), we can get the values for α_i's and Q.

$\zeta=\mathrm{e}^{2\pi\mathrm{i}\tau}$	m_0	m_1	m_2	m_3	U	a
$\frac{1}{2}$	$\pm\frac{i}{16\pi}$	$\pm\frac{i}{8\pi}$	$\frac{i}{2\pi}$ $-\frac{i}{2\pi}$	$\frac{i}{16\pi}$ $-\frac{i}{16\pi}$	$\frac{11}{768\pi^2}$	±0.0528623
	$\pm\frac{i}{16\pi}$	$\pm\frac{i}{8\pi}$	$\frac{i}{2\pi}$ $-\frac{i}{2\pi}$	$-\frac{i}{16\pi}$ $\frac{i}{16\pi}$	$-\frac{7}{256\pi^2}$	±0.0528623
	$\pm\frac{i}{8\pi}$	$\pm\frac{i}{4\pi}$	$\frac{i}{8\pi}$	$-\frac{i}{\pi}$	$\frac{7}{48\pi^2}$	±0.1057

	m_0	m_1	m_2	m_3	U	a
2	$\pm\frac{i}{8\pi}$	$\pm\frac{i}{4\pi}$	$\begin{matrix}-\frac{i}{8\pi}\\[2pt]\frac{i}{8\pi}\\[2pt]-\frac{i}{8\pi}\end{matrix}$	$\begin{matrix}\frac{i}{\pi}\\[2pt]\frac{i}{\pi}\\[2pt]-\frac{i}{\pi}\end{matrix}$	$\frac{23}{48\pi^2}$	± 0.1057

TABLE C.2.5: The parameters obtained from $\Gamma_0(8)$. Using (C.2.22), we can get the values for α_i's and Q.

$\zeta = \mathrm{e}^{2\pi i\tau}$	m_0	m_1	m_2	m_3	U	a
$\frac{1-i\sqrt{3}}{2}$	$\pm\frac{i}{6\sqrt{3}\pi}$	$\pm\frac{i}{6\sqrt{3}\pi}$	$\begin{matrix}\frac{i}{6\sqrt{3}\pi}\\[2pt]-\frac{i}{6\sqrt{3}\pi}\end{matrix}$	$\begin{matrix}\frac{i\sqrt{3}}{2\pi}\\[2pt]-\frac{i\sqrt{3}}{2\pi}\end{matrix}$	$-\frac{i(33i+25\sqrt{3})}{162\pi^2}$	$\pm(-0.1402495+0.0315441i)$
	$\pm\frac{i}{6\sqrt{3}\pi}$	$\pm\frac{i}{6\sqrt{3}\pi}$	$\begin{matrix}\frac{i}{6\sqrt{3}\pi}\\[2pt]-\frac{i}{6\sqrt{3}\pi}\end{matrix}$	$\begin{matrix}-\frac{i\sqrt{3}}{2\pi}\\[2pt]\frac{i\sqrt{3}}{2\pi}\end{matrix}$	$-\frac{i(3i+8\sqrt{3})}{81\pi^2}$	$\pm(-0.0887502+0.0362071i)$
$\frac{1+i\sqrt{3}}{2}$	$\pm\frac{i}{6\sqrt{3}\pi}$	$\pm\frac{i}{6\sqrt{3}\pi}$	$\begin{matrix}\frac{i}{6\sqrt{3}\pi}\\[2pt]-\frac{i}{6\sqrt{3}\pi}\end{matrix}$	$\begin{matrix}\frac{i\sqrt{3}}{2\pi}\\[2pt]-\frac{i\sqrt{3}}{2\pi}\end{matrix}$	$\frac{i(-33i+25\sqrt{3})}{162\pi^2}$	$\pm(-0.1402495-0.0315441i)$
	$\pm\frac{i}{6\sqrt{3}\pi}$	$\pm\frac{i}{6\sqrt{3}\pi}$	$\begin{matrix}\frac{i}{6\sqrt{3}\pi}\\[2pt]-\frac{i}{6\sqrt{3}\pi}\end{matrix}$	$\begin{matrix}-\frac{i\sqrt{3}}{2\pi}\\[2pt]\frac{i\sqrt{3}}{2\pi}\end{matrix}$	$\frac{i(-3i+8\sqrt{3})}{81\pi^2}$	$\pm(-0.0887502-0.0362071i)$

TABLE C.2.6: The parameters obtained from $\Gamma_0(9)$. Using (C.2.22), we can get the values for α_i's and Q.

Based on the above calculations, there are some remarks we can make:

- One may check that the elliptic curves parametrized by these m_i, ζ and U have the same j-invariants as in Table C.2.7 for the six Belyi maps. Moreover, there are two cases with

$\Gamma(3)$	0
$\Gamma_0(4)\cap\Gamma(2)$	$\frac{35152}{9}$
$\Gamma_1(5)$	$\frac{131072}{9}$
$\Gamma_0(6)$	-3072
$\Gamma_0(8)$	$\frac{21952}{9}$
$\Gamma_0(9)$	0

TABLE C.2.7: The j-invariants that correspond to the six index-12 Belyi maps.

$\zeta = (1\pm i\sqrt{3})/2$, which are the cusp points for the fundamental diagram of SL(2,$\mathbb{Z}$). They are exactly the dessins whose Belyi maps have j-invariant 0.

- It is obvious that for each dessin, the parametrizations for different ζ's are related by triality

$$\zeta \;\leftrightarrow\; \zeta' = \frac{1}{\zeta} \;\leftrightarrow\; \zeta'' = 1-\zeta. \tag{C.2.31}$$

This is explicitly listed in Table C.2.8. Modular invariance of the curve also leads to the following transformations of mass parameters:

$$\zeta \leftrightarrow \frac{1}{\zeta} : \; (m_0, m_1, m_2, m_3) \leftrightarrow \frac{1}{|\zeta|}(m_0, m_1, m_3, m_2);$$

$$\zeta \leftrightarrow 1 - \zeta : \quad (m_0, m_1, m_2, m_3) \leftrightarrow (m_0, m_2, m_1, m_3). \tag{C.2.32}$$

In particular, the two rows for $\Gamma_1(5)$ are also related by triality: $1 - \left(\frac{125}{2} + \frac{55}{2}\sqrt{5} \right) = -\frac{123}{2} -$

Dessin	ζ	ζ'	ζ''
$\Gamma(3)$	$\frac{1}{2}(1 \pm i\sqrt{3})$	$\frac{1}{2}(1 \mp i\sqrt{3})$	$\frac{1}{2}(1 \mp i\sqrt{3})$
$\Gamma_0(4) \cap \Gamma(2)$	2	$\frac{1}{2}$	-1
$\Gamma_1(5)$	$\frac{1}{2} - \frac{11}{50}\sqrt{5}$	$\frac{125}{2} + \frac{55}{2}\sqrt{5}$	$\frac{1}{2} + \frac{11}{50}\sqrt{5}$
	$-\frac{123}{2} + \frac{55}{2}\sqrt{5}$	$-\frac{123}{2} - \frac{55}{2}\sqrt{5}$	$\frac{125}{2} - \frac{55}{2}\sqrt{5}$
$\Gamma_0(6)$	2	$\frac{1}{2}$	-
$\Gamma_0(8)$	2	$\frac{1}{2}$	-
$\Gamma_0(9)$	$\frac{1}{2}(1 \pm i\sqrt{3})$	-	$\frac{1}{2}(1 \mp i\sqrt{3})$

TABLE C.2.8: The parametrizations for each case are related by triality. The hyphens indicate that such ζ either gives no solution to mass parameters ($\Gamma_0(6)$ and $\Gamma_0(8)$) or does not satisfy the transformations of masses ($\Gamma_0(9)$).

$\frac{55}{2}\sqrt{5}$.

C.2.4 Minimal Models and $\Gamma(3)$

As an example, let us match the parametrizations for $\Gamma(3)$ obtained above to 4-point CBs in minimal models. In fact, as we will see, such CB first appears for the tetracritical Ising model when $p' = 6$ and $p = 5$, that is, $c = 4/5$. As usual, we can write the 4-point CB as

$$\tag{C.2.33}$$

Then the intermediate field $\phi_{k,l}$ should satisfy the fusion rule

$$\phi_{r,s} \times \phi_{m,n} = \sum_{\substack{k=|m-r|+1 \\ k-m+r-1\in 2\mathbb{Z}}}^{\min(m+r-1,2p-1-m-r)} \sum_{\substack{l=|n-s|+1 \\ l-n+s-1\in 2\mathbb{Z}}}^{\min(n+s-1,2p'-1-n-s)} \phi_{k,l}, \tag{C.2.34}$$

where the entire conformal family of a primary is implicit in the above abuse of notation. Let ϕ_{r_i,s_i} correspond to $\alpha_{1,4}$ and ϕ_{m_i,n_i} correspond to $\alpha_{2,3}$ ($i = 1, 2$). Then the fusion rule for the 4-point CB is

$$\phi_{k,l} \in \phi_{r_1,s_1} \times \phi_{m_1,n_1}, \ \phi_{k,l} \in \phi_{r_2,s_2} \times \phi_{m_2,n_2} \tag{C.2.35}$$

with constraints on k, l indicated in (C.2.34).

Before we insert the specific values of the parametrizations, we can make some simplifications:

- Recall that the mass parameters are real or pure imaginary. If we have some parametrization with $m_i \in \mathbb{R}$, without loss of generality we can choose $\epsilon_1 < 0 < \epsilon_2$. Then since $\frac{\epsilon_1+\epsilon_2}{\sqrt{\epsilon_1\epsilon_2}} = Q = i\left(\sqrt{\frac{p'}{p}} - \sqrt{\frac{p}{p'}}\right)$, we have $\sqrt{\epsilon_1\epsilon_2} = -i\epsilon_2\sqrt{\frac{p}{p'}}$. Likewise, for some parametrization with $m_i \in i\mathbb{R}$, without loss of generality we can choose $\epsilon_1/i < 0 < \epsilon_2/i$. Such two cases related by $m_i \to im_i$ should give the same $\epsilon_{1,2}$ up to a factor of i.

- If we make the choice in the above point for some specific m_i, then $m_i \to -m_i$ should give the same CFT parameters with $\epsilon_{1,2} \to i\epsilon_{1,2}$. If we only have $m_0 \to -m_0$ or $m_1 \to -m_1$, then we should always get the same parametrization even without changing $\epsilon_{1,2}$ since the corresponding conformal dimension is $\frac{Q^2}{4} - \frac{m_{0,1}^2}{\epsilon_1\epsilon_2}$.

- Swapping $m_2 \leftrightarrow m_3$ and swapping $m_0 \leftrightarrow m_1$ simultaneously should give the same CFT parameters (for same $\epsilon_{1,2}$) due to the AGT map. This simply corresponds to read the CB (C.2.33) from the left or from the right.

In light of these points, it suffices to only contemplate one parametrization[5], say $m_0 = -m_1 = m_2 = -m_3 = -\frac{1}{2\sqrt{3}}$, for $\Gamma(3)$. When $p' = 6, p = 5$, we find that there is only one possibility for Δ_1 and Δ_4, that is,

$$\Delta_1 = \Delta_4 = \frac{1}{15}. \tag{C.2.36}$$

There are two possible solutions for the remaining mass parameters (and deformation parameters):

$$\epsilon_2 = \frac{2}{\sqrt{3}\pi}, \ \Delta_2 = \frac{1}{40}, \ \Delta_3 = \frac{1}{8}; \tag{C.2.37}$$

$$\epsilon_2 = -\frac{2}{\sqrt{3}\pi}, \ \Delta_2 = \frac{1}{8}, \ \Delta_3 = \frac{1}{40}. \tag{C.2.38}$$

Moreover, for the intermediate channel,

$$a = -\frac{1}{3\sqrt{3}\pi}, \ \Delta_{\text{int}} = \frac{1}{40}. \tag{C.2.39}$$

Hence, the intermediate channel (k, l) obtained from $\Gamma(3)$ corresponds to $(2, 2)$ or $(3, 4)$ (and another (k, l) satifying the fusion rule but not from the dessin is $(2, 4)$ or $(3, 2)$). It is not hard to see that the above two solutions both give the 8 CBs in Table C.2.9.

Δ_1	(2,3)	(2,3)	(2,3)	(2,3)	(3,3)	(3,3)	(3,3)	(3,3)
Δ_2	(2,2)	(2,2)	(3,4)	(3,4)	(2,2)	(2,2)	(3,4)	(3,4)
Δ_3	(1,2)	(4,4)	(1,2)	(4,4)	(1,2)	(4,4)	(1,2)	(4,4)
Δ_4	(3,3)	(2,3)	(2,3)	(3,3)	(2,3)	(3,3)	(3,3)	(2,3)
Δ_{int}	(3,4)	(3,4)	(2,2)	(2,2)	(2,2)	(2,2)	(3,4)	(3,4)

TABLE C.2.9: There are 8 possible combinations. Each column gives a CB. In the leftmost column, Δ_i's follow the nomenclature corresponding to (C.2.37). For (C.2.38), it just swaps $2 \leftrightarrow 3$ (and $\Delta_1 = \Delta_4$). Therefore, it essentially gives the same CBs. In other words, the two solutions just correspond to reading the 4-point CB (C.2.33) from left or from right.

In fact, this corresponds to not only a CB in the tetracritical Ising model, but also CBs in many other minimal models. In Figure C.2.1, we give the Kac tables for a few examples.

By looking at these examples, one might see some patterns of the minimal models and the positions of conformal dimensions in cyan appeared in the Kac tables. Now, we are going to show

Proposition C.2.2. *The dessin $\Gamma(3)$ gives rise to the charges/momenta of the states in 4-point conformal blocks, where the corresponding weights of the primaries satisfy the conditions in Table C.2.10, in minimal models.*

Following the specific values for m_i and a, we can define $M_0 := \frac{m_0}{\sqrt{\epsilon_1\epsilon_2}}$ so that

$$\alpha_1 = -M_0 + \frac{Q}{2}, \ \alpha_2 = -M_0, \ \alpha_3 = M_0, \ \alpha_4 = M_0 + \frac{Q}{2}, \ \alpha_{\text{int}} = \frac{2M_0}{3} + \frac{Q}{2}. \tag{C.2.40}$$

There are two possible choices for Δ_1 in the Kac table. For future convenience, let us denote them as Δ_{r_1, s_1} and Δ_{r_2, s_2}. Then

$$\frac{(p'r_i - ps_i)^2 - (p' - p)^2}{4p'p} = \frac{Q^2}{4} - M_0^2 = -\frac{(p' - p)^2}{4p'p} - M_0^2. \tag{C.2.41}$$

---

[5]Since $\Delta_1 = \Delta_4$, when considering $\zeta \leftrightarrow 1/\zeta$, it is equivalent to swapping both $m_2 \leftrightarrow m_3$ and $m_0 \leftrightarrow m_1$. Therefore, $\zeta = (1 \pm i\sqrt{3})/2$ should give the same parametrizations. Even if $|\zeta| \neq 1$, as long as $\Delta_1 = \Delta_4$, swapping $2 \leftrightarrow 3$ always gives same CFT parameters as the extra factor of $1/|\zeta|$ can be absorbed into $\sqrt{\epsilon_1\epsilon_2}$.

(A) $p'=6, p=5$

	1	2	3	4	5
4	3	$\frac{13}{8}$	$\frac{2}{3}$	$\frac{1}{8}$	0
3	$\frac{7}{5}$	$\frac{21}{40}$	$\frac{1}{15}$	$\frac{1}{40}$	$\frac{2}{5}$
2	$\frac{2}{5}$	$\frac{1}{40}$	$\frac{1}{15}$	$\frac{21}{40}$	$\frac{7}{5}$
1	0	$\frac{1}{8}$	$\frac{2}{3}$	$\frac{13}{8}$	3

(B) $p'=7, p=5$

	1	2	3	4	5	6
4	$\frac{15}{4}$	$\frac{16}{7}$	$\frac{33}{28}$	$\frac{3}{7}$	$\frac{1}{28}$	0
3	$\frac{9}{5}$	$\frac{117}{140}$	$\frac{8}{35}$	$-\frac{3}{140}$	$\frac{3}{35}$	$\frac{11}{20}$
2	$\frac{11}{20}$	$\frac{3}{35}$	$-\frac{3}{140}$	$\frac{8}{35}$	$\frac{117}{140}$	$\frac{9}{5}$
1	0	$\frac{1}{28}$	$\frac{3}{7}$	$\frac{33}{28}$	$\frac{16}{7}$	$\frac{15}{4}$

(C) $p'=7, p=6$

	1	2	3	4	5	6
5	5	$\frac{22}{7}$	$\frac{12}{7}$	$\frac{5}{7}$	$\frac{1}{7}$	0
4	$\frac{23}{8}$	$\frac{85}{56}$	$\frac{33}{56}$	$\frac{5}{56}$	$\frac{1}{56}$	$\frac{3}{8}$
3	$\frac{4}{3}$	$\frac{10}{21}$	$\frac{1}{21}$	$\frac{1}{21}$	$\frac{10}{21}$	$\frac{4}{3}$
2	$\frac{3}{8}$	$\frac{1}{56}$	$\frac{5}{56}$	$\frac{33}{56}$	$\frac{85}{56}$	$\frac{23}{8}$
1	0	$\frac{1}{7}$	$\frac{5}{7}$	$\frac{12}{7}$	$\frac{22}{7}$	5

(D) $p'=8, p=5$

	1	2	3	4	5	6	7
4	$\frac{9}{2}$	$\frac{95}{32}$	$\frac{7}{4}$	$\frac{27}{32}$	$\frac{1}{4}$	$-\frac{1}{32}$	0
3	$\frac{11}{5}$	$\frac{187}{160}$	$\frac{9}{20}$	$\frac{7}{160}$	$-\frac{1}{20}$	$\frac{27}{160}$	$\frac{7}{10}$
2	$\frac{7}{10}$	$\frac{27}{160}$	$-\frac{1}{20}$	$\frac{7}{160}$	$\frac{9}{20}$	$\frac{187}{160}$	$\frac{11}{5}$
1	0	$-\frac{1}{32}$	$\frac{1}{4}$	$\frac{27}{32}$	$\frac{7}{4}$	$\frac{95}{32}$	$\frac{9}{2}$

(E) $p'=8, p=7$

	1	2	3	4	5	6	7
6	$\frac{15}{2}$	$\frac{165}{32}$	$\frac{13}{4}$	$\frac{57}{32}$	$\frac{3}{4}$	$\frac{5}{32}$	0
5	$\frac{34}{7}$	$\frac{675}{224}$	$\frac{45}{28}$	$\frac{143}{224}$	$\frac{3}{28}$	$\frac{3}{224}$	$\frac{5}{14}$
4	$\frac{39}{14}$	$\frac{323}{224}$	$\frac{15}{28}$	$\frac{15}{224}$	$\frac{1}{28}$	$\frac{99}{224}$	$\frac{9}{7}$
3	$\frac{9}{7}$	$\frac{99}{224}$	$\frac{1}{28}$	$\frac{15}{224}$	$\frac{15}{28}$	$\frac{323}{224}$	$\frac{39}{14}$
2	$\frac{5}{14}$	$\frac{3}{224}$	$\frac{3}{28}$	$\frac{143}{224}$	$\frac{45}{28}$	$\frac{675}{224}$	$\frac{34}{7}$
1	0	$\frac{5}{32}$	$\frac{3}{4}$	$\frac{57}{32}$	$\frac{13}{4}$	$\frac{165}{32}$	$\frac{15}{2}$

FIGURE C.2.1: Here we list the first five possible examples of CBs that $\Gamma(3)$ corresponds to: (a) $p'=6, p=5$, (b) $p'=7, p=5$, (c) $p'=7, p=6$, (d) $p'=8, p=5$, (e) $p'=8, p=7$. Those appeared in the CBs are in cyan in the Kac tables. For (e), we also have another combination of CBs in green.

Therefore,

$$M_0^2 = -\frac{(p'r_i - ps_i)^2}{4p'p}. \tag{C.2.42}$$

It is also immediate from (C.2.40) that $\Delta_1 = \Delta_4$. Hence, we can denote $\Delta_{2 \text{ or } 3}$ as Δ_{m_i,n_i} without specifying whether $(m_{1,2}, n_{1,2})$ corresponds to Δ_2 or Δ_3. We can plug this into $\Delta_{m_i,n_i} = \Delta_3 = -M_0^2 + QM_0$ and get

$$(p'm_i - p'n_i + xn_2)^2 - x^2 = (p'r_j - p's_j + xs_j)^2 - 2x(p'r_j - p's_j + xs_j), \tag{C.2.43}$$

where $x := p' - p$ is some positive integer. Its expansion gives

$$p'^2(m_i-n_i)^2 + 2p'(m_i-n_i)xn_i + x^2n_i^2 - x^2 = p'^2(r_j-s_j)^2 + 2p'(r_j-s_j)(s_j-1)x + x^2s_j^2 - 2x^2s_j. \tag{C.2.44}$$

Cases	Conditions
All	$(r_1,s_1) = (p-r_2, p'-s_2) \in 3(\mathbb{Z},\mathbb{Z})$
$(r_1,s_1),(r_1+1,s_1+1),(r_1-1,s_1-1),(r_1,s_1)$	
$(r_1,s_1),(r_1+1,s_1+1),(r_2+1,s_2+1),(r_2,s_2)$	$r_1 \le \frac{3(p-1)}{4}, s_1 \le \frac{3(p'-1)}{4},$
$(r_1,s_1),(r_1-1,s_1-1),(r_2-1,s_2-1),(r_2,s_2)$	$k = \frac{2}{3}r_1, l = \frac{2}{3}s_1$
$(r_2,s_2),(r_2+1,s_2+1),(r_2-1,s_2-1),(r_2,s_2)$	
$(r_2,s_2),(r_1+1,s_1+1),(r_1-1,s_1-1),(r_2,s_2)$	$\left(\frac{p+1}{2} \le r_1 \le p-2\right.$
$(r_2,s_2),(r_1+1,s_1+1),(r_2+1,s_2+1),(r_1,s_1)$	$\left.\text{or } \frac{p+1}{2} \le r_1 \le \frac{3(p-1)}{4} \text{ or } p=2r_1\right)$
$(r_2,s_2),(r_1-1,s_1-1),(r_2-1,s_2-1),(r_1,s_1)$	and (similar relations[6] with $p \to p', r_1 \to s_1$)
$(r_1,s_1),(r_2+1,s_2+1),(r_2-1,s_2-1),(r_1,s_1)$	and $k = p - \frac{2}{3}r_1, l = p' - \frac{2}{3}s_1$

TABLE C.2.10: The possible CBs of minimal models that $\Gamma(3)$ corresponds to.

Since this is for general p', by comparing coefficients at different orders of p', we have

$$m_i - n_i = \pm(r_j - s_j), \ n_i = \pm(s_j - 1), \ n_i^2 - 1 = s_j^2 - 2s_j, \tag{C.2.45}$$

where $\pm$ can be seen from the symmetry of p'^2 and p' terms in (C.2.44). Due to a similar symmetry for $(m_i, n_i) \leftrightarrow (p - m_i, p' - n_i)$, it is possible to replace (m_i, n_i) with $(p - m_i, p' - n_i)$ or (r_j, s_j) with $(p - r_j, p' - s_j)$ in (C.2.43). It turns out that they also give the same set of equations. The third equation is actually redundant, and hence we have

$$m_i - n_i = \pm(r_j - s_j), \ n_i = \pm(s_j - 1). \tag{C.2.46}$$

Strictly speaking, in (C.2.43), we should really have $|p'r_j - p's_j + xs_j|$ on the right hand side. Taking this into account, we would obtain another set of solutions with -1 replaced by $+1$. Therefore,

$$m_i = r_j - 1, \ n_i = s_j - 1, \tag{C.2.47}$$

$$\text{or} \quad m_i = r_j + 1, \ n_i = s_j + 1. \tag{C.2.48}$$

As we also have similar relations for Δ_2 and we have seen that $\Delta_{m_1,n_1} \neq \Delta_{m_2,n_2}$ for $Q \neq 0$, we learn that

$$(m_i, n_i) = (r_j, s_j) \pm (1, 1), \ (m_1, n_1) \neq (m_2, n_2), \ (m_1, n_1) \neq (p - m_2, p' - n_2). \tag{C.2.49}$$

For the intermediate channel, using $\frac{a}{\sqrt{\epsilon_1 \epsilon_2}} = \frac{2M_0}{3}$, we have

$$(p'k - p'l + l)^2 = \frac{4}{9}(p'r_j - p's_j + s_j)^2, \tag{C.2.50}$$

so likewise,

$$k = \frac{2}{3}r_1, \ l = \frac{2}{3}s_1, \tag{C.2.51}$$

$$\text{or} \quad k = p - \frac{2}{3}r_1, \ l = p' - \frac{2}{3}s_1, \tag{C.2.52}$$

where without loss of generality we have chosen $j = 1$ for convenience. As k, l are integers, we must have $r_1, s_1 \in 3\mathbb{Z}$ (or in other words, $(p - r_2), (p' - s_2) \in 3\mathbb{Z}$). As $p = p' - 1$, it is straightforward to see that $k, l \in 2\mathbb{Z}$ for (C.2.51) while $(k, l) \in (2\mathbb{Z}, 2\mathbb{Z} + 1)$ or $(k, l) \in (2\mathbb{Z} + 1, 2\mathbb{Z})$ for (C.2.52).

We also need to take the fusion rule into account. In general, there are $2^2 \times \binom{4}{2} = 24$ possible choices of external legs, where 2^2 is the number of choices of Δ_1 and Δ_4 and $\binom{4}{2}$ corresponds to the choices of $\Delta_2 \neq \Delta_3$. Therefore, we can discuss these possibilities case by case. Here, we will provide the details for three representative cases as examples[7].

Example 1: $r_1, r_1 + 1, r_1 - 1, r_1$ In such case, the fusion rule gives

$$2 \leq k \leq \min(2r_1, 2p - 2r_1 - 2);$$
$$2 \leq k \leq \min(2r_1 - 2, 2p - 2r_1). \tag{C.2.53}$$

Putting them together, we have

$$2 \leq k \leq \min(2r_1 - 2, 2p - 2r_1 - 2). \tag{C.2.54}$$

Therefore,

$$r_1 \geq 2, \ p - r_1 \geq 2. \tag{C.2.55}$$

In fact, we can omit $r_1 \geq 2$ as we already have $r_1 \in 3\mathbb{Z}$. Furthermore, we also require $k - (r_1 + 1) + r_1 - 1 \in 2\mathbb{Z}$, that is, $k \in 2\mathbb{Z}$. We can write similar conditions for l. In particular, l should also

---

[7]Below we will use the corresponding r's for external legs to denote each case.

be even, so (k, l) should obey (C.2.51). Therefore, we also need to plug (C.2.51) into the above inequality. This gives

$$r_1 \leq \frac{3(p-1)}{4}, \ s_1 \leq \frac{3(p'-1)}{4}. \tag{C.2.56}$$

Comparing $p - 2$ with $3(p - 1)/4$, we find that $p - 2 \leq 3(p - 1)/4$ only when $p \leq 5$ (with equality at $p = 5$). However, for $p \leq 4$, we cannot have $p - r_1 \geq 2$ as $r_1 \in 3\mathbb{Z}$. Hence, $r_1 \leq \min(p - 2, 3(p - 1)/4) = 3(p - 1)/4$ and likewise for s_1. In all, the conditions for this case are

$$r_1 \leq \frac{3(p-1)}{4}, \ s_1 \leq \frac{3(p'-1)}{4}, \ k = \frac{2}{3}r_1, \ l = \frac{2}{3}s_1. \tag{C.2.57}$$

Example 2: $r_2, r_1 + 1, r_1 - 1, r_2$ In such case, it is not hard to see that k and l should satisfy (C.2.52). Besides, the fusion rule gives

$$|p - 2r_1 - 1| + 1 \leq k \leq p - 2;$$
$$|p - 2r_1 + 1| + 1 \leq k \leq p - 2. \tag{C.2.58}$$

Putting them together, we have

$$\max(|p - 2r_1 - 1| + 1, |p - 2r_1 + 1| + 1) \leq k \leq p - 2. \tag{C.2.59}$$

Since $p - 2r_1 - 1 < p - 2r_1 + 1$, there are three possibilities:

1. $p - 2r_1 - 1 \geq 0$: If

$$p \geq 2r_1 + 1, \tag{C.2.60}$$

then

$$p - 2r_1 + 2 \leq k \leq p - 2. \tag{C.2.61}$$

Plugging $k = p - \frac{2}{3}r_1$ into (C.2.61), one may check that (C.2.60) and (C.2.61) are indeed consistent (they give the conditions $r_1 \geq 2/3$ and $r_1 \geq 3$ which are automatic as $r_1 \in 3\mathbb{Z}$).

2. $p - 2r_1 + 1 \leq 0$: If

$$p \leq 2r_1 - 1, \tag{C.2.62}$$

then

$$2r_1 - p + 2 \leq k \leq p - 2. \tag{C.2.63}$$

For this inequality to hold, we need $p \geq r_1 + 2$. Plugging $k = p - \frac{2}{3}r_1$ into the inequalities, we need $r_1 \leq \frac{3(p-1)}{4}$. Following the above same reasoning, it suffices to keep $r_1 \leq \frac{3(p-1)}{4}$.

3. $p - 2r_1 = 0$: If

$$p = 2r_1, \tag{C.2.64}$$

then

$$2 \leq k \leq p - 2. \tag{C.2.65}$$

Plugging $k = p - \frac{2}{3}r_1$ into the inequalities, one may check that these inequalities are indeed consistent (they give the conditions $r_1 \geq 2/3$ and $r_1 \geq 3$ which are automatic as $r_1 \in 3\mathbb{Z}$).

The disussion for p', l, s_1 is the same.

Example 3: $r_1, r_1 + 1, r_1 - 1, r_2$ In such case, the fusion rule gives

$$2 \leq k \leq \min(2r_1, 2p - 2r_1 - 2);$$
$$2 \leq k \leq \min(r_1 + r_2 - 2, 2p - r_1 - r_2) = \min(p - 2, p) = p - 2. \tag{C.2.66}$$

Putting them together, we have

$$2 \leq k \leq \min(2r_1 - 2, 2p - 2r_1 - 2, p - 2). \tag{C.2.67}$$

Therefore,

$$r_1 \geq 2, \ p \geq 4, \ p - r_1 \geq 2, \tag{C.2.68}$$

where we can omit the first two conditions as we already have $r_1 \in 3\mathbb{Z}$. Furthermore, we also require $k - (r_1 + 1) + r_1 - 1 \in 2\mathbb{Z}$, that is, $k \in 2\mathbb{Z}$. We can write the similar conditions for l. In particular, l should also be even. However, we also have $k - (r_1 - 1) + r_2 - 1 \in 2\mathbb{Z}$, that is, $k - r_1 - r_2 = k - p = k - p' + 1 \in 2\mathbb{Z}$. Likewise, $l - p' \in 2\mathbb{Z}$. This means that k, l cannot be even at the same time (i.e., they should satisfy (C.2.52)). Hence, we reach an contradiction and this case is not possible.

In fact, we can still reduce the number of cases to be checked. Since $r_1 = p - r_2$, we have $r_1 \pm 1 = p - (r_2 \mp 1)$. Therefore, we can rule out the cases where we choose $r_1 \pm 1, r_2 \mp 1$ from the $\binom{4}{2}$ possibilities as $\Delta_2 \neq \Delta_3$. Hence, there are 16 cases (including the above three examples) overall. Moreover, just like in Example 3, we see that it fails to satisfy the fusion rule due to the parity of k, l. This can also be used to reduce the number of possible cases. One may check that

$$r = r_i, m = r_j \pm 1, i = j \ \Rightarrow \ (k, l) \in 2(\mathbb{Z}, \mathbb{Z});$$
$$r = r_i, m = r_j \pm 1, i \neq j \ \Rightarrow \ (k, l) \in (2\mathbb{Z}, 2\mathbb{Z} + 1) \text{ or } (2\mathbb{Z} + 1, 2\mathbb{Z}). \tag{C.2.69}$$

This further reduces the number of possible cases (including the first two examples) to 8. Although there are 8 distinct cases, there are only two conditions as in Example 1 and 2. This is because for the combination $r_i, r_i \pm 1, r_j \pm 1, r_j$, we always have

$$2 \leq k \leq \min(2r_1 - 2, 2p - 2r_1 - 2), \tag{C.2.70}$$

and for the combination $r_i, r_{j \neq i} \pm 1, r_\iota, r_{\kappa \neq \iota} \pm 1$, we always have

$$\max(|p - 2r_1 - 1| + 1, |p - 2r_1 + 1| + 1) \leq k \leq p - 2. \tag{C.2.71}$$

This completes the proof, and the above conditions are summarized in Table C.2.10. We can also see why the tetracritical Ising model is the one with smallest p' for $\Gamma(3)$. One way is to compute $p' = 3, 4, 5$ (with possible p) case by case, and none of them would give parametrizations from $\Gamma(3)$. Alternatively, it is straightforward to use the above conditions as well. Likewise, we can deduce that the smallest possible p is 5. Moreover, this also tells us why we cannot have $r_1 = 6$ or $s_1 = 6$ for $p' = 6, 7$ and why $s_1 = 6$ is not allowed for $(p', p) = (8, 5)$ as in Figure C.2.1 etc.

If a minimal model has CBs corresponding to $\Gamma(3)$, then $(r_1, s_1) = (3, 3)$ (and hence $(r_2, s_2) = (p - 3, p' - 3)$) must be one solution. It is not hard to find that (k, l) is $(2, 2)$ or $(p - 2, p' - 2)$, and either Δ_2 or Δ_3 corresponds to $(2, 2)$ or $(p - 2, p' - 2)$ for all the eight cases. Therefore, we may use this to solve M_0 and $\epsilon_{1,2}$. Suppose $\Delta_{\text{int}} = \Delta_3$, then

$$\frac{Q^2}{4} - \frac{4}{9}M_0^2 = -M_0^2 + QM_0. \tag{C.2.72}$$

Hence, $M_0 = \frac{3Q}{10}$ or $\frac{3Q}{2}$ with $Q = \frac{i}{\sqrt{p'(p'-1)}}$. If we consider $\Delta_{\text{int}} = \Delta_2$ (which we have seen that this would give no new CBs), then we have the opposite values, that is, $M_0 = -\frac{3Q}{10}$ or $-\frac{3Q}{2}$. Using $M_0 = \frac{m_0}{\sqrt{\epsilon_1 \epsilon_2}}$ and $\sqrt{\epsilon_1 \epsilon_2}Q = \epsilon_1 + \epsilon_2$, we may also solve $\epsilon_{1,2}$.

C.2.5 Minimal Models and $\Gamma_0(4) \cap \Gamma(2)$

Let us now discuss one more example, $\Gamma_0(4) \cap \Gamma(2)$. We first focus on the cases when $\zeta = 1/2$. In terms of the simplifications we can make as above, there are only two cases we need to consider. Again, we set $M_0 = \frac{m_0}{\sqrt{\epsilon_1 \epsilon_2}}$. In particular, one can find that the two cases only differ by Δ_3. However, after some calculations, the fusion rule would always lead to $p', p \in 2\mathbb{Z}$, which is impossible for coprime p' and p.

Next, for $\zeta = 2$, it is very similar to $\zeta = 1/2$ but with a swap of m_2, m_3 and an overall rescaling. We also have two distinct cases. For $(+, +, -, -)$ [8], using the same method yields the CBs in minimal models with conditions in Table C.2.11.

Cases	Conditions
$2r_0, 2r_0 \pm 1, r_0 \pm 1, r_0$	
$2r_0, 2r_0 \pm 1, p - (r_0 \pm 1), p - r_0$	$r_0 \leq \frac{p-1\pm1}{3},$
$p - 2r_0, p - (2r_0 \pm 1), r_0 \pm 1, r_0$	$k = 2r_0$
$p - 2r_0, p - (2r_0 \pm 1), p - (r_0 \pm 1), p - r_0$	
$p - 2r_0, 2r_0 \pm 1, p - (r_0 \pm 1), r_0$	$\left(r_0 < \frac{p\mp1}{4} \text{ or} \right.$
$p - 2r_0, 2r_0 \pm 1, r_0 \pm 1, p - r_0$	$\frac{p\mp1}{4} \leq r_0 \leq \frac{p-1/2\mp1/2}{3} \text{ or } r_0 = \frac{p-1}{2} \Big)$
$2r_0, p - (2r_0 \pm 1), p - (r_0 \pm 1), r_0$	and $k = p - 2r_0$
$2r_0, p - (2r_0 \pm 1), r_0 \pm 1, p - r_0$	

TABLE C.2.11: One set of possible CBs in minimal models that $\Gamma_0(4) \cap \Gamma(2)$ corresponds to. There are similar relations for s_0, l, p' by a simple substitution of the corresponding letters, where we have set $\alpha_4 = \alpha_{r_0, s_0}$.

Likewise, the other case with $(-, +, -, +)$ gives the conditions in Table C.2.12.

Cases	Conditions
$2r_0, 2r_0 \pm 1, r_0 \mp 1, r_0$	
$2r_0, 2r_0 \pm 1, p - (r_0 \mp 1), p - r_0$	$r_0 \leq \frac{p-1\pm1}{3},$
$p - 2r_0, p - (2r_0 \pm 1), r_0 \mp 1, r_0$	$k = 2r_0$
$p - 2r_0, p - (2r_0 \pm 1), p - (r_0 \mp 1), p - r_0$	
$p - 2r_0, 2r_0 \pm 1, p - (r_0 \mp 1), r_0$	$\left(r_0 < \frac{p\mp1}{4} \text{ or} \right.$
$p - 2r_0, 2r_0 \pm 1, r_0 \mp 1, p - r_0$	$\frac{p\mp1}{4} \leq r_0 \leq \frac{p-1/2\mp1/2}{3} \text{ or } r_0 = \frac{p-1}{2} \Big)$
$2r_0, p - (2r_0 \pm 1), p - (r_0 \mp 1), r_0$	and $k = p - 2r_0$
$2r_0, p - (2r_0 \pm 1), r_0 \mp 1, p - r_0$	

TABLE C.2.12: The other set of possible CBs in minimal models that $\Gamma_0(4) \cap \Gamma(2)$ corresponds to. There are similar relations for s_0, l, p' by a simple substitution of the corresponding letters, where we have set $\alpha_4 = \alpha_{r_0, s_0}$.

It is not hard to see that for $(+, +, -, -)$, the first CB appears in the minimal model with $p' = 5, p = 4$, viz, the tricritical Ising model. For $(-, +, -, +)$, the first CB appears in the minimal model with $p' = 4, p = 3$, viz, the (critical) Ising model. The Kac tables and corresponding CBs are shown in Figure C.2.2.

Finally, let us consider $\zeta = -1$. Since a always vanishes, $\Delta_{\text{int}} = \frac{Q^2}{4} = -\frac{(p'-p)^2}{4p'p}$. Hence, $p'k - pl = 0$, that is, $p'/p = l/k$. However, as $\gcd(p', p) = 1$ and $k < p, l < p'$, this is impossible.

Now that we have found two dessins that corresponds to CBs in minimal models, we can consider their CBs in the same minimal model. Such example would first appear when $p' = 6, p = 5$ as in Figure C.2.3.

---

[8]Here, it is still sufficient to choose two representatives for the two distinct cases. As different parametrizations of the masses would only differ by signs of m_i's, we will only use their signs to denote (m_0, m_1, m_2, m_3).
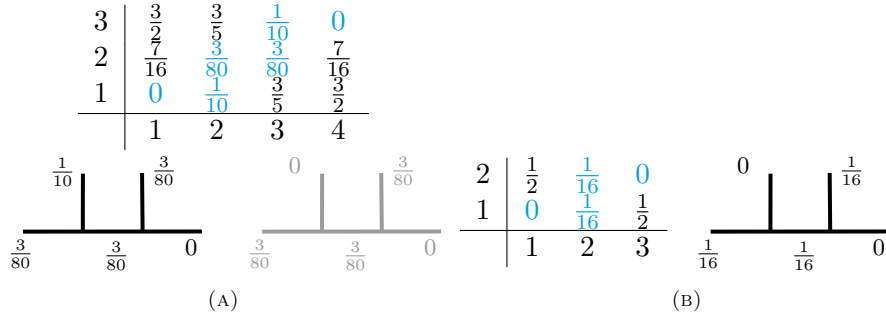
FIGURE C.2.2: Here we list the first possible examples of CBs that $\Gamma_0(4) \cap \Gamma(2)$ corresponds to: (a) The first CB for $(+, +, -, -)$. For reference, the one in grey is the CB from $(-, +, -, +)$ for this minimal model. (b) The first CB for $(-, +, -, +)$.
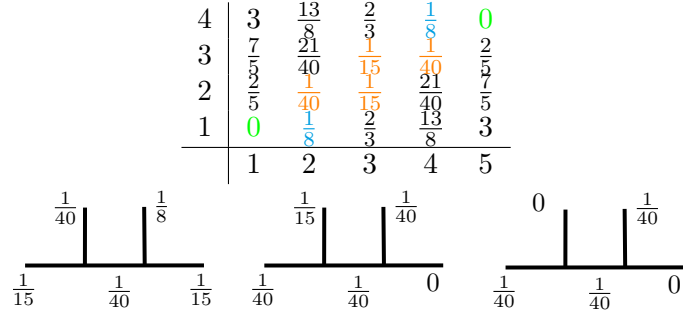
FIGURE C.2.3: The CBs from $\Gamma(3)$ (cyan) and $\Gamma_0(4) \cap \Gamma(2)$ (green) in the tetracritical Ising model. The ones in orange appear for both of the dessins. The three CBs, from left to right, come from $\Gamma(3)$, $(+, +, -, -)$ and $(-, +, -, +)$ in $\Gamma_0(4) \cap \Gamma(2)$ respectively.

C.2.6 Minimal Models and General Dessins

Following the above steps, we can derive the results for any dessin in general.

Proposition C.2.3. *Suppose for a dessin, we have the gauge theory parameters with relation*

$$m_1 = \pm/\mp k_1 m_0, \ m_2 = \pm/\mp k_2 m_0, \ m_3 = \pm/\mp k_3 m_0, \ a = \pm/\mp k_{\text{int}} m_0, \tag{C.2.73}$$

where $k_{i,\text{int}} > 0$. Then the dessin corresponds to the states of 4-point CBs satisfying conditions in Table C.2.13 in minimal models.

Cases	Conditions
$k_1 r_0, k_2 r_0 \pm 1, k_3 r_0 \pm / \mp 1, r_0$	$\max(\lvert \blacktriangle \pm 1 \rvert, \lvert \triangle \pm 1 \rvert) + 1$
$k_1 r_0, k_2 r_0 \pm 1, p - (k_3 r_0 \pm / \mp 1), p - r_0$	$\leq k_{\text{int}} r_0 \leq \frac{1}{2} \min(\bigstar - 3, 4p - 3 - \bigstar),$
$p - k_1 r_0, p - (k_2 r_0 \pm 1), k_3 r_0 \pm / \mp 1, r_0$	and $k = k_{\text{int}} r_0$
$p - k_1 r_0, p - (k_2 r_0 \pm 1), p - (k_3 r_0 \pm / \mp 1), p - r_0$	
$p - k_1 r_0, k_2 r_0 \pm 1, p - (k_3 r_0 \pm / \mp 1), r_0$	$\max(\lvert (k_1 + k_2) r_2 \pm 1 \rvert, \lvert (k_3 + 1) r_2 \pm 1 \rvert) + 1$
$p - k_1 r_0, k_2 r_0 \pm 1, k_3 r_0 \pm / \mp 1, p - r_0$	$\leq k_{\text{int}} r_0 \leq \min(p - 2 - \lvert \blacktriangle \rvert, p - 2 - \lvert \triangle \rvert),$
$k_1 r_0, p - (k_2 r_0 \pm 1), p - (k_3 r_0 \pm / \mp 1), r_0$	and $k = p - k_{\text{int}} r_0$
$k_1 r_0, p - (k_2 r_0 \pm 1), k_3 r_0 \mp 1, p - r_0$	

TABLE C.2.13: The set of possible CBs in minimal models that a general dessin corresponds to. There are similar relations for s_0, l, p' by a simple substitution of the corresponding letters, where we have set $\alpha_4 = \alpha_{r_0, s_0}$ and $\blacktriangle = (k_2 - k_1) r_0$, $\triangle = (1 - k_3) r_0$, $\bigstar = \left(-\lvert k_1 + k_2 - k_3 - 1 \rvert + \sum_i k_i \right) r_0$. In particular, $k_{i,\text{int}} r_0 \in \mathbb{N}^*$ is a necessary condition.

In fact, we may further make the following conjecture.

Conjecture C.2.4. *For a dessin satisfying the conditions in Proposition C.2.6, it corresponds to a family of 4-point CBs whose states follow Table C.2.13.*

So far, we have already discussed how a dessin can reproduce the charges/momenta of the states in a 4-point CB of a minimal model. However, as ζ is fixed for each dessin and we are only obtaining ζ by relating the Strebel and SW differentials rather than describing it as a concrete mathematical object in the language of dessins, further study on whether/how dessins could fully recover the CBs and the spectra is required.

With the conditions in Table C.2.13, we can check what CBs in minimal models we can obtain from a dessin. For instance, when $\zeta = \frac{1}{2} + \frac{11}{50}\sqrt{5}$ for $\Gamma_1(5)$, we have $k_2 = 1, k_1 = k_3 = 5, k_{\text{int}} = 2$. It is not hard to find that the first CB it corresponds to appears when $p' = 7, p = 6$ as in Figure C.2.4.
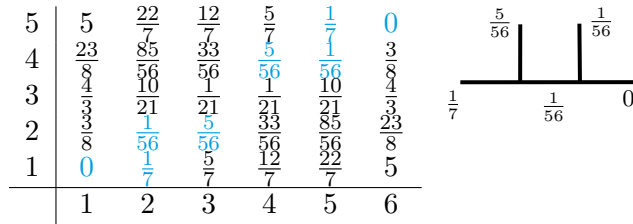
FIGURE C.2.4: The CB on the right has conformal dimensions coloured cyan in the Kac table.

Examples not giving minimal models   From Proposition C.2.6, it is straightforward to see that there could be dessins that do not correspond to CBs in minimal models. Besides the inequalities in Table C.2.13, a necessary condition is that $k_{i,\text{int}}r_0$ and $k_{i,\text{int}}s_0$ should be positive integers. Let us verify this with some examples.

For $\Gamma_0(6)$, there are two big classes of parametrizations. If m_2 or m_3 has the factor $\sqrt{109}$, then we cannot get the rational conformal dimensions for all the external legs. If instead m_1 has the factor $\sqrt{109}$, all the conformal dimensions can be rational since $\Delta_1 = \frac{Q^2}{4} - M_0^2$. However, if we now express M_0 in terms of the labels (r_2, s_2) for Δ_4 and insert this into Δ_1, we find that

$$(p'r_1 - ps_1)^2 = 4 \times 109(p'r_2 - ps_2)^2, \tag{C.2.74}$$

where 109 is not a square number, and hence no integer solutions (except when $0 = 0$ which is excluded for minimal models). Therefore, it is not possible to get CBs in minimal models for $\Gamma_0(6)$.

For $\Gamma_0(8)$, m_i and a are non-zero and cannot simultaneously be real/pure imaginary as in Table C.2.5. Without loss of generality, suppose $\frac{m_i}{\sqrt{\epsilon_1\epsilon_2}}$ is pure imaginary and then $\frac{a}{\sqrt{\epsilon_1\epsilon_2}}$ is real. This yields

$$\Delta_{\text{int}} = \frac{Q^4}{4} - \frac{a^2}{\epsilon_1\epsilon_2} < \frac{Q^2}{4}. \tag{C.2.75}$$

Therefore,

$$\frac{(p'k - pl)^2 - (p' - p)^2}{4p'p} < \frac{Q^2}{4} = -\frac{(p' - p)^2}{4p'p}. \tag{C.2.76}$$

In other words,

$$(p'k - pl)^2 < 0. \tag{C.2.77}$$

Hence, it is not possible to get CBs in minimal models for $\Gamma_0(8)$.

For $\Gamma_0(9)$, since the a's are not real or pure imaginary, it should not give CBs in minimal models.

Appendix D

Minimally Tempered Newton Polynomials

In Table D.0.1, we list all the maximally and minimally tempered Newton polynomials for the reflexive polygons.

Polygon	Maximally tempered polynomial	Minimally tempered polynomial
No.1	$k - \frac{w^2}{z} - \frac{z^2}{w} - \frac{3w}{z} - \frac{3z}{w} - \frac{1}{wz} - 3w - \frac{3}{w} - 3z - \frac{3}{z}$	$k - \frac{w^2}{z} - \frac{z^2}{w} - \frac{1}{wz}$
No.2	$k - \frac{w^3}{z} - \frac{4w^2}{z} - \frac{6w}{z} - \frac{z}{w} - \frac{1}{wz} - 2w - \frac{2}{w} - \frac{4}{z}$	$k - \frac{w^3}{z} - \frac{z}{w} - \frac{1}{wz}$
No.3	$k - \frac{w^2}{z} - \frac{3w}{z} - \frac{z}{w} - \frac{1}{wz} - 2w - \frac{2}{w} - z - \frac{3}{z}$	$k - \frac{w^2}{z} - \frac{z}{w} - \frac{1}{wz} - z$
No.4	$k - wz - \frac{z}{w} - \frac{w}{z} - \frac{1}{wz} - 2w - \frac{2}{w} - 2z - \frac{2}{z}$	$k - wz - \frac{z}{w} - \frac{w}{z} - \frac{1}{wz}$
No.5	$k - \frac{w^2}{z} - \frac{3w}{z} - \frac{1}{wz} - 2w - \frac{1}{w} - z - \frac{3}{z}$	$k - \frac{w^2}{z} - \frac{1}{wz} - \frac{1}{w} - z$
No.6	$k - \frac{w^2}{z} - \frac{2w}{z} - \frac{z}{w} - 2w - \frac{1}{w} - z - \frac{1}{z}$	$k - \frac{w^2}{z} - \frac{z}{w} - \frac{1}{w} - z - \frac{1}{z}$
No.7	$k - \frac{w^2}{z} - \frac{3w}{z} - \frac{1}{wz} - 2w - z - \frac{3}{z}$	$k - \frac{w^2}{z} - \frac{1}{wz} - z$
No.8	$k - \frac{w^2}{z} - \frac{2w}{z} - 2w - \frac{1}{w} - z - \frac{1}{z}$	$k - \frac{w^2}{z} - \frac{1}{w} - z - \frac{1}{z}$
No.9	$k - \frac{w}{z} - \frac{1}{wz} - w - \frac{1}{w} - z - \frac{2}{z}$	$k - \frac{w}{z} - \frac{1}{wz} - w - \frac{1}{w} - z$
No.10	$k - \frac{z}{w} - \frac{w}{z} - w - \frac{1}{w} - z - \frac{1}{z}$	$k - \frac{z}{w} - \frac{w}{z} - w - \frac{1}{w} - z - \frac{1}{z}$
No.11	$k - \frac{w}{z} - \frac{1}{wz} - \frac{1}{w} - z - \frac{2}{z}$	$k - \frac{w}{z} - \frac{1}{wz} - \frac{1}{w} - z$
No.12	$k - \frac{1}{wz} - w - \frac{1}{w} - z - \frac{1}{z}$	$k - \frac{1}{wz} - w - \frac{1}{w} - z - \frac{1}{z}$
No.13	$k - \frac{w}{z} - \frac{1}{wz} - z - \frac{2}{z}$	$k - \frac{w}{z} - \frac{1}{wz} - z$
No.14	$k - \frac{1}{wz} - w - \frac{1}{w} - z$	$k - \frac{1}{wz} - w - \frac{1}{w} - z$
No.15	$k - w - \frac{1}{w} - z - \frac{1}{z}$	$k - w - \frac{1}{w} - z - \frac{1}{z}$
No.16	$k - z - w - \frac{1}{zw}$	$k - z - w - \frac{1}{zw}$

TABLE D.0.1: The maximally and minimally tempered Newton polynomials for reflexive polygons.

D.1 Elliptic Curves for Minimally Tempered Coefficients

Although not as physically interesting as the maximally tempered coefficients, let us list the results for minimally tempered coefficients for comparison and reference. As the reflexive polygons No.10, 12, 14, 15 and 16 do not have any boundary points other than vertices, the minimally tempered

coefficients coincide with the maximially tempered coefficients. Hence, we will not repeat their results here.

As shown in Table D.1.1, the elliptic curves for minimally tempered coefficients are not the same for specular duals. The reason is that these coefficients do not encode all the information of the corresponding (numbers of) perfect matchings.

Polygon	No.1	No.2	No.3	No.4
$a(k)$	$-\frac{9}{2}k$	-4	-3	$\frac{1}{3}k^2 - \frac{16}{3}$
$b(k)$	$-\frac{5}{8}k^3 - \frac{27}{4}$	$-\frac{2}{3}k^2$	$-\frac{3}{4}k^2 - 2$	$-\frac{1}{36}k^4 - \frac{4}{9}k^2 + \frac{128}{27}$
$j(k)$	$\frac{k^3(k^3+216)^3}{(k^3-27)^3}$	$\frac{(k^4+192)^3}{(k^4-64)^2}$	$\frac{(k^4+144)^3}{k^2(k^2-16)(k^2+9)^2}$	$\frac{(k^4-16k^2+256)^3}{k^4(k^2-16)^2}$

Polygon	No.5	No.6
$a(k)$	1	$\frac{1}{6}k^2 + \frac{1}{2}k + \frac{5}{3}$
$b(k)$	$-\frac{1}{12}k^2 - k - 1$	$-\frac{1}{72}k^4 - \frac{1}{24}k^3 - \frac{1}{9}k^2 - \frac{5}{6}k - \frac{125}{108}$
$j(k)$	$\frac{(k^4-48)^3}{k^7+k^6+k^4-72k^3-504k^2-864k-496}$	$\frac{(k^4-8k^2-24k-80)^3}{(k^2+4k+5)^2(k^3-6k^2+12k-35)}$

Polygon	No.7	No.8	No.9
$a(k)$	0	$\frac{1}{2}k^2 + k$	$\frac{1}{6}k^2 + k + \frac{2}{3}$
$b(k)$	-1	$-\frac{1}{24}k^4 - \frac{1}{12}k^3 + \frac{1}{4}k^2 + k + 1$	$-\frac{1}{72}k^4 - \frac{1}{12}k^3 - \frac{1}{36}k^2 + \frac{1}{3}k - \frac{7}{27}$
$j(k)$	$\frac{k^{12}}{k^6-432}$	$\frac{(k^4-8k^2-32)^3}{k^6-11k^4-32k^2-256}$	$\frac{(k^4-8k^2-48k-32)^3}{(k+1)^2(k^4-8k^2-64k-48)}$

Polygon	No.11	No.13
$a(k)$	$\frac{1}{2}k + 1$	1
$b(k)$	$-\frac{1}{24}k^3 - \frac{1}{12}k^2 + \frac{1}{4}$	$-\frac{1}{12}k^2$
$j(k)$	$\frac{(k^4-24k-48)^3}{k^5+k^4+k^3-30k^2-96k-91}$	$\frac{(k^4-48)^3}{k^4-64}$

TABLE D.1.1: The data of the elliptic curves $y^2 = x^3 + fx + g$ and j-invariants for reflexive polygons (with minimally tempered coefficients). Again, we have $f = -\frac{1}{48}k^4 + a(k)$ and $g = \frac{1}{864}k^6 + b(k)$ here.

In Figure D.1.1, we list the plots obtained from $j(k)/1728$. As we can see, this is not a Belyi map for No.8, and hence the plot is not dessin or even a bipartite graph. Moreover, although the graph for No.9 is bipartite, it is not connected, and hence the map is not Belyi as well.

One may also compute the Mahler measures for the Newton polynomials $P(z,w) = k - p(z,w)$ with those minimally tempered coefficients as series of k. We will not list them here, but we would like to point out two properties:

- There are several (but not all) reflexive pairs giving the same Mahler measures. These pairs are No.1&16, No.2&13, No.4&15 (plus the self-dual ones). The reason is that the vertices of the polygons in each pair are related by some GL$(2,\mathbb{Z})$ transformation (while the other reflexive duals are not). This can be seen by quotient gradings on the lattice or direct computations of Plücker coordinates. As the minimally tempered coefficients only contain the vertices, this then follows from the fact that Mahler measure is GL$(2,\mathbb{Z})$ invariant.

- There are four classes of polygons whose Mahler measures can be expressed compactly using some generalized hypergeometric functions $_4F_3$. Likewise, their u_0 are also simply some hypergeometric functions $_2F_1$. These four classes are classified in [50]. It turns out that the four classes are precisely No.1&16, No.2&13, No.4&15 and the self-dual No.7.

Although not all dessins (or just graphs) are associated to congruence subgroups, we may still compute the modular expansions for the k parameters and check if they give rise to any Hauptmoduln. Here we give three examples of different types. The detailed steps can be found in [183, 185].

Example 1: No.1   As this is the same as the case for dP_0 (No.16), we have computed that $k^3 = 27 + \left(\frac{\eta(\tau)}{\eta(3\tau)}\right)^{12}$. This is a Hauptmodul for $\Gamma_0(3)$. In particular, the congruence subgroup associated to the dessin in this case is $\Gamma(3)$, which is a subgroup of $\Gamma_0(3)$.

Example 2: No.13   We have

$$k^4 = q^{-1} + 40 + 276q - 2048q^2 + 11202q^3 + \cdots = 64 + \left(\frac{\eta(\tau)}{\eta(2\tau)}\right)^{24}, \tag{D.1.1}$$

where the second equality is checked perturbatively. This is a Hauptmodul for $\Gamma_0(2)$. On the other hand, the crossing dessin does not correspond to any congruence subgroup. By removing the white vertices (or black vertices), this does not even seem to be a coset graph for any group either.

Example 3: No.7   We have

$$k^6 = 864 \left(1 - \frac{E_6(\tau)}{E_4^{3/2}(\tau)}\right), \tag{D.1.2}$$

where $E_4(\tau) = 1 + 240 \sum_{n=1}^{\infty} \frac{n^3 q^n}{1-q^n}$ and $E_6(\tau) = 1 - 540 \sum_{n=1}^{\infty} \frac{n^5 q^n}{1-q^n}$ are the Eisenstein series. This is not known to be a Hauptmodul of any genus-0 congruence subgroup. On the other hand, the flower dessin does not correspond to any congruence subgroup either. By removing the white vertices, however, it could be viewed as a coset graph associated to any group with 6 generators (and the subgroup being itself). Incidentally, there are two things worth noting:

- As given in [284], we have

$$E_4^{1/4}(\tau) = {}_2F_1\left(\frac{1}{12}, \frac{5}{12}; 1; \frac{1728}{j}\right) \tag{D.1.3}$$

  in terms of j-invariant (cf. §4.2.2).

- The q-series expansion for $E_4(\tau)$ has $a_n = 240$ for $n \geq 1$. It turns out that $2a_n = 480$ are the GW invariants in the first row of Table 1 given in [192] (cf. §4.3.2).

(A) No.1: $\Gamma(3)$

(B) No.2

(C) No.3: $\Gamma_0(4) \cap \Gamma(2)$

(D) No.4: $\Gamma_0(4) \cap \Gamma(2)$

(E) No.5: $\Gamma_0(9)$

(F) No.6: $\Gamma_0(9)$

(G) No.7

(H) No.8

(I) No.9: $\Gamma_0(3) \times \Gamma_0(4)$

(J) No.11: $\Gamma_0(9)$

(K) No.13
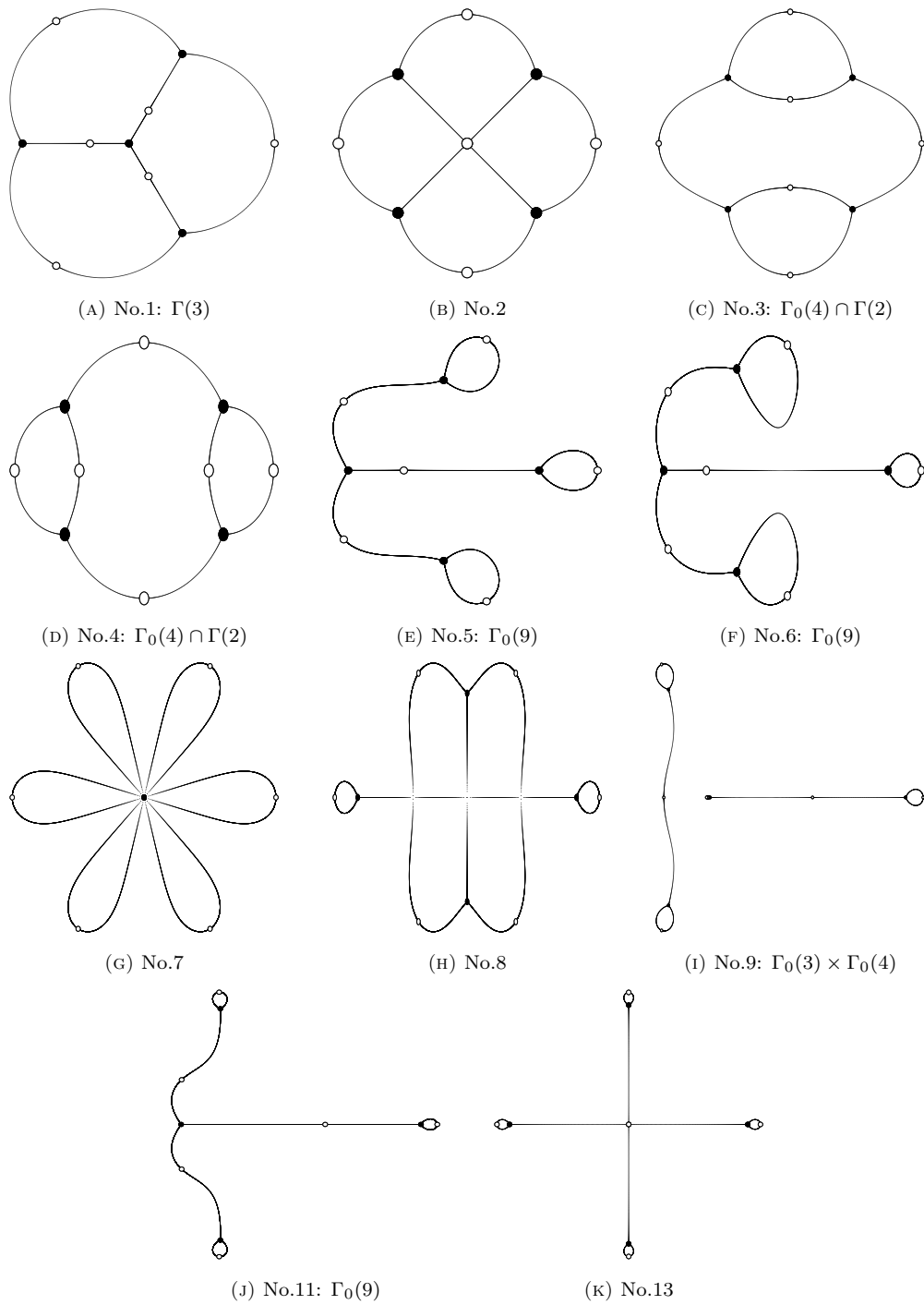
FIGURE D.1.1: The dessins (or just graphs from $j/1728$) for reflexive polygons with minimally tempered coefficients. As listed, some of them correspond to certain congruence subgroups (as coset graphs).

Appendix E

Quivers for Generalized Conifolds

Given any generalized conifold with $M + N \geq 1$, its toric diagram is

$$ \text{(E.0.1)} $$
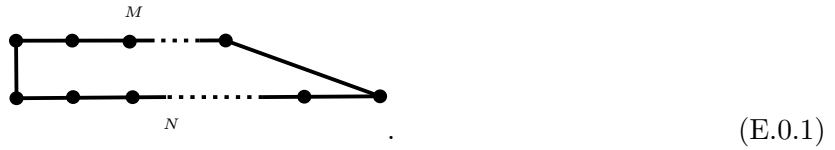
Its quivers in different toric phases can be obtained from the triangulations of the lattice polygon [285, 286]. These triangulations can in turn be encoded by a sequence of signs $\varsigma = \{\varsigma_a | a \in \mathbb{Z}/(M + N)\mathbb{Z}\}$, one for each simplex in the toric diagram. There are M minus ones and N plus ones. When two simplices are glued side by side, they have the same sign. When they are glued in the alternative way, they have opposite signs. An illustration can be found in Figure E.0.1.
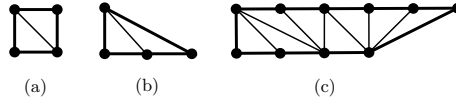
FIGURE E.0.1: In these examples, we have (a) $\varsigma = \{-1, +1\}$, (b) $\varsigma = \{-1, -1\}$ and (c) $\varsigma = \{-1, -1, +1, +1, -1, +1, +1, +1\}$.

The quiver is constructed as follows. First, there is always a pair of opposite arrows connecting node a and node $a + 1$ ($a \in \mathbb{Z}/(M + N)\mathbb{Z}$). Then the node a is bosonic/even and has a self-loop if $\varsigma_a = \varsigma_{a+1}$. If $\varsigma_a = -\varsigma_{a+1}$, then it is fermionic/odd and has no self-loops. Hence, the resulting quiver is essentially the double of the untwisted affine $\mathfrak{sl}_{M|N}$ Dynkin quiver with extra loops on the bosonic nodes. The superpotential W can be fully determined in the toric quiver gauge theory and is composed of the terms

$$ \begin{cases} \varsigma_a \mathrm{tr}(I_{a,a}I_{a,a-1}I_{a-1,a} - I_{a,a}I_{a,a+1}I_{a+1,a}), & \varsigma_a = \varsigma_{a+1}, \\ \varsigma_a \mathrm{tr}(I_{a,a+1}I_{a+1,a}I_{a,a-1}I_{a-1,a}), & \varsigma_a = -\varsigma_{a+1}, \end{cases} \qquad \text{(E.0.2)} $$

where $I_{a,b}$ denotes the arrow/field from node a to b.

Recall that from the superpotential, we have the loop constraint

$$ \sum_{I \in L} \widetilde{\epsilon}_I = 0, \qquad \text{(E.0.3)} $$

for any closed loop L in the periodic quiver. Furthermore, there are also vertex constraints:

$$ \sum_{I \in a} \mathrm{sgn}_a(I)\widetilde{\epsilon}_I = 0, \qquad \text{(E.0.4)} $$

where the sign function $\mathrm{sgn}_a(I)$ is equal to $+1$ (resp. -1) when the arrow I starts from (resp. ends at) the node a, and 0 otherwise.

Following the above rule of toric duality, it is straightforward to see that we can only dualize fermionic nodes in the toric phase. This would just change the parity of the two nodes connected to the dualized node by adding or removing the adjoint loops. Correspondingly, the Dynkin diagrams of the underlying affine Lie superalgebra are related by odd reflections.

A generalized conifold with a larger polygon can be higgsed to one with a smaller polygon. This can be decomposed into a sequence of higgsings. For each single higgsing, the leftmost or rightmost simplex is removed. In the quiver, we merge two adjacent nodes. The two nodes can be either bosonic or fermionic. Suppose that the nodes a and $a + 1$ are merged, then $|a'| = |a| + |a + 1|$, where a' denotes the corresponding node after higgsing. Let us list how the Cartan matrices would change for the three possible cases:

$$|a| = |a + 1| = 0 : \quad \begin{matrix} \\ \\ a \\ a+1 \\ \\ \end{matrix} \begin{pmatrix} \ddots & & & & \\ \cdots & 2 & -1 & \cdots & \\ \cdots & -1 & 2 & -1 & \cdots \\ & \cdots & -1 & 2 & -1 & \cdots \\ & & & -1 & 2 & \cdots \\ & & & & & \ddots \end{pmatrix} \implies a' \begin{pmatrix} \ddots & & & \\ \cdots & 2 & -1 & \cdots \\ \cdots & -1 & 2 & -1 & \cdots \\ & & -1 & 2 & \cdots \\ & & & & \ddots \end{pmatrix}, \quad (E.0.5)$$

$$|a| = 0, |a + 1| = 1 : \quad \begin{matrix} \\ \\ a \\ a+1 \\ \\ \end{matrix} \begin{pmatrix} \ddots & & & & \\ \cdots & 2 & -1 & \cdots & \\ \cdots & -1 & 2 & -1 & \cdots \\ & \cdots & -1 & 0 & 1 & \cdots \\ & & & 1 & -2 & \cdots \\ & & & & & \ddots \end{pmatrix} \implies a' \begin{pmatrix} \ddots & & & \\ \cdots & 2 & -1 & \cdots \\ \cdots & -1 & 0 & 1 & \cdots \\ & & 1 & -2 & \cdots \\ & & & & \ddots \end{pmatrix}, \quad (E.0.6)$$

$$|a| = |a + 1| = 1 : \quad \begin{matrix} \\ \\ a \\ a+1 \\ \\ \end{matrix} \begin{pmatrix} \ddots & & & & \\ \cdots & 2 & -1 & \cdots & \\ \cdots & -1 & 0 & 1 & \cdots \\ & \cdots & 1 & 0 & -1 & \cdots \\ & & & -1 & 2 & \cdots \\ & & & & & \ddots \end{pmatrix} \implies a' \begin{pmatrix} \ddots & & & \\ \cdots & 2 & -1 & \cdots \\ \cdots & -1 & 2 & -1 & \cdots \\ & & -1 & 2 & \cdots \\ & & & & \ddots \end{pmatrix}. \quad (E.0.7)$$

Therefore, the quiver Yangian constructed therefrom is a two-parameter algebra[1]. The general rule of the parameter assignment to the arrows is summarized in Figure E.0.2.

Now, according to the definition of quiver Yangians, the defining relations for the cases of generalized conifolds can be written as follows.

Definition E.0.1. *Given a quiver $Q = (Q_0, Q_1)$ and its superpotential W (with $M + N > 2$), the* non-reduced *quiver Yangian is generated by the modes $e_n^{(a)}$, $f_n^{(a)}$ and $\psi_n^{(a)}$ ($a \in Q_0$, $n \in \mathbb{N}$) satisfying the relations*

$$\left[\psi_n^{(a)}, \psi_m^{(b)} \right] = 0, \tag{E.0.8}$$

$$\left[e_n^{(a)}, f_m^{(b)} \right\} = \delta_{ab} \psi_{m+n}^{(a)}, \tag{E.0.9}$$

---

[1]In §5.7, we discuss the connection of quiver Yangians to $\mathcal{W}$-algebras. These $\mathcal{W}$-algebras only depend on the ratio ϵ_1/ϵ_2 [69]. However, the two parameters are independent for generic quiver Yangians. This is also reflected in the condition on $\epsilon_{1,2}$ in Theorem 5.7.4.
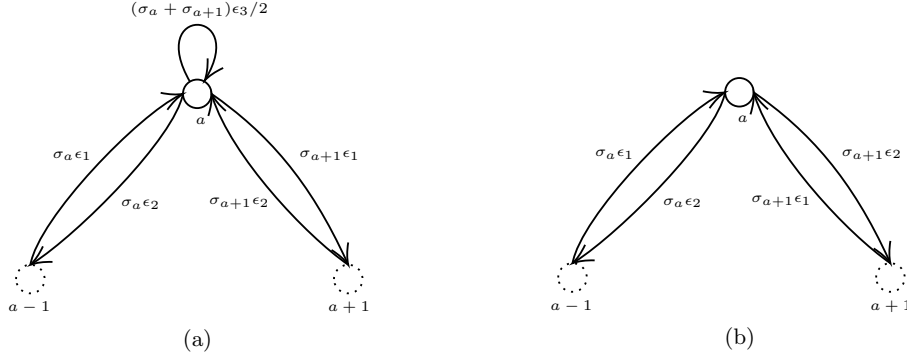
FIGURE E.0.2: The values of $\widetilde{\epsilon}_I$ associated to bifundamentals and adjoints subject to the loop and vertex constraints for generalized conifolds. We have (a) $\varsigma_a = \varsigma_{a+1}$ and (b) $\varsigma_a = -\varsigma_{a+1}$, where $\epsilon_{1,2,3}$ are parameters of the quiver Yangian.

$$\left[\psi_{n+1}^{(a)}, e_m^{(b)}\right] - \left[\psi_n^{(a)}, e_{m+1}^{(b)}\right] = \sigma_1^{ba}\psi_n^{(a)}e_m^{(b)} + \sigma_1^{ab}e_m^{(b)}\psi_n^{(a)}, \tag{E.0.10}$$

$$\left[\psi_{n+1}^{(a)}, f_m^{(b)}\right\} - \left[\psi_n^{(a)}, f_{m+1}^{(b)}\right\} = -\sigma_1^{ab}\psi_n^{(a)}f_m^{(b)} - \sigma_1^{ba}f_m^{(b)}\psi_n^{(a)}, \tag{E.0.11}$$

$$\left[e_n^{(a)}, e_m^{(b)}\right\} = \left[f_n^{(a)}, f_m^{(b)}\right\} = 0 \qquad (\sigma_1^{ab} = 0), \tag{E.0.12}$$

$$\left[e_{n+1}^{(a)}, e_m^{(b)}\right\} - \left[e_n^{(a)}, e_{m+1}^{(b)}\right\} = \sigma_1^{ba}e_n^{(a)}e_m^{(b)} + (-1)^{|a||b|}\sigma_1^{ab}e_m^{(b)}e_n^{(a)} \qquad (\sigma_1^{ab} \neq 0), \tag{E.0.13}$$

$$\left[f_{n+1}^{(a)}, f_m^{(b)}\right\} - \left[f_n^{(a)}, f_{m+1}^{(b)}\right\} = -\sigma_1^{ab}f_n^{(a)}f_m^{(b)} - (-1)^{|a||b|}\sigma_1^{ba}f_m^{(b)}f_n^{(a)} \qquad (\sigma_1^{ab} \neq 0). \tag{E.0.14}$$

The generators $e_n^{(a)}$ and $f_n^{(a)}$ have the $\mathbb{Z}_2$-grading same as the corresponding node a while $\psi_n^{(a)}$ is always bosonic. In the above relations, we also allow $\psi_{-1}^{(a)} := 1/(\epsilon_1 + \epsilon_2)$ so that

$$\left[\psi_0^{(a)}, e_m^{(b)}\right] = \frac{1}{\epsilon_1 + \epsilon_2}\left(\sigma_1^{ab} + \sigma_1^{ba}\right)e_m^{(b)}, \qquad \left[\psi_0^{(a)}, f_m^{(b)}\right] = -\frac{1}{\epsilon_1 + \epsilon_2}\left(\sigma_1^{ab} + \sigma_1^{ba}\right)f_m^{(b)} \tag{E.0.15}$$

can be deduced from the ψe and ψf relations.

Notice that for convenience, we have rescaled the generators compared to the convention in §5.2. The two sets of modes are related by $\mathsf{e}_n^{(a)} = (\epsilon_1 + \epsilon_2)^{1/2}e_n^{(a)}$, $\mathsf{f}_n^{(a)} = (\epsilon_1 + \epsilon_2)^{1/2}f_n^{(a)}$ and $\psi_n^{(a)} = (\epsilon_1 + \epsilon_2)\psi_n^{(a)}$ (including $\psi_{-1}^{(a)}$), where for clarity we have used e, f and ψ to denote the ones using the convention in §5.2.

To correctly recover the BPS degeneracies, we also need the Serre relations.

Definition E.0.2. *Given the above quiver data, the (reduced) quiver Yangian $\mathsf{Y}_{Q,W}$ is the non-reduced quiver Yangian with the Serre relations given as follows. When $MN \neq 2$, we have*

$$\text{Sym}_{n_1,n_2}\left[e_{n_1}^{(a)}, \left[e_{n_2}^{(a)}, e_m^{(a\pm1)}\right]\right\} = 0 \qquad (|a| = 0), \tag{E.0.16}$$

$$\text{Sym}_{n_1,n_2}\left[e_{n_1}^{(a)}, \left[e_{m_1}^{(a+1)}, \left[e_{n_2}^{(a)}, e_{m_2}^{(a-1)}\right\}\right\}\right\} = 0 \qquad (|a| = 1), \tag{E.0.17}$$

and the same relations with all e replaced by f. When $(M, N) = (2, 1)$ (or equivalently, $(M, N) = (1, 2)$), namely for the suspended pinch point (SPP), we have

$$\text{Sym}_{n_1,n_2}\text{Sym}_{m_1,m_2}\left[e_{n_1}^{(0)}, \left[e_{m_1}^{(2)}, \left[e_{n_2}^{(0)}, \left[e_{m_2}^{(2)}, e_k^{(1)}\right\}\right\}\right\}\right\}$$
$$=\text{Sym}_{n_1,n_2}\text{Sym}_{m_1,m_2}\left[e_{m_1}^{(2)}, \left[e_{n_1}^{(0)}, \left[e_{m_2}^{(2)}, \left[e_{n_2}^{(0)}, e_k^{(1)}\right\}\right\}\right\}\right\}, \tag{E.0.18}$$

and the same relation with all e replaced by f, where the node (1) is taken to be the single bosonic node.

For toric CYs, as the superpotential can be unambiguously determined for a given quiver, we shall abbreviate $\mathsf{Y}_{Q,W}$ as Y_Q or even Y if it would not cause confusions. Moreover, since the quiver Yangian is always a two-parameter Yangian algebra, we will omit ϵ_i as well.

Appendix F

BPS Partition Functions, Plethystics and Kac Polynomials

In this chapter, we discuss the BPS partition functions for all the toric CYs without compact 4-cycles as well as (tripled) quivers from affine type (including non-toric ones). One may check that the resuls agree with those from topological strings such as in [202, 287–291]. All of them can be expressed using (generalized) MacMahon functions[1]:

$$M(p,q) := \prod_{k=1}^{\infty} \frac{1}{(1-pq^k)^k}, \quad M(q) := M(1,q), \quad \widetilde{M}(p,q) := M(p,q)M(p^{-1},q). \tag{F.0.1}$$

In the above, $M(q)$ is the standard MacMahon function [292]. We can then also use these expressions to study the gluing process beyond two trivalent vertices in the web diagram and identify the bosonic and fermionic generators.

When studying wall crossings, it is convenient to introduce the shorthand notation

$$M_{\wedge}(p,q;k_0) := \prod_{k=k_0}^{\infty} \frac{1}{(1-pq^k)^k}, \quad M^{\wedge}(p,q;k_0) := \prod_{k=1}^{k_0} \frac{1}{(1-pq^k)^k} \tag{F.0.2}$$

as the truncated MacMahon functions from below and above. For different chambers separated by the walls of marginal stability, we shall discuss their possible crystal descriptions. For chambers $\widetilde{C}$ described by $M^{\wedge}$, the model could be constructed by combining a union of (sub-)crystals. For chambers C described by $M_{\wedge}$, the model could be constructed by peeling semi-infinite faces off the crystal.

We will also write these generating functions in terms of plethystic exponential (PE) of a multi-variable analytic function $f(t_1, \ldots, t_r)$:

$$\mathrm{PE}[f(t_1, \ldots, t_r)] = \exp\left(\sum_{k=1}^{\infty} \frac{f(t_1^k, \ldots, t_r^k) - f(0, \ldots, 0)}{k}\right). \tag{F.0.3}$$

As the PE computes the character of the symmetric algebra, this indicates that the quiver Yangians are symmetric algebras. They can then be endowed with Hopf algebra structures as one may expect.

For some cases, we shall also discuss the PE expressions in the context of (nilpotent) Kac polynomials [293] and consider the connections to different quantum algebras. More specifically, for $\mathbb{C}^3$, the partition function agrees with the Poincaré polynomial encoded by Kac polynomials for some nilpotent (sub)stack. For (tripled) affine quiver cases, the double of such Poincaré polynomial contains the partition function as a factor, and it seems that there exists some subalgebra structure. All these will be checked for both unrefined and refined expressions. It could be possible that the other cases may as well have certain interpretations in their PE expressions.

---

[1]For refined partition functions, we will use refined (generalized) MacMahon functions.

Crystal Partition Functions   In this appendix, we are considering toric diagrams without internal points. Therefore, we will count the D2 and D0 states bound to a single D6. As the dimensional reduction from 4d $\mathcal{N} = 1$ gauge theory, the effective supersymmetric quantum mechanics on the D-branes is a quiver theory. Recall that a quiver $\mathcal{Q}$ is a graph $(\mathcal{Q}_0, \mathcal{Q}_1)$ with $\mathcal{Q}_0$ denoting the set of nodes and $\mathcal{Q}_1$ its edges, and the crystal model can be thought of as the 3d uplift of the periodic quiver.

Given a molten crystal configuration $\mathfrak{C}$, we can write the crystal generating function to enumerate the possible configurations:

$$Z_{\text{crystal}}(q_j) = \sum_{\mathfrak{C}} \prod_{j \in \mathcal{Q}_0} q_j^{|\mathfrak{C}(j)|}, \tag{F.0.4}$$

where $|\mathfrak{C}(j)|$ denotes the number of atoms with colour j in $\mathfrak{C}$. For BPS states counting, we have the BPS partition function

$$Z_{\text{BPS}}(q, \boldsymbol{Q}) = \sum_{n_0, \boldsymbol{n_2}} \Omega(n_0, \boldsymbol{n_2}) q^{n_0} \prod_{i=1}^{|\mathcal{Q}_0|-1} Q_i^{n_{2,i}}, \tag{F.0.5}$$

where Ω is the Witten index for the bound states of n_0 D0s and $\boldsymbol{n_2}$ D2s inside a single non-compact D6 with $n_{2,i}$ the number of D2's wrapping the ith 2-cycle. Note that $n_0 \in \mathbb{Z}_{\geq 0}$ is a non-negative integer and $\boldsymbol{n_2} = (n_{2,i}) \in \mathbb{Z}_{\geq 0}^{|\mathcal{Q}_0|-1}$ is a vector, where $|\mathcal{Q}_0| - 1$ is the number of compact 2-cycles in the CY$_3$. In topological strings, these fugacities q and $\boldsymbol{Q} = (Q_i)$ are related to string coupling g_s and Kähler moduli respectively [131].

Roughly speaking, the partition functions for crystal and BPS states are related by a change of variables $q = \pm \prod_{j=0}^{n-1} q_j$, $Q_i = \pm Q_i$ for $n = |\mathcal{Q}_0|$ and $i = 1, \ldots, n-1$. To determine these signs, we first introduce the (Euler-)Ringel form[2]

$$\langle \boldsymbol{d}_1, \boldsymbol{d}_2 \rangle = \sum_{a \in \mathcal{Q}_0} d_{1,a} d_{2,a} - \sum_{X_{ab} \in \mathcal{Q}_1} d_{1,a} d_{2,b} \tag{F.0.6}$$

for the dimension vectors $\boldsymbol{d}_{1,2}$. Then the sign of the term $\boldsymbol{q}^{\boldsymbol{m}} = \prod_{i=0}^{n-1} q_i^{m_i}$ is given by $(-1)^{m_0 + \langle \boldsymbol{m}, \boldsymbol{m} \rangle}$ [294].

In general, we need to check the signs term by term. However, for toric diagrams without internal points, we simply have

$$(-1)^{m_0 + \langle \boldsymbol{m}, \boldsymbol{m} \rangle} = (-1)^{\sum\limits_{a \in S} m_a}, \tag{F.0.7}$$

where $S = \{a_0\} \sqcup \{a | \nexists X_{aa} \in \mathcal{Q}_1\}$. Notice the disjoint union sign here. This means the initial node is counted twice, one from $\{a_0\}$ and one from $\{a | \nexists X_{aa} \in \mathcal{Q}_1\}$ (if it does not have a loop). Therefore, the signs of variables can be determined as follows:

$$q_0 = \begin{cases} p_0, & \nexists X_{aa} \in \mathcal{Q}_1 \\ -p_0, & \exists X_{aa} \in \mathcal{Q}_1 \end{cases} ; \qquad q_{i \neq 0} = \begin{cases} p_i, & \exists X_{aa} \in \mathcal{Q}_1 \\ -p_i, & \nexists X_{aa} \in \mathcal{Q}_1 \end{cases} . \tag{F.0.8}$$

We shall call this the crystal-to-BPS map. Then we can obtain $Z_{\text{BPS}}(q, \boldsymbol{Q})$ via $q = \prod_{j=0}^{n-1} p_j$, $Q_i = p_j$.

For convenience, especially when writing the sign-changed expressions, we have simply denoted the crystal-to-BPS map as $q_j \to \pm q_j$ in the followings, with the understanding of the signs according to (F.0.8).

---

[2]Recall that X_{ab} denotes an arrow from node a to node b. Moreover, the node a_0 corresponding to the initial atom always uses the variable q_0.

Kac Polynomials   As our partition functions can also be expressed in terms of PE, we would like to see whether they could be related to Kac polynomials. Given a locally finite quiver $Q = (Q_0, Q_1)$, the Kac polynomial $A_{\boldsymbol{d}}(\mathbb{F}_p)$ is the number of absolutely indecomposable representations of the quiver over a finite field $\mathbb{F}_p$ of dimension $\boldsymbol{d} \in \mathbb{Z}_{\geq 0}^{|Q_1|}$ (and hence the name dimension vector). This is called a polynomial because there exists a unique polynomial $A_{\boldsymbol{d}}(t) \in \mathbb{Z}[t]$ such that $A_{\boldsymbol{d}}(\mathbb{F}_p) = A_{\boldsymbol{d}}(p)$ for any $\mathbb{F}_p$ [293].

One can then define the doubled quiver $\overline{Q} = (Q_0, Q_1 \sqcup Q_1^*)$ where an arrow X^* in opposite direction is added for each arrow X in the quiver Q. The preprojective algebra Π_Q is defined as the path algebra $\mathbb{C}\overline{Q}$ quotiented by the ideal generated by $\sum_{X \in Q_1} [X, X^*]$. The stack of representations of Π_Q is an abelian category denoted as $\mathrm{Rep}\Pi_Q = \bigsqcup_{\boldsymbol{d}} \mathrm{Rep}_{\boldsymbol{d}}\Pi_Q$. A representation M is called nilpotent if there exists a filtration $\{0\} = M_l \subset \cdots \subset M_1 \subset M$ such that $\Pi_Q^+(M_i) \subseteq M_{i+1}$, where $\Pi_Q^+ \subset \Pi_Q$ is the augmentation ideal [295, 296]. The substack of these nilpotent representations is called the Lusztig nilpotent variety $\Lambda_Q = \bigsqcup_{\boldsymbol{d}} \Lambda_{Q,\boldsymbol{d}}$. One may also introduce some semi-nilpotent and strongly semi-nilpotent conditions to define the Lagrangian substacks Λ_Q^0 and Λ_Q^1 respectively. We shall not expound the details here, and readers are referred to [295, 297] for these conditions. As their names suggest, $\Lambda_Q \subseteq \Lambda_Q^1 \subseteq \Lambda_Q^0$.

Consider the T-equivariant Borel-Moore homology $H_*^T(\mathrm{Rep}\Pi_Q, \mathbb{Q}) = \bigoplus_{\boldsymbol{d}} H_*^T(\mathrm{Rep}_{\boldsymbol{d}}\Pi_Q, \mathbb{Q})$ [298]. Its Poincaré polynomial[3], as shown in [295, 299], is encoded by the Kac polynomial:

$$P_Q(t, \boldsymbol{z}) = \sum_{\boldsymbol{d}} P(\mathrm{Rep}_{\boldsymbol{d}}\Pi_Q, t) t^{\langle \boldsymbol{d}, \boldsymbol{d}\rangle} \boldsymbol{z}^{\boldsymbol{d}} = \mathrm{PE}\left[\frac{1}{1 - t^{-1}} \sum_{\boldsymbol{d}} A_{\boldsymbol{d}}(t^{-1}) \boldsymbol{z}^{\boldsymbol{d}} \right], \qquad \text{(F.0.9)}$$

where $P(\mathrm{Rep}_{\boldsymbol{d}}\Pi_Q, t) = \sum_i \dim H_{2i}(\mathrm{Rep}_{\boldsymbol{d}}\Pi_Q) t^i$ and $\langle \boldsymbol{d}_1, \boldsymbol{d}_2 \rangle$ is the Ringel form. Likewise, for the Borel-Moore homology of $\Lambda_Q^\flat$ ($\flat = 0, 1$), we have[4]

$$P_Q^\flat(t, \boldsymbol{z}) = \mathrm{PE}\left[\frac{1}{1 - t^{-1}} \sum_{\boldsymbol{d}} A_{\boldsymbol{d}}^\flat(t^{-1}) \boldsymbol{z}^{\boldsymbol{d}} \right]. \qquad \text{(F.0.10)}$$

One can introduce algebra structures on these homology spaces. These "2d" COHAs are closely related to the "3d" COHAs/quiver Yangians discussed in the previous subsection. For instance, consider the Jordan quiver Q, that is, one single node with one loop X. Its tripled quiver $\widehat{Q}$ is given by $\overline{Q}$ with a loop ω added to the node. The (super)potential is then $W = \omega[X, X^*]$. Then the 2d COHAs are the dimensional reductions[5] of the corresponding versions of the 3d COHAs associated to quiver Yangian $\mathtt{Y}\left(\widehat{\mathfrak{gl}_1}\right)$ of $\widehat{Q}$ [208, 301, 302].

More generally, given a quiver Q, its tripled quiver $\widehat{Q}$ is the doubled quiver $\overline{Q}$ with a loop ω_a added to each node. The superpotential is then $W = \sum_{a,x} \omega_a[x, x^*]$. For example, the quivers for $\mathbb{C} \times \mathbb{C}^2/\mathbb{Z}_n$ are tripled quivers $\widehat{Q}$ of the affine A-type quivers Q. As the expressions here associated to both Q and $\widehat{Q}$ are in the form of PE and the Kac polynomials encode certain graded characters, it would be natural to compare them and expect some relations between them. In general, for other toric CY 3-folds, the quivers are not tripled, but it might be possible that they could also have some interpretations in terms of something similar to Kac polynomials and lead to possible connections between various algebras.

---

[3] Since we have infinitely generated homology, this should really be a series, but we shall always refer to it as Poincaré polynomial.

[4] Similarly, $A_{\boldsymbol{d}}^\flat(p)$ gives the number of absolutely indecomposable representations satifying the corresponding nilpotency condition over a finite field $\mathbb{F}_p$ [295].

[5] This dimensional reduction is in the sense that the 3d COHAs were defined in the framework of 3-dimensional CY categories in [300] while the 2d ones come from 2-dimensional CY categories in [86].

F.1 Examples Galore

We now discuss the BPS partition functions for all toric CY_3 without compact 4-cycles and some non-toric examples, along with various relevant aspects. Let us start with the simplest case $\mathbb{C}^3$ which is most well-studied in literature.

F.1.1 Plane Partition: $\mathbb{C}^3$

The toric diagram for $\mathbb{C}^3$ is the simplex with vertices $(0,0)$, $(1,0)$ and $(0,1)$. Its dual web is just the trivalent vertex. There is no compactly supported D2-branes in this case. The generating function is enumerated by plane partitions, given by the MacMahon function [303]:

$$Z_{\text{crystal}} = M(q_0) = \prod_{k=1}^{\infty} \frac{1}{(1-q_0^k)^k}. \tag{F.1.1}$$

The BPS partition function of D0-branes follows the map $q = -q_0$, that is, $Z_{\text{BPS}} = M(-q)$. For future convenience[6], let us also introduce the variable $x = -q$, and then $Z_{\text{BPS}} = M(x)$. The MacMahon function is precisely the vacuum character of the affine Yangian $\text{Y}\left(\widehat{\mathfrak{gl}_1}\right)$.

It is straightforward to write the generating function as

$$M(x) = \text{PE}\left[\frac{x}{(1-x)^2}\right]. \tag{F.1.2}$$

It is curious to see that the Hilbert series (HS) for $\mathbb{C}^2$, namely $1/(1-x)^2$, appears inside PE (rather than $\mathbb{C}^3$). Incidentally, $\mathbb{C}^2$ frequently appears in relevant study of instantons and VOAs. The COHA of the $\mathbb{C}^2$ quiver is also isomorphic to the positive part $\text{Y}^+\left(\widehat{\mathfrak{gl}_1}\right)$ of the affine Yangian [302]. Although similar features are not observed in other cases, the factor $1/(1-x)^2$ is universal in all the examples we consider[7].

We may now use the method in [26,304–306] (see also [12, Appendix B] for a short summary) to get the asymptotics for the generating function. For plane partitions, this is a well-known result [307]. At large n, the asymptotic expansion of MacMahon function has coefficient

$$Z_n \sim \frac{\zeta(3)^{7/36}}{\sqrt{12\pi}} \left(\frac{n}{2}\right)^{-25/36} \exp\left(3\zeta(3)^{1/3}\left(\frac{n}{2}\right)^{2/3} + \zeta'(-1)\right). \tag{F.1.3}$$

Since $\text{PE}[1+f] = \text{PE}[1]\text{PE}[f] = \text{PE}[f]$, we may also write the expression as

$$M(x) = \text{PE}\left[1 + \frac{x}{(1-x)^2}\right] = \text{PE}\left[\frac{1-x+x^2}{(1-x)^2}\right]. \tag{F.1.4}$$

Now the expression inside PE is purely an HS whose Taylor expansion starts from 1. In fact, this is the HS for the complete intersection defined by $\mathcal{X}_1^6 + \mathcal{X}_2^3 + \mathcal{C}_3^2 = 0$. By virtue of PE, this gives a one-to-one correspondence between the BPS states labelled by boxes in the plane partition and single-/multi-trace operators generated by $\mathcal{X}_{1,2,3}$. Nevertheless, it is not clear whether this does imply anything non-trivial in physics and mathematics[8].

---

[6]It seems to be redundant to write $M(q_0)$ (or $M(-q)$) as $M(x)$, but this notation would be easier for our discussions on cases with more variables q_i.

[7]Here, we use x instead of q as it stands for different (but patterned) products of variables for D-branes in different cases.

[8]It is worth noting that this defining equation could be labelled by E_{10} following [308] though it does not fit in the usual McKay correspondence or belong to the exceptional unimodal singularities. This could probably be in line with the McKay correspdence as equivanlence of derived categories [309,310]. Moreover, $(1-x+x^2)/(1-x)^2$ was also studied in [311] in the context of Hasse-Weil zeta functions and Dirichlet series.

Kac polynomials and Poincaré polynomials On the other hand, we find some connections to certain Kac polynomials. Consider the Jordan quiver Q whose doubled quiver $\overline{Q}$ leads to the preprojective algebra $\Pi_Q = \mathbb{C}\overline{Q}/[X, X^*]$. The tripled quiver $\widehat{Q}$ is then the quiver for $\mathbb{C}^3$ having one node with 3 loops X, X^*, ω and superpotential $W = \omega[X, X^*]$. For the T-equivariant Borel-Moore homology $H^T_*(\Lambda^\flat_Q, \mathbb{Q})$, we have [295]

$$P^\flat_Q(t, x) = \text{PE}\left[\frac{tx}{(t-1)(1-x)}\right] = \prod_{d=1}^\infty \prod_{k=0}^\infty \frac{1}{1 - t^{-k}x^d} \tag{F.1.5}$$

with Kac polynomials $A^\flat_d(t) = 1$ for both $\flat = 0$ and $\flat = 1$. In this case, $\Lambda^1_Q = \Lambda^0_Q$. Under the unrefinement $t = x^{-1}$, we find that this agrees with the MacMahon function $M(x) = \text{PE}[x/(1-x)^2]$. This reflects [297, 312] the fact that the COHA of the moduli stack of coherent sheaves on $\mathbb{C}^2$ with zero-dimensional support is isomorphic to $\text{Y}^+\left(\widehat{\mathfrak{gl}_1}\right)$. One may also check that in this case the Poincaré polynomial [86] of Y^+ is $\text{PE}\left[\frac{tx}{(t-1)(1-x)}\right]$. For reference, we also have

$$P_Q(t, x) = \text{PE}\left[\frac{x}{(t-1)(1-x)}\right] = \prod_{d=1}^\infty \prod_{k=1}^\infty \frac{1}{1 - t^{-k}x^d} \tag{F.1.6}$$

with Kac polynomials $A_d(t) = t$.

F.1.2 Conifold

Instead of directly move on to $\mathbb{C}^3$ orbifolds, we shall first consider another very well-studied case, that is, the conifold $\mathcal{C}$. The toric diagram is the square enclosed by the four vertices (p_1, p_2) with $p_{1,2} = \{0, 1\}$. As the quiver has two nodes with two pairs of opposite arrows, the atoms in the crystal (aka pyramid partition) should have two colours $q_{0,1}$. The generating function is well-known from [202, 203]:

$$Z_\text{crystal} = \frac{M(q_0 q_1)^2}{M(-q_1, q_0 q_1) M(-q_1^{-1}, q_0 q_1)} = M(q_0 q_1)^2 \widetilde{M}(-q_1, q_0 q_1)^{-1}. \tag{F.1.7}$$

We may write this in terms of PE as

$$
\begin{aligned}
Z_\text{crystal} &= \text{PE}\left[\sum_{k \in 2\mathbb{Z}_{\geq 0}+1} k q_1^{k-1}(1+q_1)^2 q_0^k\right] \text{PE}\left[\sum_{k \in 2\mathbb{Z}_{>0}} \frac{k}{2} q_1^{k-2}(-1 + 2q_1 + 4q_1^2 + 2q_1^3 - q_1^4) q_0^k\right] \\
&= \text{PE}\left[\frac{q_0((1+q_1)^2 + q_0^2 q_1^2(1+q_1)^2 + q_0(-1 + 2q_1 + 4q_1^2 + 2q_1^3 - q_1^4))}{(1 - q_0 q_1)^2}\right].
\end{aligned}
\tag{F.1.8}
$$

Setting $q_0 = q_1 = \mathfrak{q}$, we get the pyramid partition without any colouring:

$$Z = \text{PE}\left[\frac{\mathfrak{q}(1 + \mathfrak{q} + 3\mathfrak{q}^2 + 4\mathfrak{q}^3 + 3\mathfrak{q}^4 + \mathfrak{q}^5 + \mathfrak{q}^6)}{(1 - \mathfrak{q}^4)^2}\right]. \tag{F.1.9}$$

This has asymptotic behaviour

$$Z_n \sim \frac{(7\zeta(3))^{\frac{2}{9}}}{\sqrt{3}\pi} 2^{-\frac{25}{36}} n^{-\frac{13}{18}} \exp\left(\frac{2}{3}(7\zeta(3))^{\frac{1}{3}}\left(\frac{n}{2}\right)^{\frac{2}{3}} + 2\zeta'(-1)\right). \tag{F.1.10}$$

We can use the map $q = -q_0 q_1$ for D0s and $Q = -q_1$ for D2s to obtain the BPS partition function:

$$Z_\text{BPS}(q, Q) = M(-q)^2 \widetilde{M}(Q, -q)^{-1}. \tag{F.1.11}$$

In terms of PE, we get

$$
\begin{aligned}
Z_{\text{BPS}}(q,Q) &= \text{PE}\left[\sum_{\substack{k=1 \\ k \notin 4\mathbb{Z}+2}}^{\infty} (-1)^{k+1} k \frac{(1-Q)^2}{Q} q^k \right] \text{PE}\left[\sum_{k \in 4\mathbb{Z}_{\geq 0}+2} -\frac{k}{2} \frac{(1-Q)^2(1+4Q+Q^2)}{Q^2} q^k \right] \\
&= \text{PE}\left[\frac{q(1-Q)^2(Q - q(1+4Q+Q^2) + 3q^2 Q - 4q^3 Q + 3q^4 Q - q^5(1+4Q+Q^2) + q^6 Q)}{Q^2(1-q^4)^2} \right].
\end{aligned}
$$
$$(\text{F.1.12})$$

The expressions in PE are rather tedious in this case. Besides, it is not easy to instantaneously transform between the MacMahon expressions and the PE ones. However, if we change the signs properly, namely getting rid of the minus signs in the arguments of (generalized) MacMahon functions, we can easily get

$$
\widetilde{Z}_c = M(q_0 q_1)^2 \widetilde{M}(q_1, q_0 q_1)^{-1} = \text{PE}\left[-\frac{q_0(1-q_1)^2}{(1-q_0 q_1)^2} \right], \tag{F.1.13}
$$

where $\widetilde{Z}_c$ is the sign-changed expression from Z_{crystal}. As we will see, when writing the generating functions in terms of PE, the patterns are more straightforward for generalized conifolds with the signs properly changed. The coefficients in the expansions of $\widetilde{Z}_c$ and Z_{crystal} also agree up to signs. One can simply multiply $(-1)^{n_0+n_1}$ for the terms $q_0^{n_0} q_1^{n_1}$ in $\widetilde{Z}_c$ to recover[9] the correct signs in Z_{crystal}. Alternatively, one may consider the twisted PE introduced in [313]. We find that in general given $\widetilde{Z}_c = \text{PE}[\tilde{g}]$, the twisted PE of $\tilde{g}$ is precisely Z_{crystal}.

Likewise, using $x = -q = q_0 q_1$, we have

$$
Z_{\text{BPS}}(x,Q) = M(x)^2 \widetilde{M}(Q,x)^{-1} = \text{PE}\left[-\frac{x(1-Q)^2}{Q(1-x)^2} \right]. \tag{F.1.14}
$$

In general given $Z_{\text{BPS}}(x,Q) = \text{PE}[\tilde{g}]$, the twisted PE of $\tilde{g}$ is precisely $Z_{\text{BPS}}(q,Q)$. Henceforth, we shall always abbreviate $Z_{\text{BPS}}(x,Q)$ as Z_{BPS}.

Gluing operators In [314–316], the vacuum character for the $\mathcal{N}=2$ affine Yangian and its generalization were studied through certain gluing process. Likewise, we may also identify the gluing operators for the affine Yangians discussed in this paper. For the $\mathfrak{u}(1) \oplus \mathcal{W}_\infty^{\mathcal{N}=2}$ algebra, it contains two copies of affine Yangians of $\mathfrak{gl}_1$ as subalgebra. Therefore, in its vacuum character

$$
\chi(x,y) = M(x)^2 \widetilde{M}(-yx^\rho, x)^{-1}, \tag{F.1.15}
$$

the factor $M(x)^2$ is identified with the generators contributed from the two $\mathcal{W}_{1+\infty}$ with 't Hooft couplings λ_a, λ_b and central charges c_a, c_b. Then the factor

$$
\widetilde{M}(-yx^\rho, x)^{-1} = \prod_{k=1}^{\infty} (1 + yx^{k+\rho})^k (1 + y^{-1}x^{k+\rho})^k \tag{F.1.16}
$$

can be interpreted as gluing operators whose conformal dimensions are controlled by the shifting modulus ρ. More precisely, we have $\Delta = 1 + \rho$. For the $\mathcal{N}=2$ affine Yangian, $\rho = 1/2$.

Compared to the vacuum character of affine Yangian of $\mathfrak{gl}_{1|1}$ for the conifold, we find that $M(x)^2$ with $x = q_0 q_1 = -q$ (and $y = q_1 = -Q$) again comes from the two trivalent vertices while their

---

[9]Since the coefficients in the expansion of Z_{crystal} are all positive as they simply count the numbers of atoms, this is equivalent to just taking absolute values for the coefficients in the expansion of $\widetilde{Z}_c$.

gluing yields the gluing operators with contribution $\widetilde{M}(-y, x)^{-1}$ with no shift, viz, $\rho = 0$. Therefore, we may write the character identity

$$\prod_{k=1}^{\infty} (1 + yx^k)^k = \sum_R y^{|R|} \chi_R^{\wedge, [\lambda_a]}(x) \chi_{R^*}^{\wedge, [\lambda_b]}(x), \tag{F.1.17}$$

where the representation R runs over all Young tableaux and $R^* := \overline{R^{\mathrm{T}}}$ is the conjugate of R^{T}. Moreover, $\chi_R^{\wedge, [\lambda]}(x)$ is the wedge part of the character for representation R of $\mathcal{W}_{1+\infty}[\lambda]$, that is [314, 317],

$$\chi_R^{[\lambda]}(x) = \chi_{\mathrm{pp}}(x) \chi_R^{\wedge, [\lambda]}(x) = M(x) \chi_R^{\wedge, [\lambda]}(x), . \tag{F.1.18}$$

where $\chi_{\mathrm{pp}} = \chi_{\text{plane partitions}}$ is the MacMahon function $M(x)$. With a similar decomposition for the second part in $\widetilde{M}(-yx^\rho, x)^{-1}$, we arrive at

$$\chi_{\mathrm{vac}, \mathcal{C}}(x, y) = M(x)^2 \widetilde{M}(-y, x)^{-1}$$

$$= \chi_{\mathrm{pp}}(x)^2 \left(\sum_{R_1} y^{|R_1|} \chi_{R_1}^{\wedge, [\lambda_a]}(x) \chi_{R_1^*}^{\wedge, [\lambda_b]}(x) \right) \left(\sum_{R_2} y^{-|R_2|} \chi_{R_2^*}^{\wedge, [\lambda_a]}(x) \chi_{R_2}^{\wedge, [\lambda_b]}(x) \right) \tag{F.1.19}$$

$$= \chi_{\mathrm{pp}}(x)^2 + \sum_{R_1} y^{|R_1|} \chi_{R_1}^{[\lambda_a]}(x) \chi_{R_1^*}^{[\lambda_b]}(x) + \sum_{R_2} y^{-|R_2|} \chi_{R_2^*}^{[\lambda_a]}(x) \chi_{R_2}^{[\lambda_b]}(x) + \dots.$$

In particular, the fermionic gluing generators transform as $(R_1, R_1^*) \oplus (R_2^*, R_2)$ under the left and right $\mathcal{W}_{1+\infty}$ algebras[10]. This is reflected by the negative power on $\widetilde{M}$ and the minus signs of the arguments therein, as well as the minus signs in the sign-changed $\widetilde{Z}_{c,b}$. The ways of triangulations/gluing simplices in the toric diagrams are also in line with this. It will become more obvious when we discuss those with bosonic generators in the next subsection.

F.1.3 Coloured Plane Partitions: $\mathbb{C} \times \mathbb{C}^2 / \mathbb{Z}_n$

In such cases, they are all plane partitions but with multiple colours, one for each node. Therefore, we have n variables $q_{0,1,\dots,n-1}$, and the generating function would reduce to the MacMahon function under $q_0 = \dots = q_{n-1}$.

The other bicoloured crystal: $n = 2$ Let us start with the simplest case $\mathbb{C} \times \mathbb{C}^2 / \mathbb{Z}_2$. When writing the generating functions for the conifold, we observe that they are of form $\mathrm{PE}[q_0(1+q_1)^2 g_1]$ and $\mathrm{PE}\left[\frac{q(1-Q)^2}{Q} g_2 \right]$, where $g_{1,2}$ have expansion $1 + \dots$. In particular, the two extra factors satisfy $q_0(1+q_1)^2 = q(1-Q)^2/Q$ under the matching of variables for conifolds. As one of the only two cases with two colours, it is natural to wonder whether $\mathbb{C} \times \mathbb{C}^2 / \mathbb{Z}_2$ would also follow the same pattern with the same extra factor $q_0(1+q_1)^2$ or $q(1-Q)^2/Q$. Recall that we have $\mathrm{PE}[xg_1]$ with $g_1 = 1/(1-x)^2$ for the plane partition with extra factor x. Replacing this extra factor with $q_0(1+q_1)^2$, we obtain

$$Z_{\mathrm{crystal}} = \mathrm{PE}\left[\frac{q_0(1+q_1)^2}{(1-q_0q_1)^2} \right] = M(q_0q_1)^2 \widetilde{M}(q_1, q_0q_1), \tag{F.1.20}$$

where we have also substitute x in the denominator with q_0q_1 similar to the conifold expression. Indeed, one may check that when taking $q_0 = q_1 = \mathfrak{q}$, we get $M(\mathfrak{q}) = \mathrm{PE}[\mathfrak{q}/(1-\mathfrak{q})^2]$ and recover the plane partition with single colour. As there are no minus signs to be removed in (F.1.20), $\widetilde{Z}_c = Z_{\mathrm{crystal}}$ in this case.

For $\mathbb{C} \times \mathbb{C}^2 / \mathbb{Z}_2$, the D-brane variables follow $q = -q_0q_1$ and $Q = q_1$. Therefore, the extra factor should be $-q(1+Q)^2/Q = q_0(1+q_0q_1)^2$ instead of $q(1-Q)^2/Q$ in this case. Either applying this

---

[10] In [315], this was denoted as $(R_1 \otimes R_2^*, R_1^* \otimes R_2)$, where the notation $R \otimes S^*$ indicates the representation has "box" part described by R and "anti-box" part described by S^{T}. In [316], it was denoted as $(R_1 \oplus R_2^*, R_1^* \oplus R_2)$. Here, we shall use the notation which resembles the branching rule.

extra factor to PE$[x/(1-x)^2]$ (with $\mathfrak{q}$ in the denominator changed to q) or directly writing (F.1.20) in q, Q, we can get

$$
\begin{aligned}
Z_{\text{BPS}}(q, Q) =& \text{PE}\left[\frac{-q(1-Q)^2}{Q^2(1-q^4)^2}(Q(1+Q)^2 - q(1+2Q+6Q^2+2Q^3+Q^4) + 3q^2Q(1+Q)^2\right. \\
& \left. -4q^3Q(1+Q)^2 + 3q^4Q(1+Q)^2 - q^5(1+2Q+6Q^2+2Q^3+Q^4) + q^6Q(1+Q)^2))\right] \\
=& \text{PE}\left[\sum_{\substack{k=1 \\ k\notin 4\mathbb{Z}+2}}^{\infty}(-1)^{k+1}k\frac{(1+Q)^2}{Q}q^k\right] \text{PE}\left[\sum_{k\in 4\mathbb{Z}_{\geq 0}+2}\frac{k}{2}\frac{(1-Q)^2(1+2Q+6Q^2+2Q^3+Q^4)}{Q^2}q^k\right] \\
=& M(-q)^2\widetilde{M}(Q, -q).
\end{aligned}
$$

$$(\text{F.1.21})$$

In fact, the generating functions for $\mathbb{C}\times\mathbb{C}^2/\mathbb{Z}_n$ were obtained in [287, 288]. One can check that (F.1.20) and (F.1.21) do give the correct expressions.

As before, it is more concise to use $x = -q$:

$$Z_{\text{BPS}} = M(x)^2\widetilde{M}(Q, x) = \text{PE}\left[\frac{x(1+Q)^2}{Q(1-x)^2}\right].\tag{F.1.22}$$

More importantly, comparing $\widetilde{Z}_c$ for $\mathbb{C}\times\mathbb{C}^2/\mathbb{Z}_2$ with the ones for the conifold, or equivalently their $Z_{\text{crystal,BPS}}$ in (generalized) MacMahon functions, we can see that they only differ by certain minus signs. This is in fact consistent with the analysis of bosonic and fermionic gluing operators. In terms of toric diagrams, they correspond to the two different ways of gluing two simplices. More specifically, here we have

$$\chi_{\text{vac},\mathbb{C}\times\mathbb{C}^2/\mathbb{Z}_2} = \prod_{k=1}^{\infty}\frac{1}{(1-x^k)^{2k}(1-yx^k)^k(1-y^{-1}x^k)^k},\tag{F.1.23}$$

where $x = q_0 q_1 = -q$ and $y = q_1 = Q$. This leads to the bosonic gluing operators with character identity

$$\prod_{k=1}^{\infty}(1+yx^k)^{-k} = \sum_R y^{|R|}\chi_R^{\wedge,[\lambda_a]}(x)\chi_{\overline{R}}^{\wedge,[\lambda_b]}(x).\tag{F.1.24}$$

As a result, the vacuum character decomposes as

$$
\begin{aligned}
\chi_{\text{vac},\mathbb{C}\times\mathbb{C}^2/\mathbb{Z}_2}(x, y) &= \chi_{\text{pp}}(x)^2\left(\sum_{R_1}y^{|R_1|}\chi_{R_1}^{\wedge,[\lambda_a]}(x)\chi_{\overline{R}_1}^{\wedge,[\lambda_b]}(x)\right)\left(\sum_{R_2}y^{-|R_2|}\chi_{\overline{R}_2}^{\wedge,[\lambda_a]}(x)\chi_{R_2}^{\wedge,[\lambda_b]}(x)\right) \\
&= \chi_{\text{pp}}(x)^2 + \sum_{R_1}y^{|R_1|}\chi_{R_1}^{[\lambda_a]}(x)\chi_{\overline{R}_1}^{[\lambda_b]}(x) + \sum_{R_2}y^{-|R_2|}\chi_{\overline{R}_2}^{[\lambda_a]}(x)\chi_{R_2}^{[\lambda_b]}(x) + \dots.
\end{aligned}
$$

$$(\text{F.1.25})$$

In particular, the bosonic gluing generators transform as $(R_1, \overline{R}_1)\oplus(\overline{R}_2, R_2)$ under the left and right $\mathcal{W}_{1+\infty}$ algebras.

General n We may generalize the above discussion to any n. The extra factor now becomes $q_0(1 + q_1 + q_1q_2 + \cdots + q_1q_2 \ldots q_{n-1})(1 + q_{n-1} + q_{n-1}q_{n-2} + \cdots + q_{n-1}q_{n-2} \ldots q_1)$. Therefore,

$$
\begin{aligned}
Z_{\text{crystal}} &= \text{PE} \left[\frac{q_0 \left(1 + \sum\limits_{i=1}^{n-1} \prod\limits_{j=1}^{i} q_j \right) \left(1 + \sum\limits_{i=1}^{n-1} \prod\limits_{j=1}^{i} q_{n-j} \right)}{\left(1 - \prod\limits_{i=0}^{n-1} q_i \right)^2} \right] \\
&= M \left(\prod\limits_{i=0}^{n-1} q_i \right)^n \prod\limits_{0 < r \le s < n} \widetilde{M} \left(\prod\limits_{i=r}^{s} q_i, \prod\limits_{j=0}^{n-1} q_j \right).
\end{aligned}
\tag{F.1.26}
$$

As a sanity check, this reduces to the MacMahon function $M(\mathfrak{q})$ under $q_{0,\ldots,n-1} = \mathfrak{q}$. More generally, if $m|n$, then Z_{BPS} for n can be reduced to the one for m by identifying all $q_i = q_j$ when $i \equiv j \pmod{m}$.

Now that the crystal-to-BPS map reads $q_0 \to -q_0$, $q_{i \ne 0} \to q_i$, we have $q = -\prod\limits_{i=0}^{n-1} q_i$ and $Q_i = q_i$. Thus,

$$
Z_{\text{BPS}}(q, Q) = M(-q)^n \prod\limits_{0 < r \le s < n} \widetilde{M} \left(\prod\limits_{i=r}^{s} Q_i, -q \right).
\tag{F.1.27}
$$

One may check that (F.1.26) and (F.1.27) agree with the results in [287, 288]. By using $x = -q$, we can also get a simpler PE form for Z_{BPS}:

$$
\begin{aligned}
Z_{\text{BPS}} &= M(x)^n \prod\limits_{0 < r \le s < n} \widetilde{M} \left(\prod\limits_{i=r}^{s} Q_i, x \right) \\
&= \text{PE} \left[\frac{x \left(1 + \sum\limits_{i=1}^{n-1} \prod\limits_{j=1}^{i} Q_j \right) \left(1 + \sum\limits_{i=1}^{n-1} \prod\limits_{j=1}^{i} Q_{n-j} \right)}{(1-x)^2 \prod\limits_{i=0}^{n-1} Q_i} \right].
\end{aligned}
\tag{F.1.28}
$$

Remarkably, it was observed in [313] that

$$
Z_{\text{crystal}} = \text{PE} \left[\frac{x}{(1-x)^2} \left(n + \sum\limits_{\boldsymbol{\alpha} \in \Psi} \boldsymbol{q}_*^{\boldsymbol{\alpha}} \right) \right],
\tag{F.1.29}
$$

where $x = \prod\limits_{i=0}^{n-1} q_i$ and $\boldsymbol{q}_*^{\boldsymbol{\alpha}} = \prod\limits_{i=1}^{n-1} q_i^{\alpha_i}$ while Ψ is the root system of the Lie algebra of type A_{n-1}. In particular, $\left(n + \sum\limits_{\boldsymbol{\alpha} \in \Phi} \boldsymbol{q}_*^{\boldsymbol{\alpha}} \right)$ is the character of the adjoint representation. This reflects the enhanced gauge symmetry when the target spaces of type IIA strings have A_{n-1} singularities [318].

General gluings Given the vacuum characters for affine Yangians $\text{Y}\left(\widehat{\mathfrak{gl}}_n \right)$, we are now able to generalize the gluing process to n trivalent vertices. In (F.1.26), the factor $M(x)^n$ arises from n disjoint trivalent vertices. This corresponds to the subalgebra of n copies of $\mathcal{W}_{1+\infty}$. Hence, the remaining product of generalized MacMahon functions are contributions from the gluing operators.

Suppose we only have the first two vertices and glue them. Then we obtain

$$
M(x)^2 \widetilde{M}(q_1, x) = \chi_{\text{pp}}(x)^2 \left(\sum\limits_{R_1} q_1^{|R_1|} \chi_{R_1}^{\wedge, [\lambda_a]}(x) \chi_{\overline{R}_1}^{\wedge, [\lambda_b]}(x) \right) \left(\sum\limits_{R_2} q_1^{-|R_2|} \chi_{\overline{R}_2}^{\wedge, [\lambda_a]}(x) \chi_{R_2}^{\wedge, [\lambda_b]}(x) \right)
\tag{F.1.30}
$$

as in the $\mathbb{C} \times \mathbb{C}^2/\mathbb{Z}_{n=2}$ case, where the blue part corresponds to the two bosonic gluing operators.

Now let us glue a third vertex. We should expect different non-trivial factors as this is not a gluing of two trivalent vertices any more. According to the vacuum character in the $n = 3$ case, we should get

$$
\begin{aligned}
M(x)^3 \widetilde{M}(q_1, x) \widetilde{M}(q_2, x) \widetilde{M}(q_1 q_2, x) = {} & \chi_{\mathrm{pp}}^3 \left(\sum_{R_1} q_1^{|R_1|} \chi_{R_1}^{\wedge} \chi_{\overline{R}_1}^{\wedge} \right) \left(\sum_{R_2} q_1^{-|R_2|} \chi_{\overline{R}_2}^{\wedge} \chi_{R_2}^{\wedge} \right) \\
& \times \left(\sum_{R_3} q_2^{|R_3|} \chi_{R_3}^{\wedge} \chi_{\overline{R}_3}^{\wedge} \right) \left(\sum_{R_4} q_2^{-|R_4|} \chi_{\overline{R}_4}^{\wedge} \chi_{R_4}^{\wedge} \right) \\
& \times \left(\sum_{R_5} (q_1 q_2)^{|R_5|} \chi_{R_5}^{\wedge} \chi_{\overline{R}_5}^{\wedge} \right) \left(\sum_{R_6} (q_1 q_2)^{-|R_6|} \chi_{\overline{R}_6}^{\wedge} \chi_{R_6}^{\wedge} \right),
\end{aligned}
$$
(F.1.31)

where we have omitted the superscripts coming from the three copies $\mathcal{W}_{1+\infty}[\lambda_{a,b,c}]$ in $\chi^{\wedge}$ for brevity. In particular, the red part corresponds to the bosonic operators when the second and third vertices are glued together (ignoring the first vertex). On the other hand, the purple part indicates that there are new bosonic generators arising from blue and red ones. For convenience, we shall refer to the generators like those in blue and red as "basic" gluing operators while the ones like those in purple as "derived" gluing operators. The vacuum character can be decomposed as

$$
\begin{aligned}
\chi_{\mathrm{pp}_3} = {} & \chi_{\mathrm{pp}}^3 + \sum_{R_1} q_1^{|R_1|} \chi_{R_1} \chi_{\overline{R}_1} \chi_{\mathrm{pp}} + \sum_{R_2} q_1^{-|R_2|} \chi_{\overline{R}_2} \chi_{R_2} \chi_{\mathrm{pp}} \\
& + \sum_{R_3} q_2^{|R_3|} \chi_{\mathrm{pp}} \chi_{R_3} \chi_{\overline{R}_3} + \sum_{R_4} q_2^{-|R_4|} \chi_{\mathrm{pp}} \chi_{\overline{R}_4} \chi_{R_4} \\
& + \sum_{R_5} (q_1 q_2)^{|R_5|} \chi_{R_5} \chi_{\overline{R}_5} \chi_{\mathrm{pp}} + \sum_{R_4} (q_1 q_2)^{-|R_6|} \chi_{\overline{R}_6} \chi_{R_6} \chi_{\mathrm{pp}} + \dots,
\end{aligned}
$$
(F.1.32)

where pp_n denotes the n-coloured plane partitions. Here, some generators transform as $(R_1, \overline{R}_1, 1) \oplus (\overline{R}_2, R_2, 1)$ and $(1, R_3, \overline{R}_3) \oplus (1, \overline{R}_4, R_4)$. The remaining ones transform as $(R_5, \overline{R}_5, 1) \oplus (\overline{R}_6, R_6, 1)$ under a subalgebra composed of three different copies of $\mathcal{W}'_{1+\infty}$ (which can be thought of as a mixing of $\mathcal{W}_{1+\infty}[\lambda_{a,b,c}]$). We shall illustrate this gluing in the shorthand notation

$$
q_1 \quad \boxed{q_2 \quad q_1 q_2} \,,
$$
(F.1.33)

where those in the dashed box correspond to the new bosonic gluing operators.

Moving on to $n = 4$, we further glue another vertex. According to (F.1.26),

$$
\chi_{\mathrm{pp}_4} = M(x)^4 \widetilde{M}(q_1, x) \widetilde{M}(q_2, x) \widetilde{M}(q_1 q_2, x) \widetilde{M}(q_3, x) \widetilde{M}(q_2 q_3, x) \widetilde{M}(q_1 q_2 q_3, x).
$$
(F.1.34)

As we can see, gluing the third and fourth vertices (while ignoring the other two) leads to the bosonic operators of the green part. Then the blue and green operators give rise to the new cyan bosonic gluing operators while the red and green parts yield the new yellow ones. The character decomposition can be obtained likewise as before. In the above shorthand notation,

$$
q_1 \quad \boxed{q_2 \quad q_1 q_2} \quad \boxed{q_3 \quad q_2 q_3 \quad q_1 q_2 q_3} \,.
$$
(F.1.35)

As we can see, we have $q_{1,2,3}$ corresponding to basic operators while $q_1 q_2$ and $q_2 q_3$ corresponds to derived operators arising from basic ones. Furthermore, we also have derived ones that are derived from both basic and derived generators.

We can thence get the gluing operators for any n. For instance, at the next level, in the shorthand notation we have

$$q_1 \quad q_2 \quad q_1 q_2 \quad \boxed{q_3 \quad q_2 q_3 \quad q_1 q_2 q_3} \quad \boxed{q_4 \quad q_3 q_4 \quad q_2 q_3 q_4 \quad q_1 q_2 q_3 q_4} \tag{F.1.36}$$

Here, we only have bosonic gluing operators, so we do not need to worry about their $\mathbb{Z}_2$-gradings. When considering any generalized conifolds, we will also have fermionic gluing operators. Although the process is the same, we will discuss the way to determine their $\mathbb{Z}_2$-gradings for multiple vertices.

Kac polynomials and Poincaré polynomials As in the $\mathbb{C}^3$ case, let us view the quiver for $\mathbb{C} \times \mathbb{C}^2/\mathbb{Z}_n$ as the tripled quiver $\widetilde{Q}$ of some quiver Q. Then the quiver Q is simply the cyclic affine $\hat{A}_{n-1}$ quiver with arrows in the same orientation. From [295], we know that

$$P_Q^0(t, \boldsymbol{q}) = \mathrm{PE}\left[\sum_{\boldsymbol{d} \in \Phi_0^+} \frac{t \boldsymbol{q}^{\boldsymbol{d}}}{(t-1)(1-\boldsymbol{q}^{\boldsymbol{\delta}})} \right] \mathrm{PE}\left[\frac{nt\boldsymbol{q}^{\boldsymbol{\delta}}}{(t-1)(1-\boldsymbol{q}^{\boldsymbol{\delta}})} \right] \mathrm{PE}\left[\sum_{\boldsymbol{d} \in \Phi_0^-} \frac{t \boldsymbol{q}^{\boldsymbol{d}+\boldsymbol{\delta}}}{(t-1)(1-\boldsymbol{q}^{\boldsymbol{\delta}})} \right], \tag{F.1.37}$$

where $\boldsymbol{q}^{\boldsymbol{d}} = \prod_{i=0}^{n-1} q_i^{d_i}$. Here, let $\Phi^+ = \Phi_{\mathrm{Re}}^+ \sqcup \Phi_{\mathrm{Im}}^+$ denote the set of positive roots with real and imaginary roots $\Phi_{\mathrm{Re}}^+ = \{\Phi_0^+ + \boldsymbol{\delta}\mathbb{Z}_{\geq 0}\} \sqcup \{\Phi_0^- + \boldsymbol{\delta}\mathbb{Z}_{>0}\}$ and $\Phi_{\mathrm{Im}}^+ = \boldsymbol{\delta}\mathbb{Z}_{>0}$ respectively, where $\boldsymbol{\delta}$ is the minimal positive imaginary root. For affine A-type, we simply have $\boldsymbol{\delta} = (1, \ldots, 1) = \mathbf{1}_n$. Then Φ_0 is the root system of the underlying finite type quiver $Q_0 \subset Q$. For reference, we also have

$$P_Q(t, \boldsymbol{q}) = P_Q^1(t, \boldsymbol{q}) = \mathrm{PE}\left[\sum_{\boldsymbol{d} \in \Phi_0^+} \frac{t \boldsymbol{q}^{\boldsymbol{d}}}{(t-1)(1-\boldsymbol{q}^{\boldsymbol{\delta}})} \right] \mathrm{PE}\left[\frac{(1 + (n-1)t)\boldsymbol{q}^{\boldsymbol{\delta}}}{(t-1)(1-\boldsymbol{q}^{\boldsymbol{\delta}})} \right] \mathrm{PE}\left[\sum_{\boldsymbol{d} \in \Phi_0^-} \frac{t \boldsymbol{q}^{\boldsymbol{d}+\boldsymbol{\delta}}}{(t-1)(1-\boldsymbol{q}^{\boldsymbol{\delta}})} \right].$$
$$\tag{F.1.38}$$

The Kac polynomials are

$$\begin{cases} A_{\boldsymbol{d}}(t) = A_{\boldsymbol{d}}^\flat(t) = 1, & \boldsymbol{d} \in \Phi_{\mathrm{Re}}^+ \\ A_{\boldsymbol{d}}(t) = A_{\boldsymbol{d}}^1(t) = t + n - 1, \ A_{\boldsymbol{d}}^0(t) = n, & \boldsymbol{d} \in \Phi_{\mathrm{Im}}^+ \end{cases}. \tag{F.1.39}$$

To compare this with the character of the affine Yangian, let us further introduce a "negative" counterpart of the COHA associated to Λ_Q^0 such that the Poincaré polynomial takes the sum over $\Phi^- = \Phi_{\mathrm{Re}}^- \sqcup \Phi_{\mathrm{Im}}^-$ with $\Phi_{\mathrm{Re}}^- = \{\Phi_0^- - \boldsymbol{\delta}\mathbb{Z}_{\geq 0}\} \sqcup \{\Phi_0^+ - \boldsymbol{\delta}\mathbb{Z}_{>0}\}$ and $\Phi_{\mathrm{Im}}^- = -\boldsymbol{\delta}\mathbb{Z}_{>0}$. This simply takes $q_i \to q_i^{-1}$ in (F.1.37). Notice that $A_{\boldsymbol{d}}^0$ is independent of t, and the t dependence in P_Q^0 only comes from the factor $1/(1 - t^{-1})$ in (F.0.10). Therefore, we also treat t as a formal variable and take $t \to t^{-1}$. Then

$$\widetilde{P}_Q^0(t, \boldsymbol{q}) = \mathrm{PE}\left[\sum_{\boldsymbol{d} \in \Phi_0^+} \frac{t^{-1} \boldsymbol{q}^{-\boldsymbol{d}}}{(t^{-1}-1)(1-\boldsymbol{q}^{-\boldsymbol{\delta}})} \right] \mathrm{PE}\left[\frac{nt^{-1}\boldsymbol{q}^{-\boldsymbol{\delta}}}{(t^{-1}-1)(1-\boldsymbol{q}^{-\boldsymbol{\delta}})} \right] \mathrm{PE}\left[\sum_{\boldsymbol{d} \in \Phi_0^-} \frac{t^{-1} \boldsymbol{q}^{-\boldsymbol{d}-\boldsymbol{\delta}}}{(t^{-1}-1)(1-\boldsymbol{q}^{-\boldsymbol{\delta}})} \right]$$

$$= \mathrm{PE}\left[\sum_{\boldsymbol{d} \in \Phi_0^-} \frac{\boldsymbol{q}^{\boldsymbol{d}}}{(1-t)(1-\boldsymbol{q}^{-\boldsymbol{\delta}})} \right] \mathrm{PE}\left[\frac{n\boldsymbol{q}^{-\boldsymbol{\delta}}}{(1-t)(1-\boldsymbol{q}^{-\boldsymbol{\delta}})} \right] \mathrm{PE}\left[\sum_{\boldsymbol{d} \in \Phi_0^+} \frac{\boldsymbol{q}^{\boldsymbol{d}-\boldsymbol{\delta}}}{(1-t)(1-\boldsymbol{q}^{-\boldsymbol{\delta}})} \right]$$

$$= \mathrm{PE}\left[\sum_{\boldsymbol{d} \in \Phi_0^-} \frac{\boldsymbol{q}^{\boldsymbol{d}+\boldsymbol{\delta}}}{(t-1)(1-\boldsymbol{q}^{\boldsymbol{\delta}})} \right] \mathrm{PE}\left[\frac{n}{(t-1)(1-\boldsymbol{q}^{\boldsymbol{\delta}})} \right] \mathrm{PE}\left[\sum_{\boldsymbol{d} \in \Phi_0^+} \frac{\boldsymbol{q}^{\boldsymbol{d}}}{(t-1)(1-\boldsymbol{q}^{\boldsymbol{\delta}})} \right].$$
$$\tag{F.1.40}$$

Consider the product

$$
\begin{aligned}
P_Q^0(t,\boldsymbol{q})\widetilde{P}_Q^0(t,\boldsymbol{q}) =& \mathrm{PE}\left[\sum_{\boldsymbol{d}\in\Phi_0^+}\frac{\boldsymbol{q}^{\boldsymbol{d}}}{(t-1)(1-\boldsymbol{q}^{\boldsymbol{\delta}})}\right]\mathrm{PE}\left[\frac{nt\boldsymbol{q}^{\boldsymbol{\delta}}}{(t-1)(1-\boldsymbol{q}^{\boldsymbol{\delta}})}\right]\mathrm{PE}\left[\sum_{\boldsymbol{d}\in\Phi_0^-}\frac{t\boldsymbol{q}^{\boldsymbol{d}+\boldsymbol{\delta}}}{(t-1)(1-\boldsymbol{q}^{\boldsymbol{\delta}})}\right]\\
&\times\mathrm{PE}\left[\sum_{\boldsymbol{d}\in\Phi_0^+}\frac{t\boldsymbol{q}^{\boldsymbol{d}}}{(t-1)(1-\boldsymbol{q}^{\boldsymbol{\delta}})}\right]\mathrm{PE}\left[\sum_{\boldsymbol{d}\in\Phi_0^-}\frac{\boldsymbol{q}^{\boldsymbol{d}+\boldsymbol{\delta}}}{(t-1)(1-\boldsymbol{q}^{\boldsymbol{\delta}})}\right]\mathrm{PE}\left[\frac{n}{(t-1)(1-\boldsymbol{q}^{\boldsymbol{\delta}})}\right]\\
=& \mathrm{PE}\left[\left(\sum_{\boldsymbol{d}\in\Phi_0^+}\frac{\boldsymbol{q}^{\boldsymbol{d}}}{(t-1)(1-x)}\right)+\frac{ntx}{(t-1)(1-x)}+\left(\sum_{\boldsymbol{d}\in\Phi_0^-}\frac{tx\boldsymbol{q}^{\boldsymbol{d}}}{(t-1)(1-x)}\right)\right]\\
&\times\mathrm{PE}\left[\left(\sum_{\boldsymbol{d}\in\Phi_0^+}\frac{t\boldsymbol{q}^{\boldsymbol{d}}}{(t-1)(1-x)}\right)+\frac{n}{(t-1)(1-x)}+\left(\sum_{\boldsymbol{d}\in\Phi_0^-}\frac{x\boldsymbol{q}^{\boldsymbol{d}}}{(t-1)(1-x)}\right)\right],
\end{aligned}
$$
$$(\text{F.1.41})$$

where we have again used $x=\prod_{i=0}^{n-1}q_i$. Henceforth, we shall abbreviate the second PE in the last equality as an ellipsis. As before, taking $t=x^{-1}$, we get

$$
P_Q^0(1/x,\boldsymbol{q})\widetilde{P}_Q^0(1/x,\boldsymbol{q}) = \mathrm{PE}\left[\frac{x}{(1-x)^2}\left(n+\sum_{\boldsymbol{d}\in\Phi_0}\boldsymbol{q}^{\boldsymbol{d}}\right)\right]\times\ldots . \qquad (\text{F.1.42})
$$

Recall the character of the affine Yangian $\mathtt{Y}\left(\widehat{\mathfrak{gl}}_n\right)$ in (F.1.26) and especially in (F.1.29). Inside PE, we have the root system Ψ of A_{n-1} while Φ_0 here is the root system of A_n. Hence, Ψ is the subset of Φ_0 with $d_0=0$. As a result, we obtain

$$
\begin{aligned}
P_Q^0(1/x,\boldsymbol{q})\widetilde{P}_Q^0(1/x,\boldsymbol{q}) =& \mathrm{PE}\left[\frac{x}{(1-x)^2}\left(n+\sum_{\substack{\boldsymbol{d}\in\Phi_0\\d_0=0}}\boldsymbol{q}^{\boldsymbol{d}}\right)\right]\mathrm{PE}\left[\frac{x}{(1-x)^2}\left(\sum_{\substack{\boldsymbol{d}\in\Phi_0\\d_0\neq0}}\boldsymbol{q}^{\boldsymbol{d}}\right)\right]\times\ldots\\
=& \chi_{\mathrm{PP}_n}\mathrm{PE}\left[\frac{x}{(1-x)^2}\left(\sum_{\substack{\boldsymbol{d}\in\Phi_0\\d_0\neq0}}\boldsymbol{q}^{\boldsymbol{d}}\right)\right]\times\ldots .
\end{aligned}
$$
$$(\text{F.1.43})$$

Therefore, it is tempting to conjecture that the double copy of the COHA associated to Λ_Q^0 contains (the positive part of) the affine Yangian as a subalgebra. We will also check this with the refined partition functions below.

Let us illustrate this with a concrete example. Consider $n=2$, then we have

$$
\chi_{\mathrm{PP}_2} = \mathrm{PE}\left[\frac{q_0(1+q_1)^2}{(1-q_0q_1)^2}\right] = \mathrm{PE}\left[\frac{q_0q_1(q_1+2+q_1^{-1})}{(1-q_0q_1)^2}\right] \qquad (\text{F.1.44})
$$

while

$$
P_Q^0(1/x,\boldsymbol{q})\widetilde{P}_Q^0(1/x,\boldsymbol{q}) = \mathrm{PE}\left[\frac{q_0q_1}{(1-q_0q_1)^2}(q_1+2+q_1^{-1}+q_0+q_0^{-1}+q_0q_1+q_0^{-1}q_1^{-1})\right]\times\ldots .
$$
$$(\text{F.1.45})$$

F.1.4 Generalized Conifolds

The generalized conifold is defined by $xy = z^m w^n$. Its crystal melting partition function will give the vacuum character of the affine Yangian $\mathsf{Y}\left(\widehat{\mathfrak{gl}_{m|n}}\right)$. From the information of the (triangulations of the) toric diagrams and their quivers in Appendix E, we can deduce that the crystal-to-BPS map reads $q_0 \to (-1)^{\frac{\sigma_0 + \sigma_1}{2}} q_0$ and $q_a \to (-1)^{\frac{\sigma_a - \sigma_{a+1}}{2}} q_a$ for $a \neq 0$. Now we can write our ansatz for $\widetilde{Z}_c$ which recovers Z_{crystal} under the crystal-to-BPS map. The sign-changed expression is $\widetilde{Z}_c = \text{PE}\left[\frac{g}{(1-x)^2}\right]$, where $x = \prod\limits_{i=0}^{m+n-1} q_i$. The extra factor g is

$$g = (-1)^{\frac{\sigma_0 + \sigma_1}{2}} q_0 \left(1 + \sum_{i=1}^{m+n-1} (-1)^{\frac{\sigma_1 - \sigma_{i+1}}{2}} \prod_{j=1}^{i} q_j\right) \left(1 + \sum_{i=1}^{m+n-1} (-1)^{\frac{\sigma_{m+n-i} - \sigma_0}{2}} \prod_{j=1}^{i} q_{m+n-j}\right).$$
(F.1.46)

In the expansion of $\widetilde{Z}_c$, the coefficients are equal to the numbers of atoms given by Z_{crystal} up to signs. As Z_{crystal} always has positive coefficients in its expansion, the correct signs are recovered simply by taking absolute values.

Write $\widetilde{Z}_c$ using (generalized) MacMahon functions and apply the crystal-to-BPS map, we find

$$Z_{\text{crystal}} = M\left(\prod_{i=0}^{m+n-1} q_i\right)^{m+n} \prod_{0 < r \leq s < m+n} \widetilde{M}\left((-1)^{\frac{\sigma_r - \sigma_{s+1}}{2}} \prod_{j=r}^{s} q_j, \prod_{i=0}^{m+n-1} q_i\right)^{(-1)^{\frac{\sigma_r - \sigma_{s+1}}{2}}}. \quad \text{(F.1.47)}$$

As we can see, such expression in terms of (generalized) MacMahon functions also follows a nice pattern. One may check that all the cases discussed before obey this expression.

Now from the crystal-to-BPS map, we obtain $q = -\prod\limits_{i=0}^{m+n-1} q_i$, $Q_j = (-1)^{\frac{\sigma_j - \sigma_{j+1}}{2}} q_j$. Therefore,

$$Z_{\text{BPS}}(q, Q) = M(-q)^{m+n} \prod_{0 < r \leq s < m+n} \widetilde{M}\left(\prod_{i=r}^{s} Q_i, -q\right)^{(-1)^{\frac{\sigma_r - \sigma_{s+1}}{2}}}. \quad \text{(F.1.48)}$$

In terms of $x = -q$, $Z_{\text{BPS}} = \text{PE}\left[\frac{\tilde{g}}{(1-x)^2}\right]$, where the extra factor $\tilde{g}$ reads

$$\tilde{g} = \frac{x\left(1 + \sum\limits_{i=1}^{m+n-1} (-1)^{\frac{\sigma_1 - \sigma_{i+1}}{2}} \prod\limits_{j=1}^{i} Q_j\right)\left(1 + \sum\limits_{i=0}^{m+n-1} (-1)^{\frac{\sigma_{m+n-i} - \sigma_0}{2}} \prod\limits_{j=1}^{i} Q_{m+n-j}\right)}{\prod\limits_{i=1}^{m+n-1} Q_i}. \quad \text{(F.1.49)}$$

One may expect that these expressions agree with the topological vertex formalism in [290, 291] as well as the results in [319] from a more mathematical approach. They should also satisfy the following properties:

- The perturbative expansion would recover the number of configurations at each level in the crystal in light of the melting rule.

- As a self-consistency check, we can make identifications among the variables $q_{0,...,m+n-1}$. This should reduce to Z_{crystal} with fewer colours of the same crystal configuration.

- The general gluing operators should be consistent with the factors in the character.

The gluing process Let us explain the gluings in more detail. When gluing two "free" vertices, there will be fermionic or bosonic generators depending on the way of gluing them. More generally, when there are multiple vertices glued together, the $\mathbb{Z}_2$-gradings of the basic generators are determined via σ. In other words, if $\sigma_a = \sigma_{a+1}$, the basic gluing operators are bosonic for q_a. If $\sigma_a = -\sigma_{a+1}$, the basic gluing operators are fermionic for q_a. As a result, we cannot separate the two triangles/trivalent vertices and treat them as two "free" building blocks to determine the $\mathbb{Z}_2$-grading of the basic generators. Therefore, for the conifold $\mathcal{C}$, we have fermionic gluing operators since $\sigma_1 = -\sigma_{2\equiv0}$. On the other hand, we only have bosonic ones for $\mathbb{C} \times \mathbb{C}^2/\mathbb{Z}_n$ since $\sigma_1 = \sigma_2 = \cdots = \sigma_{n-1} = \sigma_{n\equiv0}$.

Recall the criterion of adding adjoint loops to quiver nodes. We find that a yields bosonic gluing operators when it has an odd number of adjoint loops while it gives fermionic ones when it has no adjoint loop[11]. This is exactly the same as the grading rule in [57] for determining whether $e_n^{(a)}$ and $f_n^{(a)}$ are bosonic or fermionic generators.

Moreover, there will also be derived gluing operators as discussed before. These extra generators can be simply determined by the usual $\mathbb{Z}_2$-grading, namely, $b \times b = f \times f = b$ and $b \times f = f$. One may check that the generalized MacMahon functions in the characters do follow the discussions here.

Example: SPP As an example, let us consider the SPP as in Figure F.1.1; this corresponds to $m = 1, n = 2$ from the above.

(a)   (b)   (c)
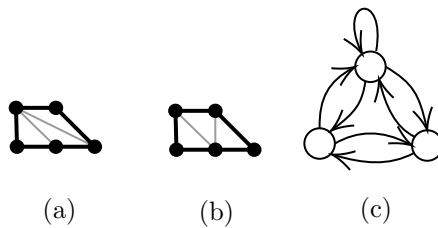
FIGURE F.1.1: The toric diagram with two different triangulations is shown in (a), (b). They give the same quiver as in (c). In the crystals, (a) has the initial atom corresponding to the node with an adjoint while (b) has the initial atom corresponding to one of the nodes without adjoints.

For the crystal from Figure F.1.1(a), the crystal partition function reads

$$
\begin{aligned}
Z_{\text{crystal}} =& M(q_0q_1q_2)\widetilde{M}(-q_1, q_0q_1q_2)^{-1}\widetilde{M}(-q_2, q_0q_1q_2)^{-1}\widetilde{M}(q_1q_2, q_0q_1q_2) \\
=& \text{PE}\left[\frac{q_0}{\left(1 - q_0^2q_1^2q_2^2\right)^2} \left(q_0q_2^2 \left(q_0q_2 \left(q_2 + 1\right) - 1\right) q_1^4 + q_0q_2^2 \left(q_0q_2^2 + 3q_0q_2 + 2q_2 + q_0 + 2\right) q_1^3 \right.\right. \\
& \left.\left. + \left(q_2 + 1\right) \left(q_0^2q_2^2 + q_2 - q_0 \left(q_2^3 - 3q_2^2 - 3q_2 + 1\right)\right) q_1^2 + \left(\left(2q_0 + 1\right) q_2^2 + \left(2q_0 + 3\right) q_2 + 1\right) q_1 \right.\right. \\
& \left.\left. - q_0q_2^2 + q_2 + 1\right) \right].
\end{aligned}
$$

$$(\text{F}.1.50)$$

The sign-changed expression is

$$
\begin{aligned}
\widetilde{Z}_c =& M(q_0q_1q_2)\widetilde{M}(q_1, q_0q_1q_2)^{-1}\widetilde{M}(q_2, q_0q_1q_2)^{-1}\widetilde{M}(q_1q_2, q_0q_1q_2) \\
=& \text{PE}\left[\frac{q_0 \left(q_2^2q_1^2 - q_2q_1^2 - q_2^2q_1 + 3q_2q_1 - q_1 - q_2 + 1\right)}{\left(1 - q_0q_1q_2\right)^2} \right].
\end{aligned}
$$

$$(\text{F}.1.51)$$

---

[11]Here, the "odd number" is used to include the $\mathbb{C}^3$ case. We can likewise extend the fermionic case to even number of adjoints. Of course, for generalized conifolds, this even number can only be zero. It seems that a non-zero even number of adjoints does not exist for physical quiver theories [57].

They have perturbative expansions

$$Z_{\text{crystal}} = 1 + q_0 + (q_0^2 + q_0q_1 + q_0q_2) + (q_0^3 + q_0^2q_1 + q_0^2q_2 + 3q_0q_1q_2) + \dots \tag{F.1.52}$$

and

$$\widetilde{Z}_c = 1 + q_0 + (q_0^2 - q_0q_1 - q_0q_2) + (q_0^3 - q_0^2q_1 - q_0^2q_2 + 3q_0q_1q_3) + \dots . \tag{F.1.53}$$

Indeed, the terms only differ by signs. We may take $\mathfrak{q} = q_0 = q_1 = q_2$ to get the monochrome crystal[12]:

$$Z = \text{PE}\left[\frac{\mathfrak{q}(1 + 2\mathfrak{q} + 3\mathfrak{q}^2 + 2\mathfrak{q}^3 + 5\mathfrak{q}^4 + 6\mathfrak{q}^5 + 5\mathfrak{q}^6 + 2\mathfrak{q}^7 + 3\mathfrak{q}^8 + 2\mathfrak{q}^9 + \mathfrak{q}^{10})}{(1 - \mathfrak{q}^6)^2}\right]$$
$$= 1 + \mathfrak{q} + 3\mathfrak{q}^2 + 6\mathfrak{q}^3 + \dots . \tag{F.1.54}$$

As a byproduct, its asymptotic behaviour is

$$Z_n \sim \frac{e^{\frac{7}{3}\zeta'(-1)}\Gamma\left(\frac{1}{6}\right)^{\frac{2}{3}}\zeta(3)^{\frac{17}{108}}}{2^{\frac{23}{54}}3^{\frac{47}{54}}\pi^{\frac{5}{6}}}n^{-\frac{71}{108}}\exp\left(6^{\frac{1}{3}}\zeta(3)^{\frac{1}{3}}n^{\frac{2}{3}}\right). \tag{F.1.55}$$

Under $q = -q_0q_1q_2$ and $Q_{1,2} = -q_{1,2}$, we have

$$Z_{\text{BPS}}(q, Q) = M(-q)^3\widetilde{M}(Q_1, -q)^{-1}\widetilde{M}(Q_2, -q)^{-1}\widetilde{M}(Q_1Q_2, -q)$$

$$= \text{PE}\left[\frac{q}{Q_1^2Q_2^2(1-q^4)^2}(-q^6Q_1^3Q_2^3 + q^6Q_1^2Q_2^3 + q^6Q_1^3Q_2^2 - 3q^6Q_1^2Q_2^2\right.$$
$$+ q^6Q_1Q_2^2 + q^6Q_1^2Q_2 - q^6Q_1Q_2 + q^5Q_1^4Q_2^4 - q^5Q_1^2Q_2^4 + 2q^5Q_1^3Q_2^3 - 2q^5Q_1^2Q_2^3$$
$$- q^5Q_1^2 - q^5Q_1^4Q_2^2 - 2q^5Q_1^3Q_2^2 + 9q^5Q_1^2Q_2^2 - 2q^5Q_1Q_2^2 - q^5Q_2^2 - 2q^5Q_1^2Q_2$$
$$+ 2q^5Q_1Q_2 + q^5 - 3q^4Q_1^3Q_2^3 + 3q^4Q_1^2Q_2^3 + 3q^4Q_1^3Q_2^2 - 9q^4Q_1^2Q_2^2 + 3q^4Q_1Q_2^2$$
$$+ 3q^4Q_1^2Q_2 - 3q^4Q_1Q_2 + 4q^3Q_1^3Q_2^3 - 4q^3Q_1^2Q_2^3 - 4q^3Q_1^3Q_2^2 + 12q^3Q_1^2Q_2^2 - 4q^3Q_1Q_2^2$$
$$- 4q^3Q_1^2Q_2 + 4q^3Q_1Q_2 - 3q^2Q_1^3Q_2^3 + 3q^2Q_1^2Q_2^3 + 3q^2Q_1^3Q_2^2 - 9q^2Q_1^2Q_2^2 + 3q^2Q_1Q_2^2$$
$$+ 3q^2Q_1^2Q_2 - 3q^2Q_1Q_2 + qQ_1^4Q_2^4 - qQ_1^2Q_2^4 + 2qQ_1^3Q_2^3 - 2qQ_1^2Q_2^3 - qQ_1^2 - qQ_1^4Q_2^2$$
$$- 2qQ_1^3Q_2^2 + 9qQ_1^2Q_2^2 - 2qQ_1Q_2^2 - qQ_2^2 - 2qQ_1^2Q_2 + 2qQ_1Q_2 + q - Q_1^3Q_2^3 + Q_1^2Q_2^3$$

$$\left.+ Q_1^3Q_2^2 - 3Q_1^2Q_2^2 + Q_1Q_2^2 + Q_1^2Q_2 - Q_1Q_2)\right]$$

$$= 1 + \left(-3 + Q_1 + Q_2 + \frac{1}{Q_1} + \frac{1}{Q_2} - Q_1Q_2 - \frac{1}{Q_1Q_2}\right)q + \dots . \tag{F.1.56}$$

More concisely, with $x = -q$, we have

$$Z_{\text{BPS}} = M(x)^3\widetilde{M}(Q_1, x)^{-1}\widetilde{M}(Q_2, x)^{-1}\widetilde{M}(Q_1Q_2, x) = \text{PE}\left[\frac{x(1 - Q_1 + Q_1Q_2)(1 - Q_2 + Q_1Q_2)}{Q_1Q_2(1-x)^2}\right]. \tag{F.1.57}$$

From the generalized MacMahon functions, it is straightforward to find out the gluing operators. In particular, the basic generators for $\widetilde{M}(q_1, q_0q_1q_2)^{-1}$ and $\widetilde{M}(q_2, q_0q_1q_2)^{-1}$ are both fermionic. This is consistent with $\sigma_1 = -\sigma_2$ and $\sigma_2 = -\sigma_{3\equiv 0}$. Their derived gluing operators $\widetilde{M}(q_1q_2, q_0q_1q_2)$ are thus bosonic as expected. The shorthand notation is simply

$$-q_1 \quad -q_2 \quad q_1q_2 \tag{F.1.58}$$

---

[12]Of course, $\widetilde{Z}_c(\mathfrak{q}) = 1 + \mathfrak{q} - \mathfrak{q}^2 + 2\mathfrak{q}^3 + \dots$ would have different coefficients.

where the minus signs indicate the fermionic generators.

Likewise, for Figure F.1.1(b), we have

$$
\begin{aligned}
Z_{\text{crystal}} &= M(q_0 q_1 q_3)^3 \widetilde{M}(-q_1, q_0 q_1 q_2)^{-1} \widetilde{M}(q_2, q_0 q_1 q_2) \widetilde{M}(-q_1 q_2, q_0 q_1 q_2)^{-1} \\
&= 1 + q_0 + (q_0 q_1 + q_0 q_2) + (3 q_0 q_1 q_2 + q_0^2 q_1 + q_0^2 q_2) + \dots
\end{aligned}
\tag{F.1.59}
$$

and

$$
\begin{aligned}
Z_{\text{BPS}}(q, Q) &= M(-q)^3 \widetilde{M}(Q_1, -q)^{-1} \widetilde{M}(Q_2, -q) \widetilde{M}(Q_1 Q_2, -q)^{-1} \\
&= 1 + \left(-3 + Q_1 - Q_2 + \frac{1}{Q_1} - \frac{1}{Q_2} + Q_1 Q_2 + \frac{1}{Q_1 Q_2} \right) q + \dots .
\end{aligned}
\tag{F.1.60}
$$

One may also check that the gluing operators follow our discussions above.

As another check, let us consider for instance two copies of the (triangulated) trapezia in Figure F.1.1(a) glued together. This is SPP/$\mathbb{Z}_2$ with action $(1, 0, 0, 1)$. Its defining equation is $xy = z^2 w^4$. Its crystal has four colours with generating function

$$
\begin{aligned}
Z_{\text{BPS}} =& M(x)^6 \widetilde{M}(-q_1, x)^{-1} \widetilde{M}(-q_2, x)^{-1} \widetilde{M}(q_3, x) \widetilde{M}(-q_4, x)^{-1} \widetilde{M}(-q_5, x)^{-1} \widetilde{M}(q_1 q_2, x) \\
&\times \widetilde{M}(-q_2 q_3, x)^{-1} \widetilde{M}(-q_3 q_4, x)^{-1} \widetilde{M}(q_4 q_5, x) \widetilde{M}(q_1 q_2 q_3, x) \widetilde{M}(q_2 q_3 q_4, x) \widetilde{M}(q_3 q_4 q_5, x) \\
&\times \widetilde{M}(-q_1 q_2 q_3 q_4, x)^{-1} \widetilde{M}(-q_2 q_3 q_4 q_5, x)^{-1} \widetilde{M}(q_1 q_2 q_3 q_4 q_5, x),
\end{aligned}
\tag{F.1.61}
$$

where $x = \prod_{i=0}^{5} q_i$. One may check that under $q_0 = \dots = q_5 = \mathfrak{q}$, this reduces to the SPP partition without colouring as in (F.1.54). Moreover, taking $q_0 = q_3$, $q_1 = q_4$ and $q_2 = q_5$, we get the crystal partition function (F.1.50) for SPP, that is, the SPP partition with three colours.

F.1.5   The Remaining Case: $\mathbb{C}^3/(\mathbb{Z}_2 \times \mathbb{Z}_2)$

Besides generalized conifolds, there is another one which does not have compact four cycles, that is, $\mathbb{C}^3/(\mathbb{Z}_2 \times \mathbb{Z}_2)$ as shown in Figure F.1.2. We have
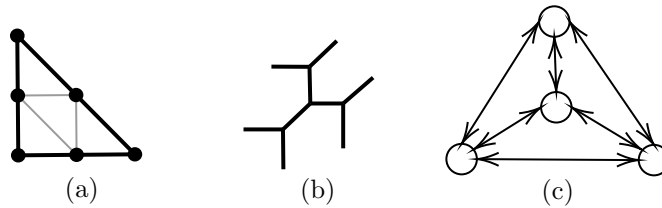
FIGURE F.1.2: (a) The toric diagram for $\mathbb{C}^3/(\mathbb{Z}_2 \times \mathbb{Z}_2)$. (b) Its dual web diagram. (c) The corresponding quiver (the Mercedes-Benz quiver).

$$
\begin{aligned}
Z_{\text{crystal}} =& M(q_0 q_1 q_2 q_3)^4 \widetilde{M}(-q_1, q_0 q_1 q_2 q_3)^{-1} \widetilde{M}(-q_2, q_0 q_1 q_2 q_3)^{-1} \widetilde{M}(-q_3, q_0 q_1 q_2 q_3)^{-1} \\
&\times \widetilde{M}(q_1 q_2, q_0 q_1 q_2 q_3) \widetilde{M}(q_1 q_3, q_0 q_1 q_2 q_3) \widetilde{M}(q_2 q_3, q_0 q_1 q_2 q_3) \widetilde{M}(-q_1 q_2 q_3, q_0 q_1 q_2 q_3)^{-1}
\end{aligned}
\tag{F.1.62}
$$

and

$$
\begin{aligned}
Z_{\text{BPS}}(q, Q) =& M(-q)^4 \widetilde{M}(Q_1, -q)^{-1} \widetilde{M}(Q_2, -q)^{-1} \widetilde{M}(Q_3, -q)^{-1} \widetilde{M}(Q_1 Q_2, -q) \widetilde{M}(Q_1 Q_3, -q) \\
&\times \widetilde{M}(Q_2 Q_3, -q) \widetilde{M}(Q_1 Q_2 Q_3, -q)^{-1}.
\end{aligned}
\tag{F.1.63}
$$

The expressions in terms of PE are rather tedious. Hence, we shall not list them here. Instead, by removing the minus signs, the sign-changed expression $\widetilde{Z}_c$ is more concise:

$$\widetilde{Z}_c = \text{PE}\left[\frac{q_0}{(1 - q_0 q_1 q_2 q_3)^2}(-q_2^2 q_3^2 q_1^2 + q_2 q_3^2 q_1^2 + q_2^2 q_3 q_1^2 - q_2 q_3 q_1^2 + q_2^2 q_3^2 q_1 - q_2 q_3^2 q_1\right.$$
$$\left. - q_2 q_1 - q_2^2 q_3 q_1 + 4 q_2 q_3 q_1 - q_3 q_1 + q_1 + q_2 - q_2 q_3 + q_3 - 1)\right].$$

(F.1.64)

Likewise, again with $x = -q$,

$$Z_{\text{BPS}} = \text{PE}\left[\frac{x}{Q_1 Q_2 Q_3 (1 - x)^2}(Q_2^2 Q_3^2 Q_1^2 + Q_2 Q_3^2 Q_1^2 + Q_2^2 Q_3 Q_1^2 + Q_2 Q_3 Q_1^2 + Q_2^2 Q_3^2 Q_1\right.$$
$$\left. + Q_2 Q_3^2 Q_1 + Q_2 Q_1 + Q_2^2 Q_3 Q_1 + 4 Q_2 Q_3 Q_1 + Q_3 Q_1 + Q_1 + Q_2 + Q_2 Q_3 + Q_3 + 1)\right].$$

(F.1.65)

One may check that Z_{crystal} reduces to $\text{PE}\left[\frac{\mathfrak{q}}{(1-\mathfrak{q})^2}\right]$, namely the (monochrome) crystal for $\mathbb{C}^3$, when taking $q_{0,1,2,3} = \mathfrak{q}$.

Moreover,

$$Z_{\text{BPS}} = \text{PE}\left[\frac{x}{(1 - x)^2}\left(2 + \prod_{i=1}^{4}\left(Q_i^{1/2} + Q_i^{-1/2}\right)\right)\right],$$

(F.1.66)

where $Q_4 := Q_1 Q_2 Q_3$. In particular, it contains the fundamental representation of $\text{SU}(2)^4$. Physically, the web diagram decribes the $T[A_{N-1}]$ theory where N M5-branes wrap a sphere with three full punctures when $N = 2$ [320]. Therefore, it should have $\text{SU}(2)^3$ flavour symmetry [321], which is reflected by the factors with $Q_{1,2,3}$. On the other hand, the Q_4 part should indicate the $\mathbb{Z}_3$ action on the brane web which reduces the above $\text{SU}(2)^3$ to a single $\text{SU}(2)$ as discussed in [322][13].

The gluing process As shown in Figure F.1.2, there is one trivalent vertex glued to each leg of the centre one. As a result, the gluing operators in this picture would also be different[14]. This is again indicated by the vacuum character. From (F.1.62), we see that the basic gluing operators are all fermionic. Furthermore, we have gluing operators associated to $q_i q_j$ for all pairs (i, j) with $i < j$ and $q_1 q_2 q_3$ all derived from the basic operators. In our shorthand notation, we have

$$-q_1 \quad -q_2 \quad -q_3 \quad q_1 q_2 \quad q_1 q_3 \quad q_2 q_3 \quad -q_1 q_2 q_3 \qquad \text{.}$$

(F.1.67)

F.1.6   Some Non-Toric Examples

Based on the discussions on A-type singularities, we may try to generalize to D- and E-type singularities. Now, $\mathbb{C} \times \mathbb{C}^2/\Gamma$ are not toric, where $\Gamma \in \{\text{Dic}_r, \text{BT}, \text{BO}, \text{BI}\}$ is the binary dihedral/tetrahedral/octaheral/icosahedral group, i.e., the D_r and $E_{6,7,8}$ subgroups of $\text{SU}(2)$. Nevertheless, they should still admit quiver descriptions which are the tripled quivers $\widehat{Q}$ of the affine D-/E-type quivers Q [323].

---

[13]Notice that the full flavour symmetry under gauging this $\mathbb{Z}_3$ discrete symmetry would further have an extra $\text{SU}(3)$ factor.

[14]However, we should emphasize that the gluing process here is essentially in line with the ones for generalized conifolds. The algebraic gluing rules we have still consist of the corresponding holomorphic curves on the geometric side for topological string amplitudes.

Similar to (F.1.26) and (F.1.29), we may conjecture that the parititon function in such case is

$$\chi_r = \mathrm{PE}\left[\frac{x}{(1-x)^2}\left(r + \sum_{\boldsymbol{\alpha}\in\Psi}\boldsymbol{q}_*^{\boldsymbol{\alpha}}\right)\right], \tag{F.1.68}$$

where $x := \prod_{i=0}^{r-1} q_i^{\delta_i}$ and $\boldsymbol{q}_*^{\boldsymbol{\alpha}} = \prod_{i=1}^{r-1} q_i^{\alpha_i}$ while Ψ is the root system of the Lie algebra of type D_r or $E_{6,7,8}$. In particular, $\left(r + \sum_{\boldsymbol{\alpha}\in\Phi}\boldsymbol{q}_*^{\boldsymbol{\alpha}}\right)$ is the character of the adjoint representation.

Notice that here we let the convention to be $x = \prod_{i=0}^{r-1} q_i^{\delta_i}$ due to the non-trivial minimal positive imaginary root $\boldsymbol{\delta}$. For the affine ADE types, $\boldsymbol{\delta}$ are the Dynkin labels (dual Coxeter numbers) [324]:

$$\tag{F.1.69}$$

Then $\delta_{0,\dots,r-1}$ should take the values associated to the nodes of the underlying finite quiver.

This is in line with the discussions on Kac polynomials. For affine DE's, the Kac polynomials are [295]

$$\begin{cases} A_{\boldsymbol{d}}(t) = A_{\boldsymbol{d}}^{\flat}(t) = 1, & \boldsymbol{d}\in\Phi_{\mathrm{Re}}^+ \\ A_{\boldsymbol{d}}(t) = A_{\boldsymbol{d}}^1(t) = t + r, & \boldsymbol{d}\in\Phi_{\mathrm{Im}}^+ \end{cases}. \tag{F.1.70}$$

The Poincaré polynomials are

$$P_Q^{\flat}(t,\boldsymbol{q}) = P_Q(t,\boldsymbol{q}) = \mathrm{PE}\left[\sum_{\boldsymbol{d}\in\Phi_0^+}\frac{t\boldsymbol{q}^{\boldsymbol{d}}}{(t-1)(1-\boldsymbol{q}^{\boldsymbol{\delta}})}\right]\mathrm{PE}\left[\frac{(1+rt)\boldsymbol{q}^{\boldsymbol{\delta}}}{(t-1)(1-\boldsymbol{q}^{\boldsymbol{\delta}})}\right]\mathrm{PE}\left[\sum_{\boldsymbol{d}\in\Phi_0^-}\frac{t\boldsymbol{q}^{\boldsymbol{d}+\boldsymbol{\delta}}}{(t-1)(1-\boldsymbol{q}^{\boldsymbol{\delta}})}\right]. \tag{F.1.71}$$

Again, the double copy $P_Q^0(t,\boldsymbol{q})\widetilde{P}_Q^0(t,\boldsymbol{q})$ contains χ_r as a factor:

$$P_Q^0(t,\boldsymbol{q})\widetilde{P}_Q^0(t,\boldsymbol{q}) = \mathrm{PE}\left[\frac{x}{(1-x)^2}\left(r + \sum_{\substack{\boldsymbol{d}\in\Phi_0 \\ d_0=0}}\boldsymbol{q}^{\boldsymbol{d}}\right)\right]\times\cdots = \chi_r\times\dots \tag{F.1.72}$$

under the unrefinement $t^{-1} = x$. This seems to indicate some subalgebra struture. In §F.2.1, we will check this with the refined partition functions.

It is worth noting that the partition functions Z_{DT} and Z_{PT} for DT and Pandharipande-Thomas (PT) invariants were obtained in [325, 326] for ADE singularities $\mathbb{C}\times\mathbb{C}^2/\Gamma$ with $\Gamma\subset\mathrm{SU}(2)$ finite. One may then verify that (F.1.68) agrees with these results under wall crossings discussed in the next section. More generally, one may also consider all the other affine quivers as classified in [324, Table Aff 1-3]. Although the 3-fold geometry may not be clear, it would be natural to conjecture that (F.1.68) would still give the partition functions for the tripled quivers of these affine quivers. Moreover, the Kac polynomials and Poincaré polynomials would again follow (F.1.70)~(F.1.72).

F.2   Wall Crossings

Having presented in detail, in the previous section, explicit expressions for Z_{crystal} and Z_{BPS} for a variety of examples, let us now move on to discuss the wall-crossing phenomena which have been intensively studied for such partition functions.

It is well-known that there are walls of marginal stability of codimension 1 in the moduli space of the quiver theory. When BPS particles cross a wall from one chamber to another, they might decay due to the stability conditions. So far, we have only focused on the BPS states in the NCDT chamber [202]. It is related to the toplogical string amplitudes by $Z_{\text{BPS}} = Z_{\text{top}}(x, \boldsymbol{Q}) Z_{\text{top}}(x, \boldsymbol{Q}^{-1})$. On the other hand, the BPS parition function in the core chamber is trivially $Z_{\text{BPS}} = 1$. There are many other chambers between these two where the (anti-)D2s on different 2-cycles form stable states with various numbers of D0s.

For example, the most well-studied conifold case has the chamber structure which can be depicted as[15] [44, 45]

(F.2.1)

The BPS partition function Z_{BPS} in the NCDT/Szendröi chamber is the one discussed above while $Z_{\text{BPS}} = Z_{\text{DT}} = Z_{\text{top}}(x, Q)$ in the DT chamber. Therefore, one loses a factor $(1 - x^k Q^{-1})^k$ when crossing the wall from the chamber C_{k-1} to C_k. In the other half, if we start from the core chamber, one obtains a factor $(1 - x^k Q)^k$ when crossing the wall from the chamber $\widetilde{C}_{k-1}$ to $\widetilde{C}_k$, and in the PT chamber, we have $Z_{\text{BPS}} = M(Q, x)^{-1}$ such that the BPS invariants are identified with PT invariants. Let R denote the inverse D0-brane central charge (up to some complex constant)[16], and let B denote the NS-NS B-field through the 2-cycles wrapped by the D2s in the CY manifold. Then $R > 0$ from NCDT to DT chambers while $R < 0$ from PT to core chambers. The B-fields satisfy $k - 1 < B < k$ and $-k - 1 < B < -k$ respectively. In fact, there is another half with flopped geometry going from NCDT to core chambers. Together the two pieces form a closed circle.

More generally, for any toric CYs without compact 4-cycles, one would obtain/lose a factor $\left(1 - x^k \mathbf{Q}^{\pm 1}\right)^{\pm k}$ every time we cross a wall of marginal stability similar to the conifold case. Here, $\mathbf{Q} = \left(\prod\limits_{i \in J} Q_i\right)$ where J refers to the set of indices for any possible combination of Q_i's that would appear in Z_{NCDT}.

For generalized conifolds $xy = z^m w^n$, the BPS partition function in any chamber can be written as [285, 327]

$$Z_{\text{BPS}} = \prod_{(k, \boldsymbol{\beta}) : \mathcal{Z}(k, \boldsymbol{\beta}) > 0} \left(1 - x^k \boldsymbol{Q}^{\boldsymbol{\beta}}\right)^{k N_{\boldsymbol{\beta}}^0}, \tag{F.2.2}$$

where $\mathcal{Z}$ denotes the central charge and $N_{\boldsymbol{\beta}}^0$ is the genus-0 Gopakumar-Vafa invariant specified by the 2-cycle $\boldsymbol{\beta} = \sum\limits_{i \leq l \leq j} \alpha_l$ with α_l the basis of 2-cycles. Therefore, $N_0^0 = |\mathcal{Q}_0| - 1 = m + n$ and $N_{-\boldsymbol{\beta}}^0 = N_{\boldsymbol{\beta}}^0$. The central charge is $\mathcal{Z} = (k + B(\boldsymbol{\beta}))/R$ where $B(\boldsymbol{\beta})$ is the B-field flux through the 2-cycle $\boldsymbol{\beta}$. Recall that $\sigma = \{\sigma_l\}$ denotes the signs of simplices in the triangulation. Then [285, 286]

$$N_{\boldsymbol{\beta}}^0 = (-1)^{1 + \#\{l \in [i,j]: \ \alpha_l \text{ is an } \mathcal{O}(-1,-1)\text{-curve}\}} = (-1)^{1 + \#\{l \in [i,j]: \ \sigma_l \neq \sigma_{l+1}\}}. \tag{F.2.3}$$

The BPS partition function is therefore

$$Z_{\text{BPS}} = M(x)^{m+n} \prod_{0 < r \leq s < m+n} \left(M\left(\prod_{i=r}^s Q_i, x\right) M_{\wedge}\left(\prod_{i=r}^s Q_i^{-1}, x; B_{r,\dots,s}\right) \right)^{(-1)^{\frac{\sigma_r - \sigma_{s+1}}{2}}} \tag{F.2.4}$$

---

[15]This can be understood as follows. Starting from the region where only the D6 itself is stable (which is known as the core chamber), every time one crosses a wall labeled by D2 + ND0, an arbitrary number of D2 + ND0 can bind to the D6. Then one encounters the D0 wall where any number of D0s can bind to the D6. After that, $\overline{\text{D2}} + N$D0 particles start to bind to the D6 every time one crosses a $\overline{\text{D2}} + N$D0 wall.

[16]This notation R comes from the Taub-NUT circle in the M-theory uplift [327].

or

$$Z_{\text{BPS}} = \prod_{0 < r \le s < m+n} M^{\wedge} \left(\prod_{i=r}^{s} Q_i, x; B_{r,\dots,s} \right)^{(-1)^{\frac{\sigma_r - \sigma_{s+1}}{2}}} \tag{F.2.5}$$

based on the chamber, where $B_{r,\dots,s} := [B(\alpha_r + \cdots + \alpha_s)]$, which labels the chamber, is the integer part of the value of the B-field through the 2-cycle $\boldsymbol{\beta} = \alpha_r + \cdots + \alpha_s$.

The remarkable result in [286] says that $[B]$ are not completely independent and can be determined by the map $\theta : \frac{1}{2}\mathbb{Z}_{\text{odd}} \to \frac{1}{2}\mathbb{Z}_{\text{odd}}$ such that $\theta(h + m + n) = \theta(h) + m + n$ for any half-integer h and $\sum_{i=1}^{m+n} \theta(i - \frac{1}{2}) = \sum_{i=1}^{m+n} (i - \frac{1}{2})$. If $\theta(1/2) < \theta(3/2) < \cdots < \theta(m + n - 1/2)$, then

$$[B_\theta(\alpha_r + \cdots + \alpha_s)] = \#\{k \in \mathbb{Z} | \theta(r - 1/2) < k(m + n) < \theta(s + 1/2)\}. \tag{F.2.6}$$

If θ is not increasing, then we can choose a permutation $\tau \in \mathfrak{S}_{m+n}$ such that $\theta(\tau(1/2)) < \theta(\tau(3/2)) < \cdots < \theta(\tau(m + n + 1/2))$ and replace θ by $\theta \circ \tau$. For instance, in the SPP example in Figure F.1.1, if $\theta(1/2) = 11/2, \theta(3/2) = 3/2, \theta(5/2) = -5/2$, then $[B_{\theta\circ\tau}(\alpha_1)] = [B_{\theta\circ\tau}(\alpha_2)] = 1, [B_{\theta\circ\tau}(\alpha_1 + \alpha_2)] = 2$ where $\tau = (132)$. This specifies the truncations of MacMahon functions in (F.2.4) and (F.2.5). Notice that $\theta(1/2) = -5/2, \theta(3/2) = 3/2, \theta(5/2) = 11/2$ gives $[B_\theta]$ of the same values, but generically they parametrize different chambers [286].

It is also straightforward to write Z_{BPS} in different chambers using PE. This simply follows from

$$M_{\wedge}(p, q; k_0) = \text{PE}\left[\sum_{k=k_0}^{\infty} kpq^k \right], \quad M^{\wedge}(p, q; k_0) = \text{PE}\left[\sum_{k=1}^{k_0} kpq^k \right], \tag{F.2.7}$$

along with $\text{PE}[f]\text{PE}[g] = \text{PE}[f + g]$ and $\text{PE}[f]^{-1} = \text{PE}[-f]$.

F.2.1 Refined Partition Functions

For any chamber $\mathbb{C}$, the refined BPS index/(protected) spin character is $\Omega(n_0, \boldsymbol{n_2}; \mathtt{y}; \mathbb{C}) = \text{Tr}_{\mathcal{H}_{n_0, \boldsymbol{n_2}}(\mathbb{C})}(-\mathtt{y})^{J_3}$, where $\mathcal{H}$ is the (reduced) Hilbert space of BPS states and $\mathtt{y}$ tracks the spin information J_3. In the limit $\mathtt{y} \to 1$, one recovers the unrefined index. In the following, it would be more convenient to take $t_1 = q\mathtt{y}$ and $t_2 = q/\mathtt{y}$.

It is fairly straightforward to refine the partition functions discussed above:

$$Z_{\text{BPS}} = M_R(t_1, t_2)^{m+n} \prod_{0 < r \le s < m+n} \widetilde{M}_R \left(\prod_{i=r}^{s} Q_i; t_1, t_2 \right)^{(-1)^{\frac{\sigma_r - \sigma_{s+1}}{2}}} \tag{F.2.8}$$

for the generalized conifold $xy = z^m w^n$ [328, 329] and

$$Z_{\text{BPS}} = M_R(t_1, t_2)^4 \prod_{I \in \mathcal{P}\{1,2,3\}} \widetilde{M}_R \left(\prod_{i \in I} Q_i; t_1, t_2 \right)^{(-1)^{|I|}} \tag{F.2.9}$$

for $\mathbb{C}^3/(\mathbb{Z}_2 \times \mathbb{Z}_2)$ where $\mathcal{P}\{1, 2, 3\}$ is the power set of $\{1, 2, 3\}$. Here,

$$M_R(p; t_1, t_2) = \prod_{k,l=0}^{\infty} \frac{1}{1 - pt_1^{k+1}t_2^l} = \text{PE}\left[\frac{pt_1}{(1 - t_1)(1 - t_2)} \right], \tag{F.2.10}$$

$$M_R(t_1, t_2) = M_R(1; t_1, t_2), \quad \widetilde{M}_R(p; t_1, t_2) = M_R(p; t_1, t_2)M_R(p^{-1}; t_1, t_2)$$

are the refined (generalized) MacMahon functions. In terms of PE, we have $Z_{\text{BPS}} = \text{PE}[g]$, where

$$g = \frac{t_1 \left(m + n + \sum_{0 < r \le s < m+n} (-1)^{\frac{\sigma_r - \sigma_{s+1}}{2}} \left(\prod_{i=r}^{s} Q_i + \prod_{i=r}^{s} Q_i^{-1} \right) \right)}{(1 - t_1)(1 - t_2)} \tag{F.2.11}$$

for the generalized conifold and

$$g = \frac{t_1 \left(4 + \sum\limits_{I \in \mathcal{P}\{1,2,3\}} (-1)^{|I|} \left(\prod\limits_{i \in I} Q_i + \prod\limits_{i \in I} Q_i^{-1} \right) \right)}{(1 - t_1)(1 - t_2)} \tag{F.2.12}$$

for $\mathbb{C}^3/(\mathbb{Z}_2 \times \mathbb{Z}_2)$.

Recall that in the unrefined case, one would obtain/lose a factor of $\left(1 - x^N \mathtt{Q}^{\pm 1} \right)^{\pm N}$ when crossing a wall of marginal stability, where $\mathtt{Q} = \left(\prod\limits_{i \in J} Q_i \right)$ for a set J of indices whose combination would appear in Z_{NCDT}. Likewise, in the refinement, one would obtain/lose a factor of $\left(\prod\limits_{k+l+1=N} (1 - t_1^{k+1} t_2^l \mathtt{Q}^{\pm 1}) \right)^{\pm 1}$ every time we cross a wall[17].

We can also directly compare the refined partition functions with the previous discussions on Kac polynomials and Poincaré polynomials. Indeed, the refined $\mathbb{C}^3$ partition function is $M_R(t_1, t_2)$, which is exactly (F.1.5) under the change of variables $x = t_1$ and $t^{-1} = t_2$. One may also check that the results for all the affine ADE quiver cases still hold. The partition function is

$$\chi_r = \mathrm{PE} \left[\frac{t_1}{(1 - t_1)(1 - t_2)} \left(r + \sum_{\boldsymbol{\alpha} \in \Psi} \boldsymbol{Q}^{\boldsymbol{\alpha}} \right) \right]. \tag{F.2.13}$$

This is precisely a factor of $P_Q^0(t, \boldsymbol{q}) \widetilde{P}_Q^0(t, \boldsymbol{q})$ under $x = \boldsymbol{q}^{\boldsymbol{\delta}} = t_1$, $t^{-1} = t_2$ and $q_i = Q_i$.

A comment of D4-D2-D0 bound states Based on [152, 330–333], it would be straightforward to write the generating functions for certain D4-D2-D0 brane bound states similar to the above discussions. Mathematically, they are related to curve counting on surfaces in the CY 3-fold [289, 334].

As argued in [152], the D4-D2-D0 bound states can be enumerated by 2-dimensional crystals as opposed to the 3d crystals for D6-D2-D0 bound states. As a result, they should be counted via 2d Young tableaux instead of 3d plane partitions. Indeed, it turns that the (generalized) MacMahon functions should be replaced by the inverse (generalized) Euler functions $\phi(x, q)^{-1}$ counting integer partitions. See [12, §5] for more details.

---

[17]It is conjectured that there does not exist walls invisible to unrefined indices such that only refined indices would jump [45].

Appendix G

Examples of $\mathcal{R}$-Matrices Acting on Higher Levels

Here, we shall consider some examples at higher levels using the contour integral expressions for the matrix elements of $\mathcal{T}$.

G.0.1 Example 1: Conifold

Let us first consider the conifold whose 2d crystal description can be found in [152, Figure 29 and 30]. In particular, there is one atom of colour a (or $b \neq a$) at the first level and only one atom of colour b (or a) can be added at the second level. Following the $\mathcal{R}\mathcal{T}\mathcal{T}$ relation, we can write

$$\langle \mathfrak{C}_{(a)}, \varnothing_{(c)} | \mathcal{R}_{12}(u-v)\mathcal{T}_1(u)\mathcal{T}_2(v)|\varnothing_{(a)}, \varnothing_{(c)}\rangle = \langle \mathfrak{C}_{(a)}, \varnothing_{(c)} | \mathcal{T}_2(v)\mathcal{T}_1(u)\mathcal{R}_{12}(u-v)|\varnothing_{(a)}, \varnothing_{(c)}\rangle, \quad \text{(G.0.1)}$$

where c is either a or b and $\mathfrak{C}_{(a)}$ here stands for the 2d crystal with two atoms whose initial atom is of colour a. Based on the first part of contour integral conjecture (§5.3.2), the right hand side is then

$$\mathcal{T}_{\varnothing_{(c)}, \varnothing_{(c)}}(v)\mathcal{T}_{\mathfrak{C}_{(a)}, \varnothing_{(a)}} = \frac{1}{2\pi i} \oint_{\infty+u} \mathrm{d}z F(z)h^{(c)}(v)f^{(b)}(z)f^{(a)}(u)h^{(a)}(u), \quad \text{(G.0.2)}$$

where we have used the fact that $\mathcal{T}_{\square_{(a)}, \varnothing_{(a)}}(u) = f^{(a)}(u)h^{(a)}(u)$. Suppose $a = c \neq b$. After applying the current relations, we have

$$\langle \mathfrak{C}_{(a)}, \varnothing_{(a)} | \mathcal{R}_{12}\mathcal{T}_1\mathcal{T}_2|\varnothing_{(a)}, \varnothing_{(a)}\rangle = \left(\frac{v-u-\epsilon_3}{v-u} - \epsilon_3^2\right) \frac{1}{2\pi i} \oint_{\infty+u} \mathrm{d}z F(z)f^{(b)}(z)f^{(a)}(u)h^{(a)}(u)h^{(a)}(v)$$
$$+ \frac{(u-v)\epsilon_3}{u-v-\epsilon_3} \frac{1}{2\pi i} \oint_{\infty+u} \mathrm{d}z F(z)f^{(b)}(z)h^{(a)}(u)f^{(a)}(v)h^{(a)}(v). \quad \text{(G.0.3)}$$

The first term clearly leads to a bra vector $\langle \mathfrak{C}_{(a)}, \varnothing_{(a)}|$. For the second term, suppose the contour integral gives

$$\oint_{\infty+u} \mathrm{d}z F(z)f^{(b)}(z) = P(u)f^{(b)}(u) + \sum_j Q_j(u)f_j^{(b)}, \quad \text{(G.0.4)}$$

where $P(u)$ comes from $-\mathrm{Res}_u(F(z)f^{(b)}(z)) = P(u)f^{(b)}(u) + \dots$ with the ellipsis denoting terms only with modes of $f^{(b)}$ (if $F(z)$ has a higher order pole at $z = u$). The terms with $Q_j(u)$ then include both such terms and those from the residue at infinity. Thus, using the hf relation and writing the modes as contour integrals of the current, the second term in (G.0.3) becomes

$$\frac{(u-v)\epsilon_3}{u-v-\epsilon_3} h^{(a)}(u)P(u)\left(f^{(b)}(v) + \frac{1}{P(u)}\sum_j Q_j(u)f_j^{(b)}\right)f^{(a)}(v)h^{(a)}(v). \quad \text{(G.0.5)}$$

However, since this must become some matrix element(s) composed of allowed states/2d molten crystal configurations (with levels no greater than 2), we propose that $Q_j(u)$ must vanish or equal $P(u)$. Therefore,

$$\frac{(u-v)\epsilon_3}{u-v-\epsilon_3}\frac{1}{2\pi i}\oint_{\infty+v}\mathrm{d}zF(z)\frac{P(u)}{P(v)}h^{(a)}(u)f^{(b)}(z)f^{(a)}(v)h^{(a)}(v). \tag{G.0.6}$$

Hence, we get

$$\langle\mathfrak{C}_{(a)},\varnothing_{(a)}|\mathcal{R}_{12}=\langle\mathfrak{C}_{(a)},\varnothing_{(a)}|\left(\frac{v-u-\epsilon_3}{v-u}-\epsilon_3^2\right)+\langle\varnothing_{(a)},\mathfrak{C}_{(a)}|\frac{(u-v)\epsilon_3 P(u)}{(u-v-\epsilon_3)P(v)}. \tag{G.0.7}$$

Now let us consider the case $b=c\neq a$. Then (G.0.2) becomes

$$\frac{1}{2\pi i}\oint_{\infty+u}\mathrm{d}zF(z)\frac{v-z-\epsilon_3}{v-z}f^{(b)}(z)f^{(a)}(u)h^{(a)}(u)h^{(b)}(v). \tag{G.0.8}$$

The residue of the contour integral would be

$$P(u)\frac{v-u-\epsilon_3}{v-u}f^{(b)}(u)+\sum_j Q'_j(u)f_j^{(b)}. \tag{G.0.9}$$

Therefore, $Q'_j(u)$ should be equal to either $P(u)(v-u-\epsilon_3)/(v-u)$ or 0. As a result,

$$\langle\mathfrak{C}_{(a)},\varnothing_{(b)}|\mathcal{R}_{12}=\langle\mathfrak{C}_{(a)},\varnothing_{(b)}|\frac{v-u-\epsilon_3}{v-u}P(u). \tag{G.0.10}$$

As the two-atom configuration is $e_0^{(b)}e_0^{(a)}|\varnothing_{(a)}\rangle$ (and $\langle\varnothing_{(a)}|f_0^{(a)}f_0^{(b)}$) for $a\neq b$, we can use the second part of the contour integral conjecture (§5.4) to write[1]

$$\begin{aligned}\langle\varnothing_{(a)}|f_0^{(a)}f_0^{(b)}\mathcal{T}|\varnothing_{(a)}\rangle&=\frac{1}{2\pi i}\oint_{\infty+u}\mathrm{d}z\frac{1}{\epsilon_3}\left(1-\frac{u-z-\epsilon_3}{u-z}\frac{(u-z-\epsilon_2)(u-z+\epsilon_2)}{(u-z-\epsilon_1)(u-z+\epsilon_1)}\right)f^{(b)}(z)f^{(a)}(u)h^{(a)}(u)\\&=-\frac{\epsilon_2^2}{\epsilon_1^2}f^{(b)}(u)f^{(a)}(u)h^{(a)}(u).\end{aligned} \tag{G.0.11}$$

Therefore, $P(u)=\epsilon_2^2/\epsilon_1^2$ (and indeed Q_j, Q'_j vanish). Hence,

$$\langle\mathfrak{C}_{(a)},\varnothing_{(b)}|\mathcal{R}_{12}=\begin{cases}\langle\mathfrak{C}_{(a)},\varnothing_{(a)}|\left(\frac{u-v+\epsilon_3}{u-v}-\epsilon_3^2\right)+\langle\varnothing_{(a)},\mathfrak{C}_{(a)}|\frac{(u-v)\epsilon_3}{(u-v-\epsilon_3)},&a=b\\\langle\mathfrak{C}_{(a)},\varnothing_{(b)}|\frac{\epsilon_2^2}{\epsilon_1^2}\frac{u-v+\epsilon_3}{u-v},&a\neq b.\end{cases} \tag{G.0.12}$$

G.0.2   Example 2: $\mathbb{C}\times\mathbb{C}^2/\mathbb{Z}_3$

Now, let us discuss $\mathbb{C}\times\mathbb{C}^2/\mathbb{Z}_3$ with the specific state, say, $e_1^{(2)}e_0^{(3)}e_0^{(1)}|\varnothing_{(1)}\rangle$. At level 1, we simply have $\mathcal{T}_{\varnothing_{(1)},\square_{(1)}}=h^{(1)}(u)e^{(1)}(u)$. At level 2, we have

$$\begin{aligned}\langle\varnothing_{(1)}|\mathcal{T}e_0^{(3)}e_0^{(1)}|\varnothing_{(1)}\rangle&=\frac{1}{2\pi i}\oint_{\infty+u}\mathrm{d}z\frac{1}{\epsilon_3}\left(1-\frac{u-z-\epsilon_3}{u-z}\frac{u-z-\epsilon_1}{u-z+\epsilon_2}\right)h^{(1)}(u)e^{(1)}(u)e^{(3)}(z)\\&=-\frac{\epsilon_1}{\epsilon_2}h^{(1)}(u)e^{(1)}(u)e^{(3)}(u).\end{aligned} \tag{G.0.13}$$

Then at level 3, recall that

$$e_1^{(2)}=\frac{1}{2\epsilon_3}\left[\psi_1^{(2)}-\frac{1}{2}\left(\psi_0^{(2)}\right)^2,e_0^{(2)}\right] \tag{G.0.14}$$

---

[1]Notice that here the convention of f is the one for YB instead of Y.

following the results in §5.4. Therefore,

$$e_1^{(2)}e_0^{(3)}e_0^{(1)}|\varnothing_{(1)}\rangle = \frac{1}{2\epsilon_3}\left(\psi_1^{(2)}e_0^{(2)} - \frac{1}{2}\psi_0^{(2)}\psi_0^{(2)}e_0^{(2)} - e_0^{(2)}\psi_1^{(2)} + \frac{1}{2}e_0^{(2)}\psi_0^{(2)}\psi_0^{(2)}\right)e_0^{(3)}e_0^{(1)}|\varnothing_{(1)}\rangle.$$
(G.0.15)

By considering the action of the current $\psi^{(2)}(z)$ and taking the contour integral around ∞, we get

$$\psi_0^{(2)}e_0^{(3)}e_0^{(1)}|\varnothing_{(1)}\rangle = (4u - 2\epsilon_3)\,e_0^{(3)}e_0^{(1)}|\varnothing_{(1)}\rangle, \quad \psi_0^{(2)}e_0^{(2)}e_0^{(3)}e_0^{(1)}|\varnothing_{(1)}\rangle = 6u e_0^{(2)}e_0^{(3)}e_0^{(1)}|\varnothing_{(1)}\rangle,$$
$$\psi_1^{(2)}e_0^{(3)}e_0^{(1)}|\varnothing_{(1)}\rangle = \left(8u^2 - 8\epsilon_3 u + \epsilon_3^2\right)e_0^{(3)}e_0^{(1)}|\varnothing_{(1)}\rangle, \quad \psi_1^{(2)}e_0^{(2)}e_0^{(3)}e_0^{(1)}|\varnothing_{(1)}\rangle = 18u^2 e_0^{(2)}e_0^{(3)}e_0^{(1)}|\varnothing_{(1)}\rangle.$$
(G.0.16)

Moreover,

$$\langle\varnothing_{(1)}|\mathcal{T}e_0^{(2)}e_0^{(3)}e_0^{(1)}|\varnothing_{(1)}\rangle$$
$$= \frac{1}{2\pi i}\oint_{\infty+u}dz\frac{-\epsilon_1}{\epsilon_2\epsilon_3}\left(1 - \frac{u-z-\epsilon_3}{u-z}\frac{u-z-\epsilon_1}{u-z+\epsilon_2}\frac{u-z-\epsilon_2}{u-z+\epsilon_1}\right)h^{(1)}(u)e^{(1)}(u)e^{(3)}(u)e^{(2)}(z)$$
(G.0.17)
$$= -\frac{\epsilon_1}{\epsilon_2}h^{(1)}(u)e^{(1)}(u)e^{(3)}(u)e^{(2)}(u).$$

Hence,

$$\langle\varnothing_{(1)}|\mathcal{T}(u)e_1^{(2)}e_0^{(3)}e_0^{(1)}|\varnothing_{(1)}\rangle = -\frac{\epsilon_1\epsilon_3}{2\epsilon_2}h^{(1)}(u)e^{(1)}(u)e^{(3)}(u)e^{(2)}(u).$$
(G.0.18)

One can then obtain, for example, $\mathcal{R}_{12}(u-v)\left(e_1^{(2)}e_0^{(3)}e_0^{(1)}|\varnothing_{(1)}\rangle\right)\otimes|\varnothing_{(a)}\rangle$ using the $\mathcal{R}\mathcal{T}\mathcal{T}$ relation and the relations among the currents.

Appendix H

Rectangular $\mathcal{W}$-Algebras

In literature, the rectangular $\mathcal{W}$-algebra (of type A) is often defined based on the distinguished case for the Kac-Moody superalgebra where the number of fermionic nodes is minimized. Nevertheless, we can certainly consider $\mathcal{W}$-algebras with any underlying root systems/Dynkin diagrams as we are going to discuss now. Proposition 5.7.2 then ensures that they are isomorphic for a given generalized conifold.

In this appendix only, we will use $\mathfrak{g}$ to denote the algebra $\mathfrak{gl}(Ml|Nl)$ for some positive integer l. We shall choose the convention such that the basis matrix E_{ij} has entry $(-1)^{p(j)}$ at position (i,j) with all other elements being zero[1]. Notice that we have used

$$p(i) = \begin{cases} 0, & i \text{ is bosonic} \\ 1, & i \text{ is fermionic} \end{cases} \tag{H.0.1}$$

so as to distinguish it from $|a|$ in the quiver Yangians. Given a parity sequence ς composed of $(-1)^{p(i)}$, the $\mathbb{Z}_2$-grading of E_{ij} is $p(i) + p(j)$. In particular, $E_{i_1 j_1} E_{i_2 j_2} = (-1)^{p(j_1)} \delta_{j_1 i_2} E_{i_1 j_2}$ and $\mathrm{str}(E_{i_1 j_1} E_{i_2 j_2}) = (-1)^{p(j_1)} \delta_{j_1 i_2} \delta_{i_1 j_2}$. Then

$$\mathfrak{g} = \bigoplus_{\substack{1 \le i,j \le M+N \\ 1 \le r,s \le l}} \mathbb{C} E_{(r-1)(M+N)+i,(s-1)(M+N)+j}, \tag{H.0.2}$$

and $E_{(r-1)(M+N)+i,(s-1)(M+N)+j} = E_{ij} \otimes E_{rs}$ as $\mathfrak{g}$ is isomorphic to $\mathfrak{gl}(M|N) \otimes \mathfrak{gl}(l)$ as a vector space[2]. We shall take the bosonic nilpotent matrix $x^- = \sum_{s=1}^{l-1} \sum_{i=1}^{M+N} E_{s(M+N)+i,(s-1)(M+N)+i}$ which can be written as $\left(\sum_{i=1}^{M+N} E_{ii} \right) \otimes \left(\sum_{s=1}^{l-1} E_{s,s-1} \right)$. This nilpotent matrix is of Jordan type with the rectangle Young tableau $\left(l^{(M|N)} \right)$ (and hence the name rectangular $\mathcal{W}$-algebra). Given a complex number k, there is an inner product of $\mathfrak{g}$ given by

$$(u|v) = \begin{cases} k\mathrm{str}(uv), & u \in \mathfrak{sl}(Ml|Nl) \text{ or } v \in \mathfrak{sl}(Ml|Nl) \\ k\mathrm{str}(uv) + (-1)^{p(i)+p(j)}(1-c), & u = E_{ii} \otimes E_{rr} \text{ and } v = E_{jj} \otimes E_{ss} \end{cases} \tag{H.0.3}$$

for some $c \in \mathbb{C}$.

Now, $\mathfrak{g}$ has a good grading in the sense of [76] for the nilpotent element with

$$\mathfrak{g}_r := \bigoplus_{\substack{1 \le i,j \le M+N \\ 0 \le s \le l-1 \\ 0 \le s+r \le l-1}} \mathbb{C} E_{s(M+N)+i,(s+r)(M+N)+j}. \tag{H.0.4}$$

---

[1]Another convention often adopted in literature would naturally be 1 at entry (i,j).
[2]Notice that the $\mathfrak{gl}(l)$ part (with subscripts r, s) is always bosonic.

We then have an $\mathfrak{sl}_2$ triple (h, x^+, x^-) such that $\mathfrak{g}_r = \{y \in \mathfrak{g} | [h, y] = ry\}$. Define the subalgebras $\mathfrak{b} = \mathfrak{g}_{\leq 0} = \bigoplus_{r \leq 0} \mathfrak{g}_r$ and $\mathfrak{g}_0 = \mathfrak{g}_{r=0}$. We have an inner product on $\mathfrak{b}$ which reads

$$\kappa(u, v) = (u|v) + \frac{1}{2}(\kappa_{\mathfrak{g}}(u, v) - \kappa_{\mathfrak{g}_0}(\mathrm{pr}(u), \mathrm{pr}(v))) \tag{H.0.5}$$

for any $u, v \in \mathfrak{b}$, where $\kappa_{\mathfrak{g}}$ (resp. $\kappa_{\mathfrak{g}_0}$) is the Killing form on $\mathfrak{g}$ (resp. $\mathfrak{g}_0$) and $\mathrm{pr} : \mathfrak{b} \to \mathfrak{g}_0$ is the projection map. Recall that in general, the Killing form is $\kappa_{\mathfrak{gl}(M|N)}(x, y) = 2(M - N)\mathrm{str}(xy) - 2\mathrm{str}(x)\mathrm{str}(y)$. Then

$$\kappa(E_{r_1(M+N)+i_1, s_1(M+N)+j_1}, E_{r_2(M+N)+i_2, s_2(M+N)+j_2})$$
$$= \delta_{r_1, s_2}\delta_{r_2, s_1}\delta_{i_1, j_2}\delta_{i_2, j_1}(-1)^{p(j)}\varkappa + \delta_{r_1, s_1}\delta_{r_2, s_2}\delta_{i_1, j_1}\delta_{i_2, j_2}(\delta_{r_1, r_2} - c), \tag{H.0.6}$$

where $\varkappa := k + (l - 1)(M - N)$. Consider the affinization $\hat{\mathfrak{b}} = \mathfrak{b}[t^{\pm 1}] \oplus \mathbb{C}\mathbf{1}$ (with $\mathbf{1}$ central). The commutation relation reads $[at^m, bt^n] = [a, b]t^{m+n} + \delta_{m, -n}m\kappa(a, b)\mathbf{1}$. The associated (universal affine) vertex algebra $V^k(\mathfrak{b})$ is defined to be $U(\hat{\mathfrak{b}})/U(\hat{\mathfrak{b}})(\mathfrak{b}[t] \oplus \mathbb{C}(\mathbf{1} - 1)) \cong U(\hat{\mathfrak{b}}) \otimes_{U(\mathfrak{b}[t] \oplus \mathbb{C}\mathbf{1})} \mathbb{C}$. Here, $\mathbb{C}$ denotes the one-dimensional representation of $\mathfrak{b}[t] \oplus \mathbb{C}\mathbf{1}$ where $\mathfrak{b}[t]$ acts trivially as 0 and $\mathbf{1}$ acts as 1. This is isomorphic to $U(\mathfrak{b}[t^{-1}]t^{-1})$ as a vector space by PBW theorem. Here, we shall take the mode expansion of a current $a(z)$ in the vertex algebra depending on its spin s:

$$a(z) = \sum_{n \in \mathbb{Z}} \frac{a[n]}{z^{n+s}}, \tag{H.0.7}$$

where we have denoted at^n as $a[n]$ to avoid potential clutter of subscripts later on. In this paper, we use the normal ordered product with the convention[3]

$$: a(z)b(z) : = a(z)_{\leq}b(z) + (-1)^{p(a)+p(b)}b(z)a(z)_{>},$$
$$\text{where } a(z)_{\leq} = \sum_{n \leq -s} \frac{a[n]}{z^{n+s}} \text{ and } a(z)_{>} = \sum_{n > -s} \frac{a[n]}{z^{n+s}}. \tag{H.0.8}$$

In terms of modes, we have

$$: a[n]b[m] : = \begin{cases} a[n]b[m], & n \leq -s \\ (-1)^{p(a)+p(b)}b[m]a[n], & n > -s. \end{cases} \tag{H.0.9}$$

In the main context and below, we shall use (ab) instead of $:ab:$ to denote the normal ordering for convenience when it would not cause confusions. Of course, different conventions of the normal ordered product would not change our results in §5.7. For instance, if we "split" the normal ordering at the zero modes, one may check that the homomorphism Φ from $\mathtt{Y}$ to $\mathcal{W}$ would remain the same.

Let us also consider the Lie superalgebra $\mathfrak{a} = \left(\bigoplus_{u \in \mathfrak{b}} \mathbb{C}\mathcal{A}^{(u)}\right) \oplus \left(\bigoplus_{u \in \mathfrak{g}_{<0}} \mathbb{C}\mathcal{A}_{(u)}\right)$ with $p(\mathcal{A}^{(u)}) = p(u)$ and $p(\mathcal{A}_{(u)}) = p(u) + 1$. The commutation relations are

$$\left[\mathcal{A}^{(u)}, \mathcal{A}^{(v)}\right\} = \mathcal{A}^{([u, v])}, \quad \left[\mathcal{A}_{(u)}, \mathcal{A}_{(v)}\right\} = 0,$$
$$\left[\mathcal{A}^{(E_{i_1 j_1})}, \mathcal{A}_{(E_{i_2 j_2})}\right\} = \delta_{j_1, i_1}\mathcal{A}_{(E_{i_1, j_2})} - \delta_{i_1, j_2}(-1)^{(p(i_1)+p(j_1))(p(i_2)+p(j_2)+1)}\mathcal{A}_{(E_{i_2, j_1})}. \tag{H.0.10}$$

---

[3]One can also define the n-product given by

$$(a_{(n)}b)(z) = a(z)_{(n)}b(z) = \begin{cases} \mathrm{Res}_w(w - z)^n[a(w), b(z)], & n \geq 0 \\ \frac{1}{(n+1)!} : \partial^{n+1}a(z)b(z) :, & n < 0, \end{cases}$$

as well as the λ-bracket $[a_\lambda b] = \sum_{n \in \mathbb{Z}_+} \frac{\lambda^n}{n!} a_{(n)}b$ which enjoys certain properties such as the noncommutative Wick formula. See for example [335] for more details. The pair of fields is local if $(a_{(n)}b)(z)$ vanishes for sufficiently large (positive) n. It is clear that the (-1)-product coincides with the normal ordered product.

Suppose $u = \sum_i a_i u_i$ $(a_i \in \mathbb{C})$, then $\mathcal{A}^{(u)}$ is $\sum_i a_i \mathcal{A}^{(u_i)}$ (and similarly for $\mathcal{A}_{(u)}$). We can write the inner product determined by

$$\kappa_{\mathfrak{a}}\left(\mathcal{A}^{(u)}, \mathcal{A}^{(v)}\right) = \kappa_{\mathfrak{b}}(u, v), \quad \kappa_{\mathfrak{a}}\left(\mathcal{A}^{(u)}, \mathcal{A}_{(v)}\right) = \kappa_{\mathfrak{a}}\left(\mathcal{A}_{(u)}, \mathcal{A}_{(v)}\right) = 0, \tag{H.0.11}$$

and likewise consider the affinization of $\mathfrak{a}$. Then the associated vertex algebra $V^k(\mathfrak{a})$ contains $V^k(\mathfrak{b})$ as a subalgebra. Both of the vertex algebras can be regarded as non-associative algebras with respect to the normal ordered product.

The $\mathcal{W}$-algebra is then the collection of elements in $V^k(\mathfrak{b})$ that are annihilated by the BRST charge. More specifically, the BRST cohomology has fermionic derivation $Q : V^k(\mathfrak{a}) \to V^k(\mathfrak{a})$ commuting with the translation operator ∂ of the vertex algebra. The other commutation relations Q should satisfy can be found for example in [336, §3] and in [224, §3] (with the convention therein).

Definition H.0.1. *Given the above data, the rectangular $\mathcal{W}$-algebra is $\mathcal{W}^k\left(\mathfrak{gl}(M|N), \left(l^{(M|N)}\right)\right) :=$* $\{v \in V^k(\mathfrak{b}) \subset V^k(\mathfrak{a}) | Qv = 0\}$.

Notice that we have omitted the parity sequence ς in the notation as different ς give isomorphic $\mathcal{W}$-algberas by Proposition 5.7.2. For our discussions, it would be of great help to obtain the generators of the $\mathcal{W}$-algebra. This can be constructed by considering the non-associative free algebra $T\left(\mathfrak{gl}(l)_{\leq 0}\left[t^{-1}\right]t^{-1}\right) \otimes \mathbb{C}[\tau]$ with the even element τ commuting with $\mathbf{1}$ and $[\tau, y[m]] = -my[m-1]$ for $y \in \mathfrak{gl}(l)_{\leq 0}$. We then have an algebra homomorphism $\mathfrak{T} : T\left(\mathfrak{gl}(l)_{\leq 0}\left[t^{-1}\right]t^{-1}\right) \otimes \mathbb{C}[\tau] \to$ $\mathfrak{gl}(M|N) \otimes V^k(\mathfrak{b}) \otimes \mathbb{C}[\tau]$ such that

$$\mathfrak{T}(x) = \sum_{i,j=1}^{M+N} (-1)^{p(i)p(j)} E_{ij} \otimes \mathfrak{T}_{ij}(x), \quad \mathfrak{T}(\tau) = \tau, \tag{H.0.12}$$

where

$$\mathfrak{T}_{ij}(x) = x \otimes E_{ji} \in \mathfrak{gl}(l)_{\leq 0}\left[t^{-1}\right]t^{-1} \otimes \mathfrak{gl}(M|N) = \mathfrak{b}\left[t^{-1}\right]t^{-1}. \tag{H.0.13}$$

Since $\mathfrak{T}(xy) = \mathfrak{T}(x)\mathfrak{T}(y)$, we find that

$$\mathfrak{T}_{ij}(xy) = \sum_{r=1}^{M+N} \mathfrak{T}_{ir}(x)\mathfrak{T}_{rj}(y). \tag{H.0.14}$$

Let us now consider the $l \times l$ matrix

$$B = \begin{pmatrix} \varkappa\tau + E_{11}[-1] & -1 & 0 & \dots & 0 \\ E_{21}[-1] & \varkappa\tau + E_{22}[-1] & -1 & \dots & 0 \\ \vdots & \vdots & \ddots & \vdots & \vdots \\ E_{l-1,1}[-1] & E_{l-1,2}[-1] & \dots & \varkappa\tau + E_{l-1,l-1}[-1] & -1 \\ E_{l1}[-1] & E_{l2}[-1] & \dots & E_{l,l-1}[-1] & \varkappa\tau + E_{ll}[-1] \end{pmatrix} \tag{H.0.15}$$

and compute its column determinant

$$\mathrm{cdet}(B) = \sum_{\sigma \in \mathfrak{S}_l} \mathrm{sgn}\sigma \, b_{\sigma(1)1}(b_{\sigma(2)2}(b_{\sigma(3)3} \dots (b_{\sigma(l-1),l-1}b_{\sigma(l),l})\dots)). \tag{H.0.16}$$

As the entries b_{rs} of B are in $T\left(\mathfrak{gl}(l)_{\leq 0}\left[t^{-1}\right]t^{-1}\right) \otimes \mathbb{C}[\tau]$, we can write

$$\mathfrak{T}_{ij}(\mathrm{cdet}(B)) = \sum_{r=0}^{l} \widetilde{U}_{ji}^{(r)}(\varkappa\tau)^{l-r}. \tag{H.0.17}$$

We then have the remarkable results from [224, 336]:

Theorem H.0.1. *The rectangular $\mathcal{W}$-algebra $\mathcal{W}^k\left(\mathfrak{gl}(M|N),\left(l^{(M|N)}\right)\right)$ is freely generated by $\widetilde{U}_{ij}^{(r)}$ for $1 \leq r \leq l$ and $1 \leq i, j \leq M + N$. Moreover, when $M \neq N$, $M + N \geq 2$ (and $\varkappa \neq 0$), it is generated by $\widetilde{U}_{ij}^{(1)}$ and $\widetilde{U}_{ij}^{(2)}$.*

Following [336, 337], the projection $\mathfrak{b} \to \mathfrak{l} = (\mathfrak{gl}_l)_0 \otimes \mathfrak{gl}_{M|N}$ induces an injective algebra homomorphism $\mu : \mathcal{W}^k\left(\mathfrak{gl}(M|N),\left(l^{(M|N)}\right)\right) \to V^k(\mathfrak{l})$ known as the (quantum) Miura transformation. Under the Miura transformation, we have

$$\sum_{r=0}^{l} \mu\left(\widetilde{U}_{ji}^{(r)}\right)(\varkappa\tau)^{l-r} = \mathfrak{T}_{ij}\left((\varkappa\tau + E_{11}[-1])(\varkappa\tau + E_{22}[-1])\ldots(\varkappa\tau + E_{ll}[-1])\right). \quad \text{(H.0.18)}$$

Let us write[4]

$$\mathcal{J}_{ij}^s = -E_{(s-1)(M+N)+i,(s-1)(M+N)+j}[-1], \quad \partial\mathcal{J}_{ij}^s = -E_{(s-1)(M+N)+i,(s-1)(M+N)+j}[-2]. \quad \text{(H.0.19)}$$

This gives the same convention as in [69]. The generators of the $\mathcal{W}$-algebra can be written as

$$U_{ij}^{(1)} = \sum_{1 \leq s \leq l} \mathcal{J}_{ij}^s, \qquad U_{ij}^{(2)} = \varkappa \sum_{1 \leq s \leq l}(s-1)\partial\mathcal{J}_{ij}^s + \sum_{\substack{1 \leq s_1 < s_2 \leq l \\ 1 \leq n \leq M+N}}\left(\mathcal{J}_{in}^{s_1}\mathcal{J}_{nj}^{s_2}\right). \quad \text{(H.0.20)}$$

By definition of the vertex algebra, the OPE of $\mathcal{J}_{ij}^s$ reads

$$\begin{aligned}
\mathcal{J}_{i_1j_1}^{s_1}(z)\mathcal{J}_{i_2j_2}^{s_2}(w) \sim &\frac{\kappa(E_{(s_1-1)(M+N)+i_1,(s_1-1)(M+N)+j_1}, E_{(s_2-1)(M+N)+i_2,(s_1-2)(M+N)+j_2})}{(z-w)^2}\\
&\frac{[E_{(s_1-1)(M+N)+i_1,(s_1-1)(M+N)+j_1}, E_{(s_2-1)(M+N)+i_2,(s_1-2)(M+N)+j_2}][-1](w)}{z-w}\\
= &\frac{\delta_{s_1 s_2}\delta_{j_1 i_2}\delta_{i_1 j_2}(-1)^{(p(j_1))}\varkappa + \delta_{i_1 j_1}\delta_{i_2 j_2}(\delta_{s_1 s_2} - c)}{(z-w)^2}\\
&+ \frac{(-1)^{p(i_1)p(j_1)+p(i_2)p(j_2)+p(j_1)p(i_2)}\delta_{s_1 s_2}\delta_{i_1 j_2}\mathcal{J}_{i_2j_1}^{s_1} - (-1)^{p(j_1)}\delta_{s_1 s_2}\delta_{i_2 j_1}\mathcal{J}_{i_1j_2}^{s_1}}{z-w}.
\end{aligned}$$
$$\text{(H.0.21)}$$

The OPEs for $U_{ij}^{(r)}$ can then be obtained from this, as well as the commutation relations for their modes via

$$\left[U_{i_1j_1}^{(r)}[m], U_{i_2j_2}^{(s)}[n]\right\} = \frac{1}{(2\pi i)^2}\oint_0 \mathrm{d}w \oint_w \mathrm{d}z\, z^{m+r-1}w^{n+s-1}U_{i_1j_1}^{(r)}(z)U_{i_2j_2}^{(s)}(w). \quad \text{(H.0.22)}$$

In this paper, we shall focus on the case when the parameter $c = 0$. The commutation relations used in this paper are listed in Lemma 5.7.1.

To relate the non-associative $\mathcal{W}$-algebra with the quiver Yangian, we shall consider the universal enveloping algebra $U(\mathcal{W})$. In general, for any vertex algebra V, its universal enveloping algebra $U(V)$ is an associative algebra topologically generated by ut^m (or ut^{m+s-1} depending on the convention) for $u \in V$ and $m \in \mathbb{Z}$ which correspond to the modes $u[m]$ in the vertex algebra. Therefore, we shall slightly abuse the notation and write $u[m]$ as well for the elements in $U(V)$. For more details on vertex algebras and their universal enveloping algebras, see for example [338].

---

[4]Notice that we could have also started with $-E_{ij}$ as our basis matrix from the very beginning.

Appendix I

Conventions of Heisenberg Modes

In the main context, we introduced the modes k_r (and l_r) for the $\psi_\pm$ currents. Here, we mention some alternative convention to define these Heisenberg modes. It could be possible that this would be more convenient when considering certain aspects of the algebras such as their representations and the AGT correspondence.

Let us consider the toroidal algebras for non-chiral quivers as an example. The other cases can be redefined in a similar manner. First, we rescale the e, f modes as

$$e_n^{(a)} = \left(\mathsf{q} - \mathsf{q}^{-1}\right)^{1/2} \mathsf{e}_n^{(a)}, \quad f_n^{(a)} = \left(\mathsf{q} - \mathsf{q}^{-1}\right)^{1/2} \mathsf{f}_n^{(a)}, \tag{I.0.1}$$

where we have suggestively written $\mathsf{q} = \exp(\beta h_1) = H_1$. Notice that this does not change the ee and ff relations. Then the $e_0 f_0$ relations (as well as the $e_n f_{-n}$ relations) would become

$$\left[\mathsf{e}_0^{(a)}, \mathsf{f}_0^{(a)}\right\} = \delta_{ab} \frac{\mathsf{q}^{k_0^{(a)}} - \mathsf{q}^{-k_0^{(a)}}}{\mathsf{q} - \mathsf{q}^{-1}} = \delta_{ab} \left[k_0^{(a)}\right]_{\mathsf{q}}. \tag{I.0.2}$$

Here, $[x]_{\mathsf{q}} = \frac{\mathsf{q}^x - \mathsf{q}^{-x}}{\mathsf{q} - \mathsf{q}^{-1}}$ is the standard q-number. On the other hand, the $k_0 e_n$ (resp. $k_0 f_n$) relations remain the same as the ones for $k_0 e_n$ (resp. $k_0 f_n$). As we can see, the relations among the zero modes resemble the ones appeared in quantum groups.

Likewise, we can write

$$\psi_\pm^{(a)}(U) = \psi_{\pm,0}^{(a)} \exp\left(\left(\mathsf{q} - \mathsf{q}^{-1}\right) \sum_{n=0}^{\infty} \mathsf{k}_{\pm n}^{(a)} U^{\mp n}\right) \tag{I.0.3}$$

such that $k_r^{(a)} = \left(\mathsf{q} - \mathsf{q}^{-1}\right) \mathsf{k}_r^{(a)}$. Therefore,

$$\psi_{\pm,n}^{(a)} = \psi_{\pm,0}^{(a)} \sum_{m=1}^{n} \frac{\left(\mathsf{q} - \mathsf{q}^{-1}\right)^m}{m!} \sum_{\substack{r_1,\dots,r_m > 0 \\ r_1 + \cdots + r_m = n}} \mathsf{k}_{\pm r_1}^{(a)} \mathsf{k}_{\pm,r_2}^{(a)} \dots \mathsf{k}_{\pm,r_m}^{(a)}. \tag{I.0.4}$$

The commutation relations involving $\mathsf{k}_r^{(a)}$ can be obtained with the substitutions

$$H_1^{rA_{ab}} - H_1^{-rA_{ab}} \to [rA_{ab}]_{\mathsf{q}}, \quad C^{-r} - C^r \to \frac{C^{-r} - C^r}{\mathsf{q} - \mathsf{q}^{-1}} = -[rc/h_1]_{\mathsf{q}} \tag{I.0.5}$$

in the relations for $\mathsf{k}_r^{(a)}$.

Sometimes, it is also conventional to define the Heisenberg modes with signs inside the exponentials. In other words, we have $\exp\left(\pm \sum_n k_{\pm n} U^{\mp n}\right)$ in the expressions for $\psi_\pm$. This is simply a redefinition of $k_{-n} \to -k_{-n}$.

Appendix J

Gröbner Bases & Hilbert Series

Since our chiral rings can be realized as quotient rings of polynomial rings over $\mathbb{C}$ by defining ideals arising from the likes of polynomial F-terms, it is important for us to systematically study such objects. The first step toward any serious investigation of an ideal I within a graded ring is the establishment of its Gröbner basis $\mathrm{GB}(I)$; constituting the pillar of computational algebraic geometry [339, 340] (cf. [341] for recent advances and applications in the context of gauge/string theories).

Briefly [339, 342], for the polynomial ring $R = \mathbb{C}[x_1, x_2, \ldots, x_n]$ to any monomial $\vec{x}^{\vec{\alpha}} := x_1^{\alpha_1} x_2^{\alpha_2} \ldots x_n^{\alpha_n}$ with each $\alpha_i \in \mathbb{Z}_{\geq 0}$ (the short-hand notation of raising the exponent is standard) in R, we can associate the exponent vector $\vec{\alpha}$; this defines a monomial ordering $\succ$ such that

1. $\succ$ is a total order on R, i.e., for any elements $\vec{\alpha}, \vec{\beta}$, one and only one of the three possibilities $\vec{\alpha} \succ \vec{\beta}$, or $\vec{\beta} \succ \vec{\alpha}$, or $\vec{\alpha} = \vec{\beta}$ occurs;

2. for any $\vec{\gamma}$, if $\vec{\alpha} \succ \vec{\beta}$, then $\vec{\alpha} + \vec{\gamma} \succ \vec{\beta} + \vec{\gamma}$;

3. $\succ$ is a well-ordering in that any nonempty subset has a smallest element.

Of course, these properties are no more than the axiomatization of how we usually manipulate degrees in monomials. Indeed, we will denote total degree of a monomial as $|\vec{\alpha}| = \sum\limits_{i=1}^{n} \alpha_i$.

We emphasize that there are many possible choices of this ordering and the most typical are

- Lexicographic: this is just dictionary ordering, i.e., $\vec{\alpha} \succ_{\mathrm{Lex}} \vec{\beta}$ if the leftmost nonzero entry of $\vec{\alpha} - \vec{\beta}$ is positive;

- Graded Lexicographic: this is sorting by total degree first and then by lexicographic, i.e., $\vec{\alpha} \succ_{\mathrm{grLex}} \vec{\beta}$ if $|\vec{\alpha}| > |\vec{\beta}|$ or, when $|\vec{\alpha}| = |\vec{\beta}|$, we have $\vec{\alpha} \succ_{\mathrm{Lex}} \vec{\beta}$. There is a reverse version of this where one sorts by total degree first and then if they are equal, then $\vec{\alpha} \succ_{\mathrm{grevLex}} \vec{\beta}$ if the rightmost nonzero entry of $\vec{\alpha} - \vec{\beta}$ is negative;

- General Weighted Lexicographic: We can weight each variable x_i. For example, choose a weight vector $\vec{w} = (w_1, w_2, \ldots, w_n)$ for the variables x_i. Usually, the weight is taken to be $w_i \in \mathbb{Z}_{\geq 0}$. This weight can, for example, be prescribed by the R-charges. Here, the total degree is obviously $|\vec{\alpha}| = w \cdot \vec{\alpha}$.

  In fact, one is not restricted to just weighting each variable by some non-negative integer but in general by some vector, say of length $k \leq n$, so that we have some *weight matrix* $W_{k \times n}$. Then we could sort as: $\vec{\alpha} \succ_W \vec{\beta}$ if $W \cdot \vec{\alpha} \succ_{\mathrm{Lex}} W \cdot \vec{\beta}$. This multi-weighting can be used as a *refinement* of possible charges and variables thus graded are called fugacities [26, 28].

An example, taken from [339], would illustrate the above. Suppose $R = \mathbb{C}[x, y, z]$, and we weight x, y, z with the standard base vectors $(1, 0, 0)$, $(0, 1, 0)$ and $(0, 0, 1)$, then $x \succ_{\mathrm{Lex}} yz^2$ since $(1, 0, 0) - (0, 1, 2)$ has the leftmost entry 1 which is positive. On the other hand, $yz^2 \succ_{\mathrm{grLex}} x$ since the

degrees are $|x| = 1$ and $|yz^2| = 3$; this graded lexicographic ordering is one perhaps most familiar to us.

Having fixed a monomial ordering $\succ$ on R, then we have

Definition J.0.1. *For any multivariate polynomial $f = \sum_{\vec{\alpha}} c_{\vec{\alpha}} \vec{x}^{\vec{\alpha}} \in R$, the* initial monomial $\text{in}(f)$ *is the largest (with respective to $\succ$) monomial term in f. We can always make the coefficient of this term to be 1 so that f is monic.*

Thus prepared, we are finally at the crux of our subject:

Definition J.0.2. *A subset $\{g_1, g_2, \ldots, g_m\}$ for an ideal I is a Gröbner basis $\text{GB}(I)$ for I if the ideal generated by the initial monomials of the elements of I is generated by $\{\text{in}(g_1), \ldots, \text{in}(g_m)\}$, i.e., if*

$$\text{in}(I) = \langle \text{in}(g_i) \rangle.$$

Computationally, we have the important result that

Theorem J.0.1. *A set G is a Gröbner basis iff the S-polynomial (or syzygy pair) defined as*

$$S(g_i, g_j) := \frac{\text{lcm}\big(\text{in}(g_i),\ \text{in}(g_j)\big)}{\text{in}(g_i)} g_i - \frac{\text{lcm}\big(\text{in}(g_i),\ \text{in}(g_j)\big)}{\text{in}(g_j)} g_j$$

reduces modolo G for all *pairs $g_i, g_j \in G$.*

This gives a practical - albeit exponential-running-time - algorithm, the so-called *Buchberger algorithm* for computing $\text{GB}(I)$ given an ideal $I = \langle f_i \rangle_{i=1,\ldots,N}$:

1. Set $G = \{f_1, \ldots, f_N\}$ and compute $S(f_i, f_j)$ for each of the pairs with respect to a chosen ordering $\succ$;

2. Compute the remainder of each $S(f_i, f_j)$ upon division by each of the elements of G. If the remainder is not zero, then include this $S(f_i, f_j)$ as a new element of G;

3. Repeat until all remainders with respect to all elements are 0; this final list (which could have much more than N elements) is a Gröbner basis for I.

J.0.1 Hilbert Series: Revisited

In light of the discussions above, more properties, especially from a computational perspective, of the HS emerge. Most importantly, we have a the classical result of Macaulay [343] that

Theorem J.0.2. *The Hilbert series of $\text{in}(I)$ is the same as that of the ideal I itself.*

Thus explicit computation of the HS reduces to finding the Gröbner basis: given the ideal I, we simply (1) compute its Gröbner basis $\text{GB}(I) = \{g_i\}$ with respect to some monomial ordering; (2) find the initial ideal $\langle \text{in}(g_i) \rangle$ (this is a Gröbner basis guarantees that this ideal is equal to $\text{in}(I)$); (3) importantly each generator $\text{in}(g_i)$ is monomial and we thus only need to compute the basis of monomials modulo these monomials at each degree and sum the generating series to obtain the HS for $\text{in}(I)$, which by the above theorem is then the HS for I.

Moreover, one can *refine* the HS: this means we can assign not just a single weight to the variable t, but, instead, a vector of weights for multi-variables t_i. In other words, the polynomial ring will be multi-graded. For example, for $\mathbb{C}^3$, the (unrefined) HS is $\text{HS}(t; \mathbb{C}^3) = (1 - t)^{-3}$ and the refined series can be, for instantce, $\text{HS}(t_1, t_2, t_3; \mathbb{C}^3) = ((1 - t_1)(1 - t_2)(1 - t_3))^{-1}$.

Appendix K

Genus for Lopsided Amoebae

Using lopsidedness, we can write the conditions for the number of genus for any $\mathcal{LA}_{\tilde{P}_n}$. We now derive such conditions for some lopsided amoebae where $n = 1$.

Example 1: F_0 As one of the simplest examples, let us determine the genus of the lopsided amoeba for F_0 with $P(z, w) = c_1 z + c_2 w + c_3 z^{-1} + c_4 w^{-1} + c_5$ which could have at most one genus corresponding to its sole interior point[1]. Straight away, we can find the centre of the amoeba, which always lie in the hole if $g = 1$. We can find the spectral curve (spines) by considering the asymptotic behaviour as

- $z, w \to \infty, z/w \sim \mathcal{O}(1)$: this yields $\mathrm{Log}|w| = \mathrm{Log}|z| - \mathrm{Log}\left|\frac{c_2}{c_1}\right|$.

- $1/z, 1/w \to \infty, z/w \sim \mathcal{O}(1)$: this yields $\mathrm{Log}|w| = \mathrm{Log}|z| + \mathrm{Log}\left|\frac{c_4}{c_3}\right|$.

- $z, 1/w \to \infty, zw \sim \mathcal{O}(1)$: this yields $\mathrm{Log}|w| = -\mathrm{Log}|z| - \mathrm{Log}\left|\frac{c_1}{c_4}\right|$.

- $1/z, w \to \infty, zw \sim \mathcal{O}(1)$: this yields $\mathrm{Log}|w| = -\mathrm{Log}|z| + \mathrm{Log}\left|\frac{c_3}{c_2}\right|$.

In particular, the first two lines are parallel to each other, and so are the other two. The remaining 4 pairs give rise to 4 intersection points (which may or may not coincide). In other words, we have obtained the equations for the four spines of the amoeba and how they surround a rectangle with these 4 intersection points as vertices. One can check that this rectangle is centred at $\left(\frac{1}{2}\mathrm{Log}\left|\frac{c_3}{c_1}\right|, \frac{1}{2}\mathrm{Log}\left|\frac{c_4}{c_2}\right|\right)$.

In general, to determine the genus, we should find all possibilities for the lopsided lists. Here, using (7.2.1), we have that $P\{x_1, x_2\} = \{|c_1 z|, |c_2 w|, |c_3/z|, |c_4/w|, |c_5|\}$. Suppose $|c_5|$ is the largest number, then we have the lopsided condition:

$$|c_5| > |c_1 z| + |c_2 w| + |c_3/z| + |c_4/w|. \tag{K.0.1}$$

However, the right hand side reaches a minimum when $|c_1 z| = |c_3/z|, |c_2 w| = |c_4/w|$, i.e., $|z| = |c_3/c_1|^{1/2}, |w| = |c_4/c_2|^{1/2}$, which is exactly the aforementioned centre of the amoeba. Therefore, $|c_5|$ should at least be greater than this minimum for genus 1, and this bound is precisely $|c_5| > a := 2|c_1 c_3|^{1/2} + 2|c_2 c_4|^{1/2}$. In other words,

$$g = \begin{cases} 0, & |c_5| \le a \\ 1, & \text{otherwise} \end{cases}. \tag{K.0.2}$$

In particular, the centre point is precisely the point where the right hand side of (K.0.1) reaches its minimum.

---

[1] Here, all the coefficients can be any complex numbers. To avoid degenerate cases, we also require $c_{1,2,3,4} \neq 0$.

For completeness, there are four more possibilities for $P\{x_1, x_2\}$ to be lopsided, but we can see that they would not lead to a non-zero genus by the same argument. For example, suppose the largest is

$$|c_1 z| > |c_2 w| + |c_3/z| + |c_4/w| + |c_5|. \tag{K.0.3}$$

Let us now fix $|w|$, viz, contemplating a horizontal line on the Log plane. If we keep increasing $|z|$ (or equivalently Log$|z|$), this inequality would always hold. Therefore, this region, as a complementary component of the amoeba on the Log plane, would go to infinity. Hence, it is not bounded and cannot be a hole of the amoeba. Likewise, the other three inequalities would not give a hole either by considering the asymptotic behaviour of $|w|$ (or $|z|$) going to infinity or zero while keeping $|z|$ (or $|w|$) fixed. This also verifies that the lopsided amoeba for F_0 can have at most genus 1.

Example 2: $L^{3,3,2}$ Let us now consider $L^{3,3,2}$ as it is a non-reflexive polytopes (see [2]) and hence has more interior points. Its Newton polynomial is $P = c_1 z + c_2 w + c_3 z^{-1} + c_4 w^{-1} + c_5 z^2 + c_6 = 0$. Therefore, $P\{x\} = \{|c_1 z|, |c_2 w|, |c_3/z|, |c_4/w|, |c_5 z^2|, |c_6|\}$. One possibility for these numbers to be lopsided is

$$|c_1 z| > |c_2 w| + |c_3/z| + |c_4/w| + |c_5 z^2| + |c_6|. \tag{K.0.4}$$

As $|z|$ cannot be zero, we can divide both sides by $|z|$ and then find the minimum for the right hand side. For $|w|$, it is easy to see that this requires $|w| = w_0 \equiv (|c_4/c_2|)^{1/2}$. Then for $|z|$, we have the cubic equation

$$|c_5||z|^3 - \left(2|c_2 c_4|^{1/2} + |c_6|\right)|z| - 2|c_3| = 0. \tag{K.0.5}$$

Write

$$p = -\frac{\left(2|c_2 c_4|^{1/2} + |c_6|\right)}{|c_5|}, \quad q = -2\left|\frac{c_3}{c_5}\right|,$$
$$\Delta = \left(\frac{q}{2}\right)^2 + \left(\frac{p}{3}\right)^3 = \left|\frac{c_3}{c_5}\right|^2 - \frac{\left(2|c_2 c_3|^{1/2} + |c_6|\right)^3}{27|c_5|^3}. \tag{K.0.6}$$

Based on the sign of the discriminant, we have three different cases. If $\Delta > 0$, or equivalently, $27\left|c_3^2 c_5\right| > \left(2|c_2 c_4|^{1/2} + |c_6|\right)^3$, then there is only one real root to this equation:

$$z_0 = \sqrt[3]{-\frac{q}{2} + \sqrt{\Delta}} + \sqrt[3]{-\frac{q}{2} - \sqrt{\Delta}}. \tag{K.0.7}$$

Since $q < 0$, z_0 is always positive. If $\Delta = 0$, there are three real roots. Again, due to negative q, we always have a positive root

$$z_0 = -2\sqrt[3]{\frac{q}{2}}. \tag{K.0.8}$$

If $\Delta < 0$, then we would have three distinct roots, $z_{1,2,3}$. Since $z_1 + z_2 + z_3 = 0$, there must be at least one positive root, which we shall still call z_0. Hence, there would be (at least) one hole if

$$|c_1| > a_1 := |c_2|w_0/z_0 + |c_3|/z_0^2 + |c_4|/(z_0 w_0) + |c_5|z_0 + |c_6|/z_0. \tag{K.0.9}$$

It is also possible that these numbers are lopsided as

$$|c_6| > |c_1 z| + |c_2 w| + |c_3/z| + |c_4/w| + |c_5 z^2|. \tag{K.0.10}$$

Likewise, the right hand side reaches its minimum when $|w| = w_0 = (|c_4/c_2|)^{1/2}$ and $|z| = z_0'$ where z_0' is a positive number satisfying[2]

$$2|c_5|z_0'^3 + |c_1|z_0'^2 - |c_3| = 0. \tag{K.0.11}$$

---

[2]One can show that there is always a positive root for this cubic equation. A quick way to see this is to consider the function $y = x^2(2|c_5|x + |c_1|)$, which is a cubic curve tangent to the x-axis at the origin (and always increasing for positive x). It also crosses the negative x-axis once while increasing. Then we can simply move this curve down along the y-axis to get $y = x^2(2|c_5|x + |c_1|) - |c_3|$. Hence, this would always give a positive root. Using this method, one can also check that both z_0 and z_0' give local minima in the two cases.

Then there would be (at least) one hole if

$$|c_6| > a_2 := |c_1|z_0' + |c_2|w_0 + |c_3|/z_0' + |c_4|/w_0 + |c_5|z_0'^2. \tag{K.0.12}$$

One may check that other ways for $P\{x\}$ to be lopsided would lead to unbounded complementary regions. To summarize[3],

$$g = \begin{cases} 0, & |c_1| \le a_1 \text{ and } |c_6| \le a_2 \\ 1, & (|c_1| > a_1 \text{ and } |c_6| \le a_2) \text{ or } (|c_1| \le a_1 \text{ and } |c_6| > a_2) . \\ 2, & |c_1| > a_1 \text{ and } |c_6| > a_2 \end{cases} \tag{K.0.13}$$

The punchline is that in this example, we are dealing with cubic (and quadratic) equations. Hence, we can always write down a full analytic condition for the genus. In general, for most of the polygons (even including reflexive ones) as well as $\tilde{P}_n$, we can always write certain equations to determine the genus for any coefficients, but there may not be general formulae to solve them analytically.

---

[3]If different holes combined with each other, then there would be a point (i.e., fixed $|z|, |w|$) in the hole satisfying more than one inequality. However, this is not possible for fixed $|z|, |w|$.

References

[1] J. Bao, Y.-H. He, E. Hirst, and S. Pietromonaco, "Lectures on the Calabi-Yau Landscape," `arXiv:2001.01212 [hep-th]`.

[2] J. Bao, G. Beaney Colverd, and Y.-H. He, "Quiver Gauge Theories: Beyond Reflexivity," *JHEP* **20** (2020) 161, `arXiv:2004.05295 [hep-th]`.

[3] J. Bao, S. Franco, Y.-H. He, E. Hirst, G. Musiker, and Y. Xiao, "Quiver Mutations, Seiberg Duality and Machine Learning," *Phys. Rev. D* **102** no. 8, (2020) 086013, `arXiv:2006.10783 [hep-th]`.

[4] J. Bao, Y.-H. He, and Y. Xiao, "Chiral rings, Futaki invariants, plethystics, and Gröbner bases," *JHEP* **21** (2020) 203, `arXiv:2009.02450 [hep-th]`.

[5] J. Bao, O. Foda, Y.-H. He, E. Hirst, J. Read, Y. Xiao, and F. Yagi, "Dessins d'enfants, Seiberg-Witten curves and conformal blocks," *JHEP* **05** (2021) 065, `arXiv:2101.08843 [hep-th]`.

[6] J. Bao, Y.-H. He, E. Hirst, J. Hofscheier, A. Kasprzyk, and S. Majumder, "Hilbert series, machine learning, and applications to physics," *Phys. Lett. B* **827** (2022) 136966, `arXiv:2103.13436 [hep-th]`.

[7] J. Bao, Y.-H. He, and E. Hirst, "Neurons on Amoebae," `arXiv:2106.03695 [math.AG]`.

[8] J. Bao, A. Hanany, Y.-H. He, and E. Hirst, "Some Open Questions in Quiver Gauge Theory," *Proyecciones Journal of Mathematics* **41** no. 2, (2022) , `arXiv:2108.05167 [hep-th]`.

[9] J. Bao, Y.-H. He, and A. Zahabi, "Mahler Measure for a Quiver Symphony," *Commun. Math. Phys.* (2022) , `arXiv:2108.13903 [hep-th]`.

[10] J. Bao, Y.-H. He, E. Hirst, J. Hofscheier, A. Kasprzyk, and S. Majumder, "Polytopes and Machine Learning," `arXiv:2109.09602 [math.CO]`.

[11] J. Bao, Y.-H. He, and A. Zahabi, "Reflexions on Mahler: Dessins, Modularity and Gauge Theories," `arXiv:2111.03655 [hep-th]`.

[12] J. Bao, Y.-H. He, and A. Zahabi, "Crystal melting, BPS quivers and plethystics," *JHEP* **06** (2022) 016, `arXiv:2202.12850 [hep-th]`.

[13] J. Bao, Y.-H. He, E. Heyes, and E. Hirst, "Machine Learning Algebraic Geometry for Physics," `arXiv:2204.10334 [hep-th]`.

[14] J. Bao, "A Note on Quiver Yangians and $\mathcal{R}$-Matrices," *JHEP* **08** (2022) 219, `arXiv:2206.06186 [hep-th]`.

[15] J. Bao, "Quiver Yangians and $\mathcal{W}$-Algebras for Generalized Conifolds," `arXiv:2208.13395 [hep-th]`.

[16] J. Bao, "A Survey of Toric Quivers and BPS Algebras," `arXiv:2301.00663 [hep-th]`.

[17] D. Harlow *et al.*, "TF1 Snowmass Report: Quantum gravity, string theory, and black holes," `arXiv:2210.01737 [hep-th]`.

[18] H. Nakajima, "Instantons on ALE spaces, quiver varieties, and Kac-Moody algebras," *Duke Math. J.* **76** no. 2, (1994) 365–416.

[19] M. R. Douglas and G. W. Moore, "D-branes, quivers, and ALE instantons," `arXiv:hep-th/9603167`.

[20] A. Hanany and K. D. Kennaway, "Dimer models and toric diagrams," `arXiv:hep-th/0503149 [hep-th]`.

[21] S. Franco, A. Hanany, K. D. Kennaway, D. Vegh, and B. Wecht, "Brane dimers and quiver gauge theories," *JHEP* **01** (2006) 096, `arXiv:hep-th/0504110 [hep-th]`.

[22] B. Feng, Y.-H. He, K. D. Kennaway, and C. Vafa, "Dimer models from mirror symmetry and quivering amoebae," *Adv. Theor. Math. Phys.* **12** no. 3, (2008) 489–545, `arXiv:hep-th/0511287 [hep-th]`.

[23] R. Kenyon, "Local statistics of lattice dimers," *Annales de L'Institut Henri Poincare Section (B) Probability and Statistics* **33** no. 5, (Jan., 1997) 591–618, `arXiv:math/0105054 [math.CO]`.

[24] R. Kenyon, "An introduction to the dimer model," *arXiv Mathematics e-prints* (Oct., 2003) math/0310326, `arXiv:math/0310326 [math.CO]`.

[25] S. Benvenuti, B. Feng, A. Hanany, and Y.-H. He, "Counting BPS Operators in Gauge Theories: Quivers, Syzygies and Plethystics," *JHEP* **11** (2007) 050, `arXiv:hep-th/0608050 [hep-th]`.

[26] B. Feng, A. Hanany, and Y.-H. He, "Counting gauge invariants: The Plethystic program," *JHEP* **03** (2007) 090, `arXiv:hep-th/0701063`.

[27] J. Gray, A. Hanany, Y.-H. He, V. Jejjala, and N. Mekareeya, "SQCD: A Geometric Apercu," *JHEP* **05** (2008) 099, `arXiv:0803.4257 [hep-th]`.

[28] D. Forcella, A. Hanany, Y.-H. He, and A. Zaffaroni, "The Master Space of N=1 Gauge Theories," *JHEP* **08** (2008) 012, `arXiv:0801.1585 [hep-th]`.

[29] A. Hanany, C. Hwang, H. Kim, J. Park, and R.-K. Seong, "Hilbert Series for Theories with Aharony Duals," *JHEP* **11** (2015) 132, `arXiv:1505.02160 [hep-th]`. [Addendum: JHEP 04, 064 (2016)].

[30] V. Braun, *Counting Points and Hilbert Series in String Theory*, pp. 225–236. 6, 2012. `arXiv:1206.2236 [hep-th]`.

[31] D. Rodríguez-Gómez and G. Zafrir, "On the 5d instanton index as a Hilbert series," *Nucl. Phys. B* **878** (2014) 1–11, `arXiv:1305.5684 [hep-th]`.

[32] S. Cremonesi, A. Hanany, N. Mekareeya, and A. Zaffaroni, "Coulomb branch Hilbert series and Hall-Littlewood polynomials," *JHEP* **09** (2014) 178, `arXiv:1403.0585 [hep-th]`.

[33] A. Hanany, E. E. Jenkins, A. V. Manohar, and G. Torri, "Hilbert Series for Flavor Invariants of the Standard Model," *JHEP* **03** (2011) 096, `arXiv:1010.3161 [hep-ph]`.

[34] J. Gray, Y.-H. He, V. Jejjala, and B. D. Nelson, "Exploring the vacuum geometry of N=1 gauge theories," *Nucl. Phys. B* **750** (2006) 1–27, `arXiv:hep-th/0604208`.

[35] Y.-H. He, V. Jejjala, C. Matti, and B. D. Nelson, "Veronese Geometry and the Electroweak Vacuum Moduli Space," *Phys. Lett. B* **736** (2014) 20–25, `arXiv:1402.3312 [hep-th]`.

[36] Y.-H. He, V. Jejjala, C. Matti, B. D. Nelson, and M. Stillman, "The Geometry of Generations," *Commun. Math. Phys.* **339** no. 1, (2015) 149–190, `arXiv:1408.6841 [hep-th]`.

[37] Y.-H. He, V. Jejjala, C. Matti, and B. D. Nelson, "Testing R-parity with Geometry," *JHEP* **03** (2016) 079, `arXiv:1512.00854 [hep-th]`.

[38] B. Henning, X. Lu, T. Melia, and H. Murayama, "Hilbert series and operator bases with derivatives in effective field theories," *Commun. Math. Phys.* **347** no. 2, (2016) 363–388, `arXiv:1507.07240 [hep-th]`.

[39] L. Lehman and A. Martin, "Low-derivative operators of the Standard Model effective field theory via Hilbert series methods," *JHEP* **02** (2016) 081, `arXiv:1510.00372 [hep-ph]`.

[40] Y. Xiao, Y.-H. He, and C. Matti, "Standard Model Plethystics," *Phys. Rev. D* **100** no. 7, (2019) 076001, `arXiv:1902.10550 [hep-th]`.

[41] A. Okounkov, N. Reshetikhin, and C. Vafa, "Quantum Calabi-Yau and classical crystals," *Prog. Math.* **244** (2006) 597, `arXiv:hep-th/0309208`.

[42] A. Iqbal, N. Nekrasov, A. Okounkov, and C. Vafa, "Quantum foam and topological strings," *JHEP* **04** (2008) 011, `arXiv:hep-th/0312022`.

[43] H. Ooguri and M. Yamazaki, "Crystal Melting and Toric Calabi-Yau Manifolds," *Commun. Math. Phys.* **292** (2009) 179–199, `arXiv:0811.2801 [hep-th]`.

[44] M. Yamazaki, "Crystal Melting and Wall Crossing Phenomena," *Int. J. Mod. Phys. A* **26** (2011) 1097–1228, `arXiv:1002.1709 [hep-th]`.

[45] T. D. Dimofte, *Refined BPS Invariants, Chern-Simons Theory, and the Quantum Dilogarithm*. PhD thesis, Caltech, 2010.

[46] Y.-H. He, R.-K. Seong, and S.-T. Yau, "Calabi–Yau Volumes and Reflexive Polytopes," *Commun. Math. Phys.* **361** no. 1, (2018) 155–204, `arXiv:1704.03462 [hep-th]`.

[47] K. Mahler, "On some inequalities for polynomials in several variables," *Journal of the London Mathematical Society* **1** no. 1, (1962) 341–344.

[48] A. Grothendieck, "Esquisse d'un Programme," 1984.

[49] G. Belyi, "On galois extensions of a maximal cyclotomic field," *Mathematics of the USSR-Izvestiya* **14** no. 2, (1980) 247.

[50] F. R. Villegas, "Modular mahler measures i," in *Topics in number theory*, pp. 17–48. Springer, 1999.

[51] E. B. Bogomolny, "Stability of Classical Solutions," *Sov. J. Nucl. Phys.* **24** (1976) 449.

[52] M. K. Prasad and C. M. Sommerfield, "An Exact Classical Solution for the 't Hooft Monopole and the Julia-Zee Dyon," *Phys. Rev. Lett.* **35** (1975) 760–762.

[53] M. Kontsevich and Y. Soibelman, "Stability structures, motivic Donaldson-Thomas invariants and cluster transformations," `arXiv:0811.2435 [math.AG]`.

[54] Y.-H. Kiem and J. Li, "Categorification of donaldson-thomas invariants via perverse sheaves," `arXiv:1212.6444 [math.AG]`.

[55] D. Gaiotto, G. W. Moore, and E. Witten, "Algebra of the Infrared: String Field Theoretic Structures in Massive $\mathcal{N} = (2,2)$ Field Theory In Two Dimensions," `arXiv:1506.04087 [hep-th]`.

[56] D. Gaiotto, G. W. Moore, and E. Witten, "An Introduction To The Web-Based Formalism," `arXiv:1506.04086 [hep-th]`.

[57] W. Li and M. Yamazaki, "Quiver Yangian from Crystal Melting," *JHEP* **11** (2020) 035, `arXiv:2003.08909 [hep-th]`.

[58] D. Galakhov, W. Li, and M. Yamazaki, "Gauge/Bethe correspondence from quiver BPS algebras," *JHEP* **11** (2022) 119, `arXiv:2206.13340 [hep-th]`.

[59] D. Maulik and A. Okounkov, "Quantum groups and quantum cohomology," `arXiv:1211.1287 [math.AG]`.

[60] K. Costello, "Supersymmetric gauge theory and the Yangian," `arXiv:1303.2632 [hep-th]`.

[61] K. Costello, E. Witten, and M. Yamazaki, "Gauge Theory and Integrability, I," *ICCM Not.* **06** no. 1, (2018) 46–119, `arXiv:1709.09993 [hep-th]`.

[62] K. Costello, E. Witten, and M. Yamazaki, "Gauge Theory and Integrability, II," *ICCM Not.* **06** no. 1, (2018) 120–146, `arXiv:1802.01579 [hep-th]`.

[63] K. Costello and M. Yamazaki, "Gauge Theory And Integrability, III," `arXiv:1908.02289 [hep-th]`.

[64] A. B. Zamolodchikov, "Infinite Additional Symmetries in Two-Dimensional Conformal Quantum Field Theory," *Theor. Math. Phys.* **65** (1985) 1205–1213.

[65] T. Procházka and M. Rapčák, "Webs of W-algebras," *JHEP* **11** (2018) 109, `arXiv:1711.06888 [hep-th]`.

[66] T. Procházka and M. Rapčák, "$\mathcal{W}$-algebra modules, free fields, and Gukov-Witten defects," *JHEP* **05** (2019) 159, `arXiv:1808.08837 [hep-th]`.

[67] T. Creutzig and Y. Hikida, "Rectangular W-algebras, extended higher spin gravity and dual coset CFTs," *JHEP* **02** (2019) 147, `arXiv:1812.07149 [hep-th]`.

[68] T. Creutzig and Y. Hikida, "Rectangular W algebras and superalgebras and their representations," *Phys. Rev. D* **100** no. 8, (2019) 086008, `arXiv:1906.05868 [hep-th]`.

[69] M. Rapčák, "On extensions of $\widehat{\mathfrak{gl}(m|n)}$ Kac-Moody algebras and Calabi-Yau singularities," *JHEP* **01** (2020) 042, `arXiv:1910.00031 [hep-th]`.

[70] L. Eberhardt and T. Procházka, "The matrix-extended $W_{1+\infty}$ algebra," *JHEP* **12** (2019) 175, `arXiv:1910.00041 [hep-th]`.

[71] D. J. Gross, "High-Energy Symmetries of String Theory," *Phys. Rev. Lett.* **60** (1988) 1229.

[72] M. Henneaux and S.-J. Rey, "Nonlinear $W_{infinity}$ as Asymptotic Symmetry of Three-Dimensional Higher Spin Anti-de Sitter Gravity," *JHEP* **12** (2010) 007, `arXiv:1008.4579 [hep-th]`.

[73] A. Campoleoni, S. Fredenhagen, S. Pfenninger, and S. Theisen, "Asymptotic symmetries of three-dimensional gravity coupled to higher-spin fields," *JHEP* **11** (2010) 007, `arXiv:1008.4744 [hep-th]`.

[74] M. R. Gaberdiel and R. Gopakumar, "Higher Spins & Strings," *JHEP* **11** (2014) 044, `arXiv:1406.6103 [hep-th]`.

[75] T. Creutzig, Y. Hikida, and P. B. Ronne, "Extended higher spin holography and Grassmannian models," *JHEP* **11** (2013) 038, `arXiv:1306.0466 [hep-th]`.

[76] V. G. Kac, S.-S. Roan, and M. Wakimoto, "Quantum reduction for affine superalgebras," *Commun. Math. Phys.* **241** (2003) 307–342, `arXiv:math-ph/0302015`.

[77] V. G. Kac and M. Wakimoto, "Quantum reduction and representation theory of superconformal algebras," `arXiv:math-ph/0304011`.

[78] V. G. Kac and M. Wakimoto, "Corrigendum to "Quantum reduction and representation theory of superconformal algebras": [Adv. Math. 185 (2004) 400-458]," *Advances in Mathematics* **193** (2005) 453–455.

[79] L. F. Alday, D. Gaiotto, and Y. Tachikawa, "Liouville Correlation Functions from Four-dimensional Gauge Theories," *Lett. Math. Phys.* **91** (2010) 167–197, `arXiv:0906.3219 [hep-th]`.

[80] N. Wyllard, "A(N-1) conformal Toda field theory correlation functions from conformal N = 2 SU(N) quiver gauge theories," *JHEP* **11** (2009) 002, `arXiv:0907.2189 [hep-th]`.

[81] C. Briot and E. Ragoucy, "RTT presentation of finite W algebras," *J. Phys. A* **34** (2001) 7287–7310, `arXiv:math/0005111`.

[82] J. Brundan and A. Kleshchev, "Shifted Yangians and finite W-algebras," `arXiv:math/0407012`.

[83] C. Briot and E. Ragoucy, "Yangians and $\mathcal{W}$-Algebras," *Theoretical and Mathematical Physics* **127** no. 3, (2001) 709–718, `arXiv:1305.4100 [math-ph]`.

[84] M. R. Gaberdiel, R. Gopakumar, W. Li, and C. Peng, "Higher Spins and Yangian Symmetries," *JHEP* **04** (2017) 152, `arXiv:1702.05100 [hep-th]`.

[85] T. Procházka, "Instanton R-matrix and $\mathcal{W}$-symmetry," *JHEP* **12** (2019) 099, `arXiv:1903.10372 [hep-th]`.

[86] O. Schiffmann and E. Vasserot, "Cherednik algebras, w-algebras and the equivariant cohomology of the moduli space of instantons on a 2," *Publications mathématiques de l'IHÉS* **118** no. 1, (2013) 213–342, `arXiv:1202.2756 [math.QA]`.

[87] A. Braverman, M. Finkelberg, and H. Nakajima, "Instanton moduli spaces and $\mathcal{W}$-algebras," `arXiv:1406.2381 [math.QA]`.

[88] D. Gaiotto and M. Rapčák, "Vertex Algebras at the Corner," *JHEP* **01** (2019) 160, `arXiv:1703.00982 [hep-th]`.

[89] T. C. Collins, D. Xie, and S.-T. Yau, "K stability and stability of chiral ring," arXiv:1606.09260 [hep-th].

[90] B. Feng, A. Hanany, and Y.-H. He, "D-brane gauge theories from toric singularities and toric duality," *Nucl. Phys. B* **595** (2001) 165–200, arXiv:hep-th/0003085.

[91] B. Feng, Y.-H. He, and F. Lam, "On correspondences between toric singularities and (p,q) webs," *Nucl. Phys.* **B701** (2004) 334–356, arXiv:hep-th/0403133 [hep-th].

[92] D. R. Gulotta, "Properly ordered dimers, R-charges, and an efficient inverse algorithm," *JHEP* **10** (2008) 014, arXiv:0807.3012 [hep-th].

[93] B. Feng, A. Hanany, Y.-H. He, and A. M. Uranga, "Toric duality as Seiberg duality and brane diamonds," *JHEP* **12** (2001) 035, arXiv:hep-th/0109063 [hep-th].

[94] J. M. Maldacena, "The Large N limit of superconformal field theories and supergravity," *Int. J. Theor. Phys.* **38** (1999) 1113–1133, arXiv:hep-th/9711200 [hep-th]. [Adv. Theor. Math. Phys.2,231(1998)].

[95] B. S. Acharya, J. M. Figueroa-O'Farrill, C. M. Hull, and B. J. Spence, "Branes at conical singularities and holography," *Adv. Theor. Math. Phys.* **2** (1999) 1249–1286, arXiv:hep-th/9808014 [hep-th].

[96] D. R. Morrison and M. R. Plesser, "Nonspherical horizons. 1.," *Adv. Theor. Math. Phys.* **3** (1999) 1–81, arXiv:hep-th/9810201 [hep-th].

[97] W. Fulton, *Introduction to Toric Varieties.* Annals of mathematics studies. Princeton University Press, 1993.

[98] D. Cox, J. Little, and H. Schenck, *Toric Varieties.* Graduate studies in mathematics. American Mathematical Soc., 2011.

[99] G. S. Guralnik, C. R. Hagen, and T. W. B. Kibble, "Global conservation laws and massless particles," *Phys. Rev. Lett.* **13** (11, 1964) 585–587. https://link.aps.org/doi/10.1103/PhysRevLett.13.585.

[100] P. W. Higgs, "Broken symmetries and the masses of gauge bosons," *Phys. Rev. Lett.* **13** (10, 1964) 508–509. https://link.aps.org/doi/10.1103/PhysRevLett.13.508.

[101] F. Englert and R. Brout, "Broken symmetry and the mass of gauge vector mesons," *Phys. Rev. Lett.* **13** (8, 1964) 321–323. https://link.aps.org/doi/10.1103/PhysRevLett.13.321.

[102] B. Feng, S. Franco, A. Hanany, and Y.-H. He, "UnHiggsing the del Pezzo," *JHEP* **08** (2003) 058, arXiv:hep-th/0209228 [hep-th].

[103] M. Yamazaki, "Brane Tilings and Their Applications," *Fortsch. Phys.* **56** (2008) 555–686, arXiv:0803.4474 [hep-th].

[104] E. Witten, "Phases of N=2 theories in two-dimensions," *Nucl. Phys.* **B403** (1993) 159–222, arXiv:hep-th/9301042 [hep-th]. [AMS/IP Stud. Adv. Math.1,143(1996)].

[105] A. Hanany and R.-K. Seong, "Brane Tilings and Reflexive Polygons," *Fortsch. Phys.* **60** (2012) 695–803, arXiv:1201.2614 [hep-th].

[106] N. Seiberg, "Electric - magnetic duality in supersymmetric nonAbelian gauge theories," *Nucl. Phys.* **B435** (1995) 129–146, arXiv:hep-th/9411149 [hep-th].

[107] C. E. Beasley and M. R. Plesser, "Toric duality is Seiberg duality," *JHEP* **12** (2001) 001, arXiv:hep-th/0109053 [hep-th].

[108] S. Fomin and A. Zelevinsky, "Cluster algebras I: foundations," *Journal of the American Mathematical Society* **15** no. 2, (2002) 497–529, arXiv:math/0104151.

[109] A. Hanany, Y.-H. He, V. Jejjala, J. Pasukonis, S. Ramgoolam, and D. Rodriguez-Gomez, "Invariants of Toric Seiberg Duality," *Int. J. Mod. Phys.* **A27** (2012) 1250002, arXiv:1107.4101 [hep-th].

[110] S. Franco, A. Hanany, Y.-H. He, and P. Kazakopoulos, "Duality walls, duality trees and fractional branes," arXiv:hep-th/0306092 [hep-th].

[111] A. Hanany, Y.-H. He, C. Sun, and S. Sypsas, "Superconformal Block Quivers, Duality Trees and Diophantine Equations," *JHEP* **11** (2013) 017, `arXiv:1211.6111 [hep-th]`.

[112] D. Forcella, A. Hanany, Y.-H. He, and A. Zaffaroni, "Mastering the Master Space," *Lett. Math. Phys.* **85** (2008) 163–171, `arXiv:0801.3477 [hep-th]`.

[113] D. Martelli, J. Sparks, and S.-T. Yau, "The Geometric dual of a-maximisation for Toric Sasaki-Einstein manifolds," *Commun. Math. Phys.* **268** (2006) 39–65, `arXiv:hep-th/0503183 [hep-th]`.

[114] D. Martelli, J. Sparks, and S.-T. Yau, "Sasaki-Einstein manifolds and volume minimisation," *Commun. Math. Phys.* **280** (2008) 611–673, `arXiv:hep-th/0603021 [hep-th]`.

[115] S. S. Gubser, "Einstein manifolds and conformal field theories," *Phys. Rev.* **D59** (1999) 025006, `arXiv:hep-th/9807164 [hep-th]`.

[116] K. A. Intriligator and B. Wecht, "The Exact superconformal R symmetry maximizes a," *Nucl. Phys.* **B667** (2003) 183–200, `arXiv:hep-th/0304128 [hep-th]`.

[117] A. Butti and A. Zaffaroni, "R-charges from toric diagrams and the equivalence of a-maximization and Z-minimization," *JHEP* **11** (2005) 019, `arXiv:hep-th/0506232 [hep-th]`.

[118] A. Butti and A. Zaffaroni, "From toric geometry to quiver gauge theory: The Equivalence of a-maximization and Z-minimization," *Fortsch. Phys.* **54** (2006) 309–316, `arXiv:hep-th/0512240 [hep-th]`.

[119] M. Henningson and K. Skenderis, "The Holographic Weyl anomaly," *JHEP* **07** (1998) 023, `arXiv:hep-th/9806087`.

[120] D. Freedman, S. Gubser, K. Pilch, and N. Warner, "Renormalization group flows from holography supersymmetry and a c theorem," *Adv. Theor. Math. Phys.* **3** (1999) 363–417, `arXiv:hep-th/9904017`.

[121] R. Altman, J. Gray, Y.-H. He, V. Jejjala, and B. D. Nelson, "A Calabi-Yau Database: Threefolds Constructed from the Kreuzer-Skarke List," *JHEP* **02** (2015) 158, `arXiv:1411.1418 [hep-th]`.

[122] B. Nill, "Gorenstein toric Fano varieties," *arXiv Mathematics e-prints* (May, 2004) , `arXiv:math/0405448 [math.AG]`.

[123] X. Wei and R. Ding, "Lattice polygons with two interior lattice points," *Mathematical Notes* **91** (05, 2012) .

[124] G. Balletti and A. M. Kasprzyk, "Three-dimensional lattice polytopes with two interior lattice points," `arXiv:1612.08918 [math.CO]`.

[125] V. V. Batyrev, "TOROIDAL FANO 3-FOLDS," *Mathematics of the USSR-Izvestiya* **19** no. 1, (Feb, 1982) 13–25. `https://doi.org/10.1070%2Fim1982v019n01abeh001404`.

[126] V. V. Batyrev and L. A. Borisov, "On Calabi-Yau complete intersections in toric varieties," `arXiv:alg-geom/9412017 [alg-geom]`.

[127] M. Kreuzer and H. Skarke, "On the classification of reflexive polyhedra," *Commun. Math. Phys.* **185** (1997) 495–508, `arXiv:hep-th/9512204 [hep-th]`.

[128] M. Kreuzer and H. Skarke, "Classification of reflexive polyhedra in three-dimensions," *Adv. Theor. Math. Phys.* **2** (1998) 853–871, `arXiv:hep-th/9805190 [hep-th]`.

[129] M. Kreuzer and H. Skarke, "Complete classification of reflexive polyhedra in four-dimensions," *Adv. Theor. Math. Phys.* **4** (2002) 1209–1230, `arXiv:hep-th/0002240 [hep-th]`.

[130] M. Kreuzer and H. Skarke, "PALP: A Package for analyzing lattice polytopes with applications to toric geometry," *Comput. Phys. Commun.* **157** (2004) 87–106, `arXiv:math/0204356 [math.NA]`.

[131] H. Ooguri and M. Yamazaki, "Emergent Calabi-Yau Geometry," *Phys. Rev. Lett.* **102** (2009) 161601, `arXiv:0902.3996 [hep-th]`.

[132] Y.-H. He, M. L. Ge, C. Bai, J. Bao, and E. Hirst, eds., *Nankai Symposium on Mathematical Dialogues: Celebrating the 110th anniversary of the birth of Prof. S.-S. Chern.* Springer, Singapore, 9, 2022.

[133] S. Vandervelde, "The mahler measure of parametrizable polynomials," *Journal of Number Theory* **128** no. 8, (2008) 2231–2250, `arXiv:math/0611159`.

[134] A. Schinzel, *Polynomials over an algebraically closed field*, p. 201–262. Encyclopedia of Mathematics and its Applications. Cambridge University Press, 2000.

[135] D. W. Boyd and M. J. Mossinghoff, "Small limit points of mahler's measure," *Experimental Mathematics* **14** no. 4, (2005) 403–414.

[136] D. W. Boyd and F. Rodriguez-Villegas, "Mahler's measure and the dilogarithm (i)," *Canadian Journal of Mathematics* **54** no. 3, (2002) 468–492.

[137] D. W. Boyd, F. Rodriguez-Villegas, and N. Dunfield, "Mahler's measure and the dilogarithm (ii)," `arXiv:math/0308041`.

[138] P. A. Griffiths, "On the periods of certain rational integrals: I, ii," *Annals of Mathematics* (1969) 461–541.

[139] R. Kenyon, A. Okounkov, and S. Sheffield, "Dimers and amoebae," `arXiv:math-ph/0311005`.

[140] P. Kasteleyn, "Graph theory and crystal physics," *Graph Theory and Theoretical Physics* (1967) 43–110.

[141] R. Kenyon, "The laplacian and dirac operators on critical planar graphs," *Inventiones mathematicae* **150** no. 2, (Nov, 2002) 409–439, `arXiv:math-ph/0202018`. `http://dx.doi.org/10.1007/s00222-002-0249-4`.

[142] S. Franco and D. Vegh, "Moduli spaces of gauge theories from dimer models: Proof of the correspondence," *JHEP* **11** (2006) 054, `arXiv:hep-th/0601063`.

[143] R. Kenyon and A. Okounkov, "Planar dimers and Harnack curves," `arXiv:math/0311062`.

[144] M. Passare and H. Rullgård, *Amoebas, Monge-Ampere measures and triangulations of the Newton polytope.* Matem. inst., SU, 2000.

[145] G. Mikhalkin, "Real algebraic curves, the moment map and amoebas," *Annals of Mathematics* (2000) 309–326, `arXiv:math/0010018`.

[146] G. Mikhalkin and H. Rullgård, "Amoebas of maximal area," *International mathematics research notices* **2001** no. 9, (2001) 441–451, `arXiv:math/0010087`.

[147] L. Ronkin, "On zeros of almost periodic functions generated by holomorphic functions in a multicircular domain," *Complex Analysis in Modern Mathematics, Fazis, Moscow* (2000) 243–256.

[148] M. Forsberg, M. Passare, and A. Tsikh, "Laurent determinants and arrangements of hyperplane amoebas," *Advances in mathematics* **151** no. 1, (2000) 45–70.

[149] G. Mikhalkin, "Amoebas of algebraic varieties and tropical geometry," *Different faces of geometry* (2004) 257–300, `arXiv:math/0108225`.

[150] R. J. Szabo, "Instantons, Topological Strings and Enumerative Geometry," *Adv. Math. Phys.* **2010** (2010) 107857, `arXiv:0912.1509 [hep-th]`.

[151] M. Aganagic and K. Schaeffer, "Wall Crossing, Quivers and Crystals," *JHEP* **10** (2012) 153, `arXiv:1006.2113 [hep-th]`.

[152] T. Nishinaka, S. Yamaguchi, and Y. Yoshida, "Two-dimensional crystal melting and D4-D2-D0 on toric Calabi-Yau singularities," *JHEP* **05** (2014) 139, `arXiv:1304.6724 [hep-th]`.

[153] T. Theobald, "Computing amoebas," *Experimental Mathematics* **11** no. 4, (2002) 513–526.

[154] M. Bogaard, "Introduction to amoebas and tropical geometry," *Masters thesis, U. Amsterdam* (2015) . `https://scripties.uba.uva.nl/download?fid=564840`.

[155] S. Chen, Y.-H. He, E. Hirst, A. Nestor, and A. Zahabi, "Mahler Measuring the Genetic Code of Amoebae," `arXiv:2212.06553 [hep-th]`.

[156] K. Hori and C. Vafa, "Mirror symmetry," `arXiv:hep-th/0002222`.

[157] K. Hori, A. Iqbal, and C. Vafa, "D-branes and mirror symmetry," `arXiv:hep-th/0005247`.

[158] M. Yamazaki, "Quivers, YBE and 3-manifolds," *JHEP* **05** (2012) 147, `arXiv:1203.5784 [hep-th]`.

[159] B. de Tilière, "Partition function of periodic isoradial dimer models," *Probability theory and related fields* **138** no. 3-4, (2007) 451–462, `arXiv:math/0605583`.

[160] T. C. Collins and G. Szekelyhidi, "K-Semistability for irregular Sasakian manifolds," *J. Diff. Geom.* **109** no. 1, (2018) 81–109, `arXiv:1204.2230 [math.DG]`.

[161] T. Collins and G. Székelyhidi, "Sasaki–einstein metrics and k–stability," *Geometry & Topology* **23** no. 3, (2019) 1339–1413, `arXiv:1512.07213 [math.DG]`.

[162] A. Hanany and R.-K. Seong, "Brane Tilings and Specular Duality," *JHEP* **08** (2012) 107, `arXiv:1206.2386 [hep-th]`.

[163] A. Hanany and D. Vegh, "Quivers, tilings, branes and rhombi," *JHEP* **10** (2007) 029, `arXiv:hep-th/0511063`.

[164] Y. Terashima and M. Yamazaki, "Emergent 3-manifolds from 4d Superconformal Indices," *Phys. Rev. Lett.* **109** (2012) 091602, `arXiv:1203.5792 [hep-th]`.

[165] H. Ooguri, A. Strominger, and C. Vafa, "Black hole attractors and the topological string," *Phys. Rev. D* **70** (2004) 106007, `arXiv:hep-th/0405146`.

[166] Y.-H. He, J. McKay, and J. Read, "Modular Subgroups, Dessins d'Enfants and Elliptic K3 Surfaces," *LMS J. Comp. Math.* **16** (2013) 271–318, `arXiv:1211.1931 [math.AG]`.

[167] Y.-H. He and J. Read, "Hecke Groups, Dessins d'Enfants and the Archimedean Solids," *Front. in Phys.* **3** (2015) 91, `arXiv:1309.2326 [math.AG]`.

[168] Y.-H. He and J. Read, "Dessins d'enfants in $\mathcal{N} = 2$ generalised quiver theories," *JHEP* **08** (2015) 085, `arXiv:1503.06418 [hep-th]`.

[169] V. Tatitscheff, Y.-H. He, and J. McKay, "Cusps, Congruence Groups and Monstrous Dessins," `arXiv:1812.11752 [math.NT]`.

[170] Y.-H. He, E. Hirst, and T. Peterken, "Machine-learning dessins d'enfants: explorations via modular and Seiberg–Witten curves," *J. Phys. A* **54** no. 7, (2021) 075401, `arXiv:2004.05218 [hep-th]`.

[171] S. K. Ashok, F. Cachazo, and E. Dell'Aquila, "Children's drawings from Seiberg-Witten curves," *Commun. Num. Theor. Phys.* **1** (2007) 237–305, `arXiv:hep-th/0611082`.

[172] J. Stienstra, "Hypergeometric Systems in two Variables, Quivers, Dimers and Dessins d'Enfants," *Fields Inst. Commun.* **54** (2008) 125–162, `arXiv:0711.0464 [math.AG]`.

[173] V. Jejjala, S. Ramgoolam, and D. Rodriguez-Gomez, "Toric CFTs, Permutation Triples and Belyi Pairs," *JHEP* **03** (2011) 065, `arXiv:1012.2351 [hep-th]`.

[174] S. Bose, J. Gundry, and Y.-H. He, "Gauge theories and dessins d'enfants: beyond the torus," *JHEP* **01** (2015) 135, `arXiv:1410.2227 [hep-th]`.

[175] S. Franco, A. Hanany, D. Martelli, J. Sparks, D. Vegh, and B. Wecht, "Gauge theories from toric geometry and brane tilings," *JHEP* **01** (2006) 128, `arXiv:hep-th/0505211 [hep-th]`.

[176] M. Kontsevich and D. Zagier, "Periods," in *Mathematics unlimited—2001 and beyond*, pp. 771–808. Springer, 2001.

[177] T. Shioda, "On elliptic modular surfaces," *Journal of the Mathematical Society of Japan* **24** no. 1, (1972) 20–59.

[178] Y.-H. He and J. McKay, "N=2 Gauge Theories: Congruence Subgroups, Coset Graphs and Modular Surfaces," *J. Math. Phys.* **54** (2013) 012301, `arXiv:1201.3633 [hep-th]`.

[179] J. Davey, A. Hanany, and J. Pasukonis, "On the Classification of Brane Tilings," *JHEP* **01** (2010) 078, arXiv:0909.2868 [hep-th].

[180] A. Hanany, V. Jejjala, S. Ramgoolam, and R.-K. Seong, "Consistency and Derangements in Brane Tilings," *J. Phys. A* **49** no. 35, (2016) 355401, arXiv:1512.09013 [hep-th].

[181] E. Goins, "Drawing Planar Graphs via Dessins d'Enfants," 2013.

[182] C. Closset and H. Magureanu, "The U-plane of rank-one 4d $\mathcal{N} = 2$ KK theories," arXiv:2107.03509 [hep-th].

[183] D. Samart, *Mahler measures of hypergeometric families of Calabi-Yau varieties*. PhD thesis, 2014.

[184] D. Zagier, "Integral solutions of apéry-like recurrence equations," *Groups and Symmetries: from Neolithic Scots to John McKay, CRM Proc. Lecture Notes* **47** (2009) 349–366.

[185] J. Stienstra, "Mahler measure variations, Eisenstein series and instanton expansions," in *Workshop on Calabi-Yau Varieties and Mirror Symmetry*, pp. 139–150. 2, 2005. arXiv:math/0502193.

[186] G. Diaz, "Mahler's conjecture and other transcendence results," in *Introduction to Algebraic Independence Theory*, pp. 13–26. Springer, 2001.

[187] A. Hanany, Y.-H. He, V. Jejjala, J. Pasukonis, S. Ramgoolam, and D. Rodriguez-Gomez, "The Beta Ansatz: A Tale of Two Complex Structures," *JHEP* **06** (2011) 056, arXiv:1104.5490 [hep-th].

[188] Y.-H. He, V. Jejjala, and D. Rodriguez-Gomez, "Brane Geometry and Dimer Models," *JHEP* **06** (2012) 143, arXiv:1204.1065 [hep-th].

[189] A. Sen, "F theory and orientifolds," *Nucl. Phys. B* **475** (1996) 562–578, arXiv:hep-th/9605150.

[190] A. Sen, "Orientifold limit of F theory vacua," *Phys. Rev. D* **55** (1997) R7345–R7349, arXiv:hep-th/9702165.

[191] M. R. Gaberdiel, T. Hauer, and B. Zwiebach, "Open string-string junction transitions," *Nucl. Phys. B* **525** (1998) 117–145, arXiv:hep-th/9801205.

[192] A. Klemm, P. Mayr, and C. Vafa, "BPS states of exceptional noncritical strings," *Nucl. Phys. B Proc. Suppl.* **58** (1997) 177, arXiv:hep-th/9607139.

[193] W. Lerche, P. Mayr, and N. P. Warner, "Noncritical strings, Del Pezzo singularities and Seiberg-Witten curves," *Nucl. Phys. B* **499** (1997) 125–148, arXiv:hep-th/9612085.

[194] H. Jockers, V. Kumar, J. M. Lapan, D. R. Morrison, and M. Romo, "Two-Sphere Partition Functions and Gromov-Witten Invariants," *Commun. Math. Phys.* **325** (2014) 1139–1170, arXiv:1208.6244 [hep-th].

[195] J. A. Harvey and G. W. Moore, "Algebras, BPS states, and strings," *Nucl. Phys. B* **463** (1996) 315–368, arXiv:hep-th/9510182.

[196] J. A. Harvey and G. W. Moore, "On the algebras of BPS states," *Commun. Math. Phys.* **197** (1998) 489–519, arXiv:hep-th/9609017.

[197] D. Galakhov and M. Yamazaki, "Quiver Yangian and Supersymmetric Quantum Mechanics," *Commun. Math. Phys.* **396** no. 2, (2022) 713–785, arXiv:2008.07006 [hep-th].

[198] D. Galakhov, W. Li, and M. Yamazaki, "Shifted quiver Yangians and representations from BPS crystals," *JHEP* **08** (2021) 146, arXiv:2106.01230 [hep-th].

[199] D. Galakhov, W. Li, and M. Yamazaki, "Toroidal and elliptic quiver BPS algebras and beyond," *JHEP* **02** (2022) 024, arXiv:2108.10286 [hep-th].

[200] G. Noshita and A. Watanabe, "A note on quiver quantum toroidal algebra," *JHEP* **05** (2022) 011, arXiv:2108.07104 [hep-th].

[201] G. Noshita and A. Watanabe, "Shifted quiver quantum toroidal algebra and subcrystal representations," *JHEP* **05** (2022) 122, arXiv:2109.02045 [hep-th].

[202] B. Szendroi, "Non-commutative Donaldson–Thomas invariants and the conifold," *Geom. Topol.* **12** no. 2, (2008) 1171–1202, `arXiv:0705.3419 [math.AG]`.

[203] B. Young, "Computing a pyramid partition generating function with dimer shuffling," *Journal of Combinatorial Theory, Series A* **116** no. 2, (2009) 334–350, `arXiv:0709.3079 [math.CO]`.

[204] W.-y. Chuang and D. L. Jafferis, "Wall Crossing of BPS States on the Conifold from Seiberg Duality and Pyramid Partitions," *Commun. Math. Phys.* **292** (2009) 285–301, `arXiv:0810.5072 [hep-th]`.

[205] A. Neguţ, "Reduced quiver quantum toroidal algebras," `arXiv:2301.00703 [hep-th]`.

[206] A. Litvinov and I. Vilkoviskiy, "Liouville reflection operator, affine Yangian and Bethe ansatz," *JHEP* **12** (2020) 100, `arXiv:2007.00535 [hep-th]`.

[207] V. Drinfeld, "Hopf algebras and the quantum yang-baxter equation," *Proceedings of the USSR Academy of Sciences* **32** (1985) 254–258.

[208] B. Davison, "The critical CoHA of a quiver with potential," *Quart. J. Math. Oxford Ser.* **68** no. 2, (2017) 635–703, `arXiv:1311.7172 [math.AG]`.

[209] E. Chistyakova, A. Litvinov, and P. Orlov, "Affine Yangian of $\mathfrak{gl}(2)$ and integrable structures of superconformal field theory," *JHEP* **03** (2022) 102, `arXiv:2110.05870 [hep-th]`.

[210] N. Wang and K. Wu, "Yang–Baxter algebra and MacMahon representation," *J. Math. Phys.* **63** no. 2, (2022) 021702.

[211] T. Procházka, "$\mathcal{W}$-symmetry, topological vertex and affine Yangian," *JHEP* **10** (2016) 077, `arXiv:1512.07178 [hep-th]`.

[212] N. A. Nekrasov and S. L. Shatashvili, "Supersymmetric vacua and Bethe ansatz," *Nucl. Phys. B Proc. Suppl.* **192-193** (2009) 91–112, `arXiv:0901.4744 [hep-th]`.

[213] N. A. Nekrasov and S. L. Shatashvili, "Quantum integrability and supersymmetric vacua," *Prog. Theor. Phys. Suppl.* **177** (2009) 105–119, `arXiv:0901.4748 [hep-th]`.

[214] N. A. Nekrasov and S. L. Shatashvili, "Quantization of Integrable Systems and Four Dimensional Gauge Theories," in *16th International Congress on Mathematical Physics*, pp. 265–289. 8, 2009. `arXiv:0908.4052 [hep-th]`.

[215] N. Guay, H. Nakajima, and C. Wendlandt, "Coproduct for Yangians of affine Kac–Moody algebras," *Advances in Mathematics* **338** (2018) 865–911, `arXiv:1701.05288 [math.QA]`.

[216] M. Ueda, "Affine Super Yangian," `arXiv:1911.06666 [math.RT]`.

[217] V. G. Drinfeld, "A New realization of Yangians and quantized affine algebras," *Sov. Math. Dokl.* **36** (1988) 212–216.

[218] V. Chari and A. N. Pressley, *A guide to quantum groups.* Cambridge university press, 1995.

[219] V. G. Drinfeld, "Hopf algebras and the quantum Yang-Baxter equation," *Sov. Math. Dokl.* **32** (1985) 254–258.

[220] S. Kumar, *Kac-Moody groups, their flag varieties and representation theory*, vol. 204. Springer Science & Business Media, 2012.

[221] V. Serganova, "Kac–Moody superalgebras and integrability," in *Developments and trends in infinite-dimensional Lie theory*, pp. 169–218. Springer, 2011.

[222] V. V. Serganova, "Automorphisms of simple Lie superalgebras," *Mathematics of the USSR-Izvestiya* **24** no. 3, (1985) 539.

[223] C. Hoyt and V. Serganova, "Classification of finite-growth general Kac–Moody superalgebras," *Communications in Algebra* **35** no. 3, (2007) 851–874, `arXiv:0810.2637 [math.RT]`.

[224] M. Ueda, "Affine super Yangians and rectangular W-superalgebras," *Journal of Mathematical Physics* **63** no. 5, (2022) 051701, `arXiv:2002.03479 [math.RT]`.

[225] R. Kodera and M. Ueda, "Coproduct for affine Yangians and parabolic induction for rectangular W-algebras," *Letters in Mathematical Physics* **112** no. 1, (2022) 1–37, `arXiv:2107.00780 [math.RT]`.

[226] N. Genra, "Screening operators and parabolic inductions for affine W-algebras," *Advances in Mathematics* **369** (2020) 107179, `arXiv:1806.04417 [math.RT]`.

[227] B. Feigin, M. Jimbo, T. Miwa, and E. Mukhin, "Quantum toroidal and Bethe ansatz," *Journal of Physics A: Mathematical and Theoretical* **48** no. 24, (2015) 244001, `arXiv:1502.07194 [math.QA]`.

[228] A. Garbali and J. De Gier, "The R-Matrix of the Quantum Toroidal Algebra $U_{q,t}\left(\ddot{\mathrm{gl}}_1\right)$ in the Fock Module," *Communications in Mathematical Physics* **384** no. 3, (2021) 1971–2008, `arXiv:2004.09241 [math-ph]`.

[229] T. Kojima, "Elliptic Deformed Superalgebra $u_{q,p}(\hat{sl}(M|N))$," *J. Phys. A* **44** (2011) 485205, `arXiv:1103.5527 [nlin.SI]`.

[230] M. Jimbo and T. Miwa, "Solitons and Infinite Dimensional Lie Algebras," *Publ. Res. Inst. Math. Sci. Kyoto* **19** (1983) 943.

[231] P. Sulkowski, "Wall-crossing, free fermions and crystal melting," *Commun. Math. Phys.* **301** (2011) 517–562, `arXiv:0910.5485 [hep-th]`.

[232] M. Wakimoto, "Fock representations of the affine lie algebra A1(1)," *Commun. Math. Phys.* **104** (1986) 605–609.

[233] B. L. Feigin and E. V. Frenkel, "Affine Kac-Moody algebras and semiinfinite flag manifolds," *Commun. Math. Phys.* **128** (1990) 161–189.

[234] D. Kolyaskin, A. Litvinov, and A. Zhukov, "R-matrix formulation of affine Yangian of $\widehat{\mathfrak{gl}}(1|1)$," `arXiv:2206.01636 [hep-th]`.

[235] A. Litvinov and L. Spodyneiko, "On W algebras commuting with a set of screenings," *JHEP* **11** (2016) 138, `arXiv:1609.06271 [hep-th]`.

[236] S. M. Khoroshkin and V. N. Tolstoy, "Universal r-matrix for quantized (super) algebras," *Communications in Mathematical Physics* **141** no. 3, (1991) 599–617.

[237] S. Khoroshkin and V. Tolstoy, "The c art an-weyl basis and the universal r-matrix for quantum kac-moody algebras and superalgebras," *Quantum symmetries* (1993) 336.

[238] K. Harada, Y. Matsuo, G. Noshita, and A. Watanabe, "q-deformation of corner vertex operator algebras by Miura transformation," *JHEP* **04** (2021) 202, `arXiv:2101.03953 [hep-th]`.

[239] S. Cremonesi, A. Hanany, and R.-K. Seong, "Double Handled Brane Tilings," *JHEP* **10** (2013) 001, `arXiv:1305.3607 [hep-th]`.

[240] T. C. Collins and G. Székelyhidi, "Sasaki-Einstein metrics and K-stability," `arXiv:1512.07213 [math.DG]`.

[241] A. Futaki, "An obstruction to the existence of einstein kähler metrics." *Inventiones mathematicae* **73** (1983) 437–444.

[242] W. Ding and G. Tian, "Kähler-einstein metrics and the generalized futaki invariant." *Inventiones mathematicae* **110** no. 2, (1992) 315–336.

[243] S. Donaldson, "Scalar curvature and stability of toric varieties," *J. Differential Geom.* **62** no. 2, (10, 2002) 289–349.

[244] J. P. Gauntlett, D. Martelli, J. Sparks, and S.-T. Yau, "Obstructions to the existence of Sasaki-Einstein metrics," *Commun. Math. Phys.* **273** (2007) 803–827, `arXiv:hep-th/0607080`.

[245] F. Cachazo, B. Fiol, K. A. Intriligator, S. Katz, and C. Vafa, "A Geometric unification of dualities," *Nucl. Phys. B* **628** (2002) 3–78, `arXiv:hep-th/0110028`.

[246] F. Cachazo, M. R. Douglas, N. Seiberg, and E. Witten, "Chiral rings and anomalies in supersymmetric gauge theory," *JHEP* **12** (2002) 071, `arXiv:hep-th/0211170`.

[247] F. Cachazo, N. Seiberg, and E. Witten, "Chiral rings and phases of supersymmetric gauge theories," *JHEP* **04** (2003) 018, `arXiv:hep-th/0303207`.

[248] M. A. Luty and W. Taylor, "Varieties of vacua in classical supersymmetric gauge theories," *Phys. Rev. D* **53** (1996) 3399–3405, `arXiv:hep-th/9506098`.

[249] J. Hauenstein, Y.-H. He, and D. Mehta, "Numerical elimination and moduli space of vacua," *JHEP* **09** (2013) 083, `arXiv:1210.6038 [hep-th]`.

[250] A. Bergman and C. P. Herzog, "The Volume of some nonspherical horizons and the AdS / CFT correspondence," *JHEP* **01** (2002) 030, `arXiv:hep-th/0108020`.

[251] R. P. Stanley, "Hilbert functions of graded algebras," *Advances in Mathematics* **28** no. 1, (1978) 57 – 83.

[252] G. Székelyhidi, *An Introduction to Extremal Kahler Metrics.* Graduate Studies in Mathematics. American Mathematical Society, 2014.

[253] D. Bayer and D. Mumford, "What can be computed in algebraic geometry?," `alg-geom/9304003 [math.AG]`.

[254] M. Artin, C. Seshadri, and A. Tannenbaum, *Lectures on Deformations of Singularities.* Lectures on Mathematics and Physics. Tata Institute of Fundamental Research, 1976.

[255] C. Li, "Some notes on Futaki invariant,". `https://www.math.purdue.edu/~li2285/notes/Futaki.pdf`.

[256] C. Li and C. Xu, "Special test configurations and K-stability of Fano varieties," `arXiv:1111.5398 [math.AG]`.

[257] M. Fazzi and A. Tomasiello, "Holography, Matrix Factorizations and K-stability," *JHEP* **05** (2020) 119, `arXiv:1906.08272 [hep-th]`.

[258] N. Ilten and H. Süß, "K-Stability for Fano Manifolds with Torus Action of Complexity One," `arXiv:1507.04442 [math.AG]`.

[259] D. Xie and S.-T. Yau, "Singularity, Sasaki-Einstein manifold, Log del Pezzo surface and $\mathcal{N} = 1$ AdS/CFT correspondence: Part I," `arXiv:1903.00150 [hep-th]`.

[260] J. McKay, "Graphs, singularities, & finite groups," *Proc. Symp. Pure Math* **37** (1980) .

[261] J. Gonzalez-Sanchez, M. Harrison, I. Polo-Blanco, and J. Schicho, "Algorithms for Del Pezzo Surfaces of Degree 5 (Construction, Parametrization)," `arXiv:1009.4044 [math.AG]`.

[262] K. Devleming, "Notes on K-stability,". `http://www.math.ucsd.edu/~kdevleming/research/K_stability_notes.pdf`.

[263] N. Kaplan, *Rational Point Counts for Del Pezzo Surfaces Over Finite Fields and Coding Theory.* Harvard University, 2013. `https://www.math.uci.edu/~nckaplan/research_files/kaplanthesis.pdf`.

[264] S. Benvenuti, A. Hanany, and N. Mekareeya, "The Hilbert Series of the One Instanton Moduli Space," *JHEP* **06** (2010) 100, `arXiv:1005.3026 [hep-th]`.

[265] O. Aharony, A. Hanany, K. A. Intriligator, N. Seiberg, and M. Strassler, "Aspects of N=2 supersymmetric gauge theories in three-dimensions," *Nucl. Phys. B* **499** (1997) 67–99, `arXiv:hep-th/9703110`.

[266] I. Affleck, M. Dine, and N. Seiberg, "Dynamical Supersymmetry Breaking in Four-Dimensions and Its Phenomenological Implications," *Nucl. Phys. B* **256** (1985) 557–599.

[267] N. Seiberg, "Exact results on the space of vacua of four-dimensional SUSY gauge theories," *Phys. Rev. D* **49** (1994) 6857–6863, `arXiv:hep-th/9402044`.

[268] S. Benvenuti and S. Giacomelli, "Supersymmetric gauge theories with decoupled operators and chiral ring stability," *Phys. Rev. Lett.* **119** no. 25, (2017) 251601, `arXiv:1706.02225 [hep-th]`.

[269] Y.-H. He, "Deep-Learning the Landscape," `arXiv:1706.02714 [hep-th]`.

[270] Y.-H. He, *The Calabi–Yau Landscape: From Geometry, to Physics, to Machine Learning*. Lecture Notes in Mathematics. 5, 2021. `arXiv:1812.02893 [hep-th]`.

[271] D. Sommerville, *Introduction to the Geometry of N Dimensions*. Dover Books on Mathematics. Dover Publications, 2020. `https://books.google.co.uk/books?id=4vXDDwAAQBAJ`.

[272] E. Miller and B. Sturmfels, "Ehrhart polynomials," *Combinatorial Commutative Algebra* (2005) 229–246.

[273] K. Purbhoo, "A nullstellensatz for amoebas," `arXiv:math/0603201`.

[274] J. Forsgård, L. F. Matusevich, N. Mehlhop, and T. de Wolff, "Lopsided approximation of amoebas," `arXiv:1608.08663 [cs.SC]`.

[275] B. Bengfort and R. Bilbro, "Yellowbrick: Visualizing the Scikit-Learn Model Selection Process,". `http://joss.theoj.org/papers/10.21105/joss.01075`.

[276] T. Eguchi and K. Maruyoshi, "Penner Type Matrix Model and Seiberg-Witten Theory," *JHEP* **02** (2010) 022, `arXiv:0911.4797 [hep-th]`.

[277] C. Kozcaz, S. Pasquetti, and N. Wyllard, "A & B model approaches to surface operators and Toda theories," *JHEP* **08** (2010) 042, `arXiv:1004.2025 [hep-th]`.

[278] M. Bershtein and O. Foda, "AGT, Burge pairs and minimal models," *JHEP* **06** (2014) 177, `arXiv:1404.7075 [hep-th]`.

[279] K. B. Alkalaev and V. A. Belavin, "Conformal blocks of W_N minimal models and AGT correspondence," *JHEP* **07** (2014) 024, `arXiv:1404.7094 [hep-th]`.

[280] M. Mulase and M. Penkava, "Ribbon graphs, quadratic differentials on riemann surfaces, and algebraic curves defined over $\bar{q}$," *Asian J. Math.* **2** (11, 1998) .

[281] J. McKay and A. Sebbar, "J-invariants of arithmetic semistable elliptic surfaces and graphs," *CRM Proceedings and Lecture Notes* (2001) 119–130.

[282] Y. Tachikawa, *N=2 supersymmetric dynamics for pedestrians*, vol. 890. 2014. `arXiv:1312.2684 [hep-th]`.

[283] P. Francesco, P. Mathieu, and D. Sénéchal, *Conformal field theory*. Springer Science & Business Media, 2012.

[284] F. Klein and R. Fricke, *Lectures on the Theory of Elliptic Modular Functions*.

[285] K. Nagao, "Derived categories of small toric calabi-yau 3-folds and counting invariants," `arXiv:0809.2994 [math.AG]`.

[286] K. Nagao and M. Yamazaki, "The Non-commutative Topological Vertex and Wall Crossing Phenomena," *Adv. Theor. Math. Phys.* **14** no. 4, (2010) 1147–1181, `arXiv:0910.5479 [hep-th]`.

[287] B. Young and J. Bryan, "Generating functions for colored 3D Young diagrams and the Donaldson-Thomas invariants of orbifolds," *Duke Math. J.* **152** (2010) 115–153, `arXiv:0802.3948 [math.CO]`.

[288] M. Cirafici, A. Sinkovics, and R. J. Szabo, "Instantons, Quivers and Noncommutative Donaldson-Thomas Theory," *Nucl. Phys. B* **853** (2011) 508–605, `arXiv:1012.2725 [hep-th]`.

[289] M. Cirafici and R. J. Szabo, "Curve counting, instantons and McKay correspondences," *J. Geom. Phys.* **72** (2013) 54–109, `arXiv:1209.1486 [hep-th]`.

[290] M. Aganagic, A. Klemm, M. Marino, and C. Vafa, "The Topological vertex," *Commun. Math. Phys.* **254** (2005) 425–478, `arXiv:hep-th/0305132`.

[291] A. Iqbal and A.-K. Kashani-Poor, "The Vertex on a strip," *Adv. Theor. Math. Phys.* **10** no. 3, (2006) 317–343, `arXiv:hep-th/0410174`.

[292] P. A. MacMahon, *Combinatory Analysis, Volumes I and II*, vol. 137. American Mathematical Soc., 2001.

[293] V. G. Kac, "Infinite root systems, representations of graphs and invariant theory," *Inventiones mathematicae* **56** no. 1, (1980) 57–92.

[294] S. Mozgovoy and M. Reineke, "On the noncommutative donaldson–thomas invariants arising from brane tilings," *Advances in mathematics* **223** no. 5, (2010) 1521–1544, `arXiv:0809.0117 [math.AG]`.

[295] T. Bozec, O. Schiffmann, and E. Vasserot, "On the number of points of nilpotent quiver varieties over finite fields," `arXiv:1701.01797 [math.RT]`.

[296] O. G. Schiffmann, "Kac polynomials and lie algebras associated to quivers and curves," in *Proceedings of the International Congress of Mathematicians: Rio de Janeiro 2018*, pp. 1393–1424, World Scientific. 2018. `arXiv:1802.09760 [math.RT]`.

[297] O. Schiffmann and E. Vasserot, "On cohomological hall algebras of quivers: Yangians," `arXiv:1705.07491 [math.RT]`.

[298] A. Borel and J. C. Moore, "Homology theory for locally compact spaces." *Michigan Mathematical Journal* **7** no. 2, (1960) 137–159.

[299] B. Davison, "The integrality conjecture and the cohomology of preprojective stacks," `arXiv:1602.02110 [math.AG]`.

[300] M. Kontsevich and Y. Soibelman, "Cohomological Hall algebra, exponential Hodge structures and motivic Donaldson-Thomas invariants," *Commun. Num. Theor. Phys.* **5** (2011) 231–352, `arXiv:1006.2706 [math.AG]`.

[301] K. Behrend, J. Bryan, and B. Szendroi, "Motivic degree zero Donaldson-Thomas invariants," `arXiv:0909.5088 [math.AG]`.

[302] M. Rapcak, Y. Soibelman, Y. Yang, and G. Zhao, "Cohomological Hall algebras, vertex algebras and instantons," *Commun. Math. Phys.* **376** no. 3, (2019) 1803–1873, `arXiv:1810.10402 [math.QA]`.

[303] R. Stanley and S. Fomin, *Enumerative Combinatorics: Volume 2*. Cambridge Studies in Advanced Mathematics. Cambridge University Press, 1997.

[304] G. Meinardus, "Asymptotische aussagen über partitionen," *Mathematische Zeitschrift* **59** no. 1, (1953) 388–398.

[305] C. Haselgrove and H. Temperley, "Asymptotic formulae in the theory of partitions," in *Mathematical Proceedings of the Cambridge Philosophical Society*, vol. 50, pp. 225–241, Cambridge University Press. 1954.

[306] L. B. Richmond, "Some general problems on the number of parts in partitions," *Acta Arithmetica* **66** no. 4, (1994) 297–313.

[307] E. Wright, "Asymptotic partition formulaei. plane partitions," *The Quarterly Journal of Mathematics* no. 1, (1931) 177–189.

[308] V. I. Arnol'd, "Critical points of smooth functions and their normal forms," *Russian Mathematical Surveys* **30** no. 5, (1975) 1.

[309] T. Bridgeland, A. King, and M. Reid, "The mckay correspondence as an equivalence of derived categories," *Journal of the American Mathematical Society* **14** no. 3, (2001) 535–554, `arXiv:math/9908027`.

[310] M. Kobayashi, M. Mase, and K. Ueda, "A note on exceptional unimodal singularities and k3 surfaces," *International Mathematics Research Notices* **2013** no. 7, (2013) 1665–1690, `arXiv:1107.2169 [math.AG]`.

[311] Y.-H. He, "On Fields over Fields," `arXiv:1003.2986 [hep-th]`.

[312] O. Schiffmann and E. Vasserot, "On cohomological hall algebras of quivers: generators," *Journal für die reine und angewandte Mathematik (Crelles Journal)* **2020** no. 760, (2020) 59–132, `arXiv:1705.07488 [math.RT]`.

[313] B. Davison, J. Ongaro, and B. Szendroi, "Enumerating coloured partitions in 2 and 3 dimensions," *Math. Proc. Cambridge Phil. Soc.* **169** no. 3, (2020) 479–505, `arXiv:1811.12857 [math.AG]`.

[314] M. R. Gaberdiel, W. Li, C. Peng, and H. Zhang, "The supersymmetric affine Yangian," *JHEP* **05** (2018) 200, `arXiv:1711.07449 [hep-th]`.

[315] M. R. Gaberdiel, W. Li, and C. Peng, "Twin-plane-partitions and $\mathcal{N} = 2$ affine Yangian," *JHEP* **11** (2018) 192, `arXiv:1807.11304 [hep-th]`.

[316] W. Li and P. Longhi, "Gluing two affine Yangians of $\mathfrak{gl}_1$," *JHEP* **10** (2019) 131, `arXiv:1905.03076 [hep-th]`.

[317] M. R. Gaberdiel and R. Gopakumar, "String Theory as a Higher Spin Theory," *JHEP* **09** (2016) 085, `arXiv:1512.07237 [hep-th]`.

[318] S. H. Katz, D. R. Morrison, and M. R. Plesser, "Enhanced gauge symmetry in type II string theory," *Nucl. Phys. B* **477** (1996) 105–140, `arXiv:hep-th/9601108`.

[319] S. Mozgovoy and B. Pioline, "Attractor invariants, brane tilings and crystals," `arXiv:2012.14358 [hep-th]`.

[320] F. Benini, S. Benvenuti, and Y. Tachikawa, "Webs of five-branes and N=2 superconformal field theories," *JHEP* **09** (2009) 052, `arXiv:0906.0359 [hep-th]`.

[321] D. Gaiotto, "N=2 dualities," *JHEP* **08** (2012) 034, `arXiv:0904.2715 [hep-th]`.

[322] B. Acharya, N. Lambert, M. Najjar, E. E. Svanes, and J. Tian, "Gauging Discrete Symmetries of T_N-theories in Five Dimensions," `arXiv:2110.14441 [hep-th]`.

[323] A. E. Lawrence, N. Nekrasov, and C. Vafa, "On conformal field theories in four-dimensions," *Nucl. Phys. B* **533** (1998) 199–209, `arXiv:hep-th/9803015`.

[324] V. G. Kac, *Infinite-dimensional Lie algebras*. Cambridge university press, 1990.

[325] A. Gholampour and Y. Jiang, "Counting invariants for the ADE McKay quivers," `arXiv:0910.5551 [math.AG]`.

[326] S. Mozgovoy, "Motivic Donaldson-Thomas invariants and McKay correspondence," `arXiv:1107.6044 [math.AG]`.

[327] M. Aganagic, H. Ooguri, C. Vafa, and M. Yamazaki, "Wall Crossing and M-theory," *Publ. Res. Inst. Math. Sci. Kyoto* **47** (2011) 569, `arXiv:0908.1194 [hep-th]`.

[328] A. Iqbal, C. Kozcaz, and C. Vafa, "The Refined topological vertex," *JHEP* **10** (2009) 069, `arXiv:hep-th/0701156`.

[329] M. Taki, "Refined Topological Vertex and Instanton Counting," *JHEP* **03** (2008) 048, `arXiv:0710.1776 [hep-th]`.

[330] T. Nishinaka and S. Yamaguchi, "Wall-crossing of D4-D2-D0 and flop of the conifold," *JHEP* **09** (2010) 026, `arXiv:1007.2731 [hep-th]`.

[331] T. Nishinaka, "Multiple D4-D2-D0 on the Conifold and Wall-crossing with the Flop," *JHEP* **06** (2011) 065, `arXiv:1010.6002 [hep-th]`.

[332] T. Nishinaka and S. Yamaguchi, "Statistical model and BPS D4-D2-D0 counting," *JHEP* **05** (2011) 072, `arXiv:1102.2992 [hep-th]`.

[333] T. Nishinaka and Y. Yoshida, "A Note on statistical model for BPS D4-D2-D0 states," *Phys. Lett. B* **711** (2012) 132–138, `arXiv:1108.4326 [hep-th]`.

[334] A. Gholampour, A. Sheshmani, and R. Thomas, "Counting curves on surfaces in Calabi-Yau 3-folds," *Math. Ann.* **360** (2014) 67–78, `arXiv:1309.0051 [math.AG]`.

[335] V. G. Kac, *Vertex algebras for beginners*. No. 10. American Mathematical Soc., 1998.

[336] T. Arakawa and A. Molev, "Explicit generators in rectangular affine $\mathcal{W}$-algebras of type A," *Letters in Mathematical Physics* **107** no. 1, (2017) 47–59, `arXiv:1403.1017 [math.RT]`.

[337] T. Arakawa, "Introduction to W-algebras and their representation theory," in *Perspectives in Lie theory*, pp. 179–250. Springer, 2017. `arXiv:1605.00138 [math.RT]`.

[338] E. Frenkel and D. Ben-Zvi, *Vertex Algebras and Algebraic Curves*. Mathematical surveys and monographs. American Mathematical Society, 2004.

[339] H. Schenck, *Computational Algebraic Geometry*. London Mathematical Society Student Texts. Cambridge University Press, 2003.

[340] D. R. Grayson and M. E. Stillman, "Macaulay2, a software system for research in algebraic geometry." Available at `http://www.math.uiuc.edu/Macaulay2/`.

[341] Y.-H. He, P. Candelas, A. Hanany, A. Lukas, and B. Ovrut, "Computational algebraic geometry in string and gauge theory," *Advances in High Energy Physics* **2012** (03, 2012) .

[342] B. Sturmfels, "Gröbner bases of toric varieties," *Tohoku Math. J. (2)* **43** no. 2, (1991) 249–261. `https://doi.org/10.2748/tmj/1178227496`.

[343] D. Bayer and M. Stillman, "Computation of hilbert functions," *Journal of Symbolic Computation* **14** no. 1, (1992) 31 − 50.